

Utah State University

DigitalCommons@USU

---

All Graduate Theses and Dissertations

Graduate Studies

---

12-2008

## Analysis of Chemical Bonding in Clusters by Means of The Adaptive Natural Density Partitioning

Dmitry Yu Zubarev

Follow this and additional works at: <https://digitalcommons.usu.edu/etd>

 Part of the [Physical Chemistry Commons](#)

---

### Recommended Citation

Zubarev, Dmitry Yu, "Analysis of Chemical Bonding in Clusters by Means of The Adaptive Natural Density Partitioning" (2008). *All Graduate Theses and Dissertations*. 13.  
<https://digitalcommons.usu.edu/etd/13>

This Dissertation is brought to you for free and open access by the Graduate Studies at DigitalCommons@USU. It has been accepted for inclusion in All Graduate Theses and Dissertations by an authorized administrator of DigitalCommons@USU. For more information, please contact [digitalcommons@usu.edu](mailto:digitalcommons@usu.edu).



ANALYSIS OF CHEMICAL BONDING IN CLUSTERS BY MEANS OF THE  
ADAPTIVE NATURAL DENSITY PARTITIONING

by

Dmitry Yu. Zubarev

A dissertation submitted in partial fulfillment  
of the requirements for the degree

of

DOCTOR OF PHILOSOPHY

in

Chemistry

(Physical Chemistry)

Approved:

---

Dr. Alexander I. Boldyrev  
Major Professor

---

Dr. Steve Scheiner  
Committee Member

---

Dr. Stephen E. Bialkowski  
Committee Member

---

Dr. Lisa M. Berreau  
Committee Member

---

Dr. T.-C. Shen  
Committee Member

---

Byron R. Burnham  
Dean of Graduate Studies

UTAH STATE UNIVERSITY  
Logan, Utah

2008

Copyright © Dmitry Yu. Zubarev 2008  
All Rights Reserved

## ABSTRACT

Analysis of Chemical Bonding in Clusters by Means of the  
Adaptive Natural Density Partitioning

by

Dmitry Yu. Zubarev, Doctor of Philosophy

Utah State University, 2008

Major Professor: Dr. Alexander I. Boldyrev  
Department: Chemistry and Biochemistry

Models of chemical bonding are essential for contemporary chemistry. Even the explosive development of the computational resources including, both hardware and software, cannot eliminate necessity of compact, intuitive, and efficient methods of representing chemically relevant information. The Lewis model of chemical bonding, which was proposed eleven years before the formulation of quantum theory and preserves its pivotal role in chemical education and research for more than ninety years, is a vivid example of such a tool. As chemistry shifts to the nanoscale, it is becoming obvious that a certain shift of the paradigms of chemical bonding is inescapable. For example, none of the currently available models of chemical bonding can correctly predict structures and properties of sub-nano and nanoclusters. Clusters of main-group elements and transition metals are of major interest for nanotechnology with potential applications including catalysis, hydrogen storage, molecular conductors, drug development, nanodevices, etc. Thus, the goals of this dissertation were three-fold. Firstly, the dissertation introduces a

novel approach to the description of chemical bonding and the algorithm of the software performing analysis of chemical bonding, which is called Adaptive Natural Density Partitioning. Secondly, the dissertation presents a series of studies of main-group element and transition-metal clusters in molecular beams, including obtaining their photoelectron spectra, establishing their structures, analyzing chemical bonding, and developing generalized model of chemical bonding. Thirdly, the dissertation clarifies and develops certain methodological aspects of the quantum chemical computations dealing with clusters. This includes appraisal of the performance of several computational methods based on the Density Functional Theory and the development of global optimization software based on the Particle Swarm Optimization algorithm.

(431 pages)

## CONTENTS

	Page
ABSTRACT.....	iii
LIST OF TABLES.....	xii
LIST OF FIGURES.....	xiv
CHAPTER	
1. INTRODUCTION.....	1
References.....	4
2. LITERATURE REVIEW.....	5
2-1. Introduction.....	5
2-2. Chemical Bonding Models for Clusters.....	7
2-2.1. Jellium Model.....	8
2-2.2. Aromaticity/Antiaromaticity.....	10
2-3. Conclusion.....	13
References.....	14
3. DEVELOPING PARADIGMS OF CHEMICAL BONDING: ADAPTIVE NATURAL DENSITY PARTITIONING.....	20
Abstract.....	20
3-1. Introduction.....	20
3-2. Adaptive Natural Density Partitioning (AdNDP) Algorithm.....	24
3-3. Theoretical Methods.....	30
3-4. Numerical Application and Discussion.....	30
3-4.1. Li <sub>4</sub> cluster.....	31
3-4.2. B <sub>4</sub> cluster.....	31
3-4.3. B <sub>5</sub> <sup>-</sup> cluster.....	33
3-4.4. B <sub>6</sub> <sup>2-</sup> cluster.....	36
3-4.5. B <sub>9</sub> <sup>-</sup> cluster.....	38
3-4.6. B <sub>11</sub> <sup>-</sup> cluster.....	40
3-4.7. B <sub>13</sub> <sup>+</sup> cluster.....	42

3-5.	Conclusion.....	44
	References.....	46
4.	COMPREHENSIVE ANALYSIS OF CHEMICAL BONDING IN BORON CLUSTERS.....	53
	Abstract.....	53
4-1.	Introduction.....	54
4-2.	Theoretical Methods.....	56
4-3.	Chemical Bonding Analysis.....	57
	4-3.1. $B_3^+$ and $B_3^-$ Clusters.....	60
	4-3.2. $B_4$ and $B_4^{2-}$ Clusters.....	62
	4-3.3. $B_5^+$ and $B_5^-$ Clusters.....	65
	4-3.4. $B_6^{2+}$ , $B_6$ and $B_6^{2-}$ Clusters.....	68
	4-3.5. $B_7^+$ and $B_7^-$ Clusters.....	73
	4-3.6. $B_8$ , $B_8^{2-}$ and $B_9^-$ Clusters.....	76
	4-3.7. $B_{10}$ , $B_{11}^+$ and $B_{11}^-$ Clusters.....	80
	4-3.8. $B_{12}$ and $B_{13}^+$ Clusters.....	84
	4-3.9. $B_{14}$ and $B_{15}^-$ Clusters.....	87
4-4.	Overview.....	90
	References.....	93
5.	AROMATICITY AND ANTIAROMATICITY IN TRANSITION-METAL SYSTEMS.....	101
	Abstract.....	101
5-1.	Introduction.....	102
5-2.	s-AO based $\sigma$ -aromaticity and $\sigma$ -antiaromaticity in transition metal systems.....	107
	5-2.1. s-AO based $\sigma$ -aromaticity and $\sigma$ -antiaromaticity in $M_3$ clusters.....	107
	5-2.2. s-AO based $\sigma$ -aromaticity in $M_4^{2-}$ clusters.....	110
	5-2.3. s-AO based $\sigma$ -aromaticity in the $Au_5Zn^+$ cluster and $Au_6$ .....	111
	5-2.4. s-AO based $\sigma$ -aromaticity in the cyclo- $M_nH_n$ ( $M = Cu, Ag, Au; n = 3-6$ ), cyclo- $Au_3L_nH_{3-n}$ ( $L = CH_3, NH_2, OH, \text{ and } Cl; n = 1-3$ ), cyclo- $Cu_nAg_{k-n}H_n$ ( $n = 1-k, k = 3-5$ ) clusters.....	113
5-3.	p-AO based aromaticity and antiaromaticity	

in transition metal systems.....	117
5-3.1. p-AO based multiple aromaticity in the $\text{Hg}_4^{6-}$ cluster.....	117
5-3.2. p-AO based multiple aromaticity in the $\text{M}_3^{2-}$ , $\text{NaM}_3^-$ , $\text{Na}_2\text{M}_3$ (M = Zn, Cd, Hg) clusters.....	119
5-4. d-AO based aromaticity and antiaromaticity in transition metal systems.....	120
5-4.1. d-AO based $\sigma$ -aromaticity in the $\text{Mo}_3\text{O}_9^{2-}$ and $\text{W}_3\text{O}_9^{2-}$ clusters.....	121
5-4.2. d-AO based $\sigma$ -and $\pi$ - double aromaticity in $\text{X}_3^-$ (X = Sc, Y, La) clusters.....	124
5-4.3. d-AO based $\pi$ -and $\delta$ - double aromaticity in the $\text{Ta}_3\text{O}_3^-$ cluster.....	125
5-4.4. d-AO based $\sigma$ -, $\pi$ -and $\delta$ - triple aromaticity in the $\text{Hf}_3$ cluster.....	127
5-5. Summary and Overview.....	127
References.....	131
6. $\delta$ -AROMATICITY IN $[\text{Ta}_3\text{O}_3]^-$ .....	137
Abstract.....	137
6-1. Introduction.....	138
6-2. Experimental Method.....	139
6-3. Theoretical Methods.....	140
6-4. Results and Discussion.....	141
6-5. Conclusion.....	145
References.....	146
7. OBSERVATION OF TRIATOMIC SPECIES WITH CONFLICTING AROMATICITY: $\text{AlSi}_2^-$ AND $\text{AlGe}_2^-$ .....	150
Abstract.....	150
7-1. Introduction.....	150
7-2. Experimental Method.....	152
7-3. Theoretical Methods.....	152
7-4. Results and Discussion.....	153
7-5. Conclusion.....	159
References.....	159
8. GOLD APES HYDROGEN. THE STRUCTURE AND BONDING IN THE PLANAR $\text{B}_7\text{Au}_2^-$ AND $\text{B}_7\text{Au}_2$ CLUSTERS.....	163



	Abstract.....	163
8-1.	Introduction.....	163
8-2.	Experimental Method.....	165
8-3.	Theoretical Methods.....	166
8-4.	Results and Discussion.....	169
8-5.	Conclusion.....	172
	References.....	173
9.	ON THE CHEMICAL BONDING OF GOLD IN AURO-BORON OXIDE CLUSTERS $Au_nBO^-$ ( $n = 1-3$ ).....	176
	Abstract.....	176
9-1.	Introduction.....	177
9-2.	Experimental and Computational Methods.....	180
	9-2.1. Photoelectron Spectroscopy.....	180
	9-2.2. Computational Methods.....	181
9-3.	Experimental Results.....	182
	9-3.1. $AuBO^-$ .....	182
	9-3.2. $Au_2BO^-$ .....	187
	9-3.3. $Au_3BO^-$ .....	187
9-4.	Theoretical Results.....	188
	9-4.1. $AuBO^-$ and $HBO^-$ .....	188
	9-4.2. $Au_2BO^-$ and $H_2BO^-$ .....	191
	9-4.3. $Au_3BO^-$ and $H_3BO^-$ .....	191
9-5.	Interpretation of the Experimental Photoelectron Spectra.....	192
	9-5.1. $AuBO^-$ .....	192
	9-5.2. $Au_2BO^-$ .....	193
	9-5.3. $Au_3BO^-$ .....	194
9-6.	Chemical Bonding in $Au_nBO^-$ and $H_nBO^-$ ( $n = 1-3$ ).....	196
	9-6.1. $AuBO^-$ and $HBO^-$ .....	196
	9-6.2. $Au_2BO^-$ and $H_2BO^-$ .....	198
	9-6.3. $Au_3BO^-$ and $H_3BO^-$ .....	203
	9-6.4. $Au_nBO^-$ vs $Au_nCO$ .....	206
9-7.	Conclusion.....	207
	References.....	208

10. THEORETICAL PROBING OF DELTAHEDRAL CLOSO-AURO-BORANES $B_xAu_x^{2-}$ ( $x = 5-12$ ) .....	215
Abstract.....	215
10-1. Introduction.....	215
10-2. Theoretical Methods.....	217
10-3. Results and Discussion.....	219
10-4. Conclusion.....	221
References.....	223
11. $Sn_{12}^{2-}$ : STANNASPHERE.....	226
Abstract.....	226
11-1. Introduction and Experimental Method.....	226
11-2. Results and Discussion.....	227
11-3. Conclusion.....	231
References.....	231
12. CHEMICAL BONDING IN $Si_5^{2-}$ AND $NaSi_5^-$ VIA PHOTOELECTRON SPECTROSCOPY AND AB INITIO CALCULATIONS.....	234
Abstract.....	234
12-1. Introduction.....	235
12-2. Experimental Method.....	237
12-3. Theoretical Methods.....	237
12-4. Experimental Results.....	238
12-4.1. Photoelectron spectroscopy of $Si_5^-$ .....	238
12-4.2. Photoelectron spectroscopy $NaSi_5^-$ .....	241
12-5. Theoretical Results.....	244
12-5.1. $Si_5^{2-}$ .....	246
12-5.2. $Si_5^-$ and $Si_5$ .....	249
12-5.3. $NaSi_5^-$ .....	252
12-6. Interpretation of the Photoelectron Spectra of $Si_5^-$ and $NaSi_5^-$ .....	255
12-6.1. $Si_5^-$ .....	255
12-6.2. $NaSi_5^-$ .....	258
12-7. Chemical Bonding in $Si_5$ , $Si_5^-$ and $Si_5^{2-}$ .....	260

12-7.1. NPA analysis.....	261
12-7.2. Molecular orbital analysis.....	261
12-7.3. ELF analysis.....	261
12-7.4. NICS analysis.....	264
12-8. Conclusion.....	266
12-9. References.....	266
13. ON THE STRUCTURE AND CHEMICAL BONDING OF Si <sub>6</sub> <sup>2-</sup> AND Si <sub>6</sub> <sup>2-</sup> IN NaSi <sub>6</sub> <sup>-</sup> UPON Na <sup>+</sup> COORDINATION.....	277
Abstract.....	277
13-1. Introduction.....	278
13-2. Experimental Methods.....	280
13-3. Theoretical Methods.....	281
13-4. Experimental Results.....	282
13-4.1. Photoelectron Spectroscopy of Si <sub>6</sub> <sup>-</sup> .....	282
13-4.2. Photoelectron Spectroscopy of NaSi <sub>6</sub> <sup>-</sup> .....	286
13-5. Theoretical Results.....	288
13-5.1. Si <sub>6</sub> <sup>-</sup> .....	288
13-5.2. Si <sub>6</sub> <sup>2-</sup> .....	288
13-5.3. LiSi <sub>6</sub> <sup>-</sup> and NaSi <sub>6</sub> <sup>-</sup> .....	292
13-6. Interpretation of the Photoelectron Spectra.....	294
13-6.1. Si <sub>6</sub> <sup>-</sup> .....	294
13-6.2. NaSi <sub>6</sub> <sup>-</sup> .....	298
13-6.2.1. NaSi <sub>6</sub> <sup>-</sup> (C <sub>2v</sub> , <sup>1</sup> A <sub>1</sub> ).....	298
13-6.2.2. NaSi <sub>6</sub> <sup>-</sup> (C <sub>3v</sub> , <sup>1</sup> A <sub>1</sub> ).....	299
13-7. Chemical Bonding in Si <sub>6</sub> <sup>2-</sup> and NaSi <sub>6</sub> <sup>-</sup> .....	300
13-7.1. NBO Analysis.....	300
13-7.2. MO Analysis.....	302
13-7.3. ELF Analysis.....	304
13-7.4. Protonation as a Way to Increase the Relative Stability of the Octahedral Si <sub>6</sub> <sup>2-</sup> ?.....	309
13-8. Conclusions.....	310
References.....	311

14. APPRAISAL OF THE PERFORMANCE OF NONHYBRID DENSITY FUNCTIONAL METHODS IN CHARACTERIZATION OF THE $Al_4C$ MOLECULE.....	317
Abstract.....	317
14-1. Introduction.....	318
14-2. Theoretical Methods.....	322
14-3. Results of Calculations and Discussion.....	324
14-4. Conclusions.....	333
References.....	334
15. GLOBAL MINIMUM STRUCTURE SEARCHES VIA PARTICLE SWARM OPTIMIZATION.....	337
Abstract.....	337
15-1. Introduction.....	337
15-2. Size of the Search Space.....	341
15-3. Current Techniques for Finding Global Minimum Structures.....	344
15-4. Particle Swarm Optimization.....	346
15-4.1. Generalized Particle Swarm Optimization.....	346
15-4.2. Particle Swarm Optimization for Finding Stable Chemical Structures.....	347
15-4.3. Random Initialization of Chemical Structures.....	348
15-4.4. Enforcing Minimum Distance Constraints in PSO.....	351
15-4.5. Using a Local-Neighborhood with PSO.....	352
15-4.6. Distance Metric Comparing Pairs of Structures.....	353
15-4.7. Attraction and Repulsion Phases to Preserve Diversity.....	354
15-5. Computational Results.....	356
15-6. Conclusion.....	361
References.....	362
16. SUMMARY.....	372
References.....	378
APPENDIX.....	380
CURRICULUM VITAE.....	404

## LIST OF TABLES

Table	Page
3-1. Results of the NBO analysis for B <sub>4</sub> D <sub>2h</sub> ( <sup>1</sup> A <sub>g</sub> ) cluster.....	34
4-1. Computed features of the chemical bonding in boron clusters.....	59
4-2. Localized MOs of the D <sub>2h</sub> <sup>1</sup> A <sub>g</sub> structure of B <sub>4</sub> .....	63
5-1. Criteria for π-Aromaticity and π-Antiaromaticity.....	104
5-2. Binding Energies ΔE <sub>1</sub> and ΔE <sub>2</sub> , GIAO-SCF NICS and Electrophilicity of Cu <sub>n</sub> H <sub>n</sub> (n = 3-6).....	115
6-1. Experimental VDEs [eV] for [Ta <sub>3</sub> O <sub>3</sub> ] <sup>-</sup> compared with those calculated for the D <sub>3h</sub> global minimum.....	140
7-1. Experimental ADEs and VDEs of AlCGe <sup>-</sup> , AlSi <sub>2</sub> <sup>-</sup> , and AlGe <sub>2</sub> <sup>-</sup> compared with computed VDEs at different levels of theory.....	155
8-1. Experimental Vertical Detachment Energies (VDEs) of B <sub>7</sub> Au <sub>2</sub> <sup>-</sup> from the Photoelectron Spectra, Compared with Theoretical Calculations.....	168
9-1. Experimental and Theoretical Vertical Detachment Energies for Au <sub>n</sub> BO <sup>-</sup> (n = 1-3). All energies are in eV.....	186
9-2. Calculated molecular properties of the lowest-energy structures of auro-borane oxides Au <sub>n</sub> BO <sup>-</sup> (n = 1-3).....	190
12-1. Experimental VDEs compared with the calculated VDEs for the D <sub>3h</sub> ( <sup>2</sup> A <sub>2</sub> '') Si <sub>5</sub> <sup>-</sup> .....	242
12-2. Experimental VDEs compared with the calculated VDEs for the C <sub>s</sub> ( <sup>1</sup> A') NaSi <sub>5</sub> <sup>-</sup> .....	245
12-3. Calculated molecular properties of Si <sub>5</sub> <sup>2-</sup> D <sub>3h</sub> ( <sup>1</sup> A <sub>1</sub> ').....	248
12-4. Calculated molecular properties of Si <sub>5</sub> <sup>-</sup> D <sub>3h</sub> ( <sup>2</sup> A <sub>2</sub> '').....	250
12-5. Calculated molecular properties of Si <sub>5</sub> D <sub>3h</sub> ( <sup>1</sup> A <sub>1</sub> ').....	251
12-6. Calculated molecular properties of NaSi <sub>5</sub> <sup>1-</sup> C <sub>s</sub> ( <sup>1</sup> A').....	254

12-7.	Calculated NICS (ppm) indices for $\text{Si}_5^{2-}$ , $\text{Si}_5^-$ , $\text{Si}_5$ at B3LYP/6-311+G*.....	265
13-1.	Experimental and theoretical Vertical Detachment Energies for $\text{Si}_6^-$ . All energies are in eV.....	285
13-2.	Experimental and theoretical Vertical Detachment Energies for $\text{NaSi}_6^-$ . All energies are in eV.....	289
13-3.	Calculated molecular properties of $\text{C}_{2v}$ ( $^2\text{B}_2$ ) and $\text{D}_{4h}$ ( $^2\text{A}_{2u}$ ) isomers of $\text{Si}_6^-$ .....	291
13-4.	Calculated molecular properties of $\text{O}_h$ ( $^1\text{A}_{1g}$ ) and $\text{C}_{2v}$ ( $^1\text{A}_1$ ) isomers of $\text{Si}_6^{2-}$ .....	293
13-5.	Calculated molecular properties of $\text{C}_{2v}$ ( $^1\text{A}_1$ ) and $\text{C}_{3v}$ ( $^1\text{A}_1$ ) isomers of $\text{NaSi}_6^-$ .....	295
14-1.	Calculated molecular properties of the $\text{T}_d$ ( $^1\text{A}_1$ ) structure of $\text{Al}_4\text{C}$ .....	326
14-2.	Calculated molecular properties of the $\text{D}_{4h}$ ( $^1\text{A}_{1g}$ ) structure of $\text{Al}_4\text{C}$ .....	327
14-3.	Calculated molecular properties of the $\text{C}_{2v,\text{I}}$ ( $^1\text{A}_1$ ) structure of $\text{Al}_4\text{C}$ .....	328
14-4.	Calculated molecular properties of the $\text{C}_{2v,\text{II}}$ ( $^1\text{A}_1$ ) structure of $\text{Al}_4\text{C}$ .....	330
14-5.	Calculated molecular properties of the $\text{C}_s$ , ( $^1\text{A}'$ ) structure of $\text{Al}_4\text{C}$ .....	332
15-1.	PSO Search Results for $\text{LJ}_{26}$ , $\text{Si}_2\text{H}_5$ , and $\text{OH}(\text{H}_2\text{O})_3$ .....	359

## LIST OF FIGURES

Figure	Page
3-1. a) Structure and CMOs of $\text{Li}_4 \text{D}_{2h} (^1\text{A}_g)$ cluster; b) results of the AdNDP localization.....	32
3-2. a) Structure and CMOs of $\text{B}_4 \text{D}_{2h} (^1\text{A}_g)$ cluster; b) results of the AdNDP localization.....	33
3-3. a) Structure and CMOs of $\text{B}_5^- \text{C}_{2v} (^1\text{A}_1)$ cluster; b) results of the AdNDP localization.....	35
3-4. a) Structure and CMOs of $\text{B}_6^{2-} \text{D}_{2h} (^1\text{A}_g)$ cluster; b) results of the AdNDP localization.....	37
3-5. a) Structure and CMOs of $\text{B}_9^- \text{D}_{8h} (^1\text{A}_{1g})$ cluster; b) results of the AdNDP localization.....	39
3-6. a) Structure and CMOs of $\text{B}_{11}^- \text{C}_{2v} (^1\text{A}_1)$ cluster; b) results of the AdNDP localization.....	41
3-7. a) Structure and CMOs of $\text{B}_{13}^+ \text{C}_{2v} (^1\text{A}_1)$ cluster; b) results of the AdNDP localization.....	43
4-1. Global minimum structures of $\text{B}_3^+$ , $\text{B}_3^-$ , $\text{B}_4$ , $\text{B}_5^+$ , $\text{B}_5^-$ , $\text{B}_6^{2+}$ , $\text{B}_6$ , $\text{B}_6^{2-}$ , $\text{B}_7^+$ , $\text{B}_7^-$ , $\text{B}_8^{2-}$ , $\text{B}_9^-$ , $\text{B}_{10}$ , $\text{B}_{11}^+$ , $\text{B}_{11}^-$ , $\text{B}_{12}$ , $\text{B}_{13}^+$ , $\text{B}_{14}$ , and $\text{B}_{15}^-$ as reported in ref. 63.....	58
4-2. Molecular orbitals of the $\text{B}_3^+$ cation.....	61
4-3. Molecular orbitals of the $\text{B}_4$ cluster.....	64
4-4. Molecular orbitals of the $\text{B}_5^+$ cation.....	66
4-5. (a) Molecular orbitals of the $\text{D}_{6h} (^1\text{A}_{1g})$ structure of the $\text{B}_6^{2+}$ cluster; (b) molecular orbitals of the $\text{C}_{5v} (^1\text{A}_1)$ structure of the $\text{B}_6$ cluster; (c) molecular orbitals of the $\text{D}_{5h} (^1\text{A}_1')$ structure of the $\text{B}_6$ cluster; (d) molecular orbitals of the $\text{B}_6^{2-}$ dianion.....	69
4-6. Nonidentical circuits in $\text{B}_6^{2-}$ (adopted from ref. 20).....	73
4-7. (a) Molecular orbitals of the $\text{C}_{6v} (^1\text{A}_1)$ structure of the $\text{B}_7^+$ cluster; (b) molecular orbitals of the $\text{D}_{6h} (^1\text{A}_{1g})$ structure of the	

	$B_7^+$ cluster.....	74
4-8.	Molecular orbitals of the $D_{7h}$ ( $^1A_1'$ ) structure of the $B_8^{2-}$ dianion.....	77
4-9.	Molecular orbitals of the $D_{8h}$ ( $^1A_{1g}$ ) structure of the $B_9^-$ anion.....	79
4-10.	Molecular orbitals of the $D_{2h}$ ( $^1A_g$ ) structure of the $B_{10}$ cluster.....	81
4-11.	(a) Molecular orbitals of the $C_{2v}$ ( $^1A_1$ ) structure of the $B_{11}^+$ cation; (b) Molecular orbitals of the $C_{2v}$ ( $^1A_1$ ) structure of the $B_{11}^-$ anion....	83
4-12.	Molecular orbitals of the $D_{3h}$ ( $^1A_1'$ ) structure of the $B_{12}$ cluster.....	86
4-13.	Molecular orbitals of the $C_{2v}$ ( $^1A_1$ ) structure of the $B_{13}^+$ cation.....	88
4-14.	Molecular orbitals of the $D_{2h}$ ( $^1A_g$ ) structure of the $B_{14}$ cluster.....	89
4-15.	Molecular orbitals of the $C_{2v}$ ( $^1A_1$ ) structure of the $B_{15}^-$ anion.....	90
5-1.	(a) The $3a_1'$ -HOMO of $Cu_3^+$ and its schematic representation as a linear combination of 4s-AOs of Cu atoms, (b) $1a_2''$ -HOMO of $C_3H_3^+$ and its schematic representation as a linear combination of $2p_z$ -AOs of C atoms.....	108
5-2.	Optimized structures of $Cu_4Li_2$ , $Ag_4Li_2$ , and $Au_4Li_2$ . <sup>59</sup> .....	111
5-3.	Three reported isomers of $Au_5Zn^+$ . <sup>58</sup> .....	112
5-4.	Pictures of valence MOs of $Au_5Zn^+$ isomers shown in Figure 3 a and b.....	112
5-5.	Optimized planar cyclic structures of $Cu_nH_n$ clusters. <sup>54</sup> .....	114
5-6.	(a) s-MOs, (b) p-MOs, and (c) d-MOs composed out of d-AOs of Cu in $Cu_4H_4$ ( $D_{4h}$ , $^1A_{1g}$ ).....	116
5-7.	Valence molecular orbitals of $Hg_4^{6-}$ .....	118
5-8.	Molecular orbital diagram for a) $\pi$ -MOs and b) $\sigma$ -MOs for $Hg_4^{6-}$ .....	118
5-9.	Optimized structures for $M_3O_9$ (a, d) $M_3O_9^-$ (b, e) and $M_3O_9^{2-}$ (c, f) (M = Mo, W) clusters. <sup>64</sup> .....	122
5-10.	HOMOs in the $M_3O_9^-$ and $M_3O_9^{2-}$ species (M = Mo and W). <sup>64</sup> .....	123



5-11.	Valence MOs of $X_3^-$ ( $X = \text{Sc}, \text{Y}, \text{La}$ ) anions.....	124
5-12.	Optimized structure (a) and valence MOs (b) of $\text{Ta}_3\text{O}_3^-$ . <sup>65</sup> .....	125
5-13.	Optimized structure (a) and valence MOs (b) of the $\text{Hf}_3$ cluster in the $D_{3h}, ^1A_1'$ state.....	128
6-1.	Photoelectron spectra of $[\text{Ta}_3\text{O}_3]^-$ . a) 193 nm (6.424 eV); b) 157 nm (7.866 eV).....	139
6-2.	Optimized structures for the global minimum of $[\text{Ta}_3\text{O}_3]^-$ ( $D_{3h}, ^1A_1'$ ) and selected low-lying isomers. The relative energies $\Delta E_{\text{total}}$ [ $\text{kcal mol}^{-1}$ ] and interatomic distances [ $\text{\AA}$ ] were calculated at the B3LYP/Ta/Stuttgart+2flg/O/aug-cc-pvTZ level of theory ( $\Delta E_{\text{total}}$ at the B3PW91/Ta/Stuttgart+2flg/O/aug-cc-pvTZ level is shown in brackets).....	142
6-3.	The five valence MOs responsible for the metal–metal bonding in $[\text{Ta}_3\text{O}_3]^-$ ( $D_{3h}, ^1A_1'$ ).....	143
7-1.	Computationally found isomers for $\text{AlC}_2^-$ , $\text{AlCSi}^-$ , $\text{AlCGe}^-$ , $\text{AlSi}_2^-$ , $\text{AlSiGe}^-$ , $\text{AlGe}_2^-$ , $\text{Si}_3^{2+}$ , and $\text{Si}_3$ . Effective atomic charges were calculated using NBO analysis.....	154
7-2.	Photoelectron spectra of $\text{AlCGe}^-$ (a), $\text{AlSi}_2^-$ (b), and $\text{AlGe}_2^-$ (c) at 355 nm (3.496 eV) and 266 nm (4.661 eV). The vertical bars represent the calculated VDEs for the global minimum for each species at the ROVGF level of theory (Table 7-1).....	156
7-3.	Molecular orbitals of $\text{Si}_3^{2+}$ (a), $\text{Si}_3$ (b), and $\text{AlSi}_2^-$ (c).....	158
8-1.	(a) Low-energy isomers of the $\text{B}_7^-$ cluster at the B3LYP/6-311+G* level of theory (relative energies computed at the CCSD(T)/6-311+G(2df) level are shown in square brackets). <sup>12</sup> (b) The global minimum and two low-lying isomers of $\text{B}_7\text{H}_2^-$ at B3LYP/6-311+G* level. <sup>16</sup> .....	164
8-2.	Photoelectron spectra of $\text{Au}_2\text{B}_7^-$ at (a) 266 nm (4.661 eV) and (b) 193 nm (6.424 eV). The 193 nm spectrum of $\text{B}_7^-$ (c) is also included for comparison. <sup>12</sup> .....	167
8-3.	The global minimum and low-lying isomers of $\text{B}_7\text{Au}_2^-$ at B3LYP/B/cc-pvDZ/Au/ level.....	169
8-4.	Molecular orbitals (B3LYP/B/cc-pvDZ/Au/LANL2DZ)	

	of Au <sub>2</sub> B <sub>7</sub> <sup>-</sup> C <sub>2v</sub> ( <sup>1</sup> A <sub>1</sub> ). MOs are ordered according to the TD-B3LYP/B/aug-cc-pvTZ/Au/ Stuttgart_rsc_1997_ecp level of theory.....	170
9-1.	Photoelectron spectra of AuBO <sup>-</sup> at (a) 532 nm, (b) 355 nm, and (c) 193 nm. Vertical bars in (a) represent vibrational structures.....	183
9-2.	Photoelectron spectra of Au <sub>2</sub> BO <sup>-</sup> at (a) 266 nm and (b) 193 nm.....	184
9-3.	Photoelectron spectra of Au <sub>3</sub> BO <sup>-</sup> at (a) 355 nm, (b) 266 nm, and (c) 193 nm.....	185
9-4.	Structures of the most stable isomers of auro-borane oxides Au <sub>n</sub> BO <sup>-</sup> (n = 1-3) and boron hydride oxides H <sub>n</sub> BO <sup>-</sup> (n = 1-3): (a) AuBO <sup>-</sup> and HBO <sup>-</sup> , (b) Au <sub>2</sub> BO <sup>-</sup> and H <sub>2</sub> BO <sup>-</sup> , (c) Au <sub>3</sub> BO <sup>-</sup> and H <sub>3</sub> BO <sup>-</sup> .....	189
9-5.	Molecular orbitals of AuBO <sup>-</sup> C <sub>∞v</sub> ( <sup>2</sup> Σ <sup>+</sup> ).....	197
9-6.	Molecular orbitals of Au <sub>2</sub> BO <sup>-</sup> C <sub>2v</sub> ( <sup>1</sup> A <sub>1</sub> ).....	199
9-7.	Molecular orbitals of Au <sub>2</sub> BO <sup>-</sup> C <sub>∞v</sub> ( <sup>1</sup> Σ <sup>+</sup> ).....	202
9-8.	Molecular orbitals of Au <sub>3</sub> BO <sup>-</sup> C <sub>2v</sub> ( <sup>2</sup> B <sub>2</sub> ).....	204
9-9.	Molecular orbitals of Au <sub>3</sub> BO <sup>-</sup> C <sub>s</sub> ( <sup>2</sup> A').....	205
10-1.	Optimized geometric structures of B <sub>x</sub> H <sub>x</sub> <sup>2-</sup> and B <sub>x</sub> Au <sub>x</sub> <sup>2-</sup> (x = 5-12) with selected B-B distances in Å (Yellow – Au; Blue – B; Orange – H).....	220
10-2.	Calculated natural bond effective atomic charges in  e  (at B3LYP/ LANL2DZ) for B <sub>x</sub> H <sub>x</sub> <sup>2-</sup> and B <sub>x</sub> Au <sub>x</sub> <sup>2-</sup> (x = 5-12).....	222
11-1.	Photoelectron spectra of (a) Sn <sub>12</sub> <sup>-</sup> and (b) KSn <sub>12</sub> <sup>-</sup> at 193 nm. (c) Scalar relativistic (SR) energy levels of the 5p-based valence molecular orbitals of the I <sub>h</sub> Sn <sub>12</sub> <sup>2-</sup> and the correlation to the spin-orbit (SO) coupled levels of I <sub>h</sub> * Sn <sub>12</sub> <sup>2-</sup> , where the asterisk indicates the double-group symmetry.....	228
11-2.	Optimized structures: (a) Sn <sub>12</sub> <sup>-</sup> ; (b) Sn <sub>12</sub> <sup>2-</sup> ; (c) KSn <sub>12</sub> <sup>-</sup> . The bond distances and cage diameters are in Å.....	230

12-1. Photoelectron spectra of $\text{Si}_5^-$ at (a) 355 nm (3.496 eV), (b) 266 nm (4.661 eV), (c) 193 nm (6.424 eV), and (d) 157 nm (7.766 eV).....	239
12-2. Photoelectron spectra of $\text{NaSi}_5^-$ at (a) 355 nm (3.496 eV), (b) 266 nm (4.661 eV), and (c) 193 nm (6.424 eV).....	243
12-3. Optimized geometries (B3LYP/6-311+G*) of $\text{Si}_5^{2-}$ (a, b, c), $\text{Si}_5^-$ (d, e, f), $\text{Si}_5$ (g, h), and $\text{NaSi}_5^-$ (i, j). Relative geometries are given at CCSD(T)/6-311+G(2df)//B3LYP/6-311+G*. NIMAG – number of imaginary frequencies.....	247
12-4. Valence molecular orbitals of (a) $\text{Si}_5^{2-}$ ( $D_{3h}$ , $^1A_1'$ ) and (b) $\text{B}_5\text{H}_5^{2-}$ ( $D_{3h}$ , $^1A_1'$ ) at the RHF/6-311+G* level of theory.....	256
12-5. The ELF bifurcations for (a) $\text{B}_5\text{H}_5^{2-}$ ( $D_{3h}$ , $^1A_1'$ ), (b) $\text{Si}_5^{2-}$ ( $D_{3h}$ , $^1A_1'$ ) and $\text{Si}_5$ ( $D_{3h}$ , $^1A_1'$ ) calculated at the B3LYP/6-311+G* level of theory.....	263
13-1. Photoelectron spectra of $\text{Si}_6^-$ at (a) 355nm (3.496 eV), (b) 266 nm (4.661 eV), and (c) 193 nm (6.424 eV).....	284
13-2. Photoelectron spectra of $\text{NaSi}_6^-$ at (a) 355nm (3.496 eV), (b) 266 nm (4.661 eV), and (c) 193 nm (6.424 eV).....	287
13-3. Structures of isomers for $\text{Si}_6^-$ (I, II), $\text{Si}_6^{2-}$ (III, IV), $\text{NaSi}_6^-$ (V, VI), $\text{B}_6\text{H}_6^{2-}$ (VII, VIII), and $\text{Si}_6\text{H}_6^{4+}$ (IX, X).....	290
13-4. Molecular orbitals of $\text{Si}_6^{2-}$ $C_{2v}$ ( $^1A_1$ ) and $\text{NaSi}_6^-$ $C_{2v}$ ( $^1A_1$ ).....	303
13-5. Molecular orbitals of $\text{B}_6\text{H}_6^{2-}$ $O_h$ ( $^1A_{1g}$ ) and $\text{Si}_6^{2-}$ $O_h$ ( $^1A_{1g}$ ).....	305
13-6. Bifurcations of ELF for $\text{B}_6\text{H}_6^{2-}$ ( $O_h$ , $^1A_{1g}$ ), $\text{Si}_6^{2-}$ ( $O_h$ , $^1A_{1g}$ ), $\text{Si}_6^{2-}$ ( $C_{2v}$ , $^1A_1$ ), and $\text{NaSi}_6^-$ ( $C_{2v}$ , $^1A_1$ ).....	308
14-1. Optimized alternative structure of an $\text{Al}_4\text{C}$ molecule. Relative energies are given at the CCSD(T)/6-311+G(2df)// CCSD(T)/6-311+G* and at the CASSCF(8,10)-MRCISD(Q)/ 6-311+G* levels of theory (in parentheses). NIMAG is the number of imaginary frequencies.....	320
15-1. Example illustrations of (a) fragmented structures, (b) partially non-fragmented structures, and (c) completely non-fragmented (connected) structures.....	350

- 15-2. Diagram, illustrating how unit 1 is positioned relative to unit 2 along the line L. Atom 1 and atom 2 are the closest atoms in the two units..... 351
- 15-3. Global minimum structures of the test systems:  
a)  $\text{LJ}_{26}$ , (b)  $\text{Si}_2\text{H}_5$ , and (c)  $\text{OH}(\text{H}_2\text{O})_3$ ..... 360

## CHAPTER 1

### INTRODUCTION

The concept of a pair of electrons with antiparallel spins as the central object of the chemical bonding theory<sup>1</sup> is the cornerstone of contemporary chemistry. Recent commemoration<sup>2</sup> of the general theory of chemical bonding proposed by Lewis, which has been forming the landscape of chemistry for more than ninety years, demonstrated both the viability of this model and the existing tendency to go beyond its framework. The search for new approaches to define and describe chemical bonding is motivated both by conceptual difficulties of the issue, such as the lack of observables directly associated with chemical bonds,<sup>3-6</sup> the constant development of basic quantum chemical theoretical techniques,<sup>7</sup> and the existence of chemical objects that can't be satisfactorily described by any of the currently available models of bonding.

Clusters of the main group elements and transition metals represent one of the biggest challenges to modern theoretical and experimental chemistry. Clusters are generally metastable and their synthesis and characterization under ambient conditions is extremely difficult. Studies of clusters in mass spectrometer ion sources and molecular beams do not provide structural information. The structure and properties of clusters strongly depend on their size and even a difference in one atom or one electron can lead to tremendous structural rearrangements and change of properties, both chemical and physical.<sup>8-13</sup> The forces responsible for holding clusters together range from van der Waals to ionic. The intermediate position of clusters with respect to single molecules on one side, and condensed phase on the other, makes it difficult to utilize theoretical tools

applicable in the limiting cases. Actually, all of the stages of cluster research pose very puzzling problems, ranging from distinguishing multiple isomers in the photoelectron spectra to the rationalization of the patterns of cluster growth. But all these difficulties are worth overcoming because the advent of the nano-era is impossible without fully understanding nano-objects that include clusters among others.

This dissertation deals with the complete cycle of sub-nanocluster research. Chapter 2 is a review of previously performed studies in the field of models of chemical bonding in clusters. Chapter 3 is dedicated to the Adaptive Natural Density Partitioning (AdNDP) algorithm, which is a conceptually new approach to the description of chemical bonding in main-group element and transition metal clusters. The concept, theoretical formalism, and the algorithm implemented in the developed software are discussed together with examples of application of this method. Chapters 4 and 5 are literature review of application of the concepts of localized and delocalized (aromaticity/antiaromaticity) bonding to certain chemical systems. Comprehensive analysis of chemical bonding in planar and quasi-planar boron clusters is performed in Chapter 4. It is shown that the rationalization of the structures and properties of the family of planar boron clusters requires considering  $\sigma$ -localized and  $\sigma$ - and  $\pi$ -delocalized bonding. The topic of Chapter 5 is utilization of the concepts of aromaticity and antiaromaticity in the description of chemical bonding in transition-metal systems. The possible origin and types of the aromatic/antiaromatic bonding encountered in transition metal systems are discussed with consideration and analysis of examples of the various bonding situations reported previously.

Chapter 6 opens the part of the dissertation dealing with studies of individual clusters. The studies combine photoelectron spectroscopy of clusters in molecular beams and ab-initio or Density Functional Theory (DFT) calculations. The emphasis is made on the development of chemical bonding models for the systems under investigation. The identification of  $\delta$ -aromaticity in the  $\text{Ta}_3\text{O}_3^-$  cluster, which is a new mode of chemical bonding, is the topic of Chapter 6. Chapter 7 describes the observation and theoretical characterization of the conflicting aromaticity in triatomic  $\text{AlSi}_2^-$  and  $\text{AlGe}_2^-$  species. Chapter 8 reports analyses of the interesting phenomenon of gold atoms “aping” hydrogen in bonding with planar boron units within  $\text{B}_7\text{Au}_2^-$  and  $\text{B}_7\text{Au}_2$  clusters. Chapter 9 contains a further study of the analogy between gold and hydrogen in bonding with boron atoms in the case of auro-boron oxide clusters  $\text{Au}_x\text{BO}^-$  ( $x=1-3$ ). The utilization of the analogy between gold and hydrogen atoms for the theoretical prediction of a new class of boron compounds – deltahedral closo-auro-boranes  $\text{B}_x\text{Au}_x^{2-}$  ( $x=5-12$ ), is discussed in Chapter 10. Chapter 11 reports the observation and theoretical characterization of the spherical  $\text{Sn}_{12}^-$  species “stannaspherene,” which is analogous to the famous deltahedral closo-borane  $\text{B}_{12}\text{H}_{12}^{2-}$ . Chapters 12 and 13 present a series of studies into the chemical bonding in 3-dimensional silicon anionic clusters. The peculiarity of the  $\text{Si}_x^{2-}$  clusters is a strong deviation of the geometry of most of the systems from the highly symmetric spherical cages typical of the isoelectronic deltahedral closo-boranes  $\text{B}_x\text{H}_x^{2-}$ . Thus, Chapter 12 reports study of  $\text{Si}_5^-$  and  $\text{NaSi}_5^-$  by means of the combination of photoelectron spectroscopy and theoretical calculations and Chapter 13 reports joint experimental and theoretical study of the structure and chemical bonding of  $\text{Si}_6^{2-}$  and  $\text{Si}_6^{2-}$  in  $\text{NaSi}_6^-$  upon  $\text{Na}^+$  coordination.

## References

1. Lewis, G. N. *J. Am. Chem. Soc.* **1931**, *53*, 1367.
2. Frenking, G.; Shaik, S. *J. Comput. Chem.* **2007**, *28*, 1.
3. Bader, R. F. W. *Atoms in Molecules: A Quantum Theory*; Oxford University Press: Oxford, **1990**.
4. Luken, W. L.; Culberson, J. C. *Int. J. Quant. Chem.* **1982**, *16*, 265.
5. Becke, A. D.; Edgecombe, K. E.; *J. Chem. Phys.* **1990**, *92*, 5397.
6. Silvi, B.; Savin, A. *Nature*, **1994**, *371*, 683.
7. Hiberty, P. C.; Shaik, S. *J. Comput. Chem.* **2007**, *28*, 137 and references therein.
8. Jena, P.; Khanna, S. N.; Rao, B. K., eds. *Physics and Chemistry of Small Metal Clusters*; Plenum, New York, **1987**.
9. Sugano, S. *Microcluster Physics*; Springer, Berlin, **1991**.
10. Haberland, H., ed. *Clusters of Atoms and Molecules*; Springer, Berlin, **1994**.
11. Khanna, S. N.; Castleman, A. W., Jr., eds., *Quantum Phenomena in Clusters and Nanostructures*; Springer, Berlin, **2003**.
12. Mark, T. D.; Castleman, A. W., Jr. *Adv. Atomic Mol. Phys.* **1985**, *20*, 65.
13. Castleman, A. W., Jr.; Keesee, R. G. *Chem. Rev.* **1986**, *86*, 589.



## CHAPTER 2

### LITERATURE REVIEW

#### 2-1. Introduction

The theory of chemical bonding is the language of chemistry. It is being enhanced constantly through the entire history of chemical science in order to meet the challenges of contemporary research. This evolutionary process occurs through shifts of paradigms of chemical bonding and the formulation of more and more sophisticated models of chemical bonding. From the earliest attempts to understand how substances are formed and transformed, leading to ideas of “elective affinities” (Lemery, 1675)<sup>1</sup> and “chemical affinities” (Geoffroy, 1718)<sup>1</sup>, through the “dualistic” chemical theories of Davy and Berzelius,<sup>2</sup> the theory of chemical bonding evolved into theory of electronic structure in the form of the Lewis bonding model.<sup>3</sup> The emergence and development of quantum mechanics led to reformulation and to deeper theoretical understanding of the Lewis hypothesis in the works of Heitler and London,<sup>4</sup> Pauling,<sup>5</sup> Slater,<sup>6</sup> and others. One way or another, the Lewis model of chemical bonding, operating with lone-pairs (LP) and 2-center 2-electron (2c-2e) bonds according to the octet rule, has been dominating both chemical education and research for more than ninety years. The key to this long-standing success is the intuitive simplicity of the idea of the localized bonding (or non-bonding) pair of electrons, availability of the rules for constructing Lewis structures (simple enough to be taught in freshmen chemistry class), very clear graphical representation of the bonding pattern. The obtained picture of chemical bonding can be

easily connected with properties of the species and its reactivity, providing the Lewis model of the bonding with not only descriptive, but also predictive power.

Nevertheless, there are situations when chemical bonding and, thus, properties of chemical species, can't be satisfactorily described by a set of lone-pairs or 2c-2e (localized) bonds. Studies of a huge classes of compounds now are impossible without the concept of aromatic/antiaromatic (or delocalized) bonding, initially used to explain properties of benzene.<sup>7</sup> This concept has been extensively reviewed<sup>8</sup> and the discussion of its general aspects is far beyond the scope of the present work. Another example of non-Lewis systems is boron hydrides (boranes) with 3-center 2-electron bonds.<sup>9</sup>

In chemistry, the word "cluster" is used for a group of atoms or molecules held together by a range of interactions, with weak van der Waals forces on one end and strong ionic bonds on the other. Active studies of clusters started in the 1950's, though related phenomena were referred to even in the 1930's. Clusters are usually produced using mass spectrometer ion sources<sup>10</sup> or the laser vaporization technique.<sup>11</sup> The latter allows a researcher to "assemble" species of virtually any composition and go beyond studies of clusters of volatile materials. From the structural point of view, clusters constitute a form of matter intermediate between atoms and the solid phase. The properties of clusters are extremely sensitive to their composition and charge and can be altered dramatically due to the difference of a single atom or electron.<sup>12</sup> This peculiarity makes it especially hard to create bulk counterparts of the species observed in molecular beams. For example, among doubly charged anionic clusters of silicon only  $\text{Si}_5^{2-}$  and  $\text{Si}_9^{2-}$  have been synthesized and characterized by X-ray crystallography.<sup>13</sup> Photoelectron spectroscopy in molecular beams can be carried out for clusters of any size.

On the way from atoms to solid phase a deficiency of electrons available for bonding occurs. In other words, in covalently bound clusters there are not enough electron pairs to form two-center two-electron (2c-2e) bonds between each pair of atoms that are located close enough to each other. When structures of clusters are reported in the scientific literature, the lines connecting atoms in the pair-wise manner are drawn on the basis of interatomic distances. These structures thus do not necessarily represent any bonding pattern and should be seen only as connectivity diagrams in the geometric sense. The application of the Natural Bonding Orbital (NBO) analysis,<sup>14,15</sup> which recovers the Lewis structural description from the charge density distribution in a priori manner, usually leads to chemically senseless results. Very often NBO software fails to finish the analysis at all when dealing with clusters. The electron deficiency of clusters is the main source of difficulty for those who try to relate their geometries and properties to their electronic structure in some rational manner.

## **2-2. Chemical Bonding Models for Clusters**

A fine line exists where the electronic structure methods for quantum chemical calculations should be separated from the models of chemical bonding in clusters. For example, in this dissertation the canonical molecular orbitals of the Hartree-Fock-Roothaan method will not be viewed as a model for chemical bonding unless they are used within the concept of aromaticity/antiaromaticity applicable in the case of delocalized bonding. In the same way, the Valence Bonding method of the quantum chemical computations will not be viewed as a model for chemical bonding, unless the

resonance structures emerging in this approach are used for description of the delocalized bonding.

### 2-2.1. Jellium Model

To work satisfactorily, a model of chemical bonding in clusters should be able to deal with delocalization of valence electrons in these species. Somewhat similar behavior of electrons is encountered in surface regions of metals, which can be considered as nearly-free-electron systems. It was shown that the lattice of positive ions in a model metal surface could be replaced by a uniform background charge (jellium).<sup>16</sup> The positive background representing smeared ions, can be written as follows

$$n_+(\mathbf{r}) = \bar{n} \Theta(\mathbf{r}) \quad (2.1)$$

with average valence-electron density

$$\bar{n} = 3/(4\pi r_s^3) \quad (2.2)$$

where  $r_s$  is Wigner-Seitz radius (bulk density parameter). In the expression (2.1)  $\Theta(\mathbf{r})$  is 1 inside and 0 outside a zero-thickness surface. The jellium background is neutralized by the valence electrons with density  $n(\mathbf{r})$  everywhere but a region of atomic thickness around the surface. The jellium is stable for  $r_s \approx 4$  bohr and gives a good description of cohesive and surface properties of simple metals, but anomalies are encountered in the non-equilibrium regions: for  $r_s \approx 2$  bohr the jellium surface energy is negative,<sup>16a</sup> and for  $r_s \approx 6$  bohr the jellium bulk modulus is negative.<sup>17</sup> The introduction of pseudopotential corrections<sup>16-19</sup> helps to fight the deficiencies of the jellium model, but eliminates its simplicity and universality since they introduce the dependence of properties on the

valence, crystal structure, and  $r_s$ , or at least  $r_s$  in the case of a structureless pseudopotential.<sup>20</sup>

The pioneering work on the application of the jellium model to metal clusters was performed by Knight et. al.<sup>21</sup> The relative abundance of the neutral sodium clusters in mass spectra was explained on the basis of a one-electron shell model in which independent delocalized valence electrons were bound in a spherically symmetric potential well. Since then the studies of clusters on the basis of the jellium model have been reviewed.<sup>12e,22-27</sup> The nature of the jellium model suggests that the most reliable results should be expected for systems with near-free behavior of the valence electrons, such as metal clusters, or systems at the nano-scale with developed surfaces and electronic structure close to the structure of bulk metals. Limitations on the success of the jellium model for metal clusters were reviewed by Jena and co-workers.<sup>28</sup> In recent years the jellium model has been utilized in studies of metalloid (elementoid) clusters,<sup>29</sup> structural and electronic properties of medium-size gold clusters,<sup>30</sup> shape evolution of intermediate size silver clusters,<sup>31</sup> stability and symmetry breaking in metal nanowires,<sup>32</sup> evolution of electronic structure and properties of aluminum clusters,<sup>33</sup> and so on. It proved to be useful in the description of “superatomic” systems – certain clusters behaving like atoms of certain elements in the periodic table.<sup>34</sup>

Though the jellium model is more “physical” than “chemical” and does not introduce “chemical bonds” per se, it is one of the major theoretical tools used nowadays in depicting electronic structure of clusters and revealing their structure-property relationships.

### 2-2.2. Aromaticity/Antiaromaticity

A long-standing tradition of dealing with delocalized bonding exists in organic chemistry. The concept of aromaticity was initially introduced to explain the unusual structural and chemical properties of benzene.<sup>7,35</sup> As a property, aromaticity does not have a clear definition. Discussions of the criteria of aromaticity<sup>8a,36-38</sup> as well as its types<sup>8a,38-42</sup> are extensive. From the theoretical point of view, aromatic/antiaromatic bonding can be approached via either resonance structures of the Valence Bonding method<sup>4a,6,43</sup> or delocalized canonical molecular orbitals (CMO) of the Hartree-Fock-Roothaan self-consistent field (SCF) method.<sup>44</sup> Resonance structures are Lewis (classical) structures. The system with delocalized bonding can be seen as intermediate (or “resonating”) with two or more such limiting structures. When CMO language is used, aromatic bonding emerges as the result of occupation of a certain set of CMOs and this fact can be expressed through counting rules for the amount of electrons involved in the delocalized bonding (e.g. rules of Huckel,<sup>45</sup> Zintl,<sup>46</sup> Mingos,<sup>47</sup> Wade,<sup>48</sup> Jemmis,<sup>49</sup> graph-theoretical approach<sup>50</sup> etc.).

The discovery of aromaticity/antiaromaticity in clusters was made on the basis of CMO analysis.<sup>51,52</sup> To identify a certain cluster as aromatic/antiaromatic it is necessary to outline the sets of the CMOs that can't be transformed into the classical Lewis bonding objects, such as LPs and 2c-2e bonds. These orbitals are compared with prototypical aromatic systems on the basis of overlap type and separated into subsets, corresponding to different types of aromatic bonding (e.g. s-, p-, d-). Then aromaticity/antiaromaticity is established on the basis of counting rules specific for the delocalized bonding of each type.<sup>53-56</sup> In this way numerous clusters were recognized as aromatic (multiple-aromatic,

spherical aromatic), antiaromatic (multiple-antiaromatic, spherical antiaromatic), and conflicting aromatic. The binary lanthanide hydride clusters  $\text{Ln}_3\text{H}_9$  and  $\text{Ln}_4\text{H}_{12}$  ( $\text{Ln} = \text{La}, \text{Gd}, \text{and Lu}$ ) were predicted to be stable and significantly aromatic.<sup>57</sup> The five-membered cyclic tellurium species  $\text{Te}_2\text{N}_2\text{S}$  was studied with the purpose of analysis and quantification of the electron delocalization.<sup>58</sup> The  $\text{Hf}_3^-$  anionic cluster was shown to possess unique triple (s-, p-, and d-) aromaticity.<sup>59</sup> The study of  $\text{Al}_7\text{C}^-$  and  $\text{Al}_7\text{O}^-$  was performed to analyze the possibility of aromatic behavior, stability and reactivity of these systems.<sup>60</sup> The double-aromatic character of selected monocyclic carbon, boron, and borocarbon rings was demonstrated.<sup>61</sup> A new class of “all-metal” aromatic hydrido-bridged binary coinage metal heterocycles was predicted by Tsipis et al.<sup>62</sup> Sandwich-like compounds were theoretically designed using all-metal aromatic  $\text{Al}_4^{2-}$  unit and the main group metals (Li, Na, K, Be, Mg, Ca) as building blocks.<sup>63</sup> Apparently, the utilization of the concepts of aromaticity/antiaromaticity for the description of electronic structure of clusters is very beneficial. The amount of the cluster research using these concepts to explain properties of clusters is constantly increasing.

Certain difficulties of the analysis of delocalized bonding using CMOs exist though. It is not a trivial task to separate “localizable” CMOs from those responsible for the delocalized bonding. It is also tricky to determine the pattern of the localized bonding derived from the “localizable” CMOs. There are no tools created specifically to solve this problem, though NBO can be tricked into doing this in some cases. Separation of the subsets of CMOs according to the overlap type is not always possible. For example, a cluster has to be planar to have  $\sigma/\pi$  separation;  $\sigma$ -MOs originating from s-atomic orbitals can always mix with  $\sigma$ -MOs originating from p-atomic functions;  $\sigma$ -radial CMOs can

mix with  $\sigma$ -tangential CMOs etc. Taking into account the overwhelmingly huge number of low-symmetry three-dimensional clusters ( $C_1$  point group), the overlap-type separation of CMOs is, in fact, generally impossible. The electron counting rules derived for certain chemical systems might not work in the case of other systems. An excellent example is the counting rules for spherically aromatic species (i.e. Wade-Mingos, Hirsch). While closo-borane  $B_{12}H_{12}^{2-}$  is an icosahedral cage, the valence isoelectronic silicon cluster  $Si_{12}^{2-}$  is not, nor is  $Ge_{12}^{2-}$ . The most stable isomers of  $Sn_{12}^{2-}$  and  $Pb_{12}^{2-}$  are icosahedra again. All of these species have identical structures of the occupied CMOs and thus electron counting, but different stability of the icosahedral isomers. Another example is the  $Al_6^{2-}$  octahedral cluster,<sup>64</sup> which violates Wade's rule by having only eight instead of fourteen  $\pi$ -electrons responsible for the skeletal bonding. It is also hard to expect the counting rules to be applicable and CMO analysis to be feasible when dealing with clusters of large size (hundreds of atoms) with distinguishable external ("surface") and internal ("bulk") regions.

The approach utilizing ideas of aromatic/antiaromatic bonding in the description of clusters is in general the most successful in bringing "chemistry" into studies of clusters. There is a very strong correlation between the delocalized bonding pattern, the structure of the species, and its properties. For example, aromaticity pronounces itself in a highly symmetric geometry, high first singlet vertical excitation energies, highly negative NICS values, high atomization energies, and high abundance in molecular beams. Antiaromaticity is related to the first-order Jahn-Teller effect and geometric distortions leading to the formation of islands of aromaticity, low first singlet vertical excitation energies, NICS values close to zero or positive, and low atomization energies.



There are attempts to use Valence Bond theory for the description of the delocalized bonding in clusters. The  $Al_4^{2-}$  system was studied by Zhan et al.<sup>65</sup> and Havenith et al.<sup>66</sup> The first group reported 16 relevant resonance structures, the second only 6 with highest contribution from 2 Dewar-type structures. Description of the delocalized bonding in fullerene  $C_{60}$  in terms of valence bond representation would require 12500 resonance structures.<sup>67</sup> As the Valence Bond method can be successfully used for electronic structure calculations of small and medium-size clusters, the above-mentioned examples demonstrate its apparent deficiency from the point of view of chemical bonding analysis. When a single existing structure has to be represented by a handful of non-existing resonance structures, it is neither a simple, nor intuitive way to solve the problem.

### **2-3. Conclusion**

Initially studies of clusters were concentrated on obtaining relative abundances of species of different size in mass spectra and finding “magic” numbers. The discovery of fullerenes definitely shifted the interest towards establishing structures of the observed clusters and studying structure-property relationships. It should be realized though, that the fast development of computational techniques (including algorithms, software, and hardware) makes it simpler to use a brute force approach to the theoretical studies of clusters, which is based on the extensive amount of calculations without analysis of the obtained results. The number of publications reporting just sets of isomers (local minima) for a cluster of given size and composition is still higher than the number of papers trying to explain structures of different clusters and families of clusters on the unified

conceptual basis. The field of models of chemical bonding for clusters is not too rich. There is the “jellium model” originating from physical theory of the solid state and reflecting the physical origin of cluster research. The “aromaticity/antiaromaticity model” is of a chemical nature since it is rooted in the concept actively and successfully used in organic chemistry. The incredible diversity of clusters inevitably leads to the development of this concept. The result of such development is a new approach to the description of chemical bonding in clusters as described in the following chapters.

### References

1. Siegrid, R. *From Elements to Atoms: A History of Chemical Composition*; American Philosophical Society: Philadelphia, 2002.
2. Bensaude-Vincent, B.; Stengers, I. *A History of Chemistry* (van Dam, D., English translation); Harvard University Press: Cambridge, 1996.
3. Lewis, G. N. *J. Am. Chem. Soc.* **1916**, *38*, 762.
4. (a) Heitler, W.; London, F. *Zeits fur Physik* **1927**, *44*, 455. (b) Heitler, W.; London, F. *Quantum Chemistry Classic Scientific Paper* (Hetteema, H. English Translation); World Scientific: Singapore, 2000, p. 140.
5. Pauling, L. *Proc. Natl. Acad. Sci. USA* **1928**, *14*, 359.
6. Slater, J. C. *Phys. Rev.* **1931**, *37*, 481.
7. Kekule, A. *Bull. Soc. Chim. Fr.* **1865**, *3*, 98.
8. (a) Minkin, V. I.; Glukhovtsev, M. N.; Simkin, B. Ya. *Aromaticity and Antiaromaticity. Electronic and Structural Aspects*; Wiley & Sons: New York, 1994; (b) Special edition on aromaticity. P. v. R. Schleyer, ed. *Chem. Rev.* **2001**,

- 101, No. 5; (c) Special edition on delocalization pi and sigma. P. v. R. Schler ed. 2005, 105, No. 10.
9. (a) Lipscomb, W. N. *Boron Hydrides*, Benjamin: New York, 1963; (b) Muetterties, E. L. *Boron Hydride Chemistry*, Academic Press: New York, 1975.
10. Becker, E. W. *Metal Clusters* (eds. Trager, F. and Putlitz, G.); Springer: Berlin, 1986.
11. Dietz, T. G.; Duncan, M. A.; Powers, D. E.; Smalley, R. E. *J. Chem. Phys.* **1981**, *74*, 6511.
12. (a) Jena, P.; Khana, S. N.; Rao, B. K. *Physics and Chemistry of Small Clusters*; Plenum: New York, 1987; (b) Sugano, S. *Microcluster Physics*; Springer: Berlin, 1991; (c) Haberland, H. *Clusters of Atoms and Molecules*; Springer: Berlin; (d) Khanna, S. N.; Castleman, A. W., Jr. *Quantum Phenomena in Clusters and Nanostructures*; Springer: Berlin, 2003; (e) *Proc. Natl. Acad. Sci. USA, Cluster Chemistry and Dynamics Special Feature* **2006**, *103*, 10553.
13. (a) Goicoechea, J. M.; Sevov, S. C. *J. Am. Chem. Soc.* **2004**, *126*, 6860; (b) Goicoechea, J. M.; Sevov, S. C. *Inorg. Chem.* **2005**, *44*, 2654
14. (a) Foster, J. P.; Weinhold, F. *J. Am. Chem. Soc.* **1980**, *102*, 7211; (b) Reed, A. E.; Curtiss, L. A.; Weinhold, F. *Chem. Rev.* **1988**, *88*, 899.
15. Glendening, E. D.; Badenhop, J. K.; Reed, A. E.; Carpenter, J. E.; Bohmann, J. A.; Morales, C. M.; Weinhold, F. Theoretical Chemistry Institute, NBO 5.0, University of Wisconsin, Madison, 2001.
16. (a) Lang, N. D.; Kohn, W. *Phys. Rev. B* **1970**, *1*, 4555; (b) Lang, N. D.; Kohn, W. *Phys. Rev. B* **1971**, *3*, 1215.

17. Ashcroft, N. W.; Langreth, D. C. *Phys. Rev.* **1967**, *155*, 682.
18. Manninen, M. *Phys. Rev. B* **1986**, *34*, 6886.
19. Ashcroft, N. W. *Phys. Lett.* **1966**, *23*, 48.
20. Perdew, P. J.; Tran, H. Q.; Smith, E. D. *Phys. Rev. B* **1990**, *42*, 11627.
21. Knight, W. D.; Clemenger, K.; de Heer, W. A.; Saunders, W. A.; Chou, M. Y.; Cohen, M. L. *Phys. Rev. Lett.* **1984**, *52*, 2141.
22. Rao, B. K.; Jena, P. *Phys. Rev. B* **1985**, *32*, 2058.
23. Bonacic-Koutecky, V.; Fantucci, P.; Koutecky, J. *Chem. Rev.* **1991**, *91*, 1035.
24. (a) Brack, M. *Rev. Mod. Phys.* **1993**, *65*, 677; (b) de Heer, W. A. *Rev. Mod. Phys.* **1993**, *65*, 611.
25. Alonso, J.A.; Balbas, L.C. *Density Functional Theory III*, **1996**, *182*, 119.
26. Kuleff, A. I.; Maruani, J.; Raychev, P. P. *Advances In Quantum Chemistry, Vol 40: New Perspectives In Quantum Systems In Chemistry And Physics, PT2*, **2001**, *40*, 279.
27. von Issendorff, B.; Cheshnovsky, O. *Annu. Rev. Phys. Chem.* **2005**, *56*, 549.
28. Magaud, L.; Khanna, S. N.; Jena, P. *Chem. Phys. Lett.* **1991**, *183*, 333.
29. Hartig, J.; Stosser, A.; Hauser, P.; Schnockel, H. *Angew. Chem. Int. Ed.* **2007**, *46*, 1658.
30. Dong, Y.; Springborg, M. *J. Phys. Chem. C* **2007**, *111*, 12528.
31. Yang, M.; Jackson, K. A.; Jellinek, J. *J. Chem. Phys.* **2006**, *125*, 144308.
32. (a) A I Mares, A. I.; Urban, D. F.; Bürki, J.; Grabert, H.; Stafford, C. A.; van Ruitenbeek, J. M. *Nanotechnology* **2007**, *18*, 265403; (b) Urban, D. F.; Bürki, J.; Stafford, C. A.; Grabert, H. *Phys. Rev. B.* **2006**, *74*, 245414.

33. Rao, B. K.; Jena, P. *J. Chem. Phys.* **1999**, *111*, 1890.
34. (a) Reber, A. C.; Khanna, S. N.; Castleman, A. W. *J. Am. Chem. Soc.* **2007**, *129*, 10189; (b) Chattaraj PK, Giri S. *J. Phys. Chem. A* **2007**, *111*, 11116; (c) Reveles, J. U.; Khanna, S. N.; Roach, P. J.; Castleman, A. W., Jr. *Proc. Natl. Acad. Sci. USA* **2006**, *103*, 18405.
35. Armit, J. W.; Robinson, R. *J. Chem. Soc.* **1925**, *127*, 1604.
36. Garratt, P. J. *Aromaticity*; Wiley, Inc.: New York, 1986.
37. Lloyd, D. *Non-Benzoid Conjugated Carbocyclic Compounds*; Elsevier: Amsterdam, 1984.
38. Lewis, D. Peters, D. *Facts and Theories of Aromaticity*; Macmillan: London, 1975.
39. Balaban, A. T.; Banciu, M.; Ciorba, V. *Annulenes, Benzo-, Hetero-, Homo-Derivatives and their Valence Isomers*, Vols. 1-3; CRC Press: Boca Raton, FL, 1986.
40. *Pseudoaromaticity and Antiaromaticity*, Proceedings of an International Symposium, Bergmann, E. D.; Pullman, D.; Eds. (Israel Academy of Sciences and Humanities, Jerusalem, 1971).
41. Lloyd, D. *The Chemistry of Conjugated Cyclic Compounds*, In *To Be or Not To Be Like Benzene*; Wiley: New York, 1989.
42. Schleyer, P. v. R. *Chem. Rev.* **2001**, *101*, 1115.
43. Pauling, L. *The Nature of the Chemical Bond*; Cornell University Press: Ithaca, New York, 1939.

44. (a) Hartree, D. R. *The Calculations of Atomic Structures*; John Wiley & Sons, Inc: New York, Chapman & Hall: London; 1957; (b) Roothaan, C. C. J. *Rev. Mod. Phys.* **1951**, *23*, 69; (c) Hall, G. G. *Proc. R. Soc. (London)* **1951**, *A205*, 541.
45. Huckel, E. *Z. Phys.* **1931**, *70*, 204.
46. Zintl, E.; Goubeau, J.; Dullenkopf, W. *Z. Phys. Chem. Abt. A* **1931**, *154*, 1.
47. Mingos, D. M. *Nature* **1972**, *236*, 99.
48. Wade, K. *Adv. Inorg. Chem. Radiochem.* **1976**, *18*, 1.
49. Baslakrishnarajan, M. M.; Jemmis, E. D. *J. Am. Chem. Soc.* **2000**, *122*, 4516.
50. King, R. B. *Chem. Rev.* **2001**, *101*, 1119.
51. Li, X.; Kuznetsov, A. E.; Zhang, H. F.; Boldyrev, A. I.; Wang, L. S. *Science* **2001**, *291*, 859.
52. Kuznetsov, A. E.; Birch, K. A.; Boldyrev, A. I.; Zhai, H. J.; Wang, L. S. *Science* **2003**, *300*, 622.
53. Boldyrev, A. I.; Wang, L. S. *Chem. Rev.* **2005**, *106*, 3716.
54. Alexandrova, A. N.; Boldyrev, A. I.; Zhai, H. J.; Wang, L. S. *Coord. Chem. Rev.* **2006**, *250*, 2811.
55. Zubarev, D. Yu.; Boldyrev, A. I. *J. Comput. Chem.* **2007**, *28*, 251.
56. Zubarev, D. Yu.; Averkiev, B. B.; Zhai, H. J.; Wang, L. S.; Boldyrev, A. I. *Phys. Chem. Chem. Phys.* **2008**, *10*, 257.
57. Luo, Y; Hou, Z.M. *J. Phys. Chem. C* **2008**, *112*, 635.
58. Bandeira, N. A. G.; Corminboeuf, C.; Calhorda, M. J. *Struc. Chem.* **2007**, *18*, 841.
59. Averkiev, B. B.; Boldyrev, A. I. *J. Phys. Chem. A* **2007**, *111*, 11885.
60. Chattaraj, P. K.; Giri, S. *J. Phys. Chem. A* **2007**, *111*, 11116.

61. Wodrich, M. D.; Corminboeuf, C.; Park, S. S.; Schleyer, P. V. *Chem. Eur. J.* **2007**, *13*, 4582.
62. Tsipis, A. C.; Stalikas, A.V. *New Jour. Chem.* **2007**, *31*, 852.
63. Yang, L. M.; Ding, Y. H.; Sun, C. C. *Chem. Eur. J.* **2007**, *13*, 2546.
64. Kuznetsov, A. E.; Boldyrev, A. I.; Zhai, H. J.; Wang, L. S. *J. Am. Chem. Soc.* **2002**, *124*, 11791.
65. Zhan, C. G.; Zhang, F.; Dixon, D. A. *J. Am. Chem. Soc.* **2002**, *124*, 14795.
66. Havenith, R. W. A.; van Lenthe, J. H. *Chem. Phys. Lett.* **2004**, *385*, 1998.
67. Buhl, M.; Hirsch, A. *Chem. Rev.* **2001**, *101*, 1153.

## CHAPTER 3

DEVELOPING PARADIGMS OF CHEMICAL BONDING:  
ADAPTIVE NATURAL DENSITY PARTITIONING<sup>1</sup>**Abstract**

A method of description of the chemical bonding combining the compactness and intuitive simplicity of Lewis theory with the flexibility and generality of Canonical Molecular Orbital theory is presented, which is called Adaptive Natural Density Partitioning. The objects of chemical bonding in this method are n-center 2-electron bonds, where n goes from one (lone-pair) to the maximum number of atoms in the system (completely delocalized bonding). The algorithm is a generalization of the Natural Bonding Orbital analysis and is based on the diagonalization of the blocks of the first-order density matrix written in the basis of Natural Atomic Orbitals. The results obtained by the application of the algorithm to the systems with non-classical bonding can be readily interpreted from the point of view of aromaticity/antiaromaticity concepts. The considered examples include Li<sub>4</sub> cluster and a family of planar boron clusters observed in molecular beams.

**3-1. Introduction**

It has been slightly more than 90 years since G. N. Lewis proposed the most successful and generally accepted theory of chemical bonding.<sup>1</sup> Almost a century later the development of the general theory of chemical bonding is still far from completion.<sup>2</sup> The

---

<sup>1</sup> Coauthored by Dmitry Yu. Zubarev and Alexander I. Boldyrev. Reproduced with permission from *Phys. Chem. Chem. Phys.* **2008**, 10, 1-10.



diversity of ideas and concepts co-existing in this area is absolutely remarkable. The theory of molecular orbitals (MO) by Mulliken and Hund<sup>3</sup> leading to delocalized description of electrons in the chemical systems turned out to be compatible with more intuitive and practically applicable Lewis description after utilizing various localization techniques. The possibility of such localization procedures proposed by Foster and Boys,<sup>4</sup> Edmiston and Ruedenberg,<sup>5</sup> Pipek and Mezey<sup>6</sup> is based on the fact that the wave function is invariant under unitary transformations. Valence bond (VB) theory coined by Heitler, London, Slater, and Pauling,<sup>7, 8</sup> being an alternative to the MO theory, naturally incorporates such important bonding concepts as hybridization and resonance structures. It can be very useful for the explanation of the systems with multireference character, representation of the potential energy surfaces for chemical dynamics, quantitative characterization of the electron delocalization, etc.<sup>9, 10</sup> A huge segment of the chemical bonding field belongs to the theories, avoiding references to the “chemical bonds” as objects that do not have physical definition and are imprecise. Instead, they rely on different forms of analysis of charge density, such as studies of the topological properties of the Laplacian of the electron density within the framework of Quantum Theory of Atoms in Molecules (QTAIM),<sup>11</sup> or local quantum-mechanical functions, related to the Pauli exclusion principle such as Fermi Hole (FH), Electron Localization Function (ELF) and their various flavors.<sup>12-20</sup> Analysis of chemical bonding can be performed according to Coulson’s definition<sup>21</sup> of bond order in polyatomic molecules, which was extended beyond the  $\pi$ -electron level by Wiberg,<sup>22</sup> who used the term bond index instead of bond order. For nonorthogonal basis sets, the appropriate definition of bond order/index was proposed by Mayer.<sup>23,24</sup> The three-center bond index was first proposed by Giambiagi et

al.<sup>25</sup> and independently also by Sannigrahi and Kar.<sup>26</sup> Various electron sharing indexes such as Fulton's Electron Sharing Index (ESI),<sup>27,28</sup> Mayer's bond-orders,<sup>23,24,29-31</sup> and Delocalization Indexes (DI)<sup>32,33</sup> were reviewed by E. Matito et al.<sup>34</sup> One of the most important tools in the chemical bonding toolbox is Natural Bonding Orbital (NBO) analysis by Weinhold.<sup>35</sup> Developed to construct Lewis structure of a given molecule in an a priori manner and being extremely computationally efficient, the method is the first choice in dealing with the widest range of systems.<sup>36</sup>

Without comprehensive reviewing the existing methods of chemical bonding analysis it should be clear that there is a great diversity of views on the topic and very different paradigms can be chosen to meet conceptual/motivational requirements of a particular scientist or scientific task. None of them can be regarded as ultimate though due to the conceptual difficulties, interpretational subtleties, computational demands etc. As a reference point of the localized description of chemical bonding Lewis theory has a well-known deficiency. Sometimes single Lewis structure is not sufficient for the adequate representations of the electronic structure of a system and multiple resonance Lewis structures are necessary. These cases are also dealt with utilizing idea of delocalized or aromatic/antiaromatic bonding.<sup>37</sup> From the physical point of view, aromaticity and antiaromaticity are even more ill-defined than the chemical bond itself. The literature dedicated to these concepts is truly enormous and its reviewing as well discussing the concepts themselves is far beyond the scope of this paper. The most recent discussion of aromaticity and antiaromaticity can be found in Ref. 38-41 Aromaticity as an electronic structure related phenomenon can also be described using various aromaticity indices, for example para-delocalization index (PDI),<sup>42a</sup> the aromatic

fluctuation index (FLU),<sup>42b</sup> and MO multicenter bond index (MCI).<sup>43</sup> Using a slightly different approach, Ponec and coworkers<sup>44-47</sup> confirmed that six-center bond index indeed a useful quantity to measure aromaticity. Ponec et al.<sup>48</sup> further demonstrated that the multi-center bond index can be used for the quantitative characterization of homoaromaticity, non-homoaromatic and anti-homoaromatic systems. Normalized variants of MCI as a measure of aromaticity were proposed by Cioslowski et al.<sup>49</sup> Among widely used probes for aromaticity/antiaromaticity there are ones based on the response to the presence of external magnetic field such as Nuclear Independent Chemical Shifts (NICS) pioneered by Schleyer and co-workers,<sup>50</sup> the Aromatic Ring-Current Shieldings (ARCS)<sup>51</sup> and the Gauge-Including Magnetically Induced Current (GIMIC)<sup>52</sup> proposed by Sundholm and co-workers, and maps of current density induced by a perpendicular magnetic field developed by Fowler and co-workers.<sup>53</sup> From the practical point of view, the comparison of a given system with prototypical one within MO theory is often enough to assign some certain type of the delocalized bonding, as it is done in the case of main-group elements or transition-metal clusters.<sup>54,55</sup>

Another significant adjustment is that due to the development of the chemical bonding theory for boron hydrides<sup>56</sup> the set of Lewis objects of the localized bonding was extended to include three-center two-electron (3c-2e) bonds in addition to lone-pairs (LP) and two-center two-electron (2c-2e) bonds. What has to be kept in mind is that the Lewis theory, formulated eleven years prior the emergence of quantum theory, has assumed the central role as chemical language in education and research. So, it is good idea for the new approaches to the extraction and representation of the chemically relevant information to preserve connection with the Lewis theory by perhaps generalizing the

latter. It was shown lately,<sup>54,55,57,58</sup> that combination of the localized and delocalized (aromatic/antiaromatic) description can consistently explain structures and properties of the main group element and transition metal clusters. The objects of bonding in this case have to be lone-pairs, 2c-2e bonds, and electron pairs, localized over bigger fragments, such as 3-, 4-, and more atomic, up to the entire cluster. The electron pairs that are localized over the maximum available number of atoms should actually be called “delocalized” and their presence is a sign of aromatic/antiaromatic bonding. The assignment of aromaticity or antiaromaticity in this case can be performed on the basis of counting rules. Electron pairs, localized over smaller molecular fragments usually point to the island aromaticity in globally antiaromatic systems. In this way Lewis description is extended to include n-center 2-electron bonds and can be naturally reconciled with concepts of aromaticity and antiaromaticity. The procedure of obtaining such a description of chemical bonding, which we call Adaptive Natural Density Partitioning (AdNDP) and examples of its application are presented below.

### 3-2. Adaptive Natural Density Partitioning (AdNDP) Algorithm

From the computational point of view AdNDP is a generalization of NBO analysis by Weinhold.<sup>35</sup> The latter is based on some optimal transformation of a many-electron wavefunction into a localized form consistent with Lewis-theoretical picture. If the spinless first-order reduced density operator  $\gamma(1|1')$  for a closed-shell system

$$\gamma(1|1') = N \int \psi(1,2,\dots,N)\psi^*(1',2,\dots,N)d2\dots dN \quad (3-1)$$

where 1 and 1' are abbreviations for  $\mathbf{x}_1$  and  $\mathbf{x}_{1'}$  and the matrix element is

$$P_{kl} = \int \chi_k^*(1)\gamma(1|1')\chi_l(1')d1d1' \quad (3-2)$$

then  $\gamma(1|1')$  can be expanded in a complete orthonormal basis set of atomic orbitals  $\{\chi_k\}$  as follows

$$\gamma(1|1') = \sum_{kl} P_{kl} \chi_k(1) \chi_l^*(1') \quad (3-3)$$

Diagonal elements  $P_{kk}$  of the density matrix  $\mathbf{P}=\{P_{kl}\}$  correspond to the occupation numbers (ON) of the orbitals  $\chi_k$ . If  $\chi_k$  are bond orbitals with maximum occupancies, the set of the atomic hybrids forming them should be considered as optimal in the sense that the approximate wavefunction constructed using the found bond orbitals will have the best overlap with the original wavefunction. The search for these “maximum-occupancy” hybrids can be performed numerically based on the condition of maximum occupancy but it is computationally expensive procedure, so alternative approach is used.

The density matrix  $\mathbf{P}$  is represented in the block form

$$\mathbf{P} = \begin{bmatrix} \mathbf{P}_{11} & \mathbf{P}_{12} & \dots & \mathbf{P}_{1N} \\ \mathbf{P}_{21} & \mathbf{P}_{22} & \dots & \mathbf{P}_{2N} \\ \dots & \dots & \dots & \dots \\ \mathbf{P}_{i1} & \mathbf{P}_{i2} & \dots & \mathbf{P}_{iN} \\ \dots & \dots & \dots & \dots \\ \mathbf{P}_{N1} & \mathbf{P}_{N2} & \dots & \mathbf{P}_{NN} \end{bmatrix} \quad (3-4)$$

where block  $\mathbf{P}_{jj}$  corresponds to the  $j$ -th atomic center. As natural spin orbitals with maximum occupancies are eigenvectors of the full density matrix  $\mathbf{P}$ , it is possible to obtain hybrid orbitals, maximizing the occupancy on a given atomic center by diagonalizing sub-blocks of  $\mathbf{P}$ , involving this center. If the following eigenproblem

$$\mathbf{P}_{jj} \mathbf{h}_l^{(j)} = n_l^{(j)} \mathbf{S}_{jj} \mathbf{h}_l^{(j)} \quad (3-5)$$

where  $\mathbf{P}_{jj}$  is the density matrix sub-block on the  $j$ -th center,  $\mathbf{S}_{jj}$  is overlap matrix,  $\mathbf{h}_l^{(j)}$  and  $n_l^{(j)}$  are the  $l$ -th eigenvector and eigenvalue of  $\mathbf{P}_{jj}$ , respectively, gives  $n_l^{(j)}$  close to 2, the

eigenvector  $\mathbf{h}_l^{(j)}$  can be seen as describing a lone-pair on center j (of course, if core electrons are already removed from the picture and the density due to the valence electrons is considered). Eigenvalues significantly lower than 2 correspond to the vectors available for the bonding with other centers. The vectors describing these bonds can be recovered, in their turn, by diagonalizing the density matrix sub-blocks, including the centers of interest and corresponding off-diagonal blocks, i.e. 2 x 2 sub-blocks of the form

$$\mathbf{P}^{(ij)} = \begin{bmatrix} \mathbf{P}_{ii} & \mathbf{P}_{ij} \\ \mathbf{P}_{ji} & \mathbf{P}_{jj} \end{bmatrix} \quad (3-6)$$

can reveal 2c-2e bonds between centers i and j (eigenvectors  $\mathbf{h}_l^{(ij)}$  with eigenvalues  $n_l^{(ij)}$  close to 2), 3 x 3 sub-blocks

$$\mathbf{P}^{(ijk)} = \begin{bmatrix} \mathbf{P}_{ii} & \mathbf{P}_{ij} & \mathbf{P}_{ik} \\ \mathbf{P}_{ji} & \mathbf{P}_{jj} & \mathbf{P}_{jk} \\ \mathbf{P}_{ki} & \mathbf{P}_{kj} & \mathbf{P}_{kk} \end{bmatrix} \quad (3-7)$$

can reveal 3c-2e bonds between centers i, j and k, and so on. After n-center eigenvectors (on the centers i,j,...,k – total n) are obtained, it is necessary to deplete the full density matrix  $\mathbf{P}$  from the density associated with the found bonding objects (n-center eigenvectors with eigenvalues close to 2)

$$\tilde{\mathbf{P}} \equiv \mathbf{P} - n_l^{(ij\dots k)} \mathbf{h}_l^{(ij\dots k)} \mathbf{h}_l^{(ij\dots k)\dagger} \quad (3-8)$$

After depletion the search for (n+1)-center occurs without mixing near degenerate n- and (n+1)-center eigenvectors. Found in this manner bonding orbitals are generally nonorthogonal and can be orthogonalized using Löwdin symmetric transformation.<sup>59</sup>

So, NBOs are obtained as local block eigenfunctions of the one-electron density

matrix and have optimal convergence properties for describing the electron density. From this point of view the obtained orbitals are “natural” in Löwdin sense.<sup>60</sup> The procedure is numerically efficient since it involves only a series of diagonalizations of density matrix blocks. It is unbiased in the sense that no preliminary ideas of the bonding pattern are required to perform analysis. In the mean time, the presumption that bonding in the most general systems can be satisfactorily described using the set of Lewis theoretical objects (LP, 2c-2e, and 3c-2e bonds) makes the method inflexible. When delocalized bonding is encountered only one of the possible resonance structures is reported or delocalized part is represented in the form of low-occupancy lone-pairs. In its current implementation<sup>61</sup> NBO analysis does not go beyond 3c-2e bonds, but apparently the search can be easily extended to any number of atomic centers in the way it is described above. The implementation of the algorithm for the search of n-center 2-electron bonding objects is called Adaptive Natural Density Partitioning. AdNDP is based on the diagonalization of the n-atomic sub-block of the density matrix (full or depleted) of N-atomic molecular system written in the basis of Natural Atomic Orbitals (NAO). NAO are the orthonormal one-center orbitals of the maximal occupancy for the given molecular wavefunction, derived from atomic sub-blocks of the density matrix.<sup>62</sup> The blocks are formed for all the possible combinations of n elements out of N available. In this way the obtained eigenvectors are consistent with the point-group symmetry of the molecule since the full density matrix has the symmetry of the molecule. For the given n-atomic block those eigenvectors are picked out whose occupation numbers (eigenvalues) exceed the established threshold value, usually close to 2. The threshold values are set individually for each n (number of centers in the atomic block) to ensure flexibility of the algorithm.

When search over all  $n$ -center blocks is over, the picked eigenvectors are ranked according to their occupation numbers again. Ranking is performed to form the set of vectors with the highest occupancies within some preset tolerance. This group of vectors is then accepted as  $n$ -center 2-electron bonds and the full density matrix is depleted of their density. For the rest of the  $n$ -center eigenvectors with high initial occupancies the diagonalization is performed again to obtain corrected eigenvalues and thus avoid overcounting the density associated with the shared elements of the different  $n \times n$  density sub-blocks. If the corrected occupation numbers are still above the threshold, the vectors are picked out to go through the ranking again and so on. When no  $n$ -center eigenvectors with acceptable occupancies are found, the search starts for  $(n+1)$ -center blocks. If some part of the density cannot be localized into  $n < N$  center bonds, the  $N$ -center eigenvectors or completely delocalized bonds are reported. They usually closely resemble the canonical MOs (CMO), that are regarded as aromatic when the description of the bonding in the particular system is given on the basis of MO theory and the concept of aromaticity. It should be mentioned that the accepted  $n$ -center vectors are not orthogonalized in the current implementation of the AdNDP algorithm. The primary goal of the code *is not to form an orthonormal basis set* for subsequent perturbation theory analysis, multireference calculations etc. The goal is to reveal the regions of the localization of electron pairs. Certainly, the orthogonalization can be performed if necessary using some of the existing algorithms.<sup>59</sup> Also, the accepted eigenvectors are allowed to have overlaps with each other within the AdNDP procedure. These overlaps can be projected out but we believe that they are manifestations of the delocalized bonding and thus can be used for qualitative characterization of the degree of



delocalization. More rigorous analysis of the possible overlaps of localized nc-2e bonds and its connection with aromatic nature of bonding is subject of the future work. If the standard NBO method were extended to nc-2e blocks, it would still produce resonance structures in certain cases, because it rejects vectors with significant overlaps. As the result these resonance structure would have bonding patterns inconsistent with the point group symmetry of the studied system. The AdNDP avoids this problem. By accepting overlapping eigenvectors it produces bonding pattern, which is always consistent with the symmetry of the system. “Bonding pattern” here is the set of all bonding elements recovered by the AdNDP analysis and placed on the molecular framework. Results of the AdNDP analysis are dependent on the choice of the threshold values for the occupation numbers. This kind of dependence is inherited from the parental NBO analysis. The results of the application of the standard NBO code also depend on the occupation number threshold, which can be adjusted using documented features of the code. The only difference is that NBO can operate in “black-box” manner changing thresholds without participation of the user, while AdNDP requires explicit specification of the thresholds. If inappropriate threshold values are selected, the analysis cannot be successfully accomplished, because the amount of accepted bonds exceeds the amount of valence electron pairs. Though the dependence on the threshold values is intrinsic for “Natural Orbital” – based methods, there are all the reasons to expect, that AdNDP provides unique partitioning of electron density into nc-2e bonds. Apparently, acceptance of a certain set of n-center vectors and consequent depletion of the density matrix influences results of the search for (n+1)-center vectors. With individual threshold values for each size of the atomic block AdNDP algorithm provides high flexibility.

### 3-3. Theoretical Methods

The AdNDP algorithm is implemented using Fortran 77 standard. The geometry optimization and normal mode analysis for the studied systems were carried out using hybrid density functional B3LYP<sup>63-65</sup> method with 6-311+G\*<sup>66-68</sup> polarized split-valence basis set as implemented in Gaussian 03<sup>69</sup> software package. The full density matrix in the basis of the natural atomic orbitals as well as the transformation between atomic orbital and natural atomic orbital basis sets were generated at RHF/STO-3G<sup>70,71</sup> level of theory by means of NBO 3.0<sup>35,36,62,72-74</sup> code incorporated into Gaussian 03. It is known, that the results of NBO analysis do not generally depend on the quality of the basis set, so the choice of the level of theory for AdNDP application is adequate. In the most general case, the results might be dependent on the basis set. However, in all our calculation we found that the pattern of nc-2e bonding remains qualitatively the same, when we used STO-3G, 3-21G or 6-31G\* basis sets. The only difference was the variation of the values of the occupation numbers, which did not exceed 0.1 |e|. The visualization of the results of calculations is performed using MOLEKEL 4.3<sup>75</sup> and MOLDEN 3.4<sup>76</sup> software.

### 3-4. Numerical Application and Discussion

The choice of the systems for the analysis by means of AdNDP code was made based on their non-classical chemical bonding. “Non-classical” in the context of the present work means that the bonding cannot be satisfactorily represented by a single Lewis structure and normally requires either invoking description in terms of resonant structures (within the paradigm of the localized bonding) or in terms of CMO and aromaticity/antiaromaticity concepts (within the paradigm of the completely delocalized

bonding). AdNDP leads to the description, combining these two paradigms. For instance, the application of the AdNDP to the benzene molecule leads to the textbook description with six 2c-2e C-C bonds with the occupation number 1.99 |e|, six 2c-2e C-H bonds with the occupation number 1.99 |e| and three completely delocalized  $\pi$ -bonds closely resembling Hartree-Fock  $\pi$ -MOs. The application of AdNDP to organic molecules will be discussed in forthcoming paper. For the present paper we selected systems, which are particularly complex and cannot be described in a straightforward manner.

### 3-4.1. $Li_4$ cluster

The first system to be considered is neutral  $Li_4$  cluster. In its rhombus  $D_{2h}$ , ( $^1A_g$ ,  $1a_g^2 1b_{1u}^2$ ) (Fig. 3-1a) configuration the cluster is  $\sigma$ -antiaromatic.<sup>54,77,78</sup> Antiaromaticity originates from the bonding HOMO-1  $1a_g$  and antibonding HOMO  $1b_{1u}$  and is expected to lead to the formation of the islands of  $\sigma$ -aromaticity. AdNDP shows these 3-center regions of island  $\sigma$ -aromaticity as two 3c-2e bonds with occupation numbers 2.0 |e| (Fig. 3-1b). Standard NBO software also cracks this case, since the bonds are 3-center.

### 3-4.2. $B_4$ cluster

The second system  $B_4$   $D_{2h}$ , ( $^1A_g$ ,  $1a_g^2 1b_{1u}^2 1b_{2u}^2 1b_{3g}^2 1b_{3u}^2 2a_g^2$ ) (Fig. 3-2a) belongs to the family of planar all-boron clusters extensively studied before and recently reviewed (Ref. 57, 58 and references therein). The rhombus shape of the global minimum structure<sup>79</sup> in this case is the result of the second-order Jahn-Teller effect and even at moderate temperatures the cluster is effectively square.<sup>80,81</sup> Most general considerations of the structure of CMOs lead to the conclusion that the bonding can be

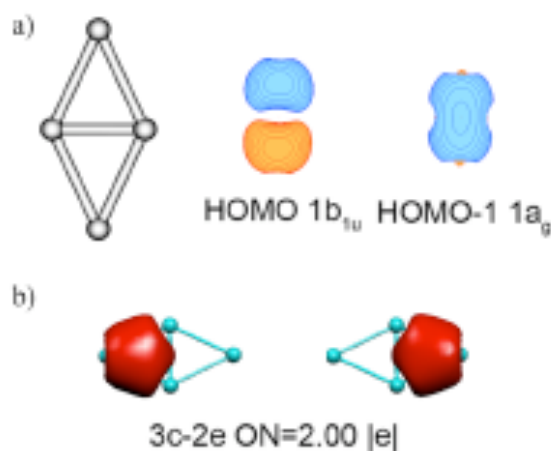


Figure 3-1. a) Structure and CMOs of Li<sub>4</sub> D<sub>2h</sub>, (<sup>1</sup>A<sub>g</sub>) cluster; b) results of the AdNDP localization.

described as the combination of four 2c-2e peripheral B-B bonds, a completely delocalized  $\sigma$ -aromatic bond (originating from the completely bonding HOMO 2a<sub>g</sub>), and a completely delocalized  $\pi$ -aromatic bond (originating from the completely bonding HOMO-1 1b<sub>3u</sub>). These predictions are confirmed by the results of AdNDP analysis (Fig. 3-2b). The part of the electron density due to the valence electrons is partitioned into four 2c-2e B-B bonds with occupancies 1.99 |e|, one aromatic 4c-2e  $\sigma$ -bond (ON = 2.0 |e|), and one aromatic 4c-2e  $\pi$ -bond (ON = 2.0 |e|). The completely delocalized bonds obviously are very close to the corresponding CMOs.

The overall bonding pattern is consistent with D<sub>2h</sub> symmetry of the cluster, description of which would otherwise require several resonance structures. Standard NBO software in this case does report classical 2c-2e bonds, but represents two

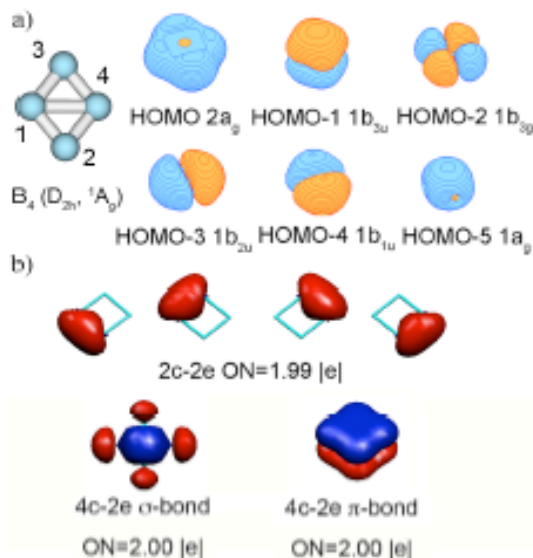


Figure 3-2. a) Structure and CMOs of B<sub>4</sub> D<sub>2h</sub>, (<sup>1</sup>A<sub>g</sub>) cluster; b) results of the AdNDP localization.

completely delocalized bonds as a set of eight lone-pairs with occupation numbers around 0.5 |e| (see Table 3-1).

### 3-4.3.B<sub>5</sub><sup>-</sup> cluster

The C<sub>2v</sub> (<sup>1</sup>A<sub>1</sub>, 1a<sub>1</sub><sup>2</sup>1b<sub>2</sub><sup>2</sup>2a<sub>1</sub><sup>2</sup>3a<sub>1</sub><sup>2</sup>1b<sub>1</sub><sup>2</sup>2b<sub>2</sub><sup>2</sup>4a<sub>1</sub><sup>2</sup>3b<sub>2</sub><sup>2</sup>) global minimum structure of B<sub>5</sub><sup>-</sup> cluster (Fig. 3-3a) is a system with conflicting aromaticity as it follows from the analysis of CMOs.<sup>58</sup> The σ-antiaromaticity originates from the completely bonding HOMO-1 4a<sub>1</sub> and partially bonding HOMO 3b<sub>2</sub>, the π-aromaticity - from the completely bonding HOMO-3 1b<sub>1</sub>. The remaining five valence CMOs are expected to be transformable into five 2c-2e peripheral B-B bonds. These five localized bonds can be recovered by standard NBO, together with one 3c-2e bond involving atoms 1, 2, and 3, two low-occupancy LPs

Table 3-1. Results of the NBO analysis for B<sub>4</sub> D<sub>2h</sub>, (<sup>1</sup>A<sub>g</sub>) cluster.

Type	ON,  e	Center (contribution, %)	Hybrids composition, (function, %)
2c-2e	1.98	1 (49)	s 49, p 51
		2 (51)	s 50, p 50
	1.98	1 (49)	s 49, p 51
		3 (51)	s 50, p 50
	1.98	2 (51)	s 50, p 50
	4 (49)	s 49, p 51	
	1.98	3 (51)	s 50, p 50
		4 (49)	s 49, p 51
LP	0.57	1	s 0, p 100
	0.54	1	s 2, p 98
	0.46	2	s 0, p 100
	0.43	2	s 0, p 100
	0.46	3	s 0, p 100
	0.43	3	s 0, p 100
	0.57	4	s 0, p 100
	0.54	4	s 2, p 98

NBO, together with one 3c-2e bond involving atoms 1, 2, and 3, two low-occupancy LPs on atoms 4 and 5 (ON = 1.57 |e|, composed out of 65% of 2s and 35% of 2p functions each), and five low-occupancy LPs on atoms 1, 2, 3, 4, and 5 (ONs from 0.18 |e| to 0.62 |e|, almost pure p-functions). Application of AdNDP algorithm leads to chemically reasonable results (Fig. 3-3b).

Indeed, five peripheral 2c-2e bonds are recovered. Antiaromatic  $\sigma$ -system gives rise to two islands of  $\sigma$ -aromaticity which reveal themselves as two 3c-2e  $\sigma$ -bonds (centered on atoms 1, 3, 5 and 1, 2, 4). The completely delocalized 5c-2e  $\pi$ -bond is the consequence of the aromaticity in the  $\pi$ -system of the cluster. One important remark should be made here. The difference of the results of NBO and AdNDP analyses for the number of centers higher than 3 is understandable, since NBO does not carry out localization for more than 3 centers in principle. The difference for the 3c-2e bonds is due

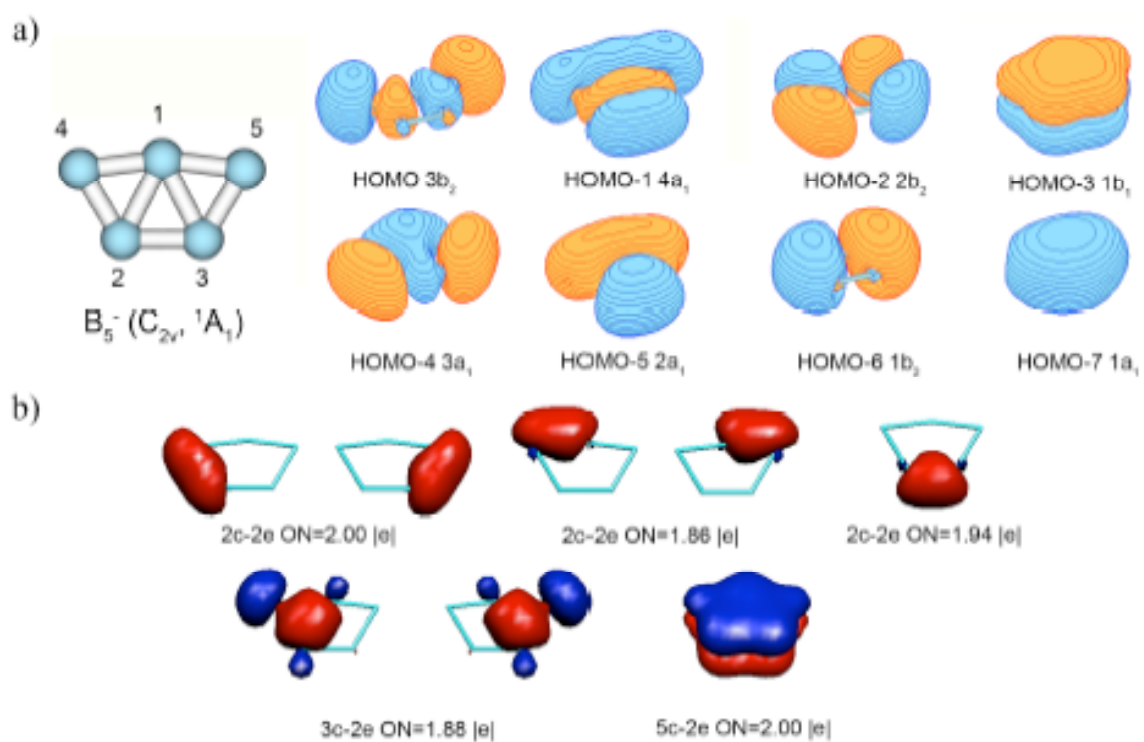


Figure 3-3. a) Structure and CMOs of  $B_5^- C_{2v} (^1A_1)$  cluster; b) results of the AdNDP localization.

to the fact that NBO does not accept eigenvectors with significant mutual overlaps. We believe that for the multi-center bonds derived from aromatic or antiaromatic MOs the overlap of the conjugated n-center bonds is a phenomenon closely related to the nature of aromaticity/antiaromaticity in the particular system and thus should not be removed from the bonding picture but preserved and studied.

#### 3-4.4. $B_6^{2-}$ cluster

$D_{2h}$  ( $^1A_g, 1a_g^2 1b_{1u}^2 2a_g^2 1b_{2u}^2 1b_{3g}^2 1b_{3u}^2 3a_g^2 2b_{2u}^2 2b_{1u}^2 1b_{2g}^2$ ) structure is the global minimum for  $B_6^{2-}$  dianion (Fig. 3-4a).<sup>82,83</sup> Analysis of the chemical bonding in this system on the basis of ring currents,<sup>83a</sup> CMOs,<sup>83b</sup> and topological resonance energy (TRE)<sup>84</sup> leads to the conclusion that the cluster is doubly antiaromatic with HOMO-3  $3a_g$  (completely bonding) and HOMO-1  $2b_{1u}$  (partially bonding) responsible for the  $\sigma$ -antiaromaticity, and HOMO-4  $1b_{3u}$  (completely bonding) and HOMO  $1b_{2g}$  (partially bonding) responsible for the  $\pi$ -antiaromaticity. Double antiaromaticity (in  $\sigma$ - and  $\pi$ -systems) is expected to lead to the formation of the islands of  $\sigma$ - and  $\pi$ - aromaticity, so that the globally antiaromatic system nevertheless has large resonance energy.<sup>58</sup> In addition to the island-aromatic bonding, analysis of CMOs suggests formation of six peripheral 2c-2e bonds. AdNDP results for  $B_6^{2-}$  cluster are shown in Figure 3-4b. The bonding picture clearly supports the idea of formation of two doubly aromatic ( $\sigma$ - and  $\pi$ -) triangular subunits within globally antiaromatic cluster. Two 3c-2e  $\sigma$ -bonds and two 3c-2e  $\pi$ -bonds recovered during the analysis do not contribute to the bonding between two 3-atomic units but are responsible for the doubly aromatic bonding within each of them. Six 2c-2e B-B bonds responsible for the peripheral bonding and holding two aromatic subunits together are also present in



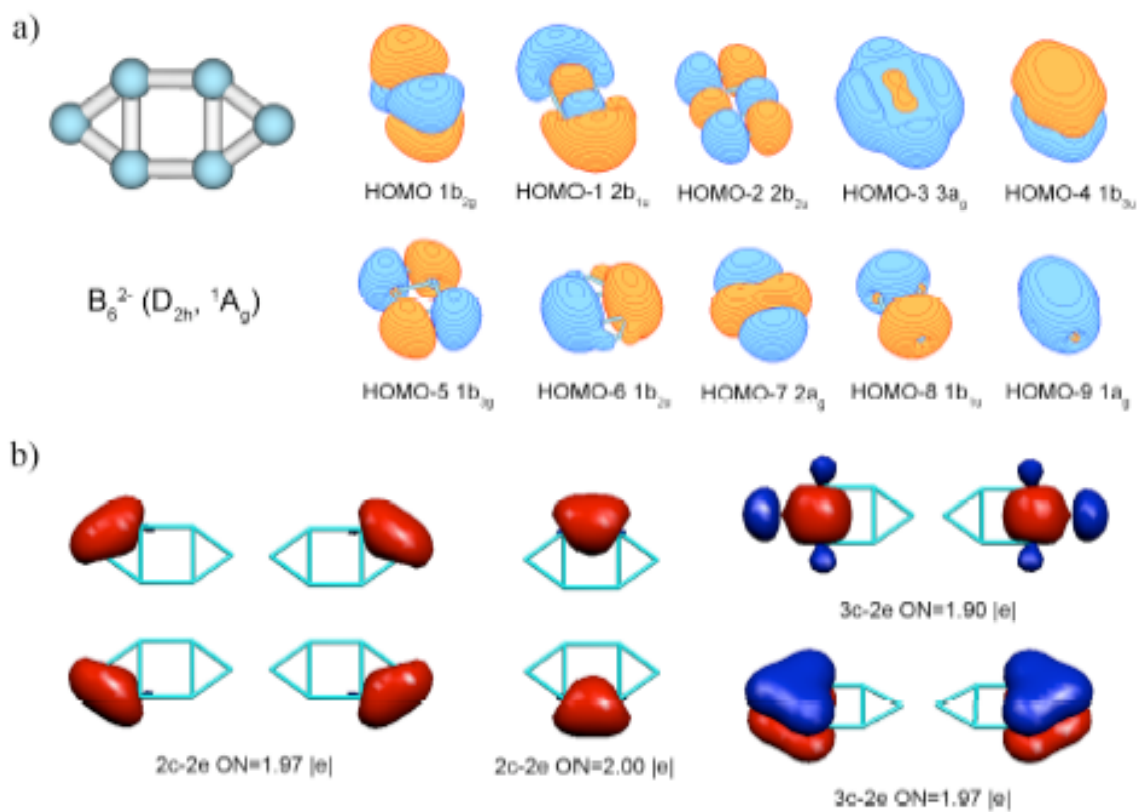


Figure 3-4. a) Structure and CMOs of  $B_6^{2-} (D_{2h}, {}^1A_g)$  cluster; b) results of the AdNDP localization.

the picture. There is consistency between the AdNDP and NBO results in this case, since bonding can be described by a combination of 2c-2e and 3c-2e bonds. NBO analysis is indeed considered as a standard within the ranges of its applicability, so the above-mentioned consistency is very important for the benchmarking the performance of the new tool. Our conclusion on antiaromaticity of the  $B_6^{2-} D_{2h} (^1A_g)$  structure is supported by the results of Havenith et al.<sup>82</sup> who studied the induced ring current maps. They demonstrated that in both the  $\pi$ -only and  $(\sigma+\pi)$  maps, a strong paramagnetic current is discernible in the inner square of the molecule, consistent with the expected anti-aromatic nature of this system.

#### 3-4.5. $B_9^-$ cluster

The outlandish global minimum  $D_{8h} (1a_{1g}^2 1e_{1u}^4 1e_{2g}^4 1e_{3u}^4 2a_{1g}^2 1b_{2g}^2 1a_{2u}^2 2e_{1u}^4 1e_{1g}^4)$  wheel-shaped structure and CMOs of the  $B_9^-$  cluster are shown at Figure 3-5a. The system is doubly  $\sigma$ - and  $\pi$ -aromatic according to the analysis of CMO structure.<sup>85</sup> Three  $\sigma$ -radial MOs (HOMO-1, HOMO-1'  $2e_{1u}$ , and HOMO-4  $2a_{1g}$ ) are responsible for  $\sigma$ -aromaticity and three  $\pi$ -MOs (HOMO, HOMO'  $1e_{1g}$ , and HOMO-2  $1a_{2u}$ ) are responsible for  $\pi$ -aromaticity. The rest of the CMOs are responsible for the peripheral bonding and are expected to be localizable into eight 2c-2e B-B bonds. Localization by AdNDP algorithm shows that this expectation is correct (Fig. 3-5b) and these eight 2c-2e bonds are recovered. At the current state-of-art on the aromaticity research field it is not clear if the description of the aromatic system, including not only completely but also partially bonding orbitals, is possible in terms of some localized bonding objects. Thus AdNDP reports three completely delocalized 9c-2e  $\sigma$ -radial “bonds” and three completely

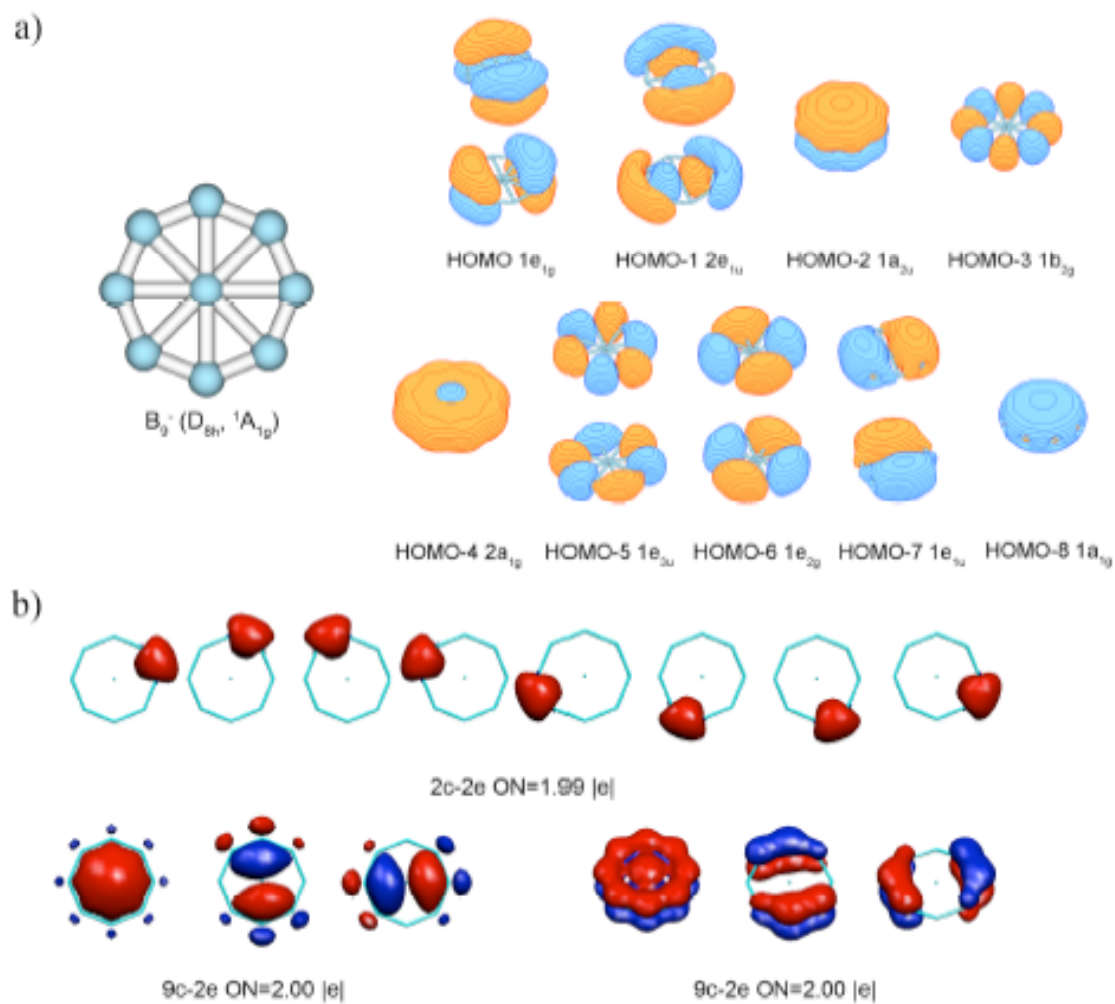


Figure 3-5. a) structure and CMOs of  $B_9^- D_{8h} (^1A_{1g})$  cluster; b) results of the AdNDP localization.

delocalized 9c-2e  $\pi$ -“bonds” that closely resemble parental  $\sigma$ -aromatic and  $\pi$ -aromatic CMOs. The discussion of the peculiarities of the aromatic bonding due to both completely and partially bonding MOs is far beyond the scope of the present study, but it is remarkable that localized and delocalized descriptions now complement each other in a seamless manner.

#### 3-4.6. $B_{11}^-$ cluster

According to Zhai et al.<sup>86</sup>  $B_{11}^-$  cluster has  $C_{2v}$  ( $^1A_1$ ,  $1a_1^2 1b_2^2 2a_1^2 3a_1^2 2b_2^2 3b_2^2 4a_1^2 5a_1^2 4b_2^2 6a_1^2 1b_1^2 5b_2^2 7a_1^2 8a_1^2 1a_2^2 6b_2^2 2b_1^2$ ) global minimum structure (Fig. 3-6a). Structure of CMOs suggests, that ten of them (from HOMO-7 to HOMO-16) should give rise to ten 2c-2e bonds (nine peripheral and one between two internal atoms) after localization, four  $\sigma$ -MOs (HOMO-1  $6b_2$ , HOMO-3  $8a_1$ , HOMO-4  $7a_1$ , and HOMO-5  $5b_2$ ) make the systems  $\sigma$ -antiaromatic, and three  $\pi$ -MOs (HOMO  $2b_1$ , HOMO-2  $1a_2$ , and HOMO-6  $1b_1$ ) make the system  $\pi$ -aromatic. According to this tentative assignment<sup>58</sup>  $B_{11}^- C_{2v}$  cluster is a system with conflicting aromaticity. The AdNDP localization (Fig. 3-6b) produces somewhat different bonding pattern. First, only nine 2c-2e peripheral bonds are encountered, all between the peripheral boron atoms. Second, five 3c-2e  $\sigma$ -bonds on five locally aromatic fragments suggest that there are totally five  $\sigma$ -CMOs involved into the  $\sigma$ -aromatic bonding, so the cluster should be considered as  $\sigma$ -aromatic. Finally, three completely delocalized 11c-2e  $\pi$ -“bonds” originate from three  $\pi$ -aromatic CMOs and closely resemble them. So, our previously made assignment<sup>58</sup> of conflicting aromaticity to  $B_{11}^- C_{2v}$  ( $^1A_1$ ) cluster, which was based on the visual analysis of the CMOs structure, structure, should be corrected and the

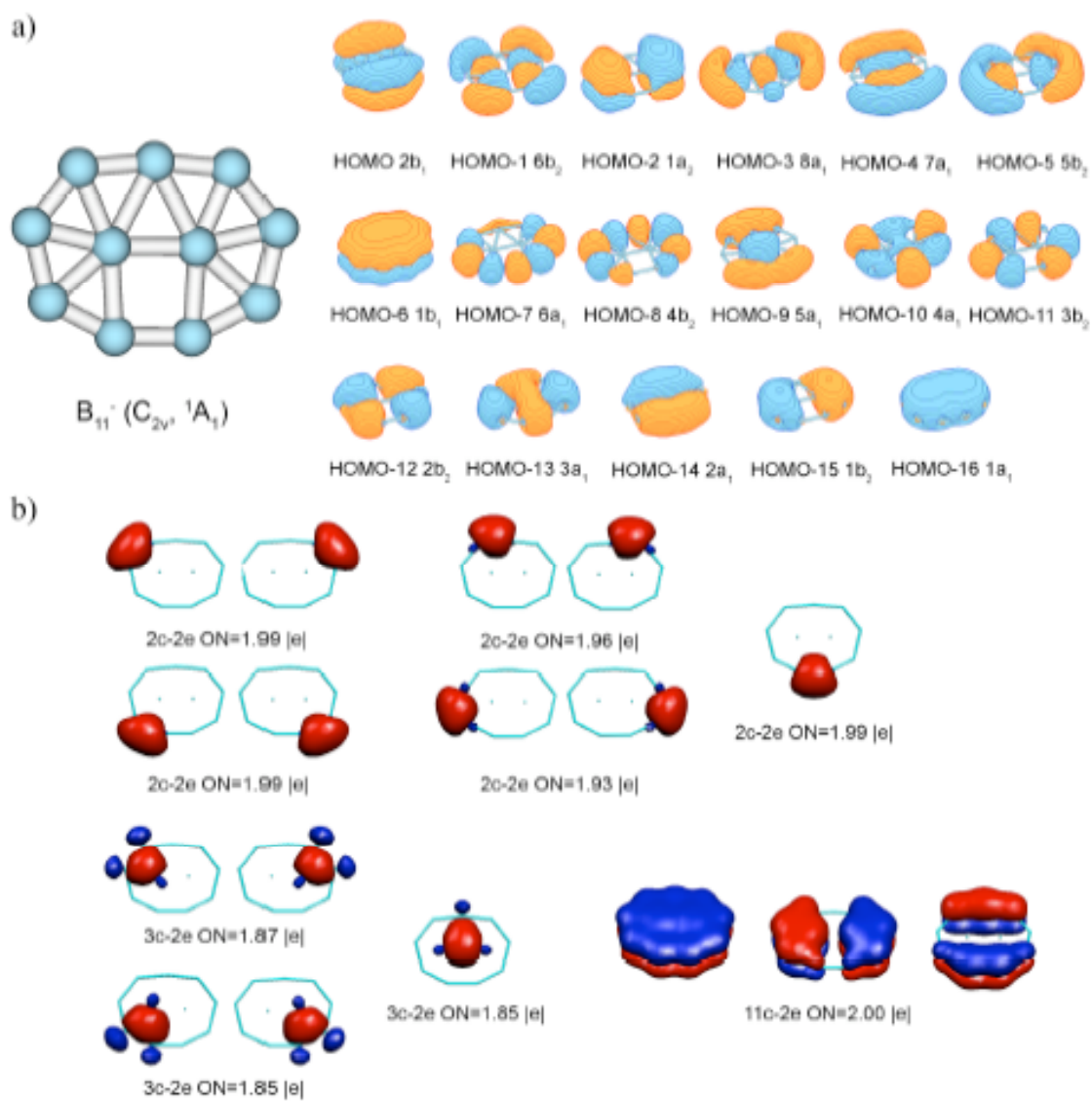


Figure 3-6. a) structure and CMOs of  $B_{11}^- C_{2v} (^1A_1)$  cluster; b) results of the AdNDP localization.

system should be considered as doubly ( $\sigma$ - and  $\pi$ -) aromatic according to the results of AdNDP analysis. Again, the question why  $\pi$ -aromatic system does not give rise to bonds with higher degree of localization in this low-symmetry structure is left open till further research.

### 3-4.7. $B_{13}^+$ cluster

Figure 3-7a represents the famous  $C_{2v}$  ( $^1A_1$ ,  $1a_1^2 1b_2^2 2a_1^2 3a_1 2^2 b_2^2 4a_1^2 3b_2^2 5a_1^2 4b_2^2 6a_1^2 7a_1^2 5b_2^2 1b_1^2 8a_1^2 9a_1^2 6b_2^2 1a_1^2 2b_1^2 10a_1^2$ ) global minimum structure<sup>87</sup> and CMOs of  $B_{13}^+$  cluster. The remarkably high stability and low reactivity in comparison with other cationic boron clusters has been reported by Anderson and co-workers.<sup>88-94</sup> First Fowler and Ugalde,<sup>95</sup> and later Aihara<sup>96</sup> related this exceptional stability to the aromatic character of the  $\pi$ -electronic system of the cluster. It has been demonstrated recently<sup>58</sup> that aromaticity of the  $\sigma$ -electronic system should also be taken into account. Tentative description of the chemical bonding in  $B_{13}^+$   $C_{2v}$  ( $^1A_1$ ) based on the visual analysis of its CMOs<sup>58</sup> is as follows. Three orbitals (HOMO-4  $9a_1$ , HOMO-3  $6b_2$ , and HOMO  $10a_1$ ) are assumed to belong to  $\sigma$ -aromatic system, three more (HOMO-6  $1b_1$ , HOMO-2  $1a_2$ , and HOMO-1  $2b_1$ ) – to  $\pi$ -aromatic system, and remaining ten CMOs are supposed to be transformable to ten 2c-2e peripheral bonds. The cluster is therefore doubly ( $\sigma$ - and  $\pi$ -) aromatic. Again, the application of AdNDP in this case leads to a different bonding picture (Fig. 3-7b). Eleven lowest CMOs (from HOMO-18 to HOMO-8) are localized into ten 2c-2e bonds between peripheral boron atoms and one 3c-2e bond (I, Fig. 3-7b) between three internal boron atoms. Remaining five  $\sigma$ -CMOs (HOMO-7, HOMO-5, HOMO-4, HOMO-3, and HOMO) are transformed into five 3c-2e

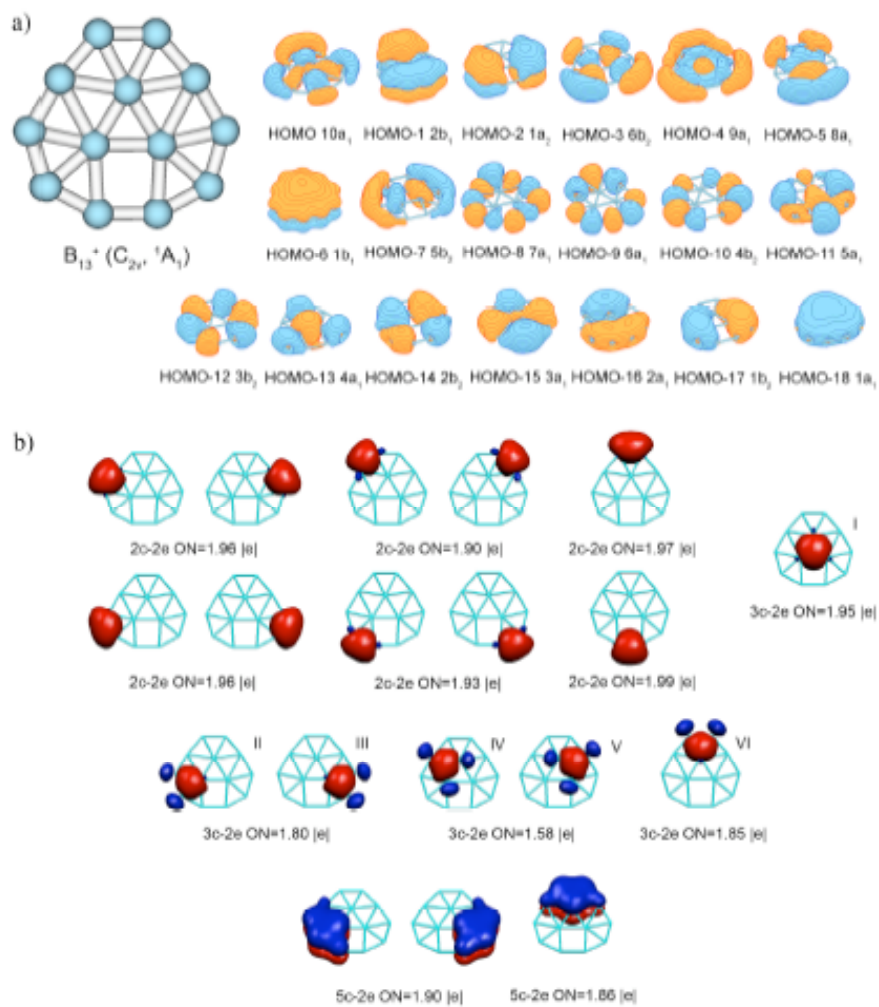


Figure 3-7. a) structure and CMOs of  $B_{13}^+ C_{2v} (^1A_1)$  cluster; b) results of the AdNDP localization.

$\sigma$ -bonds (II, III, IV, V, and VI, Fig. 3-7b) binding internal three-atomic and external ten-atomic cycles. Finally, three  $\pi$ -CMOs (HOMO-6, HOMO-2, and HOMO-1) are localized into three 5c-2e conjugated  $\pi$ -bonds. While  $\pi$ -system is now fragmented into three 5c-2e conjugated  $\pi$ -bonds, it remains overall globally aromatic similarly to the coronene, where three Clar's sextets are associated with individual six-membered rings preserving global aromaticity of this system. Similar logic applies to the  $\sigma$ -delocalized bonding in  $B_{13}^+$ : five 3c-2e  $\sigma$ -bonds responsible for bonding between the external ten-membered ring and the internal three-membered ring should be considered as forming globally aromatic  $\sigma$ -framework with ten electron satisfying the  $4n+2$  rule. Finally, there is one more 3c-2e bond within the internal three-atomic cycle responsible for local  $\sigma$ -aromaticity of this fragment. In spite of some difference in details both the previous tentative assignment on the basis of visual inspection of CMOs and "instrumental" analysis using AdNDP agree with each other on the globally doubly  $\sigma$ - and  $\pi$ -aromatic nature of the  $B_{13}^+$  cluster.

### 3-5. Conclusion

The newly developed Adaptive Natural Density Partitioning algorithm is an attempt to combine the ideas of Lewis theory and aromaticity. If the bonding is essentially due to a pair of electrons with antiparallel spins and description of a huge number of molecules can be given in terms of electron pairs localized at one (LP) or two (2c-2e bonds) atoms, then it seems only natural to assume that "localized bonds" should not be limited to two atoms (or three, as in the case of boron hydrates). This approach leads to partitioning of the charge density into the elements with highest possible degree of localization of electron pairs – nc-2e bonds. If some part of the density cannot be



localized in this manner, it is left “delocalized” (localized on the maximal number of the available centers) thus incorporating the idea of a completely delocalized (globally aromatic) bonding. Thus, AdNDP achieves seamless description of the chemical bonding in the systems of the most general type. AdNDP was developed to have a philosophy of a pry-bar rather than a black-box. It is intended to help a researcher to get inside the studied system and analyze it and work with it, but simultaneously provide certain level of the conceptual and interpretational comfort. From the computational point of view, AdNDP is a generalization of the Natural Bonding Orbital analysis and inherits pros and cons of the latter. The method is resource-efficient, since essentially involves only eigenproblem solving by diagonalization. It can be paired with any quantum chemical software that reports electron density matrix. The found bonding objects can be easily visualized using existing graphical software. It should be kept in mind, that just like its parent, AdNDP is sensitive to the choice of the occupation number threshold. This fact leaves the researcher responsible for the choice of the search strategy and acceptance of the final bonding pattern. The reported eigenvectors with high eigenvalues should not be regarded as “orbitals” in the sense of NBO, since they are not orthonormalized. This is the reason for the choice of the name of the algorithm. Its primary task is to provide partitioning of the electron density consistent with the concept of electron pair responsible for the bonding via technique related to the “natural orbitals” of Löwdin. The reported examples show, that indeed the approach, allowing for the  $nc-2e$  bonds, works consistently. The results of the AdNDP application agree with the NBO results for the systems that can be treated by both methods. For other systems, the results agree with earlier made predictions and in some case clarify or correct them. Consideration of the

chemical bonding in this article is limited to clusters only, since the purpose of the paper is to introduce a new tool for the analysis of chemical bonding. Also, only closed-shell systems have been analyzed due to the current limitations of the code. The extension of the method to the analysis of the open-shell and multiconfigurational systems is possible and will be done in the subsequent papers. For open-shell systems  $\alpha$ - and  $\beta$ - density matrices are analyzed separately with maximum occupation numbers being equal to one instead of two. Indeed, AdNDP can be applied to any chemical system. Moreover, we expect that it would help to get theoretical insight into the nature of the delocalized bonding. We strongly believe that AdNDP will find its place in the toolboxes of both theoreticians and experimentalists.

## References

1. G. N. Lewis, *J. Am. Chem. Soc.* 1931, **53**, 1367.
2. G. Frenking and S. J. Shaik, *J. Comput. Chem.* 2007, **28**, 1.
3. (a) F. Hund, *Zeits. f. Physik*, 1931, **73**, 1; (b) R. S. Mulliken, *Phys. Rev.* 1932, **41**, 49.
4. J. M. Foster and S. F. Boys, *Rev. Mod. Phys.* 1960, **32**, 300.
5. C. Edmiston and K. Ruedenberg, *Rev. Mod. Phys.* 1963, **35**, 457.
6. J. Pipek and P. G. Mezey, *J. Chem. Phys.* 1989, **90**, 4916.
7. W. Heitler and F. London, *Z. Phys.* 1927, **44**, 455.
8. (a) J. C. Slater, *Phys. Rev.* 1931, **37**, 481; J. C. Slater, *Phys. Rev.* 1931, **37**, 1109; (b) L. Pauling, *J. Am. Chem. Soc.* 1931, **53**, 1367; (c) L. Pauling, *J. Am. Chem. Soc.* 1931, **53**, 3225;

9. D. G. Truhlar, *J. Comput. Chem.* 2007, **28**, 73 and references therein.
10. Y. Mo, L. Song and Y. Lin, *J. Phys. Chem. A* 2007, **111**, 8291.
11. R. F. W. Bader, *Atoms in Molecules: A Quantum Theory*; Oxford University Press: Oxford, 1990.
12. K. Z. Artman, *Naturforsch.* 1946, **1**, 426.
13. J. Lennard-Jones, *Proc. R. Soc.* 1949, **A198**, 1; J. Lennard-Jones, *Proc. R. Soc.* 1949, **A198**, 14.
14. R. Daudel, *Quantum Theory of the Chemical Bond*; Reidel, Dordrecht, 1974.
15. R. F. W. Bader and M. E. Stephens, *J. Am. Chem. Soc.* 1975, **97**, 7391.
16. W. L. Luken and J. C. Culberson, *Int. J. Quant. Chem.* 1982, **16**, 265.
17. A. D. Becke and K. E. Edgecombe, *J. Chem. Phys.* 1990, **92**, 5397.
18. B. Silvi and A. Savin, *Nature*, 1994, **371**, 683.
19. P. Fuentealba, *Int. J. Quant. Chem.* 1998, **69**, 559.
20. R. Ponec and D. L. Cooper, *J. Phys. Chem. A* 2007, **111**, 11294.
21. C. A. Coulson, *Proc. Roy. Soc. (London)*, 1938, **A169**, 413.
22. K. B. Wiberg, *Tetrahedron*, 1968, **24**, 1083.
23. I. Mayer, *Chem. Phys. Lett.* 1983, **97**, 270.
24. I. Mayer, *Int. J. Quantum Chem.* 1986, **29**, 73.
25. M. Giambiagi, M. S. Giambiagi and M. S. Mundim, *Struct. Chem.* 1990, **1**, 123.
26. A. B. Sannigrahi and T. Kar, *Chem. Phys. Lett.* 1990, **173**, 569.
27. R. L. Fulton and S. T. Mixon, *J. Phys. Chem.* 1993, **97**, 7530.
28. R. L. Fulton, *J. Phys. Chem.* 1993, **97**, 7516.
29. I. Mayer, *Int. J. Quantum Chem.* 1986, **29**, 477.

30. I. Mayer, *Int. J. Quantum Chem.* 1985, **28**, 419.
31. I. Mayer, *Int. J. Quantum Chem.* 1984, **26**, 151.
32. X. Fradera, M. A. Austen and R. F. W. Bader, *J. Phys. Chem. A*, 1999, **103**, 304.
33. R. F. W. Bader and M. E. Stephens, *J. Am. Chem. Soc.* 1975, **97**, 7391.
34. E. Matito, M. Sola, P. Salvador and M. Duran, *Faraday Discuss.* 2007, **135**, 325.
35. (a) J. P. Foster and F. Weinhold, *J. Am. Chem. Soc.* 1980, **102**, 7211. (b) A. E. Reed, L. A. Curtiss and F. Weinhold, *Chem. Rev.* 1988, **88**, 899.
36. F. Weinhold and C. R. Landis, *Valency and Bonding: A Natural Bond Orbital Donor-Acceptor Perspective*; Cambridge University Press: Cambridge, UK, 2005.
37. A. Kekule, *Bull. Soc. Chim. Fr. (Paris)*, 1865, **3**, 98.
38. Minkin, V. I.; Glukhovtsev, M. N.; Simkin, B. Ya. *Aromaticity and Antiaromaticity. Electronic and Structural Aspects*; Wiley & Sons: New York, 1994.
39. Special edition on aromaticity. P. v. R. Schleyer, ed. *Chem. Rev.* 2001, **101**, No. 5.
40. Special edition on heterocycles. A. Katritzky, ed. *Chem. Rev.* 2004, **104**, No. 5.
41. Special edition on delocalization pi and sigma. P. v. R. Schleyer ed. *Chem. Rev.* 2005, **105**, No. 10.
42. (a) J. Poater, X. Fradera, M. Duran and M. Sola, *Chem. – Eur. J.* 2003, **9**, 1113; (b) E. Matito, M. Duran and M. Sola, *J. Chem. Phys.* 2005, **122**, 014109.
43. (a) M. S. Giambiagi, M. Giambiagi and M. S. Fortes, *J. Mol. Struc. (Theochem)*, 1997, **391**, 141; (b) M. Giambiagi, M. S. Giambiagi, C. D. Santos Silva and A. P. Figueiredo, *Phys. Chem. Chem. Phys.* 2000, **2**, 3381.

44. P. Bultinck, R. Ponec and S. V. Dammme, *J. Phys. Org. Chem.* 2005, **18**, 706.
45. P. Bultinck, S. Fias and R. Ponec, *Chem. Eur. J.* 2006, **12**, 8813.
46. P. Bultinck, R. Ponec and R. Carbo-Dorca, *J. Comput. Chem.* 2007, **28**, 152.
47. P. Bultinck, M. Rafat, R. Ponec, B. V. Gheluwe, R. Carbo-Dorca and P. Popelier, *J. Phys. Chem. A*, 2006, **110**, 7642.
48. R. Ponec, P. Bultinck and A. G. Saliner, *J. Phys. Chem. A*, 2005, **109**, 6606.
49. J. Cioslowski, E. Matito and M. Sola, *J. Phys. Chem.* 2007, **111**, 6521.
50. (a) P. v. R. Schleyer, C. Maerker, A. Dransfeld, H. Jiao and N. J. R. van Eikema Hommes, *J. Am. Chem. Soc.* 1996, **118**, 6317; (b) for recent review NICS application see Z, Chen, C. S. Wannere, C. Corminboeuf, R. Puchta and P. v. R. Schleyer, *Chem. Rev.* 2005, **105**, 3842.
51. J. Juselius and D. Sundholm, *Phys. Chem. Chem. Phys.* 1999, **1**, 3429.
52. J. Juselius, D. Sundholm and J. Gauss, *J. Chem. Phys.* 2004, **121**, 3952.
53. E. Steiner and P. W. Fowler, *J. Phys. Chem. A*, 2001, **105**, 9553.
54. A. I. Boldyrev and L. S. Wang, *Chem. Rev.* 2005, **106**, 3716.
55. D. Yu. Zubarev, B. B. Averkiev, H. J. Zhai, L. S. Wang and A. I. Boldyrev, *Phys. Chem. Chem. Phys.* 2008, **10**, 257.
56. W. N. Lipscomb, *Boron Hydrides*; Benjamin, New York, 1963.
57. A. N. Alexandrova, A. I. Boldyrev, H. J. Zhai and L. S. Wang, *Coord. Chem. Rev.* 2006, **250**, 2811.
58. D. Yu. Zubarev and A. I. Boldyrev, *J. Comput. Chem.* 2007, **28**, 251.

59. P. O. Löwdin, *J. Chem. Phys.* 1950, **18**, 365.
60. P. O. Löwdin, *Phys. Rev.* 1955, **97**, 1474.
61. E. D. Glendening, J. K. Badenhop, A. E. Reed, J. E. Carpenter, J. A. Bohmann, C. M. Morales and F. Weinhold, Theoretical Chemistry Institute, *NBO 5.0.*, University of Wisconsin, Madison, 2001.
62. A. E. Reed, R. B. Weinstock and F. Weinhold, *J. Chem. Phys.* 1985, **83**, 735.
63. R. G. Parr and W. Yang, *Density-Functional Theory of Atoms and Molecules*; Oxford University Press, Oxford, 1989.
64. A. D. Becke, *J. Chem. Phys.* 1993, **98**, 5648.
65. J. P. Perdew, J. A. Chevary, S. H. Vosko, K. A. Jackson, M. R. Pederson, D. J. Singh and C. Fiolhais, *Phys. Rev. B*, 1992, **46**, 6671.
66. R. Krishnan, J. S. Binkley, R. Seeger and J. A. Pople, *J. Chem. Phys.* 1980, **72**, 650.
67. A. D. McLean and G. S. Chandler, *J. Chem. Phys.* 1980, **72**, 5639.
68. T. Clark, J. Chandrasekhar, G. W. Spitznagel and P. v. R. Schleyer, *J. Comput. Phys.* 1983, **4**, 294.
69. M. J. Frisch, G. M. Trucks, H. B. Schlegel et al., *GAUSSIAN 03*, Revision A.1, Gaussian, Inc., Pittsburgh, PA, 2003.
70. W. J. Hehre, R. F. Stewart and J. A. Pople, *J. Chem. Phys.* 1969, **51**, 2657.
71. J. B. Collins, P. v. R. Schleyer, J. S. Binkley and J. A. Pople, *J. Chem. Phys.* 1976, **64**, 5142.
72. J. E. Carpenter and F. Weinhold, *J. Mol. Struct. (Theochem)*, 1988, **169**, 41.
73. J. E. Carpenter, PhD thesis, University of Wisconsin, Madison, WI, 1987.

74. A. E. Reed and F. Weinhold, *J. Chem. Phys.* 1983, **78**, 4066.
75. S. Portmann, *MOLEKEL*, Version 4.3., CSCS/ETHZ, 2002.
76. G. Schaftenaar, *MOLDEN 3.4*, CAOS/CAMM Center, The Netherlands, 1998.
77. A. N. Alexandrova and A. I. Boldyrev, *J. Phys. Chem. A*, 2003, **107**, 554.
78. L. Yong, S. D. Wu and X. X. Chi, *Int. J. Quant. Chem.* 2007, **107**, 722.
79. J. M. L. Martin, J. P. Francois and R. Gijbels, *Chem. Phys. Lett.* 1992, **189**, 52.
80. H. J. Zhai, L. S. Wang, A. N. Alexandrova, A. I. Boldyrev and V. G. Zakrzewski, *J. Phys. Chem. A* 2003, **107**, 9319.
81. C. Gillery, R. Linguerri, P. Rosmus and J. P. Maier, *Z. Phys. Chem.* 2005, **219**, 467.
82. R. W. A. Havenith, P. W. Fowler and E. Steiner, *Chem.-Eur. J.* 2002, **8**, 1068.
83. (a) A. N. Alexandrova, A. I. Boldyrev, H. J. Zhai, L. S. Wang, E. Steiner and P. W. Fowler, *J. Phys. Chem. A*, 2003, **107**, 1359; (b) A. N. Alexandrova, A. I. Boldyrev, H.-J. Zhai and L. S. Wang, *J. Chem. Phys.* 2005, **122**, 054313.
84. J. Aihara, H. Kanno and T. Ishida, *J. Am. Chem. Soc.* 2005, **127**, 13324.
85. H.-J. Zhai, A. N. Alexandrova, K. A. Birch, A. I. Boldyrev and L. S. Wang, *Angew. Chem. Int. Ed.* 2003, **42**, 6004.
86. H. J. Zhai, B. Kiran, J. Li and L. S. Wang, *Nat. Mater.* 2003, **2**, 827.
87. A. Ricca and C. W. Bauschlicher, *J. Chem. Phys.* 1996, **208**, 233.
88. L. Hanley, and S. L. Anderson, *J. Phys. Chem.* 1987, **91**, 5161.
89. L. Hanley and S. L. Anderson, *J. Chem. Phys.* 1988, **89**, 2848.
90. L. Hanley, J. L. Whitten and S. L. Anderson, *J. Phys. Chem.* 1988, **92**, 5803.
91. P. A. Hintz, S. A. Ruatta and S. L. Anderson, *J. Chem. Phys.* 1990, **92**, 292.

92. S. A. Ruatta, P. A. Hintz and S. L. Anderson, *J. Chem. Phys.* 1991, **94**, 2833.
93. P. A. Hintz, M. B. Sowa, S. A. Ruatta and S. L. Anderson, *J. Chem. Phys.* 1991, **94**, 6446.
94. M. B. Sowa-Resat, J. Smolanoff, A. Lapiki and S. L. Anderson, *J. Chem. Phys.* 1997, **106**, 9511.
95. J. E. Fowler, J. M. Ugalde, *J. Phys. Chem. A*, 2000, **104**, 397.
96. J. Aihara, *J. Phys. Chem. A*, 2001, **105**, 5486.



CHAPTER 4  
COMPREHENSIVE ANALYSIS OF CHEMICAL BONDING  
IN BORON CLUSTERS<sup>1</sup>

**Abstract**

We present a comprehensive analysis of chemical bonding in pure boron clusters. It is now established in joint experimental and theoretical studies that pure boron clusters are planar or quasi-planar at least up to twenty atoms. Their planarity or quasi-planarity was usually discussed in terms of  $\pi$ -delocalization or  $\pi$ -aromaticity. In the current article we demonstrated, that one cannot ignore  $\sigma$ -electrons and that the presence of two-center two-electron (2c-2e) peripheral B-B bonds together with the globally delocalized  $\sigma$ -electrons must be taken into consideration when the shape of pure boron cluster is discussed. The global aromaticity (or global antiaromaticity) can be assigned on the basis of the  $4n+2$  (or  $4n$ ) electron counting rule for either  $\pi$ - or  $\sigma$ - electrons in the planar structures. We showed that pure boron clusters could have double ( $\sigma$ - and  $\pi$ -) aromaticity ( $B_3^-$ ,  $B_4$ ,  $B_5^+$ ,  $B_6^{2+}$ ,  $B_7^+$ ,  $B_7^-$ ,  $B_8$ ,  $B_8^{2-}$ ,  $B_9^-$ ,  $B_{10}$ ,  $B_{11}^+$ ,  $B_{12}$ , and  $B_{13}^+$ ), double ( $\sigma$ - and  $\pi$ -) antiaromaticity ( $B_6^{2-}$ ,  $B_{15}$ ); or conflicting aromaticity ( $B_5^-$ ,  $\sigma$ -antiaromatic and  $\pi$ -aromatic and  $B_{14}$ ,  $\sigma$ -aromatic and  $\pi$ -antiaromatic). Appropriate geometric fit is also an essential factor, which determines the shape of the most stable structures. In all boron clusters considered here the peripheral atoms form planar cycles. Peripheral 2c-2e B-B bonds are built up from s-p hybrid atomic orbitals and this enforces the planarity of the cycle. If the

---

<sup>1</sup> Coauthored by Dmitry Yu. Zubarev and Alexander I. Boldyrev. Reproduced with permission from *J. Comput. Chem.* **2007**, 28, 251-268.

given number of central atoms (1, 2, 3, or 4) can perfectly fit the central cavity then the overall structure is planar. Otherwise, central atoms come out of the plane of the cycle and the overall structure is quasi-planar.

#### **4-1. Introduction**

In organic chemistry a vast majority of molecules can be represented by a single Lewis structure (classical molecules) with either single or multiple two-center two-electron (2c-2e) bonds and with an appropriate number of lone pairs on electron-rich atoms. Chemical bonding in many inorganic molecules also can be represented by a single Lewis structure, but generally in inorganic chemistry such a description encounters significant problems. If, however, a single Lewis structure description is not sufficient, then the resonance of Lewis structures is used. The last approach is particularly important for description of the chemical bonding in aromatic compounds. The major advantage of the above mentioned chemical bonding model is that we can predict possible isomers of classical molecules using just paper and pencil and with high certainty we can also predict which isomer could be the most stable one for a given stoichiometry. We can also draw a possible mechanism of chemical reaction using the above mentioned chemical bonding models, which makes them irreplaceable in chemistry.

Homoatomic and heteroatomic clusters today represent the final frontier for developing unified chemical bonding theory. However, we do not have similar chemical bonding models allowing us to use the “paper and pencil” approach for predicting isomers of homoatomic and heteroatomic clusters. The brute-force techniques based on genetic algorithm, molecular dynamics, and hopping models can help us to find global

minima of small clusters as well as their low-lying isomers, but they quickly run into computational problems in larger systems. Without robust chemical bonding models capable of predicting global minimum structures and stable isomers of clusters our progress in understanding cluster structure and the rational design of molecular/cluster-level electronic and mechanical devices is seriously limited.

There was some progress in recent years in developing chemical bonding models for clusters.<sup>1-13</sup> Boron clusters are the best understood clusters of the main group elements. Today we are capable of explaining and predicting their geometric structures and other molecular and spectroscopic properties, because of recent advances in developing chemical bonding model for these systems.<sup>5a,6,7b,14-24</sup>

Pioneering works on pure boron cations have been done by Anderson and co-workers.<sup>25-31</sup> These authors produced boron cluster cations in molecular beams using laser vaporization and studied their chemical reactivity and fragmentation properties. They initially postulated the three-dimensional structures for boron clusters. Subsequent quantum chemical calculations<sup>32-62</sup> have shown that boron clusters prefer planar or quasi-planar structures. However, these computational predictions were not verified experimentally. In a series of recent articles joint experimental and theoretical studies have been reported for a number of boron clusters,  $B_3^-$  and  $B_4^-$ ,<sup>14</sup>  $B_5^-$ ,<sup>15</sup>  $B_6^-$ ,<sup>16</sup>  $B_7^-$ ,<sup>17</sup>  $B_8^-$  and  $B_9^-$ ,<sup>18</sup>  $B_{10}^-$ - $B_{15}^-$ ,<sup>19</sup> and their neutrals. The structures of these clusters have been studied computationally and verified through comparisons of experimental and theoretical photoelectron spectra. These studies have confirmed the two-dimensional or quasi two-dimensional structures of all these clusters. Pure boron clusters have been recently reviewed.<sup>63</sup>

The planarity of boron clusters has been primarily discussed in terms of  $\pi$ -delocalization<sup>43,44</sup> and  $\pi$ -aromaticity.<sup>5a,6,7b,14-24</sup> It has been shown that high symmetric planar boron clusters  $B_3^-$  ( $D_{3h}$ ),  $B_4$  (effectively  $D_{4h}$ ),  $B_8^{2-}$  ( $D_{7h}$ ),  $B_9^-$  ( $D_{8h}$ ) have either 2 ( $B_3^-$  and  $B_4$ ) or 6 ( $B_8^{2-}$  and  $B_9^-$ )  $\pi$ -electrons similar to the prototypical hydrocarbons  $C_3H_3^+$  ( $D_{3h}$ , with 2  $\pi$ -electrons) and  $C_6H_6$  ( $D_{6h}$ , with 6  $\pi$ -electrons). Thus they formally satisfy the  $4n+2$  Huckel rule and could be considered as  $\pi$ -aromatic clusters. Boron clusters with  $4n$   $\pi$ -electrons such as  $B_6^{2-}$  (4  $\pi$ -electrons) and  $B_{14}$  (8  $\pi$ -electrons) can be considered as  $\pi$ -antiaromatic. Aihara and co-workers<sup>20</sup> recently performed analysis of the aromaticity of boron clusters  $B_x$  ( $x=3-15$ ) in terms of the topological resonance energy (TRE) and concluded that all boron clusters are highly  $\pi$ -aromatic including systems with  $4n$   $\pi$ -electrons.

In order to resolve the controversy about aromaticity or antiaromaticity of closed shell boron clusters with  $4n$  electrons and also to include  $\sigma$ -electrons into the discussion, in the current work we present a comprehensive chemical bonding analysis of the pure boron clusters  $B_x^{0,+1,+2,-1,-2}$  ( $x=2-15$ ). We will consider here only clusters with an even number of electrons. For neutral and anionic boron clusters with 3-9 atoms, the  $\sigma$ -aromaticity has been previously considered,<sup>14-18,21-24</sup> however, the influence of the  $\sigma$ -electrons on the geometric structure of boron clusters with 10-15 atoms has not been discussed yet.<sup>5a,6,19,20</sup> Also, the use of the concept of aromaticity in cationic boron clusters was limited primarily to the  $B_{13}^+$  cluster.<sup>5a,6</sup>

## 4-2. Theoretical Methods

In our current study we used previously determined geometries for  $B_3^+$ ,  $B_3^-$ ,  $B_4$ ,

$B_4^{2-}$ ,  $B_5^+$ ,  $B_5^-$ ,  $B_6$ ,  $B_6^{2-}$ ,  $B_7^-$ ,  $B_8$ ,  $B_8^{2-}$ ,  $B_9^-$  clusters which have been summarized in a recent review.<sup>63</sup> Their structures are shown in Figure 4-1. Chemical bonding analysis was performed using the Natural Bond Analysis (NBO)<sup>64</sup> (at the B3LYP/6-311+G\* level of theory<sup>65-69</sup>), pictures of Hartree-Fock canonical MOs (RHF/6-311+G\*), and Nuclear Independent Chemical Shift (NICS)<sup>70</sup> (B3LYP/6-311+G\*). We also calculated the first singlet vertical excitation energies at TD-B3LYP/6-311+G\*<sup>71,72</sup> as a probe of the aromaticity or antiaromaticity. All calculations were performed using the Gaussian 03 program.<sup>73</sup> MO pictures were made using the Molden 3.4 program.<sup>74</sup> Results of our calculations are summarized in Table 4-1.

### 4-3. Chemical Bonding Analysis

In our chemical bonding analysis we adopt the following approach. First, we use the NBO analysis to determine which canonical MOs can be localized into 2c-2e chemical bonds. Second, MOs, which cannot be localized into 2c-2e bonds, are identified as  $\sigma$ -delocalized or  $\pi$ -delocalized. Third, the  $\pi$ -aromaticity (or  $\pi$ -antiaromaticity) and the  $\sigma$ -aromaticity (or  $\sigma$ -antiaromaticity) is assigned to a cluster on the basis of counting of the delocalized electrons according to the  $4n+2$  rule for aromaticity (the singlet coupling of the electrons) and the  $4n$  rule for antiaromaticity (the singlet coupling of the electrons). For the triplet coupling of electrons we use the inverse  $4n$  counting rules for aromaticity. Thus in our analysis we mix two ways of describing chemical bonding in boron clusters: localized MOs and delocalized MOs. In the result chemical bonding is expressed in terms of 2c-2e bonds and lone pairs as well as multiple aromaticity, multiple antiaromaticity or conflicting ( $\sigma$ -aromaticity and  $\pi$ -antiaromaticity or  $\sigma$ -antiaromaticity and  $\pi$ -aromaticity)

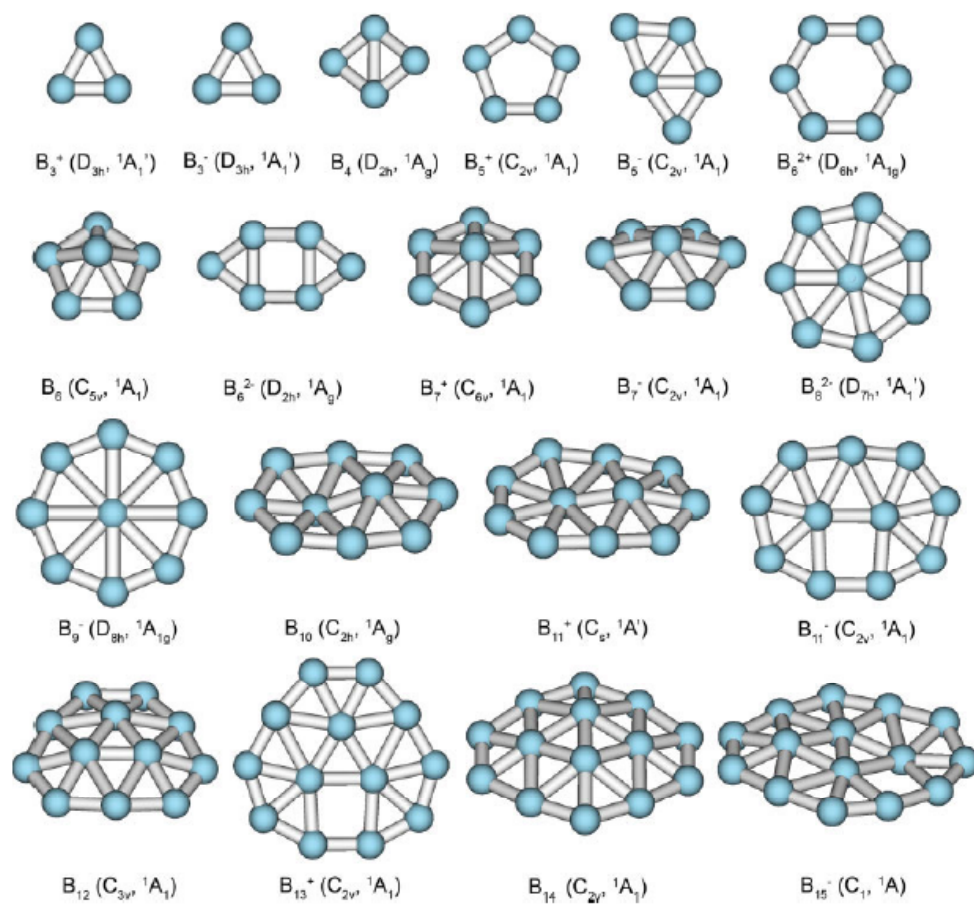


Figure 4-1. Global minimum structures of  $B_3^+$ ,  $B_3^-$ ,  $B_4$ ,  $B_5^+$ ,  $B_5^-$ ,  $B_6^{2+}$ ,  $B_6$ ,  $B_6^{2-}$ ,  $B_7^+$ ,  $B_7^-$ ,  $B_8^{2-}$ ,  $B_9^-$ ,  $B_{10}$ ,  $B_{11}^+$ ,  $B_{11}^-$ ,  $B_{12}$ ,  $B_{13}^+$ ,  $B_{14}$ , and  $B_{15}^-$  as reported in ref. 63.

Table 4-1. Computed features of the chemical bonding in boron clusters.<sup>a</sup>

Cluster	N <sub>B-B</sub>	Totally delocalized s-MOs	Totally delocalized p-MOs	NICS, ppm	First singlet vertical excitation energy, eV	E <sub>atomiz</sub> , kcal/mol per atom
B <sub>3</sub> <sup>+</sup> D <sub>3h</sub> ( <sup>1</sup> A <sub>1</sub> ' )	3	0	1	-66.3 (0.0) -46.3 (0.5) -15.9 (1.0)	0.77	56.4
B <sub>3</sub> <sup>-</sup> D <sub>3h</sub> ( <sup>1</sup> A <sub>1</sub> ' )	3	1	1	-73.6 (0.0) -57.9 (0.5) -28.2 (1.0)	2.65	88.43
B <sub>4</sub> D <sub>2h</sub> ( <sup>1</sup> A <sub>g</sub> )	4	1	1	-35.6 (0.0) -24.5 (0.5) 7.7 (1.0)	3.08	79.65
B <sub>5</sub> <sup>+</sup> D <sub>5h</sub> ( <sup>1</sup> A <sub>1</sub> ' )	5	1	1	-36.2 (0.0) -31.0 (0.5) -18.8 (1.0)	2.97	88.04
B <sub>5</sub> <sup>-</sup> C <sub>2v</sub> ( <sup>1</sup> A <sub>1</sub> )	5	2	1	-10.8 (0.0) -16.9 (0.5) -14.3 (1.0)	1.10	98.10
B <sub>6</sub> <sup>2+</sup> D <sub>6h</sub> ( <sup>1</sup> A <sub>1g</sub> )	6	1	1	-29.6 (0.0) -26.2 (0.5) -17.8 (1.0)	1.94	70.02
B <sub>6</sub> <sup>0</sup> C <sub>5v</sub> ( <sup>1</sup> A <sub>1</sub> )	8	3	1	-59.1 (-0.15) -41.9 (-0.65) -23.3 (-1.15)	2.34	89.18
B <sub>6</sub> <sup>-2</sup> D <sub>2h</sub> ( <sup>1</sup> A <sub>g</sub> )	6	3	2	-3.6 (0.0) 3.4 (0.5) 8.9 (1.0)	0.88	93.57
B <sub>7</sub> <sup>+</sup> C <sub>6v</sub> ( <sup>1</sup> A <sub>1</sub> )	6	3	1	-42.3 (-0.1) -36.0 (-0.6) -20.4 (-1.1)	1.99	98.74
B <sub>8</sub> <sup>2-</sup> D <sub>7h</sub> ( <sup>1</sup> A <sub>1</sub> ' )	7	3	3	-84.7 (0.0) -27.0 (0.5) -24.8 (1.0)	1.75	106.31
B <sub>9</sub> <sup>-</sup> D <sub>8h</sub> ( <sup>1</sup> A <sub>1g</sub> )	8	3	3	-28.3 (0.0) -23.3 (0.5) -13.7 (1.0)	2.79	110.62
B <sub>10</sub> <sup>0</sup> C <sub>2h</sub> ( <sup>1</sup> A <sub>g</sub> )	9	3	3	-17.0 (0.0) -15.2 (0.5) -13.3 (1.0)	1.95	105.19
B <sub>11</sub> <sup>+</sup> C <sub>s</sub> ( <sup>1</sup> A')	10	3	3	-19.6 (-0.0) -20.0 (-0.5) -15.3 (1.0)	1.34	108.20
B <sub>11</sub> <sup>-</sup> C <sub>2v</sub> ( <sup>1</sup> A <sub>1</sub> )	10	4	3	-18.5 (0.0) -20.1 (0.5) -17.0 (1.0)	1.81	114.27
B <sub>12</sub> <sup>0</sup> C <sub>3v</sub> ( <sup>1</sup> A <sub>1</sub> )	9	6	3	-28.4 (-0.04) -27.1 (-0.54) -19.9 (-1.04)	2.57	107.24
B <sub>13</sub> <sup>+</sup> C <sub>2v</sub> ( <sup>1</sup> A <sub>1</sub> )	10	6	3	-17.2 (0.0) -21.5 (0.5) -20.2 (1.0)	2.09	111.21
B <sub>14</sub> C <sub>2v</sub> ( <sup>1</sup> A <sub>1</sub> )	10	7	4	-14.5 (0.6) -19.0 (0.1) -11.9 (-0.4)	1.50	108.74
B <sub>15</sub> <sup>-</sup> C <sub>1</sub> ( <sup>1</sup> A)	11	8	4	-11.4 (0.0) -12.0 (0.5) -8.8 (1.0)	1.02	114.5

<sup>a</sup> All data at B3LYP/6-311+G\*

aromaticity. Such a mixed analysis is not new in chemistry. It is constantly used in organic chemistry. For example, in benzene,  $\sigma$ -electrons are treated as forming localized 2c-2e C-C bonds, while  $\pi$ -electrons are treated as completely delocalized over six carbon atoms.

The concept of “double aromaticity” was initially introduced in 1979 by Schleyer and co-workers to explain the chemical bonding in the 3,5-didehydrophenyl cation.<sup>75</sup> Double aromaticity and antiaromaticity in small carbon rings was discussed by Martin-Santamaria and Rzepa.<sup>76</sup> ( $\pi+\sigma$ )-Double aromaticity and ( $\pi,\sigma$ )-mixed aromaticity have been used by Berndt and co-workers for explaining the chemical bonding in planar boron compounds.<sup>77</sup>

#### 4-3.1. $B_3^+$ and $B_3^-$ Clusters

The  $B_3^+$  cluster is a perfect triangle in the closed shell ground spectroscopic state ( $D_{3h}$ ,  $^1A_1'$ ,  $1a_1'^2 1e'^4 1a_2''^2$ )<sup>35,36,39,42,49</sup> (Figure 4-1). The molecular orbital picture of four valence MOs is presented in Figure 4-2. The HOMO ( $1a_2''$ ) is a  $\pi$ -MO, formed by the out-of-plane overlap of  $2p_z$ -AOs of the three B atoms. We localized the remaining set of valence MOs ( $1e'$ -HOMO-2 and  $1a_1'$ -HOMO-3) into three 2c-2e B-B bonds with the occupation numbers (ON) 1.89 | e | using NBO analysis at the B3LYP/6-311+G\* level of theory in the putative  $B_3^{3+}$  cation ( $1a_1'^2 1e'^4$  electronic configuration) at the geometry of the  $B_3^+$  cluster. The strong s-p hybridization in the  $B_3^{3+}$  cation (occupation numbers are  $2s^{0.96} 2p^{1.03}$ ) is responsible for bonding character of the lowest three valence MOs [correction to our statement in the Ref. 14a where we stated that the bonding effect from these MOs should be small]. The two electrons in the fully delocalized  $\pi$ -HOMO make



$B_3^+$   $\pi$ -aromatic, obeying the  $4n+2$  Hückel rule for  $n = 0$ . Three other MOs represent 2c-2e bonds, even though their ON ( $1.89 |e|$ ) are somewhat lower than  $2.00 |e|$  for the classical 2c-2e bonds. Its aromatic character is confirmed by highly symmetric structure and highly negative NICS values: NICS(0)=-66.3 ppm; NICS(0.5)=-46.3 ppm, and NICS(1.0)=-15.9 ppm (Table 4-1). The small first singlet vertical excitation energy (0.77 eV, Table 4-1) reflects the presence of low-lying completely bonding  $\sigma$ -aromatic LUMO ( $2a_1'$ ).

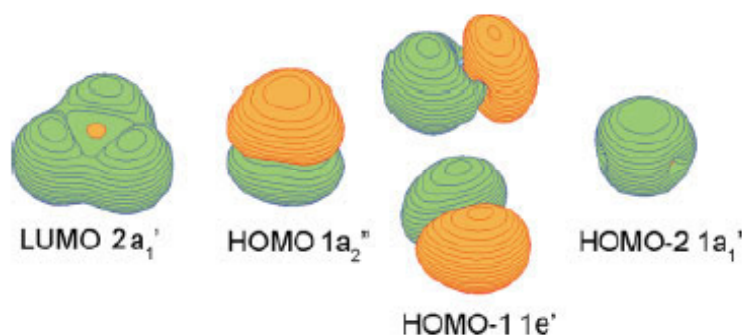


Figure 4-2. Molecular orbitals of the  $B_3^+$  cation.

In the triangular ground electronic state of the  $B_3^-$  cluster,<sup>14,49,55</sup> the extra pair of electrons occupies the  $2a_1'$ -MO (LUMO in  $B_3^+$ , Figure 4-2) which is a  $\sigma$ -molecular orbital formed by the radial overlap of the 2p-atomic orbitals on boron atoms (Figure 4-2). The two electrons in the fully delocalized  $\sigma$ -HOMO make  $B_3^-$   $\sigma$ -aromatic. The doubly occupied  $\pi$ -HOMO-1 is responsible for  $\pi$ -aromaticity in  $B_3^-$ . The  $1a_1'$  HOMO-3 and the  $1e'$  HOMO-2 can be transformed into three 2c-2e B-B bonds. Thus,  $B_3^-$  is a doubly ( $\sigma$ - and  $\pi$ -) aromatic system. Its doubly aromatic character is confirmed by NICS

value: NICS(0)=-73.6 ppm; NICS(0.5)=-57.9 ppm, and NICS(1.0)=-28.2 ppm (Table 4-1). High symmetry and a rather high first singlet vertical excitation energy (2.65 eV at TD-B3LYP/6-311+G\*, Table 4-1) also confirm the doubly-aromatic character of  $B_3^-$ .

#### 4-3.2. $B_4$ and $B_4^{2-}$ Clusters

The structure of neutral  $B_4$  was carefully studied by Martin et al.<sup>35</sup> They predicted the  $D_{2h}$   $^1A_g$  rhombus global minimum structure (Figure 4-1). Such a distortion from the perfect square comes from the second-order (or “pseudo”) Jahn-Teller effect, as discussed by Martin et al.<sup>35</sup> Because of the nature of the distortion, the barrier for “squareness” is rather small (0.7-0.8 kcal/mol<sup>14a,58</sup>) and even at moderate temperature the  $B_4$  cluster is effectively square.

The molecular orbitals of the  $D_{2h}$  ( $^1A_g$ ,  $1a_g^2 1b_{1u}^2 1b_{2u}^2 1b_{3g}^2 1b_{3u}^2 2a_g^2$ ) structure of  $B_4$  are shown in Figure 4-3. The lowest four MOs (HOMO-2 ( $1b_{3g}$ ), HOMO-3 ( $1b_{2u}$ ), HOMO-4 ( $1b_{1u}$ ), HOMO-5 ( $1a_g$ )) can be localized, as it has been shown by NBO analysis, into four classical peripheral 2c-2e B-B bonds (Table 4-2). Again, the strong s-p hybridization on the both types of boron atoms:  $2s^{0.95}2p^{1.14}$  and  $2s^{1.04}2p^{0.83}$  (from HOMO-2 through HOMO-5) is responsible for the formation of four classical B-B bonds. The remaining two MOs are globally delocalized and participate in the global bonding in the cluster. NBO analysis in this case shows eight lone pairs with the occupation number 0.5 e (Table 4-2) on each atom. The HOMO-1 ( $1b_{3u}$ ) is a completely bonding  $\pi$ -molecular orbital formed by the out-of-plane overlap of  $2p_z$ -AOs on the B atoms. The two electrons populating this MO make the cluster  $\pi$ -aromatic. The HOMO ( $2a_g$ ) of  $B_4$  is a  $\sigma$ -radial molecular orbital, just like the HOMO ( $2a_1'$ ) of  $B_3^-$ , formed by the radial overlap of  $2p$ -

Table 4-2. Localized MOs<sup>1</sup> of the D<sub>2h</sub>, <sup>1</sup>A<sub>g</sub> structure of B<sub>4</sub>.

LMO type	Occupation number  e	Composition
1. B <sub>1</sub> -B <sub>2</sub>	1.977	50.49% B <sub>1</sub> : 2s – 47.79%; 2p – 52.03 %
		49.51% B <sub>2</sub> : 2s – 49.93%; 2p – 49.91 %
1. B <sub>1</sub> -B <sub>3</sub>	1.977	50.49% B <sub>1</sub> : 2s – 47.79%; 2p – 52.03 %
		49.51% B <sub>3</sub> : 2s – 49.93%; 2p – 49.91 %
1. B <sub>2</sub> -B <sub>4</sub>	1.977	49.51% B <sub>2</sub> : 2s – 49.93%; 2p – 49.91 %
		50.49% B <sub>4</sub> : 2s – 47.79%; 2p – 52.03 %
1. B <sub>3</sub> -B <sub>4</sub>	1.977	49.51% B <sub>3</sub> : 2s – 49.93%; 2p – 49.91 %
		50.49% B <sub>4</sub> : 2s – 47.79%; 2p – 52.03 %
5. Lone pair B <sub>1</sub>	0.576	B <sub>1</sub> : 2s – 0.0%; 2p – 99.5 %
6. Lone pair B <sub>1</sub>	0.529	B <sub>1</sub> : 2s – 5.1%; 2p – 93.9 %
7. Lone pair B <sub>4</sub>	0.576	B <sub>4</sub> : 2s – 0.0%; 2p – 99.5 %
8. Lone pair B <sub>4</sub>	0.529	B <sub>4</sub> : 2s – 5.1%; 2p – 93.9 %
9. Lone pair B <sub>2</sub>	0.503	B <sub>2</sub> : 2s – 1.6%; 2p – 97.7 %
10. Lone pair B <sub>2</sub>	0.424	B <sub>2</sub> : 2s – 0.0%; 2p – 99.6 %
11. Lone pair B <sub>3</sub>	0.503	B <sub>3</sub> : 2s – 1.6%; 2p – 97.7 %
12. Lone pair B <sub>3</sub>	0.424	B <sub>3</sub> : 2s – 0.0%; 2p – 99.6 %

<sup>1</sup> LMO calculated at B3LYP/6-311+G\* using the NBO analysis.

AOs. The system thus can be characterized as  $\sigma$ -aromatic, i.e.,  $B_4$  is a doubly-aromatic molecule as it was first recognized by Zhai et al.<sup>14a</sup> This conclusion is supported by an effective highly symmetric (square) structure, calculated the first singlet vertical excitation energy (3.08 eV  $X^1A_g \rightarrow A^1B_{3g}$  at TD-B3LYP/6-311+G\*, Table 4-1) and calculated NICS index, which is highly negative at the center of the cluster (-35.7 ppm), but quickly diminishes and changes the sign at 1.0 Å above the center (+7.7 ppm) (Table 4-1).

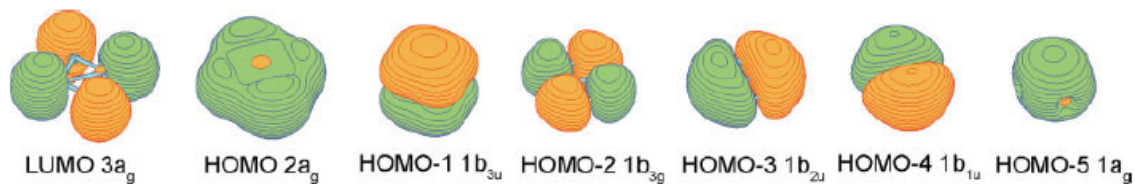


Figure 4-3 Molecular orbitals of the  $B_4$  cluster.

The doubly charged  $B_4^{2-}$  cluster has a square planar  $D_{4h}$   $^1A_{1g}$  ( $1a_{1g}^2 1e_u^4 1b_{1g}^2 1b_{2g}^2 2a_{1g}^2 1a_{2u}^2$ ) structure according to Sundholm and co-workers<sup>8a</sup> who used the isoelectronic analogy with  $Al_4^{2-}$ , where an extensive search for the global minimum structure has been performed<sup>1a,1b</sup> and the  $D_{4h}$   $^1A_{1g}$  square planar structure was found to be the most stable isomer. The  $Al_4^{2-}$  dianion has been studied extensively and it was shown using a variety of criteria that it is a doubly ( $\sigma$ - and  $\pi$ -) aromatic system [1a and references therein]. Thus, the isoelectronic, isostructural  $B_4^{2-}$  is also a doubly ( $\sigma$ - and  $\pi$ -) aromatic system with four 2c-2e peripheral B-B bonds. Sundholm et al.<sup>8a</sup> also confirmed aromaticity in  $B_4^{2-}$  by calculating the ring-current susceptibility, which was

found to be  $7.4 \text{ nAT}^{-1}$ . That is only 10% smaller than the value of the prototypical aromatic benzene molecule, thus confirming the aromatic nature of the dianion.

#### 4-3.3. $B_5^+$ and $B_5^-$ Clusters

Kato et al.<sup>36</sup> and Rica and Bauschlicher<sup>42</sup> reported that in the global minimum  $B_5^+$  adopts a  $C_{2v}$  structure, which is a slightly distorted planar pentagon. Rica and Bauschlicher stated that the  $D_{5h}$  ( ${}^1A_1'$ ,  $1a_1'^2 1e_1'^4 1e_2'^4 1a_2''^2 2a_1'^2$ ) planar pentagon has two imaginary frequencies at the B3LYP/cc-pvTZ level of theory and in the global minimum  $C_{2v}$  ( ${}^1A_1$ ,  $1a_1^2 1b_2^2 2a_1^2 3a_1^2 1b_1^2 2b_2^2 4a_1^2 3b_2^2$ ) structure B-B bonds are only slightly distorted. This distortion is due to the second order Jahn-Teller effect. According to our calculations (CCSD(T)/6-311+G\*), the global minimum  $C_{2v}$  ( ${}^1A_1$ ) structure (Figure 4-1) is only 0.365 kcal/mol lower in energy than the second-order saddle point  $D_{5h}$  ( ${}^1A_1'$ ) planar pentagon structure and after ZPE correction (harmonic frequencies at CCSD(T)/6-311+G\*), the vibrationally averaged  $D_{5h}$  ( ${}^1A_1'$ ) structure is actually lower in energy than the vibrationally averaged  $C_{2v}$  ( ${}^1A_1$ ) structure by 0.010 kcal/mol. Thus, for all practical purposes we can consider the  $B_5^+$  cluster as a planar pentagon.

The beautiful planar pentagonal structure of  $B_5^+$  can be understood from its molecular orbital analysis (Figure 4-4). The NBO analysis showed that HOMO-2 and HOMO-2' ( $1e_2'$ ), HOMO-3 and HOMO-3' ( $1e_1'$ ), and HOMO-4 ( $1a_1'$ ) can be localized into five peripheral 2c-2e B-B bonds. The HOMO ( $2a_1'$ ) in  $B_5^+$  is a globally bonding  $\sigma$ -MO and HOMO-1 ( $1a_2''$ ) is a globally bonding  $\pi$ -MO. Thus, they make the cation doubly ( $\sigma$ - and  $\pi$ -) aromatic. Double aromaticity in conjunction with the presence of five 2c-2e B-B peripheral bonds is responsible for the vibrationally averaged highly symmetry  $D_{5h}$

structure of the  $B_5^+$  cluster. Also, double aromaticity in  $B_5^+$  manifests itself in the high first singlet vertical excitation energy (2.97 eV at TD-B3LYP/6-311+G\*, Table 1), highly negative values of NICS: NICS(0)=-36.2 ppm; NICS(0.5)=-31.0 ppm, and NICS(1.0)=-18.8 ppm (Table 4-1) and most importantly it explains why  $B_5^+$  is a magic cluster in collision induced dissociation (CID) experiments by Anderson and co-workers.<sup>23</sup> The distortion of the  $D_{5h}$  ( $^1A_1'$ ) structure can be explained by the second-order Jahn-Teller effect, because there is nothing in occupied MOs (Figure 4-4) of the pentagon indicating the deviation from high symmetry. That case is similar to the distortion of the  $B_4$  cluster into rhombus and like in that case, the second-order distortion makes the  $B_5^+$  potential energy surface very shallow.

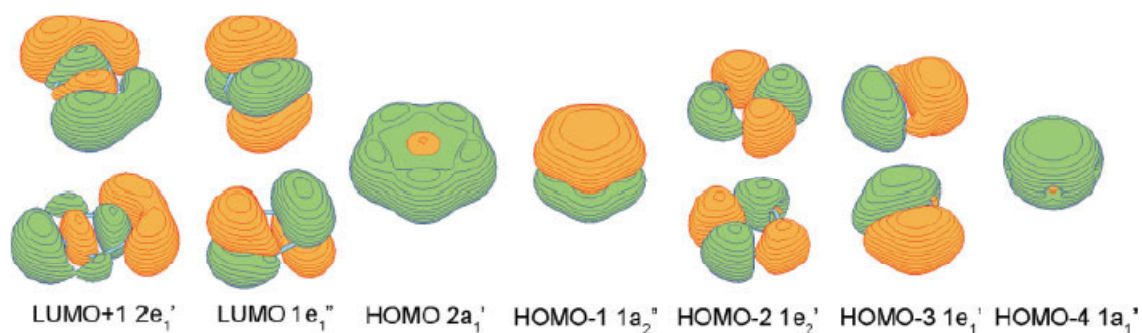


Figure 4-4. Molecular orbitals of the  $B_5^+$  cation.

For the  $B_5^-$  cluster we can predict the global minimum structure if we start with the  $B_5^+$  cluster. The  $1e_1''$ -LUMO in  $B_5^+$   $D_{5h}$  ( $^1A_1'$ ) is a doubly degenerate  $\pi$ -MO which is a partially bonding/antibonding orbital related to the completely bonding  $1a_2''$ -HOMO-1  $\pi$ -MO. These three MOs are a part of the set of 5 MOs formed by the  $2p_z$ -AOs of B and responsible for global  $\pi$ -bonding. Occupation of one of the doubly degenerate LUMO by

two electrons should lead to distortion of the  $D_{5h}$  structure to the  $C_{2v}$  structure due to the first order Jahn-Teller effect. Our calculations have shown that the resulting  $C_{2v}$  ( ${}^1A_1$ ,  $1a_1^2 1b_2^2 2a_1^2 3a_1^2 1b_1^2 2b_2^2 4a_1^2 1a_2^2$ ) structure is 50.6 (B3LYP/6-311+G\*) kcal/mol higher than the global minimum and it is a first order saddle point. Geometry optimization following the imaginary frequency normal mode led eventually to the global minimum structure.

In the global minimum structure the LUMO+1 ( $2e_1'$ -MO) is partially occupied instead of LUMO ( $1e_1''$ ). The singlet  $1a_1^2 1e_1'^4 1e_2'^4 1a_2'^2 2a_1^2 1e_1''^2$  electronic configuration of the  $D_{5h}$  structure of  $B_5^-$  should also lead to the first order Jahn-Teller distortion. Indeed it was shown that the  $C_{2v}$  ( ${}^1A_1$ ,  $1a_1^2 1b_2^2 2a_1^2 3a_1^2 1b_1^2 2b_2^2 4a_1^2 2b_2^2$ ) planar structure is the  $B_5^-$  global minimum structure. The LUMO+1 in  $B_5^+$  belongs to a partially bonding/antibonding  $\sigma$ -orbital related to the completely bonding  $\sigma$ -HOMO ( $2a_1'$ ). These three MOs are a part of the set of five MOs formed by the 2p-radial AOs of B and responsible for global  $\sigma$ -bonding. Thus,  $B_5^-$  has four electrons on globally  $\sigma$ -delocalized HOMO-1 ( $4a_1$ ) and HOMO ( $3b_2$ ) and two electrons on globally delocalized HOMO-3 ( $1b_1$ ), which makes  $B_5^-$  a system with conflicting aromaticity ( $\sigma$ -antiaromatic and  $\pi$ -aromatic). NBO analysis for the  $B_5^{5+}$  cation at the geometry of  $B_5^-$  and with the  $1a_1^2 1b_2^2 2a_1^2 3a_1^2 2b_2^2$  electronic configuration shows that there are five 2c-2e B-B peripheral bonds ( $ON=1.76-1.91 |e|$ ). The  $C_{2v}$   ${}^1A_1$  structure of  $B_5^-$  has been experimentally established in a joint photoelectron and ab initio study by Zhai et al.<sup>9</sup> Because the geometric structure of the  $\sigma$ -antiaromatic and  $\pi$ -aromatic  $B_5^-$  anion has lower symmetry we believe that antiaromaticity overwhelms aromaticity in this case and we prefer to call this cluster “net antiaromatic.” The low first singlet vertical excitation

energy (1.10 eV, at TD-B3LYP/6-311+G\*) provides us additional support in our overall assignment of aromaticity in spite of negative values of NICS in this case (Table 4-1). The  $B_5^-$  anion is a remarkable example showing that if we would limit our chemical bonding analysis to  $\pi$ -electrons only, we will not be able to explain why the  $\pi$ -aromatic (2  $\pi$ -electrons)  $B_5^-$  cluster has low  $C_{2v}$  symmetry and a low first singlet vertical excitation energy.

#### 4-3.4. $B_6^{2+}$ , $B_6$ , and $B_6^{2-}$ Clusters

The six-atomic cyclic analog of the  $B_5^+$  cluster should be the  $B_6^{2+}$  dication. It has 16 valence electrons and assuming the formation of six peripheral 2c-2e B-B bonds out of HOMO-2 ( $1b_{2u}$ ), HOMO-3 and HOMO-3' ( $1e_{2g}$ ), HOMO-4 and HOMO-4' ( $1e_{1u}$ ), and HOMO-5 ( $1a_{1g}$ ) we should have four electrons on two completely bonding  $\sigma$ -HOMO ( $2a_{1g}$ ) and  $\pi$ -HOMO-1 ( $1a_{2u}$ ) (Figure 4-5a). This makes the  $B_6^{2+}$  dication doubly aromatic. Our calculations proved that the  $B_6^{2+}$   $D_{6h}$  ( $^1A_{1g}$ ) structure indeed is a minimum at three levels of theory (B3LYP/6-311+G\*, MP2/6-311+G\*, and CCSD(T)/6-311+G\*).

In the  $B_6$  cluster in addition to cyclic structures we observe the emergence of a new type of structure - pentagonal pyramid, which now corresponds to the global minimum.<sup>16</sup> The planar pentagonal structure with the boron atom located at the center of the five-atomic ring is not a minimum because the cavity inside of the pentagon is too small to favorably accommodate a boron atom at the center. However, as we will see in the large boron clusters ( $B_8$  and  $B_9^-$ ), with the increase of the size of the central cavity a boron atom can be favorably accommodated at the center of the appropriate polygon leading to planar highly symmetric global minimum structures. The most accurate



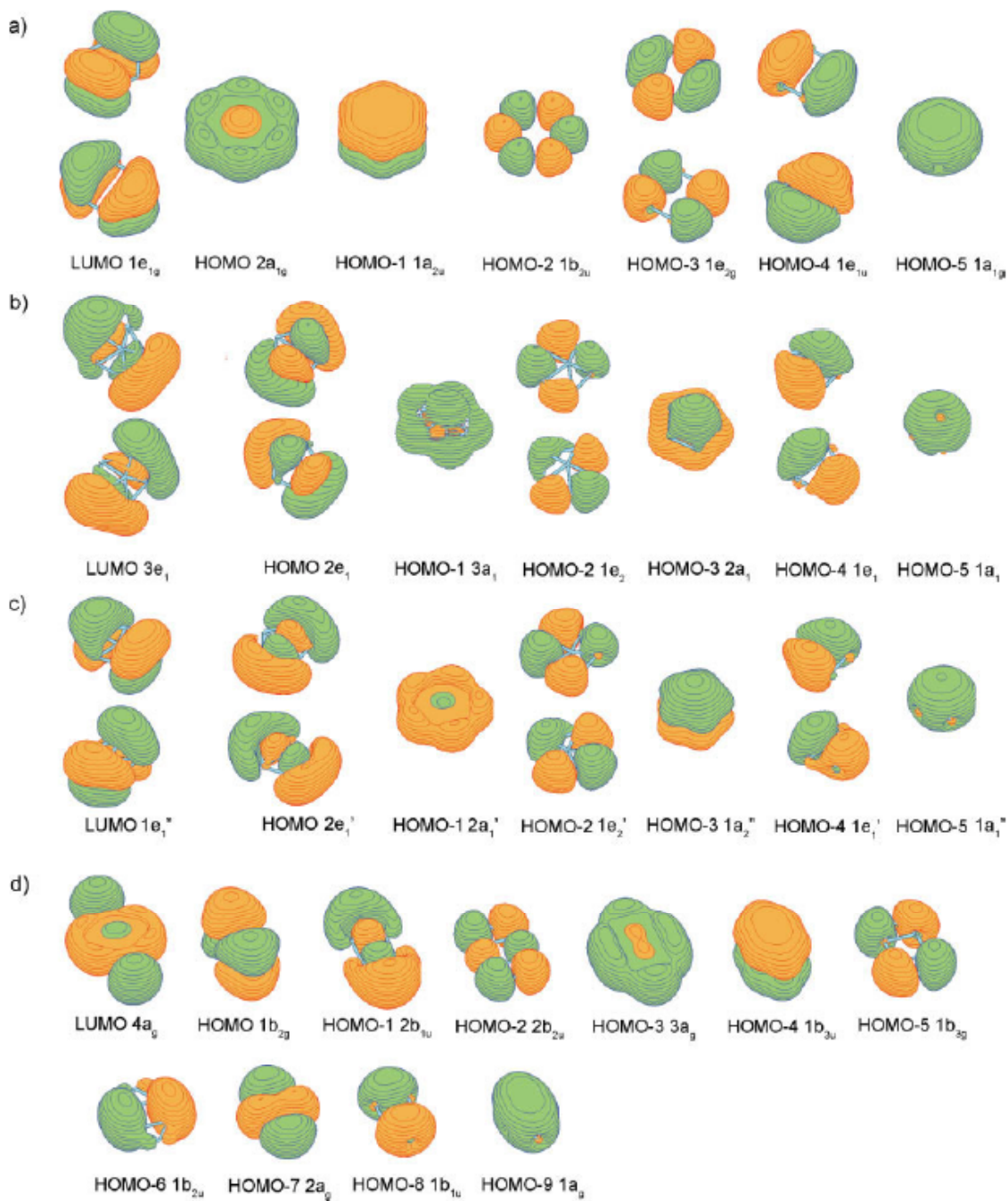


Figure 4-5. (a) Molecular orbitals of the  $D_{6h}$  ( $^1A_{1g}$ ) structure of the  $B_6^{2+}$  cluster; (b) molecular orbitals of the  $C_{5v}$  ( $^1A_1$ ) structure of the  $B_6$  cluster; (c) molecular orbitals of the  $D_{5h}$  ( $^1A_1'$ ) structure of the  $B_6$  cluster; (d) molecular orbitals of the  $B_6^{2-}$  dianion.

calculations<sup>16</sup> reveal that the global minimum structure of B<sub>6</sub> is the pyramid C<sub>5v</sub> (<sup>1</sup>A<sub>1</sub>, 1a<sub>1</sub><sup>2</sup>1e<sub>1</sub><sup>4</sup>2a<sub>1</sub><sup>2</sup>1e<sub>2</sub><sup>4</sup>3a<sub>1</sub><sup>2</sup>2e<sub>1</sub><sup>4</sup>) structure with the boron atom located 0.94 Å above the center of the B<sub>5</sub> perfect pentagon. The triplet C<sub>2h</sub> <sup>3</sup>A<sub>u</sub> (1a<sub>g</sub><sup>2</sup>1b<sub>u</sub><sup>2</sup>2a<sub>g</sub><sup>2</sup>2b<sub>u</sub><sup>2</sup>3a<sub>g</sub><sup>2</sup>1a<sub>u</sub><sup>2</sup>3b<sub>u</sub><sup>2</sup>4a<sub>g</sub><sup>2</sup>4b<sub>u</sub><sup>1</sup>1b<sub>g</sub><sup>1</sup>) and the singlet C<sub>2</sub> <sup>1</sup>A (1a<sup>2</sup>1b<sup>2</sup>2b<sup>2</sup>2a<sup>2</sup>3a<sup>2</sup>4a<sup>2</sup>3b<sup>2</sup>5a<sup>2</sup>4b<sup>2</sup>) structures originating from the cyclic B<sub>6</sub> geometry upon Jahn-Teller distortions were found to be 7.2 kcal/mol and 8.2 kcal/mol (CCSD(T)/6-311+G(2df)//B3LYP/6-311+G\*), respectively, higher in energy.<sup>16</sup>

In order to simplify the interpretation of the molecular orbitals let us first perform MO analysis for the D<sub>5h</sub> (<sup>1</sup>A<sub>1</sub><sup>'</sup>, 1a<sub>1</sub><sup>'2</sup>1e<sub>1</sub><sup>'4</sup>1a<sub>2</sub><sup>'2</sup>1e<sub>2</sub><sup>'2</sup>2a<sub>1</sub><sup>'2</sup>2e<sub>1</sub><sup>'4</sup>) structure (Figure 4-5) in which the central atom is pushed into the center. The set of five MOs (HOMO-2 and HOMO-2' (1e<sub>2</sub><sup>'</sup>), HOMO-4 and HOMO-4' (1e<sub>1</sub><sup>'</sup>), and HOMO-5 (1a<sub>1</sub><sup>'</sup>)) can be localized into five 2c-2e B-B bonds, so they are responsible for the peripheral bonding. The HOMO-3 (1a<sub>2</sub><sup>'</sup>) is formed by 2p<sub>z</sub>-AOs and it is responsible for the global π-bonding. The HOMO and HOMO' (2e<sub>1</sub><sup>'</sup>), and HOMO-1 (2a<sub>1</sub><sup>'</sup>) are formed from 2p-radial AOs and they are responsible for global σ-bonding in the B<sub>6</sub> cluster. Thus, B<sub>6</sub> in the D<sub>5h</sub> <sup>1</sup>A<sub>1</sub><sup>'</sup> configuration is a doubly (σ- and π-) aromatic system with 2π- and 6σ-electrons. However, as we mentioned above, the central cavity in the B<sub>5</sub> pentagon is too small to favorably accommodate the central boron atom and therefore a C<sub>5v</sub> <sup>1</sup>A<sub>1</sub> pyramidal structure corresponds to the global minimum. While in the pyramidal structure σ- and π-MOs are mixed, we believe that the bonding picture developed for the D<sub>5h</sub> <sup>1</sup>A<sub>1</sub><sup>'</sup> structure is still qualitatively valid and can explain why the B<sub>6</sub> cluster adopts such a structure.

When two extra electrons are added, the planar D<sub>2h</sub> <sup>1</sup>A<sub>g</sub> (1a<sub>g</sub><sup>2</sup>1b<sub>1u</sub><sup>2</sup>2a<sub>g</sub><sup>2</sup>1b<sub>2u</sub><sup>2</sup>1b<sub>3g</sub><sup>2</sup>1b<sub>3u</sub><sup>2</sup>3a<sub>g</sub><sup>2</sup>2b<sub>2u</sub><sup>2</sup>2b<sub>1u</sub><sup>2</sup>1b<sub>2g</sub><sup>2</sup>) structure becomes the global minimum for the B<sub>6</sub><sup>2-</sup> dianion.<sup>7b,16</sup> This structure is originating from the D<sub>6h</sub> hexagon, which

underwent the first order Jahn-Teller distortion. Molecular orbital analysis helps us to interpret the chemical bonding in  $B_6^{2-}$  (Figure 4-5d). Six MOs (HOMO-2 ( $2b_{2u}$ ), HOMO-5 ( $1b_{3g}$ ), HOMO-6 ( $1b_{2u}$ ), HOMO-7 ( $2a_g$ ), HOMO-8 ( $1b_{1u}$ ), and HOMO-9 ( $1a_g$ )) can be localized into six 2c-2e B-B bonds so they are responsible for the peripheral bonding in this cluster. The remaining four MOs are responsible for the global bonding in the  $B_6^{2-}$  cluster. The HOMO-1 ( $2b_{1u}$ ) and HOMO-3 ( $3a_g$ ) are  $\sigma$ -radial MOs, with the HOMO-3 being completely bonding, and the HOMO-1 being partially antibonding. Thus,  $B_6^{2-}$  has two globally delocalized  $\sigma$ -MOs, which makes this dianion  $\sigma$ -antiaromatic. The two other delocalized orbitals HOMO-4 ( $1b_{3u}$ ) and HOMO ( $1b_{2g}$ ) are  $\pi$ -MOs. The HOMO-4 is completely bonding, and the HOMO is a partially bonding orbital. The  $B_6^{2-}$  dianion has 4  $\sigma$ - and 4  $\pi$ -electrons on the globally delocalized MOs and six 2c-2e peripheral B-B bonds. Thus, we can assign  $B_6^{2-}$  to doubly ( $\sigma$ - and  $\pi$ -) antiaromatic systems. The question may arise, why a doubly antiaromatic structure is the global minimum. We believe this is because the  $B_6^{2-}$  cannot favorably support six delocalized electrons in either  $\sigma$ - or  $\pi$ -subsystems. Electrostatic field from the screened boron nuclei does not provide enough stabilization for six electrons in either  $\sigma$ - and  $\pi$ -subsystems and that leads to a compromised globally doubly antiaromatic structure.

In recent paper Aihara et al.<sup>20</sup> claimed that the boron  $B_6^{2-}$  cluster is highly aromatic on the basis of topological resonance energy (TRE). The calculated TRE for  $B_6^{2-}$  in terms of the resonance integral between two bonded boron atoms ( $|\beta_{BB}|$ ) is  $0.549 |\beta_{BB}|$ . This value expressed in terms of the resonance integral between two bonded carbon atoms ( $|\beta_{CC}|$ ) is  $0.478 |\beta_{CC}|$ . For reference the TRE for benzene is  $0.273 |\beta_{CC}|$ . Thus, according to Aihara et al.<sup>20</sup> the  $B_6^{2-}$  cluster is clearly showing the presence

of aromaticity. However, this large resonance energy does not contradict our assignment of  $B_6^{2-}$  to a doubly antiaromatic system. Our assignment of  $B_6^{2-}$  to a  $\pi$ -antiaromatic system is based on the presence of four  $\pi$ -electrons, its highly distorted ( $D_{2h}$ ) structure, and paratropic ring currents calculated by Fowler and co-workers (see ref. 16 for details). We see this cluster as being *antiaromatic globally*. It does not however mean that this cluster cannot have positive resonance energy. In fact, according to our MO analysis, we can consider the  $\pi$ -system in  $B_6^{2-}$  as being split into two subsystems, with two  $\pi$ -electrons localized over each of two triangular regions.  $\pi$ -MOs of  $B_6^{2-}$  cluster can be viewed as composed of two aromatic  $B_3^-$  clusters (see ref. 16 for detailed discussion). Indeed,  $1b_{2g}$ -HOMO and  $1b_{3u}$ -HOMO-4 are a pair of bonding and antibonding  $\pi$ -MOs in  $B_3^-$ . Thus,  $\pi$ -MOs do not contribute to chemical bonding between two  $B_3^-$  groups. That allows us to speculate that  $\pi$ -MOs in  $B_6^{2-}$  give rise to an island  $\pi$ -aromaticity in this cluster. Similar analysis for the delocalized  $\sigma$ -MOs reveals that we also have an island  $\sigma$ -aromaticity in  $B_6^{2-}$ . Thus, the globally antiaromatic  $B_6^{2-}$  system can be considered as having two island aromatic subunits. The island  $\pi$ -aromaticity is responsible for positive TRE in  $B_6^{2-}$  in the Aihara et al.<sup>20</sup> calculations. Indeed, Aihara et al.<sup>20</sup> stated that three (a2-a4) out of four circuit currents (Figure 4-6), are paratropic indicating antiaromaticity and the a1 circuit current, which is located over triangular region, is highly diatropic. It overwhelms the antiaromatic contributions from the a2-a4 a1 circuit currents and results in the overall positive TRE. This result clearly supports the presence of island aromaticity in  $B_6^{2-}$ . Alexandrova et al.<sup>21</sup> have shown that for  $Li_2B_6$  molecule in the gas phase, the global minimum structure is  $C_{2h}$  ( $^1A_1$ ) with two  $Li^+$  ions located above and below the  $B_3^-$  triangular areas in  $B_6^{2-}$ . The  $D_{2h}$  ( $^1A_g$ ) structure, containing one  $Li^+$  cation above and

another  $\text{Li}^+$  below the plane of  $\text{B}_6^{2-}$  dianion, was found to be a saddle point on the potential energy surface. These results confirmed the presence of the  $\pi$ -island aromaticity in the globally antiaromatic system.

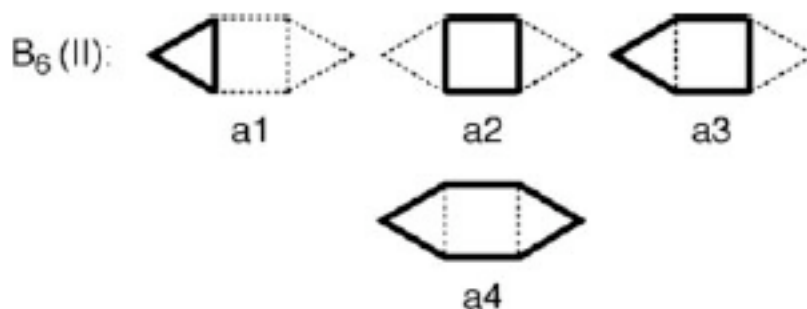


Figure 4-6. Nonidentical circuits in  $\text{B}_6^{2-}$  (adopted from ref. 20).

#### 4-3.5. $\text{B}_7^+$ and $\text{B}_7^-$ Clusters

The global minimum structure of the cationic  $\text{B}_7^+$  cluster is the  $\text{C}_{6v}$   $^1\text{A}_1$  ( $1a_1^2 1e_1^4 1e_2^4 2a_1^2 1b_1^2 3a_1^2 2e_1^4$ ) pyramid<sup>36,39,41,55,60</sup> with the central boron atom located 0.72 Å above the plane (Figure 4-1). In order to simplify the interpretation of the molecular orbitals we performed MO analysis of the  $\text{D}_{6h}$  ( $^1\text{A}_{1g}$ ,  $1a_{1g}^2 1e_{1u}^4 1e_{2g}^4 1b_{2u}^2 2a_{1g}^2 1a_{2u}^2 2e_{1u}^4$ ) structure (Figure 4-7), in which the central atom is pushed into the plane. The set of six MOs (HOMO-3 ( $1b_{2u}$ ), HOMO-4 and HOMO-4' ( $1e_{2g}$ ), HOMO-5 and HOMO-5' ( $1e_{1u}$ ) and HOMO-6 ( $1a_{1g}$ )) is responsible for the peripheral bonding and can be localized into six 2c-2e B-B bonds. The HOMO-1 ( $1a_{2u}$ ) is formed by  $2p_z$ -AOs and is responsible for the global  $\pi$ -bonding. The HOMO and HOMO' ( $2e_{1u}$ ), and HOMO-2 ( $2a_{1g}$ ) are formed from  $2p$ -radial AOs and they are responsible for global  $\sigma$ -bonding in the  $\text{B}_7^+$  cluster. Thus,  $\text{B}_7^+$  in the  $\text{D}_{6h}$   $^1\text{A}_{1g}$  configuration is doubly ( $\sigma$ - and  $\pi$ -) aromatic system with  $2\pi$ -

and 6 $\sigma$ -electrons. However, the central cavity in the B<sub>6</sub> hexagon is too small to favorably accommodate the central boron atom and therefore the C<sub>6v</sub> <sup>1</sup>A<sub>1</sub> pyramidal structure corresponds to the global minimum. While in the pyramidal C<sub>6v</sub> <sup>1</sup>A<sub>1</sub> structure  $\sigma$ - and  $\pi$ -MOs are now mixed, we believe that the bonding picture we developed for the D<sub>6h</sub> <sup>1</sup>A<sub>1g</sub> structure is still qualitatively valid.

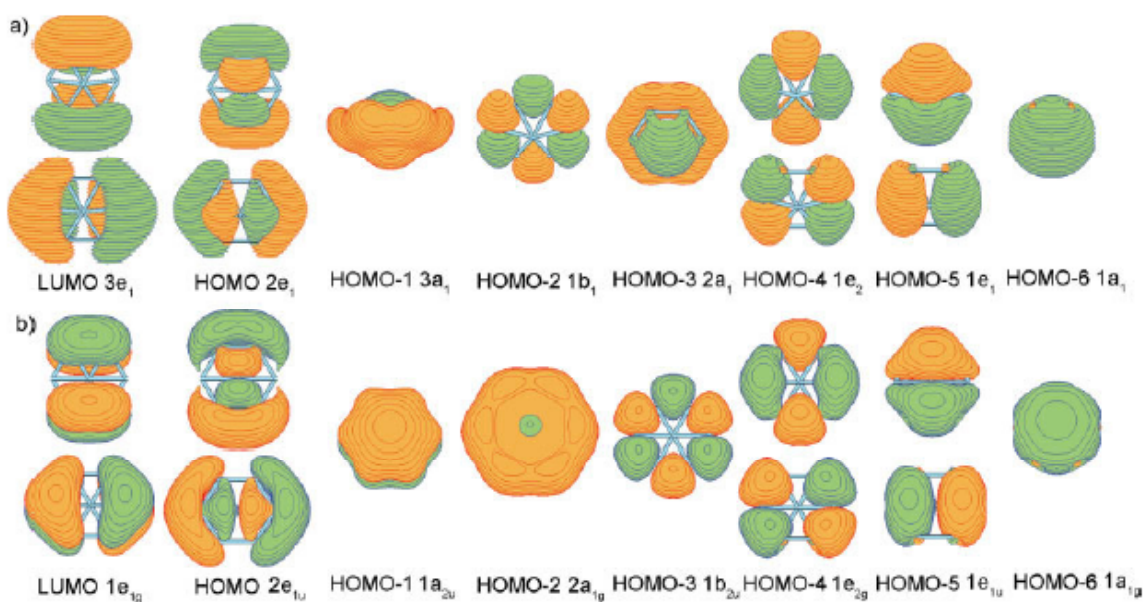


Figure 4-7. (a) Molecular orbitals of the C<sub>6v</sub> (<sup>1</sup>A<sub>1</sub>) structure of the B<sub>7</sub><sup>+</sup> cluster; (b) molecular orbitals of the D<sub>6h</sub> (<sup>1</sup>A<sub>1g</sub>) structure of the B<sub>7</sub><sup>+</sup> cluster.

The seven-atomic cyclic structure of the B<sub>7</sub><sup>+</sup> cluster is a local minimum with the <sup>3</sup>A<sub>2</sub>' (1a<sub>1</sub>'<sup>2</sup>1e<sub>1</sub>'<sup>4</sup>1e<sub>2</sub>'<sup>4</sup>1e<sub>3</sub>'<sup>4</sup>1a<sub>2</sub>'<sup>2</sup>2a<sub>1</sub>'<sup>2</sup>1e<sub>1</sub>'<sup>2</sup>) spectroscopic state. It has 20 valence electrons and assuming the formation of seven peripheral 2c-2e B-B bonds from HOMO-3 and HOMO-3' (1e<sub>3</sub>'), HOMO-4 and HOMO-4'(1e<sub>2</sub>'), HOMO-5 and HOMO-5' (1e<sub>1</sub>') and HOMO-6 (1a<sub>1</sub>') we should have six electrons for global bonding. Two of them occupy the completely bonding  $\sigma$ -HOMO-1 (2a<sub>1</sub>'). Two electrons occupy the completely

bonding  $\pi$ -HOMO-2 ( $1a_2''$ ) and two electrons occupy the partially bonding doubly degenerate  $\pi$ -HOMO ( $1e_1''$ ) with the triplet coupling. This makes the  $B_7^+$  dication doubly aromatic in the cyclic structure. However, the  $B_7^+ D_{7h}$  ( ${}^3A_2'$ ) structure is significantly higher (63.4 kcal/mol at B3LYP/6-311+G\*) in energy than the global minimum  $C_{6v}$  ( ${}^1A_1'$ ) structure because of unsupported dangling electron density at the center of the cycle. Thus, the cyclic structures are not favorable anymore beyond six boron atoms.

According to the Alexandrova et al.<sup>17</sup> calculations the  $B_7^-$  cluster has a very flat triplet  $C_{6v}$   ${}^3A_2$  ( $1a_1^2 1e_1^4 1e_2^4 2a_1^2 3a_1^2 1b_1^2 2e_1^4 3e_1^2$ )<sup>78</sup> pyramidal structure similar to the  $B_7^+$  structure as the global minimum. The second lowest  $C_{2v}$   ${}^1A_1$  ( $1a_1^2 1b_2^2 1b_1^2 2a_1^2 1a_2^2 3a_1^2 2b_1^2 4a_1^2 2b_2^2 3b_1^2 3b_2^2$ ) structure (Figure 4-1) was found to be just 0.7 kcal/mol higher (RCCSD(T)/6-311+G(2df)//RCCSD(T)/6-311+G\*) in energy than the global minimum structure. Thus, these two structures are almost degenerate. The combined photoelectron spectroscopic and ab initio study<sup>17</sup> suggests that at least two isomers  $C_{6v}$   ${}^3A_2$  and  $C_{2v}$   ${}^1A_1$  could coexist in the  $B_7^-$  beam and contribute to the photoelectron spectra of  $B_7^-$ .

MO analysis was performed for the planar  $B_7^- D_{6h}$   ${}^3A_{2g}$  ( $1a_{1g}^2 1e_{1u}^4 1e_{2g}^4 1b_{2u}^2 2a_{1g}^2 1a_{2u}^2 2e_{1u}^4 1e_{1g}^2$ )<sup>78</sup> model system (In ref. 17 the  ${}^3A_1$  spectroscopic state was reported for the  $1a_1^2 1e_1^4 1e_2^4 2a_1^2 3a_1^2 1b_1^2 2e_1^4 3e_1^2$  electronic configuration of the  $B_7^- C_{6v}$  structure as determined by the Gaussian 03 program. However, the correct spectroscopic state for such electronic configuration is  ${}^3A_2$ . Similarly, in ref. 17 the  ${}^3A_{1g}$  was reported for the  $1a_{1g}^2 1e_{1u}^4 1e_{2g}^4 1b_{2u}^2 2a_{1g}^2 1a_{2u}^2 2e_{1u}^4 1e_{1g}^2$  configuration of the  $B_7^- D_{6h}$  structure, while the correct spectroscopic state is  ${}^3A_{2g}$ .) NBO analysis showed that the set of low-energy MOs (Figure 4-6): HOMO-7 ( $1a_{1g}$ ), HOMO-6 and HOMO-6' ( $1e_{1u}$ ), HOMO-5

and HOMO-5' ( $1e_{2g}$ ) and HOMO-3 ( $1b_{2u}$ ) can be localized into six peripheral 2c-2e B-B bonds, forming the hexagonal framework. HOMO-2 ( $1a_{2u}$ ) which is a completely bonding  $\pi$ -MO and partially antibonding and partially occupied HOMO and HOMO' ( $1e_g$ ) make this cluster  $\pi$ -aromatic with four  $\pi$ -electrons according to the inverse  $4n$  rule for triplet states. HOMO-2 ( $2a_g$ ) and HOMO-1 and HOMO-1' ( $2e_{1u}$ ) are delocalized  $\sigma$ -MOs which make this cluster  $\sigma$ -aromatic. Thus, the  $B_7^-$  cluster is a doubly ( $\sigma$ - and  $\pi$ -) aromatic system with six peripheral B-B bonds.

#### 4-3.6. $B_8$ , $B_8^{2-}$ , and $B_9^-$ Clusters

The neutral  $B_8$  cluster has a triplet perfect heptagon structure  $D_{7h} \ ^3A_2'$  ( $1a_1''^2 1e_1''^4 1e_2''^4 2a_1''^2 1e_3''^4 1a_2''^2 2e_1''^4 1e_1''^2$ ) in its ground electronic state (correction to the previous statement in ref. 18) as it was established by Zhai et al.<sup>18</sup> Another wheel-type structure  $C_s \ ^1A'$  was identified as a low-lying isomer.<sup>18</sup> The  $C_s \ ^1A'$  isomer is a Jahn-Teller distorted heptagon, because in the heptagon singlet structure only one out of two doubly degenerate  $1e_1''$ -HOMOs is occupied.

In the triplet  $D_{7h} \ ^3A_2'$  perfect heptagon structure HOMO-3 and HOMO-3' ( $1e_3''$ ), HOMO-5 and HOMO-5' ( $1e_2''$ ), HOMO-6 and HOMO-6' ( $1e_1''$ ), and HOMO-7 ( $1a_1''$ ) (Figure 4-8) can be localized into seven 2c-2e B-B bonds, HOMO and HOMO' ( $1e_1''$ ), and HOMO-2 ( $1a_2''$ ) (Figure 4-8) are formed from  $2p_z$ -AOs and they are responsible for the global  $\pi$ -bonding. The HOMO-1 and HOMO-1' ( $2e_1''$ ) and HOMO-4 ( $2a_1''$ ) are formed from  $2p$ -radial AOs and they are responsible for global  $\sigma$ -bonding in the  $B_8$  cluster. Thus, the  $D_{7h} \ ^3A_2'$  structure is a doubly ( $\sigma$ - and  $\pi$ -) aromatic system with 4  $\pi$ -electron (satisfying the inverse rule  $4n$  rule for aromaticity for triplet coupled electrons),



with six  $\sigma$ -electrons (satisfying the  $4n+2$  rule for aromaticity for singlet coupled electrons), and with seven 2c-2e peripheral B-B bonds.

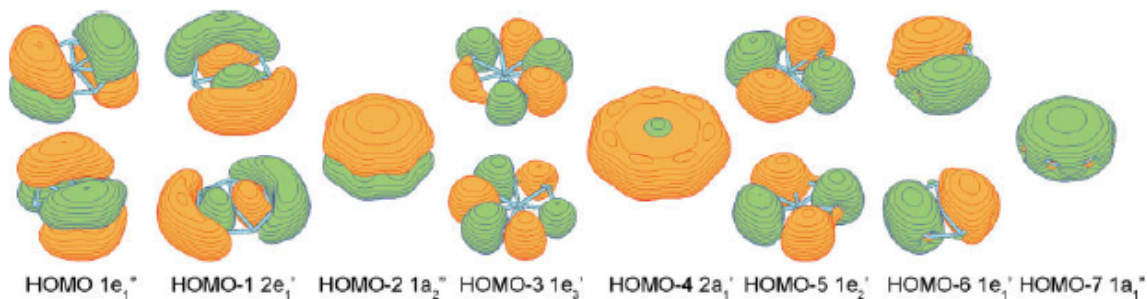


Figure 4-8. Molecular orbitals of the  $D_{7h}$  ( $^1A_1'$ ) structure of the  $B_8^{2-}$  dianion.

In the singlet  $C_s$   $^1A'$  isomer, one of the doubly degenerate HOMOs is now occupied by a pair of electrons with another one being empty, which results in the Jahn-Teller distortion. This system is the one with conflicting aromaticity: there are four  $\pi$ -electron (satisfying  $4n$  rule for antiaromaticity for a singlet coupled electrons) and six  $\sigma$ -electrons (satisfying  $4n+2$  rule for aromaticity for a singlet coupled electrons), and seven 2c-2e peripheral B-B bonds.

We also optimized the cyclic  $B_8$  ( $D_{8h}$ ,  $^5A_1'$ ,  $1a_{1g}^2 1e_{1u}^4 1e_{2g}^4 1e_{3u}^4 2a_{1g}^2 1b_{2g}^2 1a_{2u}^2 2e_{1u}^2 1e_{1g}^2$ ) doubly aromatic structure and found that it is a local minimum at B3LYP/6-311+G\*. However, it is about 98 kcal/mol higher in energy than the boron-centered  $B_8$  ( $D_{7h}$ ,  $^3A_2'$ ) doubly aromatic global minimum structure.

Thus, the cyclic structures even being doubly aromatic and corresponding to local minima are getting less and less stable with the increase of the size of the cluster starting from  $B_7^+$  and cannot be considered even as low-energy isomers.

The doubly-charged  $B_8^{2-}$  anion has a planar  $D_{7h}$   $^1A_1'$  ( $1a_1'^2 1e_1'^4 1e_2'^4 2a_1'^2 1e_3'^4 1a_2''^2 2e_1''^4 1e_1''^4$ ) singlet global minimum structure (Figure 4-1), in which high symmetry is restored again because the doubly degenerate  $1e_3''$ -HOMO is now occupied by four electrons. While the isolated dianion was not studied experimentally, its high-symmetric structure was experimentally confirmed in a joint photoelectron spectroscopy and ab initio calculations of the  $LiB_8^-$  cluster by Alexandrova et al.<sup>21</sup> It was shown that the calculated photoelectron spectrum of the half-sandwich structure of  $LiB_8^-$  in which  $Li^+$  cation is located above the slightly distorted  $B_8^{2-}$  heptagon agrees well with the experimentally recorded spectra of the anion.

The singlet  $D_{7h}$   $^1A_1'$  structure of  $B_8^{2-}$  is a doubly ( $\sigma$ - and  $\pi$ -) aromatic system with 6  $\pi$ -electron, 6  $\sigma$ -electrons, and seven 2c-2e peripheral B-B bonds. This analysis of chemical bonding for  $B_8^{2-}$  was first proposed by Zhai et al.<sup>18</sup> Its double aromaticity is also confirmed by very high values of NICS: NICS(0) = -84.7 ppm, NICS(0.5) = -27.0 ppm, and NICS(1.0) = -24.8 ppm (Table 4-1).

The anionic  $B_9^-$  has the perfect planar  $D_{8h}$  ( $^1A_{1g}$ ,  $1a_{1g}^2 1e_{1u}^4 1e_{2g}^4 1e_{3u}^4 2a_{1g}^2 1b_{2g}^2 1a_{2u}^2 2e_{1u}^4 1e_{1g}^4$ ) wheel-shaped structure as the global minimum (Figure 4-1), which was established in a joint photoelectron and ab initio study by Zhai et al.<sup>18</sup> The perfect octagon structure of  $B_9^-$  is unprecedented in chemistry and represents the first example of octacoordinated atom in a planar environment.

The remarkable planar octagon structure of  $B_9^-$  can be easily rationalized on the basis of the presence of double ( $\sigma$ - and  $\pi$ -) aromaticity (Figure 4-9). The chemical bonding in  $B_9^-$  is remarkably similar to the bonding pattern in  $B_8^{2-}$ . As before eight MOs (Figure 4-9): HOMO-3 ( $1b_{2g}$ ), HOMO-5, HOMO-5' ( $1e_{3u}$ ), HOMO-6, HOMO-6' ( $1e_{2g}$ ),

HOMO-7, HOMO-7' ( $1e_{1u}$ ), and HOMO-8 ( $1a_{1g}$ ) can be localized into eight 2c-2e B-B peripheral bonds. The other valence MOs are delocalized over the octagon and they are responsible for global bonding between the central B atom and peripheral B atoms. The three  $\pi$ -MOs HOMO, HOMO' ( $1e_{1g}$ ) and HOMO-2 ( $1a_{2u}$ ) are responsible for  $\pi$ -aromaticity and the three  $\sigma$ -MOs HOMO-1, HOMO-1' ( $2e_{1u}$ ) and HOMO-4 ( $2a_{1g}$ ) are responsible for  $\sigma$ -aromaticity in  $B_9^-$ . Again, such chemical bonding analysis for  $B_9^-$  was first proposed by Zhai et al.<sup>18</sup> The double ( $\sigma$ - and  $\pi$ -) aromaticity in  $B_9^-$  is supported by high symmetry, high first singlet vertical excitation energy (2.79 eV at TD-B3LYP/6-311+G\*), and highly negative NICS values: NICS(0)=-28.3 ppm, NICS(0.5)=-23.3 ppm, and NICS(1.0)=-13.7 ppm (Table 4-1).

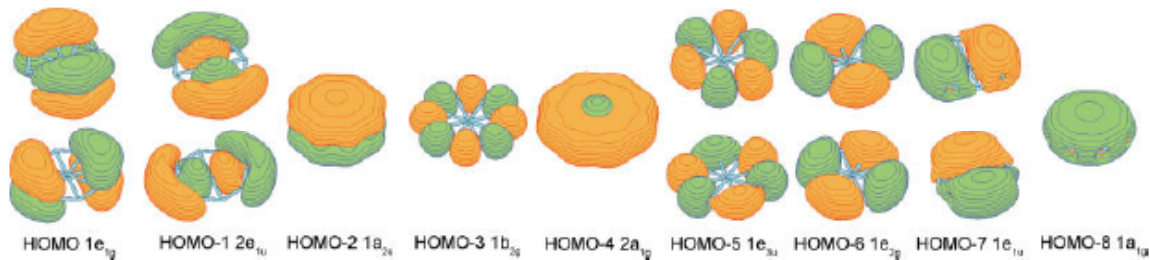


Figure 4-9. Molecular orbitals of the  $D_{8h}$  ( $^1A_{1g}$ ) structure of the  $B_9^-$  anion.

In addition to the wheel planar structure of  $B_9^-$ , Minkin and co-workers<sup>79,80</sup> reported planar structures and  $\pi$ -aromatic character in the  $CB_8$ ,  $SiB_8$ , and  $PB_8^+$  species. The authors found, however, that in the case of octacoordinated carbon, the central cavity is now too big to be stabilized through the accommodation of only one boron nucleus. The  $D_{8h}$  structure of  $CB_8$  is a second-order saddle point. The normal mode displacements lead to a  $C_{2v}$  ( $^1A_1$ ) structure, in which the central C-atom is shifted to the side. However,

the barrier on the intramolecular rearrangement is rather small and it allows one to consider the fluxional  $\text{CB}_8$  system as one with effective octacoordination of the central atom. The  $\text{SiB}_8$  and  $\text{PB}_8^+$  clusters were found to have a perfect octagonal structure. We would like to stress that on the basis of our analysis of chemical bonding in  $\text{B}_9^-$ , the valence isoelectronic  $\text{CB}_8$ ,  $\text{SiB}_8$ , and  $\text{PB}_8^+$  species are also  $\sigma$ -aromatic with six  $\sigma$ -electrons and they also have eight 2c-2e peripheral B-B bonds.  $\pi$ - and  $\sigma$ -aromaticity together with eight peripheral B-B bonds are responsible for the beautiful octagonal structure of these species.

#### 4-3.7. $\text{B}_{10}$ , $\text{B}_{11}^+$ , and $\text{B}_{11}^-$ Clusters

The  $\text{B}_{10}$ ,  $\text{B}_{11}^+$  and  $\text{B}_{11}^-$  clusters in their global minimum structures (Figure 4-1) have a common feature – two boron atoms located inside either eight- ( $\text{B}_{10}$ ) or nine- ( $\text{B}_{11}^+$  and  $\text{B}_{11}^-$ ) membered ring. Therefore, we will consider chemical bonding in these clusters together.

The global minimum of  $\text{B}_{10}$  according to Zhai et al.<sup>19</sup> and Boustani<sup>44</sup> is the  $\text{C}_{2h}$ ,  $^1\text{A}_g$  structure (Figure 4-1), which is nonplanar with eight boron atoms forming a planar cycle around two atoms at the center, with one of the central atoms located above the plane and the other one below the plane. The chemical bonding analysis of the global minimum structure of  $\text{B}_{10}$  was performed by Zhai et al.<sup>19</sup> only for the  $\pi$ -system and it was shown that this structure has six  $\pi$ -electrons and thus it is  $\pi$ -aromatic. We propose here an explanation of chemical bonding in  $\text{B}_{10}$  including both  $\sigma$ - and  $\pi$ -electrons. As before, let us first flatten the  $\text{C}_{2h}$   $^1\text{A}_g$  structure into the planar  $\text{D}_{2h}$   $^1\text{A}_g$  structure for simplicity and perform MO analysis (Figure 4-10) for the planar structure. NBO analysis shows eight

peripheral 2c-2e B-B bonds ( $ON=1.87-1.93 |e|$ ) and one 2c-2e B-B bond ( $ON=1.52 |e|$ ) between central atoms, which could be approximately assigned to HOMO-5 ( $2b_{3g}$ ), HOMO-7 ( $2b_{2u}$ ), HOMO-8 ( $3a_g$ ), HOMO-9 ( $2b_{1u}$ ), HOMO-10 ( $1b_{3g}$ ), HOMO-11 ( $2a_g$ ), HOMO-12 ( $1b_{2u}$ ), HOMO-13 ( $1b_{1u}$ ), and HOMO-14 ( $1a_g$ ). Rather low occupation number for the central B-B bond shows that we should treat the existence of this bond with caution. Three MOs (HOMO ( $1b_{1g}$ ), HOMO-1 ( $1b_{2g}$ ) and HOMO-6 ( $1b_{3u}$ )) are responsible for the global  $\pi$ -bonding and the remaining three  $\sigma$ -MOs (HOMO-2 ( $4a_g$ ), HOMO-3 ( $3b_{1u}$ ), and HOMO-4 ( $3b_{2u}$ )) are responsible for the global  $\sigma$ -bonding. Thus,  $B_{10}$  is a doubly ( $\sigma$ - and  $\pi$ -) aromatic cluster with eight peripheral 2c-2e B-B bonds and one 2c-2e central B-B bond. A relatively high first singlet vertical excitation energy (1.95 eV, at TD-B3LYP/6-311+G\*) and negative NICS values (Table 4-1) support our description of the chemical bonding in  $B_{10}$ .

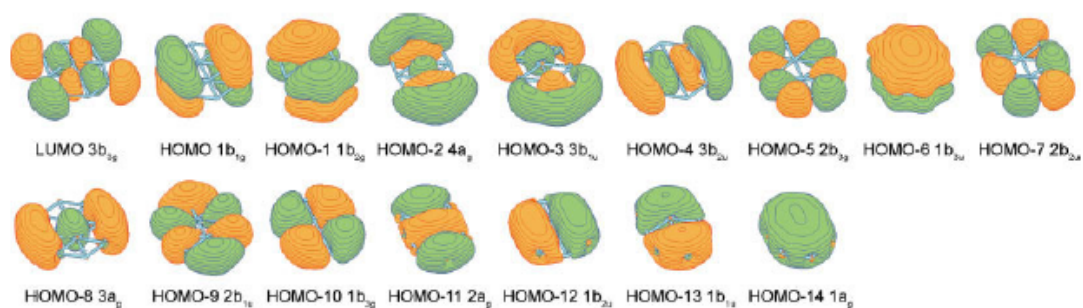


Figure 4-10. Molecular orbitals of the  $D_{2h}$  ( $^1A_g$ ) structure of the  $B_{10}$  cluster.

We calculated the  $B_{10}$  ( $D_{9h}$ ,  $^1A_1'$ ) planar structure with only one boron atom at the center of the nine-atom ring. The radius of the external ring was found to be 2.202 Å (B3LYP/6-311+G\*) and the central cavity is now too big to be stabilized through the

accommodation of only one boron nucleus. Because of that this structure is 60.5 kcal/mol higher than the global minimum structure with two boron nuclei at the center. Also, this structure is the fourth order saddle point. Thus, starting from B<sub>10</sub> cluster, the structures with one boron atom at the center are not low energy isomers anymore. However, the eight membered ring is still small to favorably accommodate two boron atoms within the plane.

Ricca and Bauschlicher<sup>42</sup> reported a quasi-planar C<sub>s</sub> <sup>1</sup>A' structure for the B<sub>11</sub><sup>+</sup> cluster (Figure 4-1). In this case, the nine-atomic ring is again too small to accommodate two boron atoms within the plane. We plotted MOs of B<sub>11</sub><sup>+</sup> for the flattened C<sub>2v</sub> <sup>1</sup>A<sub>1</sub> (1a<sub>1</sub><sup>2</sup>2a<sub>1</sub><sup>2</sup>1b<sub>2</sub><sup>2</sup>3a<sub>1</sub><sup>2</sup>2b<sub>2</sub><sup>2</sup>4a<sub>1</sub><sup>2</sup>3b<sub>2</sub><sup>2</sup>5a<sub>1</sub><sup>2</sup>6a<sub>1</sub><sup>2</sup>4b<sub>2</sub><sup>2</sup>1b<sub>1</sub><sup>2</sup>7a<sub>1</sub><sup>2</sup>5b<sub>2</sub><sup>2</sup>8a<sub>1</sub><sup>2</sup>2b<sub>1</sub><sup>2</sup>1a<sub>2</sub><sup>2</sup>) structure in Figure 4-11a. NBO analysis reveals nine 2c-2e peripheral B-B bonds (ON=1.81-1.94 |e|) and one central B-B bond (ON=1.53 |e|) which could be approximately assigned to the ten lowest canonical MOs (from HOMO-6 to HOMO-15). Three MOs HOMO (1a<sub>2</sub>), HOMO-1 (2b<sub>1</sub>) and HOMO-5 (1b<sub>1</sub>) are responsible for the global π-bonding and three MOs HOMO-2 (8a<sub>1</sub>), HOMO-3 (5b<sub>2</sub>), and HOMO-4 (7a<sub>1</sub>) are responsible for the global σ-bonding. Thus, the B<sub>11</sub><sup>+</sup> cation is a doubly aromatic system with 6 σ- and 6 π-delocalized electrons, nine 2c-2e B-B peripheral bonds and somewhat less pronounced central B-B bond. The global minimum structure C<sub>2v</sub> <sup>1</sup>A<sub>1</sub> for B<sub>11</sub><sup>-</sup> was reported by Zhai et al<sup>19</sup> (Figure 4-1). Our MO plots for this dianion are shown in Figure 4-11b. NBO analysis reveals nine 2c-2e peripheral B-B bonds (ON=1.93-1.96 |e|) and one B-B bond between central atoms (ON=1.56 |e|). We believe that the lowest ten canonical MOs (from HOMO-7 to HOMO-16) are approximately responsible for the formation of these ten B-B bonds. Three MOs: HOMO (2b<sub>1</sub>), HOMO-2 (1a<sub>2</sub>) and HOMO-6 (1b<sub>1</sub>) are

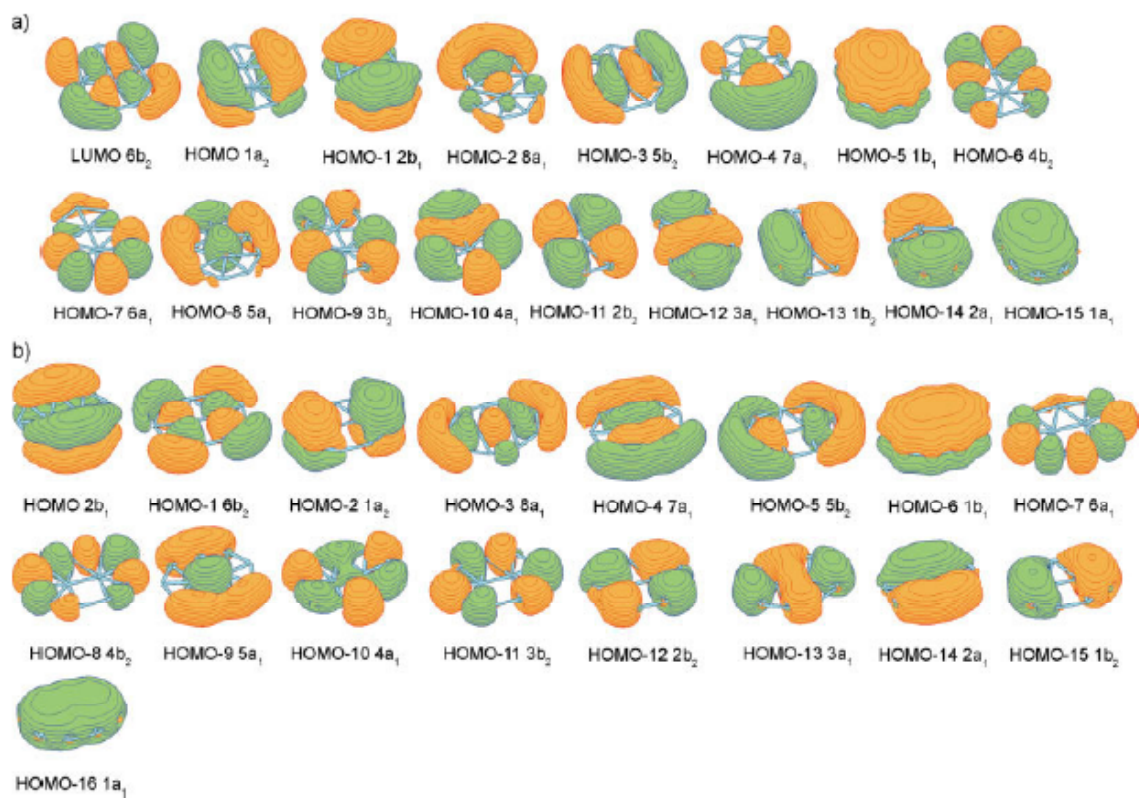


Figure 4-11. (a) Molecular orbitals of the  $C_{2v}$  ( $^1A_1$ ) structure of the  $B_{11}^+$  cation; (b) molecular orbitals of the  $C_{2v}$  ( $^1A_1$ ) structure of the  $B_{11}^-$  anion.

responsible for the global  $\pi$ -bonding, making this cluster  $\pi$ -aromatic as it was initially reported by Zhai et al.<sup>19</sup> Four MOs: HOMO-1 ( $6b_2$ ), HOMO-3 ( $8a_1$ ), HOMO-4 ( $7a_1$ ) and HOMO-5 ( $5b_2$ ) are approximately responsible for the global  $\sigma$ -bonding, making this system formally  $\sigma$ -antiaromatic.

However, the shape of HOMO-1, HOMO-3, HOMO-4 and HOMO-5 hints that the globally delocalized electrons may in fact break into four localized areas (giving rise to island  $\sigma$ -aromaticity) over the  $B_{11}^-$  cluster, similar to  $\sigma$ -delocalized electrons in the  $B_6^{2-}$  cluster, where they are split into two subsystems each localized over three boron atoms. At this point it is hard to point out which atoms in the  $B_{11}^-$  clusters belong to which regions of island  $\sigma$ -aromaticity.

#### 4-3.8. $B_{12}$ and $B_{13}^+$ Clusters

Zhai et al.<sup>19</sup> and Boustani<sup>39</sup> reported that the global minimum for  $B_{12}$  is the quasi-planar convex structure  $C_{3v} \ ^1A_1$  (Figure 4-1). In this case, three central boron atoms cannot fit into the plane of the nine-membered ring. As before, let us first flatten the  $C_{3v} \ ^1A_1$  structure into the planar  $D_{3h} \ ^1A_1'$  structure for simplicity and perform MO analysis for the planar structure. NBO analysis shows nine peripheral 2c-2e B-B bonds (ON=1.89-1.94 |e|). Unlike in  $B_{10}$ ,  $B_{11}^+$  and  $B_{11}^-$ , in  $B_{12}$  NBO analysis does not show 2c-2e B-B bonds between three central atoms. Instead, NBO analysis shows the presence of three “lone pairs” with the average occupation number about 1.1 |e| and with the total accumulation of 3.2 |e| on each of three central atoms. Such unusual accumulation of electron density could be a deficiency of the employed NBO method and a hint that two electrons on every central boron atoms could be involved into the formation of three 2c-



2e B-B bonds. Let us for now assume that indeed, we have also three 2c-2e B-B bonds between central atoms. That makes the total number of 2c-2e B-B bonds twelve. These twelve bonds take twenty four out of thirty six valence electrons. Molecular orbital picture (Figure 4-12) also shows the presence of three globally delocalized  $\pi$ -MOs: HOMO-5 ( $1a_2''$ ), HOMO-1 and HOMO-1' ( $1e''$ ), which reveals  $\pi$ -aromaticity, as it was initially reported by Zhai et al.<sup>19</sup> We have also six electrons on globally delocalized  $\sigma$ -MOs: HOMO-2 ( $4a_1'$ ), HOMO and HOMO' ( $5e'$ ), which reveals  $\sigma$ -aromaticity. With our previous assumptions, we can assign the  $B_{12}$  cluster as being doubly ( $\sigma$ - and  $\pi$ -) aromatic with nine 2c-2e peripheral B-B bonds and three 2c-2e central B-B bonds. We would like to stress that this description is tentative at this point. The presence of double aromaticity in  $B_{12}$  is supported by high first singlet vertical excitation energy (2.57 eV, at TD-B3LYP/6-311+G\*) and highly negative NICS values (all in Table 4-1).

In alternative explanation of  $\sigma$ -bonding in  $B_{12}$ , one may consider that central boron atoms donate their electrons to form islands of  $\sigma$ -aromaticity where each pair of delocalized  $\sigma$ -electrons is affiliated with three or four boron atoms. We need to develop new software tools for making  $\sigma$ -bonding analysis in such systems more precise.

The  $B_{13}^+$  cationic cluster attracted a lot of attention, because Anderson and co-workers<sup>25-31</sup> reported that it has anomalously high stability and low reactivity in comparison with other cationic boron clusters. Initially this high stability was attributed to  $B_{13}^+$  having a filled icosahedron structure.<sup>28</sup> Kawai and Weare<sup>34</sup> have shown that a filled icosahedra of  $B_{13}^+$  is not even a minimum on the potential energy surface using Car-Parrinello ab initio molecular dynamics simulations. The global minimum structure

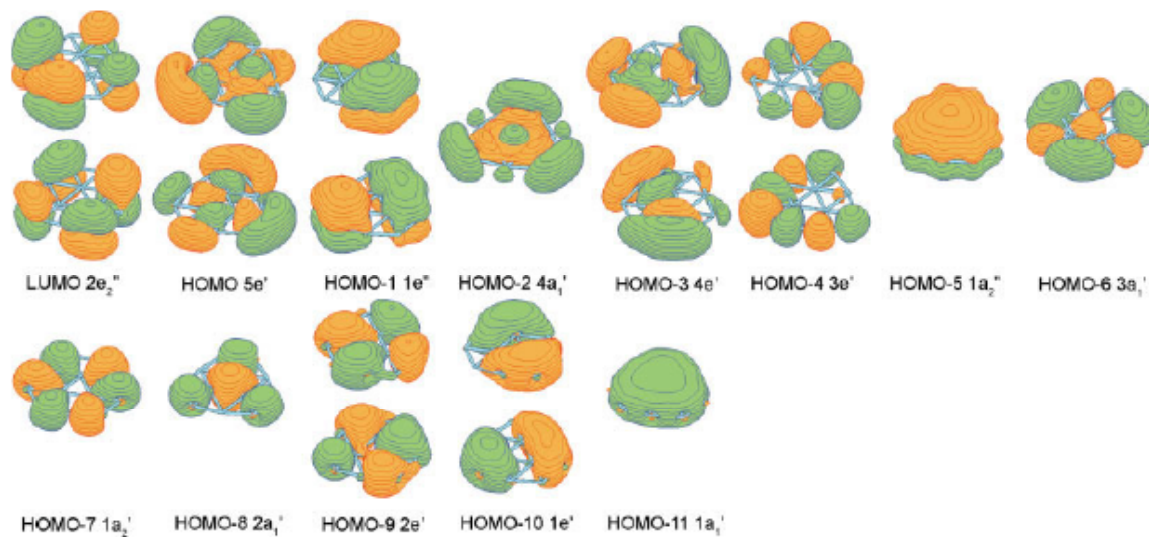


Figure 4-12. Molecular orbitals of the  $D_{3h}$  ( $^1A_1'$ ) structure of the  $B_{12}$  cluster.

of  $B_{13}^+$  was established by Ricca and Bauschlicher,<sup>42</sup> who predicted the planar  $C_{2v}$   $^1A_1$  structure (Figure 4-1). Three boron atoms can fit perfectly into the plane of the ten-membered ring. Fowler and Ugalde<sup>5a</sup> were the first who proposed that exceptional stability and low reactivity of  $B_{13}^+$  is related to its aromatic character. On the basis of plotted MOs Fowler and Ugalde concluded that three doubly occupied  $\pi$ -MOs give six  $\pi$ -electrons in a round system, a situation reminiscent of benzene and the Huckel aromaticity. Aihara<sup>6</sup> evaluated the topological resonance energy (TRE) for  $\pi$ -electrons using his graph theory of aromaticity. He found that the TRE of  $B_{13}^+$  is positive in sign and very large in magnitude:  $TRE = 2.959 |\beta_{BB}|$ . This number can be compared to the aromatic hydrocarbons of similar size such as the phenalenium ( $C_{13}H_9^+$ )  $TRE = 0.410 |\beta_{BB}|$ , anthracene ( $C_{14}H_{10}$ )  $TRE = 0.475 |\beta_{BB}|$ , and phenanthrene ( $C_{14}H_{10}$ )  $TRE = 0.576$

$|\beta_{\text{BB}}|$ . On the basis of the TRE value,  $\text{B}_{13}^+$  is much more aromatic than polycyclic aromatic hydrocarbons of the similar size.

However, like in case of other large boron clusters, the  $\sigma$ -bonding has not been discussed. Molecular orbitals for the  $\text{B}_{13}^+$  cation are plotted in Figure 4-13. NBO analysis shows ten 2c-2e B-B peripheral bonds ( $\text{ON} = 1.89\text{-}1.93 |e|$ ) and three “lone pairs” with the average occupation number about  $1.1 |e|$  and total accumulation of  $3.2 |e|$  on each of three central atoms. As before, let us assume that we have also three 2c-2e B-B bonds between central atoms, which makes the total number of 2c-2e B-B bonds thirteen. These thirteen bonds take 26 out of 38 valence electrons. Molecular orbital picture (Figure 4-13) also shows the presence of three globally delocalized  $\pi$ -MOs: HOMO-6 ( $1b_1$ ), HOMO-2 ( $1a_2$ ), and HOMO-1 ( $2b_1$ ), which reveals  $\pi$ -aromaticity, as was previously reported by Fowler and Ugalde<sup>5a</sup> and Aihara.<sup>6</sup> We can assign six remaining electrons on HOMO-4 ( $9a_1$ ), HOMO-3 ( $6b_2$ ), and HOMO ( $10a_1$ ) to globally delocalized  $\sigma$ -bonding. Again, we would like to stress that such chemical bonding description should be considered at this point as tentative. However, if we assume that our description is correct, than the presence of double aromaticity in  $\text{B}_{13}^+$  can explain high first singlet vertical excitation energy (2.09 eV, at TD-B3LYP/6-311+G\*), highly negative NICS values (all in Table 4-1), and most importantly anomalously high stability and low reactivity of  $\text{B}_{13}^+$  in comparison to other cationic boron clusters observed by Anderson and co-workers.<sup>25-31</sup>

#### 4-3.9. $\text{B}_{14}$ and $\text{B}_{15}^-$ Clusters

Zhai et al<sup>19</sup> reported that the global minimum for  $\text{B}_{14}$  is the quasi-planar structure  $\text{C}_{2v} \ ^1\text{A}_1$  (Figure 4-1). We performed MO analysis for the planar  $\text{D}_{2h} \ (^1\text{A}_g)$  structure

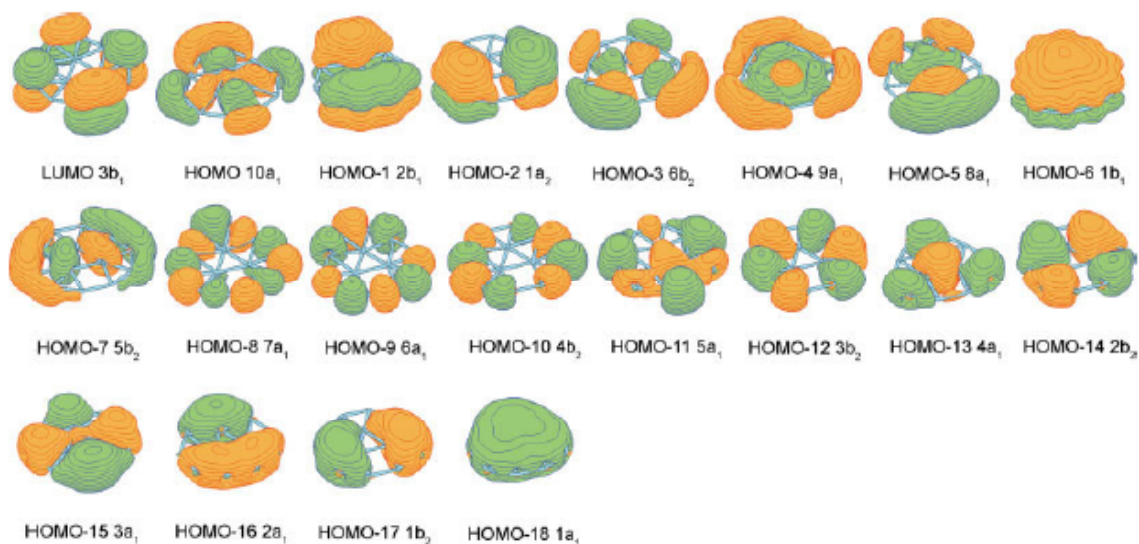


Figure 4-13. Molecular orbitals of the  $C_{2v}$  ( $^1A_1$ ) structure of the  $B_{13}^+$  cation.

(Figure 4-14). NBO analysis shows ten peripheral 2c-2e B-B bonds ( $ON=1.88-1.95$  |e|). It also shows the presence of three “lone pairs” with the average occupation number about 1.1 |e| and the total accumulation of 2.9-3.3 |e| on each of four central atoms. Like before, let us assume that there are four 2c-2e B-B bonds between central atoms. That makes total number of 2c-2e B-B bonds fourteen. These fourteen bonds account for 28 out of 42 valence electrons. Molecular orbital picture (Figure 4-14) also shows the presence of four globally delocalized  $\pi$ -MOs: HOMO-10 ( $1b_{3u}$ ), HOMO-4 ( $1b_{1g}$ ), HOMO-3 ( $1b_{2g}$ ), and HOMO (  $2b_{3u}$ ) which reveals global  $\pi$ -antiaromaticity, as it was previously reported by Zhai et al.<sup>19</sup> The global  $\pi$ -antiaromaticity results in formation of small areas of  $\pi$ -aromaticity (island aromaticity). The remaining six electrons occupy globally delocalized  $\sigma$ -MOs: HOMO-6 ( $5a_g$ ), HOMO-2 ( $5b_{2u}$ ) and HOMO-1 ( $6a_g$ ), which reveals  $\sigma$ -aromaticity. Thus, we can tentatively assign the  $B_{12}$  cluster as having

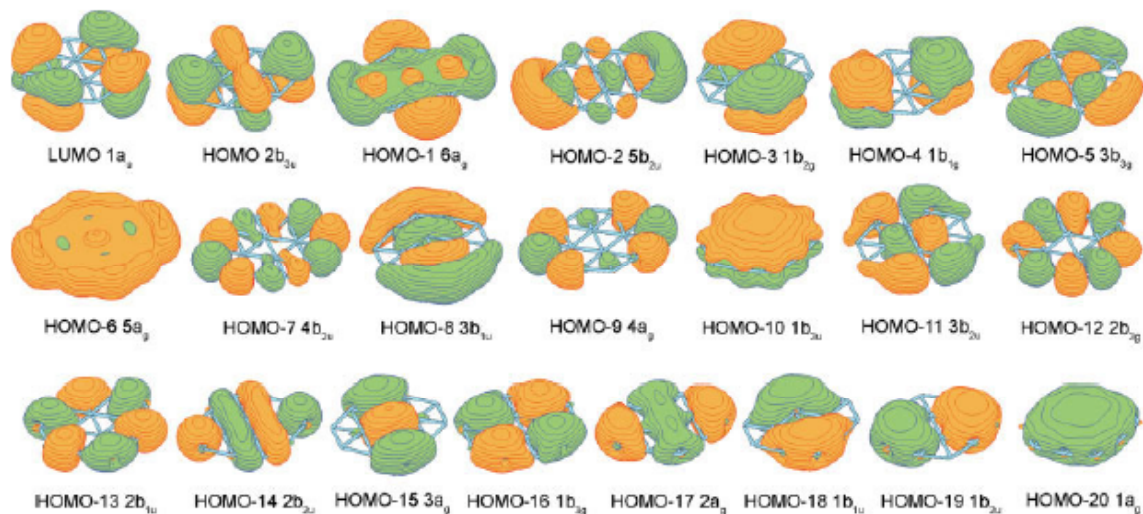


Figure 4-14. Molecular orbitals of the  $D_{2h}$  ( $^1A_g$ ) structure of the  $B_{14}$  cluster.

conflicting ( $\sigma$ -aromatic and  $\pi$ -antiaromatic) aromaticity with ten 2c-2e peripheral B-B bonds and four 2c-2e central B-B bonds.

Zhai et al.<sup>19</sup> reported that the global minimum for  $B_{15}^-$  is the quasi-planar structure  $C_1$   $^1A$  (Figure 4-1). We performed MO analysis for the planar  $C_{2v}$  ( $^1A_1$ ) structure (Figure 4-15). NBO analysis shows eleven peripheral 2c-2e B-B bonds ( $ON=1.88-1.95$  |e|). It also shows the presence of three “lone pairs” with the average occupation number about 1.1 |e| with the total accumulation of 2.9-3.3 |e| on each of three central atoms. Let us assume that we have also four 2c-2e B-B bonds between central atoms. That makes total number of 2c-2e B-B bonds fifteen. These fifteen bonds take thirty out of forty six valence electrons. Molecular orbital picture (Figure 4-15) shows the presence of four globally delocalized  $\pi$ -MOs: HOMO-11 ( $1b_1$ ), HOMO-5 ( $1a_2$ ), HOMO-2 ( $2b_1$ ), and HOMO-1 ( $3b_1$ ), which reveals global  $\pi$ -antiaromaticity. We have also eight electrons on

globally delocalized  $\sigma$ -MOs: HOMO (11a<sub>1</sub>), HOMO-3 (8b<sub>2</sub>), HOMO-4 (10a<sub>1</sub>) and HOMO-7 (9a<sub>1</sub>), which reveals global  $\sigma$ -antiaromaticity. Thus, we can tentatively consider the B<sub>15</sub><sup>-</sup> cluster as being doubly ( $\sigma$ - and  $\pi$ -) antiaromatic with eleven 2c-2e peripheral B-B bonds and four 2c-2e central B-B bonds. Again the  $\pi$ - and  $\sigma$ -antiaromaticity result in the formation of small areas of aromaticity (island aromaticity).

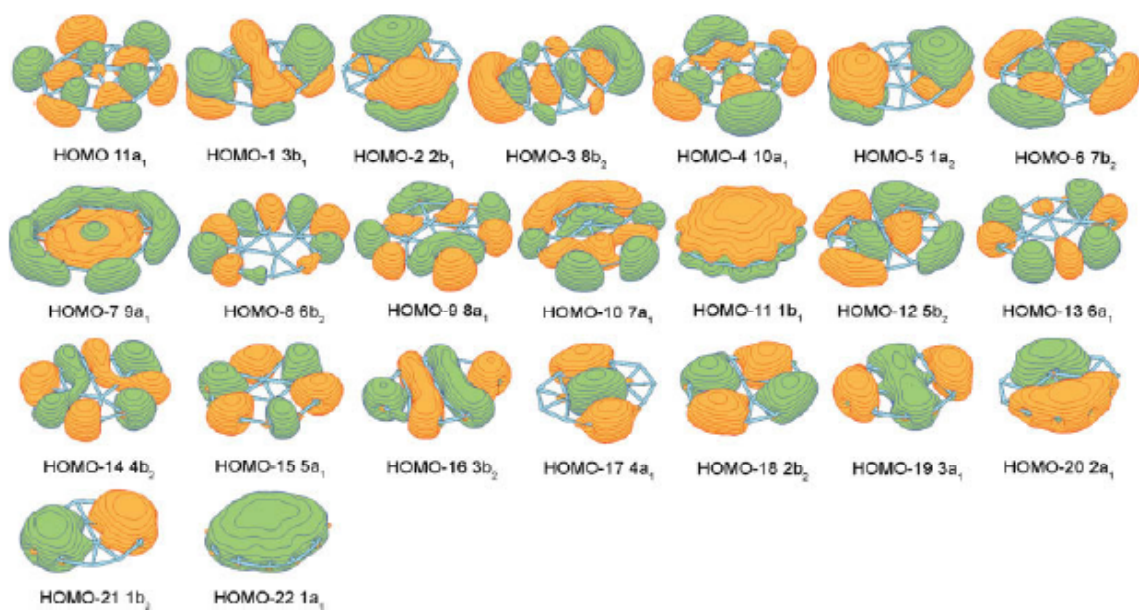


Figure 4-15. Molecular orbitals of the C<sub>2v</sub> (<sup>1</sup>A<sub>1</sub>) structure of the B<sub>15</sub><sup>-</sup> anion.

#### 4-4. Overview

On the basis of the chemical bonding analysis performed for B<sub>3</sub><sup>+</sup>, B<sub>3</sub><sup>-</sup>, B<sub>4</sub>, B<sub>4</sub><sup>-</sup>, B<sub>5</sub><sup>+</sup>, B<sub>5</sub><sup>-</sup>, B<sub>6</sub><sup>2+</sup>, B<sub>6</sub>, B<sub>6</sub><sup>2-</sup>, B<sub>7</sub><sup>+</sup>, B<sub>7</sub><sup>-</sup>, B<sub>8</sub>, B<sub>8</sub><sup>2-</sup>, B<sub>9</sub><sup>-</sup>, B<sub>10</sub>, B<sub>11</sub><sup>+</sup>, B<sub>11</sub><sup>-</sup>, B<sub>12</sub>, B<sub>13</sub><sup>+</sup>, B<sub>14</sub> and B<sub>15</sub><sup>-</sup> clusters in this work we propose the next chemical bonding model for planar or quasi-planar boron clusters:

- I. The number of 2c-2e peripheral B-B bonds in all planar or quasi-planar clusters considered here is equal to the number of peripheral edges.

- II. There are globally delocalized  $\pi$ -MOs which make a cluster either globally  $\pi$ -aromatic if it has  $4n+2$   $\pi$ -electrons or globally antiaromatic if it has  $4n$   $\pi$ -electrons for singlet coupled electrons. For triplet coupled  $\pi$ -electrons the number of electrons should satisfy the inverse  $4n$  rule for aromaticity.
- III. There are globally delocalized  $\sigma$ -MOs which make a cluster either globally  $\sigma$ -aromatic if it has  $4n+2$   $\sigma$ -electrons or globally antiaromatic if it has  $4n$   $\sigma$ -electrons for singlet coupled electrons. For triplet coupled  $\sigma$ -electrons the number of electrons should satisfy the inverse  $4n$  rule for aromatic systems.

This bonding model works well for  $B_3^+$  -  $B_9^-$  clusters. Some boron clusters can be doubly ( $\sigma$ - and  $\pi$ -) aromatic:  $B_3^-$ ,  $B_4$ ,  $B_5^+$ ,  $B_7^+$ ,  $B_7^-$ ,  $B_8$ ,  $B_8^{2-}$  and  $B_9^-$ . Some clusters can be globally doubly antiaromatic, for example,  $B_6^{2-}$ . Global antiaromaticity can be also described in terms of formation of areas of island aromaticity. In the  $B_6^{2-}$  clusters, the globally delocalized  $\pi$ - and  $\sigma$ - electrons can be localized over two areas composed of three boron atoms. Some clusters may have conflicting aromaticity, such as  $B_5^-$  (which is  $\pi$ -aromatic and  $\sigma$ -antiaromatic). For larger clusters, in addition to peripheral 2c-2e B-B bonds globally delocalized  $\pi$ -MOs, and globally delocalized  $\sigma$ -MOs, we can introduce one 2c-2e central B-B bond ( $B_{10}$ ,  $B_{11}^+$ ,  $B_{11}^-$ ), three 2c-2e central B-B bonds ( $B_{12}$ ,  $B_{13}^+$ ) or four 2c-2e central B-B bonds ( $B_{14}$ ,  $B_{15}^-$ ). The presence of central 2c-2e bonds was confirmed up to certain degree only in  $B_{10}$ ,  $B_{11}^+$  and  $B_{11}^-$  clusters. In other large clusters it was postulated. There is an alternative approach in which electrons located at central boron atoms are thought to participate in global delocalization resulting in formation of several areas with island  $\sigma$ -aromaticity.

We also would like to point out that there is no conflict between our assignment of planar boron clusters with  $4n$   $\pi$ -electrons to antiaromatic and Aihara et al. assignment of the same molecules to aromatic. The disagreement is purely semantic. We are talking about global antiaromaticity of boron clusters with  $4n$   $\pi$ -electrons. We, however, agree that a globally  $\pi$ -antiaromatic molecule such as  $B_6^{2-}$  could have islands of  $\pi$ -aromaticity. The island  $\pi$ -aromaticity is responsible for the high  $TRE=0.549 |\beta_{BB}|$  energy in  $B_6^{2-}$ . However, in order to explain low symmetry ( $D_{2h}$  instead of  $D_{6h}$ ) of  $B_6^{2-}$ , we must consider this cluster as being globally  $\pi$ -antiaromatic. The same is true for larger  $\pi$ -antiaromatic clusters. Similarly, in  $B_5^-$ , the high  $TRE=1.058 |\beta_{BB}|$  cannot explain the low symmetry ( $C_{2v}$  instead of  $D_{5h}$ ) of  $B_5^-$  as well as the small first singlet vertical excitation energy. The  $\sigma$ -electrons must be included in chemical bonding analysis. When the global  $\sigma$ -antiaromaticity in the  $B_5^-$  cluster is recognized, the low symmetry  $C_{2v}$  structure and small first singlet vertical excitation energy have rather simple explanation, which is not possible if only  $\pi$ -aromaticity in this cluster is considered.

Appropriate geometric fit is also an essential factor, which determines the shape of the most stable structures. In all boron clusters considered here the peripheral atoms form planar cycles. Peripheral  $2c-2e$  B-B bonds are built up from s-p hybrid atomic orbitals and this enforces the planarity of the cycle. If the given number of central atoms (1, 2, 3, or 4) can perfectly fit the central cavity then the overall structure is planar. Otherwise, central atoms come out of the plane of the cycle.

Initially, from  $B_3$  to  $B_6$  the cyclic (perfect or distorted depending on their aromatic or antiaromatic character) structures correspond to global minima. In the  $B_6$  cluster in addition to cyclic structures we observe the emergence of a new type of structure,



pentagonal pyramid, which now corresponds to the global minimum. The planar pentagon structure with the boron atom located at the center of the pentagon is not a minimum because the cavity inside of the pentagon is too small to favorably accommodate a boron atom at the center. The cyclic  $B_7^+$   $D_{7h}$  ( $^3A_2'$ ) structure is significantly higher (63.4 kcal/mol at B3LYP/6-311+G\*) in energy than the global minimum  $C_{6v}$  ( $^1A_1'$ ) structure because of unsupported dangling electron density at the center of the cycle. Thus, the cyclic structures are not favorable anymore beyond six boron atoms. Starting with  $B_8$  the central cavity can favorably accommodate one boron atom at the center of the appropriate polygon leading to planar highly symmetric global minimum structures. Starting from  $B_{10}$  cluster, the structures with one boron atom at the center are not low energy isomers, because it takes more than one boron nucleus to make a good fit for the central cavity.

We believe that this approach in which we combine 2c-2e bonds (or lone pairs) with global (or island)  $\pi$ - and  $\sigma$ -aromaticity is a promising way to characterize chemical bonding in large boron clusters and could potentially become a useful tool in addition to  $\pi$ -delocalization and  $\pi$ -aromaticity in case of other new planar clusters such as hyparenes,<sup>2b,2c</sup> aromatic boron wheels with more than one carbon atom at the center,<sup>81,82</sup> and fen-shaped  $B_nE_2Si$  (E=CH, BH, or Si, n=2-5) clusters.<sup>83</sup>

## References

1. (a) Boldyrev, A. I.; Wang, L. S. *Chem. Rev.* 2005, 106, 3716; (b) Li, X.; Kuznetsov, A. E.; Zhang, H. F.; Boldyrev, A. I.; Wang, L. S. *Science* 2001, 291, 859; (c) Kuznetsov, A. E.; Birch, K. A.; Boldyrev, A. I.; Li, X.; Zhai, H.-J.;

- Wang, L. S. *Science* 2003, 300, 622; (d) Boldyrev, A. I.; Kuznetsov, A. E. *Inorg. Chem.* 2002, 41, 532; (e) Alexandrova, A. N.; Boldyrev, A. I. *J. Phys. Chem. A* 2003, 107, 554.
2. (a) Chen, Z.; Wannere, C. S.; Corminboeuf, C.; Puchta, R.; Schleyer, P. v. R. *Chem. Rev.* 2005, 106, 3842; (b) Exner, K.; Schleyer, P. v. R. *Science* 2000, 1937, 290; (c) Wang, Z.-X.; Schleyer, P. v. R. *Science* 2001, 292, 2465; (d) Tanaka, H.; Neukermans, S.; Janssens, E.; Silverans, R. E.; Lievens, P. J. *Am. Chem. Soc.* 2003, 125, 2863.
  3. (a) Tsipis, C. A. *Coord. Chem. Rev.* 2005, 249, 2740; (b) Tsipis, A. C.; Tsipis, C. A. *J. Am. Chem. Soc.* 2003, 125, 1136.
  4. (a) Jemmis, E. D.; Jayasree, E. G. *Acc. Chem. Res.* 2003, 36, 816; (b) Balakrishnarajan, M. M.; Hoffmann, R.; Pancharatna, P. D.; Jemmis, E. D. *Inorg. Chem.* 2003, 42, 4650; (c) Jemmis, E. D.; Balakrishnarajan, M. M.; Pancharatna, P. D. *Chem. Rev.* 2002, 102, 93.
  5. (a) Fowler, J. E.; Ugalde, J. M. *J. Phys. Chem. A*, 2000, 104, 397; (b) Mercero, J. M.; Ugalde, J. M. *J. Am. Chem. Soc.* 2004, 126, 3380.
  6. Aihara, J. *J. Phys. Chem. A* 2001, 105, 5486.
  7. (a) Fowler, P. W.; Havenith, R. W. A.; Steiner, E. *Chem. Phys. Lett.* 2001, 342, 85; (b) Havenith, R. W. A.; Fowler, P. W.; Steiner, E. *Chem. Eur. J.* 2002, 8, 1068; (c) Fowler, P. W.; Havenith, R. W. A.; Steiner, E. *Chem. Phys. Lett.* 2002, 359, 530; (d) Havenith, R. W. A.; van Lenthe, J. H. *Chem. Phys. Lett.* 2004, 385, 198; (e) Havenith, R. W. A.; De Proft, F.; Fowler, P. W.; Geerling, P. *Chem. Phys. Lett.* 2005, 407, 391.

8. (a) Juselius, J.; Straka, M.; Sundholm, D. *J. Phys. Chem. A*, 2001, 105, 9939; (b) Lin, Y.-C.; Juselius, J.; Sundholm, D. *J. Chem. Phys.* 2005, 122, 214308; (c) Lin, Y.-C.; Sundholm, D.; Juselius, J.; Cui, L.-F.; Li, X.; Zhai, H.-J.; Wang, L. S. *J. Phys. Chem. A* 2006, 110, 4244.
9. Zhan, C.-G.; Zheng, F.; Dixon, D. A. *J. Am. Chem. Soc.* 2002, 124, 147.
10. Santos, J. C.; Andres, J.; Aizman, A.; Fuentealba, J. *Chem. Theory Comput.* 2005, 1, 83.
11. (a) Datta, A.; Pati, S. K. *J. Phys. Chem. A* 2004, 108, 9527; (b) Datta, A.; Pati, S. K. *J. Am. Chem. Soc.* 2005, 127, 3496; (c) Datta, A.; Pati, S. K.; *J. Chem. Theory Comput.* 2005, 1, 824; (d) Datta, A.; John, N. S.; Kulkarni, G. U.; Pati, S. K. *J. Phys. Chem. A*, 2005, 109, 11647; (e) Rehaman, A.; Datta, A.; Mallajosyulu, S. S.; Pati, S. K. *J. Comput. Theory Comput.* 2006, 2, 30.
12. (a) Havenith, R. W. A.; Fowler, P. W.; Steiner, E.; Shetty, S.; Kanhere, D.; Pal, S. *Phys. Chem. Chem. Phys.* 2004, 6, 285; (b) Shetty, S.; Kar, R.; Kanhere, D. G.; Pal, S. *J. Phys. Chem. A* 2006, 110, 252.
13. (a) Hu, X. B.; Li, H. R.; Liang, W. C.; Han, S. J.; *Chem. Phys. Lett.* 2004, 397, 180; (b) Hu, X.; Li, H.; Liang, W.; Han, S. *Chem. Phys. Lett.* 2005, 402, 539; (c) Hu, X. B.; Li, H. R.; Liang, W. C.; Han, S. J. *New J. Chem.* 2005, 29, 1295; (d) Wang, F.-F.; Li, Z.-R.; Wu, D.; Sun, X.-Y.; Chen, W.; Li, Ying, Sun, C.-C. *Chem. Phys. Chem.* 2006, 7, 1136.
14. (a) Zhai, H. J.; Wang, L. S.; Alexandrova, A. N.; Boldyrev, A. I.; Zakrzewski, V. G. *J. Phys. Chem. A* 2003, 107, 9319; (b) Kuznetsov, A. E.; Boldyrev, A. I. *Struct. Chem.* 2002, 13, 141.

15. Zhai, H. J.; Wang, L. S.; Alexandrova, A. N.; Boldyrev, A. I. *J. Chem. Phys.* 2002, 117, 7917.
16. Alexandrova, A. N.; Boldyrev, A. I.; Zhai, H. J.; Wang, L. S.; Steiner, E.; Fowler, P. W. *J. Phys. Chem. A* 2003, 107, 1359.
17. Alexandrova, A. N.; Boldyrev, A. I.; Zhai, H. J.; Wang, L. S. *J. Phys. Chem. A* 2004, 108, 3509.
18. Zhai, H. J.; Wang, L. S.; Alexandrova, A. N.; Boldyrev, A. I. *Angew. Chem. Int. Ed.* 2003, 42, 6004.
19. Zhai, H. J.; Kiran, B.; Li, J.; Wang, L. S. *Nature Materials* 2003, 2, 827.
20. Aihara, J.; Kanno, H.; Ishida, T. *J. Am. Chem. Soc.* 2005, 127, 13324.
21. Alexandrova, A. N.; Zhai, H.-J.; Wang, L. S.; Boldyrev, A. I. *Inorg. Chem.* 2004, 43, 3588.
22. Alexandrova, A. N.; Boldyrev, A. I.; Zhai, H.-J.; Wang, L. S. *J. Chem. Phys.* 2005, 122, 054313.
23. Alexandrova, A. N.; Kayle, E.; Boldyrev, A. I. *J. Mol. Mod.* In press.
24. Zhai, H.-J.; Wang, L. S.; Zubarev, D. Yu.; Boldyrev, A. I. *J. Phys. Chem. A*, 2006, 110, 1689.
25. Hanley, L.; Anderson, S. L. *J. Phys. Chem.* 1987, 91, 5161.
26. Hanley, L.; Anderson, S. L. *J. Chem. Phys.* 1988, 89, 2848.
27. Hanley, L.; Whitten, J. L.; Anderson, S. L. *J. Phys. Chem.* 1988, 92, 5803.
28. Hintz, P. A.; Ruatta, S. A.; Anderson, S. L. *J. Chem. Phys.* 1990, 92, 292.
29. Ruatta, S. A.; Hintz, P. A.; Anderson, S. L. *J. Chem. Phys.* 1991, 94, 2833.

30. Hintz, P. A.; Sowa, M. B.; Ruatta, S. A.; Anderson, S. L. *J. Chem. Phys.* 1991, 94, 6446.
31. Sowa-Resat, M. B.; Smolanoff, J.; Lapiki, A.; Anderson, S. L. *J. Chem. Phys.* 1997, 106, 9511.
32. Kawai, R.; Weare, J. H. *J. Chem. Phys.* 1991, 95, 1151.
33. La Placa, S. J.; Roland, P. A.; Wynne, J. J. *Chem. Phys. Lett.* 1992, 190, 163.
34. Kawai, R.; Weare, J. H. *Chem. Phys. Lett.* 1992, 191, 311.
35. Martin, J. M. L.; François, J. P.; Gijbels, R. *Chem. Phys. Lett.* 1992, 189, 52.
36. Kato, H.; Yamashita, K.; Morokuma, K. *Chem. Phys. Lett.* 1992, 190, 361.
37. Roland, P. A.; Wynne, J. J. *J. Chem. Phys.* 1993, 99, 8599.
38. Kato, H.; Yamashita, K.; Morokuma, K. *Bull. Chem. Soc. Jpn.* 1993, 66, 3358.
39. Boustani, I. *Int. J. Quantum Chem.* 1994, 52, 1081.
40. Boustani, I. *Chem. Phys. Lett.* 1995, 233, 273.
41. Boustani, I. *Chem. Phys. Lett.* 1995, 240, 135.
42. Ricca, A.; Bauschlicher, C. W. Jr. *Chem. Phys.* 1996, 208, 233.
43. Boustani, I. *Surf. Sci.* 1997, 370, 355.
44. Boustani, I. *Phys. Rev. B* 1997, 53, 16426.
45. Nie, J.; Rao, B. K.; Jena, P. J. *Chem. Phys.* 1997, 107, 132.
46. Gu, F. L.; Yang, X.; Tang, A.-C.; Jiao, H.; Schleyer, P. v. R. *J. Comput. Chem.* 1998, 19, 203.
47. Reis, H.; Papadopoulos, M. G.; Boustani, I. *Int. J. Quant. Chem.* 2000, 78, 131.
48. Yang, C. L.; Zhu, Z. H. *J. Mol. Struct. (Theochem)* 2001, 571, 225.

49. Cao, P.-L.; Zhao, W.; Li, B.; Song, X.-B.; Zhou, X.-Y.; J. Phys.: Condens. Matter, 2001, 13, 5065.
50. Li, Q. S.; Jin, H. W. J. Phys. Chem. A, 2002, 106, 7042.
51. Ma, J.; Li, Z.; Fan, K.; Zhou, M. Chem. Phys. Lett. 2003, 372, 708.
52. Jin, H. W.; Li, Q. S.; Phys. Chem. Chem. Phys. 2003, 5, 1110.
53. Li, Q. S.; Jin, Q. J. Phys. Chem. A 2004, 108, 855.
54. Li, Q. S.; Jin, Q.; Luo, Q.; Tang, A. C.; Yu, J. K.; Zhang, H. X. Int. J. Quant. Chem. 2003, 94, 269.
55. Wyss, M.; Riaplov, E.; Batalov, A.; Maier, J. P.; Weber, T.; Meyer, W.; Rosmus, P.; J. Chem. Phys. 2003, 119, 9703.
56. Cias, P.; Araki, M.; Denisov, A.; Maier, J. P. J. Chem. Phys. 2004, 121, 6776.
57. Batalov, A.; Fulara, J.; Shnitko, I.; Maier, J. P. Chem. Phys. Lett. 2005, 404, 315.
58. Gillery, C.; Linguerri, R.; Rosmus, P.; Maier, J. P. Z. Phys. Chem. 2005, 219, 467.
59. Li, Q.-S.; Gong, L.-F. J. Phys. Chem. A, 2004, 108, 4322.
60. Li, Q.-S.; Gong, L.-F.; Gao, Z.-M. Chem. Phys. Lett. 2004, 390, 220.
61. Li, Q.; Zhao, Y.; Xu, W.; Li, N. Int. J. Quant. Chem. 2005, 101, 219.
62. Lau, K. C.; Deshpande, M.; Pandey, R. Int. J. Quant. Chem. 2005, 102, 656.
63. Alexandrova, A. N.; Boldyrev, A. I.; Zhai, H.-J.; Wang, L. S. Coord. Chem. Rev. in press.
64. Reed, A. E.; Curtiss, L. A.; Weinhold, F. Chem. Rev. 1988, 88, 899.
65. Parr, R. G.; Yang, W. *Density-functional Theory of Atoms and Molecules*. 1989, Oxford Univ. Press, Oxford.

66. Becke, A. D. *J. Chem. Phys.* 1993, 98, 5648.
67. Perdew, J. P.; Chevary, J. A.; Vosko, S. H.; Jackson, K. A.; Pederson, M. R.; Singh, D. J.; Fiolhais, C. *Phys. Rev. B* 1992, 46, 6671.
68. Clark, T.; Chandrasekhar, J.; Spitznagel, G.W.; Schleyer, P. v. R. *J. Comput. Chem.* 1983, 4, 294.
69. Frisch, M. J.; Pople, J. A.; Binkley, J. S. *J. Chem. Phys.* 1984, 80, 3265.
70. Schleyer, P. v. R.; Maerker, C.; Dransfeld, A.; Jiao, H.; Hommes, N. J. R. v. E. *J. Am. Chem. Soc.* 1996, 118, 6317.
71. Bauernshmitt, R.; Alrichs, R. *Chem. Phys. Lett.* **1996**, 256, 454.
72. Casida, M.E.; Jamorski, C.; Casida, K.C.; Salahub, D.R. *J. Chem. Phys.* **1998**, 108, 4439.
73. Gaussian 03 (revision A.1). Frisch, M. J.; Trucks, G. M.; Schlegel, H. B.; Scuseria, G. E.; Robb, M. A.; Cheeseman, J. R.; Montgomery, Jr., J. A.; Vreven, T.; Kudin, K. N.; Burant, J. C.; Millam, J. M.; Iyengar, S. S.; Tomasi, J.; Barone, V.; Mennucci, B.; Cossi, M.; Scalmani, G.; Rega, N.; Petersson, G. A.; Nakatsuji, H.; Hada, M.; Ehara, M.; Toyota, K.; Fukuda, R.; Hasegawa, J.; Ishida, M.; Nakajima, T.; Honda, Y.; Kitao, O.; Nakai, H.; Klene, M.; Li, X.; Knox, J. E.; Hratchian, H. P.; Cross, J. B.; Adamo, C.; Jaramillo, J.; Gomperts, R.; Stratmann, R. E.; Yazyev, O.; Austin, A. J.; Cammi, R.; Pomelli, C.; Ochterski, J. W.; Ayala, P. Y.; Morokuma, K.; Voth, G. A.; Salvador, P.; Dannenberg, J. J.; Zakrzewski, V. G.; Dapprich, S.; Daniels, A. D.; Strain, M. C.; Farkas, O.; Malick, D. K.; Rabuck, A. D.; Raghavachari, K.; Foresman, J. B.; Ortiz, J. V.; Cui, Q.; Baboul, A. G.; Clifford, S.; Cioslowski, J.; Stefanov, B. B.; Liu, G.; Liashenko, A.;

- Piskorz, P.; Komaromi, I.; Martin, R. L.; Fox, D. J.; Keith, T.; Al-Laham, M. A.; Peng, C. Y.; Nanayakkara, A.; Challacombe, M.; Gill, P. M. W.; Johnson, B. G.; Chen, W.; Wong, M. W.; Gonzales, C. ; Pople, J. A., Gaussian, Inc., Pittsburgh PA, 2003.
74. Schaftenaar, G. MOLDEN3.4, CAOS/CAMM Center, The Netherlands, 1998.
75. (a) Chandrasekhar, J.; Jemmis, E. D.; Schleyer, P. v. R. *Tetrahedron Lett.* 1979, 3707; (b) Schleyer, P. v. R.; Jiao, H.; Glukhovtsev, M. N.; Chandrasekhar, J.; Kraka, E. J. *Am. Chem. Soc.* 1994, 116, 10129.
76. Martin-Santamaria, S.; Rzepa, H. S. *Chem. Commun.* 2000, 1503.
77. Präsang, C.; Hofmann, M.; Geiseler, G.; Massa, W.; Berndt, A. *Angew. Chem. Int. Ed.* 2002, 41, 1526; (b) Präsang, C.; Młodzianowska, A.; Sahin, Y.; Hofmann, M.; Geiseler, G.; Massa, W.; Berndt, A. *Angew. Chem. Int. Ed.* 2002, 41, 3380; (c) Mesbah, W.; Präsang, C.; Hofmann, M.; Geiseler, G.; Massa, W.; Berndt, A. *Angew. Chem. Int. Ed.* 2003, 42, 1717; (e) Hofmann, M.; Berndt, A. *Heteroatom Chem.* 2006, 17, 224.
78. Minkin, V. I.; Minyaev, R. M. *Mendeleev Comm.* 2004, 14, 43.
79. Minyaev, R. M. Gribanova, T. N.; Starikov, A. G.; Minkin, V. I. *Medeleev Comm.* 2001, 11, 213.
80. Erhardt, S.; Frenking, G.; Chen, Z.; Schleyer, P. v. R. *Angew. Chem. Int. Ed.* 2005, 44, 1078.
81. Wu, Y.-B.; Yuan, C.-X.; Yang, P. J. *Molecular Structure, Theochem*, (in press)
82. Li, S.-D.; Miao, C.-C.; Guo, J.-C.; Ren, G.-M. *J. Am. Chem. Soc.* 2004, 126, 16227.



CHAPTER 5  
AROMATICITY AND ANTIAROMATICITY IN  
TRANSITION-METAL SYSTEMS<sup>1</sup>

**Abstract**

Aromaticity is an important concept in chemistry primarily for organic compounds, but it has been extended to compounds containing transition-metal atoms. Recent findings of aromaticity and antiaromaticity in all-metal clusters have stimulated further researches in describing the chemical bonding, structures, and stability in transition-metal clusters and compounds on the basis of aromaticity and antiaromaticity, which are reviewed here. The presence of d-orbitals endows much more diverse chemistry, structure, and chemical bonding to transition-metal clusters and compounds. One interesting feature is the existence of a new type of aromaticity -  $\delta$ -aromaticity, in addition to  $\sigma$ - and  $\pi$ -aromaticity that are only possible for main group compounds. Another striking characteristic in the chemical bonding of transition-metal systems is the multi-fold nature of aromaticity, antiaromaticity, or even conflicting aromaticity. Separate sets of counting rules have been proposed for cyclic transition-metal systems to account for the three types of  $\sigma$ -,  $\pi$ -, and  $\delta$ -aromaticity/antiaromaticity. The diverse transition-metal clusters and compounds reviewed here indicate that multiple aromaticity and antiaromaticity may be much more common in chemistry than one would anticipate. It is hoped that the current review will stimulate interest in further understanding the structure and bonding, on the basis of aromaticity and antiaromaticity, of other known or

---

<sup>1</sup> Coauthored by Dmitry Yu. Zubarev, Boris B. Averkiev, Hua-Jin Zhai, Lai-Sheng Wang and Alexander I. Boldyrev. Reproduced with permission from *Phys. Chem. Chem. Phys.* **2008**, 10, 257-267.

unknown transition-metal systems, such as the active sites of enzymes or other biomolecules, which contain transition-metal atoms and clusters.

### 5-1. Introduction

Aromaticity in compounds containing a transition-metal atom was first considered in a pioneering paper in 1979 by Thorn and Hoffmann<sup>1</sup> on six-membered ring metallocyclic compounds, that are derived from the prototypical aromatic benzene molecule with one C-H moiety replaced by an isolobal transition-metal fragment. Just three years later the first example of a stable, isolable metallobenzene — osmabenzene — was reported by Elliott *et al.*<sup>2</sup> A large family of metallobenzenes — the iridabenzenes — was synthesized by Bleeke and co-workers;<sup>3-5</sup> whereas a series of dimetallobenzenes with two metal atoms incorporated into the benzene ring was synthesized and characterized by Rothwell *et al.*<sup>6,7</sup> Recent advances in metallobenzenes have been reviewed by Bleeke,<sup>8</sup> He *et al.*,<sup>9</sup> Wright,<sup>10</sup> and Landorf and Haley.<sup>11</sup> A thorough chemical bonding analysis of metallobenzene has been recently performed by Fernandez and Frenking.<sup>12</sup> However, aromaticity in transition metal compounds is not restricted to metallobenzene molecules. Other molecules, in which the aromatic cycle composed of transition-metal atoms only and are not based on the prototypical benzene molecule, have also been reported recently, and they are the subject of the current article.

Before discussing in detail the aromaticity in transition-metal systems, let us briefly review the concept of aromaticity, since it has been rather controversial, despite the fact that it is taught routinely in general chemistry. Many books<sup>13-21</sup> and numerous reviews<sup>22-29</sup> have been published, and several conferences<sup>30-32</sup> have been dedicated to deciphering

the concept of aromaticity. We would like to adopt a view of aromaticity with which we hope that most chemists can agree. Aromaticity was initially introduced into chemistry to describe the lack of reactivity of benzene and its derivatives, in spite of the apparent unsaturated nature of the carbon-carbon bonds in these molecules. Because all these molecules have an aroma, the property of chemical stability of the unsaturated bonds in the cyclic systems was called aromaticity. Nowadays most molecules, which are considered to be aromatic, do not have any aroma and in order to characterize them as aromatic a variety of criteria have been proposed in the literature based on molecular orbital or other considerations. They are summarized in Table 5-1 (we adopt a list of the properties proposed by Krygowski *et al.*<sup>33</sup> with some small modifications and additions).

These criteria have been proposed for  $\pi$ -aromatic and  $\pi$ -antiaromatic organic systems, but we will see that many of them are also applicable to  $\sigma$ -aromatic and  $\sigma$ -antiaromatic systems, as well as to  $\delta$ -aromatic and  $\delta$ -antiaromatic systems. We stress that one should not expect that aromaticity/antiaromaticity in transition metal systems will manifest itself exactly the same way as in organic chemistry. Many specific deviations are expected. Nevertheless, we believe that the overall delocalized chemical bonding and most of the molecular properties in certain transition metal species could be understood using the aromaticity/antiaromaticity concepts.

The discovery and experimental generation of the first all-metal aromatic and antiaromatic clusters using photoelectron spectroscopy and *ab initio* calculations<sup>34,35</sup> have stimulated much interest in extending these ideas to other metal systems, including transition metals.<sup>36,37</sup> It has been understood that aromaticity/antiaromaticity in metal systems has very specific flavors if compared with organic compounds. The striking

Table 5-1. Criteria for  $\pi$ -Aromaticity and  $\pi$ -Antiaromaticity.<sup>33</sup>

Property	Aromatic	Olefinic/Classical	Antiaromatic
<b>(i) Electronic nature</b>	$(4n + 2)$ $\pi$ -electron cyclic conjugation	No cyclic conjugation	$4n$ $\pi$ -electron cyclic conjugation
<b>(ii) Energy</b>			
Cyclic conjugation	Stabilization	Standard	Destabilization
Delocalization	Enhanced	Standard	Decreased
HOMO-LUMO gap	Large	Standard	Small
<b>(iii) Geometry</b>			
Bond lengths	Equalization	Alternation	Alternation
<b>(iv) Magnetic properties</b>			
Anisotropy of diamagnetic susceptibility	Enhanced		Small
Susceptibility exaltation	High		Low
<sup>1</sup> H NMR shifts	Diatropic (low-field shift)		Paratropic (high-field shift)
NICS (nucleus independent chemical shift)	Large negative	Close to zero	Large positive
<b>(v) Reactivity</b>			
Chemical example	e.g., benzene	e.g., cyclohexadiene	e.g., cyclooctatetraene
Retention of structure	Electrophilic substitution	Electrophilic addition	Addition
<b>(vi) Spectroscopy</b>			
UV spectra	High energy	Standard	Low energy
IR/Raman spectra	High symmetry		Low symmetry
Photoelectron spectra	High electron detachment energies	Standard	Low electron detachment energies

feature of chemical bonding in metal systems is the possibility of the multi-fold nature of aromaticity, antiaromaticity, and conflicting aromaticity.<sup>36-39</sup> When only s-atomic orbitals (AOs) are involved in chemical bonding, one may expect only  $\sigma$ -aromaticity or  $\sigma$ -antiaromaticity. If p-AOs are involved,  $\sigma$ -tangential ( $\sigma_t$ -),  $\sigma$ -radial ( $\sigma_r$ -), and  $\pi$ -aromaticity/antiaromaticity could occur.<sup>36</sup> In this case, there can be multiple ( $\sigma$ - and  $\pi$ -) aromaticity, multiple ( $\sigma$ - and  $\pi$ -) antiaromaticity, and conflicting aromaticity (simultaneous  $\sigma$ -aromaticity and  $\pi$ -antiaromaticity or  $\sigma$ -antiaromaticity and  $\pi$ -aromaticity). If d-AOs are involved in chemical bonding,  $\sigma$ -tangential ( $\sigma_t$ -),  $\sigma$ -radial ( $\sigma_r$ -),  $\pi$ -tangential ( $\pi_t$ -),  $\pi$ -radial ( $\pi_r$ -), and  $\delta$ -aromaticity/antiaromaticity could occur. In this case, there can be multiple ( $\sigma$ -,  $\pi$ -, and  $\delta$ -) aromaticity, multiple ( $\sigma$ -,  $\pi$ -, and  $\delta$ -) antiaromaticity, and conflicting aromaticity (simultaneous aromaticity and antiaromaticity among the three types of  $\sigma$ ,  $\pi$ , and  $\delta$  bonds).

One would expect that doubly and triply aromatic molecules would be significantly more stable with higher resonance energies, shortened bond lengths, enhanced ring currents, more negative NICS values, and a higher average bifurcation value of the electron localization function (ELF) than in conventional singly aromatic molecules. Indeed, Boldyrev and Kuznetsov,<sup>40</sup> and Zhan et al.<sup>41</sup> showed that the doubly ( $\sigma$ - and  $\pi$ -) aromatic species  $Al_4^{2-}$  has a very high resonance energy  $\sim 48$  kcal/mol<sup>40</sup> and  $\sim 73$  kcal/mol<sup>41</sup>, respectively. For the prototypical singly aromatic benzene molecule the resonance energy is only 20 kcal/mol.<sup>13</sup> The ring-current susceptibilities for the doubly aromatic  $Al_4^{2-}$  dianion was also found to be  $10$  nA T<sup>-1</sup>, which is higher than  $8$  nA T<sup>-1</sup> in benzene.<sup>42</sup> Fowler et al demonstrated that the contribution to the ring current from  $\sigma$ -delocalized electrons is significantly higher than from  $\pi$ -electrons.<sup>43,44</sup> According to Chen

et al.,<sup>45</sup>  $\text{Al}_4^{2-}$  has significant negative NICS (-30.9 ppm) compared to that in benzene (-9.7 ppm).<sup>46</sup> Santos et al.<sup>47</sup> showed that  $\text{Al}_4^{2-}$  has the highest average bifurcation value of  $\text{ELF}_\sigma$  and  $\text{ELF}_\pi$  among the set of various singly aromatic systems. Establishing the overall aromaticity or antiaromaticity in molecules with conflicting aromaticity is especially challenging task, because of the simultaneous presence of aromaticity and antiaromaticity in different electronic subsystems.<sup>35,45,48</sup> Studies of magnetic properties of systems with conflicting aromaticity such as  $\text{Li}_3\text{Al}_4^-$  and  $\text{Li}_4\text{Al}_4$  can lead to contradictory conclusions on the overall aromaticity or antiaromaticity of the system.<sup>35,49-51</sup> Conflicting aromaticity also results in floppy geometries of the  $\text{Li}_3\text{Al}_4^-$  and  $\text{Li}_4\text{Al}_4$  clusters.<sup>50</sup> One of the most interesting features of molecules with conflicting aromaticity is the possibility of large linear and nonlinear optical properties such as linear polarizability, first hyperpolarizability, and second hyperpolarizability.<sup>52</sup>

In the following sections we will consider in details the cases of multiple aromaticity, multiple antiaromaticity and conflicting aromaticity in recent examples of transition metal clusters and compounds, including  $\text{Cu}_3^+$ ,<sup>53</sup> *cyclo*- $\text{Cu}_n\text{H}_n$  ( $n = 3-6$ ),<sup>54</sup> *cyclo*- $\text{M}_n\text{H}_n$  ( $\text{M} = \text{Ag}, \text{Au}; n = 3-6$ ),<sup>55</sup> *cyclo*- $\text{Au}_3\text{L}_n\text{H}_{3-n}$  ( $\text{L} = \text{CH}_3, \text{NH}_2, \text{OH}, \text{and Cl}; n = 1-3$ ),<sup>56</sup> *cyclo*- $\text{Cu}_n\text{Ag}_{3-n}\text{H}_n$  ( $n = 1-3$ ), *cyclo*- $\text{Cu}_n\text{Ag}_{4-n}\text{H}_n$  ( $n = 1-4$ ), and *cyclo*- $\text{Cu}_n\text{Ag}_{5-n}\text{H}_n$  ( $n = 1-5$ ),<sup>57</sup>  $\text{Au}_5\text{Zn}^+$ ,<sup>58</sup>  $\text{M}_4\text{Li}_2$  ( $\text{M} = \text{Cu}, \text{Ag}, \text{Au}$ ),<sup>59</sup>  $\text{M}_4\text{L}_2$  and  $\text{M}_4\text{L}^-$  ( $\text{M} = \text{Cu}, \text{Ag}, \text{Au}; \text{L} = \text{Li}, \text{Na}$ ),<sup>60</sup>  $\text{Hg}_4^{6-}$ ,<sup>61</sup>  $\text{M}_3^{2-}$ ,  $\text{NaM}_3^-$ , and  $\text{Na}_2\text{M}_3$  ( $\text{M} = \text{Zn}, \text{Cd}, \text{Hg}$ ),<sup>62</sup>  $\text{M}_3^-$  ( $\text{M} = \text{Sc}, \text{Y}, \text{La}$ ),<sup>63</sup>  $\text{M}_3\text{O}_9^-$  and  $\text{M}_3\text{O}_9^{2-}$  ( $\text{M} = \text{W}, \text{Mo}$ ),<sup>64</sup>  $\text{Ta}_3\text{O}_3^-$ ,<sup>65</sup> and  $\text{Hf}_3$ .<sup>66</sup>

## 5-2. s-AO based $\sigma$ -aromaticity and $\sigma$ -antiaromaticity in transition metal systems

### 5-2.1. s-AO based $\sigma$ -aromaticity and $\sigma$ -antiaromaticity in $M_3$ clusters

The prototypical system with s-AO based  $\sigma$ -aromaticity is the  $\text{Li}_3^+$  cluster, which was initially discussed by Alexandrova and Boldyrev,<sup>67</sup> and then by Havenith et al.<sup>68</sup> and Yong et al.<sup>53</sup> The  $\text{Cu}_3^+$  has a similar  $D_{3h}$ ,  $^1A_1'$  ( $1a_1'^2 1e'^4 1a_2''^2 2a_1'^2 1e'^4 2e'^4 2a_2''^2 3e'^4 2e''^4 3a_2''^2 3a_1'^2$ ) global minimum structure.<sup>53</sup> As in the case of  $\text{Li}_3^+$ , the bonding in  $\text{Cu}_3^+$  is rooted in 4s-AOs of Cu, because all the bonding and antibonding MOs ( $1a_1'^2 1e'^4 1a_2''^2 2a_1'^2 1e'^4 2e'^4 2a_2''^2 3e'^4 2e''^4 3a_2''^2$ ) composed out of 3d-AOs of Cu are occupied, hence the contribution to bonding from 3d-AOs of Cu is negligible. The  $3a_1'$ -valence HOMO is a sum of the 4s-AOs of three Cu atoms (Fig. 5-1a). It is completely bonding and in this sense similar to the completely bonding  $\pi$ -MO in the prototypical  $\pi$ -aromatic  $\text{C}_3\text{H}_3^+$  cation (Fig. 5-1b).

The only difference is that the  $\pi$ -MO is a sum of  $2p_z$ -AOs of carbons. The delocalized  $\pi$ -MO in  $\text{C}_3\text{H}_3^+$  renders its  $\pi$ -aromaticity according to the famous  $4n+2$  Huckel rule. On the basis of the analogy between the  $\pi$ -delocalized MO in  $\text{C}_3\text{H}_3^+$  and the  $\sigma$ -delocalized MO in  $\text{Cu}_3^+$  it is reasonable to call the latter  $\sigma$ -aromatic (the  $4n+2$  rule holds for  $\sigma$ -aromatic cyclic systems with valence s-AOs participating in bonding).<sup>19</sup> Yong et al.<sup>53</sup> considered aromaticity in the  $\text{Cu}_3^+$  cation on the basis of nucleus-independent chemical shift (NICS) indexes.<sup>46</sup> Their calculations show  $\text{NICS}(0.0) = -8.22$  ppm,  $\text{NICS}(0.5) = -22.59$  ppm, and  $\text{NICS}(1.0) = -12.31$  ppm at B3LYP/6-311+G\*,

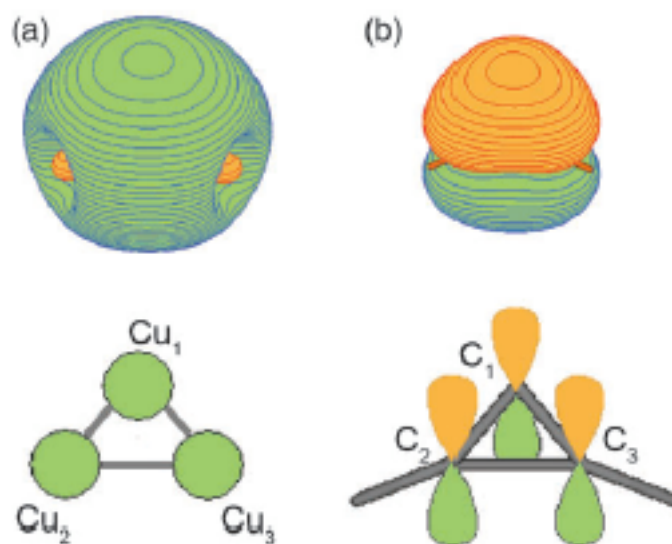


Figure 5-1. (a) The 3a<sub>1</sub>'-HOMO of Cu<sub>3</sub><sup>+</sup> and its schematic representation as a linear combination of 4s-AOs of Cu atoms, (b) 1a<sub>2</sub>''-HOMO of C<sub>3</sub>H<sub>3</sub><sup>+</sup> and its schematic representation as a linear combination of 2p<sub>z</sub>-AOs of C atoms.

clearly confirming the presence of  $\sigma$ -aromaticity in this cluster.<sup>53</sup> Yong et al.<sup>53</sup> also evaluated the resonance energy in the Cu<sub>3</sub><sup>+</sup> D<sub>3h</sub>, <sup>1</sup>A<sub>1</sub>' using the following equation:



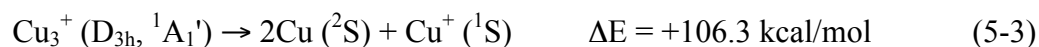
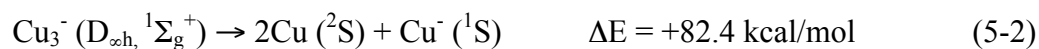
where Cu<sub>2</sub> and CuCl are reference classical molecules. According to their calculations, the energy of reaction (5-1), which is also the resonance energy for Cu<sub>3</sub><sup>+</sup>, is 36.8 kcal/mol (B3LYP/6-311+G(3df)). The calculated resonance energy is certainly very high compared to the Cu<sub>2</sub> dissociation energy (41.7 kcal/mol at the same level of theory). Thus, the use of the  $\sigma$ -aromaticity for the description of the Cu<sub>3</sub><sup>+</sup> cation is justified.



Apparently, the concept of  $\sigma$ -aromaticity based on the s-AOs should be applicable to  $\text{Ag}_3^+$  and  $\text{Au}_3^+$ , though in the last case the s-d hybridization may play a more significant role.

For  $\sigma$ -antiaromatic species (with  $ns$ -AOs participating in bonding) the counting rule is  $4n$  (singlet coupling). The  $\text{Cu}_3^-$  anion is a good example of  $\sigma$ -antiaromatic system with  $4\sigma$ -electrons. The electronic configuration for the singlet state of  $\text{Cu}_3^-$  at the  $D_{3h}$  symmetry is  $1a_1'^2 1e'^2$  (only bonding MOs are included), and the triangular structure with the singlet electronic state must undergo the Jahn-Teller distortion towards linear  $D_{\infty h}$  structure with a  $1\sigma_g^2 1\sigma_u^2$  valence electronic configuration.

Two  $\sigma$ -delocalized MOs can be approximately localized into two 2c-2e bonds and the linear structure of  $\text{Cu}_3^-$  can be formally considered as a classical structure. This situation is similar to the antiaromatic cyclobutadiene structure, which can be considered as having two double and two single carbon-carbon bonds, and thus can be described using single a Lewis structure. The antiaromaticity should manifest itself in the reduction of the stability of the molecule. Two reactions below show that the atomization energy of  $\text{Cu}_3^-$  (reaction 5-2, CCSD(T)/6-311+G(2df)//CCSD(T)6-311+G\*+ZPE/CCSD(T)/6-311+G\*) is indeed substantially lower than the atomization energy of  $\text{Cu}_3^+$  (reaction 5-3, CCSD(T)/6-311+G(2df)//CCSD(T)6-311+G\*+ZPE/CCSD(T)/6-311+G\*).



5-2.2. *s*-AO based  $\sigma$ -aromaticity in  $M_4^{2-}$  clusters

Initially aromaticity in the  $M_4^{2-}$  ( $M = \text{Cu, Ag, Au}$ ) dianions as parts of  $M_4\text{Li}_2$  ( $M = \text{Cu, Ag, Au}$ ) neutral species was studied by Wannere et al.<sup>59</sup> They found that the  $\text{Li}_2\text{M}_4$  species have distorted octahedral  $D_{4h}$ ,  $^1A_{1g}$  structures (Fig. 5-2) with the  $M_4^{2-}$  dianion forming a perfect square with two  $\text{Li}^+$  cations located above and below the square on the  $C_4$  axis. The significant charge transfer from Li to  $M_4$  was confirmed by the NPA charges. For example, in  $\text{Cu}_4\text{Li}_2$ , the NPA charge on Li is +0.8 |e|. These authors also reported the NICS values in the centers of  $\text{Cu}_4\text{Li}_2$  (-14.5 ppm),  $\text{Ag}_4\text{Li}_2$  (-14.1 ppm), and  $\text{Au}_4\text{Li}_2$  (-18.6 ppm) (all at PW91PW91/LANL2DZ) clusters which show the presence of aromaticity in the  $M_4^{2-}$  dianions. Wannere et al.<sup>59</sup> stated that the participation of p-orbitals in the bonding (and cyclic electron delocalization) in these clusters is negligible. Instead, these clusters benefit strongly from the delocalization of d and to some extent s orbitals. They also pointed out that d-orbital aromaticity of  $\text{Cu}_4\text{Li}_2$  is indicated by its high (243.2 kcal/mol) atomization energy.

Lin et al.<sup>60</sup> reported a joint photoelectron spectroscopy and theoretical study of  $\text{Cu}_4\text{Na}^-$ ,  $\text{Au}_4\text{Na}^-$  as well as theoretical results on  $\text{Cu}_4\text{Li}^-$ ,  $\text{Ag}_4\text{Li}^-$ ,  $\text{Ag}_4\text{Na}^-$ ,  $\text{Au}_4\text{Li}^-$ ,  $\text{Cu}_4\text{Li}_2$ ,  $\text{Ag}_4\text{Li}_2$ ,  $\text{Au}_4\text{Li}_2$ , and  $\text{Cu}_4^{2-}$ . They found that the  $\text{Cu}_4\text{Li}^-$ ,  $\text{Cu}_4\text{Na}^-$ ,  $\text{Ag}_4\text{Li}^-$ , and  $\text{Ag}_4\text{Na}^-$  anions have a pyramidal structure consistent with the bipyramidal structure reported by Wannere et al., while the  $\text{Au}_4\text{Li}^-$  and  $\text{Au}_4\text{Na}^-$  anions were found to be planar. The pyramidal structure of  $\text{Cu}_4\text{Na}^-$  with the  $\text{Na}^+$  cation located above the planar square  $\text{Cu}_4^{2-}$  dianion was confirmed by good agreement between theoretical and experimental VDEs for this system.

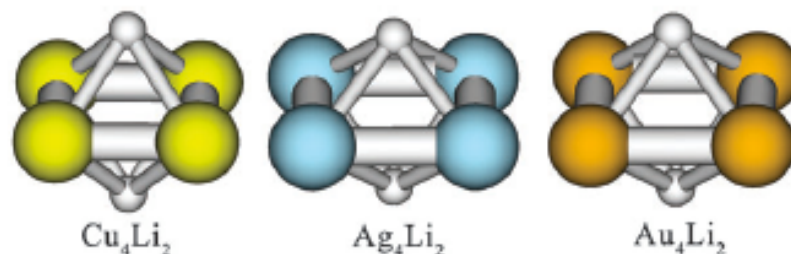


Figure 5-2. Optimized structures of  $\text{Cu}_4\text{Li}_2$ ,  $\text{Ag}_4\text{Li}_2$ , and  $\text{Au}_4\text{Li}_2$ .<sup>59</sup>

Using the Gauge-Including Magnetically Induced Current (GIMIC) method Lin et al.<sup>60</sup> concluded that strong ring currents are sustained mainly by the HOMO derived from the Cu 4s-AOs. Thus, the GIMIC calculations show that the  $\text{Cu}_4^{2-}$  ring is  $\sigma$ -aromatic due to 4s-AOs and that the d orbitals do not play any significant role for the electron delocalization effects. This study did not support the notion by Wannere et al.<sup>59</sup> that the square-planar  $\text{Cu}_4^{2-}$  is the first example of d-orbital aromatic molecules.

If bonding in the  $\text{Cu}_4^{2-}$  and  $\text{Ag}_4^{2-}$  rings is primarily due to  $\sigma$ -orbitals, then these systems are examples of systems with six valence  $\sigma$ -electrons and should be regarded as  $\sigma$ -aromatic according to the  $4n+2$  rule, similar to the  $\text{Li}_4^{2-}$ ,  $\text{Mg}_4^{2+}$  and  $\text{Li}_2\text{Mg}_2$  main group clusters with six bonding  $\sigma$ -electrons considered by Alexandrova and Boldyrev.<sup>67</sup>

### 5-2.3. *s*-AO based $\sigma$ -aromaticity in the $\text{Au}_5\text{Zn}^+$ cluster and $\text{Au}_6$

The  $\text{Au}_5\text{Zn}^+$  cation was found to be the most abundant cluster in the mass-spectrum of  $\text{Au}_n\text{Zn}^+$  ( $n = 2-44$ ) by Tanaka et al.<sup>58</sup> The authors performed MP2/Zn/6-311+G\*/Au/5s5p4d1f calculations and identified three lowest isomers I, II, and III for  $\text{Au}_5\text{Zn}^+$  (Fig. 5-3). For the two lowest isomers, Tanaka et al.<sup>58</sup> presented MO pictures

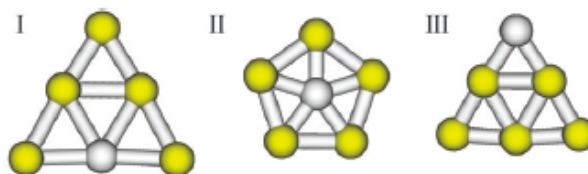


Figure 5-3. Three reported isomers of  $\text{Au}_5\text{Zn}^+$ .<sup>58</sup>

(Fig. 5-4) showing that six valence  $\sigma$ -electrons are delocalized over the whole cluster. The  $\text{Au}_5\text{Zn}^+$  cluster is isoelectronic to the  $\text{Au}_6$  cluster and its most stable structure is the same as the  $D_{3h}$  global minimum structure of  $\text{Au}_6$ , which possesses a large HOMO-LUMO gap and possesses a very stable electronic configuration.<sup>69,70</sup>

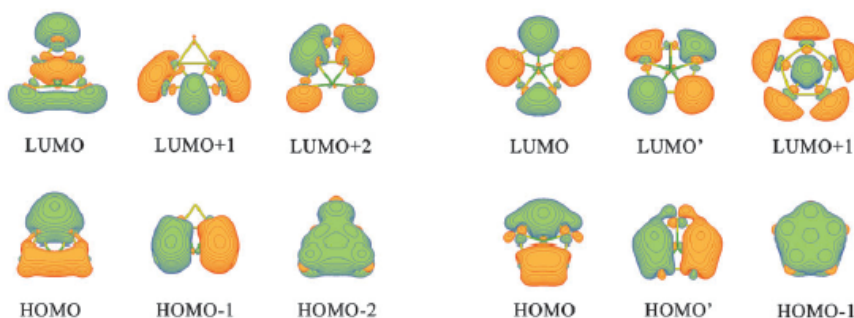


Figure. 5-4. Pictures of valence MOs of  $\text{Au}_5\text{Zn}^+$  isomers shown in Figure 5-3 a and b.

The MO pattern of  $\text{Au}_5\text{Zn}^+$  depicted in Fig. 5-4 resembles those of prototypical aromatic organic molecules  $\text{C}_6\text{H}_6$  and  $\text{C}_5\text{H}_5^-$ , except for their nodal properties in the molecular plane. The six delocalized electrons with the appropriate nodal pattern in  $\text{Au}_5\text{Zn}^+$  satisfies the  $4n+2$  rule for  $\sigma$ -aromaticity. Tanaka et al.<sup>58</sup> also performed NICS calculations for all three structures and concluded the negative NICS indexes are larger

than in the prototypical aromatic organic molecules  $C_6H_6$  and  $C_5H_5^-$ , confirming the presence of aromaticity in  $Au_5Zn^+$ . Overall the  $Au_5Zn^+$  cluster can be regarded as a  $\sigma$ -aromatic bimetallic cluster with six delocalized  $\sigma$ -electrons and that the enhanced stability of  $Au_5Zn^+$  may be ascribed to its aromaticity.

*5-2.4. s-AO based  $\sigma$ -aromaticity in the cyclo- $M_nH_n$  ( $M = Cu, Ag, Au$ ;  $n = 3-6$ ), cyclo- $Au_3L_nH_{3-n}$  ( $L = CH_3, NH_2, OH$ , and  $Cl$ ;  $n = 1-3$ ), cyclo- $Cu_nAg_{k-n}H_n$  ( $n = 1-k$ ,  $k = 3-5$ ) clusters*

Tsipis and Tsipis<sup>54</sup> performed B3LYP/6-311+G\* calculations on  $Cu_nH_n$  ( $n = 3-6$ ) cyclic species (Fig. 5) as models for the well documented cyclic organocopper (I) compounds, such as the square planar four-membered ring  $Cu_4R_4$  ( $R = CH_2SiMe_3$ ) with short Cu-Cu distances of 2.42 Å.<sup>71</sup> Tsipis and Tsipis<sup>54</sup> calculated also the 3D-structures for  $Cu_nH_n$  ( $n = 4-6$ ) and concluded that they are significantly less stable than the planar ones. In follow-up articles,<sup>55-57</sup> Tsipis and co-workers studied *cyclo- $M_nH_n$*  ( $M = Ag, Au$ ;  $n = 3-6$ ), *cyclo- $Au_3L_nH_{3-n}$*  ( $L = CH_3, NH_2, OH$ , and  $Cl$ ;  $n = 1-3$ ), *cyclo- $Cu_nAg_{3-n}H_n$*  ( $n = 1-3$ ), *cyclo- $Cu_nAg_{4-n}H_n$*  ( $n = 1-4$ ), and *cyclo- $Cu_nAg_{5-n}H_n$*  ( $n = 1-5$ ). The  $Cu_nH_n$  ( $n = 3-6$ ) cyclic species are discussed here and the other species are similar.

All  $Cu_nH_n$  ( $n = 3-6$ ) species were found to be cyclic with short Cu-Cu distances (between 2.404 Å in  $Cu_3H_3$  to 2.556 Å in  $Cu_6H_6$ ). The authors<sup>54</sup> stated that the equivalence of the Cu-Cu and Cu-H bonds in these species is indicative of the aromatic character of the cyclic hydrocoppers (I). In addition, they reported binding energies, NICS values and the electrophilicity index  $\omega$  (Table 5-2), which also support the aromatic nature of these species.

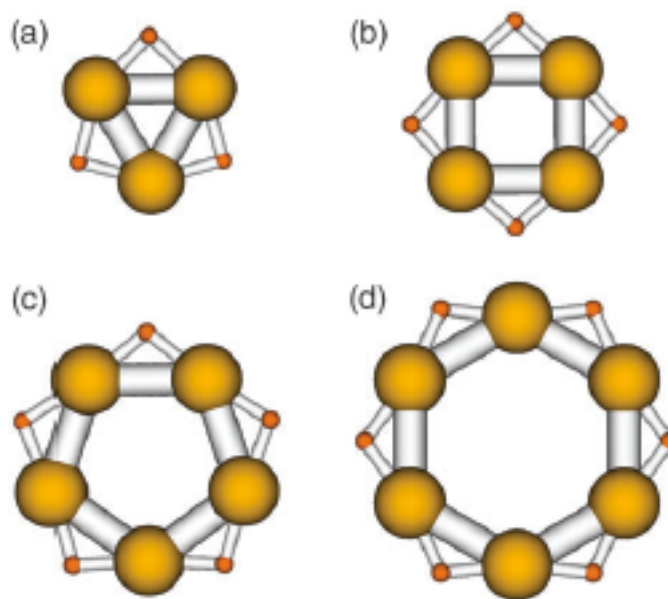


Fig. 5-5. Optimized planar cyclic structures of  $\text{Cu}_n\text{H}_n$  clusters.<sup>54</sup>

The authors<sup>21</sup> stated that all the metallocycles exhibit a composite bonding mode involving  $\sigma$ ,  $\pi$ , and  $\delta$  components on the basis of their analysis of occupied valence MOs. However, we found a rather different picture. We performed a NBO analysis of the representative  $\text{Cu}_4\text{H}_4$  ( $D_{4h}$ ,  $^1A_{1g}$ ) cluster at B3LYP/6-311++G\*\* level of theory. According to our NBO analysis the Cu atoms have  $4s^{0.56}3d^{9.91}4p^{0.02}$  valence atomic occupations and an effective atomic charge of +0.50 |e|, while the H atoms have  $1s^{1.49}$  atomic occupation and an effective atomic charge of -0.50 |e|. One can see that the 3d-AOs of Cu are almost completely occupied and thus do not significantly contribute to bonding. The bonding from completely delocalized  $\delta$ -HOMO-11,  $\pi$ -HOMO-17,  $\pi$ -HOMO-18,  $\sigma$ -HOMO-19 and  $\sigma$ -HOMO-20 (Fig. 5-6) will be offset by the effect of antibonding orbitals composed of d-AOs of Cu atoms. Thus, the net bonding effect from MOs composed of 3d-AOs cannot be significant. Rather, the bonding in the  $\text{Cu}_n\text{H}_n$  cyclic

clusters comes from an ionic contribution between  $H^{-0.501}$  and  $Cu^{+0.501}$  and from delocalized MOs composed out of 4s-AOs on Cu. In fact, NBO analysis in  $Cu_4H_4$  reveals one resonance structure (the same way as NBO produces some of the Kekule resonance structure for benzene) in which there are four Cu-H 2c-2e bonds composed of 1s-AOs of H and 4s-AOs of Cu with the occupation number 1.744 |e| alternated over the  $Cu_4H_4$  distorted planar octahedron. This confirms the aromatic nature of the  $Cu_nH_n$  clusters, but the aromaticity is due to delocalization of  $\sigma$ -bonds (composed of 1s-AOs of H and 4s-AOs of Cu) and not due to the delocalized  $\sigma$ -,  $\pi$ -, and  $\delta$ -MOs composed of 3d-AOs of Cu. Thus, aromaticity in the  $Cu_nH_n$  clusters is not  $\delta$  but rather  $\sigma$  in nature. Lin et al.,<sup>60</sup> however, reported that they did not find any strong magnetically induced ring current in  $Cu_4H_4$ . This might be a sign of the weak aromaticity in  $Cu_nH_n$  clusters. Due to relativistic effects, s-d hybridization started to play a bigger role in  $Ag_nH_n$  and  $Au_nH_n$  clusters, but additional research accounting for the relativistic effects should be performed before making any conclusions on the bonding nature in these clusters.

Table 5-2. Binding Energies  $\Delta E_1$  and  $\Delta E_2$ , GIAO-SCF NICS and Electrophilicity of  $Cu_nH_n$  ( $n = 3-6$ ).

Cluster	$\Delta E_1$ , <sup>a</sup> kcal/mol	$\Delta E_2$ , <sup>b</sup> kcal/mol	NICS, ppm	$\omega$ , eV
$Cu_3H_3$ , $D_{3h}$	81.5	260.9	-8.4	1.595
$Cu_4H_4$ , $D_{4h}$	137.0	376.1	-4.2	1.743
$Cu_5H_5$ , $D_{5h}$	180.1	479.0	-1.4	2.040
$Cu_6H_6$ , $D_{6h}$	217.5	576.2	-0.2	2.230

$$^a \Delta E_1 = E(CuH)_n - nE(CuH)$$

$$^b \Delta E_1 = E(CuH)_n - n[E(Cu) + E(H)].$$

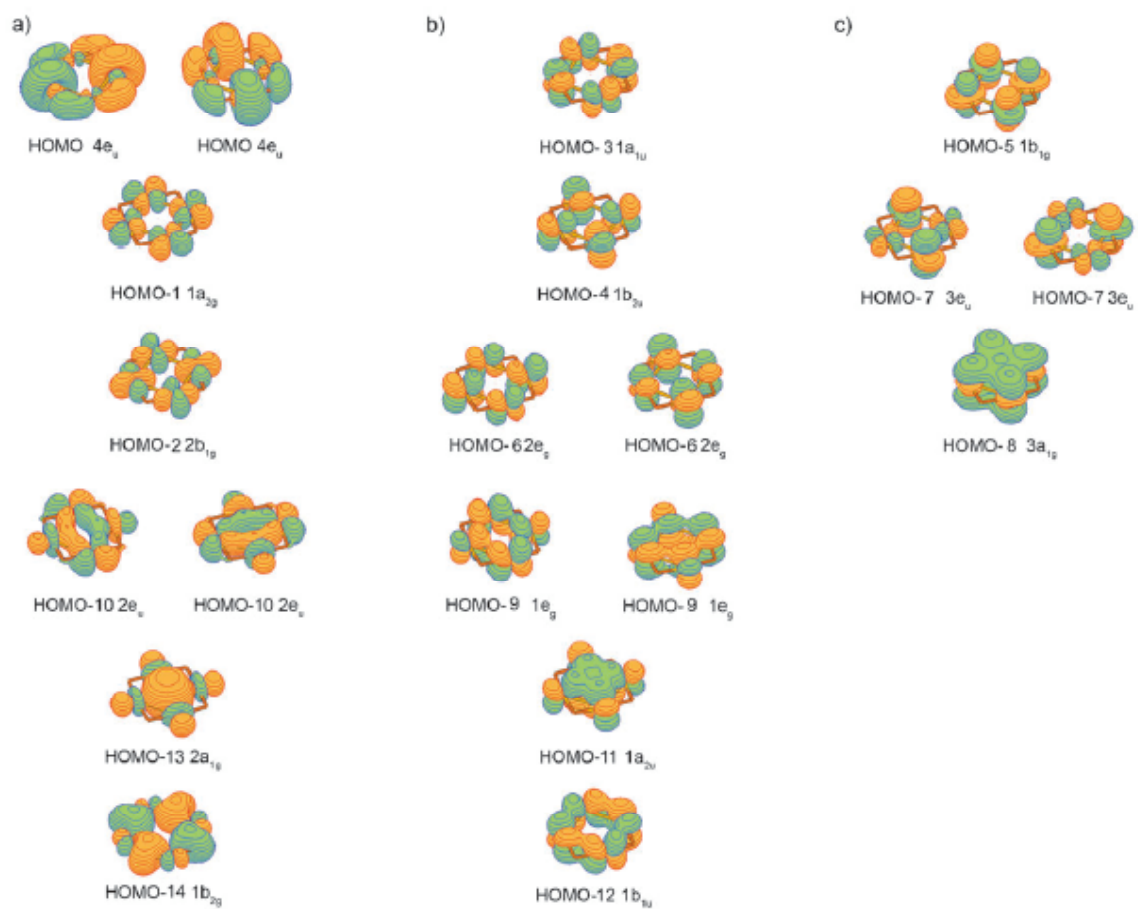


Figure 5-6. (a) s-MOs, (b) p-MOs, and (c) d-MOs composed out of d-AOs of Cu in  $\text{Cu}_4\text{H}_4$  ( $D_{4h}$ ,  $^1A_{1g}$ ).



### 5-3. p-AO based aromaticity and antiaromaticity in transition metal systems

Double aromaticity (simultaneous presence of  $\sigma$ - and  $\pi$ -aromaticity) was introduced in chemistry by Chandrasekhar et al. to explain the properties of the 3,5-dehydrophenyl cation.<sup>72</sup> Simultaneous presence of aromaticity and antiaromaticity was first used by Martin-Santamaria and Rzepa<sup>73</sup> to explain chemical bonding in small carbon rings. Präsang et al.<sup>74,75</sup> have shown that small carborane molecules containing 3- and 4-membered rings also exhibit both  $\sigma$  and  $\pi$  aromaticity. The  $\text{Hg}_4^{6-}$  cluster was the first transition metal system where double ( $\sigma$ - and  $\pi$ -) aromaticity due to p-AOs was discovered.<sup>73</sup>

#### 5-3.1. p-AO based multiple aromaticity in the $\text{Hg}_4^{6-}$ cluster

Mercury has a closed shell electron configuration ( $6s^2$ ) and therefore a neutral  $\text{Hg}_4$  cluster is expected to be a van der Waals complex. However, it was shown in the solid that one particular sodium-mercury amalgam  $\text{Na}_3\text{Hg}_2$  contains  $\text{Hg}_4^{6-}$  square units as its building blocks.<sup>61</sup> The high stability of the  $\text{Hg}_4^{6-}$  building block was explained once we recognized that it is isoelectronic to the first all-metal aromatic cluster,  $\text{Al}_4^{2-}$ .<sup>34</sup> Basically, the bonding in  $\text{Hg}_4^{6-}$  is due to Hg 6p-AO based MOs and the completely occupied Hg d-AOs do not contribute to bonding.<sup>61</sup> Fig. 5-7 displays the seven valence MOs of the square-planar  $\text{Hg}_4^{6-}$ , which are very similar to those in  $\text{Al}_4^{2-}$ .<sup>34</sup> The HOMO ( $1b_{2g}$ ), HOMO-1 ( $1a_{2u}$ ), and HOMO-2 ( $2a_{1g}$ ) are completely bonding orbitals formed from the Hg 6p-AOs and represent  $p_{\sigma-t}$ -MOs (tangential MO),  $p_{\pi}$ -MOs, and  $p_{\sigma-r}$ -MOs (radial MO), respectively. The remaining four MOs are bonding, non-bonding, and antibonding

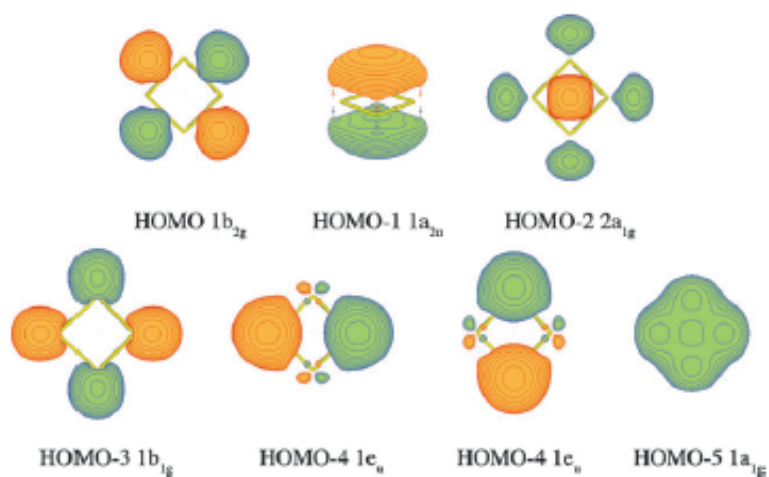


Figure 5-7. Valence molecular orbitals of  $\text{Hg}_4^{6-}$ .

orbitals formed primarily from the filled valence 6s orbitals of Hg and can be viewed as atomic  $6s^2$  lone pairs. Thus, the upper three MOs are mainly responsible for the chemical bonding in  $\text{Hg}_4^{6-}$ . If we split the  $\sigma$ - and  $\pi$ -orbitals into two separate sets, we can represent the MOs formed by the Hg 6p-AOs with the MO diagram shown in Fig. 5-8.

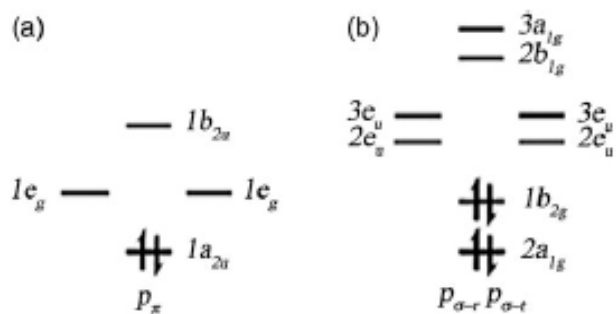


Figure 5-8. Molecular orbital diagram for a)  $\pi$ -MOs and b)  $\sigma$ -MOs for  $\text{Hg}_4^{6-}$ .

The lowest-lying  $\pi$ -MO and the two lowest-lying  $\sigma$ -MOs are completely bonding, whereas the highest-lying ones are completely antibonding. The two MOs in the  $\pi$ -set and the four MOs in the  $\sigma$ -set that are located in between the completely bonding and antibonding MOs are doubly degenerate with bonding/antibonding characters. The  $2e_u$ - and  $3e_u$ -MOs are composed of  $p_{\sigma-r}$  and  $p_{\sigma-t}$ -AOs. This is the reason why  $p_{\sigma-r}$  and  $p_{\sigma-t}$ -MOs are presented as one set in Fig. 5-8. On the basis of this mixing in the  $p_{\sigma-r}$  and  $p_{\sigma-t}$ -AOs the counting rule for  $\sigma$ -electrons for cyclic systems with even number of vertices should be  $4n+4/4n+6$  for aromaticity/antiaromaticity, but they are  $4n+2/4n$  for the cyclic systems with the odd number of vertices. On the basis of two distinct types of MOs, we can introduce one types of aromaticity:  $\pi$ -aromaticity based on the  $p_\pi$  MOs, and two types of  $\sigma$ -aromaticity based on the  $p_{\sigma-r}$  and  $p_{\sigma-t}$  MOs. The occupation of all three bonding MOs in  $\text{Hg}_4^{6-}$  makes its shape a perfect square and renders its doubly aromatic nature.

The finding of the double aromaticity in  $\text{Hg}_4^{6-}$  establishes a solid bridge between our gas-phase studies of multiply aromatic clusters and bulk materials containing such species. It is surprising that such an ancient material as amalgams can be rationalized on the basis of multiple aromaticity initially discovered in the gas phase studies of the  $\text{Al}_4^{2-}$  all-metal aromatic cluster,<sup>34,41,76,77</sup> produced in the form of  $\text{MAl}_4^-$  in the gas phase, where  $\text{M} = \text{Li}, \text{Na}, \text{Cu}$ .

*5-3.2. p-AO based multiple aromaticity in the  $\text{M}_3^{2-}$ ,  $\text{NaM}_3^-$ ,  $\text{Na}_2\text{M}_3$  ( $\text{M} = \text{Zn}, \text{Cd}, \text{Hg}$ ) clusters*

Yong and Chi<sup>62</sup> have recently shown using B3LYP, B3PW91, and CCSD(T) calculations that a series of  $\text{M}_3^{2-}$ ,  $\text{NaM}_3^-$ ,  $\text{Na}_2\text{M}_3$  ( $\text{M} = \text{Zn}, \text{Cd}, \text{Hg}$ ) clusters all have the

$M_3^{2-}$ ,  $D_{3h}$   $^1A_1'$  core, which is  $\pi$ -aromatic. Like in  $Hg_4^{6-}$ , neither 5d- nor 6s-AOs participate in the bonding in  $M_3^{2-}$ . Its bonding is due to the  $a_2''$ -HOMO, which is composed of the outer p-AOs of M. This is a completely bonding  $\pi$ -MO similar to the  $1a_2''$ -HOMO in the  $C_3H_3^+$  cation (Fig. 5-1b). Thus, in all the  $M_3^{2-}$ ,  $NaM_3^-$ ,  $Na_2M_3$  (M = Zn, Cd, Hg) systems bonding in the  $M_3^{2-}$  core is due to  $\pi$ -aromaticity only, without the formation of a  $\sigma$ -framework. Similar bonding pattern was previously reported for  $Mg_3^{2-}$ ,  $NaMg_3^-$  and  $Na_2Mg_3$  systems by Kuznetsov and Boldyrev.<sup>78</sup> Yong and Chi<sup>62</sup> also calculated a sizable resonance energy of 24.8 kcal/mol ( $Zn_3^{2-}$ ), 12.9 kcal/mol ( $Cd_3^{2-}$ ), and 12.1 kcal/mol ( $Hg_3^{2-}$ ) (either at CCSD(T)/6-311+G\* or CCSD(T)/LANL2DZ), as well as large negative values of NICS: -24.86 ppm ( $Zn_3^{2-}$ ), -19.59 ppm ( $Cd_3^{2-}$ ), and -15.40 ppm ( $Hg_3^{2-}$ ), further confirming their  $\pi$ -aromaticity

#### 5-4. d-AO based aromaticity and antiaromaticity in transition metal systems

Due to the more complicated nodal structure of d-AOs that can form  $\delta$ -bond in addition to  $\sigma$  and  $\pi$  bonds, transition-metal systems can provide a more diverse array of aromaticity-antiaromaticity combinations. We may expect  $\sigma$ -tangential ( $\sigma_t$ ),  $\sigma$ -radial ( $\sigma_r$ ),  $\pi$ -tangential ( $\pi_t$ ),  $\pi$ -radial ( $\pi_r$ ), and  $\delta$ -MOs. For  $\sigma$ - and  $\pi$ -MOs, the counting rules are  $4n+4$  (aromaticity) and  $4n+6$  (antiaromaticity) for cyclic structures with even number of atoms and  $4n+2$  (aromaticity) and  $4n$  (antiaromaticity) for cyclic structures with odd number of atoms. For  $\delta$ -MOs the counting rule is  $4n+2/4n$  for aromaticity/antiaromaticity. In general, there can be multiple ( $\sigma$ -,  $\pi$ -, and  $\delta$ -) aromaticity, multiple ( $\sigma$ -,  $\pi$ -, and  $\delta$ -) antiaromaticity, and conflicting aromaticity (simultaneous

aromaticity and antiaromaticity among the three types of  $\sigma$ ,  $\pi$ , and  $\delta$  MOs). So far only few transition metal systems with d-AO based aromaticity have been reported.<sup>63-66</sup>

#### 5-4.1. d-AO based $\sigma$ -aromaticity in the $\text{Mo}_3\text{O}_9^{2-}$ and $\text{W}_3\text{O}_9^{2-}$ clusters

The first cases of d-orbital aromaticity in 4d and 5d transition metal oxide clusters,  $\text{Mo}_3\text{O}_9^-$  and  $\text{W}_3\text{O}_9^-$ , were reported by Huang *et al.* by combining photoelectron spectroscopy and theoretical calculations.<sup>64</sup> They found that the  $\text{M}_3\text{O}_9$ ,  $\text{M}_3\text{O}_9^-$ , and  $\text{M}_3\text{O}_9^{2-}$  (M = Mo, W) clusters all have  $D_{3h}$  structures and each metal atom is bonded to two bridged O atoms and two terminal O atoms (Fig. 5-9).

The attachment of the first and second electrons to the  $\text{M}_3\text{O}_9$  species reduces the M-M distance significantly (0.25 Å for  $\text{Mo}_3\text{O}_9^-$  and 0.29 Å for  $\text{W}_3\text{O}_9^-$ ) and (0.20 Å for  $\text{Mo}_3\text{O}_9^{2-}$  and 0.19 Å for  $\text{W}_3\text{O}_9^{2-}$ ). The large geometry changes induced by addition of one or two electrons to the  $\text{M}_3\text{O}_9$  species agree with the nature of the HOMO in the singly  $\text{M}_3\text{O}_9^-$  and doubly  $\text{M}_3\text{O}_9^{2-}$  charged anions (Fig. 5-10).

The completely bonding nature of the  $\sigma$ -HOMO in  $\text{M}_3\text{O}_9^-$  and  $\text{M}_3\text{O}_9^{2-}$  species renders their  $\sigma$ -aromaticity. Calculations of NICS at the center of  $\text{Mo}_3\text{O}_9^{2-}$  (-21.5 ppm) and  $\text{W}_3\text{O}_9^{2-}$  (-20.5 ppm) also support the presence of aromaticity. Huang *et al.*<sup>64</sup> also estimated a sizable (7.6 kcal/mol) resonance energy for  $\text{W}_3\text{O}_9^-$ . These results provide solid evidence that the anionic  $\text{Mo}_3\text{O}_9^-$ ,  $\text{W}_3\text{O}_9^-$ ,  $\text{Mo}_3\text{O}_9^{2-}$  and  $\text{W}_3\text{O}_9^{2-}$  species with the  $D_{3h}$  ( $^2A_1'$  or  $^1A_1'$ ) structure are the first experimentally-confirmed d-orbital aromatic ( $\sigma$ ) species.

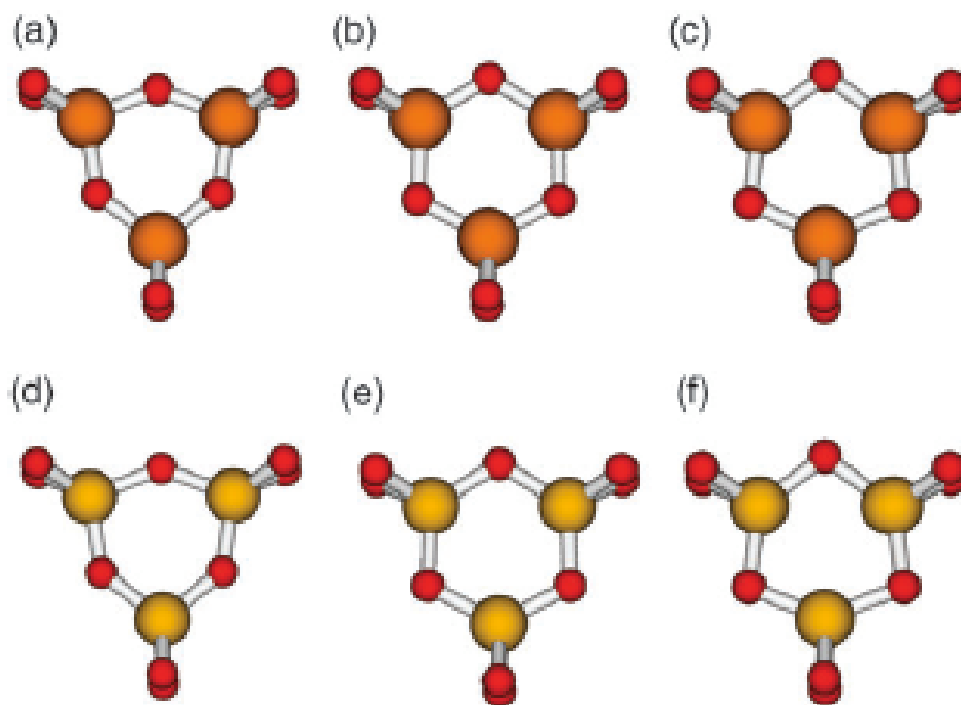


Figure 5-9. Optimized structures for  $M_3O_9$  (a, d)  $M_3O_9^-$  (b, e) and  $M_3O_9^{2-}$  (c, f) ( $M = Mo, W$ ) clusters.<sup>64</sup>

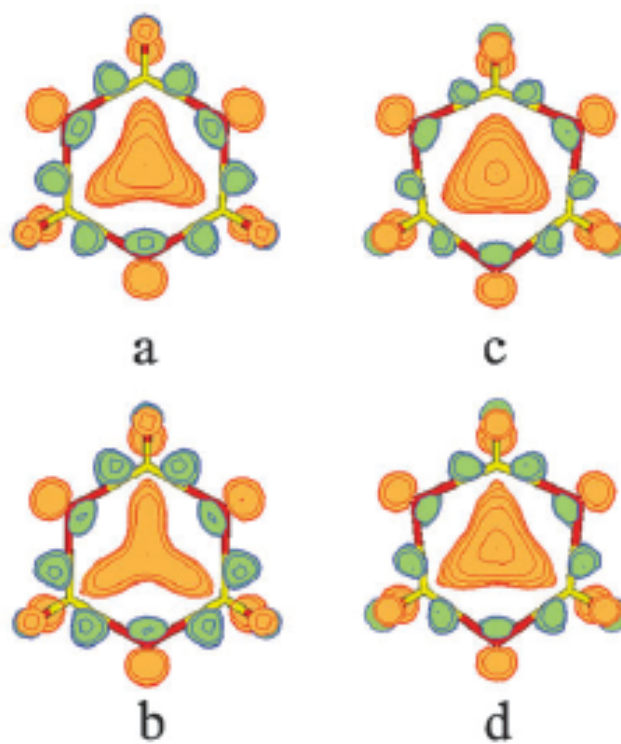


Figure 5-10. HOMOs in the  $M_3O_9^-$  and  $M_3O_9^{2-}$  species (M = Mo and W).<sup>64</sup>

5-4.2. *d*-AO based  $\sigma$ - and  $\pi$ - double aromaticity in  $X_3^-$  ( $X = \text{Sc}, \text{Y}, \text{La}$ ) clusters

The first systems with double ( $\sigma$ - and  $\pi$ -) aromaticity have been recently reported by Chi and Liu.<sup>63</sup> They demonstrated using B3LYP, B3PW91, MP2 and CCSD(T) levels of theory with 6-311+G\* basis sets for Sc and LANL2DZ basis sets with relativistic effective core potentials for Y and La, that the  $D_{3h}$  ( $^1A_1'$ ) structures are the global minimum structures for  $X_3^-$  ( $X = \text{Sc}, \text{Y}, \text{La}$ ). All three species have the same valence electronic configuration  $1a_1'^2 1e'^4 1a_2''^2 2a_1'^2$ , though the order of the MOs varies (Fig. 5-11). Here the  $1a_1'$ - and  $1e'$ -MOs are formed by the *ns*-AOs and do not contribute to bonding significantly, because all the bonding and antibonding MOs composed of the *ns*-AOs are occupied and the bonding effect from the  $1a_1'$ -MO is compensated by the antibonding effect from the  $1e'$ -MOs. Valence  $1a_2''$ - and  $2a_1'$ -MOs are responsible for bonding in the  $X_3^-$  anions. The  $1a_2''$ -MO is a completely bonding  $\pi$ -MO and it renders  $\pi$ -aromaticity. The  $2a_1'$ -MO is a completely bonding  $\sigma$ -MO and it renders  $\sigma$ -aromaticity in  $X_3^-$ . Thus all three anions are *d*-orbital doubly ( $\sigma$ - and  $\pi$ -) aromatic systems. Chi and Liu<sup>63</sup> also reported large negative NICS values for all three anions, thus supporting the presence of aromaticity in  $\text{Sc}_3^-$ ,  $\text{Y}_3^-$ , and  $\text{La}_3^-$ .

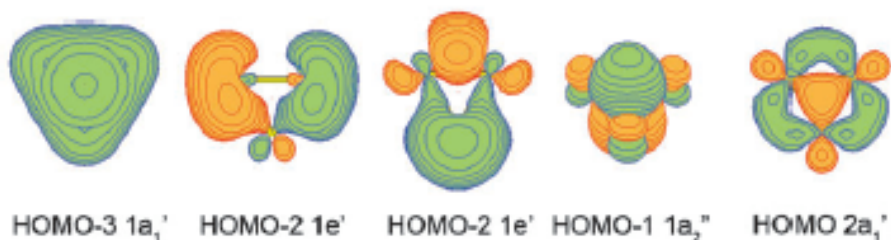


Figure 5-11. Valence MOs of  $X_3^-$  ( $X = \text{Sc}, \text{Y}, \text{La}$ ) anions.



### 5-4.3. *d*-AO based $\pi$ - and $\delta$ -double aromaticity in the $Ta_3O_3^-$ cluster

It was shown by Zhai et al.<sup>65</sup> using photoelectron spectroscopy and theoretical calculations that the  $Ta_3O_3^-$  cluster possesses a global minimum with a perfect  $D_{3h}$  ( $^1A_1'$ ) planar triangular structure (Fig. 5-12a).

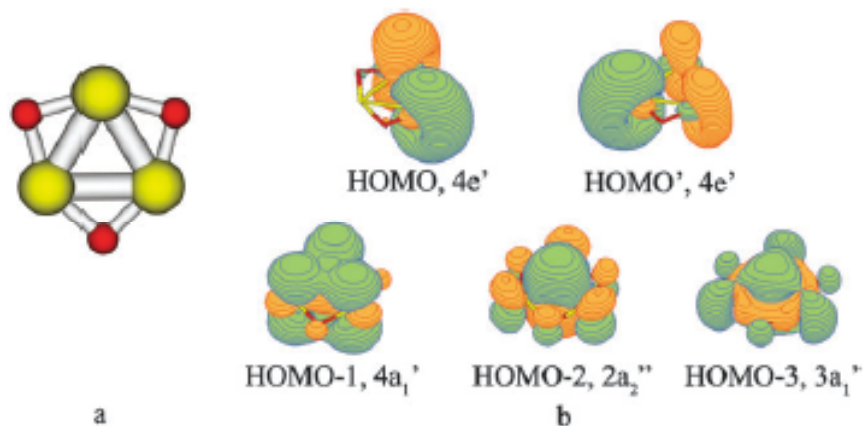


Figure 5-12. Optimized structure (a) and valence MOs (b) of  $Ta_3O_3^-$ .<sup>65</sup>

The structure and bonding in  $Ta_3O_3^-$  can be understood by analyzing their molecular orbitals (Fig. 5-12b). Out of 34 valence electrons in  $Ta_3O_3^-$ , 24 belong to either pure oxygen lone pairs or those polarized towards Ta (responsible for the covalent contributions to Ta-O bonding). The other ten valence electrons are responsible for the direct metal-metal bonding, as shown in Fig. 5-12b. Among the five upper MOs, three MOs are of  $\sigma$ -type: the partially bonding/antibonding doubly degenerate  $4e'$  HOMO and the completely bonding  $3a_1'$  HOMO-3. The antibonding nature of the completely occupied doubly degenerate HOMO significantly reduces the bonding contribution of completely bonding HOMO-3 to the  $\sigma$ -bonding in the  $Ta_3$  framework. If the HOMO

( $4e'$ ) and the HOMO-3 ( $3a_1'$ ) were composed of the same s-d hybrid functions, bonding due to these MOs would be completely canceled. However, the hybridization in the  $4e'$  and  $3a_1'$  orbitals is somewhat different. Therefore, there should remain some  $\sigma$ -aromatic bonding in  $Ta_3O_3^-$ . In the  $Ta_3O_3^-$  anion, the HOMO-2 ( $2a_2''$ ) is a completely bonding  $\pi$  orbital composed primarily out of the 5d orbitals of Ta, giving rise to  $\pi$ -aromatic character according to the  $(4n + 2)$  Hückel rule for  $\pi$ -aromaticity for ring molecules with odd numbers of atoms in the ring. Here, we apply the  $(4n + 2)$  counting rule (odd number of atoms in the metal cycle) separately for each type of aromaticity encountered in a particular planar system, i. e. separately for  $\sigma$ -,  $\pi$ -, and  $\delta$ -type molecular orbitals.

The HOMO-1 ( $4a_1'$ ), which is a completely bonding orbital mainly coming from the overlap of the  $d_z^2$  orbital on each Ta atom is in fact a  $\delta$ -aromatic orbital. This orbital has the “appearance” of a  $\pi$  orbital with major overlaps above and below the molecular plane, but it is not a  $\pi$ -type MO because it is symmetric with respect to the molecular plane. This MO possesses two nodal surfaces perpendicular to the molecular  $C_3$  axis, and thus it is a  $\delta$  orbital (see detailed discussion in ref. 65). Therefore, the  $Ta_3O_3^-$  cluster possesses an unprecedented multiple ( $\delta$  and  $\pi$ ) aromaticity, which is responsible for the metal-metal bonding and the perfect triangular  $Ta_3$  framework. The energy ordering of  $\sigma$  (HOMO-3)  $<$   $\pi$  (HOMO-2)  $<$   $\delta$  (HOMO-1)<sup>65</sup> molecular orbitals indicates that the strength of the metal-metal bonding increases from  $\delta$  to  $\pi$  to  $\sigma$ , in agreement with the intuitive expectation that  $\sigma$ -type overlap is greater than  $\pi$ -type overlap, and  $\delta$ -type overlap is expected to be the weakest.

#### 5-4.4. *d*-AO based $\sigma$ -, $\pi$ - and $\delta$ - triple aromaticity in the $\text{Hf}_3$ cluster

Averkiev and Boldyrev<sup>66</sup> theoretically predicted that the  $\text{Hf}_3$  cluster in the  $D_{3h}$ ,  $^1A_1'$  ( $1a_1'$ ,  $2a_1'$ ,  $2e'$ ,  $4a_2''$ ,  $2a_1''$ ) state possesses triple ( $\sigma$ -,  $\pi$ -, and  $\delta$ -) aromaticity. The valence  $1a_1'$ - and  $1e'$ -MOs are primarily composed out of 6s-AOs of Hf and as in  $\text{Ta}_3\text{O}_3^-$  do not contribute to bonding significantly (Fig. 5-13).

Six d-electrons populate completely bonding delocalized  $\sigma$ -MO ( $2a_1'$ ),  $\pi$ -MO ( $1a_2''$ ), and  $\delta$ -MO ( $3a_1'$ ) (Fig. 5-13b). The former three MOs render  $\sigma$ -,  $\pi$ -, and  $\delta$ -aromaticity just like the completely bonding  $\pi$ -delocalized MO in  $\text{C}_3\text{H}_3^+$  renders  $\pi$ -aromaticity in  $\text{C}_3\text{H}_3^+$ . Thus the  $\text{Hf}_3$  cluster in the  $D_{3h}$ ,  $^1A_1'$  state represents the first example of a chemical system with the triple aromaticity.

### 5-5. Summary and overview

The goal of this review is to demonstrate that the concepts of aromaticity and antiaromaticity, initially introduced in organic chemistry, can and should be applied to the description of chemical bonding in transition metal systems. At the present, systems containing transition metal clusters are being actively studied both experimentally and theoretically in chemistry and biochemistry. Apparently there is a need for convenient tools that connect electronic structure with molecular properties of such systems. We have shown that aromaticity and antiaromaticity are indeed useful tools for explaining and understanding chemical bonding in transition metal systems. Aromaticity and antiaromaticity have been established in the gas phase  $\text{Cu}_3^+$  and  $\text{Cu}_3^-$  clusters. The aromaticity in  $\text{Cu}_3^+$  helped to explain its high symmetry ( $D_{3h}$ ) structure,

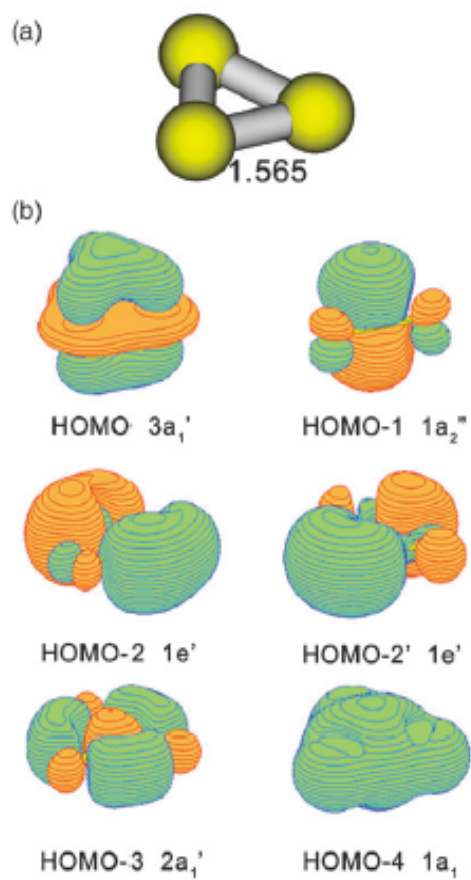


Figure 5-13. Optimized structure (a) and valence MOs (b) of the  $\text{Hf}_3$  cluster in the  $D_{3h}$ ,  $^1A_1'$  state.

high atomization and resonance energies, and high negative value of NICS. The aniaromaticity of  $\text{Cu}_3^-$  helped to explain its linear structure and low atomization energy.

Similarly, aromaticity in *cyclo*- $\text{Cu}_n\text{H}_n$  ( $n = 3-6$ ), *cyclo*- $\text{M}_n\text{H}_n$  ( $\text{M} = \text{Ag}, \text{Au}; n=3-6$ ), *cyclo*- $\text{Au}_3\text{L}_n\text{H}_{3-n}$  ( $\text{L} = \text{CH}_3, \text{NH}_2, \text{OH}, \text{and Cl}; n = 1-3$ ), *cyclo*- $\text{Cu}_n\text{Ag}_{3-n}\text{H}_n$  ( $n = 1-3$ ), *cyclo*- $\text{Cu}_n\text{Ag}_{4-n}\text{H}_n$  ( $n = 1-4$ ), and *cyclo*- $\text{Cu}_n\text{Ag}_{5-n}\text{H}_n$  ( $n = 1-5$ ) helped explain the planar cyclic structure of these species, high binding energies, and negative NICS. Also, aromaticity in these model systems was used to rationalize the planar cyclic organocopper (I) compounds in condensed phase. The recognition of aromaticity in the gas phase  $\text{Au}_5\text{Zn}^+$  cluster helped to understand high abundance observed in the mass spectrum. The presence of aromaticity in gas phase clusters  $\text{M}_4\text{Li}_2$  ( $\text{M} = \text{Cu}, \text{Ag}, \text{Au}$ ),  $\text{M}_4\text{L}_2$  and  $\text{M}_4\text{L}^-$  ( $\text{M} = \text{Cu}, \text{Ag}, \text{Au}; \text{L}=\text{Li}, \text{Na}$ ) allowed us to understand the planar square structure of  $\text{Cu}_4^{2-}$  and  $\text{Ag}_4^{2-}$  structural units. The presence of double ( $\sigma$ - and  $\pi$ -) aromaticity in the  $\text{Hg}_4^{6-}$  building block of  $\text{Na}_3\text{Hg}_2$  amalgam explains the planar square structure as well as stability of it in the stabilizing external field of  $\text{Na}^+$  cations.  $\pi$ -Aromaticity in  $\text{M}_3^{2-}$ ,  $\text{NaM}_3$ ,  $\text{Na}_2\text{M}_3$  ( $\text{M} = \text{Zn}, \text{Cd}, \text{Hg}$ ) is responsible for their stability. Double ( $\sigma$ - and  $\pi$ -) aromaticity in gas phase  $\text{M}_3^-$  ( $\text{M} = \text{Sc}, \text{Y}, \text{La}$ ) clusters is responsible for their high symmetry ( $\text{D}_{3h}$ ) structure, high atomization and resonance energies, and high negative value of NICS.

True d-orbital aromaticity was first observed in  $\text{M}_3\text{O}_9^-$  and  $\text{M}_3\text{O}_9^{2-}$  ( $\text{M} = \text{W}, \text{Mo}$ ) metal oxide clusters. The presence of  $\sigma$ -aromaticity in these anions is responsible for their high symmetry ( $\text{D}_{3h}$ ) structure, appreciable resonance energies, and high negative value of NICS. The high symmetry ( $\text{D}_{3h}$ ) of  $\text{Ta}_3\text{O}_3^-$  and high first VDE could be explained on the basis of the presence of double ( $\pi$ - and  $\delta$ -) aromaticity. This oxide cluster is the first example of  $\delta$ -aromaticity in a transition metal system. Finally, the  $\text{Hf}_3$

cluster in the  $D_{3h}$   ${}^1A_1'$  ( $1a_1'$ ,  ${}^22a_1'$ ,  ${}^21e'$ ,  ${}^41a_2''$ ,  ${}^23a_1''$ ) state is the first example of triple ( $\sigma$ -,  $\pi$ -, and  $\delta$ -) aromaticity.

It is clear that aromaticity and antiaromaticity could be very useful concepts in explaining structure, stability and other molecular properties of isolated and embedded clusters of transition metals and transition metal oxide clusters. The chemical bonding in transition metal clusters can come from s-AOs, p-AOs, and d-AOs, and can be expressed as a variety of multiple aromaticities and antiaromaticities as well as of conflicting aromaticities. We believe that transition metal systems with triple antiaromaticity and all types of conflicting aromaticity outlined in the introduction should all exist and should represent a research frontier. Furthermore, atomic f-AOs in lanthanide and actinide clusters offer additional possibility to form  $\phi$ -bonds and thus could lead to systems with even richer variety of  $\phi$ -aromaticity/antiaromaticity. Such systems have not yet been reported and may suggest new research opportunities both computationally and experimentally.

The counting rules for s-AO based  $\sigma$ -aromaticity are the same as the Huckel  $4n+2/4n$  rules for aromaticity/antiaromaticity for all cyclic structures. The counting rules for p-AO based  $\sigma$ -aromaticity are  $4n+4$  (aromaticity) and  $4n+6$  (antiaromaticity) for cyclic structures with even number of atoms and  $4n+2$  (aromaticity) and  $4n$  (antiaromaticity) for cyclic structures with odd number of atoms, because there are two types of  $\sigma$ -orbitals:  $p_{\sigma_r}$ - and  $p_{\sigma_t}$ -MOs which should be considered together. In the simplest case of the occupation of just one  $p_{\sigma_r}$ - and one  $p_{\sigma_t}$ -MO the system is also aromatic. For p-AO based  $\pi$ -aromaticity the counting rule are  $4n+2/4n$  for aromaticity/antiaromaticity for all cyclic structures. For d-AO based  $\sigma$ - and  $\pi$ -

aromaticity the counting rules are  $4n+4$  (aromaticity) and  $4n+6$  (antiaromaticity) for cyclic structures with even number of atoms and  $4n+2$  (aromaticity) and  $4n$  (antiaromaticity) for cyclic structures with odd number of atoms, because there are two types of  $\sigma$ -orbitals:  $d_{\sigma-r}$ - and  $d_{\sigma-t}$ -MOs and two types of p-orbitals:  $d_{\pi-r}$ - and  $d_{\pi-t}$ -MOs. For d-AO based  $\delta$ -aromaticity the counting rule is  $4n+2/4n$  for aromaticity/antiaromaticity, respectively

It is hoped that the introduction of the concepts of aromaticity and antiaromaticity will stimulate theoretical analysis of chemical bonding in other known or unknown chemical compounds containing transition metal atoms and clusters in both inorganic compounds and metallo-biomolecules. Such analysis may establish simple and robust rules connecting electronic and molecular structures with stability and reactivity. It may be possible that aromaticity and antiaromaticity may become as useful concepts in deciphering the chemical bonding in transition metal systems as in organic chemistry.

## References

1. D. L. Thorn, R. Hoffmann, *Nouv. J. Chim.* 1979, **3**, 39.
2. G. P. Elliot, W. R. Roper, J. M. Waters, *J. Chem. Soc. Chem. Commun.* 1982, 811.
3. J. R. Bleeker, Y.-F. Xie, W.-J. Peng, M. Chiang, *J. Am. Chem. Soc.* 1989, **111**, 4118.
4. J. R. Bleeker, R. Behm, Y.-F. Xie, T. W. Clayton, Jr., K. D. Robinson, *J. Am. Chem. Soc.* 1994, **116**, 4093.
5. J. R. Bleeker, R. Behm, Y.-F. Xie, M. Y. Chiang, K. D. Robinson, A. M. Beatty, *Organometallics* 1997, **16**, 606.
6. R. D. Profilet, P. E. Fanwick, I. P. Rothwell, *Angew. Chem., Int. Ed.* 1992, **31**, 1261.

7. P. N. Riley, R. D. Profilet, M. M. Salberg, P. E. Fanwick, I. P. Rothwell, *Polyhedron* 1998, **17**, 773.
8. J. R. Blecke, *Chem. Rev.* 2001, **101**, 1205.
9. G. He, H. Xia, G. Jia, *Chin. Sci. Bull.* 2004, **49**, 1543.
10. L. J. Wright, *Dalton Trans.* 2006, 1821.
11. W. C. Landorf, M. M. Haley, *Angew. Chem. Int. Ed.* 2006, **45**, 3914.
12. I. Fernandez, G. Frenking, *Chem. Eur. J.* 2007, **13**, 5873.
13. Minkin, V. I.; Glukhovtsev, M. N.; Simkin, B. Ya. *Aromaticity and Antiaromaticity. Electronic and Structural Aspects*; Wiley & Sons, New York, 1994.
14. R. G. Harvey, *Polycyclic Aromatic Hydrocarbons*, Wiley-VCH, New York, 1997.
15. I. Gutman, S. J. Cyvin, *Introduction to the Theory of Benzenoid Hydrocarbons*; Springer-Verlag, Berlin, 1989.
16. D. Lloyd, *The Chemistry of Conjugate Cyclic Compounds*. Wiley & Sons, Chichester, 1989.
17. S. J. Cyvin, I. Gutman, I. *Kekule Structures in Benzenoid Hydrocarbons*, Springer-Verlag, Berlin, 1988.
18. J. R. Dias, *Handbook of Polycyclic Hydrocarbons. Part A. Benzenoid Hydrocarbons*; Elsevier, Amsterdam, 1987.
19. P. J. Garrat, *Aromaticity*, Wiley & Sons, New York, 1986.
20. D. Lewis, D. Peters, *Facts and Theories of Aromaticity*; Macmillan, London, 1975.
21. E. Clar, *The Aromatic Sextet*; Wiley & Sons, London, 1972.



22. Special edition on delocalization pi and sigma. P. v. R. Schleyer ed. 2005, **105**, No. 10.
23. Special edition on aromaticity. P. v. R. Schleyer, ed. *Chem. Rev.* 2001, **101**, No. 5.
24. Special edition on heterocycles. A. Katritzky, ed. *Chem. Rev.* 2004, **104**, No. 5.
25. M. Randic, *Chem. Rev.* 2003, **103**, 3449.
26. S. Shaik, A. Shurki, D. Danovich, P. C. Hiberty, *J. Mol. Struct. (Theochem)* 1997, **155**, 398.
27. P. v. R. Schleyer, H. Jiao, *Pure & Appl. Chem.* 1996, **38**, 209.
28. J.-I. Aihara, *Pure Appl. Chem.* 1982, **54**, 1115.
29. A. T. Balaban, *Pure Appl. Chem.* 1980, **52**, 1409.
30. 4<sup>th</sup> *Int. Symp. Chem. of Novel Aromatic Compounds*, Jerusalem, 1981; Agranat, I., Ed.; *Pure Appl. Chem.* 1982, **54**, 927.
31. *Int. Symp. Aromaticity*, Dubrovnik, 1979; Graovac, A., Trinajstic, N. Eds.; *Pure Appl. Chem.* 1980, **52**, 1397.
32. E. D. Bergman, B. Pullman (Eds), *Aromaticity, Pseudoaromaticity, Antiaromaticity* (Israel Academy of Science and Humanities, Jerusalem, 1971).
33. T. M. Krygowski, M. K. Cyranski, Z. Czarnocki, G. Häfelfinger, G. A. R. Katritzky, *Tetrahedron* 2000, **56**, 1783.
34. X. Li, A. E. Kuznetsov, H. F. Zhang, A. I. Boldyrev, L. S. Wang, *Science*, 2001, **291**, 859.

35. A. E. Kuznetsov, K. A. Birch, A. I. Boldyrev, X. Li, H.-J. Zhai, L. S. Wang, *Science*, 2003, **300**, 622.
36. A. I. Boldyrev, L. S. Wang, *Chem. Rev.* 2005, **106**, 3716.
37. C. A. Tsipis, *Coord. Chem. Rev.* 2005, **249**, 2740.
38. A. N. Alexandrova, A. I. Boldyrev, H.-J. Zhai, L. S. Wang, *Coord. Chem. Rev.* 2006, **250**, 2811.
39. D. Yu. Zubarev, A. I. Boldyrev, *J. Comput. Chem.* 2007, **28**, 251.
40. A. I. Boldyrev, A. E. Kuznetsov, *Inorg. Chem.* 2002, **41**, 532.
41. C.-G. Zhan, F. Zheng, D. A. Dixon, *J. Am. Chem. Soc.* 2002, **124**, 14795.
42. J. Juselius, M. Straka, D. Sundholm, *J. Phys. Chem. A*, 2001, **105**, 9939.
43. P. W. Fowler, R. W. A. Havenith, E. Steiner, *Chem. Phys. Lett.* 2001, **342**, 85.
44. P. W. Fowler, R. W. A. Havenith, E. Steiner, *Chem. Phys. Lett.* 2002, **359**, 530.
45. Z. Chen, C. Corminboeuf, T. Heine, J. Bohmann, P. v. R. Schleyer, *J. Am. Chem. Soc.* 2003, **125**, 13930.
46. P. v. R. Schleyer, C. Maerker, A. Dransfeld, H. Jiao, N. J. v. E. Hommes, *J. Am. Chem. Soc.* 1996, **118**, 6317.
47. J. C. Santos, J. Andres, A. Aizman, P. Fuentealba, *J. Chem. Theory Comput.* 2005, **1**, 83.
48. S. K. Ritter, *Chem. & Eng. News*, 2003, **81**, 23.
49. Y.-C. Lin, J. Juselius, D. Sundholm, J. Gauss, *J. Chem. Phys.* 2005, **122**, 214308.
50. R. Islas, T. Heine, G. Merino, *J. Chem. Theory Comput.* 2007, **3**, 775.
51. R. W. A. Havenith, P. W. Fowler, E. Steiner, S. Shetty, D. Kanhere, S. Pal, *Phys. Chem. Chem. Phys.* 2004, **6**, 285.

52. A. Datta, S. S. Mallajosyula, S. K. Pati, *Acc. Chem. Res.* 2007, **40**, 213.
53. L. Yong, S. D. Wu, X. X. Chi, *Int. J. Quant. Chem.* 2007, **107**, 722.
54. A. C. Tsipis, C. A. Tsipis, *J. Am. Chem. Soc.* 2003, **125**, 1136.
55. C. A. Tsipis, E. E. Karagiannis, P. F. Kladou, A. C. Tsipis, *J. Am. Chem. Soc.* 2004, **126**, 12916.
56. A. C. Tsipis, C. A. Tsipis, *J. Am. Chem. Soc.* 2005, **127**, 10623.
57. A. C. Tsipis, A. V. Stalikas, *New. J. Chem.* 2007, **31**, 852.
58. H. Tanaka, S. Neukermans, E. Janssens, R. E. Silverans, P. Lievens, *J. Am. Chem. Soc.* 2003, **125**, 2862.
59. C. S. Wannere, C. Corminboeuf, Z.-X. Wang, M. D. Wodrich, R. B. King, P. v. R. Schleyer, *J. Am. Chem. Soc.* 2005, **127**, 5701.
- 60 Y.-C. Lin, D. Sundholm, J. Juselius, L.-F. Cui, X. Li, H. J. Zhai, L. S. Wang, *J. Phys. Chem. A*, 2006, **110**, 4244.
61. A. E. Kuznetsov, J. D. Corbett, L.-S. Wang, A. I. Boldyrev, *Angew. Chem. Int. Ed.* 2001, **40**, 3369.
62. L. Yong, C. Chi, *J. Mol. Struct. THEOCHEM*, 2007, 818, 93.
63. X. X. Chi, Y. Liu, *Int. J. Quant. Chem.* 2007, **107**, 1886.
64. X. Huang, H. J. Zhai, B. Kiran, L. S. Wang, *Angew. Chem. Int. Ed.* 2005, **44**, 7251.
65. H. J. Zhai, B. B. Averkiev, D. Yu. Zubarev, L. S. Wang, A. I. Boldyrev, *Angew. Chem. Int. Ed.* 2007, **46**, 4277.
66. B. B. Averkiev, A. I. Boldyrev, in press.
67. A. N. Alexandrova, A. I. Boldyrev, *J. Phys. Chem. A*, 2003, **107**, 554.

68. R. W. A. Havenith, F. De Proft, P. W. Fowler, P. Geerlings, *Chem. Phys. Lett.* 2004, **407**, 391.
69. H. Häkkinen, B. Yoon, U. Landman, X. Li, H. J. Zhai, and L. S. Wang, *J. Phys. Chem. A* 2003, **107**, 6168.
70. H. J. Zhai, B. Kiran, B. Dai, J. Li, and L. S. Wang, *J. Am. Chem. Soc.* 2005, **127**, 12098.
71. J. A. J. Jarvis, B. T. Kilbourn, R. Pearce, M. F. Lappert, *J. Chem. Soc., Chem. Commun.* 1973, 475.
72. J. Chandrasekhar, E. D. Jemmis, P. v. R. Schleyer, *Tetrahedron Lett.* 1979, **39**, 3707.
73. S. Martin-Santamaria, H. S. Rzepa, *Chem. Commun.* 2000, **16**, 1503.
74. C. Präsang, A. Młodzianowska, Y. Sahin, M. Hofmann, G. Geiseler, W. Massa, A. Berndt, *Angew. Chem. Int. Ed.* 2002, **41**, 3380.
75. C. Präsang, A. Młodzianowska, G. Geiseler, W. Massa, M. Hofmann, A. Berndt, *Pure Appl. Chem.* 2003, **75**, 1175.
76. A. E. Kuznetsov, A. I. Boldyrev, X. Li, L. S. Wang, *J. Am. Chem. Soc.*, 2001, **123**, 8825.
77. A. I. Boldyrev, A. E. Kuznetsov, *Inorg. Chem.* 2002, **41**, 532.
78. A. E. Kuznetsov, A. I. Boldyrev, *Chem. Phys. Lett.* 2004, **388**, 452.

## CHAPTER 6

 $\delta$ -AROMATICITY IN  $[\text{Ta}_3\text{O}_3]^{-1}$ **Abstract**

The concept of aromaticity was introduced into organic chemistry to describe delocalized p bonding in planar, cyclic, and conjugate molecules possessing  $(4n+2)$  p electrons.<sup>[1]</sup> In recent years, this concept has been advanced into main-group molecules including organometallic compounds with cyclic cores of metal atoms<sup>[2]</sup> and, in particular, all-metal clusters.<sup>[3]</sup> It has been shown that main-group clusters may exhibit multiple aromaticity ( $\sigma$  and  $\pi$ ), multiple antiaromaticity ( $\sigma$  and  $\pi$ ), and conflicting aromaticity ( $\sigma$  aromaticity and  $\pi$  antiaromaticity or  $\sigma$  antiaromaticity and  $\pi$  aromaticity).<sup>[4-6]</sup> Here, we report experimental and theoretical evidence of  $\delta$  aromaticity, which is only possible in transition-metal systems. It is discovered in the  $[\text{Ta}_3\text{O}_3]^-$  cluster through combined photoelectron spectroscopy and ab initio studies. Well-resolved low-lying electronic transitions are observed in the photoelectron spectra of  $[\text{Ta}_3\text{O}_3]^-$  and are compared with ab initio calculations, which show that the  $[\text{Ta}_3\text{O}_3]^-$  cluster has a planar  $D_{3h}$  triangular structure. Chemical-bonding analyses reveal that among the five valence molecular orbitals involved in the multicenter metal–metal bonding, there is a completely bonding  $\delta$  and  $\pi$  orbital formed from the 5d atomic orbitals of Ta. The totally delocalized multicenter  $\delta$  bond renders  $\delta$  aromaticity for  $[\text{Ta}_3\text{O}_3]^-$  and represents a new mode of chemical bonding.  $[\text{Ta}_3\text{O}_3]^-$  is the first  $\delta$ -aromatic molecule confirmed experimentally

---

<sup>1</sup> Coauthored by Hua-Jin Zhai, Boris B. Averkiev, Dmitry Yu. Zubarev, Lai-Sheng Wang and Alexander I. Boldyrev. Reproduced with permission from *Angew. Chem. Int. Ed.* **2007**, 46, 4277-4280. Copyright Wiley – VCH Verlag GmbH & Co. KGaA.

and theoretically, which suggests that  $\delta$  aromaticity may exist in many multinuclear, low oxidation- state transition-metal compounds.

### 6-1. Introduction

In 1964, Cotton and co-workers published a milestone work on  $\text{K}_2[\text{Re}_2\text{Cl}_8]\cdot 2\text{H}_2\text{O}$ ,<sup>[7]</sup> in which they showed the presence of a new type of chemical bond—a  $\delta$  bond between the two Re atoms. Since then, a branch of inorganic chemistry has been developed that involves multiple metal–metal bonding<sup>[8]</sup> with bond orders higher than three, the maximum allowed for main-group systems. Power and co-workers recently reported the synthesis of a  $\text{Cr}_2$  compound with a quintuple bond ( $\sigma^2\pi^4\delta^4$ ) between the two Cr atoms.<sup>[9]</sup> This work, along with recent quantum chemical studies of multiple bonds in  $\text{U}_2$  and  $[\text{Re}_2\text{Cl}_8]^{2-}$ ,<sup>[10]</sup> has generated renewed interest in multiple metal–metal bonding.<sup>[11–13]</sup> The presence of  $\delta$  bonds between two transition-metal atoms suggests that multicenter transition-metal species with a completely delocalized cyclic  $\delta$  bond may exist, thus raising the possibility of  $\delta$  aromaticity analogous to  $\pi$  or  $\sigma$  aromaticity in main-group systems. We have been interested in understanding the electronic structure and chemical bonding of early transition-metal oxide clusters as a function of size and composition, and in using them as potential molecular models for oxide catalysts<sup>[14–16]</sup> During our investigation of tantalum oxide clusters, we found the presence of  $\delta$  aromaticity in the  $[\text{Ta}_3\text{O}_3]^-$  cluster, in which each Ta atom is in a low oxidation state of  $\text{Ta}^{\text{II}}$  and still possesses three electrons for Ta–Ta bonding.

## 6-2. Experimental Method

The experiment was conducted by using a magnetic bottle-type photoelectron spectroscopy apparatus equipped with a laser vaporization cluster source.<sup>[17]</sup>  $[\text{Ta}_m\text{O}_n]^-$  clusters with various compositions were produced by laser vaporization of a pure tantalum disk target in the presence of a helium carrier gas seeded with  $\text{O}_2$ , and were size-separated by time-of-flight mass spectrometry. The  $[\text{Ta}_3\text{O}_3]^-$  species was mass-selected and decelerated before photodetachment by a pulsed laser beam. Photoelectron spectra were obtained at two relatively high photon energies, 193 nm (6.424 eV) and 157 nm (7.866 eV), to guarantee access to all valence electronic transitions (Figure 6-1).

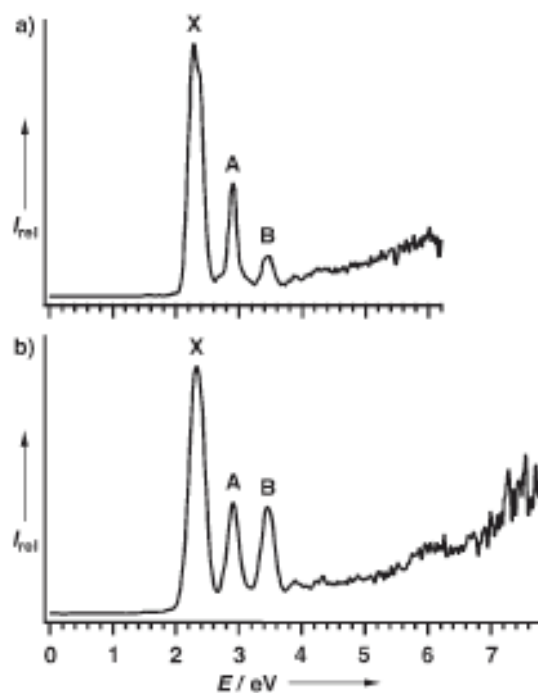


Figure 6-1. Photoelectron spectra of  $[\text{Ta}_3\text{O}_3]^-$ . a) 193 nm (6.424 eV); b) 157 nm (7.866 eV).

Three well-resolved bands (X, A, and B) were observed at the lower-binding-energy side. The X band is much more intense and shows a discernible splitting at 193 nm (Figure 6-1a). Surprisingly, no well-defined electronic transitions were observed beyond 3.7 eV, where continuous signals were present, probably as a result of multielectron transitions. The vertical detachment energies (VDEs) of the observed transitions at the low-binding energy side are given in Table 6-1, where they are compared with theoretical calculations by two different methods.

Table 6-1. Experimental VDEs [eV] for  $[\text{Ta}_3\text{O}_3]^-$  compared with those calculated for the  $D_{3h}$  global minimum.

VDE (exp.)	Final state and configuration	VDE (B3LYP) <sup>[a]</sup>	VDE (B3PW91) <sup>[a]</sup>
X $2.25 \pm 0.03$ <sup>[b]</sup>	${}^2E'$ ( $3a_1'^2 2a_2''^2 4a_1'^2 4e'^3$ )	2.27	2.25
A $2.89 \pm 0.02$	${}^2A_1'$ ( $3a_1'^2 2a_2''^2 4a_1'^1 4e'^4$ )	2.93	2.96
B $3.44 \pm 0.03$	${}^2A_2''$ ( $3a_1'^2 2a_2''^1 4a_1'^2 4e'^4$ )	3.27	3.36

[a] Using the Ta/Stuttgart+2f1g/O/aug-cc-pvTZ basis set. [b] The adiabatic electron-detachment energy was measured to be  $(2.22 \pm 0.03)$  eV.

### 6-3. Theoretical Methods

We initially performed an extensive search for the  $[\text{Ta}_3\text{O}_3]^-$  global minimum for the singlet, triplet, and quintet states at the B3LYP/LANL2DZ level of theory, and then recalculated the global minimum structure and the three lowest isomers at three other levels of theory.



#### 6-4. Results and Discussion

We found that the  $[\text{Ta}_3\text{O}_3]^-$  global minimum has a perfect  $D_{3h}$  ( $^1A_1'$ ) planar triangular structure I (Figure 6-2). The closest isomer II is 6.6 (B3LYP/Ta/Stuttgart+2f1g/O/aug-cc-pvTZ) and 1.7 kcal mol<sup>-1</sup> (B3PW91/Ta/Stuttgart+2f1g/O/aug-cc-pvTZ) higher in energy than the  $D_{3h}$  ground state. The theoretical VDEs of the global minimum at the two highest levels of theory are compared with the experimental data in Table 6-1. One can see that the calculated VDEs for the global minimum structure I agree well with the experimental results, whereas those for the three low-lying isomers (see the Supporting Information) are completely off, thus lending considerable credence to the theoretical methods and the  $D_{3h}$  structure for  $[\text{Ta}_3\text{O}_3]^-$ . The highest occupied molecular orbital (HOMO,  $4e'$ ) of the  $D_{3h}$   $[\text{Ta}_3\text{O}_3]^-$  is doubly degenerate, consistent with the intense X band observed experimentally. The splitting of the X band could be a consequence of either a Jahn–Teller effect or spin–orbit coupling.

To help understand the structure and bonding in  $[\text{Ta}_3\text{O}_3]^-$  we performed a detailed molecular orbital (MO) analysis. Out of the 34 valence electrons in  $[\text{Ta}_3\text{O}_3]^-$ , 24 belong to either pure oxygen lone pairs or those polarized towards Ta (responsible for the covalent contributions to Ta–O bonding). The remaining ten valence electrons are primarily Ta-based and are involved in direct metal–metal bonding (Figure 6-3). Among the five MOs, three are responsible for s bonding of the triangular  $\text{Ta}_3$  framework. They include the partially bonding/antibonding doubly degenerate  $4e'$  HOMO and the completely bonding  $3a_1'$  HOMO-3. The antibonding nature of the HOMO significantly reduces the s-bonding contribution to the  $\text{Ta}_3$  framework.<sup>[18]</sup> In the  $[\text{Ta}_3\text{O}_3]^-$  anion, the HOMO-2 ( $2a_2''$ ) is a completely bonding p orbital composed primarily of the 5d orbitals of Ta, thus giving

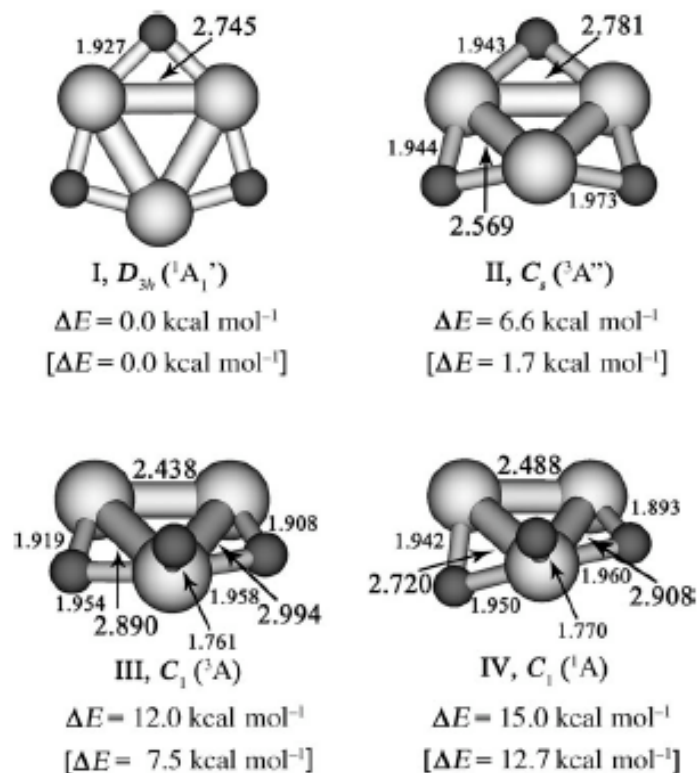


Figure 6-2. Optimized structures for the global minimum of  $[\text{Ta}_3\text{O}_3]^-$  ( $D_{3h}$ ,  $^1A_1'$ ) and selected low-lying isomers. The relative energies  $\Delta E_{\text{total}}[\text{kcal mol}^{-1}]$  and interatomic distances [ $\text{\AA}$ ] were calculated at the B3LYP/Ta/Stuttgart+2f1g/O/aug-cc-pvTZ level of theory ( $\Delta E_{\text{total}}$  at the B3PW91/Ta/Stuttgart+2f1g/O/aug-cc-pvTZ level is shown in brackets).

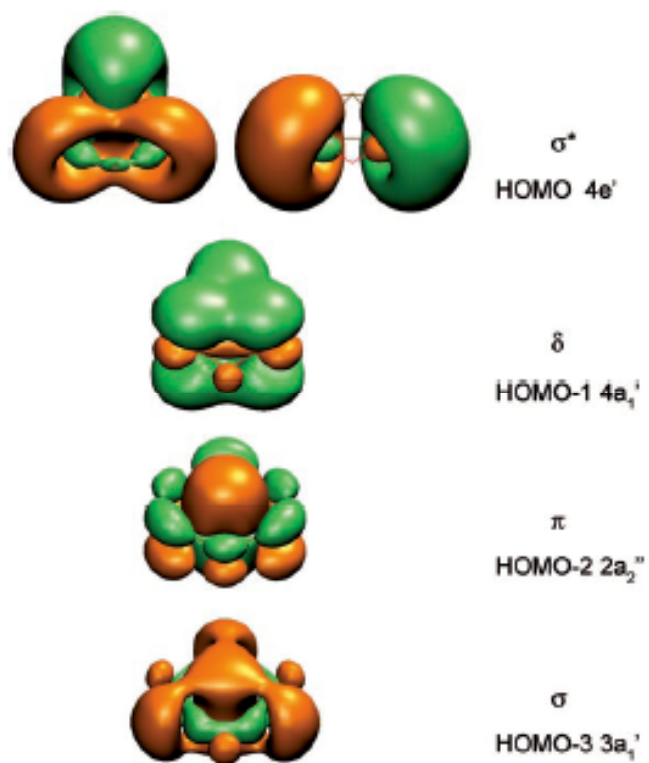


Figure 6-3. The five valence MOs responsible for the metal–metal bonding in  $[\text{Ta}_3\text{O}_3]^{3-}$  ( $D_{3h}$ ,  $^1A_1'$ ).

rise to  $\pi$ -aromatic character according to the  $(4n+2)$  Huckel rule for  $\pi$  aromaticity.<sup>[19]</sup> The most interesting MO is HOMO-1 ( $4a_1'$ ), which is a completely bonding orbital that comes mainly from the overlap of the  $d_{z^2}$  orbital on each Ta atom. This orbital has the “appearance” of a  $\pi$  orbital with major overlaps above and below the molecular plane, but it is not a  $\pi$ -type MO because it is symmetric with respect to the molecular plane. However, perpendicular to the molecular C3 axis this MO has two nodal surfaces, and thus it is a  $\delta$  orbital.<sup>[20]</sup> In fact, a similar  $\delta$ -bonding MO exists in the recently synthesized quintuple-bond  $Cr_2$  complex,<sup>[9]</sup> in which it is a two-center bond formed from a  $d_{z^2}$  orbital on each Cr atom.<sup>[13]</sup> Analogous to the circularly delocalized  $\pi$  MO over three carbon atoms, which renders  $[C_3H_3]^+$   $\pi$ -aromatic,<sup>[6]</sup> the circular delocalization and the bonding nature of the  $4a_1'$  MO give rise to  $\delta$  aromaticity in  $[Ta_3O_3]^-$ , which is also consistent with the  $(4n+2)$  Huckel rule.<sup>[19]</sup> In the  $[Ta_3O_3]^-$  cluster, the  $\delta$  MO is a three-center bond, but similar types of MOs are possible in planar tetraatomic, pentaatomic, or larger transition-metal systems. Therefore, the  $[Ta_3O_3]^-$  cluster exhibits an unprecedented multiple ( $\delta$  and  $\pi$ ) aromaticity, which is responsible for the metal–metal bonding and the perfect triangular  $Ta_3$  framework. The stability of the  $Ta_3$  triangular kernel can be seen in all the low-lying isomers of  $[Ta_3O_3]^-$  (Figure 6-2), which differ only in the coordination of the oxygen atoms to the aromatic  $Ta_3$  framework. Notably, the energy ordering of  $\sigma$  (HOMO-3) <  $\pi$  (HOMO-2) <  $\delta$  (HOMO-1) (Table 6-1 and Figure 6-3) indicates that the strength of the metal–metal bonding increases from  $\delta$  to  $\pi$  to  $\sigma$ , in agreement with the intuitive expectation that  $\sigma$ -type overlap is greater than  $\pi$ -type overlap, and that  $\delta$ -type overlap is the weakest, as is also the case in the multiple bonding of diatomic transition-

metal compounds including the classical  $[\text{Re}_2\text{Cl}_8]^{2-}$ .<sup>[7–13]</sup> Despite the expected weaker overlap in the  $\delta$  MO, it makes important contributions to the overall metal–metal bonding, as shown in the quintuple bonds in the new  $\text{Cr}_2$  complex<sup>[9, 11–13]</sup> or in the  $\text{U}_2$  dimer.<sup>[10]</sup> The three-center delocalization in the aromatic  $\delta$  MO in  $[\text{Ta}_3\text{O}_3]^-$  is expected to provide even more bonding contributions than in the cases of the metal dimers, even though it is difficult to quantify them. The three-center delocalization in the aromatic  $[\text{W}_3\text{O}_9]^{2-}$  ion that results from a d–d  $\sigma$  bond was estimated previously to provide about 1 eV additional resonance energy, similar to that estimated for benzene.<sup>[21]</sup>

## 6-5. Conclusion

Aromaticity in transition-metal systems has been discussed in the literature,<sup>[4, 5, 21–30]</sup> particularly since the discovery of aromaticity in all-metal clusters.<sup>[3]</sup> King<sup>[22]</sup> and Li<sup>[23]</sup> have considered aromaticity in transition-metal oxides as a result of metal–metal interactions through M–O–M bridges. The  $[\text{Hg}_4]^{6-}$  cluster, which is a building block of the  $[\text{Na}_3\text{Hg}_2]$  amalgam, has been shown by Kuznetsov et al.<sup>[24]</sup> to be aromatic and similar to the all-metal  $[\text{Al}_4]^{2-}$  unit.<sup>[3]</sup> Tsipis et al.<sup>[25, 26]</sup> explained the planar structure of cyclic coinage metal hydrides on the basis of their aromatic character. Aromaticity in square-planar coinage-metal clusters was discussed by Wannere et al.<sup>[27]</sup> and Lin et al.,<sup>[28]</sup> and Alexandrova et al.<sup>[29]</sup> suggested the presence of aromaticity in the  $[\text{Cu}_3\text{C}_4]^-$  cluster. Datta et al.<sup>[30]</sup> used d-orbital aromaticity to explain the metal-ring structure in tiara nickel thiolates. Recently, Huang et al.<sup>[21]</sup> demonstrated the presence of d-orbital aromaticity in the 4d and 5d transition-metal-oxide clusters  $[\text{Mo}_3\text{O}_9]^{2-}$  and  $[\text{W}_3\text{O}_9]^{2-}$ . The claim of d-orbital aromaticity in the square-planar coinage-metal clusters<sup>[27]</sup> was questioned by Lin

et al.,<sup>[28]</sup> who showed that the completely filled d orbitals do not play any significant role in the bonding in these clusters. Instead, aromaticity in these systems comes primarily from  $\sigma$ -bonding interactions of the valence s electrons. Thus, today the  $[\text{Mo}_3\text{O}_9]^{2-}$  and  $[\text{W}_3\text{O}_9]^{2-}$  clusters are the only examples in which aromaticity comes from d-bonding interactions, albeit with s character.<sup>[21]</sup>

In the  $[\text{Ta}_3\text{O}_3]^-$  cluster, we have found two new types of d-bonding interactions that lead to  $\pi$  and  $\delta$  aromaticity. The  $\delta$  aromaticity in this cluster is a new mode of chemical bonding that can only occur in multinuclear transition-metal systems. The current finding suggests that  $\delta$  aromaticity may exist in many cyclic transition-metal systems containing metal atoms in low oxidation states. The next challenge is to find  $\phi$  aromaticity, which may occur in multinuclear and cyclic f-metal systems.

## References

- [1] V. I. Minkin, M. N. Glukhovtsev, B. Ya. Simkin, *Aromaticity and Antiaromaticity*, Wiley, New York, **1994**; see also special issues: *Chem. Rev.* **2001**, 101(5) and *Chem. Rev.* **2005**, 105(10).
- [2] G. H. Robinson, *Acc. Chem. Res.* **1999**, 32, 773.
- [3] X. Li, A. E. Kuznetsov, H. F. Zhang, A. I. Boldyrev, L. S. Wang, *Science* **2001**, 291, 859.
- [4] A. I. Boldyrev, L. S. Wang, *Chem. Rev.* **2005**, 105, 3716, and references therein.
- [5] C. A. Tsipis, *Coord. Chem. Rev.* **2005**, 249, 2740.
- [6] M. Hofmann, A. Berndt, *Heteroat. Chem.* **2006**, 17, 224.

- [7] F. A. Cotton, N. F. Curtis, C. B. Harris, B. F. G. Johnson, S. J. Lippard, J. T. Mague, W. R. Robinson, J. S. Wood, *Science* **1964**, *145*, 1305.
- [8] F. A. Cotton, C. A. Murillo, R. A. Walton, *Multiple Bonds Between Metal Atoms*, 3rd ed., Springer, New York, **2005**.
- [9] T. Nguyen, A. D. Sutton, M. Brynda, J. C. Fettinger, G. J. Long, P. P. Power, *Science* **2005**, *310*, 844.
- [10] a) L. Gagliardi, O. B. Roos, *Nature* **2005**, *433*, 848; b) L. Gagliardi, O. B. Roos, *Inorg. Chem.* **2003**, *42*, 1599; c) K. Saito, Y. Nakao, H. Sato, S. Sakaki, *J. Phys. Chem. A* **2006**, *110*, 9710.
- [11] G. Frenking, *Science* **2005**, *310*, 796.
- [12] U. Radius, F. Breher, *Angew. Chem.* **2006**, *118*, 3072; *Angew. Chem. Int. Ed.* **2006**, *45*, 3006.
- [13] M. Brynda, L. Gagliardi, P.-O. Widmark, P. P. Power, B. O. Roos, *Angew. Chem.* **2006**, *118*, 3888; *Angew. Chem. Int. Ed.* **2006**, *45*, 3804.
- [14] H. J. Zhai, B. Kiran, L. F. Cui, X. Li, D. A. Dixon, L. S. Wang, *J. Am. Chem. Soc.* **2004**, *126*, 16134.
- [15] X. Huang, H. J. Zhai, J. Li, L. S. Wang, *J. Phys. Chem. A* **2006**, *110*, 85.
- [16] X. Huang, H. J. Zhai, T. Waters, J. Li, L. S. Wang, *Angew. Chem.* **2006**, *118*, 673; *Angew. Chem. Int. Ed.* **2006**, *45*, 657.
- [17] L. S. Wang, H. Wu in *Advances in Metal and Semiconductor Clusters. IV. Cluster Materials* (Ed.: M. A. Duncan), JAI, Greenwich, CT, **1998**, pp. 299 – 343.
- [18] If the HOMO ( $4e'$ ) and the HOMO-3 ( $3a_1'$ ) were composed of the same s-d hybrid functions they would cancel each other, thus resulting in negligible metal-

metal  $\sigma$  bonding. However, the hybridization in the  $4e'$  and  $3a_1'$  orbitals is somewhat different. Therefore, we cannot rule out some s-bonding contribution in the  $Ta_3$  framework; that is, there should be some  $\sigma$ -aromatic character in  $[Ta_3O_3]^-$ .

- [19] In the case of multiple aromaticity, the  $(4n+2)$  counting rule should be applied separately for each type of aromaticity encountered in a particular planar system, that is, separately for  $\sigma$ -,  $\pi$ -,  $d$ -, and  $\phi$ -type MOs.<sup>[4]</sup>
- [20] Strictly speaking, the  $\sigma$ ,  $\pi$ ,  $\delta$ , and  $\phi$  notations for MOs are only appropriate for linear systems, where they are irreducible representations of the  $C_{\infty v}$  and  $D_{\infty h}$  point groups. However, it is customary in chemistry to use  $p$  notation in planar molecules for MOs that are formed by the  $p_z$  atomic orbitals and are perpendicular to the molecular plane, even though they do not belong to the  $\pi$ -irreducible representation. For example, the orbitals responsible for the aromaticity in the prototypical aromatic molecule  $C_6H_6$  are called  $\pi$  orbitals. Following this tradition, one can introduce  $\delta$ - or  $\phi$ -type MOs in planar molecules formed from appropriate atomic orbitals.
- [21] X. Huang, H. J. Zhai, B. Kiran, L. S. Wang, *Angew. Chem.* **2005**, *117*, 7417; *Angew. Chem. Int. Ed.* **2005**, *44*, 7251.
- [22] R. B. King, *Inorg. Chem.* **1991**, *30*, 4437.
- [23] J. Li, *J. Cluster Sci.* **2002**, *13*, 137.
- [24] A. E. Kuznetsov, J. D. Corbett, L. S. Wang, A. I. Boldyrev, *Angew. Chem.* **2001**, *113*, 3473; *Angew. Chem. Int. Ed.* **2001**, *40*, 3369.
- [25] A. C. Tsipis, C. A. Tsipis, *J. Am. Chem. Soc.* **2003**, *125*, 1136.
- [26] C. A. Tsipis, E. E. Karagiannis, P. F. Kladou, A. C. Tsipis, *J. Am. Chem. Soc.*



- 2004**, *126*, 12916.
- [27] C. S. Wannere, C. Corminboeuf, Z.-X. Wang, M. D. Wodrich, R. B. King, P. von R. Schleyer, *J. Am. Chem. Soc.* **2005**, *127*, 5701.
- [28] Y.-C. Lin, D. Sundholm, J. Juselius, L. F. Cui, H. J. Zhai, L. S. Wang, *J. Phys. Chem. A* **2006**, *110*, 4244.
- [29] A. N. Alexandrova, A. I. Boldyrev, H. J. Zhai, L. S. Wang, *J. Phys. Chem. A* **2005**, *109*, 562.
- [30] A. Datta, N. S. John, G. U. Kulkarni, S. K. Pati, *J. Phys. Chem. A* **2005**, *109*, 11647.

## CHAPTER 7

## OBSERVATION OF TRIATOMIC SPECIES WITH CONFLICTING

AROMATICITY:  $\text{AlSi}_2^-$  AND  $\text{AlGe}_2^-$ <sup>1</sup>**Abstract**

We created mixed triatomic clusters,  $\text{AlCGe}^-$ ,  $\text{AlSi}_2^-$ , and  $\text{AlGe}_2^-$ , and studied their electronic structure and chemical bonding using photoelectron spectroscopy and ab initio calculations. Excellent agreement between theoretical and experimental photoelectron spectra confirmed the predicted global minimum structures for these species. Chemical bonding analysis revealed that the  $\text{AlSi}_2^-$  and  $\text{AlGe}_2^-$  anions can be described as species with conflicting ( $\sigma$ -antiaromatic and  $\pi$ -aromatic) aromaticity. The  $\text{AlCGe}^-$  anion represents an interesting example of chemical species that is between classical and aromatic.

**7-1. Introduction**

The heavier congeners of carbon with a formal triple bond ( $\text{XMM}'\text{X}$ , where M and M' are Si, Ge, Sn, and Pb and X is a monovalent ligand) have remarkably rich potential energy surfaces with many local minima close in energy to the global minimum.<sup>1,2</sup> In contrast,  $\text{C}_2\text{H}_2$  (acetylene) has the potential energy surface with the global minimum being significantly more stable than other local minima. Electropositive substitution of H in the  $\text{HMM}'\text{H}$  species can bring additional features to the chemical bonding in these species.<sup>3</sup> Previously, we have studied  $\text{AlC}_2^-$  and  $\text{AlCSi}^-$ , which can be

---

<sup>1</sup> Coauthored by Dmitry Yu. Zubarev, Alexander I. Boldyrev, Xi Li and Lai-Sheng Wang. Reproduced with permission from *J. Phys. Chem. B* **2006**, 110, 9743-9746. Copyright 2006 American Chemical Society.

viewed as  $\text{Al}^+$  bonded to a  $\text{C}_2^{2-}$  or  $\text{CSi}^{2-}$  group.<sup>3c</sup> Chemical bonding in the two isomers of  $\text{AlC}_2^-$  with the  $\pi$ - (global minimum) and  $\sigma$ -coordination of Al to  $\text{C}_2$  can be described as being rather ionic between  $\text{Al}^+$  (with a lone pair) and  $\text{C}_2^{2-}$  which in turn can be described by a Lewis structure with a triple carbon-carbon bond (see the NBO analyses in the Supporting Information). Ionic bonding between  $\text{Al}^+$  and  $\text{C}_2^{2-}$  favors a high symmetry ( $\text{C}_{2v}$ ) structure. When both carbon atoms in  $\text{AlC}_2^-$  are substituted by Si or Ge a significant electron delocalization between all three atoms occurs (the covalent character of bonding between Al and Si or Ge increases), and the chemical bonding in the resulting  $\text{AlSi}_2^-$ ,  $\text{AlSiGe}^-$ , and  $\text{AlGe}_2^-$  species cannot be described the same way as in  $\text{AlC}_2^-$  (see the Supporting Information). That delocalization results in the low symmetry  $\text{C}_s$  ( $^1\text{A}'$ ) structures (Figure 7-1). Electron delocalization can be described in terms of aromaticity or antiaromaticity. The name “aromatic compound” was initially bestowed on benzene, its derivatives, and related compounds because of their aroma. Today, the terms “aromatic” and “aromaticity” (antiaromaticity) are used to describe cyclic, planar, and conjugated molecules possessing  $4n + 2$  ( $4n$ )  $\pi$ -electrons and having specific chemical and structural stability. In addition to widely accepted  $\pi$ -aromaticity and  $\pi$ -antiaromaticity,  $\sigma$ -aromaticity and  $\sigma$ -antiaromaticity were also introduced in chemistry (see the detailed discussion in ref 4). In the current communication, we present a photoelectron spectroscopy study of  $\text{AlCGe}^-$ ,  $\text{AlSi}_2^-$ , and  $\text{AlGe}_2^-$  and ab initio calculations at the B3LYP/6-311+G\*, TD-B3LYP/6-311+G(2df), RCCSD(T)/6-311+G\*, RCCSD(T)/6-311+G(2df), and ROVGF/6-311+G(2df) levels of theory.

## 7-2. Experimental Methods

The experiment was performed using a magnetic-bottle time-of-flight photoelectron spectroscopy apparatus equipped with a laser vaporization cluster source.<sup>5</sup> The  $\text{AlCGe}^-$ ,  $\text{AlSi}_2^-$ , and  $\text{AlGe}_2^-$  anion clusters were produced using Al/C/Ge, Al/Si, and Al/Ge mixed targets, respectively. The cluster anions of interest were mass-selected before photodetachment by one of two laser beams: 355 nm (3.496 eV) and 266 nm (4.661 eV). Photoelectron spectra were measured using the magnetic-bottle time-of-flight photoelectron analyzer with an electron kinetic energy resolution of  $\Delta E_k/E_k \approx 2.5\%$ , that is, 25 meV for 1 eV electrons. The spectrometer was calibrated with the known spectra of Cu and Rh<sup>-</sup>.

## 7-3. Theoretical Methods

Theoretically, we first performed the search for the global minima on the potential energy surfaces using the B3LYP method with the 6-311+G\* basis sets. Geometries and frequencies for local minima were refined using the RCCSD(T) method with the same basis sets. Relative energies were evaluated at the RCCSD(T)/6-311+G(2df)//RCCSD(T)/6-311+G\* level of theory. We also ran CASSCF(12,12)/6-311+G\* calculations for  $\text{AlSi}_2^-$  and  $\text{AlGe}_2^-$  in order to probe the validity of the one electron approximation. These calculations showed that the Hartree-Fock configurations were dominant ( $C_{\text{HF}} = 0.914$  ( $\text{AlSi}_2^-$ ) and  $C_{\text{HF}} = 0.912$  ( $\text{AlGe}_2^-$ )) among 427 350 configurations. Thus, methods based on the one-electron approximation (B3LYP, CCSD(T), ROVGF) should perform adequately. Theoretical vertical detachment energies (VDEs) were calculated using the RCCSD(T)/6-311+G(2df), ROVGF/6-311+G(2df), and

TD-B3LYP/6-311+G(2df) levels of theory. Natural Bond Orbital (NBO) analysis was employed for detailed chemical bonding examination. Molecular orbitals (MOs) were calculated at the RHF/6-311+G\* level of theory. All HF, B3LYP, and RCCSD(T) (for closed shell species) calculations were performed using the Gaussian 03 program.<sup>6</sup> The ROVGF calculations were done using the Gaussian 98 package.<sup>7</sup> The RCCSD(T) (for open shell species) calculations were done using the MOLPRO-2000.1 package.<sup>8</sup> MO pictures were made using the MOLDEN3.4 program.<sup>9</sup>

#### 7-4. Results and Discussion

The local minimum structures are presented in Figure 7-1. For all of the anions, linear structures were found to be second order saddle points. We found only one type of minimum structure,  $C_s$  ( $1a'^2 2a''^2 3a'^2 4a''^2 1a''^2 5a'^2$ ), as shown in Figure 7-1. Surprisingly, the cyclic  $C_{2v}$  ( $^1A_1$ ) structure, which was the global minimum for  $AlC_2^-$  (Figure 7-1a), was found to be a first-order saddle point for both  $AlSi_2^-$  and  $AlGe_2^-$ , though the potential energy surfaces are rather flat. To verify the obtained global minimum structures, we compared the calculated VDEs of  $AlSi_2^-$ ,  $AlGe_2^-$ , and  $AlC_2^-$  with the experimental data in Table 7-1. As shown in Figure 7-2, the photoelectron spectra for all three species are similar, each displaying two bands (X and A). The calculated VDEs at all three levels of theory are in excellent agreement with the experimental data, confirming the predicted global minimum structures. The VDEs calculated at B3LYP/6-311+G(2df) were found to be somewhat lower.

The unusual global minimum structures of  $AlSi_2^-$ ,  $AlSiGe^-$ , and  $AlGe_2^-$  suggest new modes of chemical bonding, different from that in  $AlC_2^-$ . Straightforward application

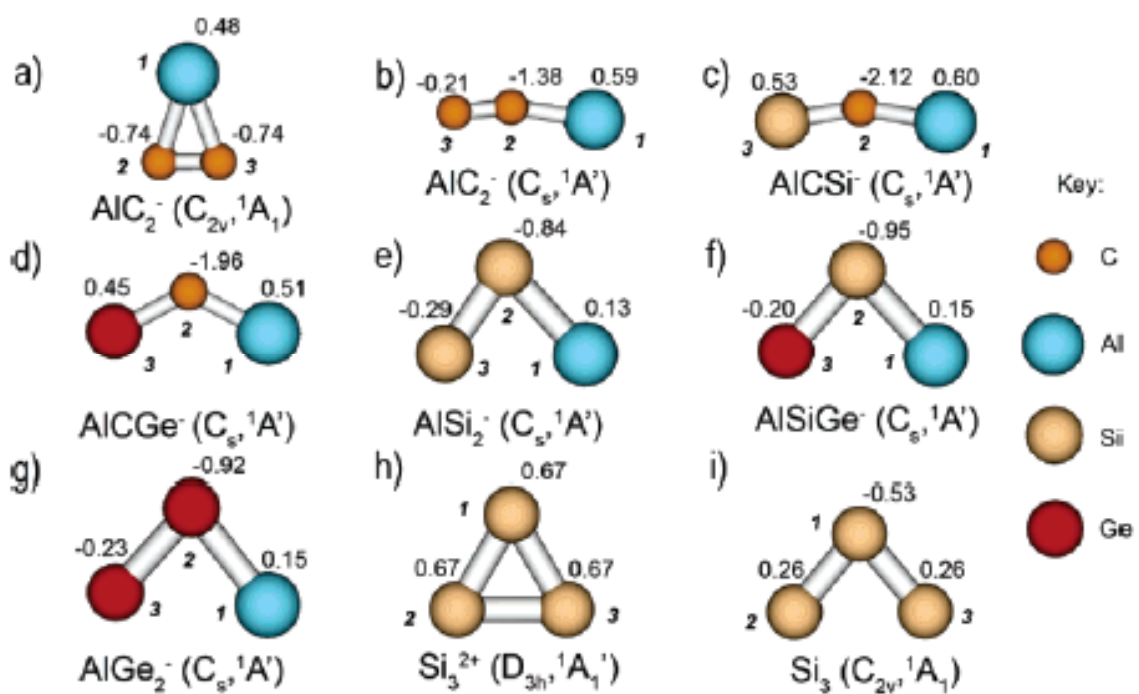


Figure 7-1. Computationally found isomers for  $\text{AlC}_2^-$ ,  $\text{AlCSi}^-$ ,  $\text{AlCGe}^-$ ,  $\text{AlSi}_2^-$ ,  $\text{AlSiGe}^-$ ,  $\text{AlGe}_2^-$ ,  $\text{Si}_3^{2+}$ , and  $\text{Si}_3$ . Effective atomic charges were calculated using NBO analysis.

Table 7-1. Experimental ADEs and VDEs of  $\text{AlGe}^-$ ,  $\text{AlSi}_2^-$ , and  $\text{AlGe}_2^-$  compared with computed VDEs at different levels of theory.

	Feature	ADE (eV) <sup>a</sup>	VDE, eV	MO	ROVGF, eV	TD-B3LYP, eV	RCCSD(T), eV
$\text{AlGe}^-$	X	$2.41 \pm 0.03$	$2.58 \pm 0.03$	$5a'$	2.688 (0.884)	2.430 <sup>b</sup>	2.625
	A		$3.07 \pm 0.02$	$1a''$	3.194 (0.877)	2.884 <sup>b</sup>	3.105
					$4a'$	3.034 (0.879)	2.930 <sup>b</sup>
$\text{AlSi}_2^-$	X	$2.19 \pm 0.03$	$2.33 \pm 0.03$	$5a'$	2.308 (0.878)	2.285	2.323
	A		$2.85 \pm 0.02$	$1a''$	2.913 (0.873)	2.725	2.955
					$4a'$	2.761 (0.863)	2.786
$\text{AlGe}_2^-$	X	$2.17 \pm 0.03$	$2.32 \pm 0.03$	$5a'$	2.294 (0.877)	2.277	2.333
	A		$2.76 \pm 0.02$	$1a''$	2.698 (0.877)	2.566	2.773
					$4a'$	2.746 (0.870)	2.672

<sup>a</sup>ADE also represents the electron affinity of the corresponding neutral molecule.

<sup>b</sup> At the CCSD(T)/6-311+G\* geometry.

of the NBO analysis to  $\text{AlSi}_2^-$ ,  $\text{AlSiGe}^-$ , and  $\text{AlGe}_2^-$  shows that there is deviation from the two-center two electron (2c-2e) picture for all three species. The occupation numbers (ONs) are just 1.80 |e| for the Si-Si, Si-Ge, and Ge-Ge bonds, and Al acquires three artificial lone pairs with ON ) 0.54, 0.22, and 0.10 |e|. In an ideal 2c-2e bond or an ideal lone pair, the ON should be 2.00 |e|. These deviations from the ideal 2c-2e bonding picture are manifestations of appreciable electron density delocalization, and in fact, these anions are  $\pi$ -aromatic and  $\sigma$ -antiaromatic systems. To prove this bonding description, let us first consider the  $D_{3h}$   $\text{Al}_3^-$  anion, which has two electrons less than  $\text{AlSi}_2^-$  and  $\text{AlGe}_2^-$ . It was recently shown<sup>10</sup> that  $\text{Al}_3^-$  is a doubly aromatic system with one completely delocalized  $\sigma$ -MO ( $2a_1'$ ) and one completely delocalized  $\pi$ -MO ( $1a_2''$ ). Dixon and co-workers<sup>10b</sup> have shown that  $\text{Al}_3^-$  has a very high resonance energy (between 56 and 79 kcal/mol), confirming the double aromaticity in  $\text{Al}_3^-$ . The various criteria of aromaticity for clusters of main group elements including metals have been recently reviewed.<sup>11</sup> In the present article, we will use only two criteria, MO analysis and geometry, because it is very difficult to find appropriate reference molecules for

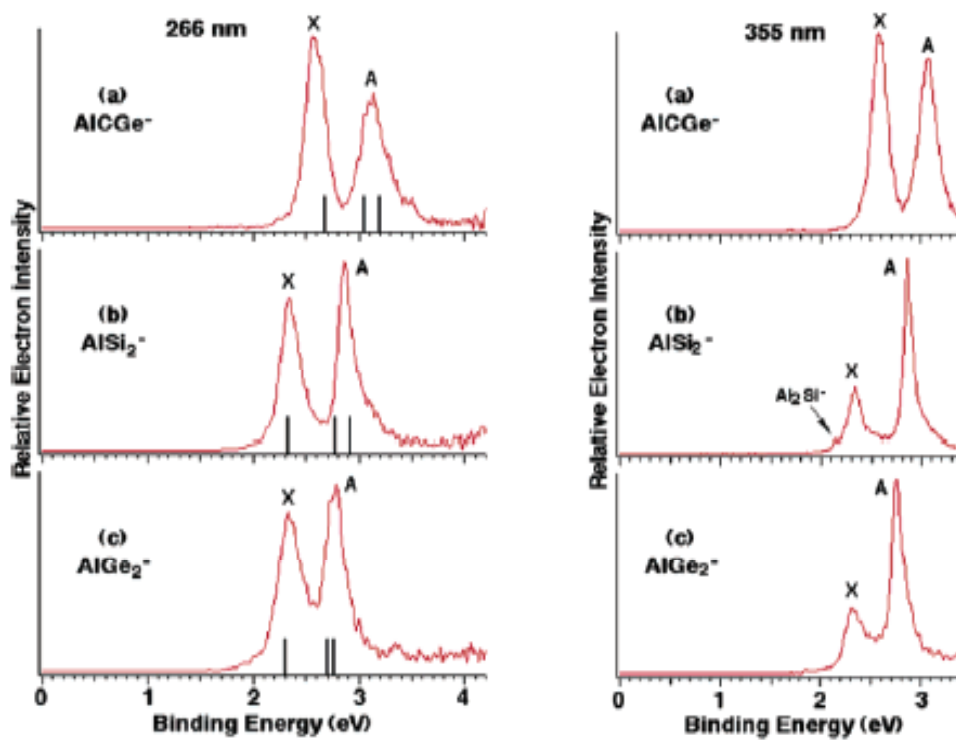


Figure 7-2. Photoelectron spectra of  $\text{AlCGe}^-$  (a),  $\text{AlSi}_2^-$  (b), and  $\text{AlGe}_2^-$  (c) at 355 nm (3.496 eV) and 266 nm (4.661 eV). The vertical bars represent the calculated VDEs for the global minimum for each species at the ROVGF level of theory (Table 7-1).



estimation of the resonance energy. We calculated an isoelectronic  $D_{3h}$  ( $^1A_1'$ )  $Si_3^{2+}$  dication as another example of double aromaticity (Figure 7-1h). Its MOs are shown in Figure 7-3a. The two upper bonding MOs are the same as those in  $Al_3^-$ , and thus,  $Si_3^{2+}$  is indeed doubly aromatic. When two additional electrons occupy the lowest unoccupied molecular orbital (LUMO) of  $Si_3^{2+}$ , forming the neutral  $Si_3$  cluster, a Jahn-Teller distortion occurs because only one of the two doubly degenerate LUMOs is occupied (Figure 7-3b). In chemical language, the highest occupied molecular orbital (HOMO) of  $Si_3$  adds antibonding character in the  $\sigma$ -framework, resulting in substantial elongation to one of the Si-Si bonds (Figure 7-1i). Four  $\sigma$ -electrons in  $Si_3$  render its  $\sigma$ -antiaromaticity, which is resulting in the  $D_{3h}$ -to- $C_{2v}$  structural distortion from  $Si_3^{2+}$  to  $Si_3$ , similar to the transition from the aromatic  $C_4H_4^{2+}$  to the antiaromatic  $C_4H_4$ . Antiaromaticity in  $C_4H_4$  manifests itself as a localization of  $\pi$ -electrons. In  $Si_3$ , antiaromaticity leads to localization of  $\sigma$ -electrons. In the pure  $\sigma$ -antiaromatic triatomic  $Li_3^-$  anion, four  $\sigma$ -electrons lead to a linear structure.<sup>12</sup> Though  $Si_3$  is a  $\sigma$ -antiaromatic system with four  $\sigma$ -electrons, it is not linear because of the important influence from the  $\pi$ -electrons. The HOMO-2 of  $Si_3$  is a completely delocalized  $\pi$ -orbital, making it  $\pi$ -aromatic. Thus,  $Si_3$  is a system with conflicting aromaticity, that is, a system with  $\sigma$ -antiaromaticity and  $\pi$ -aromaticity. When one silicon atom in  $Si_3$  is substituted by  $Al^-$  (isoelectronic to a Si atom), the resulting  $AlSi_2^-$  structure is very similar (Figure 7-1e). The isoelectronic  $AlSiGe^-$  (Figure 7-1f) and  $AiGe_2^-$  (Figure 7-1g) also have very similar structures to that of  $Si_3$ . Their valence molecular orbitals are also rather similar to those of  $Si_3$  (Figure 7-3c). Thus, these hetero-triatomic species all should be considered to possess conflicting aromaticity, similar to  $Al_4$ ,<sup>4-13</sup> which is  $\sigma$ -aromatic and  $\pi$ -antiaromatic. In systems with

conflicting aromaticity, it is difficult to make a judgment about the net aromaticity or antiaromaticity.<sup>14</sup> However, we believe that geometric criteria should be considered to be paramount relative to other criteria of aromaticity or antiaromaticity. Thus, the structural distortion in  $\text{AlSi}_2^-$ ,  $\text{AlSiGe}^-$ , and  $\text{AlGe}_2^-$  makes them net antiaromatic, again similar to  $\text{Al}_4$ ,<sup>4-13</sup> or they should be simply considered as  $\pi$ -aromatic and  $\sigma$ -antiaromatic.

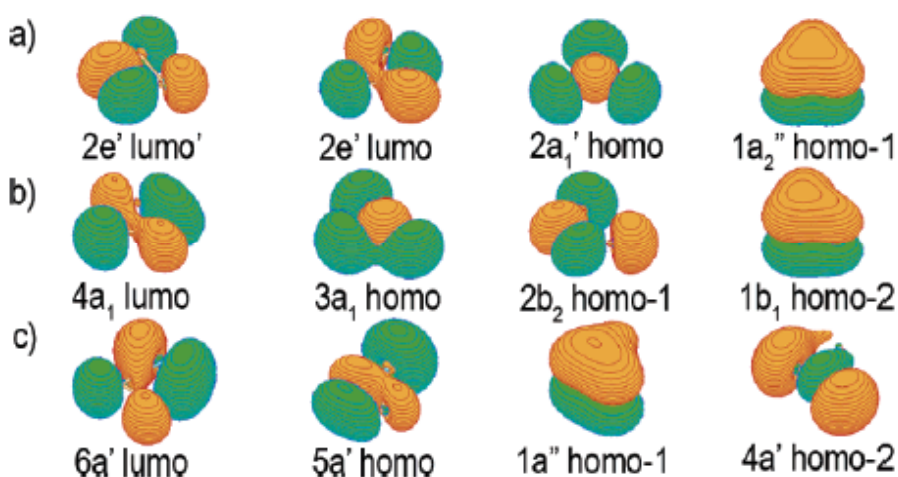


Figure 7-3. Molecular orbitals of (a)  $\text{Si}_3^{2+}$ , (b)  $\text{Si}_3$ , and (c)  $\text{AlSi}_2^-$ .

The  $\text{HCC}^-$  anion has a classical linear structure (with one 2c-2e H-C bond, three 2c-2e C-C bonds, and a lone pair on the terminal carbon atom), but its derivatives  $\text{AlCC}^-$  ( $C_s$ ,  $^1A'$ ),  $\text{AlCSi}^-$  ( $C_s$ ,  $^1A'$ ), and  $\text{AlCGe}^-$  ( $C_s$ ,  $^1A'$ ) are not linear. That deviation from linearity indicates deviation from the classical structure toward a completely delocalized aromatic structure such as that in  $\text{Si}_3^{2+}$ . The deviation from linearity increases from  $\text{AlCC}^-$  to  $\text{AlCSi}^-$  and to  $\text{AlCGe}^-$  when the electronegativity of the terminal atoms equalizes to allow electron delocalization. However, all three of these anions do not yet have conflicting aromaticity like in  $\text{AlSi}_2^-$ ,  $\text{AlSiGe}^-$ , and  $\text{AlGe}_2^-$ , because there is no

significant bonding interaction between the terminal atoms. Thus, the  $\text{AlCC}^-$ ,  $\text{AlCSi}^-$ , and  $\text{AlGe}^-$  anions are neither classical nor aromatic. They are somewhere in between.

### 7-5. Conclusion

In summary, we established the global minimum structures of  $\text{AlGe}^-$ ,  $\text{AlSi}_2^-$ , and  $\text{AlGe}_2^-$  by comparing their experimental photoelectron spectra and computed VDEs. All three anions were found to have nonlinear structures ( $C_s$ ,  $^1A'$ ). Chemical bonding analysis revealed that the  $\text{AlSi}_2^-$  and  $\text{AlGe}_2^-$  anions can be described as species with conflicting ( $\sigma$ -antiaromatic and  $\pi$ -aromatic) aromaticity. The  $\text{AlGe}^-$  anion represents an interesting example of a chemical species, which is between classical and aromatic.

### References

- (1) Power, P. P. *Chem. Commun.* **2003**, 2091.
- (2) (a) Kohler, H. J.; Lishka, H. *Chem. Phys. Lett.* **1984**, *112*, 33. (b) Luke, B. T.; Pople, J. A.; Krogh-Jespersen, M.-B.; Apoloig, Y.; Karni, M.; Chandrasekhar, J.; Schleyer, P. v. R. *J. Am. Chem. Soc.* **1986**, *108*, 270. (c) Koseki, S.; Gordon, M. S. *J. Phys. Chem.* **1988**, *92*, 364. (d) Grev, R. S.; Schaefer, H. F., III. *J. Chem. Phys.* **1992**, *97*, 7990. (d) Bogey, M.; Bovlin, H.; Demuynck, C.; Destombes, J. L. *Phys. Rev. Lett.* **1991**, *66*, 413. (e) Cordonnier, M.; Bogey, M.; Demuynck, C.; Destombes, J.-L. *J. Chem. Phys.* **1992**, *97*, 7984 and references therein.
- (3) (a) Schleyer, P. v. R. *J. Phys. Chem.* **1990**, *94*, 5560. (b) Knight, L. B., Jr.; Cobranchi, J. O.; Herlong, J. O.; Arrington, C. A. *J. Chem. Phys.* **1990**, *92*, 5856. (c) Boldyrev, A. I.; Simons, J.; Li, X.; Wang, L. S. *J. Am. Chem. Soc.* **1999**, *121*, 10193. (d) Cannon, N. A.; Boldyrev, A. I. Li, X.; Wang, L. S. *J. Chem. Phys.* **2000**, *113*, 2671.

(4) Minkin, V. I.; Glukhovtsev, M. N.; Simkin, B. Ya. *Aromaticity and Antiaromaticity: Electronic and Structural Aspects*; John Wiley & Sons: New York, 1994. See also the following special issues: *Chem. Rev.* **2001**, *101*, N5; **2005**, *105*, N10.

(5) (a) Wang, L.S.; Cheng, H. S.; Fan, J. *J. Chem. Phys.* **1995**, *102*, 9480. (b) Wang, L. S.; Wu, H. In *Advances in Metal and Semiconductor Clusters. IV. Cluster Materials*; Duncan, M. A., Ed.; JAI: Greenwich, CT, 1998; p 299.

(6) Frisch, M. J.; Trucks, G. M.; Schlegel, H. B.; Scuseria, G. E.; Robb, M. A.; Cheeseman, J. R.; Montgomery, J. A., Jr.; Vreven, T.; Kudin, K. N.; Burant, J. C.; Millam, J. M.; Iyengar, S. S.; Tomasi, J.; Barone, V.; Mennucci, B.; Cossi, M.; Scalmani, G.; Rega, N.; Petersson, G. A.; Nakatsuji, H.; Hada, M.; Ehara, M.; Toyota, K.; Fukuda, R.; Hasegawa, J.; Ishida, M.; Nakajima, T.; Honda, Y.; Kitao, O.; Nakai, H.; Klene, M.; Li, X.; Knox, J. E.; Hratchian, H. P.; Cross, J. B.; Adamo, C.; Jaramillo, J.; Gomperts, R.; Stratmann, R. E.; Yazyev, O.; Austin, A. J.; Cammi, R.; Pomelli, C.; Ochterski, J. W.; Ayala, P. Y.; Morokuma, K.; Voth, G. A.; Salvador, P.; Dannenberg, J. J.; Zakrzewski, V. G.; Dapprich, S.; Daniels, A. D.; Strain, M. C.; Farkas, O.; Malick, D. K.; Rabuck, A. D.; Raghavachari, K.; Foresman, J. B.; Ortiz, J. V.; Cui, Q.; Baboul, A. G.; Clifford, S.; Cioslowski, J.; Stefanov, B. B.; Liu, G.; Liashenko, A.; Piskorz, P.; Komaromi, I.; Martin, R. L.; Fox, D. J.; Keith, T.; Al-Laham, M. A.; Peng, C. Y.; Nanayakkara, A.; Challacombe, M.; Gill, P. M. W.; Johnson, B. G.; Chen, W.; Wong, M. W.; Gonzales, C.; Pople, J. A. *Gaussian 03*, revision A.1; Gaussian, Inc.: Pittsburgh, PA, 2003.

(7) Frisch, M. J.; Trucks, G. M.; Schlegel, H. B.; Scuseria, G. E.; Robb, M. A.; Cheeseman, J. R.; Zakrzewski, V. G.; Montgomery, J. A.; Stratmann, R. E.; Burant, J. C.; Dapprich, S.; Millam, J. M.; Daniels, A. D.; Kudin, K. N.; Strain, M. C.; Farkas, O.;

Tomasi, J.; Barone, V.; Cossi, M.; Cammi, R.; Mennucci, B.; Pomelli, C.; Adamo, C.; Clifford, S.; Ochterski, J. W.; Petersson, G. A.; Ayala, P. Y.; Cui, Q.; Morokuma, K.; Malick, D. K.; Rabuck, A. D.; Raghavachari, K.; Foresman, J. B.; Cioslowski, J.; Ortiz, J. V.; Stefanov, B. B.; Liu, G.; Liashenko, A.; Piskorz, P.; Komaromi, I.; Gomperts, R.; Martin, R. L.; Fox, D. J.; Keith, T.; Al-Laham, M. A.; Peng, C. Y.; Nanayakkara, A.; Gonzales, C.; Challacombe, M.; Gill, P. M. W.; Johnson, B. G.; Chen, W.; Wong, M. W.; Andres, J. L.; Head-Gordon, M.; Replogle, E. S.; Pople, J. A. *Gaussian 98*, revision A.1; Gaussian, Inc.: Pittsburgh, PA, 1998.

(8) Werner, H.-J.; Knowles, P. J. (with contributions from R. D. Amos, A. Bernhardsson, A. Berning, P. Celani, D. L. Cooper, M. J. O. Deegan, A. J. Dobbyn, F. Eckert, C. Hampel, G. Hetzer, T. Korona, R. Lindh, A. W. Lloyd, S. J. McNicholas, F. R. Manby, W. Meyer, M. E. Mura, A. Nicklass, P. Palmieri, R. Pitzer, G. Rauhut, M. Schutz, H. Stoll, A. J. Stone, R. Tarroni, and T. Thorsteinsson). *MOLPRO-2000.1*; University of Birmingham: UK, 1999.

(9) Schaftenaar, G. *MOLDEN3.4*; CAOS/CAMM Center: The Netherlands, 1998.

(10) (a) Kuznetsov, A. E.; Boldyrev, A. I. *Struct. Chem.* **2002**, *12*, 141. (b) Zhan, C.-G.; Zheng, F.; Dixon, D. A. *J. Am. Chem. Soc.* **2002**, *124*, 14795.

(11) Boldyrev, A. I.; Wang, L. S. *Chem. Rev.* **2005**, *105*, 3716.

(12) Alexandrova, A. N.; Boldyrev, A. I. *J. Phys. Chem. A* **2003**, *107*, 554.

(13) Kuznetsov, A. E.; Birch, K. A.; Boldyrev, A. I.; Li, X.; Zhai, H. J.; Wang, L. S. *Science* **2003**, *300*, 622.

(14) (a) Ritter, S. K. *Chem. Eng. News* **2003**, *81* (51), 23. (b) Chen, Z.; Corminboeuf, C.; Heine, T.; Bohmann, J.; Schleyer, P. v. R. *J. Am. Chem. Soc.* **2003**,

125, 13930. (c) Havenith, R. W. A.; Fowler, P. W.; Steiner, E.; Shetty, S.; Kanhere, D.; Pal, S. *Phys. Chem. Chem. Phys.* **2004**, *6*, 285. (d) Shetty, S.; Kanhere, D. G.; Pal, S. *J. Phys. Chem. A* **2004**, *108*, 628. (e) Chacko, S.; Kanhere, D. G.; Paranjape, V. V. *Phys. Rev. A* **2004**, *70*, 0123204. (f) Santos, J. C.; Andres, J.; Aizman, A.; Fuentealba, P. *J. Chem. Theory Comput.* **2005**, *1*, 83. (g) Lin, Y.-C.; Jusellius, J.; Sundholm, D. *J. Chem. Phys.* **2005**, *122*, 214308. (h) Datta, A.; Pati, S. K. *J. Am. Chem. Soc.* **2005**, *127*, 3496. (i) Datta, A.; Pati, S. K. *J. Chem. Theory Comput.* **2005**, *1*, 824.

CHAPTER 8  
GOLD APES HYDROGEN. THE STRUCTURE AND BONDING  
IN THE PLANAR  $B_7Au_2^-$  AND  $B_7Au_2$  CLUSTERS<sup>1</sup>

**Abstract**

We produced the  $B_7Au_2^-$  mixed cluster and studied its electronic structure and chemical bonding using photoelectron spectroscopy and *ab initio* calculations. The photoelectron spectra of  $B_7Au_2^-$  were observed to be relatively simple with vibrational resolution, in contrast to the complicated spectra observed for pure  $B_7^-$ , which had contributions from three isomers (Alexandrova *et al.*, *J. Phys. Chem. A* **2004**, *108*, 3509). Theoretical calculations show that  $B_7Au_2^-$  possesses an extremely stable planar structure, identical to that of  $B_7H_2^-$ , demonstrating that Au mimics H in its bonding to boron, analogous to the Au-Si bonding. The ground state structure of  $B_7Au_2^-$  ( $B_7H_2^-$ ) can be viewed as adding two Au (H) atoms to the terminal B atoms of a higher-lying planar isomer of  $B_7^-$ . The bonding and stability in the planar  $B_7Au_2^-$  ( $B_7H_2^-$ ) clusters are elucidated on the basis of the strong covalent B-Au (H) bonding and the concepts of aromaticity/antiaromaticity in these systems.

**8-1. Introduction**

Pure boron clusters have received limited attention in the literature over the past couple of decades (see 1-7 and references therein). A major breakthrough has resulted from a series of recent joint experimental and theoretical studies that have established

---

<sup>1</sup> Coauthored by Hua-Jin Zhai, Lai-Sheng Wang, Dmitry Yu. Zubarev and Alexander I. Boldyrev. Reproduced with permission from *J. Phys. Chem. A* **2006**, *110*, 1689-1693. Copyright 2006 American Chemical Society.

that all the small boron clusters are planar or quasi-planar.<sup>8-15</sup> These studies have shown that photoelectron spectroscopy in conjunction with accurate *ab initio* calculations is a powerful approach to elucidate the complex structures of atomic clusters. Furthermore, the theoretical analyses have yielded detailed information about the chemical bonding in the clusters and allowed the planarity of the boron clusters to be understood on the basis of  $\pi$  and  $\sigma$  aromaticity/antiaromaticity.

Among the small boron clusters, the  $B_7^-$  cluster is a particularly interesting and complex system because we observed the presence of three quite different isomers in its photoelectron spectra:<sup>12</sup> (1) a wheel-type quasi-planar doubly ( $\sigma$  and  $\pi$ ) aromatic triplet  $C_{6v}$  ( $^3A_1'$ ) global minimum (structure I in Figure 8-1), (2) a  $\sigma$ -aromatic and  $\pi$ -antiaromatic singlet  $C_{2v}$  ( $^1A_1$ ) isomer (structure II in Figure 8-1) with a quasi-planar shape (only 0.7 kcal/mol above the global minimum), and (3) an elongated planar doubly ( $\sigma$

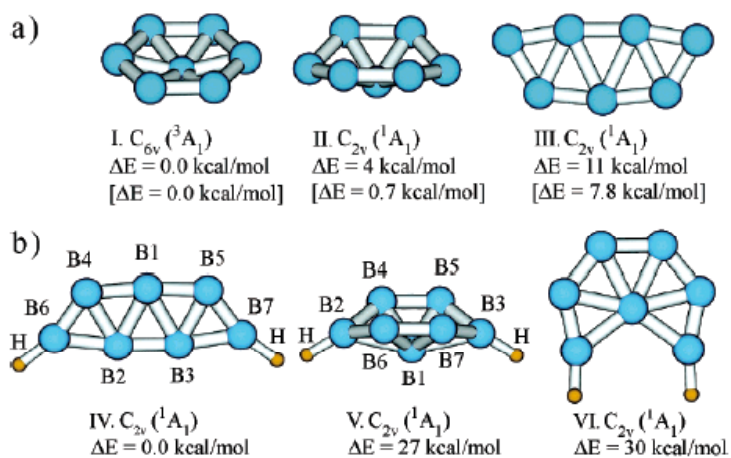


Figure 8-1. (a) Low-energy isomers of the  $B_7^-$  cluster at the B3LYP/6-311+G\* level of theory (relative energies computed at the CCSD(T)/6-311+G(2df) level are shown in square brackets).<sup>12</sup> (b) The global minimum and two low-lying isomers of  $B_7H_2^-$  at B3LYP/6-311+G\* level.<sup>16</sup>



and  $\pi$ ) antiaromatic  $C_{2v}$  ( $^1A_1$ ) isomer (structure III in Figure 8-1) (7.8 kcal/mol above the global minimum). Upon addition of two hydrogen atoms to the  $B_7^-$  cluster, it is found very recently using *ab initio* calculations that an inversion in stability occurs.<sup>16</sup> The planar  $B_7H_2^-$  ( $C_{2v}$ ,  $^1A_1$ ) isomer (structure IV in Figure 8-1), formed by the addition of two hydrogen atoms to the doubly antiaromatic  $C_{2v}$  ( $^1A_1$ )  $B_7^-$  isomer III, is overwhelmingly favored as the global minimum structure. It is 27 kcal/mol more stable than the lowest high-energy isomer V of  $B_7H_2^-$ , originated from the addition of two hydrogen atoms to the global minimum of  $B_7^-$ .

Wang and co-workers have recently discovered that gold atoms exhibit chemistry similar to that of hydrogen in Au-Si clusters, forming  $SiAu_x$  and  $Si_2Au_x$  clusters similar to the corresponding silicon hydrides,  $SiH_x$  and  $Si_2H_x$ , respectively.<sup>17,18</sup> Because of the similar electronegativity between B and Si, we conjecture that Au may also form Au-B clusters similar to the corresponding valence isoelectronic H-B clusters. If that is true, we hypothesized that the  $B_7Au_2^-$  cluster would behave similarly as the  $B_7H_2^-$  system, thus yielding a predominantly stable cluster similar to the global minimum of  $B_7H_2^-$  (IV in Figure 8-1). In this case, we would expect to obtain a somewhat simpler photoelectron spectrum for  $B_7Au_2^-$  because only the global minimum structure is expected to be present in the experiment due to its overwhelming stability.

## 8-2. Experimental Method

We produced the  $B_7Au_2^-$  anions using a laser vaporization cluster source and obtained its photoelectron spectra using a magnetic-bottle type photoelectron spectrometer.<sup>19-21</sup> The photoelectron spectra of  $B_7Au_2^-$  at 266 and 193 nm photon

energies are shown in Figure 8-2, compared with that of  $B_7^-$ . Indeed, the photoelectron spectra of  $B_7Au_2^-$  are substantially simpler and better resolved than that of  $B_7^-$  despite its larger size. Most surprisingly, despite the addition of two heavy atoms, the ground state transition (X) of  $B_7Au_2^-$  is completely vibrationally resolved at 266 nm (Figure 8-2a) with the excitation of two vibrational modes, a low frequency mode of  $790 \pm 40 \text{ cm}^{-1}$  and a high frequency mode of  $1,380 \pm 40 \text{ cm}^{-1}$ . The vibrationally resolved ground state transition yielded an accurate electron affinity (EA) of  $3.52 \pm 0.02 \text{ eV}$  for  $B_7Au_2$ . Interestingly, the EA of  $B_7Au_2$  is very close to that of isomer III for  $B_7$  ( $3.44 \pm 0.02$ ) corresponding to feature X' in the spectrum of  $B_7^-$  (Figure 8-2c).<sup>12</sup> Clearly, only one dominant isomer was present in the spectra of  $B_7Au_2^-$ . The observed detachment energies for the various detachment channels are summarized in Table 8-1. The observed  $B_7Au_2^-$  cluster is likely to correspond to the isomer III of  $B_7^-$  by adding two Au atoms to its two terminal B atoms similar to the ground state structure of  $B_7H_2^-$  as we expected.

### 8-3. Theoretical Methods

To prove our hypothesis and confirm the observed  $B_7Au_2^-$  structure, we performed quantum chemical calculations<sup>22</sup> for a variety of  $B_7Au_2^-$  structures (VII-XII, Figure 8-3), which were derived from the low-lying structures of  $B_7H_2^-$ .<sup>16</sup> We initially optimized geometries at B3LYP/B/cc-pvDZ/Au/LANL2DZ level of theory and found the structure VII of  $B_7Au_2^-$  ( $C_{2v}$ ,  $^1A_1$ ) (Figure 8-3), nearly identical to the ground state of  $B_7H_2^-$ , is indeed substantially more stable than the other structures. We then reoptimized the geometry of the  $B_7Au_2^-$  global minimum structure VII at the B3LYP/B/aug-cc-pvTZ/Au/Stuttgart\_rsc\_1997\_ecp level of theory and found that the two levels of theory

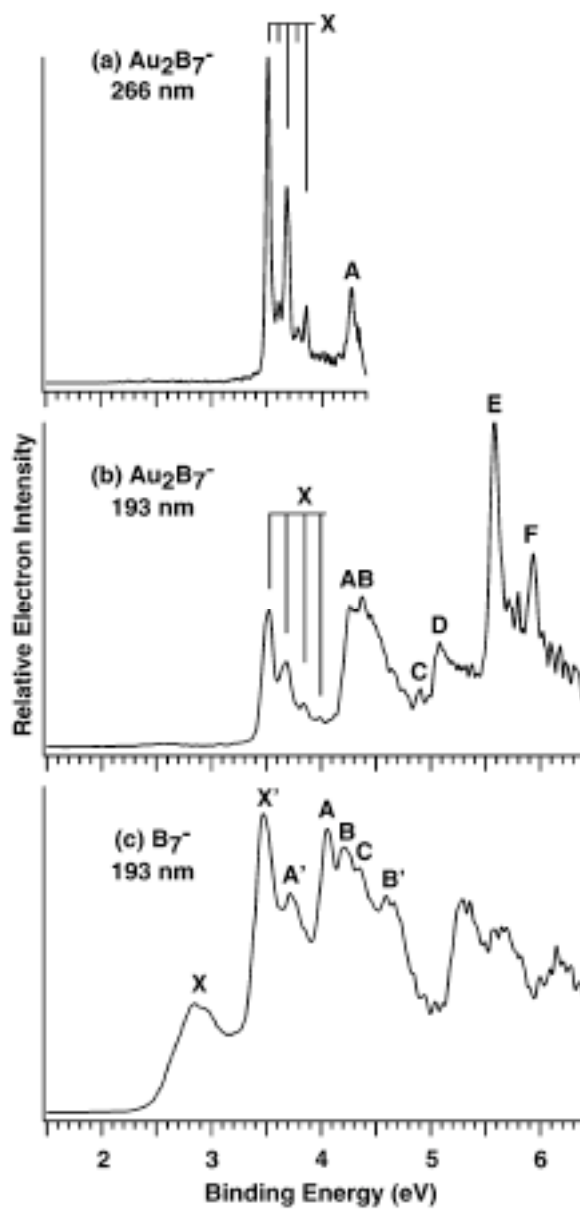


Figure 8-2. Photoelectron spectra of Au<sub>2</sub>B<sub>7</sub><sup>-</sup> at (a) 266 nm (4.661 eV) and (b) 193 nm (6.424 eV). The 193 nm spectrum of B<sub>7</sub><sup>-</sup> (c) is also included for comparison.<sup>12</sup>

Table 8-1. Experimental Vertical Detachment Energies (VDEs) of  $B_7Au_2^-$  from the Photoelectron Spectra, Compared with Theoretical Calculations.

Feature	VDE (expt), eV <sup>a</sup>	MO	VDE (theor), eV <sup>b</sup>
X <sup>c,d</sup>	3.52 (2)	3a <sub>2</sub>	3.46
A	4.27 (2)	9a <sub>1</sub>	4.21
B	4.38 (3)	8a <sub>1</sub>	4.36
C	4.90 (2)	7b <sub>2</sub>	4.92
D	5.08 (3)	6b <sub>2</sub>	5.19
E	5.58 (2)	7a <sub>1</sub>	5.31
F	5.93 (2)	3b <sub>1</sub>	5.75

- Numbers in parentheses represent experimental uncertainties in the last digit.
- At TD-B3LYP/B/aug-cc-pvTZ/Au/ Stuttgart\_rsc\_1997\_ecp level of theory.
- Electron affinity of  $B_7Au_2$ :  $3.52 \pm 0.02$  eV.
- Ground state vibrational frequencies for the  $Au_2B_7$  neutral are measured to be  $790 \pm 40$  and  $1,380 \pm 40$   $cm^{-1}$ .

give nearly identical structures. We also optimized the geometry for the neutral  $B_7Au_2$  cluster and obtained its ground state structure similar to that of the anion as summarized in Table S1. The vertical detachment energies (VDEs) from the  $B_7Au_2^-$  global minimum structure were computed using the TD-B3LYP/aug-cc-pvTZ/Au/Stuttgart\_rsc\_1997\_ecp level of theory and they are compared with the experimental data in Table 8-1. All valence molecular orbitals of the global minimum structure of  $B_7Au_2^-$  are depicted in Figure 8-4.

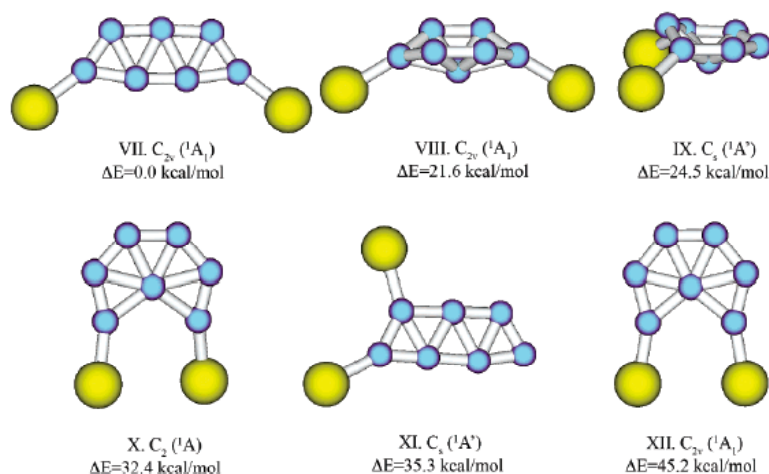


Figure 8-3. The global minimum and low-lying isomers of  $B_7Au_2^-$  at B3LYP/B/cc-pvdz/Au/ level.

#### 8-4. Results and Discussion

The ground state transition in the spectra of  $B_7Au_2^-$  (X, Figure 8-2) involves electron detachment from the  $3a_2$ -HOMO, which is a  $\pi$  bonding/antibonding orbital over the  $B_7$  moiety with some small contributions from the Au 5d orbitals (Figure 8-4). The calculated VDE of 3.46 eV agrees well with the experimental VDE (3.52 eV) of the X

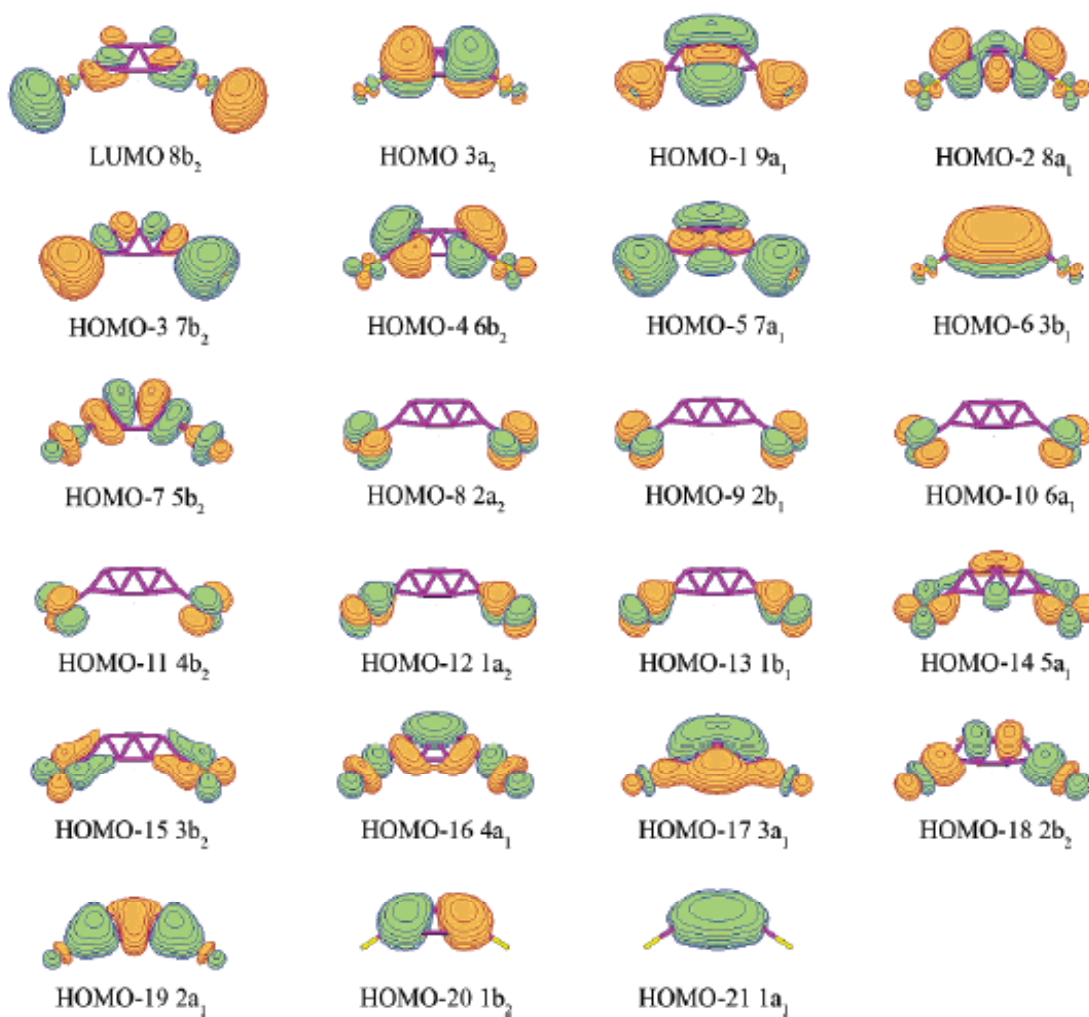


Figure 8-4. Molecular orbitals (B3LYP/B/cc-pvDZ/Au/LANL2DZ) of  $Au_2B_7^-$   $C_{2v}$  ( $^1A_1$ ). MOs are ordered according to the TD-B3LYP/B/aug-cc-pvTZ/Au/Stuttgart\_rsc\_1997\_ecp level of theory.

band (Table 8-1). Because both  $B_7Au_2^-$  and  $B_7Au_2$  have the same symmetry in their ground state, only the totally symmetric modes ( $a_1$ ) can be active in the detachment transition. The  $C_{2v}$   $B_7Au_2$  possesses eight symmetric modes, among which the  $\omega_1$  (B-B in-plane stretching) and  $\omega_3$  (B-Au stretching) modes with frequencies of 1,358 and 828  $cm^{-1}$  are in good agreement with the two observed vibrational modes ( $1,380 \pm 40 cm^{-1}$  and  $790 \pm 40 cm^{-1}$ ). The geometry changes between the anion and neutral ground states are very small, consistent with the short vibrational progressions observed. The next six detachment channels are due to electron removal from HOMO-1 to HOMO-6 (Figure 8-4), respectively, and the computed VDEs for these detachment channels are in good agreement with the experimental data (Table 8-1).

The good agreement between the experimental and theoretical VDEs confirmed the theoretical prediction of the global minimum structure VII for  $B_7Au_2^-$ , which is the same as that of  $B_7H_2^-$ . Why the structure IV is the most stable for  $B_7H_2^-$  has been discussed in detail in ref. 16. The same applies to  $B_7Au_2^-$  and can be understood from the MO pictures depicted in Figure 8-4. Among the twenty two occupied valence MOs, approximately ten are due to the Au 5d orbitals (HOMO-8 to HOMO-16 plus HOMO-18 (although a few of the lower-lying orbitals have significant mixing with the  $B_7$  backbone); seven are responsible for the formation of seven 2c-2e peripheral B-B bonds (HOMO-2, HOMO-4, HOMO-7; HOMO-17, and HOMO-19 to HOMO-21; see ref. 16 for more details); two are primarily responsible for the B-Au bonding (HOMO-3 and HOMO-5); and two are  $\pi$  orbitals (HOMO and HOMO-6). This leaves the HOMO-1 ( $9a_1$ ), which is a  $\sigma$ -orbital delocalized mainly over the five boron atoms that are not bonded to Au. Thus,  $B_7Au_2^-$  is  $\pi$ -antiaromatic ( $4\pi$  delocalized electrons) and  $\sigma$ -aromatic

(2 delocalized  $\sigma$  electrons) with all other MOs representing the two 2c-2e B-Au bonds and the seven 2c-2e B-B peripheral bonds. The planar  $B_7Au_2^-$  structure can then be viewed as originating from the mixing of the Au hybrid 6s-5d orbitals with one of the delocalized  $\sigma$  orbitals in the  $B_7^-$  isomer III, thus transforming the doubly antiaromatic  $B_7^-$  into a  $\sigma$ -aromatic but still  $\pi$ -antiaromatic  $B_7Au_2^-$ . Essentially, a delocalized  $\sigma$  orbital, forming the original  $\sigma$ -antiaromatic pair of orbitals, is transformed to two B-Au localized bonds, gaining major stabilization to the structure VII for  $B_7Au_2^-$ . The second most stable isomer for  $B_7Au_2^-$ , originated from the quasi-planar doubly aromatic isomer I of  $B_7^-$ , becomes doubly ( $\sigma$ - and  $\pi$ -) antiaromatic and thus significantly less stable. The stability of the planar structure VII of  $B_7Au_2^-$  is also reinforced by the two strong B-Au bonds formed.

### 8-5. Conclusion

The similarity in stability, structure, and bonding in the global minima of  $B_7Au_2^-$  and  $B_7H_2^-$  is analogous to the previous discovery of the Au/H analogy in Si-Au clusters.<sup>17,18</sup> Similar to the Si-Au bond, which is highly covalent, we found that the B-Au bonds in  $B_7Au_2^-$  are also highly covalent with very little charge transfer from Au to B. This is again due to the close electronegativity between B and Au, as a result of the strong relativistic effects in Au.<sup>23</sup> This study demonstrates that the Au/H analogy may be a more general phenomenon and may exist in many species involving Au. The Au/H analogy will not only extend our understanding of the chemistry of Au, but will also be highly valuable in predicting the structures and bonding of many Au-alloy clusters.



**References**

(1) (a) Hanley, L.; Anderson, S. L. *J. Phys. Chem.* **1987**, *91*, 5161; (b) Hanley, L.; Whitten, J.L.; Anderson, S.L. *J. Phys. Chem.* **1988**, *92*: 5803; (c) Ruatta, S. A.; Hintz, P. A.; Anderson, S. L. *J. Chem. Phys.* **1991**, *94*, 2833; (d) Sowa-Resat, M. B.; Smolanoff, J.; Lapiki, A.; Anderson, S. L. *J. Chem. Phys.* **1997**, *106*, 9511.

(2) Placa, S. J. L.; Roland, P.A.; Wynne, J. J. *Chem. Phys. Lett.* **1992**, *190*, 163.

(3) Bonacic-Koutecky. V.; Fantucci. P.; Koutecky, J. *Chem. Rev.* **1991**, *91*, 1035.

(4) (a) Kato, A. U.; Tanaka E. *J. Comput. Chem.* **1991**, *12*, 1097; (b) Kato, H.; Yamashita.K.; Morokuma, K. *Chem.Phys. Lett.* **1992**, *190*, 361.

(5) (a) Ricca, A.; Bauschlicher, C. W. *Chem. Phys.* **1996**, *208*, 233; (b) Ricca, A.; Bauschlicher, C. W. *J. Chem. Phys.* **1997**, *106*, 2317.

(6) (a) Boustani, I. *Int. J. Quant. Chem.* **1994**, *52*, 1081; (b) Boustani, I. *Surface Science* **1996**, *370*, 355; (c) Boustani, I. *Phys. Rev. B* **1997**, *55*, 16426.

(7) (a) Ma, J.; Li, Z. H.; Fan, K. N.; Zhou, M. F. *Chem. Phys. Lett.* **2002**, *372*, 708; (b) Jin, H. W.; Li, Q. S. *Phys. Chem. Chem. Phys.* **2003**, *5*, 1110; (c) Li, Q. S.; Jin, Q. *J. Phys. Chem. A.* **2003**, *107*, 7869.

(8) Ritter, S. K. *Chem. Eng. News*, **2004**, *82(9)*, 28.

(9) Zhai, H. J.; Wang, L. S.; Alexandrova, A. N.; Boldyrev, A. I.; Zakrzewski, V. *G. J. Phys. Chem. A* **2003**, *107*, 9319.

(10) Zhai, H. J.; Wang, L. S.; Alexandrova, A. N.; Boldyrev, A. I. *J. Chem. Phys.* **2002**, *117*, 7917.

(11) Alexandrova, A. N.; Boldyrev. A. I.; Zhai, H. J.; Wang, L. S.; Steiner, E.; Fowler, P. W. *J. Phys. Chem. A* **2003**, *107*, 1359.

(12) Alexandrova, A. N.; Boldyrev, A. I.; Zhai, H. J.; Wang, L. S. *J. Phys. Chem. A* **2004**, *108*, 3509.

(13) Zhai, H. J.; Wang, L. S.; Alexandrova, A. N.; Boldyrev, A. I. *Angew. Chem. Int. Ed.* **2003**, *42*, 6004.

(14) Zhai, H. J.; Kiran, B.; Li, J.; Wang, L. S. *Nature Materials* **2003**, *2*, 827.

(15) Kiran, B.; Bulusu, S.; Zhai, H. J.; Yoo, S.; Zeng, X. C.; Wang, L. S. *Proc. Natl. Acad. Sci. (USA)* **2005**, *102*, 961.

(16) Alexandrova, A. N.; Koyle, E.; Boldyrev, A. I. *J. Mol. Mod.* 2005, in press.

(17) Kiran, B.; Li, X.; Zhai, H. J.; Cui, L. F.; Wang, L. S. *Angew. Chem. Int. Ed.* **2004**, *43*, 2125.

(18) Li, X.; Kiran, B.; Wang, L. S. *J. Phys. Chem. A* **2005**, *109*, 4366.

(19) Details of the photoelectron spectroscopy apparatus have been described elsewhere.<sup>20,21</sup> In brief, Au-B mixed cluster anions were generated by laser vaporization of an Au/B disk target in the presence of a helium carrier gas and analyzed by time-of-flight mass spectrometry. The  $B_7Au_2^-$  anions were mass-selected and decelerated before being photodetached by a pulsed laser beam. Photoelectrons were collected at nearly 100% efficiency by a magnetic bottle and analyzed in a 3.5 m long electron flight tube. The photoelectron spectra were calibrated using the known spectra of  $Au^-$  and  $Rh^-$ , and the energy resolution was  $\Delta E_k/E_k \approx 2.5\%$ , that is, approximately 25 meV for 1 eV electrons.

(20) Wang, L. S.; Cheng, H. S.; Fan, J. *J. Chem. Phys.* **1995**, *102*, 9480.

(21) Wang, L. S.; Wu, H. In *Advances in Metal and Semiconductor Clusters. IV. Cluster Materials*, Duncan, M. A., ed.; JAI: Greenwich, CT, 1998; pp. 299-343.

(22) The B3LYP/B/cc-pvDZ/Au/LANL2DZ calculations have been performed using Gaussian 2003 program at Utah State University and the B3LYP/B/aug-cc-pvTZ/Au/ Stuttgart\_rsc\_1997\_ecp calculations have been performed using NWChem program at the W. R. Wiley Environmental Molecular Sciences Laboratory (EMSL), Pacific Northwest National Laboratory (PNNL), Richland, Washington. Molecular orbital pictures were made using the MOLDEN 3.4 program.

(23) Pyykkö, P. *Angew. Chem. Int. Ed.* **2004**, *43*, 4412.

CHAPTER 9  
ON THE CHEMICAL BONDING OF GOLD IN AURO-BORON  
OXIDE CLUSTERS  $\text{Au}_n\text{BO}^-$  ( $n = 1-3$ )<sup>1</sup>

**Abstract**

During an experiment on Au-B alloy clusters, an auro-boron oxide cluster  $\text{Au}_2\text{BO}^-$  was observed to be an intense peak dominating the Au-B mass spectra, along with weaker signals for  $\text{AuBO}^-$  and  $\text{Au}_3\text{BO}^-$ . Well-resolved photoelectron spectra have been obtained for the three new oxide clusters, which exhibit an odd-even effect in their electron binding energies.  $\text{Au}_2\text{BO}^-$  is shown to be a closed shell molecule with a very high electron binding energy, whereas  $\text{AuBO}$  and  $\text{Au}_3\text{BO}$  neutrals are shown to be closed shell species with large HOMO-LUMO gaps, resulting in relatively low electron affinities. Density functional calculations were performed for both  $\text{Au}_n\text{BO}^-$  ( $n = 1-3$ ) and the corresponding  $\text{H}_n\text{BO}^-$  species in order to evaluate the analogy in bonding between gold and hydrogen in B-Au clusters. The combination of experiment and theory allowed us to establish the structures and chemical bonding of these tertiary clusters. We find that the first gold atom does mimic hydrogen and interacts with the BO unit to produce a linear  $\text{AuBO}^-$  structure. This unit preserves its identity when interacting with additional gold atoms: a linear  $\text{Au}[\text{AuBO}]$  complex is formed when adding one extra Au atom and two isomeric  $\text{Au}_2[\text{AuBO}]$  complexes are formed when adding two extra Au atoms. Since  $\text{BO}^-$  is isoelectronic to CO, the  $\text{Au}_n\text{BO}^-$  species can be alternatively viewed as  $\text{Au}_n$

---

<sup>1</sup> Coauthored by Dmitry Yu. Zubarev, Alexander I. Boldyrev, Jun Li, Hua-Jin Zhai and Lai-Sheng Wang. Reproduced with permission from *J. Phys. Chem. A* **2007**, 111, 1648-1658. Copyright 2007 American Chemical Society.

interacting with a  $\text{BO}^-$  unit. The structures and chemical bonding in  $\text{Au}_n\text{BO}^-$  are compared to those in the corresponding  $\text{Au}_n\text{CO}$  complexes.

### 9-1. Introduction

A gold phosphine unit ( $\text{AuPPh}_3$ ) is known to participate in chemical interactions analogous to that of hydrogen. For instance, substitution of covalently bound hydrogen with  $\text{AuPPh}_3$  results in the same geometry structures in some compounds. This phenomenon made it possible to interpret various gold-carborane complexes.<sup>1,2</sup> Gold-containing closo-carboranes reported by Mitchel and Stone,<sup>1a</sup> Reid and Welch,<sup>1b</sup> and Baukova *et al.*<sup>1c</sup> represent substances where gold forms classical two-center two-electron (2c-2e) bonds with carbon. Cluster bonding between  $\text{AuPPh}_3$  and nido-carboranes was encountered in substances synthesized and characterized by Stone and co-workers.<sup>1d-1h</sup> Experimental work of Hawthorne and co-workers<sup>1i</sup> demonstrated that in aurocarboranes atoms of gold can interact with each other as well as form 2c-2e bonds with carbon. Gold-stanna-closo-borate compounds synthesized and characterized by Wesemann and co-workers have Sn-Au bonds.<sup>2</sup> More detailed information on Au-B compounds can be found in a recent review.<sup>3</sup>

The analogy between hydrogen and  $\text{AuPPh}_3$  indeed goes beyond carboranes and gives rise to various compounds with 2c-2e C-Au, N-Au, and B-Au bonds.<sup>4,5</sup> C-AuPPh<sub>3</sub> bonds are encountered in compounds containing the hypercoordinated pentagonal-bipyramidal  $\text{C}(\text{AuPPh}_3)_5^+$  and octahedral  $\text{C}(\text{AuPPh}_3)_6^{2+}$  cations.<sup>5b</sup> Model systems  $\text{BH}_n(\text{AuPH}_3)_m^k$ , where  $n + m = 3$  or 4, and charge  $k$  is  $-2, \dots, +1$ <sup>5c</sup> and model complexes  $[(\text{LAu})_6\text{X}_m]^{m+}$ ,  $[(\text{LAu})_5\text{X}_m]^{(m-1)+}$ ,  $[(\text{LAu})_4\text{X}_m]^{(m-2)+}$ , (with central atoms  $\text{X}_1 = \text{B}$ ,  $\text{X}_2 = \text{C}$ ,

and  $X_3 = N$  and ligands  $L = PH_3$  or  $P(CH_3)_3$ <sup>5d</sup> have been studied theoretically to evaluate the stabilizing effect of Au-PR<sub>3</sub> interactions in these systems. Pyykkö et al.<sup>5e</sup> investigated the effect of Au-PR<sub>3</sub> interaction on chemical bonding in  $X(AuPPh_3)_n^{m+}$  systems by considering pure  $XAu_n^{m+}$  clusters. A boron-centered gold cluster in the  $[(Cy_3P)B((AuPPh_3)_4)]^+BF_4^-$  salt has been synthesized and characterized by Schmidbaur and co-workers.<sup>5f</sup> Gold diboride AuB<sub>2</sub> compounds, which have hexagonal layers of boron atoms with gold atoms in between, are well-known as well.<sup>5g-5j</sup>

The analogy of chemical bonding between a bare gold atom and H has been recently discovered in some binary Au clusters produced in molecular beams.<sup>6-8</sup> First, SiAu<sub>4</sub>, and SiAu<sub>*n*</sub> (*n* = 2, 3) were demonstrated to have structures and bonding similar to the silane SiH<sub>4</sub> and SiH<sub>*n*</sub>, respectively.<sup>6</sup> Subsequent studies of Si<sub>2</sub>Au<sub>*n*</sub> (*n* = 2 and 4) and Si<sub>3</sub>Au<sub>3</sub> clusters revealed their similarity to Si<sub>2</sub>H<sub>*n*</sub> (*n* = 2 and 4) and Si<sub>3</sub>H<sub>3</sub>, respectively.<sup>7</sup> B-Au bonds in the Au<sub>2</sub>B<sub>7</sub><sup>-</sup> cluster<sup>8</sup> turned out to be covalent and similar to the B-H bonds in the B<sub>7</sub>H<sub>2</sub><sup>-</sup> cluster.<sup>9</sup> Very recently, we have used the concept of Au/H analogy to consider the possibility of deltahedral closo-auro-boranes B<sub>*n*</sub>Au<sub>*n*</sub><sup>2-</sup> analogous to spherically-aromatic closo-boranes B<sub>*n*</sub>H<sub>*n*</sub><sup>2-</sup> (*n* = 5-12).<sup>10</sup> The challenging question is how far the Au/H analogy can go in determining the structure and chemical bonding in other mixed clusters containing Au. Oxides of boron hydrides have been studied computationally previously<sup>11</sup> and can be used as reference systems in further exploration of the Au/H analogy.

On the other hand, highly dispersed gold nanoparticles are known to exhibit high catalytic activity in the reaction of low-temperature CO oxidation,<sup>12</sup> which made the research of gold clusters extremely attractive.<sup>13</sup> Elucidation of the nature and

mechanisms of the catalytic activity of nanogold has become a subject of significant scientific efforts.<sup>14-24</sup> While the role of the oxide support is important in nanogold catalysis,<sup>13</sup> there is evidence that the high catalytic activity of nanogold is not based on the presence of a substrate.<sup>15</sup> Therefore, chemisorbed gold cluster complexes can be viewed as molecular models of nanogold catalysts. The fact that  $\text{BO}^-$  anion and CO molecule are valent isoelectronic suggests that auro-boron oxides can be used as a model system to provide further insight into the mechanisms of CO chemisorption on nanogold and nanogold catalytic properties. Studies of the interaction of CO molecules with gold clusters and gold nanoparticles have been carried out,<sup>25-29</sup> revealing pronounced size dependence and chemisorption saturation. Such complexes as  $\text{Au}(\text{CO})_n$  ( $n = 1-5$ ) and  $\text{Au}_n(\text{CO})_2$  ( $n = 1, 2$ ) have been assigned in the study of infrared spectra of Au-CO complexes formed in a rare gas matrix.<sup>29</sup> Zhai and Wang observed several series of gold carbonyl cluster anions  $\text{Au}_m(\text{CO})_n^-$  ( $m = 2-5, n = 1-7$ ) in the gas phase and characterized their electronic structure using photoelectron spectroscopy (PES).<sup>30</sup> It was reported that for a given gold cluster CO adsorption reaches a critical number of saturation that corresponds exactly to the number of available low coordination apex sites of the respective bare gold clusters. In a subsequent work,<sup>31</sup> Wang and co-workers reported a combined PES and ab initio investigation of CO chemisorption on the planar triangular gold hexamer,  $\text{Au}_6(\text{CO})_n^-$  ( $n = 1-3$ ). They showed that the three CO molecules bind to the three apex sites with little structural distortion to the triangular  $\text{Au}_6$  parent.

In the current paper a series of auro-borane oxides  $\text{Au}_n\text{BO}^-$  ( $n = 1-3$ ) has been studied using a combination of PES and density functional calculations. Structures of the corresponding atomic assemblies are established based on the agreement between

experimental and theoretical photoelectron spectra. It turns out that the boron atom of the BO fragment tends to bind with one rather than two gold atoms. Because of this, the BO<sup>-</sup> unit behaves as a monodentate ligand with respect to gold, similar to CO interactions with Au clusters. Analyses of molecular orbitals (MO) and natural bond orbitals (NBO) were carried out to reveal the nature of the chemical bonding in the auro-boron oxides.

## 9-2. Experimental and Computational Methods

### 9-2.1. Photoelectron Spectroscopy

The experiment was carried out using a magnetic-bottle-type PES apparatus equipped with a laser vaporization supersonic cluster source. Details of the apparatus have been described elsewhere.<sup>32,33</sup> Briefly, the Au<sub>n</sub>BO<sup>-</sup> ( $n = 1-3$ ) mixed cluster anions were produced by laser vaporization of a <sup>10</sup>B/Au mixed target in the presence of a pure helium carrier gas during experiments aimed at Au-B binary alloy clusters.<sup>8</sup> In addition to the desired Au/B alloy clusters, the Au<sub>2</sub>BO<sup>-</sup> species appeared to be a particularly intense impurity peak in typical time-of-flight mass spectra and drew our attention. The oxygen impurity was most likely from the target, which was pressed from a mixture of Au and isotopically-enriched <sup>10</sup>B powders. We further noted that two other oxide impurities, Au<sub>n</sub>BO<sup>-</sup> ( $n = 1, 3$ ), were also present, albeit at lower abundance than Au<sub>2</sub>BO<sup>-</sup>. These impurity clusters were carefully studied to elucidate their structure and bonding. They were each mass-selected and decelerated before being photodetached by a pulsed laser beam. Photoelectrons were collected at nearly 100% efficiency by a magnetic bottle and analyzed in a 3.5 m long electron flight tube. The photodetachment experiment was conducted at four detachment photon energies: 532 nm (2.331 eV), 355 nm (3.496 eV),



266 nm (4.661 eV), and 193 nm (6.424 eV). The PES spectra were calibrated using the known spectra of Au<sup>-</sup> and Rh<sup>-</sup>, and the energy resolution of the apparatus was  $\Delta E_k/E_k \approx 2.5\%$ , that is, approximately 25 meV for 1 eV electrons.

### 9-2.2. Computational Methods

The search for the low-energy structures of Au<sub>n</sub>BO<sup>-</sup> ( $n = 1-3$ ) was performed manually because of the small size of the systems. We used the hybrid B3LYP method<sup>34</sup> with LANL2DZ<sup>35</sup> pseudo-potential and basis sets for the preliminary determination of the stationary points on the potential energy surface. The obtained results were refined using Stuttgart relativistic small-core pseudo-potential and valence basis set<sup>36</sup> augmented with two *f* and one *g* function on gold (Stuttgart) and aug-cc-pVTZ (AVTZ hereafter)<sup>37</sup> basis set on boron and oxygen. Computations of the structures of H<sub>n</sub>BO<sup>-</sup> ( $n = 1-3$ ) were performed at the B3LYP/AVTZ level of theory for comparison with the Au<sub>n</sub>BO<sup>-</sup> systems.

Theoretical vertical detachment energies (VDEs) were calculated using time-dependent (TD) density functional theory<sup>38</sup> at the B3LYP/Au/Stuttgart/B,O/AVTZ (at the optimized B3LYP/Au/Stuttgart/B,O/AVTZ geometries) level, which proved to be an inexpensive and reliable method for gold clusters and complexes.<sup>39</sup> In this approach, the VDEs were calculated via the lowest transitions from the ground electronic state of the anion into the ground state of the neutral species (at the B3LYP level of theory) and the vertical excitation energies in the neutral species (at the TD-B3LYP level of theory) at the anion geometry.

Chemical bonding was investigated by means of natural bond orbital (NBO 5.0)<sup>40</sup> and molecular orbital analyses. The Gaussian 03<sup>41</sup> and NWChem<sup>42</sup> software packages

were used throughout this project. The MOLDEN3.4<sup>43</sup> program was chosen for the visualization of the molecular orbitals.

### 9-3. Experimental Results

The PES spectra at various photon energies are shown in Figures 9-1 - 9-3 for  $\text{Au}_n\text{BO}^-$  ( $n = 1-3$ ), respectively. The observed adiabatic and vertical detachment energies (ADEs and VDEs) are summarized in Table 9-1 and compared to theoretical results to be described.

#### 9-3.1 $\text{AuBO}^-$

The 532 nm spectrum of  $\text{AuBO}^-$  (Figure 9-1a) revealed a partially resolved vibrational progression for the ground state transition (X) with a spacing of  $430 \pm 40 \text{ cm}^{-1}$ . The 0-0 transition defines the electron affinity (EA) of  $1.46 \pm 0.02 \text{ eV}$  for the AuBO neutral molecule, whereas the  $1 \leftarrow 0$  transition at  $1.51 \pm 0.02 \text{ eV}$  represents the ground state VDE of the anion. No additional transitions were accessible at higher binding energies in the 355 nm (Figure 9-1b) and 266 nm spectra (not shown). The first excited state (A) of AuBO turned out to be located at a rather high binding energy of  $4.78 \pm 0.03 \text{ eV}$  and was only accessed at 193 nm along with more features beyond 5 eV (Figure 9-1c). The ADE difference between features X and A defines large excitation energy ( $3.27 \text{ eV}$ ) for the first excited state of AuBO, which can also be viewed as HOMO-LUMO gap for the AuBO molecule. This HOMO-LUMO gap for AuBO is substantially greater than for any bare gold clusters<sup>39,44</sup> or bare boron clusters,<sup>45</sup> suggesting AuBO is a very stable closed shell molecule. The features beyond 5.0 eV were more congested and three well-

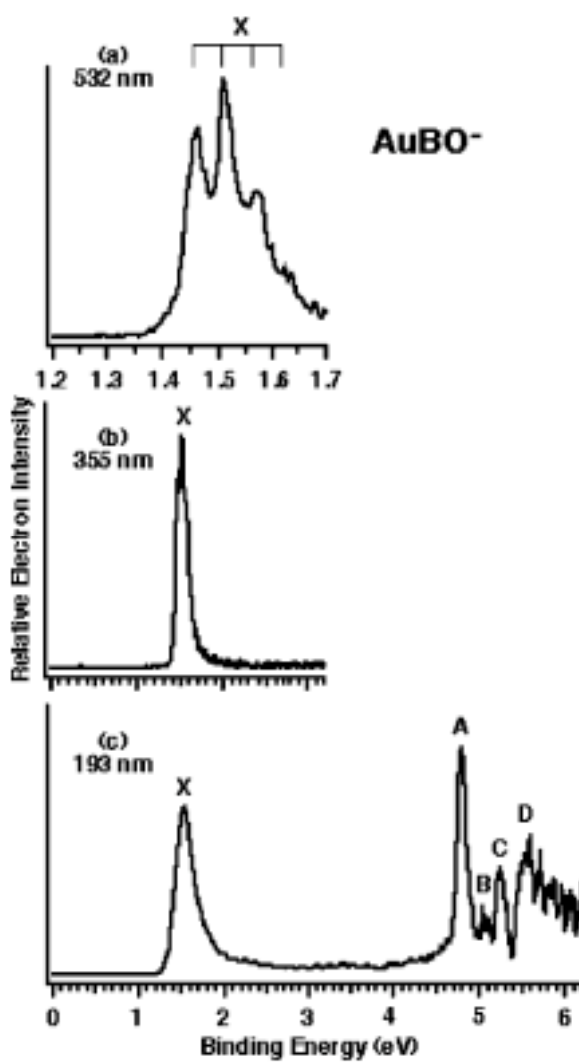


Figure 9-1. Photoelectron spectra of AuBO<sup>-</sup> at (a) 532 nm, (b) 355 nm, and (c) 193 nm. Vertical bars in (a) represent vibrational structures.

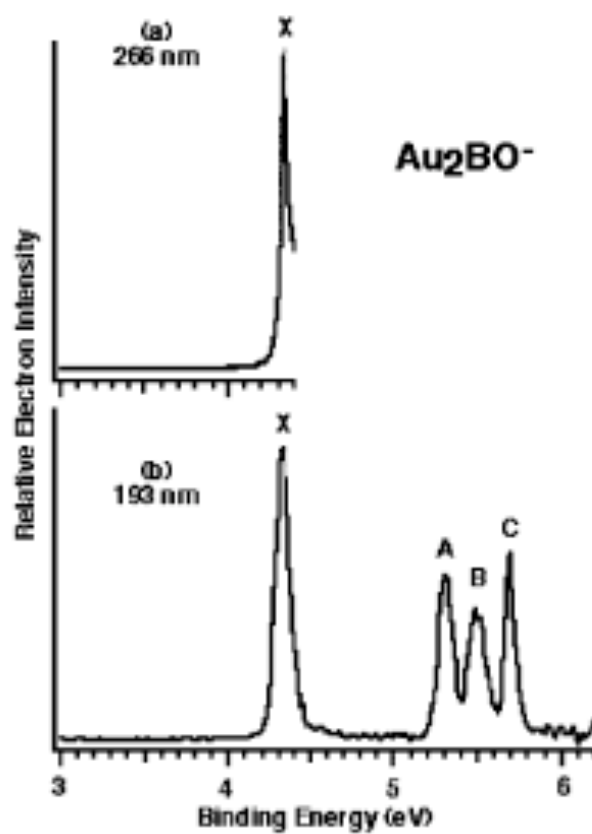


Figure 9-2. Photoelectron spectra of  $\text{Au}_2\text{BO}^-$  at (a) 266 nm and (b) 193 nm.

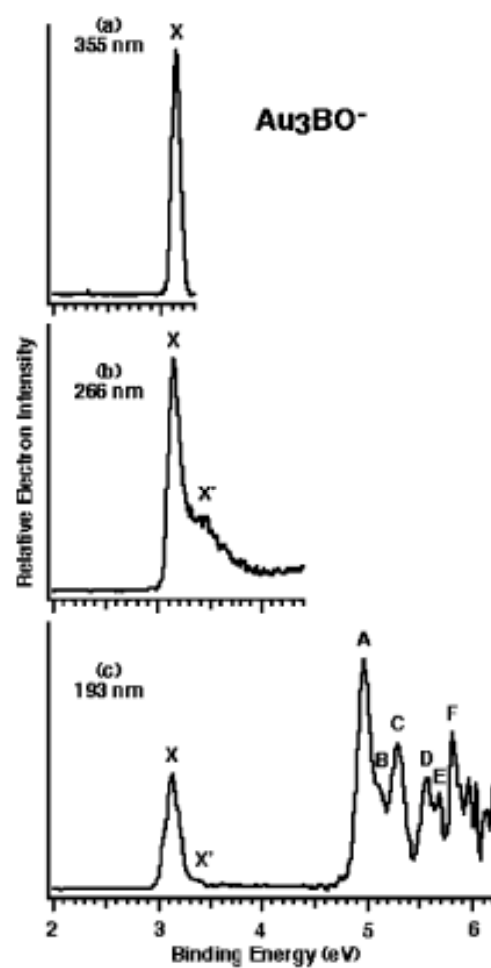


Figure 9-3. Photoelectron spectra of  $\text{Au}_3\text{BO}^-$  at (a) 355 nm, (b) 266 nm, and (c) 193 nm.

Table 9-1. Experimental and Theoretical Vertical Detachment Energies for  $\text{Au}_n\text{BO}^-$  ( $n = 1-3$ ). All energies are in eV.

Species	Feature	ADE (Exp.)	VDE (Exp.)	Final Configuration	TD-B3LYP/Au/ Stuttgart /B <sub>3</sub> O/AVTZ
<b>AuBO<sup>-</sup></b> <b>C<sub>∞v</sub> (<sup>2</sup>Σ<sup>+</sup>)</b>	X	1.46 ± 0.02	1.51 ± 0.02	<sup>1</sup> Σ <sup>+</sup> (1δ <sup>4</sup> 4σ <sup>2</sup> 5σ <sup>0</sup> )	1.48
	A		4.78 ± 0.03	<sup>3</sup> Σ <sup>+</sup> (1δ <sup>4</sup> 4σ <sup>1</sup> 5σ <sup>1</sup> )	4.56
	B		5.07 ± 0.05		
	C		5.26 ± 0.03	<sup>1</sup> Σ <sup>+</sup> (1δ <sup>4</sup> 4σ <sup>1</sup> 5σ <sup>1</sup> )	5.33
	D		5.55 ± 0.05		
<b>Au<sub>2</sub>BO<sup>-</sup></b> <b>C<sub>∞v</sub> (<sup>1</sup>Σ<sup>+</sup>)</b>	X	4.32 ± 0.02	4.33 ± 0.02	<sup>2</sup> Σ <sup>+</sup> (2δ <sup>4</sup> 3π <sup>4</sup> 5σ <sup>2</sup> 6σ <sup>1</sup> )	4.08
	A		5.31 ± 0.02	<sup>2</sup> Σ <sup>+</sup> (2δ <sup>4</sup> 3π <sup>4</sup> 5σ <sup>1</sup> 6σ <sup>2</sup> )	5.19
	B		5.50 ± 0.03	<sup>2</sup> Π (2δ <sup>4</sup> 3π <sup>3</sup> 5σ <sup>2</sup> 6σ <sup>2</sup> )	5.56
	C		5.69 ± 0.02	<sup>2</sup> Δ (2δ <sup>3</sup> 3π <sup>4</sup> 5σ <sup>2</sup> 6σ <sup>2</sup> )	5.86
<b>Au<sub>3</sub>BO<sup>-</sup></b> <b>C<sub>2v</sub> (<sup>2</sup>B<sub>2</sub>)</b>	X	3.08 ± 0.02	3.13 ± 0.02	<sup>1</sup> A <sub>1</sub> (3a <sub>2</sub> <sup>2</sup> 5b <sub>2</sub> <sup>2</sup> 9a <sub>1</sub> <sup>2</sup> 6b <sub>2</sub> <sup>0</sup> )	3.07
	A		4.96 ± 0.03	<sup>3</sup> B <sub>2</sub> (3a <sub>2</sub> <sup>2</sup> 5b <sub>2</sub> <sup>2</sup> 9a <sub>1</sub> <sup>1</sup> 6b <sub>2</sub> <sup>1</sup> )	4.77
	B		5.11 ± 0.05	<sup>1</sup> B <sub>2</sub> (3a <sub>2</sub> <sup>2</sup> 5b <sub>2</sub> <sup>2</sup> 9a <sub>1</sub> <sup>1</sup> 6b <sub>2</sub> <sup>1</sup> )	4.90
	C		5.29 ± 0.03	<sup>3</sup> A <sub>1</sub> (3a <sub>2</sub> <sup>2</sup> 5b <sub>2</sub> <sup>1</sup> 9a <sub>1</sub> <sup>2</sup> 6b <sub>2</sub> <sup>1</sup> )	5.34
	D		5.56 ± 0.03	<sup>3</sup> A <sub>1</sub> (3a <sub>2</sub> <sup>1</sup> 5b <sub>2</sub> <sup>2</sup> 9a <sub>1</sub> <sup>2</sup> 6b <sub>2</sub> <sup>1</sup> )	5.64
	E		5.68 ± 0.03	<sup>1</sup> A <sub>1</sub> (3a <sub>2</sub> <sup>2</sup> 5b <sub>2</sub> <sup>1</sup> 9a <sub>1</sub> <sup>2</sup> 6b <sub>2</sub> <sup>1</sup> )	5.75
	F		5.80 ± 0.02	<sup>1</sup> A <sub>1</sub> (3a <sub>2</sub> <sup>1</sup> 5b <sub>2</sub> <sup>2</sup> 9a <sub>1</sub> <sup>2</sup> 6b <sub>2</sub> <sup>1</sup> )	5.97
<b>Au<sub>3</sub>BO<sup>-</sup></b> <b>C<sub>s</sub> (<sup>2</sup>A')</b>	X'		~ 3.4	<sup>1</sup> A' (13a' <sup>2</sup> 14a' <sup>2</sup> 15a' <sup>0</sup> )	3.67
				<sup>3</sup> A' (13a' <sup>2</sup> 14a' <sup>1</sup> 15a' <sup>1</sup> )	4.89
				<sup>1</sup> A' (13a' <sup>2</sup> 14a' <sup>1</sup> 15a' <sup>1</sup> )	5.51
				<sup>3</sup> A' (13a' <sup>1</sup> 14a' <sup>2</sup> 15a' <sup>1</sup> )	5.60
				<sup>1</sup> A' (13a' <sup>1</sup> 14a' <sup>2</sup> 15a' <sup>1</sup> )	5.85

defined bands were discernible: B ( $5.07 \pm 0.05$  eV), C ( $5.26 \pm 0.03$ eV), and D ( $5.55 \pm 0.05$  eV).

### 9-3.2. $Au_2BO^-$

The electron binding energy of  $Au_2BO^-$  was found to be extremely high and only 266 and 193 nm photons were able to induce electron detachment, as shown in Figure 2. A sharp ground state transition (X) was observed in the 266 nm spectrum with a VDE of  $4.33 \pm 0.02$  eV. Since no vibrational structures were resolved, the ground state ADE was estimated by drawing a straight line along the leading edge of the X band and then adding the instrumental resolution to the intersection with the binding energy axis. The ADE thus evaluated is  $4.32 \pm 0.02$  eV, which also represents the electron affinity of the  $Au_2BO$  neutral species. The extremely high electron affinity suggests that the  $Au_2BO$  neutral is an open shell system, resulting in a highly stable closed-shell  $Au_2BO^-$  anion and its special mass abundance in our cluster source. The 193 nm spectrum (Figure 9-2b) further revealed three well-resolved features: A (VDE:  $5.31 \pm 0.02$  eV), B (VDE:  $5.50 \pm 0.03$  eV), and C (VDE:  $5.69 \pm 0.02$  eV). The band B appeared to be broader and contain a shoulder on the higher binding energy side, whereas band X, A, and C were relatively sharp. The overall PES pattern of  $Au_2BO^-$  is quite simple, consistent with the closed-shell nature of this anion.

### 9-3.3. $Au_3BO^-$

$Au_3BO^-$  also exhibits a rather high electron binding energy (Figure 9-3), although it is much lower than that of  $Au_2BO^-$ . The 355 nm spectrum revealed only the ground state transition X with a VDE of  $3.13 \pm 0.02$  eV and ADE of  $3.08 \pm 0.02$  eV, which also

defines the EA of neutral Au<sub>3</sub>BO. A broad shoulder (labeled X') was observed at ~3.4 eV in the 266 nm spectrum, but it became very weak at 193 nm, suggesting it was likely due to a minor isomer, as borne out from our theoretical calculations (*vide infra*). Numerous additional spectral features were observed at higher binding energies in the 193 nm spectrum (Figure 9-3c) and were reasonably well-resolved. In particular, the first excited state A is located at a rather high binding energy of  $4.96 \pm 0.03$  eV, defining a large HOMO-LUMO gap of 1.83 eV for the Au<sub>3</sub>BO neutral cluster. Beyond band A, the spectrum appears to be congested. Nevertheless, numerous well-defined sharp bands were resolved: B ( $5.11 \pm 0.05$  eV), C ( $5.29 \pm 0.03$  eV), D ( $5.56 \pm 0.03$  eV), E ( $5.68 \pm 0.03$  eV), and F ( $5.80 \pm 0.02$  eV).

## 9-4. Theoretical Results

### 9-4.1. AuBO<sup>-</sup> and HBO<sup>-</sup>

The most stable C<sub>∞v</sub> (<sup>2</sup>Σ<sup>+</sup>) structure I of AuBO<sup>-</sup> is represented in Figure 9-4a and Table 9-2. The geometry of the lowest-energy C<sub>∞v</sub> (<sup>2</sup>Σ<sup>+</sup>) structure II of HBO<sup>-</sup> (Figure 9-4a) is consistent with previous results obtained for the neutral species,<sup>11</sup> but the anion is unstable towards the spontaneous electron detachment (ADE = -0.58 eV at the level of B3LYP/H,B,O/AVTZ). Search for C<sub>∞v</sub> structures of AuOB<sup>-</sup> and HOB<sup>-</sup> where the gold/hydrogen atom is bound to the oxygen atom in both cases resulted in second-order saddle points. Further optimization along the doubly degenerate imaginary vibrational modeled to the C<sub>∞v</sub> (<sup>2</sup>Σ<sup>+</sup>) structure I in the case of AuBO<sup>-</sup>. In the case of HBO<sup>-</sup> we obtained a bent C<sub>s</sub> (<sup>2</sup>A') isomer III that is 38.6 kcal/mol higher than the C<sub>∞v</sub> (<sup>2</sup>Σ<sup>+</sup>) structure II.



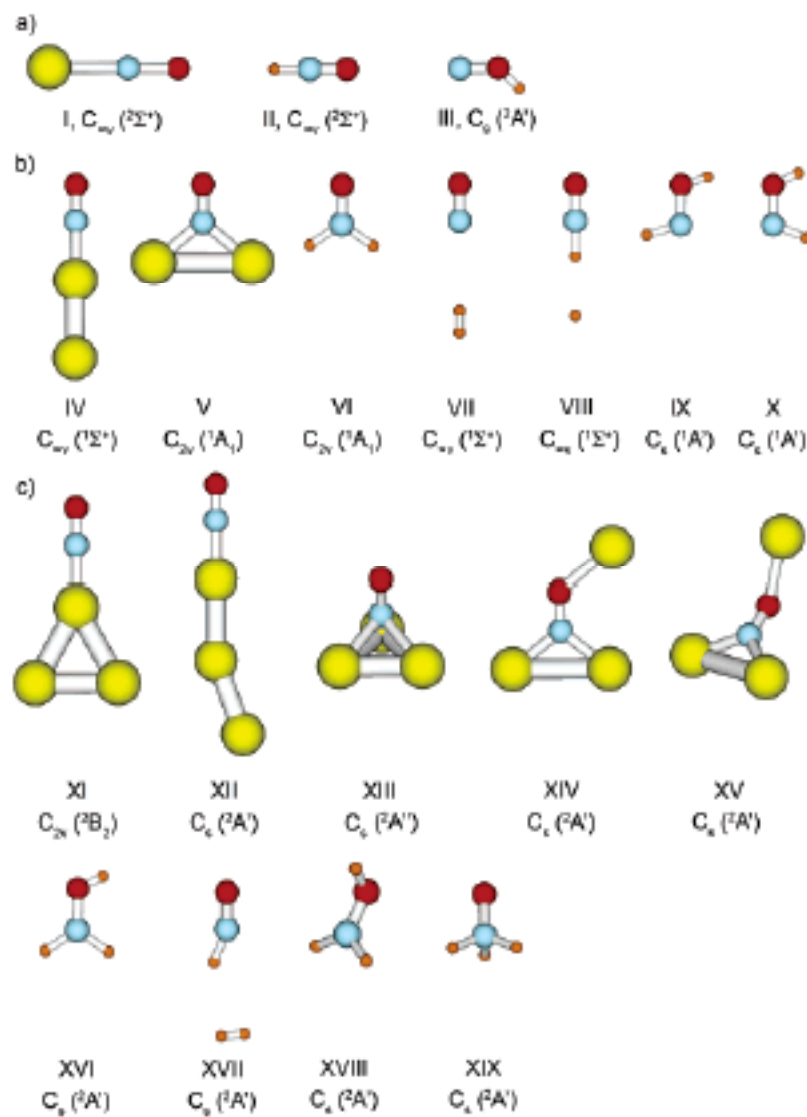


Figure 9-4. Structures of the most stable isomers of auro-borane oxides  $Au_nBO^-$  ( $n = 1-3$ ) and boron hydride oxides  $H_nBO^-$  ( $n = 1-3$ ): (a)  $AuBO^-$  and  $HBO^-$ , (b)  $Au_2BO^-$  and  $H_2BO^-$ , (c)  $Au_3BO^-$  and  $H_3BO^-$ .

Table 9-2. Calculated molecular properties of the lowest-energy structures of auro-borane oxides  $\text{Au}_n\text{BO}^-$  ( $n = 1-3$ ).

$\text{AuBO}^- \text{C}_{\infty\text{v}} (^2\Sigma^+)$ B3LYP/Au/Stuttgart/B,O/AVTZ		$\text{Au}_2\text{BO}^- \text{C}_{\infty\text{v}} (^1\Sigma^+)$ B3LYP/Au/Stuttgart/B,O/AVTZ	
-Etot, a.u.	236.150966	-Etot, a.u.	372.169882
R(B-O), Å R(Au-B), Å	1.225 2.061	R(B-O), Å R(Au <sub>1</sub> -B), Å R(Au <sub>2</sub> -Au <sub>1</sub> ), Å	1.222 2.013 2.659
$\omega_1(\sigma)$ , cm <sup>-1</sup> $\omega_2(\sigma)$ , cm <sup>-1</sup> $\omega_3(\pi)$ , cm <sup>-1</sup>	327 (42.3) <sup>a</sup> 1829 (270.3) <sup>a</sup> 188 (43.0) <sup>a</sup>	$\omega_1(\sigma)$ , cm <sup>-1</sup> $\omega_2(\sigma)$ , cm <sup>-1</sup> $\omega_3(\sigma)$ , cm <sup>-1</sup> $\omega_4(\pi)$ , cm <sup>-1</sup> $\omega_5(\pi)$ , cm <sup>-1</sup>	131 (3.2) <sup>a</sup> 386 (16.4) <sup>a</sup> 1859 (354.0) <sup>a</sup> 53 (4.6) <sup>a</sup> 356 (8.3) <sup>a</sup>
$\text{Au}_3\text{BO}^-$ B3LYP/Au/Stuttgart/B,O/AVTZ			
$\text{C}_{2\text{v}} (^2\text{B}_2)$ , -Etot, a.u.	508.111203	$\text{C}_s (^2\text{A}')$ , -Etot, a.u.	508.109561
R(B-O), Å R(Au <sub>1</sub> -B), Å R(Au <sub>2,3</sub> -Au <sub>1</sub> ), Å $\angle(\text{Au}_2\text{Au}_1\text{Au}_3)$ , °	1.220 2.004 2.809 57.8	R(B-O), Å R(Au <sub>1</sub> -B), Å R(Au <sub>2</sub> -Au <sub>1</sub> ), Å R(Au <sub>3</sub> -Au <sub>2</sub> ), Å $\angle(\text{Au}_3\text{Au}_2\text{Au}_1)$ , °	1.219 2.010 2.715 2.671 160.0
$\omega_1(\text{a}_1)$ , cm <sup>-1</sup> $\omega_2(\text{a}_1)$ , cm <sup>-1</sup> $\omega_3(\text{a}_1)$ , cm <sup>-1</sup> $\omega_4(\text{a}_1)$ , cm <sup>-1</sup> $\omega_5(\text{b}_1)$ , cm <sup>-1</sup> $\omega_6(\text{b}_1)$ , cm <sup>-1</sup> $\omega_7(\text{b}_2)$ , cm <sup>-1</sup> $\omega_8(\text{b}_2)$ , cm <sup>-1</sup> $\omega_9(\text{b}_2)$ , cm <sup>-1</sup>	88 (0.4) 127 (0.5) 395 (6.0) 1869 (437.8) 50 (4.4) 350 (7.2) 30 (7.3) 61 (0.2) 336 (1.1)	$\omega_1(\text{a}')$ , cm <sup>-1</sup> $\omega_2(\text{a}')$ , cm <sup>-1</sup> $\omega_3(\text{a}')$ , cm <sup>-1</sup> $\omega_4(\text{a}')$ , cm <sup>-1</sup> $\omega_5(\text{a}')$ , cm <sup>-1</sup> $\omega_6(\text{a}'')$ , cm <sup>-1</sup> $\omega_7(\text{a}'')$ , cm <sup>-1</sup> $\omega_8(\text{a}'')$ , cm <sup>-1</sup> $\omega_9(\text{a}'')$ , cm <sup>-1</sup>	12 (0.8) 89 (0.7) 141 (0.1) 386 (21.8) 1873 (419.5) 39 (4.4) 41 (4.4) 335 (7.2) 335 (8.4)

<sup>a</sup> Infrared intensities (km/mol) are given in parenthesis.

### 9-4.2. $Au_2BO^-$ and $H_2BO^-$

The ground state of  $Au_2BO^-$  has a linear  $C_{\infty v}$  ( $^1\Sigma^+$ ) structure IV (Figure 9-4b and Table 9-2). The energetically closest  $C_{2v}$   $^1A_1$  isomer (structure V, Figure 9-4b) is 25.0 kcal/mol less stable. On the contrary, the  $C_{2v}$   $^1A_1$  structure VI of  $H_2BO^-$  is the most stable isomer.  $H_2BO^-$  also has two higher-energy isomers with  $C_{\infty v}$  symmetry. The first one is the  $C_{\infty v}$  ( $^1\Sigma^+$ ) structure VII ( $\Delta E_{total} = 20.4$  kcal/mol) that represents a van der Waals complex between  $H_2$  and  $BO^-$ . The second one is the  $C_{\infty v}$  ( $^1\Sigma^+$ ) structure VIII ( $\Delta E_{total} = 41.6$  kcal/mol) that corresponds to a Van der Waals complex of  $H^-$  and  $HBO$ . The different energetic preference of the isomers, or the tendency of the boron atom of the  $BO$  fragment to bind to one atom of gold (monodentate behavior), but to two atoms of hydrogen (bidentate behavior) is remarkable and will be considered in details in the chemical bonding section (see below).

$H_2BO^-$  also has stable *cis* and *trans* configurations where one hydrogen atom is bound to the boron atom and the other to the oxygen atom (structures IX and X, Figure 9-4b). The *trans*-isomer IX ( $C_s$   $^1A'$ ) is found to be 56.2 kcal/mol higher than the ground state structure VI and the *cis*-isomer X ( $C_s$   $^1A'$ ) is 60.0 kcal/mol higher. Analogous isomers of  $Au_2BO^-$  were not found in our search. When starting from the corresponding *cis*- and *trans*- configurations of  $Au_2BO^-$ , our optimization led to the ground state structure IV or to an unbound Au atom and  $AuBO^-$ .

### 9-4.3. $Au_3BO^-$ and $H_3BO^-$

The  $C_{2v}$  ( $^2B_2$ ) structure XI (Figure 9-4c, Table 9-2) was found to be the most stable isomer for  $Au_3BO^-$ . The next isomer, the  $C_s$  ( $^2A'$ ) structure XII (Figure 9-4c, Table

9-2), is only 1.0 kcal/mol higher in energy and is expected to contribute to the photoelectron spectrum of  $\text{Au}_3\text{BO}^-$ . Again, while in the ground state of  $\text{Au}_3\text{BO}^-$  the boron atom behaves in a monodentate manner towards gold, it exhibits bidentate behavior towards hydrogen in the  $C_s$  ( ${}^2A'$ ) global minimum structure XVI of  $\text{H}_3\text{BO}^-$  (Figure 9-4c). The anionic  $C_s$  ( ${}^2A'$ )  $\text{H}_3\text{BO}^-$  is unstable towards spontaneous electron detachment (ADE = -0.41 eV). A similar isomer was found for  $\text{Au}_3\text{BO}^-$  ( $C_s$  ( ${}^2A'$ ) structure XIV, Figure 9-4c), but it is 39.3 kcal/mol higher than structure XI. The  $C_s$  ( ${}^2A'$ ) structure XVII of  $\text{H}_3\text{BO}^-$ , which is 15.9 kcal/mol higher, can be considered as corresponding to both structures XI and XII of  $\text{Au}_3\text{BO}^-$ . While the  $C_s$  ( ${}^2A'$ ) structure XV is another isomer of  $\text{Au}_3\text{BO}^-$  with a relative energy 40.4 kcal/mol, the similar structure XVIII  $C_s$  ( ${}^2A'$ ) for  $\text{H}_3\text{BO}^-$  is a first-order saddle point. The imaginary mode leads to the global minimum structure XVI. Two more similar structures are present among the isomers of  $\text{Au}_3\text{BO}^-$  and  $\text{H}_3\text{BO}^-$ :  $C_s$  ( ${}^2A''$ ) structure XIII ( $E_{\text{relative}} = 32.6$  kcal/mol) and  $C_s$  ( ${}^2A'$ ) structure XIX ( $E_{\text{relative}} = 21.5$  kcal/mol), respectively (Fig. 9-4c).

## 9-5. Interpretation of the Experimental Photoelectron Spectra

### 9-5.1. $\text{AuBO}^-$

The  $C_{\infty v}$  ( ${}^2\Sigma^+$ ) doublet ground state of  $\text{AuBO}^-$  cluster has a valence electron configuration of  $2\pi^4 1\delta^4 4\sigma^2 5\sigma^1$  and can give rise to either singlet or triplet final states upon electron detachment. The first calculated VDE corresponds to the removal of the unpaired electron from the  $5\sigma$  orbital, resulting in the  ${}^1\Sigma^+$  final state. The calculated VDE of 1.48 eV is in excellent agreement with the experimental value of 1.51 eV (Table 9-1).

The calculated vibrational frequency for the Au-B stretching in neutral AuBO [ $\omega_1(\sigma) = 430 \text{ cm}^{-1}$ ] also agrees well with the resolved vibrational frequency for the ground state transition ( $430 \pm 30 \text{ cm}^{-1}$ ). The second detachment channel involves the  $4\sigma$  orbital (the HOMO of the neutral species) and leads to the  $^3\Sigma^+$  final state. The computed VDE value of 4.56 eV agrees well with that of feature A at 4.78 eV (Table 9-1). There is another detachment channel for the  $4\sigma$  orbital, which results in a singlet final state. The computed VDE (5.33 eV) for this detachment channel is in excellent agreement with the observed peak C (VDE = 5.26 eV). The relative intensity ratio of bands A and C and their similar shape are consistent with the assignments that they are due to the triplet/singlet pair from detachment from the same orbital. Detachments from deeper orbitals, which correspond to features B, D, and the congested signals at higher binding energies (Figure 9-1c), involve Au 5d-based orbitals and are complicated by the strong spin-orbit coupling (SOC) effect. The calculated VDEs for detachments from the  $5\sigma$  and  $4\sigma$  orbitals are in good agreement with the experiments because these two orbitals are mainly from Au 6s orbital, which is not subject to the SOC effect. However, without including the SOC effect, the calculated electron detachment energies corresponding to removing electrons from the Au 5d-based  $1\delta$  and  $2\pi$  orbitals are inconsistent with the experiment. Calculations of VDEs including the SOC effect is beyond the scope of the current work.

### 9-5.2. $Au_2BO^-$

The ground state of  $Au_2BO^-$  is a singlet with  $C_{\infty v}$  ( $^1\Sigma^+$ ) symmetry and possesses a closed shell configuration,  $2\delta^4 3\pi^4 5\sigma^2 6\sigma^2$ , which leads only to doublet final states upon

electron detachment. The first detachment channel involves the  $6\sigma$  orbital and the computed VDE of 4.08 eV is in good agreement with the ground state transition observed experimentally at 4.33 eV (Table 9-1). The observed band A (VDE: 5.31 eV) should correspond to detachment from the  $5\sigma$  orbital and again computed VDE (5.19 eV) agrees well with the experimental VDE. The observed bands B and C should correspond to detachments from the  $3\pi$  and  $2\delta$  orbitals, respectively. Even without including the SOC effect, the computed VDEs agree fortuitously well with the observed VDEs (Table 9-1). The SOC effect is expected to be relatively small for the  ${}^2\Pi$  state because of the BO contribution to the  $3\pi$  orbital. In fact, band B appeared to contain two components with a shoulder on the higher binding energy side, which might be due to the spin-orbit splitting of the  ${}^2\Pi$  state. However, the SOC effect of the  ${}^2\Delta$  state is expected to be very large because the  $2\delta$  orbital is predominantly of Au 5d character. Thus, band C, which was fairly sharp, might correspond to one spin-orbit component of the  ${}^2\Delta$  state with the other component at a higher binding energy beyond the 193 nm photon energy.

### 9-5.3. $Au_3BO^-$

The lowest energy structure of  $Au_3BO^-$  is  ${}^2B_2$  with an electron configuration of  $3a_2^2 5b_2^2 9a_1^2 6b_2^1$ , which can lead to both singlet and triplet final states upon electron detachment (Table 9-1). The ground state transition (X) should correspond to detachment from the  $6b_2$  orbital and the calculated VDE (3.07 eV) is in excellent agreement with the experimental value of 3.13 eV (Table 9-1). The  $6b_2$  orbital is an antibonding orbital between two Au atoms (Figure 9-8) and the X band should contain an unresolved low-frequency Au-Au vibrational progression, which explains the difference

between the ADE (3.08 eV) and VDE (3.13 eV) of the ground state transition (Figure 9-3 and Table 9-1). The band A should correspond to electron detachment from the  $9a_1$  orbital leading to the triplet final state  $^3B_2$ . The computed VDE (4.77 eV) is lower than the experimental VDE (4.96 eV) by almost 0.2 eV (Table 9-1). The corresponding  $^1B_2$  singlet final state with a computed VDE of 4.90 eV (Table 9-1) should be then assigned to the B band at a VDE of 5.11 eV, which was only partially resolved from the more intense A band (Figure 9-3c). The next detachment channel is from  $5b_2$  orbital, resulting a triplet  $^3A_1$  (VDE: 5.34 eV) and singlet  $^1A_1$  (VDE: 5.75 eV) final states. The computed VDEs are in good agreement with the observed VDEs of bands C and E, respectively (Table 9-1). And the next higher binding energy photodetachment channel is from the  $3a_1$  orbital, which give rise to a triplet  $^3A_1$  (VDE: 5.64 eV) and a singlet  $^1A_1$  (VDE: 5.97 eV), which are in good agreement with the measured VDEs for bands D and F, respectively. Band F is more intense than band D, suggesting that it might contain contributions from other detachment channels

The  $C_s$  ( $^2A'$ ) isomer (structure XII, Figure 9-4c) of  $Au_3BO^-$  is very close in energy to the  $C_{2v}$  ( $^2B_2$ ) ground state and might be present experimentally. Indeed, the calculated VDE from the  $15a'$  SOMO (Figure 9-9) of the  $C_s$  ( $^2A'$ ) isomer is in reasonable agreement with the broad feature X' observed in the 266 nm (Figure 9-3b and Table 9-1). The contributions of the  $C_s$  ( $^2A'$ ) isomer to the 193 nm spectrum (Figure 9-3c) appear to be greatly diminished and should not interfere with the above assignment of the main isomer.

## 9-6. Chemical Bonding in $\text{Au}_n\text{BO}^-$ and $\text{H}_n\text{BO}^-$ ( $n = 1-3$ )

The overall agreement between the theory and experiment (Table 9-1) is gratifying for all three  $\text{Au}_n\text{BO}^-$  species, lending credence to the obtained global minimum structures. In this section, we discuss the details of the chemical bonding in  $\text{Au}_n\text{BO}^-$  and compare with that in the corresponding  $\text{H}_n\text{BO}^-$  and  $\text{Au}_n\text{CO}$  species for  $n = 1-3$ .

### 9-6.1. $\text{AuBO}^-$ and $\text{HBO}^-$

To simplify the analysis of the chemical bonding in the open-shell  $\text{AuBO}^-$ , we first consider the neutral  $\text{AuBO}$  species. Our NBO analysis of  $\text{AuBO}$  at the geometry of  $\text{AuBO}^-$  is summarized in the Table S1 of the Supporting Information. The  $5\sigma$  SOMO of  $\text{AuBO}^-$  (Figure 9-5) becomes the LUMO of  $\text{AuBO}$ , whereas the  $4\sigma$  orbital becomes the HOMO of  $\text{AuBO}$  species. NBO analysis shows a relatively simple bonding picture in  $\text{AuBO}$ , because it involves only two-center two-electron (2c-2e) bonds and lone pairs. There is a triple bond in the BO moiety and a single  $\sigma$ -bond between Au and BO. Five nearly pure d-character lone pairs are encountered on Au and one on oxygen with sp hybridization. The charge distribution is as follows: -0.84 |e| on oxygen, 0.70 |e| on boron, and 0.14 |e| on gold, indicating a fairly strong covalent bond between Au and B with only a slight charge transfer from Au to BO. In  $\text{AuBO}^-$ , the  $5\sigma$  SOMO, which is pretty much the 6s AO of Au but with antibonding character in the Au-B fragment (Figure 9-5), is singly occupied. Our NBO analysis of the open-shell  $\text{AuBO}^-$  (Table S2) shows that while the triple B-O bond, the lone pair at the oxygen, and the five lone pairs at the gold are preserved, the occupation number (OC) of the bonding orbital responsible for Au-B bond drops to only 1.00 |e| compared to 2.00 |e| in the neutral  $\text{AuBO}$ . The



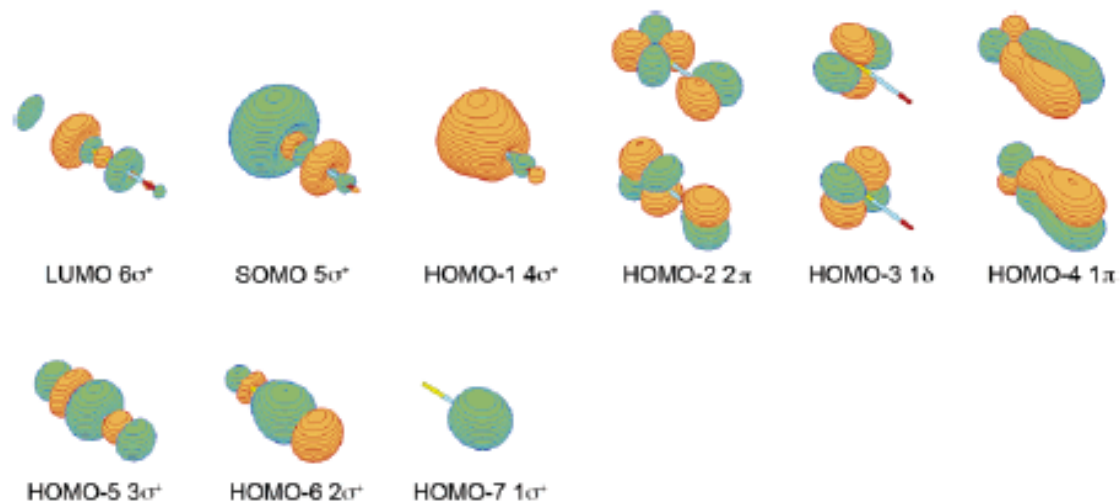


Figure 9-5. Molecular orbitals of  $\text{AuBO}^-$   $C_{\infty v}$  ( $^2\Sigma^+$ ).

oxygen atom carries a negative charge of  $-0.96 |e|$ , the Au and B have almost equal charges of opposite sign ( $-0.39 |e|$  and  $0.35 |e|$ , respectively). The additional electron is almost equally distributed over the Au ( $0.53 |e|$ ) and B ( $0.35 |e|$ ) atoms with just  $0.12 |e|$  acquired by O. The natural configuration of B is  $2s^{1.14}2p^{1.42}$ . So, in the ground state structure of  $\text{AuBO}^-$ , the Au atom is still covalently bound to the B atom of the  $\text{BO}^-$  fragment, though the chemical structure is halfway down to the elimination of the Au-B  $\sigma$ -bond and formation of a complex between Au and  $\text{BO}^-$  similar to the bonding in AuCO.

The linear anionic  $\text{HBO}^-$  (structure II, Figure 9-4a) is unstable and detachment of an electron lowers the energy of the system by approximately 13 kcal/mol. This is because the  $5\sigma$  orbital in AuBO can easily accommodate an extra electron, whereas H in HBO does not possess an equivalent accepting property. Thus, the Au/H analogy still

holds in neutral AuBO, but it reaches its limit in the anion due to the inability of hydrogen to accept any significant part of the extra electron.

### 9-6.2. $Au_2BO^-$ and $H_2BO^-$

We start our analysis of the chemical bonding in the  $Au_2BO^-$  system by first considering the  $Au_2BO^+$  cation, which has two electrons less than the anionic system. Reoptimization of the anionic structures of the  $C_{\infty v}$  ( $^1\Sigma^+$ ) isomer IV and  $C_{2v}$  ( $^1A_1$ ) isomer V at the B3LYP/Au/Stuttgart/B,O/AVTZ level of theory shows that for the cation the  $C_{\infty v}$  ( $^1\Sigma^+$ ) structure becomes a second-order saddle-point and the  $C_{2v}$  ( $^1A_1$ ) structure remains a local minimum. The same  $C_{2v}$  ( $^1A_1$ ) local minimum structure is achieved if the imaginary mode of the  $C_{\infty v}$  ( $^1\Sigma^+$ ) structure is followed. The geometry of the  $C_{2v}$  structure of the cation is more “compact” compared with the  $C_{2v}$  anion: the Au-Au distance is 2.664 Å in the cation vs. 3.235 Å in the anion, the Au-B distance is 2.103 Å vs. 2.098 Å, and the B-O distance is 1.207 Å vs. 1.240 Å. These structural changes are understandable because the HOMO ( $5b_2$ ) of the  $C_{2v}$   $Au_2BO^-$  has strong Au-Au antibonding character (Figure 9-6). Molecular orbitals of the  $C_{2v}$  ( $^1A_1$ )  $Au_2BO^+$  are similar to those of the  $C_{2v}$  ( $^1A_1$ ) structure V of  $Au_2BO^-$  (Figure 9-6), except that the  $5b_2$  orbital is no longer occupied in the cation. The fourteen lowest occupied orbitals can be attributed to the triple B-O bond, the oxygen atom lone pair, and the ten lone pairs of the two gold atoms. Even though the  $d_{z^2}$  orbitals ( $2a_1$  and  $3a_1$ ) have considerable contributions to the bonding of the  $Au_2B$  framework, the  $6a_1$  orbital is a three-center two-electron ( $3c-2e$ ) bond for the bonding in the  $Au_2B$  fragment, rendering  $\sigma$ -aromaticity to the  $Au_2BO^+$  cation. Indeed, our NBO analysis is consistent with this interpretation of the chemical

bonding in the  $C_{2v}$  ( $^1A_1$ ) structure of  $Au_2BO^+$  (Table S3), revealing a 3c-2e bond with  $OC = 2.00 |e|$  between the two Au and the B atom. The triple B-O bond, the lone pair of the oxygen, and the five lone pairs on each gold atom can be identified as well. NICS indexes calculated at the center of the  $Au_2B$  triangle support the assertion of aromaticity in  $Au_2BO^+$ :  $NICS(0) = -40.0$  ppm,  $NICS(0.5) = -29.6$  ppm, and  $NICS(1.0) = -13.8$  ppm. The estimated interaction energy between the  $Au_2$  and BO fragments in  $Au_2BO^+$  is 85.1 kcal/mol at the B3LYP/Au/Stuttgart/B,O/AVTZ level of theory, indicating that they are indeed strongly bound by chemical bonding.

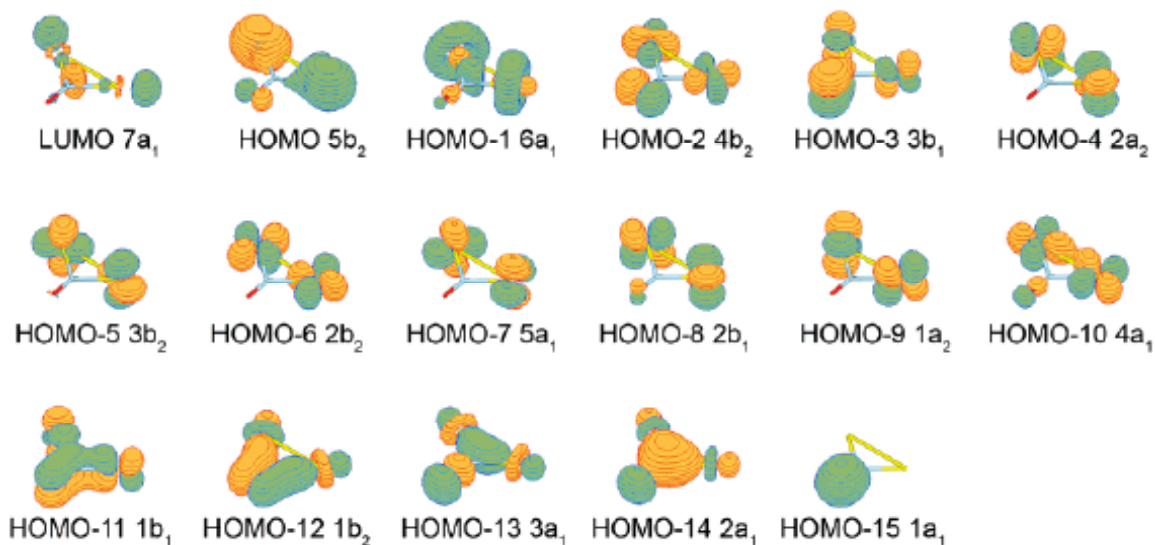


Figure 9-6. Molecular orbitals of  $Au_2BO^-$   $C_{2v}$  ( $^1A_1$ ).

It is straightforward to understand the changes in the bonding pattern as a pair of electron is added to  $Au_2BO^+$  to form  $Au_2BO^-$ . There are two options to add the pair of electrons. The first option is to have the electron pair occupy the  $5b_2$  orbital to yield the  $C_{2v}$  ( $^1A_1$ ) isomer V of  $Au_2BO^-$ . Since the  $5b_2$  is antibonding between the two gold atoms,

the  $C_{2v}$  isomer of  $Au_2BO^-$  becomes antiaromatic. Consequently, two localized 2c-2e Au-B bonds are formed in  $Au_2BO^-$ , compared to one 3c-2e  $Au_2$ -B bond in  $Au_2BO^+$ . Our NBO analysis clearly shows that this is indeed the case (Table S4). Two Au-B bonds with  $OC = 1.74 |e|$  are formed now. The triple bond between oxygen and boron undergoes some minor changes. One of the  $\pi$ -bonds becomes more polarized toward oxygen and its occupation number drops from 1.95  $|e|$  to 1.92  $|e|$ . Its composition reveals some contribution of d- and f-functions (10% and 10% respectively) on B in addition to p-functions (80%). The natural configuration of the boron atom is  $2s^{0.80}2p^{1.66}$ . Hence, the polarized  $\pi$ -bond between boron and oxygen is actually a p-lone pair of oxygen. The antiaromaticity of the Au-B-Au fragment of the  $C_{2v}$  ( $^1A_1$ ) structure V is confirmed by the obtained NICS values:  $NICS(0) = -15.0$  ppm,  $NICS(0.5) = 18.0$  ppm, and  $NICS(1.0) = 13.0$  ppm.

Alternatively, the pair of electrons can occupy the  $7a_1$  orbital (Figure 9-6), which is bonding between two gold atoms and antibonding between  $Au_2$  and BO fragments. This occupation will cause the transformation of the 3c-2e  $Au_2$ -B bond into a lone pair on the boron atom and a 2c-2e Au-Au bond. Optimization of the  $C_{2v}$  structure with this electron configuration leads to a second-order saddle point, where the Au-Au, Au-B, and B-O distances become 2.547, 3.099, and 1.230 Å, respectively. NBO analysis of this system confirms that an Au-Au bond with  $OC = 1.97 |e|$  and a lone pair on the boron atom ( $OC = 1.92 |e|$ ) are formed, instead of a 3c-2e  $Au_2$ -B bond. The presence of two imaginary normal modes can be attributed to the electrostatic instability of the system. Charge distribution shows that the  $Au_2$  unit is almost electro-neutral (total charge is -0.04  $|e|$ ; -0.02  $|e|$  on each gold atom), while  $OB^-$  unit has a dipole with strongly negative

charge of  $-1.03 |e|$  on the oxygen atom and an almost neutral boron atom ( $0.07 |e|$ ). Following the largest imaginary mode, we found that the  $C_{2v}$  geometry transforms into the  $C_{\infty v}$  ( $^1\Sigma^+$ ) global minimum structure IV of  $Au_2BO^-$ . Results of the NBO analysis show that the charge is redistributed: the terminal gold atom has negative charge of  $-0.63 |e|$ , the other gold atom is almost neutral with  $0.06 |e|$ , the boron atom becomes significantly positive ( $0.52 |e|$ ), and the oxygen basically preserves its negative charge ( $-0.94 |e|$ ). In the neutral  $C_{\infty v}$  species the charge on the terminal gold atom is  $0.12 |e|$ , the other gold is almost neutral with  $0.01 |e|$ , the charge on boron is  $0.70 |e|$  and is  $-0.84 |e|$  on oxygen. Comparison of the charge distribution in the anionic vs. neutral species clearly shows that the extra electron is almost completely acquired by the terminal gold atom ( $0.86 |e|$ ). The natural configuration of the boron atom is  $2s^{1.00}2p^{1.44}$  and the bonding pattern reflects these changes. The lone pair of the boron atom obviously transforms into the Au-B bond ( $OC = 2.00 |e|$ ) and the Au-Au bond transforms into the sixth lone pair of the terminal gold atom ( $OC = 1.64 |e|$ ). The low occupation number of this lone pair suggests that it possibly contributes to the bonding between the terminal  $Au^-$  and the AuBO unit. The estimated energy of this bond is  $57.5$  kcal/mol. The molecular orbitals of this isomer are presented at Fig. 9-7. Indeed, the  $6\sigma$  orbital is mainly responsible for the formation of the lone pair on the terminal Au, but it also has some bonding character in the Au-B region. Second order perturbation theory analysis available within NBO shows that there is significant donor-acceptor interaction between this lone pair and the low-occupation Au-B bond ( $OC = 0.34 |e|$ ). So, the ground state  $C_{\infty v}$  ( $^1\Sigma^+$ ) isomer IV of  $Au_2BO^-$  can be reasonably described as a stable neutral AuBO cluster bound with an  $Au^-$  anion by a donor-acceptor interaction.

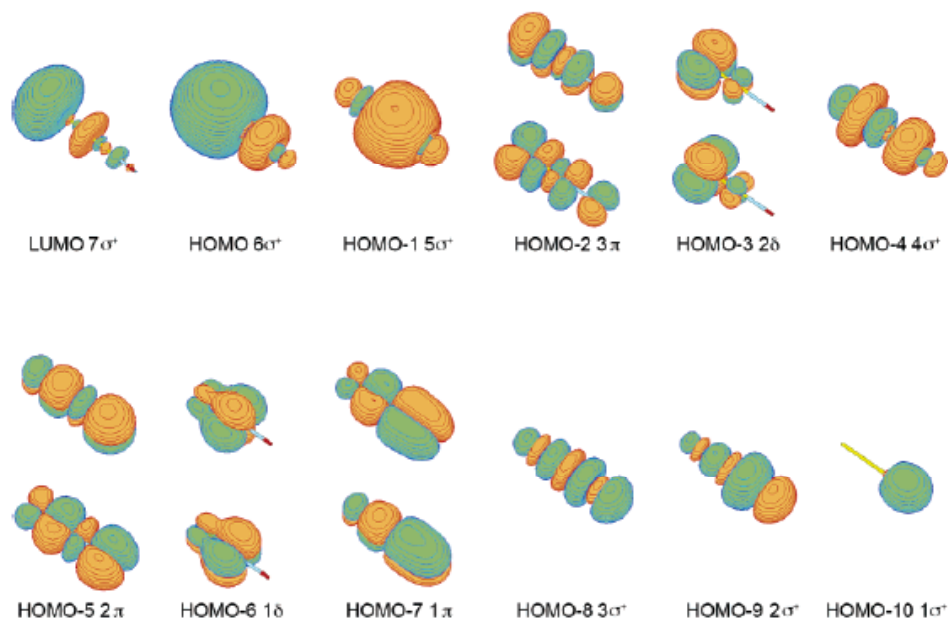


Figure 9-7. Molecular orbitals of  $\text{Au}_2\text{BO}^- C_{\infty v} (^1\Sigma^+)$ .

The  $C_{2v} (^1A_1)$  ground state structure of  $\text{H}_2\text{BO}^-$  (structure VI, Figure 9-4b) is a classical molecule and has a very simple bonding pattern, which is confirmed by our NBO analysis. There is a double bond between oxygen and boron, two B-H bonds, a lone pair with contribution from s- and p-functions (44% and 56% respectively) as well as an additional pure p-lone pair at the oxygen atom. The natural configuration of the boron atom is  $2s^{0.73}2p^{1.01}3p^{0.76}$ . Interestingly, the comparison of the charge distribution in the anionic and neutral  $C_{2v}$  species shows that the extra electron is mainly acquired by oxygen (-0.99 |e| vs. -0.44 |e|) and the two hydrogen atoms (-0.24 |e| vs. 0.00 |e|), while boron preserves its charge (0.47 |e| vs. 0.44 |e|). So the stabilization of the extra charge occurs due to its delocalization, in contrast to the  $C_{\infty v}$  isomer IV of  $\text{Au}_2\text{BO}^-$ , where the extra electron density is stabilized by the terminal gold atom.

### 9-6.3. $Au_3BO^-$ and $H_3BO^-$

$Au_3BO^-$  cluster is also an open shell system so again we first consider the neutral  $C_{2v}$   $Au_3BO$  with an electron removed from the SOMO of the  $C_{2v}$  ( $^2B_2$ ) ground state (Figure 9-8). As shown in Figure 9-8, the twenty lowest molecular orbitals consist of a triple B-O bond, a single Au-B bond in the AuBO fragment, a lone pair at the oxygen atom, and five 5d lone pairs at each gold atom. The  $9a_1$  orbital accounts mainly for Au-Au bonding between the outer gold atoms. Thus  $Au_3BO$  is a classical molecule, which is supported by our NBO analysis. The expected bond between the outer gold atoms has OC equal to 1.76 |e| and the other bonding pairs all have OCs of 2. The natural configuration of the boron atom is  $2s^{0.90}2p^{1.48}$ . Therefore, the  $C_{2v}$  structure of  $Au_3BO$  can be represented as a complex of a  $Au_2$  and a AuBO unit. The  $Au_2$  moiety carries a positive charge of 0.26 |e| equally distributed between the two atoms, and the AuBO unit has a dipole with a total charge of -0.26 |e| [O: -0.85 |e|; B: +0.58 |e|; Au: +0.01 |e|]. Thus,  $Au_3BO$  can be viewed as a  $Au_2[AuBO]$  complex. The estimated interaction energy between  $Au_2$  and AuBO is 23.0 kcal/mol. In the anion  $Au_3BO^-$ , the extra electron enters the  $6b_2$  orbital (Figure 9-8), which is antibonding between the  $Au_2$  moiety. Thus in  $Au_3BO^-$ , the bonding in the  $Au_2$  unit will be weakened, but not eliminated completely, which is consistent with our NBO analysis of the  $C_{2v}$  ( $^2B_2$ ) isomer of  $Au_3BO^-$ . The additional electron (0.98 |e|) is equally distributed over the two Au atoms in the  $Au_2$  unit. No changes occur in the bonding pattern of the AuBO unit, but in  $Au_2$  unit the OC of the Au-Au bond is decreased to 0.88 |e|. The total charge on the  $Au_2$  is -0.72 |e|, whereas that on the AuBO unit is -0.29 |e|. Thus, the  $C_{2v}$  ( $^2B_2$ ) isomer XI of  $Au_3BO^-$  can be considered

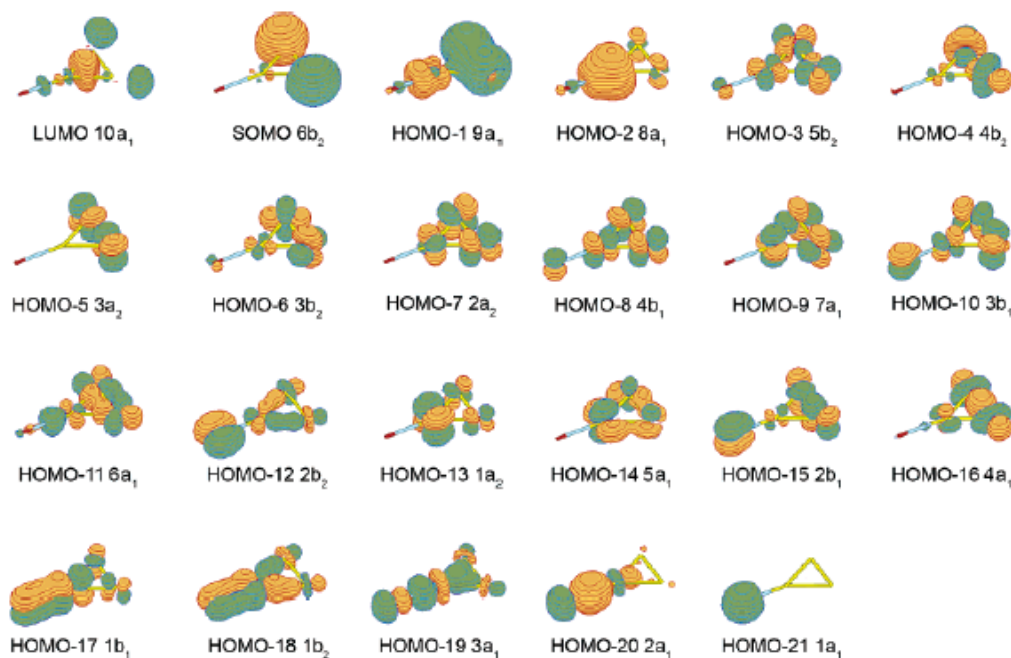


Figure 9-8. Molecular orbitals of  $\text{Au}_3\text{BO}^- C_{2v} (^2B_2)$ .

as a complex of  $\text{Au}_2^-$  and  $\text{AuBO}$ , i.e.,  $\text{Au}_2^-[\text{AuBO}]$ . The estimated interaction energy is 47.6 kcal/mol, which is twice as strong as the  $\text{Au}_2$  and  $\text{AuBO}$  interaction in  $\text{Au}_3\text{BO}$ . A second order perturbation theory analysis shows significant interaction of the Au-Au bond ( $\text{OC} = 0.88 |e|$ ) with the low-occupation Au-B bond in the  $\text{AuBO}$  fragment ( $\text{OC} = 0.26 |e|$ ).

Molecular orbitals of the low-lying  $C_s (^2A')$  isomer XII of  $\text{Au}_3\text{BO}^-$  are presented at Figure 9-9. Interestingly, our analyses show that identical sets of orbitals are occupied for both isomers XI and XII, i.e. it is not a switch of orbitals from occupied and unoccupied spaces that causes distortion of the geometry from  $C_{2v}$  to  $C_s$  symmetry. The bonding pattern revealed by the NBO analysis supports this idea. Except for the charge



redistribution, the  $C_s$  structure XII does not differ too much from the  $C_{2v}$  structure XI. We found that only low-occupancy lone-pairs at the gold atoms of the  $Au_2^-$  unit contribute to the donor-acceptor interaction with AuBO in the  $C_s$  isomer. The interaction energy is 47 kcal/mol, which is identical to that in the  $C_{2v}$   $Au_3BO^-$ .

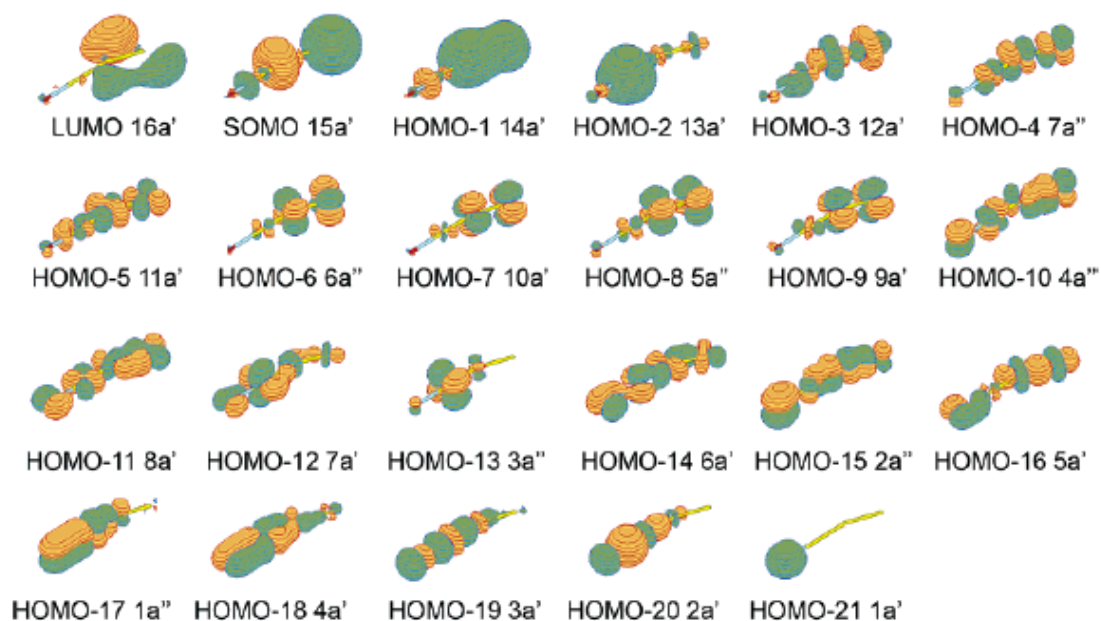


Figure 9-9. Molecular orbitals of  $Au_3BO^- C_s (^2A')$ .

The open-shell  $C_s (^2A')$  isomer XVI of  $H_3BO^-$  is electronically unstable. This explains the fact that the NBO analysis distributes one electron among several non-bonding orbitals, so that the bonding pattern in terms of lone pairs and 2c-2e bonds is identical to one of the neutral  $C_s$  species: there is a double bond between O and B, two single H-B bonds, one single H-O bond, and a lone pair at the oxygen atom. The obtained picture of Lewis bonding is related with bonding in the  $C_{2v} (^1A_1)$  ground state structure VI of  $H_2BO^-$  described in the previous section, where one lone pair of the

oxygen formed a bond with a proton. If compared with the neutral species, in the anion oxygen acquired 0.06 |e|, boron acquired 0.13 |e|, hydrogen atoms bound to boron acquired total of 0.21 |e|, and the hydrogen atom bound to oxygen got 0.59 |e|. Once again, this demonstrates that hydrogen atoms in  $\text{H}_3\text{BO}^-$  cannot electrostatically stabilize an additional electron as Au atoms do in  $\text{Au}_3\text{BO}^-$ .

#### 9-6.4. $\text{Au}_n\text{BO}^-$ vs $\text{Au}_n\text{CO}$

Since  $\text{BO}^-$  is isoelectronic with CO, it is also interesting to compare the bonding between  $\text{Au}_n\text{BO}^-$  and  $\text{Au}_n\text{CO}$ . We computed the dissociation energies of  $\text{Au}_n\text{BO}^-$  to  $\text{Au}_n + \text{BO}^-$ , as follows:



These interaction energies are significantly higher than the  $\text{Au}_n\text{CO}$  dissociation energies, which range from 18.4 kcal/mol for  $n = 1$ , to 35.2 kcal/mol for  $n = 2$ , to 37.3 kcal/mol for  $n = 3$ .<sup>46</sup> The structures of the  $\text{Au}_n\text{BO}^-$  clusters are similar to  $\text{Au}_n\text{CO}$ . The stronger interactions in  $\text{Au}_n\text{BO}^-$  are due to the charge on  $\text{BO}^-$ . From our chemical bonding analyses discussed above, we note that the  $\text{Au}_n\text{BO}^-$  clusters can all be viewed as  $\text{Au}_n[\text{BO}]$ , i.e., there is a significant charge transfer from  $\text{BO}^-$  to the  $\text{Au}_n$  clusters. This charge transfer is caused by the high electron affinities of the Au clusters. Charge transfer has also been observed to take place from CO to  $\text{Au}_n$  clusters in  $\text{Au}_n\text{CO}$  complexes and has been suggested to play a central role for understanding the catalytic mechanisms of low-temperature oxidation of CO on Au clusters and nanoparticles. Thus

the  $\text{Au}_n\text{BO}^-$  clusters are not only interesting chemical species in their own right, but they are also interesting systems to provide insight into the CO interactions with Au clusters.

### 9-7. Conclusion

Anions of auro-boron oxides with composition  $\text{Au}_n\text{BO}^-$  ( $n = 1-3$ ) have been observed in laser vaporization experiments intended to produce Au/B alloy clusters. The electronic structures and chemical bonding in these species have been investigated by photoelectron spectroscopy and theoretical calculations. Well-resolved photoelectron spectra were obtained at various photon energies and the electron affinities and low-lying electronic excited states of the neutral  $\text{Au}_n\text{BO}$  clusters were reported. Ground state structures of  $\text{Au}_n\text{BO}^-$  were identified and confirmed by comparison with the experimental data. The structures and bonding of  $\text{Au}_n\text{BO}^-$  were compared with the borane oxides  $\text{H}_n\text{BO}^-$  ( $n = 1-3$ ) to test the limit of the Au/H analogy. It was established that both  $\text{AuBO}^-$  and  $\text{Au}_2\text{BO}^-$  possess linear structures and  $\text{Au}_3\text{BO}^-$  possesses  $C_{2v}$  global minimum structure with a low-lying quasi-linear  $C_s$ . Molecular orbitals and NBO analyses showed that a single Au atom interacting with a bare BO unit indeed mimics hydrogen yielding a linear structure similar to HBO, though in anions  $\text{HBO}^-$  is not stable because the H atom does not have an equivalent accepting property compared to Au in  $\text{AuBO}$ . The neutral  $\text{AuBO}$  fragment remains unchanged as the second and third Au atom is added to form  $\text{Au}_2\text{BO}^-$  and  $\text{Au}_3\text{BO}^-$ . All the  $\text{Au}_n\text{BO}^-$  species can also be viewed as  $\text{Au}_n[\text{BO}]$  complexes, i.e., there is a significant charge transfer from  $\text{BO}^-$  to the Au clusters, analogous to that in  $\text{Au}_n\text{CO}$  complexes, although much stronger interaction exists in  $\text{Au}_n\text{BO}^-$  due to the extra charge on  $\text{BO}^-$ .

**References**

(1) (a) Mitchell, C. M.; Stone, F. G. A. *J. Chem. Soc., Chem. Commun.* **1970**, 1263; (b) Reid, B. D.; Welch, A. J. *J. Organomet. Chem.* **1992**, 438, 371; (c) Baukova, T. V.; Kuz'mina, L. G.; Dvortsova, N. V.; Porai-Koshits, M. A.; Kravtsov, D. N.; Perevalova, E. G.; *Metalloorg. Khim.* **1989**, 2, 1098; (d) Howard, J. A. K.; Jeffery, J. C.; Jelliss, P. A.; Sommerfeld, T.; Stone, F. G. A. *J. Chem. Soc., Chem. Commun.* **1991**, 1664; (e) Jeffery, J. C.; Jelliss, P. A.; Stone, F. G. A. *J. Chem. Soc., Dalton Trans.* **1993**, 1073; (f) Jeffery, J. C.; Jelliss, P. A.; Stone, F. G. A. *Inorg. Chem.* **1993**, 32, 3943; (g) Jeffery, J. C.; Jelliss, P. A.; Stone, F. G. A. *Organometallics* **1994**, 13, 2651; (h) Jeffery, J. C.; Jelliss, P. A.; Stone, F. G. A. *J. Chem. Soc., Dalton Trans.* **1994**, 25; (i) Harwell, D. E.; Mortimer, M. D.; Knobler, C. B.; Anet, F. A. L.; Hawthorne, M. F. *J. Am. Chem. Soc.* **1996**, 118, 2679.

(2) Hagen, S.; Pantenburg, I.; Weigend, F.; Wickleder, C.; Wesemann, L. *Angew. Chem. Int. Ed.* **2003**, 42, 1501; (b) Marx, T.; Mosel, B.; Pantenburg, I.; Hagen, S.; Schulze, H.; Wesemann, L. *Chem. Eur. J.* **2003**, 9, 4472; (c) Hagen, S.; Wesemann, L.; Pantenburg, I. *Chem. Commun.* **2005**, 1013.

(3) *Gold: Progress in Chemistry, Biochemistry and Technology*, Ed. Schmidbaur, H., Wiley, Chichester, UK, **1999**, and references therein.

(4) Lauher, J. W.; Wald, K.; *J. Am. Chem. Soc.* **1981**, 103, 7648.

(5) Scherbaum, F.; Grohmann, A.; Muller, G.; Schmidbaur, H. *Angew. Chem. Int. Ed.* **1989**, 28, 463; (b) Grohmann, A.; Riede, J.; Schmidbaur, H. *Nature*, **1990**, 345, 140; (c) Tamm, T.; Pyykkö, P.; *Theor. Chem. Acc.* **2000**, 103, 399; (d) Häberlen, O. D.; Schmidbaur, H.; Rösch, N. *J. Am. Chem. Soc.* **1994**, 116, 8241; (e) Pyykkö, P.; Zhao, Y.;

*Chem. Phys. Lett.* **1991**, *177*, 103; (f) Blumenthal, A.; Beruda, H.; Schmidbaur, H. *J. Chem. Soc., Chem. Comm.* **1993**, 1005; (g) Shein, I. R.; Medvedeva, N. I.; Ivanovski, A. *L. Phys. of Solid State*, **2001**, *43*, 2213; (h) Yang, F.; Han, R. S.; Tong, N. H.; Guo, W. *Chin. Phys. Lett.* **2002**, *19*, 1336; (i) Parvin, F.; Islam, A. K. M. A.; Islam, F. N. *Solid State Commun.* **2004**, *130*, 567; (j) Kwon, S. K.; Min, B. I.; Youn, S. J.; Kim, K. S. *J. Korean Phys. Soc.* **2005**, *46*, L1295.

(6) Kiran, B.; Li, X.; Zhai, H. J.; Cui, L. F.; Wang, L. S. *Angew. Chem. Int. Ed.* **2004**, *43*, 2125.

(7) Li, X.; Kiran, B.; Wang, L. S. *J. Phys. Chem. A* **2005**, *109*, 4366; (b) Kiran, B.; Li, X.; Zhai, H. J.; Wang, L. S. *J. Chem. Phys.* **2006** (in press).

(8) Zhai, H. J.; Wang, L. S.; Zubarev, D. Yu.; Boldyrev, A. I. *J. Phys. Chem. A*, **2006**, *110*, 1689.

(9) Alexandrova, A. N.; Koyle, E.; Boldyrev, A. I. *J. Mol. Mod.* **2006**, *12*, 569.

(10) Zubarev, D. Y.; Li, J.; Wang, L. S.; Boldyrev, A. I. *Inorg. Chem.* **2006**, *45*, 5269.

(11) Thomas, C.; Wishart, B. J. *Theor. Chim. Acta*, **1974**, *35*, 267. (b) Dill, J. D.; Schleyer, P. v. R.; Pople, J. A. *J. Am. Chem. Soc.* **1975**, *97*, 3402. (c) Summers, N. L.; Tyrrell, J. *J. Am. Chem. Soc.* **1977**, *99*, 3960. (d) Botschwina, P. *Chem. Phys.* **1978**, *28*, 231. (e) Tyrrell, J. *J. Phys. Chem.* **1979**, *83*, 2906. (f) Zyubina, T. S.; Charkin, O. P.; Gurvich, L. V. *Zh. Strukt. Khim.* **1979**, *20*, 3. (g) DeFrees, D. J.; Binkley, J. S.; McLean, A. D. *J. Chem. Phys.* **1984**, *80*, 3720. (h) Zyubina, T. S.; Zyubin, A. S.; Gorbik, A. A.; Charkin, O. P. *Zh. Neorg. Khim.* **1985**, *30*, 2739. (i) Peterson, K. A.; Woods, R. C. *J.*

*Chem. Phys.* **1989**, *90*, 7239. (j) Page, M. *J. Phys. Chem.* **1989**, *93*, 3639. (k) Harrison, J. A.; Maclagan, R. G. A. R. *Chem. Phys. Lett.* **1989**, *155*, 419. (l) Talaty, E. R.; Huang, Y.; Zandler, M. E. *J. Am. Chem. Soc.* **1991**, *113*, 779. (m) Mains, G. J. *J. Phys. Chem.* **1991**, *95*, 5089. (n) Yamaguchi, Y.; Vacek, G.; DeLeeuw, B. J.; Richards, C. A.; Schaefer, H. F. *J. Chem. Phys.* **1994**, *101*, 3006. (o) Richards, C. A.; Vacek, G.; DeLeeuw, B. J.; Yamaguchi, Y.; Schaefer, H. F. *J. Chem. Phys.* **1995**, *102*, 1280. (p) Lory, E. R.; Porter, R. F. *J. Am. Chem. Soc.* **1971**, *93*, 6301. (q) Kawashima, Y.; Kawaguchi, K.; Hirota, E. *Chem. Phys. Lett.* **1986**, *131*, 205. (r) Kawashima, Y.; Endo, Y.; Kawaguchi, K.; Hirota, E. *Chem. Phys. Lett.* **1987**, *135*, 441. (s) Kawashima, Y.; Endo, Y.; Hirota, E. *J. Mol. Spectrosc.* **1989**, *133*, 116.

(12) Haruta, M.; Yamada, N.; Kobayashi, T.; Iijima, S. *J. Catal.* **1989**, *115*, 301. (b) Haruta, M.; Tsubota, S.; Kobayashi, T.; Kageyama, H.; Genet, M. J.; Delmon, B. *J. Catal.* **1993**, *144*, 175.

(13) Haruta, M. *Catal. Today* **1997**, *36*, 153. (b) Haruta, M. *Chem. Rec.* **2003**, *3*, 75. (c) Bond, G. C.; Thompson, D. T. *Catal. Rev. Sci. Eng.* **1999**, *41*, 319.

(14) Valden, M.; Lai, X.; Goodman, D. W. *Science* **1998**, *281*, 1647. (b) Chen, M. S.; Goodman, D. W. *Science* **2004**, *306*, 252.

(15) Iizuka, Y.; Tode, T.; Takao, T.; Yatsu, K. I.; Takeuchi, T.; Tsubota, S.; Haruta, M. *J. Catal.* **1999**, *187*, 50.

(16) Kim, T. S.; Stiehl, J. D.; Reeves, C. T.; Meyer, R. J.; Mullins, C. B. *J. Am. Chem. Soc.* **2003**, *125*, 2018. (b) Stiehl, J. D.; Kim, T. S.; McClure S. M.; Mullins, C. B. *J. Am. Chem. Soc.* **2004**, *126*, 1606.

- (17) Guzman, J.; Gates, B. C. *Nano Lett.* **2001**, *1*, 689. (b) Guzman, J.; Gates, B. C. *J. Am. Chem. Soc.* **2004**, *126*, 2672.
- (18) Date, M.; Okumura, M.; Tsubota, S.; Haruta, M. *Angew. Chem., Int. Ed.* **2004**, *43*, 2129.
- (19) Lemire, C.; Meyer, R.; Shaikhutdinov, S.; Freund, H. J. *Angew. Chem., Int. Ed.* **2004**, *43*, 118.
- (20) Liu, Z. P.; Hu, P.; Alavi, A. *J. Am. Chem. Soc.* **2002**, *124*, 14770.
- (21) Molina, L. M.; Hammer, B. *Phys. Rev. Lett.* **2003**, *90*, 206102.
- (22) Sanchez, A.; Abbet, S.; Heiz, U.; Schneider, W. D.; Hakkinen, H.; Barnett, R. N.; Landman, U. *J. Phys. Chem. A* **1999**, *103*, 9573. (b) Yoon, B.; Hakkinen, H.; Landman, U.; Wirz, A. S.; Antonietti, J. M.; Abbet, S.; Heiz, U. *Science* **2005**, *307*, 403.
- (23) Lee, S.; Fan, C.; Wu, T.; Anderson, S. L. *J. Am. Chem. Soc.* **2004**, *126*, 5682.
- (24) Mavrikakis, M.; Stoltze, P.; Norskov, J. K. *Catal. Lett.* **2000**, *64*, 101. (b) Lopez, N.; Janssens, T. V. W.; Clausen, B. S.; Xu, Y.; Mavrikakis, M.; Bligaard, T.; Norskov, J. K. *J. Catal.* **2004**, *223*, 232.
- (25) Nygren, M. A.; Siegbahn, P. E. M.; Jin, C.; Guo, T.; Smalley, R. E. *J. Chem. Phys.* **1991**, *95*, 6181.
- (26) Lee, T. H.; Ervin, K. M. *J. Phys. Chem.* **1994**, *98*, 10023.
- (27) Wallace, W. T.; Whetten, R. L. *J. Phys. Chem. B* **2000**, *104*, 10964.

- (28) Balteanu, I.; Balaj, O. P.; Fox, B. S.; Beyer, M. K.; Bastl, Z.; Bondybey, V. E. *Phys. Chem. Chem. Phys.* **2003**, *5*, 1213; (b) Fielicke, A.; von Helden, G.; Meijer, G.; Pedersen, D. B.; Simard, B.; Rayner, D. M. *J. Am. Chem. Soc.* **2005**, *127*, 8416.
- (29) Liang, B.; Andrews, L. *J. Phys. Chem. A* **2000**, *104*, 9156; (b) Jiang, L.; Xu, Q. *J. Phys. Chem. A* **2005**, *109*, 1026.
- (30) Zhai, H. J.; Wang, L. S. *J. Chem. Phys.* **2005**, *122*, 051101.
- (31) Zhai, H. J.; Kiran, B.; Dai, B.; Li, J.; Wang, L. S. *J. Am. Chem. Soc.* **2005**, *127*, 12098.
- (32) Wang, L. S. & Wu, H. Probing the electronic structure of transition metal clusters from molecular to bulk- like using photoelectron spectroscopy in *Advances in Metal and Semiconductor Clusters. IV. Cluster Materials*, M.A. Duncan, Ed. (JAI Press, Greenwich, CT, 1998), pp.299-343.
- (33) L. S. Wang, H. S. Cheng, J. Fan, *J. Chem. Phys.* **1995**, *102*, 9480.
- (34) R. G. Parr, W. Yang, *Density-functional theory of atoms and molecules* (Oxford Univ. Press, Oxford, 1989). (b) A. D. Becke, *J. Chem. Phys.* **98**, 5648 (1993). (c) J. P. Perdew, J. A. Chevary, S. H. Vosko, K. A. Jackson, M. R. Pederson, D. J. Singh, C. Fiolhais, *Phys. Rev. B* **46**, 6671 (1992).
- (35) Hay, P. J.; Wadt, *J. Chem. Phys.* **1985**, *82*, 299.
- (36) Dolg, M.; Wedig, U.; Stoll, H.; Preuss, H. *J. Chem. Phys.* **1987**, *86*, 866.  
(b) Martin, J. M. L.; Sundermann, A. *J. Chem. Phys.* **2001**, *114*, 3408.
- (37) Dunning, Jr. T. H. *J. Chem. Phys.* **1989**, *90*, 1007. (b) Woon, D. E.; Dunning, Jr. T. H. *J. Chem. Phys.* **1993**, *98*, 1358. (c) Kendall, R. A.; Dunning, Jr. T. H.; Harrison, R. J. *J. Chem. Phys.* **1992**, *96*, 6796. (d) Peterson. K. A.; Woon, D. E.;



Dunning, Jr. T. H. *J. Chem. Phys.* **1994**, *100*, 7410. (e) Wilson, A.; van Mourik, T.; Dunning, Jr. T. H. *J. Mol. Struct. (Theochem)*, **1997**, *388*, 339. (f) Davidson, E. R. *Chem. Phys. Lett.* **1996**, *220*, 514.

(38) R. Bauernshmitt, R. Alrichs, *Chem. Phys. Lett.* **256**, 454 (1996). (b) M. E. Casida, C. Jamorski, K. C. Casida, D. R. Salahub, *J. Chem. Phys.* **108**, 4439 (1998).

(39) Li, J.; Li, X.; Zhai, H. J.; Wang, L. S. *Science* **2003**, *299*, 864; (b) Li, X.; Kiran, B.; Li, J.; Zhai, H. J.; Wang, L. S. *Angew. Chem. Int. Ed.* **2002**, *41*, 4786.

(40) *NBO 5.0*. E. D. Glendening, J. K. Badenhoop, A. E. Reed, J. E. Carpenter, J. A. Bohmann, C. M. Morales, and F. Weinhold, Theoretical Chemistry Institute, University of Wisconsin, Madison (2001).

(41) Gaussian 03 (revision A.1). M. J. Frisch, G. M. Trucks, H. B. Schlegel, G. E. Scuseria, M. A. Robb, J. R. Cheeseman, J. A. Montgomery, T. Vreven, K. N. Kudin, J. C. Burant, J. M. Millam, S. S. Iyengar, J. Tomasi, V. Barone, B. Mennucci, M. Cossi, G. Scalmani, N. Rega, G. A. Petersson, H. Nakatsuji, O. Kitao, H. Nakai, M. Klene, X. Li, J. E. Knox, H. P. Hratchian, J. B. Cross, C. Adamo, J. Jaramillo, R. Gomperts, R. E. Stratmann, O. Yazyev, A. J. Austin, R. Cammi, C. Pomelli, J. W. Ochterski, P. Y. Ayala, K. Morokuma, G. A. Voth, P. Salvador, J. J. Dannenberg, V. G. Zakrzewski, S. Dapprich, A. D. Daniels, M. C. Strain, O. Farkas, D. K. Malick, A. D. Rabuck, K. Raghavachari, J. B. Foresman, J. V. Ortiz, Q. Cui, A. G. Baboul, S. Clifford, J. Cioslowski, B. B. Stefanov, A. Liu, A. Liashenko, P. Piskorz, I. Komaromi, R. L. Martin, D. J. Fox, T. Keith, M. A. Al-Laham, C. Y. Peng, A. Nanayakkara, M. Challacombe, P. M. W. Gill, B. G. Johnson, W. Chen, M. W. Wang, C. Gonzales, and J. A. Pople (Gaussian, Inc., Pittsburgh PA, 2003).

(42) NWChem 4.7. Aprà, E.; Windus, T.L.; Straatsma, T.P.; Bylaska, E.J.; de Jong, W.; Hirata, S.; Valiev, M.; Hackler, M.; Pollack, L.; Kowalski, K.; Harrison, R.; Dupuis, M.; Smith, D.M.A; Nieplocha, J.; Tipparaju V.; Krishnan, M.; Auer, A.A.; Brown, E.; Cisneros, G.; Fann, G.; Fruchtl, H.; Garza, J.; Hirao, K.; Kendall, R.; Nichols, J.; Tsemekhman, K.; Wolinski, K.; Anchell, J.; Bernholdt, D.; Borowski, P.; Clark, T.; Clerc, D.; Dachsel, H.; Deegan, M.; Dyall, K.; Elwood, D.; Glendening, E.; Gutowski, M.; Hess, A.; Jaffe, J.; Johnson, B.; Ju, J.; Kobayashi, R.; Kutteh, R.; Lin, Z.; Littlefield, R.; Long, X.; Meng, B.; Nakajima, T.; Niu, S.; Rosing, M.; Sandrone, G.; Stave, M.; Taylor, H.; Thomas, G.; van Lenthe, J.; Wong, A.; Zhang, Z.; "NWChem, A Computational Chemistry Package for Parallel Computers, Version 4.7" (2005), (Pacific Northwest National Laboratory, Richland, Washington 99352-0999, USA).

(43) MOLDEN3.4. Schaftenaar, G. MOLDEN3.4, CAOS/CAMM Center, (The Netherlands, 1998).

(44) Hakkinen, H.; Yoon, B.; Landman, U.; Li, X.; Zhai, H. J.; Wang, L. S. *J. Phys. Chem. A* **2003**, *107*, 6168. (b) Taylor K. J.; Pettiette-Hall, C. L.; Cheshnovsky, O.; Smalley, R. E. *J. Chem. Phys.* **1992**, *100*, 7093.

(45) Zhai, H. J.; Alexandrova, A. N.; Birch, K. A.; Boldyrev, A. I.; Wang, L. S. *Angew. Chem. Int. Ed.* **2003**, *42*, 6004. (b) Zhai, H. J.; Kiran, B.; Li, J.; Wang, L. S. *Nature Mater.* **2003**, *2*, 827.

(46) Wu, X.; Senapati, L.; Nayak, S. K.; Selloni, A.; Hajaligol, M. *J. Chem. Phys.* **2002**, *117*, 4010.

## CHAPTER 10

## THEORETICAL PROBING OF DELTAHEDRAL CLOSO-

AURO-BORANES  $B_xAu_x^{2-}$  ( $x = 5-12$ )<sup>1</sup>**Abstract**

Using density functional calculations, here we show that a series of  $B_xAu_x^{2-}$  ( $x = 5-12$ ) dianions possesses structure and bonding similar to the famous deltahedral closo-borane cages,  $B_xH_x^{2-}$ . Effective atomic charges on Au in  $B_xAu_x^{2-}$  are very similar to those on H in  $B_xH_x^{2-}$ , indicating that Au in the closo-auro-boranes is indeed analogous to H in the closo-boranes. The present theoretical predictions of  $B_xAu_x^{2-}$  suggest that the closo-auro-borane species are viable new chemical building blocks that may be synthesized in the bulk. The Au atoms in the closo-auro-boranes represent highly atomically dispersed gold and may potentially exhibit novel catalytic and chemical properties.

**10-1. Introduction**

Since the discovery of boron hydrides (boranes) by Stock in 1912,<sup>1</sup> these compounds have played a major role in advancing chemical bonding theory beyond the classical idea of two-center two-electron bonds. Longuet-Higgins and Lipscomb et al.<sup>2,3</sup> first put forward the concept of three-center two-electron bonding to explain the structures of all known boron hydrides, in which the bridging B-H-B bond appeared to be the key structural unit.<sup>4</sup> This represents a milestone in establishing the validity of the molecular orbital theory.

---

<sup>1</sup> Coauthored by Dmitry Yu. Zubarev, Jun Li, Lai-Sheng Wang and Alexander I. Boldyrev. Reproduced with permission from *Inorg. Chem.* **2006**, 45, 5269-5271. Copyright 2006 American Chemical Society.

In particular, the closo-boranes ( $B_xH_x^{2-}$ ) have aesthetically pleasing symmetries because their structures are based on deltahedral boron cages. Of particular interest is the icosahedral  $B_{12}H_{12}^{2-}$  dianion, which was first synthesized by Hawthorne and Pitochelli in 1960,<sup>5</sup> shortly after its theoretical prediction by Longuet-Higgins and Roberts in 1955.<sup>6</sup> In recent years, Hawthorne and co-workers have synthesized and determined the structures of many compounds containing substituted closo- $B_{12}R_{12}^{2-}$  ( $R = Me, OH, OCH_2Ph, OCOPh$ ) dianions,<sup>7</sup> thus significantly enriching the chemistry of closo-boranes and their potential applications. Here we predict a new class of substituted closo-auro-boranes  $B_xAu_x^{2-}$  and present theoretical evidence showing that  $B_xAu_x^{2-}$  can be viable new gold-rich compounds. While, to the best of our knowledge, there are no published experimental data on  $B_xAu_x^{2-}$  closo-auro-boranes, there are many known gold-carborane complexes.<sup>8,9</sup> Mitchel and Stone,<sup>8a</sup> Reid and Welch,<sup>8b</sup> and Baukova *et al.*<sup>8c</sup> reported examples of closo-carboranes with gold bonded to carbon by 2c-2e s-bonds. Stone and co-workers reported synthesis and characterization of a series of nido-carboranes interacting with gold via cluster bonding.<sup>8d-8h</sup> Hawthorne and co-workers synthesized and characterized aurocarboranes with C-Au 2c-2e bonds with and without Au-Au interactions.<sup>8i</sup> Wesemann and co-workers reported synthesis and characterization of gold-stanna-closo-borate compounds with Sn-Au bonds.<sup>9</sup> Au-B compounds are summarized in a recent review.<sup>10</sup>

There are also a few compounds not related to boranes or carboranes, which also have 2c-2e C-Au, N-Au, and B-Au bonds.<sup>11,12</sup> The compounds containing the hypercoordinated pentagonal-bypyramidal  $C(AuPPh_3)_5^+$  and octahedral  $C(AuPPh_3)_6^{2+}$  cations are examples of interesting species with C-AuPPh<sub>3</sub> bonds.<sup>12b</sup> Theoretical studies

of model systems  $\text{BH}_n(\text{AuPH}_3)_m^k$ , where  $n+m=3$  or  $4$ , and charge  $k$  is  $-2, \dots, +1$ <sup>12c</sup> and model complexes  $[(\text{LAu})_6\text{X}_m]^{m+}$ ,  $[(\text{LAu})_5\text{X}_m]^{(m-1)+}$ ,  $[(\text{LAu})_4\text{X}_m]^{(m-2)+}$ , (with central atoms  $\text{X}_1=\text{B}$ ,  $\text{X}_2=\text{C}$ , and  $\text{X}_3=\text{N}$  and ligands  $\text{L}=\text{PH}_3$  or  $\text{P}(\text{CH}_3)_3$ )<sup>12d</sup> where the authors analyzed importance of  $\text{Au-PR}_3$  interactions for the stability of these systems have also been published. Pure  $\text{XAu}_n^{m+}$  clusters have been theoretically studied<sup>12e</sup> for the purpose of understanding the influence of  $\text{Au-PR}_3$  interaction on chemical bonding in  $\text{X}(\text{AuPPh}_3)_n^{m+}$  systems. The synthesis and characterization of the boron-centered gold cluster in the  $[(\text{Cy}_3\text{P})\text{B}((\text{AuPPh}_3)_4)^+\text{BF}_4^-]$  salt have also been reported.<sup>12f</sup> There are also several reports on gold diboride  $\text{AuB}_2$  compounds, which have hexagonal layers of boron atoms with gold atoms in between.<sup>12g-12j</sup>

Our work on the  $\text{B}_x\text{Au}_x^{2-}$  closo-auro-boranes was inspired by the recent discovery of the Au-H analogy in several binary Au-containing clusters.<sup>13</sup> It was first demonstrated that  $\text{SiAu}_4$  and  $\text{SiAu}_n$  ( $n = 2, 3$ ) have structures and bonding similar to the silane  $\text{SiH}_4$  and  $\text{SiH}_n$ , respectively.<sup>13a</sup> The  $\text{Si}_2\text{Au}_n$  ( $n = 2$  and  $4$ ) clusters were subsequently shown to be analogous to  $\text{Si}_2\text{H}_n$  ( $n = 2$  and  $4$ ).<sup>13b</sup> We have recently found that the B-Au bonds in the  $\text{Au}_2\text{B}_7^-$  cluster<sup>13c</sup> are also covalent and similar to the B-H bonds in the  $\text{B}_7\text{H}_2^-$  cluster.<sup>14</sup>

## 10-2. Theoretical Methods

On the basis of the Au-H analogy we conjectured that the closo-auro-boranes  $\text{B}_x\text{Au}_x^{2-}$  could be viable new building blocks in chemistry. To test this idea we performed quantum chemical calculations using hybrid density functional (DFT) method B3LYP<sup>15</sup> as implemented in NWChem 4.7<sup>16</sup> and Gaussian 03<sup>17</sup> with three types of basis sets using also pseudo-potential on gold: 1. LANL2DZ<sup>18</sup> on B and Au (B3LYP/LANL2DZ); 2. aug-

cc-pvTZ<sup>19</sup> on B and Stuttgart pseudo-potential and basis set<sup>20</sup> on Au (B3LYP/B/aug-cc-pvTZ/Au/Stuttgart); 3. cc-pvTZ<sup>19</sup> on B and Stuttgart pseudo-potential and basis set on Au (B3LYP/B/cc-pvTZ/Au/Stuttgart). We optimized geometry and calculated frequencies for  $B_xH_x^{2-}$  and  $B_xAu_x^{2-}$  ( $x = 5-12$ ) at B3LYP/LANL2DZ, for  $B_xH_x^{2-}$  ( $x = 5-8$ ) at B3LYP/B/H/aug-cc-pvTZ,  $B_xH_x^{2-}$  ( $x = 9-12$ ) at B3LYP/B/H/cc-pvTZ,  $B_xAu_x^{2-}$  ( $x = 5-8$ ) at B3LYP/B/aug-cc-pvTZ/Au/Stuttgart, and  $B_xAu_x^{2-}$  ( $x = 9-12$ ) at B3LYP/B/cc-pvTZ/Au/Stuttgart levels of theory. Optimized geometries, harmonic frequencies, total energies and other molecular properties of calculated species are summarized in supporting materials. B3LYP/LANL2DZ calculations have been performed at USU using the Gaussian 03 program. B3LYP/B/H/aug-cc-pvtz, B3LYP/B/H/cc-pvtz, B3LYP/B/aug-cc-pvtz/Au/Stuttgart, B3LYP/B/cc-pvtz/Au/Stuttgart calculations have been performed at the EMSL facility at PNNL using the NWChem program. The B3LYP results for  $B_6Au_6^{2-}$  were also compared with other DFT functionals and *ab initio* calculations to validate the methods used. Preliminary global minimum searches for the  $B_5Au_5^{2-}$  and  $B_6Au_6^{2-}$  clusters were performed using CPMD simulated annealing via the plane-wave DFT code of NWChem. With various starting geometries and annealing temperatures we did not find any energetically more stable structures. While a few structures of  $B_5Au_5^{2-}$  and  $B_6Au_6^{2-}$  clusters with low symmetry and Au-Au interactions were found to be lower in energy at the B3LYP level of theory than the deltahedral structures, they are significantly higher at the MP2 level of theory, indicating that the structures in Figure 10-1 are likely to be the global minima.

### 10-3. Results and Discussion

Selected geometric parameters for  $B_xH_x^{2-}$  and  $B_xAu_x^{2-}$  ( $x = 5-12$ ) calculated at our highest level of theory are summarized in Figure 10-1, with Cartesian coordinates of all these species collected in the supporting information.

Experimental geometries for the closo-borane  $B_xH_x^{2-}$  dianions from crystal data are available for  $x = 6, 8, 9, 10, 11,$  and  $12$ . Our theoretical B-B and B-H distances for the free  $B_xH_x^{2-}$  dianions agree within  $0.08 \text{ \AA}$  with the corresponding values for the same dianions in crystals. Similarly, our Au-B distances ( $2.056 - 2.072 \text{ \AA}$ ) are in reasonable agreement with the crystal Au-B distance ( $2.16-2.19 \text{ \AA}$ ) in the  $[(Cy_3P)B((AuPPh_3)_4)]^+BF_4^-$  salt.<sup>12f</sup>

According to our calculations using the B3LYP method with the largest basis sets the closo-auro-boranes  $B_xAu_x^{2-}$  with  $x = 5-12$  have minimal energy structures completely identical to the corresponding  $B_xH_x^{2-}$  species. The B-B bond lengths for the auro-boranes  $B_xAu_x^{2-}$  are indeed very similar to the corresponding boranes  $B_xH_x^{2-}$  (Figure 10-1). The shortest Au-Au distances in  $B_xAu_x^{2-}$  decrease slightly with increasing  $x$  from  $4.56 \text{ \AA}$  in  $B_5Au_5^{2-}$  to  $3.95 \text{ \AA}$  in  $B_{12}Au_{12}^{2-}$ , but they are still significantly larger than the equilibrium Au-Au distance ( $2.47 \text{ \AA}$ ) in  $Au_2$  or the Au-Au distance ( $2.884 \text{ \AA}$ ) in bulk gold, indicating that there is no direct Au-Au bonding in the closo-auro-boranes. The shortest Au-Au distances in  $B_xAu_x^{2-}$  are also outside the range  $3.00 \pm 0.25 \text{ \AA}$  for aurophilic interactions,<sup>8i</sup> suggesting that the Au-B bonding, analogous to the B-H bonding in the pure closo-boranes and the Si-Au bonding in the Si/Au binary clusters,<sup>13a,13b</sup> dominate in the  $B_xAu_x^{2-}$  molecules. While it is nearly impractical to prove if these high-symmetry minimum structures are the most stable among all the possible structures, it is conceivable that the

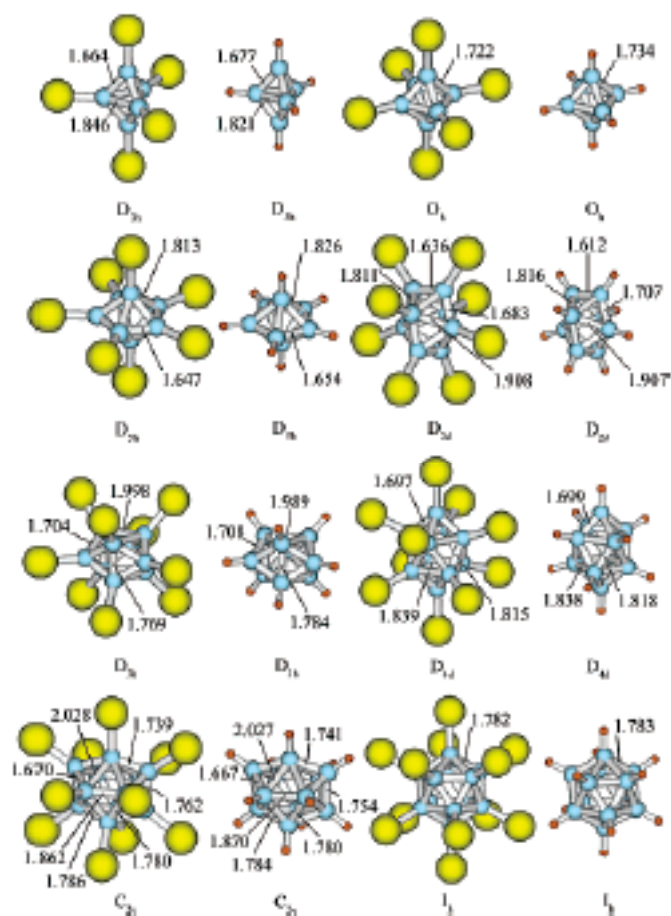


Figure 10-1. Optimized geometric structures of  $B_xH_x^{2-}$  and  $B_xAu_x^{2-}$  ( $x = 5-12$ ) with selected B-B distances in Å (Yellow – Au; Blue – B; Orange – H).



closo-auro-boranes  $B_xAu_x^{2-}$  might be made if the synthesis starts with the cage boranes or their derivatives.

To further elucidate the analogy between  $B_xAu_x^{2-}$  and  $B_xH_x^{2-}$ , we calculated the effective atomic charges using natural bond analysis (Figure 10-2). We found that the atomic charges on Au and H in every pair of  $B_xH_x^{2-}$  and  $B_xAu_x^{2-}$  dianions are indeed very similar, although the Au-B bonds are slightly more polar than the B-H bonds. Thus, the covalent B-Au bonding in the closo-auro-boranes is indeed analogous to the B-H covalent bonds in  $B_xH_x^{2-}$ , indicating that Au indeed apes H in  $B_xAu_x^{2-}$ . The relativistic effects account for the covalent character of the B-Au bonds.<sup>21</sup>

#### 10-4. Conclusion

The present research suggests that the closo-auro-borane dianions can be viable new building blocks in chemistry. We expect that  $B_xAu_x^{2-}$  clusters may undergo catenation in the solid state and thus may require ligand protections, such as the  $PPh_3$  groups. While it is hard for us to speculate if Au-B species without donor ligand protection can be isolated in condensed phase, we believe that  $B_x(AuPPh_3)_x^{2-}$  would be the most viable species to be synthesized in the condensed phase. The synthesis and characterization of the boron-centered gold cluster in the  $[(Cy_3P)B((AuPPh_3)_4)]^+BF_4^-$  salt<sup>12f</sup> provide additional hope that such synthesis might be feasible. The Au atoms in the closo-auro-boranes represent highly atomically dispersed gold and may potentially exhibit novel catalytic and chemical properties.

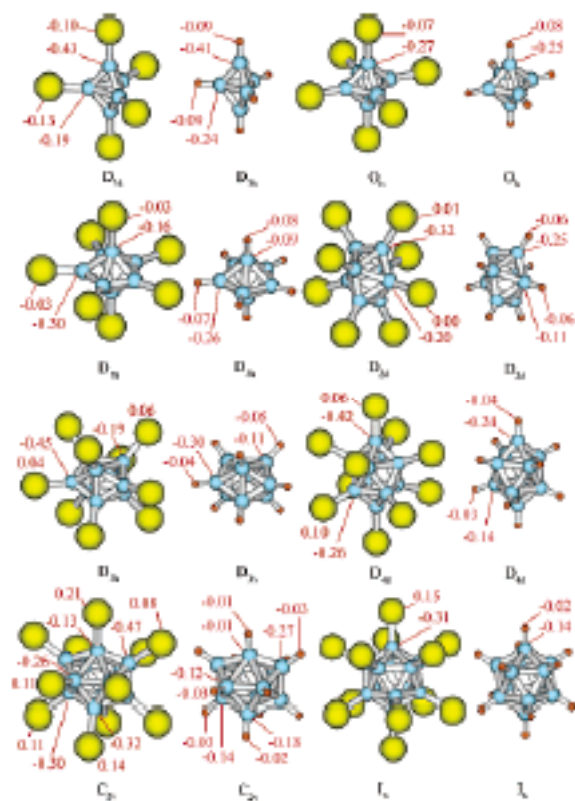


Figure 10-2. Calculated natural bond effective atomic charges in  $|e|$  (at B3LYP/LANL2DZ) for  $B_xH_x^{2-}$  and  $B_xAu_x^{2-}$  ( $x = 5-12$ ).

**References**

- (1) (a) Stock, A.; Massanez, C. *Chem. Ber.* **1912**, *45*, 3539. (b) Stock, A, Hydrides of Boron and Silicon; Cornell University Press: Ithaca, NY, 1933.
- (2) Bell, R. P.; Longuet-Higgins, H. C. *Nature* **1945**, *155*, 328.
- (3) Eberhardt, W. H.; Crawford, B.; Lipscomb, W. N. *J. Chem. Phys.* **1954**, *22*, 989.
- (4) Lipscomb, W. N. *Boron Hydride Chemistry*; Academic Press: New York, 1975.
- (5) Hawthorne, M. F.; Pitochelli, A. R. *J. Am. Chem. Soc.* **1960**, *82*, 3228.
- (6) Longuet-Higgins, H. C.; Roberts, M. de, V. *Proc. R. Soc. London, Ser. A.* **1955**, *230*, 110.
- (7) (a) Peymann, T.; Knobler, C. B.; Khan, S. I.; Hawthorne, M. F. *Inorg. Chem.* **2001**, *40*, 1291. (b) Peymann, T.; Herzog, A.; Knobler, C. B.; Hawthorne, M. F. *Angew. Chem. Int. Ed.* **1999**, *38*, 1061. (c) Bayer, M. J.; Hawthorne, M. F. *Inorg. Chem.* **2004**, *43*, 2018. (d) Farha, O. K.; Julius, R. L.; Lee, M. W.; Huertas, R. E.; Knobler, C. B.; Hawthorne, M. F. *J. Am. Chem. Soc.* **2005**, *127*, 18243.
- (8) (a) Mitchell, C. M.; Stone, F. G. A. *J. Chem. Soc., Chem. Commun.* **1970**, 1263; (b) Reid, B. D.; Welch, A. J. *J. Organomet. Chem.* **1992**, *438*, 371; (c) Baukova, T. V.; Kuz'mina, L. G.; Dvortsova, N. V.; Porai-Koshits, M. A.; Kravtsov, D. N.; Perevalova, E. G.; *Metalloorg. Khim.* **1989**, *2*, 1098; (d) Howard, J. A. K.; Jeffery, J. C.; Jelliss, P. A.; Sommerfeld, T.; Stone, F. G. A. *J. Chem. Soc., Chem. Commun.* **1991**, 1664; (e) Jeffery, J. C.; Jelliss, P. A.; Stone, F. G. A. *J. Chem. Soc., Dalton Trans.* **1993**, 1073; (f) Jeffery, J. C.; Jelliss, P. A.; Stone, F. G. A. *Inorg. Chem.* **1993**, *32*, 3943; (g) Jeffery, J. C.; Jelliss, P. A.; Stone, F. G. A. *Organometallics* **1994**, *13*, 2651; (h) Jeffery, J. C.; Jelliss, P. A.; Stone, F. G. A. *J. Chem. Soc., Dalton*

- Trans.* **1994**, 25; (i) Harwell, D. E.; Mortimer, M. D.; Knobler, C. B.; Anet, F. A. L.; Hawthorne, M. F. *J. Am. Chem. Soc.* **1996**, 118, 2679.
- (9) (a) Hagen, S.; Pantenburg, I.; Weigend, F.; Wickleder, C.; Wesemann, L. *Angew. Chem. Int. Ed.* **2003**, 42, 1501; (b) Marx, T.; Mosel, B.; Pantenburg, I.; Hagen, S.; Schulze, H.; Wesemann, L. *Chem. Eur. J.* **2003**, 9, 4472; (c) Hagen, S.; Wesemann, L.; Pantenburg, I. *Chem. Commun.* **2005**, 1013.
- (10) Gold: Progress in Chemistry, Biochemistry and Technology, Ed. Schmidbaur, H., Wiley, Chichester, UK, **1999**, and references therein.
- (11) Lauher, J. W.; Wald, K.; *J. Am. Chem. Soc.* **1981**, 103, 7648.
- (12) (a) Scherbaum, F.; Grohmann, A.; Muller, G.; Schmidbaur, H. *Angew. Chem. Int. Ed.* **1989**, 28, 463; (b) Grohmann, A.; Riede, J.; Schmidbaur, H. *Nature*, **1990**, 345, 140; (c) Tamm, T.; Pyykkö, P.; *Theor. Chem. Acc.* **2000**, 103, 399; (d) Häberlen, O. D.; Schmidbaur, H.; Rösch, N. *J. Am. Chem. Soc.* **1994**, 116, 8241; (e) Pyykkö, P.; Zhao, Y.; *Chem. Phys. Lett.* **1991**, 177, 103; (f) Blumenthal, A.; Beruda, H.; Schmidbaur, H. *J. Chem. Soc., Chem. Comm.* **1993**, 1005; (g) Shein, I. R.; Medvedeva, N. I.; Ivanovski, A. L. *Phys. of Solid State*, **2001**, 43, 2213; (h) Yang, F.; Han, R. S.; Tong, N. H.; Guo, W. *Chin. Phys. Lett.* **2002**, 19, 1336; (i) Parvin, F.; Islam, A. K. M. A.; Islam, F. N. *Solid State Commun.* **2004**, 130, 567; (j) Kwon, S. K.; Min, B. I.; Youn, S. J.; Kim, K. S. *J. Korean Phys. Soc.* **2005**, 46, L1295.
- (13) (a) Kiran, B.; Li, X.; Zhai, H. J.; Cui, L. F.; Wang, L. S. *Angew. Chem. Int. Ed.* **2004**, 43, 2125; (b) Li, X.; Kiran, B.; Wang, L. S. *J. Phys. Chem. A* **2005**, 109, 4366; (c) Zhai, H. J.; Wang, L. S.; Zubarev, D. Yu.; Boldyrev, A. I. *J. Phys. Chem. A*, **2006**, 110, 1689.

- (14) Alexandrova, A. N.; Koyle, E.; Boldyrev, A. I. *J. Mol. Mod.* 2005, published online.
- (15) (a) Parr R. G.; Yang W. *Density-functional theory of atoms and molecules* (Oxford Univ. Press, Oxford, 1989). (b) Becke A. D. *J. Chem. Phys.* **1993**, *98*, 5648. (c) Perdew J. P.; Chevary J. A.; Vosko S. H.; Jackson K. A.; Pederson M. R.; Singh D. J.; Fiolhais C. *Phys. Rev. B* **1992**, *46*, 6671
- (16) NWChem 4.7. Aprà, E. et al. "NWChem, A Computational Chemistry Package for Parallel Computers, Version 4.7" (2005), Pacific Northwest National Laboratory, Richland, Washington 99352-0999, USA.
- (17) Gaussian 03 (revision A.1). Frisch, M. J. et al. Gaussian, Inc.: Pittsburgh PA, 2003.
- (18) Hay, P. J.; Wadt, *J. Chem. Phys.* **1985**, *82*, 299.
- (19) Kendall, R. A.; Dunning, T. H. Jr. *J. Chem. Phys.* **1992**, *96*, 6796.
- (20) (a) Dolg, M.; Wedig, U.; Stoll, H.; Preuss, H. *J. Chem. Phys.* **1987**, *86*, 866. (b) Martin, J. M. L.; Sundermann, A. *J. Chem. Phys.* **2001**, *114*, 3408.
- (21) Pyykkö, P. *Angew. Chem. Int. Ed.* **2004**, *43*, 4412.

## CHAPTER 11

 $\text{Sn}_{12}^{2-}$ : STANNASPHERE<sup>1</sup>**Abstract**

During photoelectron spectroscopy (PES) experiments aimed at understanding the semiconductor-to-metal transition in tin clusters, the spectrum of  $\text{Sn}_{12}^-$  was observed to be remarkably simple and totally different from the corresponding  $\text{Ge}_{12}^-$  cluster, suggesting that  $\text{Sn}_{12}^-$  is a unique and highly symmetric cluster. Structural optimization starting from an icosahedral ( $I_h$ ) cluster led to a slightly distorted cage with  $C_{5v}$  symmetry. However, adding an electron to  $\text{Sn}_{12}^-$  resulted in a stable closed-shell  $I_h\text{-Sn}_{12}^{2-}$  cluster, which was synthesized in the form of  $\text{KSn}_{12}^-$  ( $\text{K}^+[\text{Sn}_{12}^{2-}]$ ) with a similar PES spectrum as  $\text{Sn}_{12}^-$ . The  $I_h\text{-Sn}_{12}^{2-}$  cage is shown to be bonded by four delocalized radial  $\pi$  bonds and nine delocalized on-sphere tangential  $\sigma$  bonds from the 5p orbitals of the Sn atoms, whereas the  $5s^2$  electrons remain largely localized and nonbonding. The bonding pattern in  $\text{Sn}_{12}^{2-}$  is similar to the well-known  $\text{B}_{12}\text{H}_{12}^{2-}$  cage, with the twelve  $5s^2$  localized electron pairs replacing the twelve B-H bonds. The  $\text{Sn}_{12}^{2-}$  cage has a diameter of 6.1 Å and can host most transition metal atoms in the periodic table.

**11-1. Introduction and Experimental Method**

The PES apparatus, featuring a laser vaporization supersonic cluster beam source and a magnetic bottle electron analyzer, has been described in detail previously.<sup>1</sup> A disk of pure tin was used as the laser vaporization target with a helium carrier gas. Negatively

---

<sup>1</sup> Coauthored by Li-Feng Cui, Xin Huang, Lei-Ming Wang, Dmitry Yu. Zubarev, Alexander I. Boldyrev, Jun Li and Lai-Sheng Wang. Reproduced with permission from *J. Am. Chem. Soc.* **2006**, 128, 8390-8391. Copyright 2006 American Chemical Society.

charged tin clusters ( $\text{Sn}_x^-$ ) were extracted from the cluster beam and were mass analyzed in a time-of-flight mass spectrometer. The cluster of interest was selected and then decelerated before being photodetached by a laser beam (193 nm from an excimer laser or 266 and 355 nm from a Nd:YAG laser). Photoelectrons were analyzed by the magnetic bottle time-of-flight analyzer and were calibrated by the known spectra of Cu- and Au-. The PES apparatus had an electron energy resolution of  $\Delta E/E \sim 2.5\%$ , that is, 25 meV for 1 eV electrons.

Different from its lighter congeners, Si and Ge which are semiconductors, the normal allotrope of tin under ambient conditions ( $\beta$ -Sn) is a metal with a body-centered tetragonal lattice, but it also has a small band gap semiconducting phase ( $\alpha$ -Sn) with a diamond lattice similar to Si and Ge that is stable at low temperatures.<sup>2</sup> Prior experimental<sup>3-7</sup> and theoretical<sup>8-11</sup> studies suggest that small tin clusters possess similar structures to those of Si and Ge. Small tin clusters were observed to exhibit melting temperatures exceeding that of the bulk,<sup>4</sup> consistent with the notion that small tin clusters have similar bonding configurations as those of the semiconductor Si and Ge clusters. Previous PES experiments<sup>12-14</sup> also suggested that the spectra of small  $\text{Sn}_x^-$  clusters are similar to those of the corresponding  $\text{Ge}_x^-$  clusters. However, these PES experiments were all done at low photon energies and under relatively low resolution.

## 11-2. Results and Discussion

In an effort to elucidate the semiconductor-to-metal transition as a function of size in tin clusters, we recently re-examined the PES of size-selected  $\text{Sn}_x^-$  clusters with high photon energies (up to 6.424 eV or 193 nm) and under well-controlled experimental

conditions. In the size range of  $x < 20$ , we indeed observed that the PES spectra of  $\text{Sn}_x^-$  are similar to those of the corresponding  $\text{Ge}_x^-$ , with the exception of  $\text{Sn}_{12}^-$  (Figure S1). Whereas the spectrum of  $\text{Ge}_{12}^-$  is rather congested with numerous poorly resolved features, the one of  $\text{Sn}_{12}^-$  is remarkably simple and well structured (Figure 11-1a). Four bands were resolved in the binding energy range from 3 to 4 eV, followed by a large gap and two well-resolved bands around 5 eV. The lowest energy band yielded an adiabatic detachment energy, that is, the electron affinity of neutral  $\text{Sn}_{12}$ , to be  $3.23 \pm 0.05$  eV and a vertical detachment energy (VDE) of  $3.34 \pm 0.03$  eV. Although low-symmetry structures similar to  $\text{Ge}_{12}$  have been proposed for  $\text{Sn}_{12}$ , the relatively simple and characteristic PES spectrum of  $\text{Sn}_{12}^-$  immediately suggested that it should possess a high-symmetry structure different from that of  $\text{Ge}_{12}^-$ .

In pondering the possible high-symmetry structures for  $\text{Sn}_{12}^-$ , we started from the

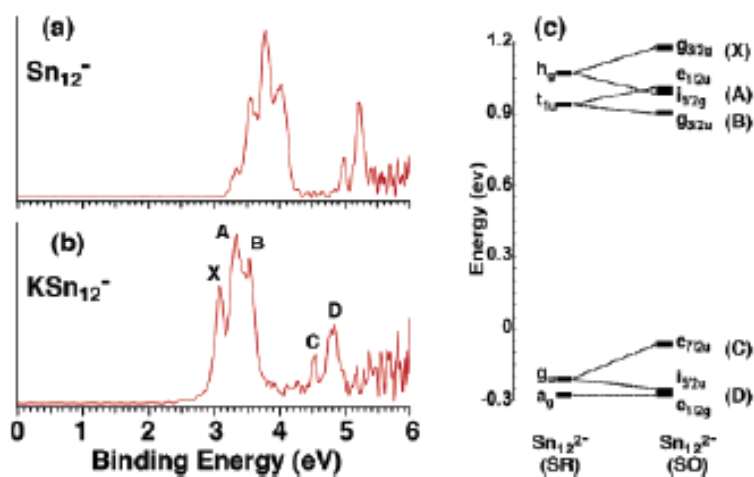


Figure 11-1. Photoelectron spectra of (a)  $\text{Sn}_{12}^-$  and (b)  $\text{KSn}_{12}^-$  at 193 nm. (c) Scalar relativistic (SR) energy levels of the  $I_h \text{Sn}_{12}^{2-}$  and the correlation to the spin-orbit (SO) coupled levels of  $I_h^* \text{Sn}_{12}^{2-}$ , where the asterisk indicates the double-group symmetry



highest symmetry possible for a twelve-atom cluster, the icosahedral cage (for computational details, see Supporting Information). However, the Jahn-Teller effect led to a slightly lower symmetry  $C_{5v}$  ( $^2A_1$ ) species (Figure 11-2a), which is only slightly distorted from the  $I_h$  structure, mainly by the depression of one apex atom. The computed first VDE (3.27 eV) of the  $C_{5v}$   $Sn_{12}^-$  is in excellent agreement with the experimental value of 3.34 eV. By adding one electron to  $Sn_{12}^-$ , we found that the resulting  $Sn_{12}^{2-}$  species is a highly stable  $I_h$  cage with a closed electron shell (Figure 11-2b).<sup>15</sup> Several other low-symmetry structures, including those suggested for  $Ge_{12}$ , have also been calculated for  $Sn_{12}^{2-}$ , but they are all much higher in energy. We were able to make  $Sn_{12}^{2-}$  in the form of  $KSn_{12}^-$  ( $K^+[Sn_{12}^{2-}]$ ) experimentally by laser vaporization of a tin target containing 15% K. The photoelectron spectrum of  $KSn_{12}^-$  (Figure 11-1b) is very similar to that of  $Sn_{12}^-$ , suggesting that the  $Sn_{12}^{2-}$  motif is not distorted greatly due to the presence of  $K^+$ . The ADE and VDE for the ground-state transition were measured as  $2.99 \pm 0.05$  and  $3.08 \pm 0.03$  eV, respectively, for  $KSn_{12}^-$ . Our calculations showed that the  $K^+$  counterion is outside the  $Sn_{12}^{2-}$  cage with a  $C_{3v}$  ( $^1A_1$ ) symmetry (Figure 11-2c). Indeed, only relatively small structural perturbations were observed in the  $Sn_{12}^{2-}$  cage as a result of the  $K^+$  coordination. The isomer with  $K^+$  inside the  $Sn_{12}^{2-}$  cage is much higher in energy by 3.1 eV because of the large size of the  $K^+$  ion, which expands the cage diameter from 6.07 Å (Figure 11-2b) to  $\sim 6.45$  Å. We also calculated K coordinated to the two lowlying isomers of  $Sn_{12}^-$ . We found they are both higher in energy and yield VDEs smaller than the experiment. Only the  $C_{3v}$   $KSn_{12}^-$  (Figure 11-2c) yields a calculated VDE (3.0 eV) in good agreement with the experiment ( $3.08 \pm 0.03$  eV), lending considerable credence to the stability of the  $Sn_{12}^{2-}$  cage. To help understand the chemical bonding in the  $I_h$ - $Sn_{12}^{2-}$

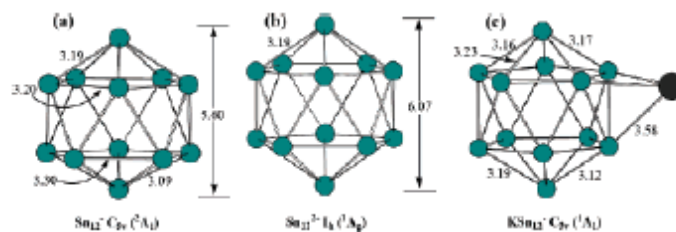


Figure 11-2. Optimized structures: (a)  $\text{Sn}_{12}^{2-}$ ; (b)  $\text{Sn}_{12}^{2-}$ ; (c)  $\text{KSn}_{12}^-$ . The bond distances and cage diameters are in Å.

cage, we analyzed its valence molecular orbitals. Sn has a valence electron configuration of  $5s^25p^2$ . We found that because of the large energy separation between the 5s and 5p shells there is little s-p hybridization in  $\text{Sn}_{12}^{2-}$ . The  $5s^2$  electron pair is largely localized on each Sn atom, leaving only the two 5p electrons responsible for bonding on the  $\text{Sn}_{12}^{2-}$  cage. Figure 11-1c shows the valence molecular orbital diagram at the scalar relativistic (SR) and spin-orbit (SO) coupled levels. It is shown that the MO levels of  $\text{Sn}_{12}^{2-}$  with the SO effect are in excellent agreement with the PES spectral pattern of  $\text{K}^+[\text{Sn}_{12}^{2-}]$ ; the observed spectral features (X, A, B, C, D) are labeled in Figure 11-1c next to the SO levels.

Among the thirteen valence orbitals, four are delocalized radial  $\pi$ -bonding orbitals ( $a_g$  and  $t_{1u}$ ) formed from the radial  $p_z$  atomic orbitals. The remaining nine orbitals ( $g_u$  and  $h_g$ ) are delocalized in-sphere  $\sigma$ -bonding orbitals from the tangential  $p_x$  and  $p_y$  atomic orbitals. The bonding pattern in  $\text{Sn}_{12}^{2-}$  is remarkably similar to that in the famous  $\text{B}_{12}\text{H}_{12}^{2-}$  molecule, which was first predicted to be a stable molecule by molecular orbital theory<sup>16</sup> and subsequently synthesized.<sup>17</sup> The  $\text{B}_{12}$  cage in  $\text{B}_{12}\text{H}_{12}^{2-}$  is also bonded similarly by four delocalized radial  $\pi$ -bonding orbitals and nine in-sphere delocalized  $\sigma$ -orbitals with 12

localized B-H bonds, which are equivalent to the  $5s^2$  electrons in the  $\text{Sn}_{12}^{2-}$  cage. Because of the delocalized  $\pi$  bonding in  $\text{Sn}_{12}^{2-}$  and its spherical symmetry, a name, stannaspherene, is suggested for this highly stable and symmetric cluster. In fact, our calculations suggest that the bare  $\text{Sn}_{12}^{2-}$  dianion is electronically stable with a 0.2 eV electron binding energy, even more stable than  $\text{C}_{60}^{2-}$  or  $\text{C}_{70}^{2-}$ .<sup>18</sup>

### 11-3. Conclusion

Small polyhedral Sn clusters are known in inorganic complexes and the Zintl phases.<sup>19,20</sup> However, the  $\text{I}_h\text{-Sn}_{12}^{2-}$  empty cage has not been known before. The high stability of this cluster suggests that it may be synthesized in the solid state using suitable ligands or counterions. More excitingly, the  $\text{Sn}_{12}^{2-}$  cage has a diameter of  $\sim 6.1$  Å, only slightly smaller than that of  $\text{C}_{60}$ , and can host an atom inside much like the endohedral fullerenes. Indeed, theoretical calculations have shown that  $\text{Cd}@\text{Sn}_{12}$  is a stable  $\text{I}_h$  cage<sup>21</sup>, and several endohedral  $\text{Pb}_{12}$  clusters, such as  $\text{Al}@\text{Pb}_{12}^+$  and  $\text{Pt}@\text{Pb}_{12}^{2-}$ , have been synthesized.<sup>22-24</sup> A recent report revealed stable Cu-Sn cluster compositions from high-temperature annealing and suggested core-shell-type structures.<sup>25</sup> The stability of the stannaspherene and its large internal volume suggest that  $\text{Sn}_{12}^{2-}$  may trap many different types of atoms to form endohedral stannaspherenes.

### References

- (1) Wang, L. S.; Wu, H. In *Advances in Metal and Semiconductor Clusters. IV. Cluster Materials*; Duncan, M. A., Ed.; JAI Press: Greenwich, CT, 1998; pp 299-343.
- (2) Burgers, W. G.; Groen, L. J. *Discuss. Faraday Soc.* **1957**, 23, 183.
- (3) Shvartsburg, A. A.; Jarrold, M. F. *Phys. Rev. A: At., Mol., Opt. Phys.* **1999**, 60, 1235.

- (4) Shvartsburg, A. A.; Jarrold, M. F. *Phys. Rev. Lett.* **2000**, *85*, 2530.
- (5) Martin, T. P.; Schaber, H. *J. Chem. Phys.* **1985**, *83*, 855.
- (6) LaiHing, K.; Wheeler, R. G.; Wilson, W. L.; Duncan, M. A. *J. Chem. Phys.* **1987**, *87*, 3401.
- (7) Yoshida, S.; Fuke, K. *J. Chem. Phys.* **1999**, *111*, 3880.
- (8) Lu, Z. Y.; Wang, C. Z.; Ho, K. M. *Phys. Rev. B: Condens. Matter* **2000**, *61*, 2329.
- (9) Majumder, C.; Kumar, V.; Mizuseki, H.; Kawazoe, Y. *Phys. Rev. B: Condens. Matter* **2001**, *64*, 233405.
- (10) Joshi, K.; Kanhere, D. G.; Blundell, S. A. *Phys. Rev. B: Condens. Matter* **2003**, *67*, 235413.
- (11) Chuang, F. C.; Wang, C. Z.; Ogut, S.; Chelikowsky, J. R.; Ho, K. M. *Phys. Rev. B: Condens. Matter* **2004**, *69*, 165408.
- (12) Gantefor, G.; Gausa, M.; Meiwes-Broer, K. H.; Lutz, H. O. *Z. Phys. D: At., Mol. Clusters* **1989**, *12*, 405.
- (13) Moravec, V. D.; Klopčič, S. A.; Jarrold, C. C. *J. Chem. Phys.* **1999**, *110*, 5079.
- (14) Negishi, Y.; Kawamata, H.; Nakajima, A.; Kaya, K. *J. Electron Spectrosc. Relat. Phenom.* **2000**, *106*, 117.
- (15) The lowest triplet state was calculated to be 34.7 kcal/mol higher at PW91/TZ2P, with spin-orbit coupling included.
- (16) Longuet-Higgins, H. C.; Roberts, M. de V. *Proc. R. Soc. London, Ser. A* **1955**, *230*, 110.
- (17) Pitochelli, A. R.; Hawthorne, M. F. *J. Am. Chem. Soc.* **1960**, *82*, 3228.

- (18) Wang, X. B.; Woo, H. K.; Huang, X.; Kappes, M. M.; Wang, L. S.; *Phys. Rev. Lett.* **2006**, *96*, 143002. Note that we could not produce the bare  $\text{Sn}_{12}^{2-}$  dianion in our laser vaporization experiment because of the coulomb repulsion between  $\text{Sn}_{12}^-$  and an electron in the process of forming  $\text{Sn}_{12}^{2-}$ . It may be produced using electrospray once synthesized in solution, like that of  $\text{C}_{70}^{2-}$ .
- (19) Wiberg, N.; Power, P. In *Molecular Clusters of the Main Group Elements*; Driess, M., Noth, H., Eds.; Wiley-VCH Verlag: Weinheim, Germany, 2004; pp 188-208.
- (20) Corbett, J. D. *Angew. Chem., Int. Ed.* **2000**, *39*, 670.
- (21) Kumar, V.; Kawazoe, Y. *Appl. Phys. Lett.* **2002**, *80*, 859.
- (22) Neukermans, S.; Janssens, E.; Chen, Z. F.; Silverans, R. E.; Schleyer, P. v. R.; Lievens, P. *Phys. Rev. Lett.* **2004**, *92*, 163401.
- (23) Esenturk, E. N.; Fettinger, J.; Lam, Y. F.; Eichhorn, B. *Angew. Chem., Int. Ed.* **2004**, *43*, 2132.
- (24) Zhang, X.; Li, G.; Xing, X.; Zhao, X.; Tang, T.; Gao, Z. *Rapid Commun. Mass Spectrom.* **2001**, *15*, 2399.
- (25) Breaux, G. A.; Hillman, D. A.; Neal, C. M.; Jarrold, M. F. *J. Phys. Chem. A* **2005**, *109*, 8755.

CHAPTER 12  
CHEMICAL BONDING IN  $\text{Si}_5^{2-}$  AND  $\text{NaSi}_5^-$  VIA  
PHOTOELECTRON SPECTROSCOPY AND  
AB INITIO CALCULATIONS<sup>1</sup>

**Abstract**

Photoelectron spectroscopy and ab initio calculations are used to investigate the electronic structure and chemical bonding of  $\text{Si}_5^-$  and  $\text{Si}_5^{2-}$  in  $\text{NaSi}_5^-$ . Photoelectron spectra of  $\text{Si}_5^-$  and  $\text{NaSi}_5^-$  are obtained at several photon energies and are compared with theoretical calculations at four different levels of theory, TD-B3LYP, R(U)OVGF, UCCSD(T), and EOM-CCSD(T), all with the 6-311+G(2df) basis sets. Excellent agreement is observed between experiment and theory, confirming the obtained ground state structures for  $\text{Si}_5^-$  and  $\text{Si}_5^{2-}$ , which are both found to be trigonal bipyramid with  $D_{3h}$  symmetry at several levels of theory. Chemical bonding in  $\text{Si}_5$ ,  $\text{Si}_5^-$ , and  $\text{Si}_5^{2-}$  is analyzed using NPA, molecular orbitals, ELF, and NICS indices. The bonding in  $\text{Si}_5^{2-}$  is compared with that in the iso-electronic and iso-structural  $\text{B}_5\text{H}_5^{2-}$  species, but is found to differ due to the involvement of electron densities, which are supposed to be lone pairs in the skeletal bonding in  $\text{Si}_5^{2-}$ .

---

<sup>1</sup> Coauthored by Dmitry Yu. Zubarev, Alexander I. Boldyrev, Xi Li, Li-Feng Cui and Lai-Sheng Wang. Reproduced with permission from *J. Phys. Chem. A* **2005**, 109, 11385-11394. Copyright 2005 American Chemical Society.

## 12-1. Introduction

The discovery of the  $C_{60}$  buckyball<sup>1</sup> has generated a great deal of interest to cage-like clusters, particularly in silicon clusters. However, the obvious valence isoelectronic  $Si_{60}$  analog does not have the same structure as  $C_{60}$ .<sup>2-9</sup> Instead of a beautiful soccer-ball shape,  $Si_{60}$  seems to adopt a rather low symmetry structure.<sup>2,4,7,9</sup> An alternative approach to searching for cage-like silicon clusters is to use the isolobal analogy between an HB unit and a Si atom<sup>10</sup> and the known fact that boranes, such as  $B_{12}H_{12}^{2-}$ , have cage-like deltahedral structures.<sup>11-13</sup> However, our preliminary ab initio calculations of the  $Si_{12}^{2-}$  cluster<sup>14</sup> indicate indeed that an icosahedral  $Si_{12}^{2-}$  cage is a local minimum, although it is not the global minimum. Our preliminary results on other  $Si_x^{2-}$  clusters<sup>14</sup> also demonstrate that many doubly charged silicon anionic clusters adopt low-symmetry structures rather than the beautiful deltahedral structures. We are interested in developing a unified chemical bonding picture for silicon clusters and understanding the deviation of the geometric structures of doubly charged silicon cluster anions from the isolobal deltahedral  $B_xH_x^{2-}$  analogs.<sup>11-13</sup>

We begin this endeavor from the  $Si_5^{2-}$  dianionic cluster, which has been recently synthesized and characterized in the solid state by Goicoechea and Sevov.<sup>15</sup> The  $Si_5^{2-}$  cluster was synthesized in the  $(Rb-crypt)_2Si_5 \cdot 4NH_3$  crystal and was shown to be a trigonal-bipyramidal cluster with equatorial distances  $d_{eq-eq} = 2.535 \text{ \AA}$  and axial distances  $d_{ax-eq} = 2.350 \text{ \AA}$ . An isolated  $Si_5^{2-}$  dianion is expected to be metastable towards autodetachment in the gas phase, but it may be stabilized by an alkali metal cation ( $M^+$ ) in  $MSi_5^-$ . Kaya and co-workers<sup>16</sup> reported experimental observation of  $NaSi_5^-$ , as well as its photoelectron spectrum at 355 nm, which displayed one broad spectral band. They

also presented theoretical calculations for  $\text{NaSi}_5^-$  and  $\text{Si}_5^{2-}$  at the MP2/6-31G\* level of theory and found a trigonal-bipyramidal structure for  $\text{Si}_5^{2-}$  and two isomers for  $\text{NaSi}_5^-$ : a  $\text{C}_{2v}$  ( $^1\text{A}_1$ ) and a  $\text{C}_{3v}$  ( $^1\text{A}_1$ ) structure. The  $\text{C}_{2v}$  structure with the  $\text{Na}^+$  cation coordinated to the edge of the triangular base was found to be more stable by 0.823 eV (at MP4/6-31G\*\*//MP2/6-31G\*) than the  $\text{C}_{3v}$  isomer, in which the  $\text{Na}^+$  cation is coordinated to one apex Si atom of the trigonal-bipyramidal  $\text{Si}_5^{2-}$  structure. The series of  $\text{ME}_5^-$  (M = Li, Na, K, and E = Si and Ge) anions have been studied by Li and co-workers,<sup>17,18</sup> who optimized the geometry for the trigonal-bipyramidal  $\text{Si}_5^{2-}$  structure using six different levels of theory. At their best density functional level of theory (B3PW91/6-311+G(3d2f)), they obtained  $d_{\text{ax-eq}} = 2.53 \text{ \AA}$  and  $d_{\text{eq-eq}} = 2.75 \text{ \AA}$  and at their best ab initio level of theory (MP2/6-311G\*) they got  $d_{\text{axx-eq}} = 2.57 \text{ \AA}$  and  $d_{\text{eq-eq}} = 2.76 \text{ \AA}$ . Both are in reasonable agreement with the  $\text{Si}_5^{2-}$  structure in the solid state:  $d_{\text{ax-eq}} = 2.48 \text{ \AA}$  and  $d_{\text{eq-eq}} = 2.69 \text{ \AA}$ .

In the current paper, we present a systematic and comprehensive study of  $\text{Si}_5^{2-}$  and  $\text{NaSi}_5^-$  using a combined experimental and theoretical approach. Photoelectron spectra of  $\text{NaSi}_5^-$  have been obtained at three photon energies, 355, 266, and 193 nm. The higher photon energy spectra yielded higher binding energy detachment features, which are better suited for comparison with the theoretical results. Molecular orbital analyses have been carried out to understand the detailed chemical bonding in the  $\text{Si}_5^{2-}$  species, which are compared with  $\text{B}_5\text{H}_5^{2-}$ . Even though  $\text{Si}_5$  and  $\text{Si}_5^-$  have been extensively studied experimentally<sup>19-50</sup> and theoretically,<sup>51-109</sup> we included them in the current study for completeness and for better evaluation of the theoretical methods, which will be used to investigate larger multiply charged silicon clusters in the future.



## 12-2. Experimental Methods

Details of the photoelectron spectroscopy apparatus have been described elsewhere.<sup>110,111</sup> Both the silicon cluster anions and Na-Si mixed cluster anions were generated by laser vaporization of a Si disk target and a Na/Si disk target in the presence of a helium carrier gas and analyzed by the time-of-flight mass spectrometry. Either the  $\text{Si}_5^-$  or  $\text{NaSi}_5^-$  anions was mass-selected and decelerated before being photodetached by a pulsed laser beam. Photoelectrons were collected at nearly 100% efficiency by a magnetic bottle and analyzed in a 3.5 m long electron flight tube. The PES spectra were calibrated by using the known spectrum of  $\text{Au}^-$ ,  $\text{Pt}^-$ , and  $\text{Rh}^-$ , and the energy resolution was  $\Delta E_k/E_k \approx 2.5\%$ , that is, approximately 25 meV for 1 eV electrons.

## 12-3. Theoretical Methods

The initial search for most stable structures was performed using our gradient embedded genetic algorithm (GEGA) program written by Alexandrova.<sup>112</sup> We used the semiempirical PM3 method for energy, gradient and force calculations. The lowest few structures in every system were recalculated using a hybrid method known in the literature as B3LYP<sup>113-115</sup> with the polarized split-valence basis sets (6-311+G\*).<sup>116-118</sup> The lowest structure in every system was then refined using the coupled-cluster method with single, double, and noniterative triple excitations (CCSD(T))<sup>119-121</sup> with the same basis sets. Total energies of these structures were also calculated using the extended 6-311+G(2df) basis sets. Some species have been calculated using the second order Moller-Plessett (MP2)<sup>122</sup> level of theory and the 6-311+G\* basis sets. In order to test the validity of the one-electron approximation, single point calculations were performed using the

multi-configuration self-consistent field method (CASSCF)<sup>123-124</sup> with 8 and 9 active electrons and 7 active molecular orbitals for  $\text{Si}_5$  and  $\text{Si}_5^-$ , respectively, [CASSCF(8,7), and CASSCF(9,7),] and with 10 active electrons and 8 active orbitals for  $\text{Si}_5^{2-}$  [CASSCF(10,8) all using the 6-311+G\* basis sets].

The vertical electron detachment energies were calculated using CCSD(T)/6-311+G(2df), the outer valence Green Function method (OVGF/6-311+G(2df))<sup>125-129</sup> and UCCSD(T)/6-311+G(2df) at the CCSD(T)/6-311+G\* geometries, as well as at the time-dependent DFT method<sup>130-131</sup> (TD B3LYP/6-311+G(2df)) at the B3LYP/6-311+G\* geometries. Core electrons were frozen in treating the electron correlation at the CCSD(T) and OVGF levels of theory.

Chemical bonding was analyzed using electron localization functions (ELF).<sup>132-134</sup> All ab initio calculations were performed using Gaussian 98 and 03 programs<sup>135,136</sup> on a 63 nodes Birch-Retford Beowulf cluster computer built at Utah State University by K. A. Birch, B. P. Retford and E. Koyle. ELF calculations have been performed using the TopMod Package.<sup>137</sup> Visualization of ELFs has been made using MOLEKEL program<sup>138</sup> and molecular orbital visualization has been done using MOLDEN3.4 program.<sup>139</sup>

## 12-4. Experimental Results

### 12-4.1. Photoelectron spectroscopy of $\text{Si}_5^-$

Figure 12-1 shows the photoelectron spectra of  $\text{Si}_5^-$  at four photon energies (355, 266, 193, and 157 nm). The photoelectron spectra of  $\text{Si}_5^-$  have been reported in a number of previous studies.<sup>25,30,31,34,36</sup> In particular, vibrationally resolved spectra have been

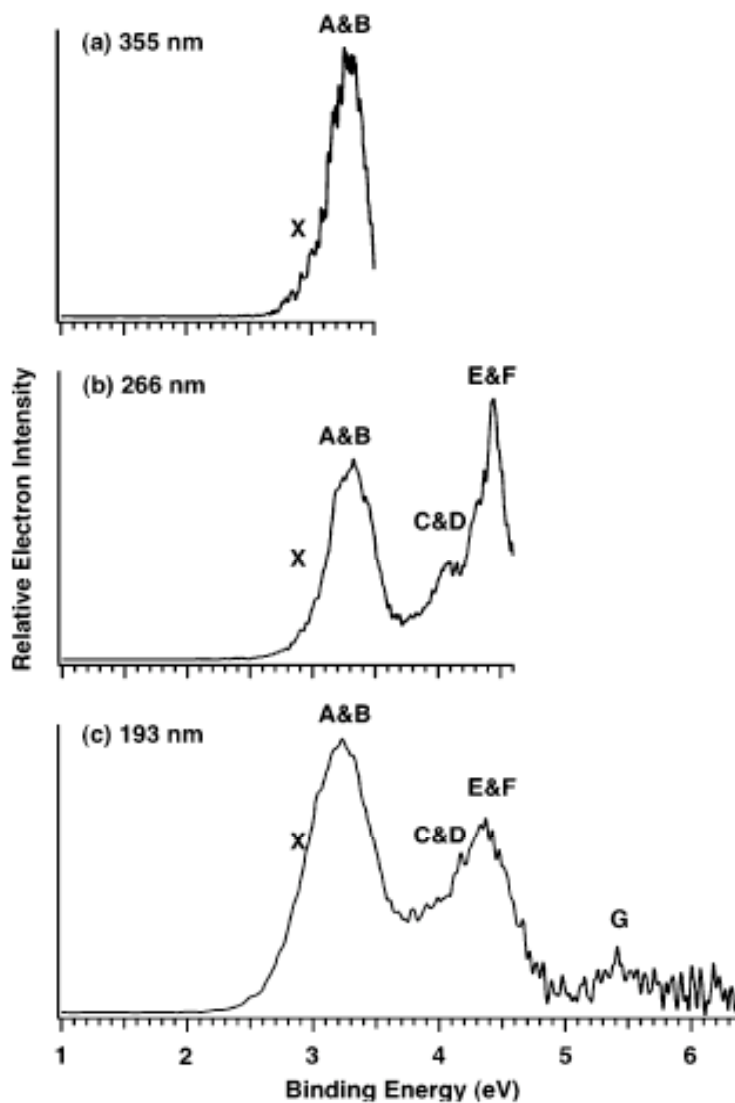


Figure 12-1. Photoelectron spectra of  $\text{Si}_5^-$  at (a) 355 nm (3.496 eV), (b) 266 nm (4.661 eV), (c) 193 nm (6.424 eV), and (d) 157 nm (7.766 eV).

obtained by Neumark and co-workers.<sup>31</sup> The current spectra agree with the previous data, but provide better resolved features beyond 3.5 eV binding energies. The 355 nm spectrum (Figure 12-1a) showed a broad band with a low binding energy tail. From their vibrationally-resolved spectra and angular dependent studies, Neumark and co-workers showed that the 355 nm spectrum contained two electronic transitions, the low energy tail (X) corresponding to the ground state transition. A long vibrational progression with an average spacing of  $233 \pm 10 \text{ cm}^{-1}$  was observed in ref. 31, suggesting a significant geometry change between the ground state of  $\text{Si}_5^-$  and  $\text{Si}_5$ . An ADE of 2.59 eV was estimated by Neumark et al. from their Franck-Condon simulation. Thus the spectral onset at  $\sim 2.7 \text{ eV}$  in the 355 nm spectrum only represents an upper limit for the ADE due to the large geometry changes between the anion and neutral ground state. The VDE of the X band is estimated to be around 3.0 eV, which is consistent with the Franck-Condon simulation by Neumark et al. The intense part of the 355 nm spectrum at the high binding energy side (A) corresponds to the detachment transition to the first excited state of  $\text{Si}_5$ . The broad nature of the A band makes it difficult to evaluate its VDE, which should be around 3.2 eV approximately.

The 266 nm spectrum (Figure 12-1b) indicates that the A band is cut off at 355 nm. This band in fact is shown to extent to around 3.6 eV, suggesting that there is likely to be another detachment transition. This is labeled as band B with a VDE around 3.4 eV approximately. As will be shown below, this band is born out in the current theoretical calculations. Although it was not recognized at the time, the 299 nm spectrum in the paper by Neumark et al.<sup>31</sup> resolved this band more clearly. The 266 nm reveals two more broad bands. A weak and broad band centered around 4 eV (C) and a more intense and

sharper band at 4.47 eV (E). A shoulder can be discerned at the lower binding energy side of the intense band at around 4.3 eV (D). At 193 nm (Figure 12-1c), the band becomes broad, suggesting an additional band around 4.6 eV, which is cut off in the 266 nm spectrum. A very weak band is also observed around 5.4 eV (G). We also took the spectrum of  $\text{Si}_5^-$  at 157 nm (Figure 12-1d), but no new detachment transitions were observed because of the poor signal-to-noise ratio in the high binding energy side.

The VDEs of all the observed detachment channels for  $\text{Si}_5^-$  are summarized in Table 12-1, where the calculated VDEs at various levels of theory are also listed.

#### *12-4.2. Photoelectron spectroscopy $\text{NaSi}_5^-$*

The photoelectron spectra of  $\text{NaSi}_5^-$  are shown in Figure 12-2 at three photon energies (355, 266, and 193 nm). The electron binding energies of  $\text{NaSi}_5^-$  are lower than those of  $\text{Si}_5^-$ , but the overall spectral patterns for the two species are quite similar. The low binding energy part of the  $\text{NaSi}_5^-$  spectra shows a very broad band, which also contains three overlapping detachment transitions (X, A, B) similar to the  $\text{Si}_5^-$  spectra. The VDE of the A band is assigned to be the most intense feature in this band at 2.67 eV in the 355 nm spectrum (Figure 12-2a). The X and B bands are assigned to be on the lower and higher binding energy side of this broad band, and their binding energies are estimated to be  $\sim 2.55$  and  $\sim 2.9$  eV, respectively. The onset of the X band is relatively sharp for  $\text{NaSi}_5^-$ , allowing us evaluate an ADE of  $2.42 \pm 0.04$  eV, which agrees with the value of  $2.45 \pm 0.05$  eV reported previously by Kaya and co-workers at 355 nm.<sup>16</sup> Following the broad band, three well resolved bands are observed (C, D, E). The bands C and D with VDEs of 3.47 and 3.71 eV, respectively, are relatively weak, whereas the

Table 12-1. Experimental VDEs compared with the calculated VDEs for the  $D_{3h}$  ( $^2A_2''$ ) $Si_5^-$ .

Final State	VDE (exp) (eV)	VDE TD B3LYP <sup>a</sup>	VDE UOVGF <sup>b</sup>	VDE CCSD(T) <sup>c</sup>	VDE EOM <sup>d</sup>
$^1A_1'$ ( $2a_1'^23a_1'^21e''^42e'^42a_2''^0$ )	~3.0 (X)	3.06	2.99 (0.91)	3.01	3.01
$^3E''$ ( $2a_1'^23a_1'^21e''^42e'^32a_2''^1$ )	~3.2 (A)	3.13	2.95 (0.90)	3.24	
$^1E''$ ( $2a_1'^23a_1'^21e''^42e'^32a_2''^1$ )	~3.4 (B)	3.52			3.26
$^3E'$ ( $2a_1'^23a_1'^21e''^32e'^42a_2''^1$ )	~4.1 (C)	4.03	3.87 (0.91)		
$^1E'$ ( $2a_1'^23a_1'^21e''^32e'^42a_2''^1$ )	~4.3 (D)	4.36			4.50
$^3A_2''$ ( $2a_1'^23a_1'^11e''^42e'^42a_2''^1$ )	$4.47 \pm 0.03$ (E)	4.29	4.31 (0.90)		
$^1A_2''$ ( $2a_1'^23a_1'^11e''^42e'^42a_2''^1$ )	~4.6 (F)	4.52			4.81
$^3A_2''$ ( $2a_1'^13a_1'^21e''^42e'^42a_2''^1$ )	~5.4 (G)	5.27	4.92 (0.88)		
$^1A_2''$ ( $2a_1'^13a_1'^21e''^42e'^42a_2''^1$ )		6.8			6.82

<sup>a</sup> The VDEs were calculated at the TD B3LYP/6-311+G(2df)//B3LYP/6-311+G\* level of theory.

<sup>b</sup> The VDEs were calculated at the UOVGF/6-311+G(2df)//CCSD(T)/6-311+G\* level of theory. The numbers in the parentheses indicate the pole strength, which characterizes the validity of the one-electron detachment picture.

<sup>c</sup> The VDEs were calculated at the CCSD(T)/6-311+G(2df)//CCSD(T)/6-311+G\* level of theory.

<sup>d</sup> The VDEs were calculated at the CCSD(T)/6-311+G(2df)//CCSD(T)/6-311+G\* level of theory.

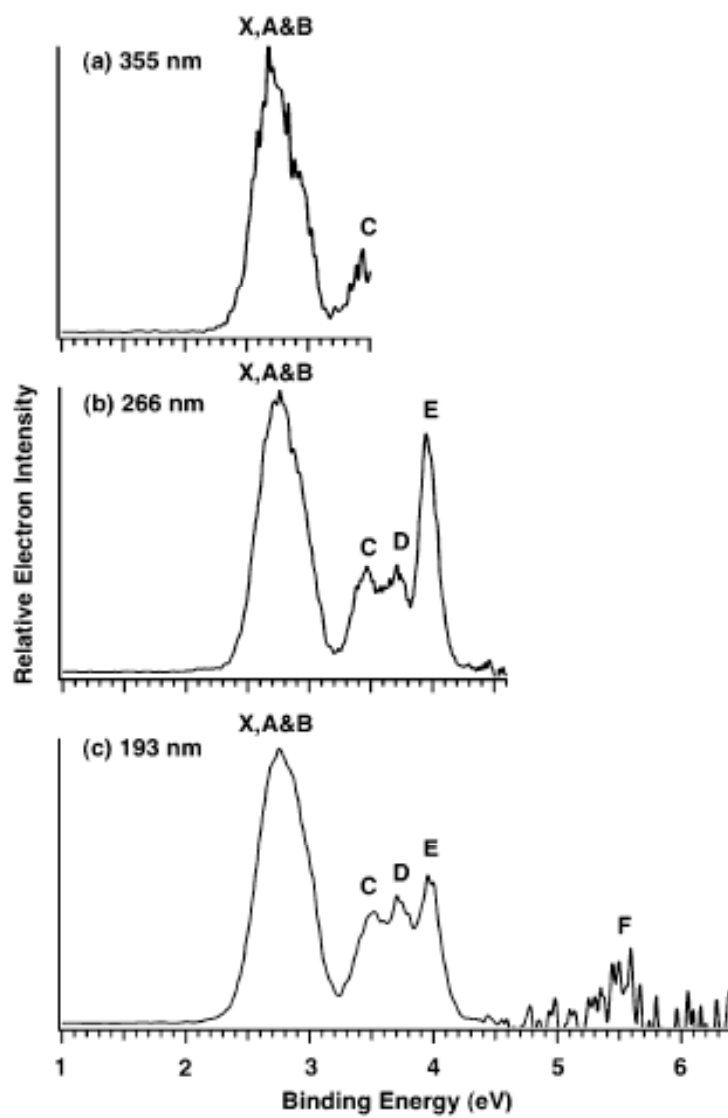


Figure 12-2. Photoelectron spectra of  $\text{NaSi}_5^-$  at (a) 355 nm (3.496 eV), (b) 266 nm (4.661 eV), and (c) 193 nm (6.424 eV).

band E at 3.95 eV is quite sharp and intense in the 266 nm spectrum (Figure 12-2b). At 193 nm (Figure 12-2c), the intensity of the E band is significantly reduced and a very weak band with relatively poor signal-to-noise ratio is observed at ~5.5 eV (F). Overall the spectral features of  $\text{NaSi}_5^-$  appeared to be slightly sharper and better resolved than the  $\text{Si}_5^-$  counterparts, suggesting that the geometry changes between  $\text{NaSi}_5^-$  and  $\text{NaSi}_5$  are relatively small. All the observed VDEs for  $\text{NaSi}_5^-$  are given in Table 12-2, where they are compared with theoretical calculations.

It has been demonstrated previously that PES combined with ab initio calculations is a powerful tool for elucidating the electronic structure and chemical bonding of novel clusters.<sup>140</sup> In the following, different levels of theories are employed to investigate the detailed structures and underlying chemical bonding of  $\text{Si}_5^-$  and  $\text{NaSi}_5^-$  ( $\text{Si}_5^{2-}$ ) and to assist the assignment of the observed photoelectron spectra.

### 12-5. Theoretical Results

The geometric structures of  $\text{Si}_5^{2-}$ ,  $\text{Si}_5^-$ , and  $\text{Si}_5$  are well established in the literature.<sup>16,51-109</sup> We still performed the search for the global minimum structures for these species primarily to test our GEGA program. While the GEGA search could potentially be performed for these species at the B3LYP/3-21G level of theory, we used the semiempirical PM3 method for the energy, gradient and force calculations. We plan to use the same level of theory for large silicon clusters, for which the B3LYP/3-21G GEGA calculations would not be possible with our computer resources.



Table 12-2. Experimental VDEs compared with the calculated VDEs for the  $C_s$  ( $^1A'$ )  $NaSi_5^-$ .

Final State	VDE(exp) (eV)	VDE (eV) ROVGF <sup>a</sup>	VDE (eV) TD B3LYP <sup>b</sup>	VDE (eV) UCCSD(T) <sup>c</sup>
$^2A'(4a'^25a'^22a''^26a'^23a''^27a'^28a'^1)$	~2.55 (X)	2.47 (0.88)	2.52	2.54
$^2A'(4a'^25a'^22a''^26a'^23a''^27a'^18a'^2)$	2.67 ± 0.04 (A)	2.68 (0.88)	2.59	
$^2A''(4a'^25a'^22a''^26a'^23a''^17a'^28a'^2)$	~2.9 (B)	2.90 (0.88)	2.74	
$^2A'(4a'^25a'^22a''^26a'^13a''^27a'^28a'^2)$	3.47 ± 0.04 (C)	3.29 (0.88)	3.40	
$^2A''(4a'^25a'^22a''^16a'^23a''^27a'^28a'^2)$	3.71 ± 0.04 (D)	3.73 (0.88)	3.43	
$^2A'(4a'^25a'^12a''^26a'^23a''^27a'^28a'^2)$	3.95 ± 0.03 (E)	3.83 (0.87)	3.74	
$^2A'(4a'^15a'^22a''^26a'^23a''^27a'^28a'^2)$	5.50 ± 0.06 (F)	5.83 (0.83)	5.66 <sup>d</sup>	

<sup>a</sup> The VDEs were calculated at the ROVGF/6-311+G(2df)//B3LYP6-311+G\* level of theory. The numbers in the parentheses indicate the pole strength, which characterizes the validity of the one-electron detachment picture.

<sup>b</sup> The VDEs were calculated at the TD B3LYP/6-311+G(2df)//B3LYP/6-311+G\* level of theory.

<sup>c</sup> The VDEs were calculated at the TD CCSD(T)/6-311+G(2df)//B3LYP/6-311+G\* level of theory.

<sup>d</sup> The electron detachment becomes a strongly multiconfigurational process.

### 12-5.1. $Si_5^{2-}$

The PM3 GEGA search yielded the bipyramidal  $D_{3h}$  ( $1A_1'$ ,  $1a_1'^2 1a_2''^2 1e'^4 2a_1'^2 3a_1'^2 1e''^4 2e''^4 2a_2''^2$ ) global minimum structure I (Figure 12-3a). Two planar isomers were also obtained II  $C_2$  ( $1A$ ) and III  $D_{2h}$  ( $1A_g$ ). We then performed B3LYP/6-311+G\* geometry optimization and frequency calculations for the structures I, II and III. Again the global minimum structure at this level of theory was found to be structure I. We also performed CCSD(T)/6-311+G\* calculations for structure I. Both geometric parameters and frequencies are in good agreement between the two methods, as shown in Table 12-3. Our optimized  $d_{eq-eq}$  (2.606 Å at B3LYP/6-311+G\* and 2.591 Å at CCSD(T)/6-311+G\*) and  $d_{ax-eq}$  (2.400 Å at B3LYP/6-311+G\* and 2.389 Å at CCSD(T)/6-311+G\*) are slightly longer than the corresponding experimental values  $d_{eq-eq} = 2.535$  Å and  $d_{ax-eq} = 2.350$  Å obtained by Goicoechea and Sevov in solid,<sup>15</sup> but they agree well with the ab initio calculations reported by Kaya and co-workers.<sup>16</sup> The isomers II,  $C_{2v}$  ( $1A_1$ ) and III,  $D_{2h}$  ( $1A_1$ ) were found to be higher in energy than the global minimum structure by 37.0 kcal/mol and 41.3 kcal/mol (all at CCSD(T)/6-311+G(2df)//B3LYP/6-311+G\*+ZPE correction at B3LYP/6-311+G\*), respectively. Optimized geometry and harmonic frequencies calculated at the CASSCF(10,8)/6-311+G\* level of theory are in good agreement with the results at B3LYP/6-311+G\* and CCSD(T)/6-311+G\* (Table 12-3). The Hartree-Fock configuration was found to be dominant ( $C_{HF} = 0.943$ ) among 1176 configurations in the CASSCF wavefunction, thus confirming the applicability of the used one-electron configuration based methods. We also performed a single point calculation with the extended active space CASSCF(12,9)/6-311+G\*. The Hartree-Fock

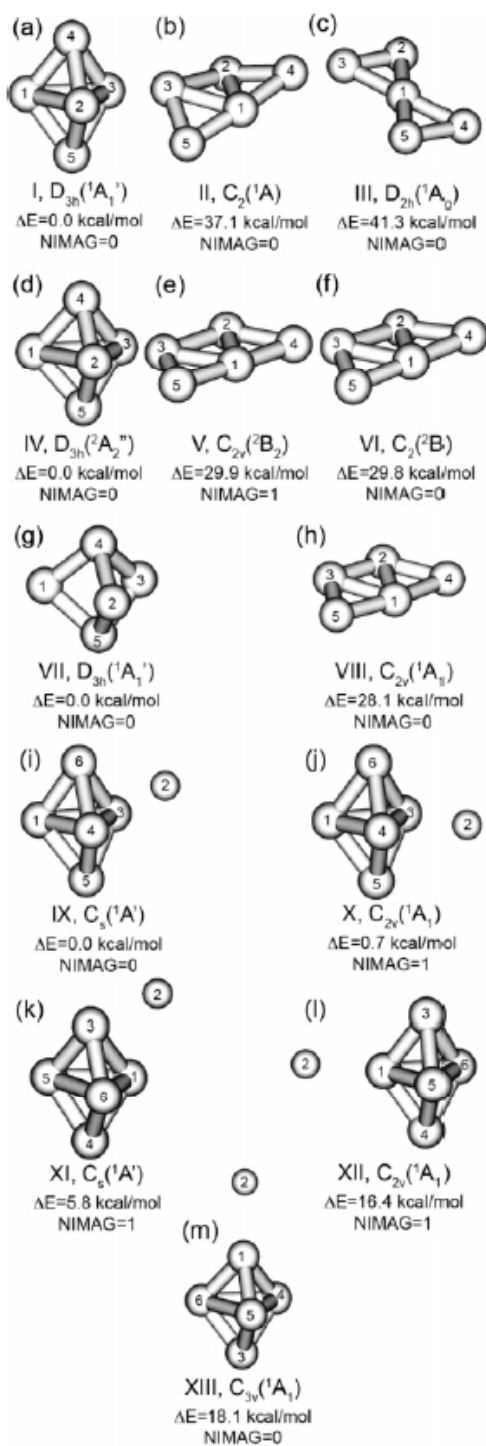


Figure 12-3. Optimized geometries (B3LYP/6-311+G\*) of  $Si_5^{2-}$  (a, b, c),  $Si_5^-$  (d, e, f),  $Si_5$  (g, h), and  $NaSi_5^-$  (i, j). Relative geometries are given at CCSD(T)/6-311+G(2df)//B3LYP/6-311+G\*. NIMAG – number of imaginary frequencies.

Table 12-3. Calculated molecular properties of  $\text{Si}_5^{2-} \text{D}_{3h} (^1\text{A}_1')$ .

Method	B3LYP/ 6-311+G*	CASSCF(10,8)/ 6-311+G*	CCSD(T)/ 6-311+G*
-E, a.u.	1447.524931	1444.582724	1445.075619
$R(\text{Si}_2\text{-Si}_5)$ , Å	2.400	2.387	2.389
$R(\text{Si}_2\text{-Si}_3)$ , Å	2.606	2.634	2.591
$\omega_1(\text{a}_1')$ , $\text{cm}^{-1}$	432 (0.0) <sup>a</sup>	464	452
$\omega_2(\text{a}_1')$ , $\text{cm}^{-1}$	332 (0.0) <sup>a</sup>	342	338
$\omega_3(\text{a}_2'')$ , $\text{cm}^{-1}$	445 (1.3) <sup>a</sup>	485	457
$\omega_4(\text{e}')$ , $\text{cm}^{-1}$	330 (0.0) <sup>a</sup>	341	336
$\omega_5(\text{e}')$ , $\text{cm}^{-1}$	180 (0.9) <sup>a</sup>	190	176
$\omega_6(\text{e}'')$ , $\text{cm}^{-1}$	301 (0.0) <sup>a</sup>	317	311

<sup>a</sup> Infrared intensities (km/mol) are given in parenthesis.

configuration was found to be almost the same ( $C_{HF} = 0.943$ ) among 3570 configurations in the CASSCF wavefunction.

### 12-5.2. $Si_5^-$ and $Si_5$ .

The similar PM3 GEGA search also yielded a bipyramidal  $D_{3h}$  ( ${}^2A_2''$ ,  $1a_1'{}^21a_2''{}^21e'{}^42a_1'{}^23a_1'{}^21e''{}^42e'{}^42a_2''{}^1$ ) global minimum structure for  $Si_5^-$  (IV, Figure 12-3d) with a lowest planar isomer VI  $C_2$  ( ${}^2B$ ) (Figure 12-3f). Subsequent B3LYP/6-311+G\* geometry optimization and frequency calculations for the structures IV, V and VI confirmed that the structure IV (Table 12-4) is the global minimum. We also performed CCSD(T)/6-311+G\* calculations for structure IV (Table 12-4). The  $D_{3h}$  ( ${}^2A_2''$ ) global minimum structure was first predicted by Raghavachari<sup>52</sup> and has been confirmed in numerous calculations later.<sup>16,51-64</sup> Our PM3 GEGA findings and the more sophisticated calculations are in excellent agreement with the previous results. The lowest  $C_2$  ( ${}^2B$ ) isomer VI (Figure 12-3f) for  $Si_5^-$  found in our calculations is substantially higher in energy (by 30 kcal/mol at CCSD(T)/6-311+G(2df)//B3LYP/6-311+G\*+ZPE corrections at B3LYP/6-311+G\*) and thus should not be significantly populated in the  $Si_5^-$  ion beam.

For  $Si_5$ , our PM3 GEGA search revealed the bipyramidal  $D_{3h}$  ( ${}^1A_1'$ ,  $1a_1'{}^21a_2''{}^21e'{}^42a_1'{}^23a_1'{}^21e''{}^42e'{}^42a_2''{}^0$ ) global minimum structure (Figure 12-3g, Table 12-5) with a low-lying singlet  $C_{2v}$  ( ${}^1A_1$ ) planar isomer VIII (Figure 12-3h). The bipyramidal  $D_{3h}$  global minimum for  $Si_5$  was also first predicted by Raghavachari and Logovinsky<sup>66</sup> and has been confirmed by numerous subsequent calculations.<sup>16,51,52,55,56,58-</sup>

<sup>109</sup> The lowest  $C_{2v}$  ( ${}^1A_1$ ) isomer VIII (Figure 12-3h) for  $Si_5$  was found to be substantially

Table 12-4. Calculated molecular properties of  $\text{Si}_5^- \text{D}_{3h} (^2\text{A}_2'')$ .

Method	B3LYP/6-311+G*	CASSCF(9,7)/6-311+G*	CCSD(T)/6-311+G*
-E, a.u.	1447.581738	1444.639338	1445.139672
$R(\text{Si}_2\text{-Si}_5)$ , Å	2.356	2.348	2.346
$R(\text{Si}_2\text{-Si}_3)$ , Å	2.778	2.730	2.751
$\omega_1(\text{a}_1')$ , $\text{cm}^{-1}$	450 (0.0) <sup>a</sup>	480	467
$\omega_2(\text{a}_1')$ , $\text{cm}^{-1}$	292 (0.0) <sup>a</sup>	310	306
$\omega_3(\text{a}_2'')$ , $\text{cm}^{-1}$	428 (2.6) <sup>a</sup>	422	445
$\omega_4(\text{e}')$ , $\text{cm}^{-1}$	360 (0.6) <sup>a</sup>	388	366
$\omega_5(\text{e}')$ , $\text{cm}^{-1}$	192 (0.7) <sup>a</sup>	200	193
$\omega_6(\text{e}'')$ , $\text{cm}^{-1}$	328 (0.0) <sup>a</sup>	333	345

<sup>a</sup> Infrared intensities (km/mol) are given in parenthesis.

Table 12-5. Calculated molecular properties of Si<sub>5</sub> D<sub>3h</sub> (<sup>1</sup>A<sub>1</sub>').

Method	B3LYP/6-311+G*	CASSCF(8,7)/6-311+G*	CCSD(T)/6-311+G*
-E, a.u.	1447.492144	1444.580865	1445.060178
R(Si <sub>2</sub> -Si <sub>5</sub> ), Å	2.330	2.330	2.316
R(Si <sub>2</sub> -Si <sub>3</sub> ), Å	3.125	3.173	3.073
ω <sub>1</sub> (a <sub>1</sub> '), cm <sup>-1</sup>	456 (0.0) <sup>a</sup>	474	477
ω <sub>2</sub> (a <sub>1</sub> '), cm <sup>-1</sup>	228 (0.0) <sup>a</sup>	216	239
ω <sub>3</sub> (a <sub>2</sub> ''), cm <sup>-1</sup>	375 (4.6) <sup>a</sup>	369	404
ω <sub>4</sub> (e'), cm <sup>-1</sup>	432 (4.5) <sup>a</sup>	457	435
ω <sub>5</sub> (e'), cm <sup>-1</sup>	170 (0.6) <sup>a</sup>	161	164
ω <sub>6</sub> (e''), cm <sup>-1</sup>	338 (0.0) <sup>a</sup>	323	364

<sup>a</sup> Infrared intensities (km/mol) are given in parenthesis.

(28 cal/mol at CCSD(T)/6-311+G(2df)//B3LYP/6-311+G\*+ZPE corrections at B3LYP/6-311+G\*) higher in energy.

We also optimized geometry and calculated harmonic frequencies at the CASSCF(9,7)/6-311+G\* ( $\text{Si}_5^-$ ) and at the CASSCF(8,7)/6-311+G\* ( $\text{Si}_5$ ) levels of theory (Tables 12-4 and 12-5). The CASSCF results are in good agreement with the results at B3LYP/6-311+G\* and CCSD(T)/6-311+G\*. The Hartree-Fock configurations were found to be dominant ( $C_{\text{HF}} = 0.969$ ) among 490 configurations in the CASSCF wavefunction for  $\text{Si}_5^-$  and ( $C_{\text{HF}} = 0.953$ ) among 490 configurations in the CASSCF wavefunction for  $\text{Si}_5$ , thus confirming the applicability of the used one-electron configuration based methods.

### 12-5.3. $\text{NaSi}_5^-$

For the  $\text{NaSi}_5^-$  anion we expected that the global minimum structure should be related to the trigonal bipyramid structure I of  $\text{Si}_5^{2-}$  (Figure 12-3a), because alternative structures for the dianion are substantially higher in energy. We placed a  $\text{Na}^+$  cation at different positions around the  $D_{3h}$   $\text{Si}_5^{2-}$ : 1) above a triangular face (Figure 12-3i), 2) above an edge between two equatorial Si atoms (Figure 12-3j), 3) above an edge between one axial and one equatorial Si atom (Figure 12-3k), 4) above an equatorial silicon atom (Figure 12-3l), and 5) above an axial Si atom (Figure 12-3m). Geometry optimization and frequency calculations for these structures were performed at the B3LYP/6-311+G\* level of theory. The lowest energy structure among those is the structure IX ( $C_s$ ,  $^1A'$ ). This structure was reoptimized at the MP2/6-311+G\* level of theory and the results agree well with the B3LYP/6-311+G\* results (Table 12-6). We were not able to converge



geometry optimization at CCSD(T)/6-311+G\* because of the numerical calculation procedure for gradients at the CCSD(T) level of theory and because of a very shallow potential energy surface. The structure X ( $C_{2v}$ ,  $^1A_1$ ) with the  $Na^+$  cation located above the edge was found to be a first order saddle point being just 0.7 kcal/mol (CCSD(T)/6-311+G(2df)//B3LYP/6-311+G\*+ZPE corrections at B3LYP/6-311+G\*) above the global minimum. Thus, the  $NaSi_5^-$  potential energy surface is very flat and the  $Na^+$  cation can almost freely move from a position over the upper face to a position over the lower face in the  $Si_5^{2-}$  trigonal bipyramid. The structure XI ( $C_s$ ,  $^1A'$ ) is also a first order saddle point corresponding to internal motions of  $Na^+$  around the upper or lower part of the  $Si_5^{2-}$  trigonal bipyramid. The barrier for this motion is appreciably higher (5.8 kcal/mol (CCSD(T)/6-311+G(2df)//B3LYP/6-311+G\*+ZPE corrections at B3LYP/6-311+G\*)). Two other optimized structures with  $Na^+$  coordinated to just one Si atom were found to be appreciably higher in energy. The structure XII ( $C_{2v}$ ,  $^1A_1$ ) is a saddle point at B3LYP/6-311+G\* being 16.4 kcal/mol (CCSD(T)/6-311+G(2df)//B3LYP/6-311+G\*+ZPE corrections at B3LYP/6-311+G\*) higher in energy than the global minimum and the structure XIII ( $C_{2v}$ ,  $^1A_1$ ) is a local minimum being 18.1 kcal/mol (CCSD(T)/6-311+G(2df)//B3LYP/6-311+G\*+ZPE corrections at B3LYP/6-311+G\*) above the global minimum.

Our finding that the  $C_s$  ( $^1A'$ ) structure IX is the global minimum for  $NaSi_5^-$  disagrees with the conclusion of Kaya and co-workers,<sup>16</sup> who reported the structure X with  $Na^+$  coordinated to an equatorial edge as the global minimum. However, the potential energy surface is very flat.

Table 12-6. Calculated molecular properties of  $\text{NaSi}_5^{1-} \text{C}_s$  ( $^1\text{A}'$ ).

Method	B3LYP/6-311+G*	MP2/6-311+G*
-E, a.u.	1609.923210	1607.003523
$\text{R}(\text{Si}_1\text{-Si}_{3,4})$ , Å	2.519	2.487
$\text{R}(\text{Si}_1\text{-Si}_5)$ , Å	2.438	2.400
$\text{R}(\text{Si}_1\text{-Si}_6)$ , Å	2.353	2.344
$\text{R}(\text{Si}_3\text{-Si}_4)$ , Å	2.698	2.638
$\text{R}(\text{Si}_5\text{-Si}_{3,4})$ , Å	2.389	2.384
$\text{R}(\text{Si}_6\text{-Si}_{3,4})$ , Å	2.456	2.439
$\text{R}(\text{Na-Si}_{3,4})$ , Å	2.831	2.842
$\text{R}(\text{Na-Si}_5)$ , Å	4.167	4.251
$\text{R}(\text{Na-Si}_6)$ , Å	2.959	2.914
$\omega_1(\text{a}')$ , $\text{cm}^{-1}$	446 (0.4) <sup>a</sup>	465 (2.4) <sup>a</sup>
$\omega_2(\text{a}')$ , $\text{cm}^{-1}$	440 (1.1) <sup>a</sup>	459 (1.1) <sup>a</sup>
$\omega_3(\text{a}')$ , $\text{cm}^{-1}$	344 (1.9) <sup>a</sup>	358 (0.7) <sup>a</sup>
$\omega_4(\text{a}')$ , $\text{cm}^{-1}$	305 (5.9) <sup>a</sup>	342 (0.8) <sup>a</sup>
$\omega_5(\text{a}')$ , $\text{cm}^{-1}$	294 (1.1) <sup>a</sup>	325 (3.6) <sup>a</sup>
$\omega_6(\text{a}')$ , $\text{cm}^{-1}$	236 (24.9) <sup>a</sup>	244 (34.9) <sup>a</sup>
$\omega_7(\text{a}')$ , $\text{cm}^{-1}$	185 (0.9) <sup>a</sup>	205 (1.3) <sup>a</sup>
$\omega_8(\text{a}')$ , $\text{cm}^{-1}$	65 (7.0) <sup>a</sup>	87 (7.4) <sup>a</sup>
$\omega_9(\text{a}'')$ , $\text{cm}^{-1}$	346 (1.7) <sup>a</sup>	365 (0.4) <sup>a</sup>
$\omega_{10}(\text{a}'')$ , $\text{cm}^{-1}$	302 (0.1) <sup>a</sup>	336 (0.9) <sup>a</sup>
$\omega_{11}(\text{a}'')$ , $\text{cm}^{-1}$	195 (5.4) <sup>a</sup>	193 (5.6) <sup>a</sup>
$\omega_{12}(\text{a}'')$ , $\text{cm}^{-1}$	97 (1.1) <sup>a</sup>	89 (0.8) <sup>a</sup>

<sup>a</sup> Infrared intensities (km/mol) are given in parenthesis.

## 12-6. Interpretation of the Photoelectron Spectra of $\text{Si}_5^-$ and $\text{NaSi}_5^-$

### 12-6.1. $\text{Si}_5^-$

The VDEs of  $\text{Si}_5^-$  were calculated at four levels of theory (TD-B3LYP, UOVGF, CCSD(T), and EOM, all with the 6-311+G(2df) basis sets), as summarized in Table 21-1. The VDEs calculated at the different levels of theory are surprisingly close to each other and agree with the experimental data very well. The ground state transition corresponds to the electron detachment from the singly occupied  $2a_2''$ -HOMO, which is the same  $2a_2''$  orbital in  $\text{Si}_5^{2-}$  as shown in Figure 12-4a. This orbital is bonding within the equatorial atoms, but antibonding between the equatorial atoms and the axial atoms. Thus detachment of the  $2a_2''$  electron leads to a considerable geometry change in neutral  $\text{Si}_5$ . It turns out the largest change is the equatorial Si-Si distances, which increases from 2.751 Å in  $\text{Si}_5^-$  to 3.073 Å in  $\text{Si}_5$  accompanied by a very small contraction of the Si-Si distances between the equatorial and axial atoms (see Tables 12-4 and 12-5). The huge geometry changes lead to a very broad band for the ground state transition. Neumark et al. resolved a long vibrational progression for this transition with an average spacing of  $233 \text{ cm}^{-1}$ , which is in excellent agreement with our calculated frequency for the  $\nu_1$  mode ( $239 \text{ cm}^{-1}$ , Table 12-5). Our calculated ADE energy, i.e., the adiabatic electron affinity of neutral  $\text{Si}_5$ , is 2.35 eV at B3LYP/6-311+G(2df) and 2.37 eV at CCSD(T)/6-311+G(2df), which is significantly lower than the calculated VDE (Table 12-1) consistent with the large geometry changes between the anion and neutral. The large geometry changes between  $\text{Si}_5^-$  and  $\text{Si}_5$  mean that the ADE may not be obtained from the PES spectra because the Franck-Condon factor for the 0-0 transition may be negligible. Neumark et al. estimated

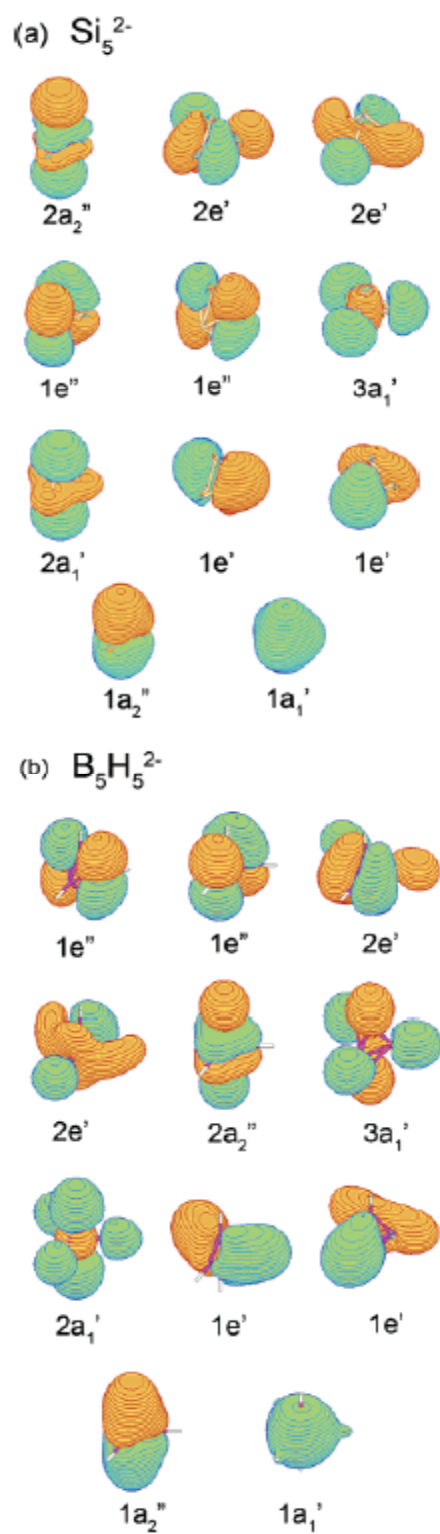


Figure 12-4. Valence molecular orbitals of (a)  $\text{Si}_5^{2-}$  ( $D_{3h}$ ,  $^1A_1'$ ) and (b)  $\text{B}_5\text{H}_5^{2-}$  ( $D_{3h}$ ,  $^1A_1'$ ) at the RHF/6-311+G\* level of theory.

and ADE of  $2.59 \pm 0.02$  eV from their Franck-Condon simulation.<sup>31</sup> Our observed detachment threshold in the 355 nm spectrum (Figure 12-1a) is around 2.7 eV. All of these should be viewed as upper limit for the ADE. We suspect that the calculated ADE may be closer to the true value.

The next detachment is from the  $2e'$  HOMO-1 orbital, which will result in two detachment channels, a triplet and a singlet final states. These states are Jahn-Teller active and are expected to give very complicated spectral features. As given in Table 12-1, the calculated VDE for the triplet state ranges from 2.95 to 3.24 eV, whereas that for the singlet state ranges from 3.26 to 3.52 eV. These VDEs are in good agreement with the estimated VDEs for the overlapping A and B bands. Thus, the first broad feature (X, A, B) in the photoelectron spectra of  $\text{Si}_5^-$  contains three detachment transitions. From their vibrationally resolved data and angular dependent study, Neumark et al. clearly resolved the A band. However, they did not recognize the third detachment channel corresponding to the singlet state ( $^1E''$ ), even though they resolved it more clearly. The complex vibrational structures observed in their spectra agree with the Jahn-Teller effects expected for these final states.

The HOMO-2 orbital ( $1e''$ ) is also a doubly degenerate MO. Detachment from this MO will again yield a triplet and singlet state, which are Jahn-Teller active. The calculated VDE for the triplet state ranges from 3.87 to 4.03 eV, whereas that for the singlet state ranges from 4.36 to 4.50 eV. These calculated VDEs are in good agreement with the estimated VDEs for the C and D bands. The HOMO-3 is a non-degenerate orbital ( $3a_1'$ ). Detachment from this orbital will also lead to a triplet ( $^3A_2''$ ) and a singlet

state ( $^1A_2''$ ). The calculated VDEs for these two states agree well with the estimated VDEs for the E and F bands, respectively.

Finally, the highest binding energy feature observed in the photoelectron spectra is the weak band G with an estimated VDE of  $\sim 5.4$  eV, which is in good agreement with the calculated VDE for the triplet final state from detachment from the  $2a_1'$  HOMO-4 (Table 12-1). The calculated VDE for the corresponding singlet final state is about 6.8 eV. However, the intensity for this detachment channel is expected to be very low, considering the weak intensity for the triplet channel (G), and is not observed in the 157 nm, which also has very poor signal-to-noise ratios in the higher binding energy part. However, overall the calculated VDEs for the  $D_{3h}$   $Si_5^-$  are in excellent agreement with the photoelectron spectra, confirming the  $D_{3h}$  structure for  $Si_5^-$  and lending credence for the TD-B3LYP and the UOVGF methods used to compute VDEs.

### 12-6.2. $NaSi_5^-$

The  $C_s$   $NaSi_5^-$  IX (Figure 12-3i) can be viewed as a  $D_{3h}$   $Si_5^{2-}$  stabilized by a  $Na^+$  cation.  $Si_5^{2-}$  is closed shell and its 11 fully occupied valence MOs are shown in Figure 4a. Thus  $NaSi_5^-$  is also closed shell and should give simpler photoelectron spectra because detachment from each occupied MO can only yield one doublet final state (Table 12-2). The HOMO of  $NaSi_5^-$  is the  $8a'$  MO, which corresponds to the  $2a_2''$ -HOMO in  $Si_5^{2-}$  (Figures 12-4a). This is also the same HOMO in  $Si_5^-$ , albeit it is singly occupied in the latter. Detachment from the  $8a'$  HOMO of  $NaSi_5^-$  yielded the ground state of  $NaSi_5$  [ $Na^+(Si_5^-)$ ]. Even though the equatorial Si-Si bond lengths are shorter in  $Si_5^{2-}$  (Table 12-3) than in  $Si_5^-$  (Table 12-4), the change between  $Si_5^{2-}$  and  $Si_5^-$  (2.591 vs. 2.751 Å) is only

half of that between  $\text{Si}_5^-$  and  $\text{Si}_5$  (2.751 vs. 3.073 Å). Thus the X band of  $\text{NaSi}_5^-$  is sharper than that in the  $\text{Si}_5^-$  spectra. The calculated VDE for the ground state transitions at all three levels of theory (ROVGF, TD-B3LYP, and CCSD(T), all with the 6-311+G(2df)) are in good agreement with the experiment.

The next two detachment channels correspond to the  $7a'$  and  $3a''$  orbitals, which can be traced to the pair of doubly degenerate  $2e'$ -MO in  $\text{Si}_5^{2-}$  (Figure 12-4a). The  $\text{Na}^+$  coordination to  $\text{Si}_5^{2-}$  splits the degeneracy of  $2e'$  orbitals. However, the calculated VDEs for these two MOs are fairly close to each other and they are also very close to the ground state detachment channel. These three closely spaced detachment channels give rise to the broad band at the lower binding energies in the photoelectron spectra (X, A, B in Figure 12-2 and Table 12-2). The photoelectron spectra of  $\text{NaSi}_5^-$  at higher binding energies exhibit four well separated bands (C, D, E, F), which correspond to detachment from the  $6a'$ ,  $2a''$ ,  $5a'$ , and  $4a'$ , respectively. The calculated VDEs are all in excellent agreement with the experimental values (Table 12-2). The  $6a'$  and  $2a''$  correspond to the  $1e''$  MO in  $\text{Si}_5^{2-}$ , whereas the  $5a'$  and  $4a'$  correspond to the  $3a_1'$  and  $2a_1'$  of  $\text{Si}_5^{2-}$ , respectively (Figure 12-4a).

The overall agreement between the experimental spectral pattern and the calculated VDEs is very good, confirming the global minimum structure for  $\text{NaSi}_5^-$  ( $C_s$ ,  $^1A'$ ), in which the  $\text{Na}^+$  counterion is coordinated to the face of the trigonal bipyramidal  $\text{Si}_5^{2-}$  (Figure 12-3i). Again, the two theoretical methods, ROVGF and TD-B3LYP, performed well for  $\text{NaSi}_5^-$  and are planned to be used in the future for large sodium coordinated silicon clusters.

### 12-7. Chemical Bonding in $\text{Si}_5$ , $\text{Si}_5^-$ and $\text{Si}_5^{2-}$

Chemical bonding in  $\text{Si}_5$  and  $\text{Si}_5^{2-}$  have been previously discussed.<sup>77,81,141</sup> In particular, Wang and Messmer,<sup>77</sup> and Patterson and Messmer<sup>81</sup> have interpreted chemical bonding in  $\text{Si}_5$  using the valence bond model, a key feature of which is that each atom is surrounded by a tetrahedrally orientated set of orbitals. Then, pairs of occupied orbitals are singlet spin coupled into electron pairs, which are spatially separated from one another due to the Pauli exclusion principle. For the  $\text{Si}_5$  cluster they obtained six symmetry equivalent bent bonds that arise from the overlap of two orbitals, one from each of two atoms. These six bonds describe 2e-2c bonding between axial and equatorial Si atoms. Every equatorial atom possesses a lone pair and the two axial Si atoms form a long bond. According to this valence bond picture the long bond is formed by two collinear tetrahedral orbitals on the two axial silicon atoms, which are pointing away from each other, but nevertheless overlap enough to form a bond. Schleyer and co-workers<sup>141</sup> pointed out that the trigonal bipyramid  $\text{Si}_5^{2-}$  is a three-dimensional aromatic cluster similar to the valence isoelectronic  $\text{B}_5\text{H}_5^{2-}$  cluster on the basis of diatropic NICS(0) values: NICS(0) = -38.5 for  $\text{Si}_5^{2-}$  and NICS(0) = -25.9 for  $\text{B}_5\text{H}_5^{2-}$ . These dianions are also aromatic according to the *styx* Lipscomb rule<sup>11,12</sup> and they also satisfy the Wade's  $2n+2$  skeletal electron rule<sup>142,143</sup> for aromatic deltahedral systems. However they do not obey the Hirsch's  $2(N+1)^2$  rule<sup>144</sup> for three-dimensional aromaticity.

In our consideration of the chemical bonding in  $\text{Si}_5$ ,  $\text{Si}_5^-$ ,  $\text{Si}_5^{2-}$ , and  $\text{B}_5\text{H}_5^{2-}$ , we used the natural population analysis (NPA), molecular orbital analysis, electron localization functions (ELF), and nuclear independent chemical shifts (NICS).



### 12-7.1. NPA analysis

According to the NPA, an electron density change upon an electron detachment from  $\text{Si}_5^{2-}$  [ $Q(\text{Si}_{\text{eq}}) = -0.40 |e|$  (hybridization  $3s^{1.63}3p^{2.71}$ ) and  $Q(\text{Si}_{\text{ax}}) = -0.40 |e|$  ( $3s^{1.65}3p^{2.70}$ )] to  $\text{Si}_5^-$  [ $Q(\text{Si}_{\text{eq}}) = -0.20 |e|$  ( $3s^{1.68}3p^{2.48}$ ) and  $Q(\text{Si}_{\text{ax}}) = -0.20 |e|$  ( $3s^{1.59}3p^{2.56}$ )] occurs on all five atoms, while upon an electron detachment from  $\text{Si}_5^-$  to  $\text{Si}_5$  [ $Q(\text{Si}_{\text{eq}}) = +0.16 |e|$  ( $3s^{1.74}3p^{2.08}$ ) and  $Q(\text{Si}_{\text{ax}}) = -0.24 e$  ( $3s^{1.59}3p^{2.60}$ )] it occurs primarily on the equatorial Si atoms.

### 12-7.2. Molecular orbital analysis

Valence molecular orbital picture for  $\text{B}_5\text{H}_5^{2-}$  is quite similar to that for  $\text{Si}_5^{2-}$  (Figure 12-4), although the order of their occupied MOs is somewhat different. This similarity at the first glance indicates that the chemical skeletal bonding in the trigonal  $\text{B}_5$  or  $\text{Si}_5$  units should be quite similar. Indeed, Schleyer and co-workers calculated NICS(0) indices at the center of both dianions and reported that they are highly negative (-25.9 ppm for  $\text{B}_5\text{H}_5^{2-}$ ) and (-38.5 ppm for  $\text{Si}_5^{2-}$ ) showing significant aromaticity in both species. The aromatic nature of deltahedral boranes have been previously discussed by King and Rouvray<sup>145</sup> and Aihara.<sup>146</sup>

### 12-7.3. ELF analysis

The ELFs calculated for  $\text{B}_5\text{H}_5^{2-}$ ,  $\text{Si}_5^{2-}$ , and  $\text{Si}_5$  are presented in Figure 12-5. The local maxima of the ELFs define “localization attractors”, of which there are only three basis types: bonding, non-bonding and core. Bonding attractors lie between the core attractors (which themselves surround the atomic nuclei) and characterize the shared-electron interactions. The spatial organization of localization attractors provides a basis

for a well-defined classification of bonds. From any point in space the ELF gradient is followed to an attractor in that region, and this point is then attributed to this attractor. The collection of all the points in the space that is assigned to a given attractor is called its basin. The criterion of discrimination between basins is provided by the reduction of reducible (containing more than one attractor) domains. The reduction of a reducible localization domain occurs at critical values (saddle points) of the bonding isosurface, over which the domain is split into domains containing fewer attractors. The localization domains are then ordered with respect to the ELF critical values, yielding bifurcations.

The ELF pictures calculated for  $B_5H_5^{2-}$  (Figure 12-5a) reveal that protonated attractor domains (sphere-like areas) are separated as the result of bifurcations at  $ELF = 0.52$  (axial domains separated) and  $ELF = 0.64$  (equatorial domains separated). These domains correspond to the 2e-2c B-H bonds. There two more bifurcations can be seen in Figure 12-5a at the  $ELF = 0.77$  and  $ELF = 0.85$ . The first bifurcation yields two reducible domains in the region of boron-boron bonding and the second bifurcation reveals the six irreducible domains corresponding to six  $B_{ax}-B_{eq}$  bonds. According to the ELF analysis, there is no  $B_{eq}-B_{eq}$  bonding. This chemical bonding picture is consistent with the *styx* Lipscomb's description of chemical bonding in  $B_5H_5^{2-}$ .

The ELF pictures calculated for the valence isoelectronic  $Si_5^{2-}$  (Figure 12-5b) are somewhat different from the  $B_5H_5^{2-}$  dianion. First, at the  $ELF = 0.65$  one can see the system of three attractors in the equatorial plane, which can be tentatively attributed to a pair of electrons delocalized in the equatorial area. At the  $ELF = 0.69$  one can see the separation of the two lone pairs corresponding to the axial Si atoms. Finally, at the  $ELF = 0.77$  one can see the separation of the three non-bonding domains corresponding to the

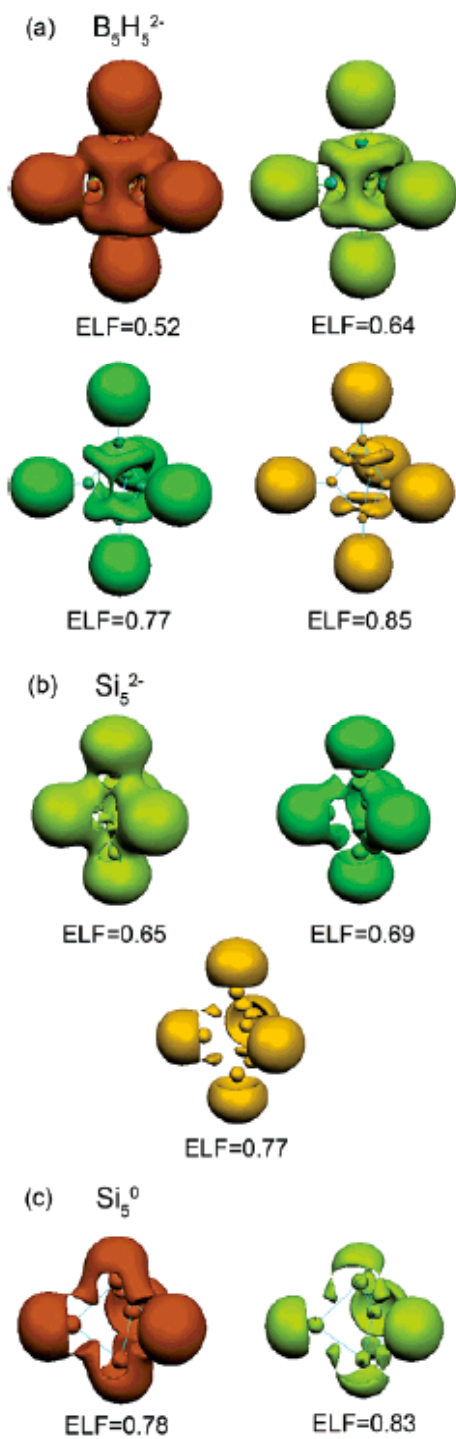


Figure 12-5. The ELF bifurcations for (a)  $B_5H_5^{2-}$  ( $D_{3h}$ ,  $^1A_1'$ ), (b)  $Si_5^{2-}$  ( $D_{3h}$ ,  $^1A_1'$ ) and  $Si_5$  ( $D_{3h}$ ,  $^1A_1'$ ) calculated at the B3LYP/6-311+G\* level of theory.

equatorial Si atoms. Simultaneously, the six bonding domains corresponding to the  $\text{Si}_{\text{eq}}\text{-Si}_{\text{ax}}$  bonds are revealed. Thus, in  $\text{Si}_5^{2-}$  if compared to  $\text{B}_5\text{H}_5^{2-}$ , one can see that some electrons, which are supposed to belong to Si equatorial lone pairs are actually participating in chemical skeletal bonding.

The bifurcations corresponding to the  $\text{Si}_5$  neutral species are shown in Figure 12-5c. The major difference in the ELF analysis between  $\text{Si}_5$  and  $\text{Si}_5^{2-}$  is the absence of the system of the three equatorial attractors in the neutral system and the significant alternation of the non-bonding domains corresponding to the axial Si atoms. It also should be pointed out that, the interaction between the bonding  $\text{Si}_{\text{ax}}\text{-Si}_{\text{eq}}$  domains and the axial non-bonding domains is appreciably stronger, because the bifurcation occurs at relatively high ELF value (0.69 for  $\text{Si}_5^{2-}$  and 0.83 for  $\text{Si}_5$ ). Thus, the change in the electron density accompanying the removal of an electron pair from  $\text{Si}_5^{2-} \rightarrow \text{Si}_5$  corresponds to the loss of electron density in the area primarily belonging to the equatorial Si atoms, and that is consistent with out NPA analysis.

#### 12-7.4. NICS analysis

We also performed calculations of the NICS indices (at B3LYP/6-311+G\*) for  $\text{Si}_5^{2-}$ ,  $\text{Si}_5^-$ , and  $\text{Si}_5$  along the normal to the triangular face of the trigonal bipyramid starting from the center of the cluster. Our results are summarized in Table 12-7. We found that the NICS(0) values at the center of the cluster are highly negative for all the  $\text{Si}_5^{2-}$ ,  $\text{Si}_5^-$ , and  $\text{Si}_5$  species clearly showing the presence of aromaticity in these clusters. The NICS(0) value is increasing along the  $\text{Si}_5^{2-}$ ,  $\text{Si}_5^-$ , and  $\text{Si}_5$  series. The NICS(0) value for the  $\text{Si}_5^{2-}$  dianion reported by Schleyer and co-workers<sup>141</sup> is very similar to our value.

We found that the NICS value is growing along the normal for the  $\text{Si}_5^{2-}$  dianion and reaching the maximum value (-41.9 ppm) at the point of crossing the triangular face. That could be a manifestation of the additional contribution from the  $\sigma$ -aromaticity (aromaticity originated from the perpendicular  $3p_x$ - and  $3p_y$ -AOs of Si) in the triangular face of the trigonal bipyramid. When one electron is detached from the  $2a_2''$ -HOMO in the  $\text{Si}_5^{2-}$ , the NICS values are substantially higher for almost all calculated points, but the NICS value at the point of crossing the triangular face is not longer the highest. Finally, when the second electron is removed from the  $2a_2''$ -HOMO in the  $\text{Si}_5^{2-}$ , the NICS values are similar to those for  $\text{Si}_5^-$ , but now they are steadily decreasing from the center. These results show that upon the detachment of an electron pair from the  $2a_2''$ -HOMO in the  $\text{Si}_5^{2-}$ , the contribution from  $\sigma$ -aromaticity in the neutral  $\text{Si}_5$  is diminished.

Table 12-7. Calculated NICS (ppm) indices for  $\text{Si}_5^{2-}$ ,  $\text{Si}_5^-$ ,  $\text{Si}_5$  at B3LYP/6-311+G\*.

Position <sup>a</sup>	NICS, $\text{Si}_5^{2-}$ ( $D_{3h}$ , $^1A_1$ )	NICS, $\text{Si}_5^{1-}$ ( $D_{3h}$ , $^2A_2''$ )	NICS, $\text{Si}_5^0$ ( $D_{3h}$ , $^1A_1'$ )
0	-37.0	-48.9	-49.0
1	-37.9	-49.1	-48.8
2	-40.0	-49.4	-47.8
3 <sup>b</sup>	-41.9	-48.2	-45.5
4	-41.4	-44.4	-41.0
5	-37.6	-37.9	-34.3

<sup>a</sup> NICS are calculated along the normal to the triangular face of the trigonal bipyramid starting from the center of the cage. Increments are 0.233 Å for  $\text{Si}_5^{2-}$ , 0.242 Å for  $\text{Si}_5^{1-}$  and 0.256 Å for  $\text{Si}_5^0$  clusters respectively.

<sup>b</sup> This point in case of all three clusters corresponds to the intersection of the normal and the triangular face of the trigonal bipyramid.

## 12-8. Conclusion

We obtained photoelectron spectra for  $\text{Si}_5^-$  and  $\text{NaSi}_5^-$  at the various photon energies. The experimental spectra have been interpreted by comparing with calculated VDEs at four different levels of theory (TD-B3LYP, R(U)OVGF, UCCSD(T), and EOM-CCSD(T), all with the 6-311+G(2df) basis sets). Excellent agreement was found between the experiment and calculations for both anions, confirming their global minimum structures for  $\text{Si}_5^-$  ( $D_{3h}$ ) and  $\text{NaSi}_5^-$  ( $C_s$ ), in which  $\text{Na}^+$  is coordinated to the face of a trigonal pyramidal  $\text{Si}_5^{2-}$ . Chemical bonding analysis of  $\text{Si}_5^{2-}$ ,  $\text{Si}_5^-$ ,  $\text{Si}_5$  and  $\text{B}_5\text{H}_5^{2-}$  was performed using the NPA, molecular orbital analysis, ELF, and NICS indices. On the basis of this analysis we concluded that  $\text{Si}_5^{2-}$  differs from the  $\text{B}_5\text{H}_5^{2-}$  by involvement of the electron density, which is supposed to be “lone pairs” in the skeletal bonding in  $\text{Si}_5^{2-}$ . The NICS indices indicated that all  $\text{Si}_5^{2-}$ ,  $\text{Si}_5^-$ ,  $\text{Si}_5$  clusters are highly aromatic. According to the higher negative NICS(0) value, the neutral and singly charged clusters are more aromatic than the doubly charged one.

## References

- (1) Kroto, H. W.; Heath, J. R.; O'Brien, S. C.; Curl, R. F.; Smalley, R. E. *Nature*, **1985**, *318*, 162.
- (2) Menon M.; Subbaswamy, K. R. *Chem. Phys. Lett.* **1994**, *219*, 219.
- (3) Gong, X. G.; Zheng, Q. Q. *Phys. Rev. B*, **1995**, *52*, 4756.
- (4) Song, J.; Ulloa, S. E.; Drabold, D. A. *Phys. Rev. B*, **1996**, *53*, 8042.
- (5) Li, B. X.; Jiang, M.; Cao, P. I. *J. Phys.: Condens. Matter*, **1999**, *11*, 8517.
- (6) Li, B. X.; Cao, P. I.; Que, D. L. *Phys. Rev. B*, **2000**, *61*, 1685.

- (7) Yu, D. K.; Zhang, R. Q.; Lee, S. T. *Phys. Rev. B* **2002**, *65*, 245417.
- (8) Chen, Z.; Jiao, H.; Seifert, G.; Horn, A. H. C.; Yu, D.; Clark, T.; Thiel, W.; Schleyer, P. v. R. *J. Comput. Chem.* **2003**, *24*, 948.
- (9) Sun, Q.; Wang, Q.; Jena, P.; Rao, B. K.; Kawazoe, Y. *Phys. Rev. Lett.* **2003**, *90*, (13), 135503.
- (10) Jemmis, E. D.; Prasad, B. V.; Tsuzuki, S.; Tanabe, K. *J. Phys. Chem.* **1990**, *94*, 5530.
- (11) Lipscomb, W. N. *Boron Hydrides*, Benjamin: New York, 1963.
- (12) Muetterties, E. L. *Boron Hydride Chemistry*, Academic Press: New York, 1975.
- (13) Cotton F. A.; Wilkinson, G.; Murillo, C. A.; Bochmann, M. *Advanced Inorganic Chemistry*, 6th ed., Wiley-Interscience: New York, 1999.
- (14) Zubarev, D. Yu.; Boldyrev, A. I. unpublished.
- (15) Goicoechea, J. M.; Sevov, S. C. *J. Am. Chem. Soc.* **2004**, *126*, 6860.
- (16) Kishi, R.; Kawamata, H.; Negishi, Y.; Iwata, S.; Nakajima, A.; Kaya, K. *J. Chem. Phys.* **1997**, *107*, 10029.
- (17) Li, S.-D.; Guo, Q.-L.; Zhao, X.-F.; Wu, H.-S.; Jin, Z.-H. *J. Chem. Phys.* **2002**, *117*, 606.
- (18) Li, S.-D.; Ren, G.-M.; Jin, Z.-H. *J. Chem. Phys.* **2003**, *119*, 10063.
- (19) Bloomfield, L. A.; Geusic, M. E.; Freeman, R. R.; Brown, W. L. *Chem. Phys. Lett.* **1985**, *121*, 33.
- (20) Reents, W. D. Jr.; Bondybey, V. E. *Chem. Phys. Lett.* **1986**, *125*, 324.

- (21) Mandich, M. L.; Reents, W. D. Jr.; Bondybey, V. E. *J. Phys. Chem.* **1986**, *90*, 2315.
- (22) Reents, W. D. Jr.; Mandich, M. L.; Bondybey, V. E. *Chem. Phys. Lett.* **1986**, *131*, 1.
- (23) Liu, Y.; Zhang, Q. L.; Tittel, F. K.; Curl, R. F.; Smalley, R. E. *J. Chem. Phys.* **1986**, *85*, 7434.
- (24) Mandich, M. L.; Bondybey, V. E.; Reents, W. D. Jr. *J. Phys. Chem.* **1987**, *86*, 4245.
- (25) Chesnovsky, O.; Yang, S. H.; Pettiette, C. L.; Craycraft, M. J.; Liu, Y.; Smalley, R. E. *Chem. Phys. Lett.* **1987**, *138*, 119.
- (26) Mandich, M. L.; Reents, W. D. Jr. *J. Chem. Phys.* **1989**, *90*, 3121.
- (27) Mandich, M. L.; Reents, W. D. Jr.; Kolenbrander, K. D. *Pure & Appl. Chem.* **1990**, *62*, 1653.
- (28) John, P. M. St.; Whetten, R. L. *Chem. Phys. Lett.* **1992**, *196*, 330.
- (29) Terasaki, A.; Yamaguchi, H.; Yasumatsu, H.; Kondow, T. *Chem. Phys. Lett.* **1996**, *262*, 269.
- (30) Kaya, K.; Nakajima, A. *Mat. Sci. and Engineering A* **1996**, *217/218*, 7.
- (31) Xu, C.; Taylor, T. R.; Burton, G. R.; Neumark, D. M. *J. Chem. Phys.* **1998**, *108*, (4), 1395.
- (32) Muller, J.; Liu, B.; Shvartsburg, A. A.; Ogut, S.; Chelikowsky, J. R.; Siu, K. W. M.; Ho, K. M.; Gantefor, G. *Phys. Rev. Lett.* **2000**, *85*, 1666.
- (33) Shvartsburg, A. A.; Hudgins, R. R.; Dugourd, P.; Jarrold, M. F. *Chem. Soc. Rev.* **2001**, *30*, 26.



- (34) Hoffmann, M. A.; Wrigge, G.; Issendorff, B. v.; Muller, J.; Gantefor, G.; Haberland, H. *Eur. Phys. J. D.* **2001**, *16*, 9.
- (35) Bergeron, D. E.; Castleman, A. W. Jr. *J. Chem. Phys.* **2002**, *117*, 3219.
- (36) Kronik, L.; Fromherz, R.; Ko, E.; Gantefor, G.; Chelikowsky, J. R. *Eur. Phys. J. D.* **2003**, *24*, 33.
- (37) Yasumatsu, H.; Kondow, T. *Rep. Prog. Phys.* **2003**, *66*, 1783.
- (38) Heath, J. R.; Liu, Y.; O'Brien, S. C.; Zhang, Q. L.; Curl, R. F.; Tittel, F. K.; Smalley, R. E. *J. Chem. Phys.* **1985**, *83*, 5520.
- (39) Creasy, W. R.; O'Keefe, A.; McDonald, J. R. *J. Phys. Chem.* **1987**, *91*, 2848.
- (40) Zhang, Q. L.; Liu, Y.; Curl, R. F.; Tittel, F. K.; Smalley, R. E. *J. Chem. Phys.* **1988**, *88*, 1670.
- (41) Jarrold, M. F.; Bower, J. E. *J. Phys. Chem.* **1988**, *92*, 5702.
- (42) Beck, S. M.; Andrews, J. M. *J. Chem. Phys.* **1989**, *91*, 4420.
- (43) Jarrold, M. F.; Honea, E. C. *J. Phys. Chem.* **1991**, *95*, 9181.
- (44) Fuke, K.; Tsukamoto, K.; Misaizu, F.; Sanekata, M. J. *J. Chem. Phys.* **1993**, *99*, 7807.
- (45) Ran, Q.; Schmude, R. W. Jr.; Miller, M.; Gingerich, K. A. *Chem. Phys. Lett.* **1994**, *230*, 337.
- (46) Li, S.; Van Zee, R. J.; Weltner, Jr. W.; Raghavachari, K. *Chem. Phys. Lett.* **1995**, *243*, 275.

- (47) Honea, E. C.; Ogura, A.; Peale, D. R.; Felix, C.; Murray, C. A.; Raghavachari, K.; Sprenger, W. O.; Jarrold, M. F.; Brown, W. L. *J. Chem. Phys.* **1999**, *110*, 12161.
- (48) Patrone, L.; Ozerov, I.; Sentis, M. L.; Marine, W. *J. Phys. IV*, **2001**, *11*, 121.
- (49) Bulgakov, A. V.; Ozerov, I.; Marine, W. *Applied Physics A*, **2004**, *79*, (4-6), 1591.
- (50) Bulgakov, A. V.; Ozerov, I.; Marine, W. *Thin Solid Films*, **2004**, *453-454*, 557.
- (51) Tomanek, D.; Schluter, M. A. *Phys. Rev. B*, **1987**, *36*, 1208.
- (52) Raghavachari, K. *Z. Phys. D*, **1989**, *12*, 61.
- (53) Raghavachari, K.; Rohlfing, C. M. *J. Chem. Phys.* **1991**, *94*, 3670.
- (54) Adamowicz, L. *Chem. Phys. Lett.* **1992**, *188*, 131.
- (55) Curtiss, L. A.; Deutsch, P. W.; Raghavachari, K. *J. Chem. Phys.* **1992**, *96*, 6868.
- (56) Binggeli, N.; Martins, J. L.; Chelikowsky, J. R. *Phys. Rev. Lett.* **1992**, *68*, 2956.
- (57) Binggeli, N.; Chelikowsky, J. R. *Phys. Rev. Lett.* **1995**, *75*, 493.
- (58) Wei, S.; Barnett, R. N.; Landman, U. *Phys. Rev. B*, **1997**, *55*, 7935.
- (59) Kishi, R.; Iwata, S.; Nakajima, A.; Kaya, K. *J. Chem. Phys.* **1997**, *107*, 3056.
- (60) Kishi, R.; Negishi, Y.; Kawamata, H.; Iwata, S.; Nakajima, A.; Kaya, K. *J. Chem. Phys.* **1998**, *108*, 8039.

- (61) Shvartsburg, A. A.; Liu, B.; Jarrold, M. F.; Ho, K. M. *J. Chem. Phys.* **2000**, *112*, 4517.
- (62) Zhao, C.; Balasubramanian, K. *J. Chem. Phys.* **2002**, *116*, 3690.
- (63) Li, B. X.; Cao, P. L.; Song, B.; Ye, Z. Z. *Phys. Lett. A*, **2003**, *307*, 318.
- (64) Ishii, S.; Ohno, K.; Kumar, V.; Kawazoe, Y. *Phys. Rev. B*, **2003**, *68*, 195412.
- (65) Weinert, C. M. *Surf. Sci.* **1985**, *156*, 641.
- (66) Raghavachari, K.; Logovinsky, V. *Phys. Rev. Lett.* **1985**, *55*, 2853.
- (67) Tomanek, D.; Schluter, M. A. *Phys. Rev. Lett.* **1986**, *56*, 1055.
- (68) Pacchioni, G.; Koutecky, J. *J. Chem. Phys.* **1986**, *84*, 3301.
- (69) Raghavachari, K. *J. Chem. Phys.* **1986**, *84*, 5672.
- (70) Feuston, B. P.; Kalia, R. K.; Vashishta, P. *Phys. Rev. B*, **1987**, *35*, 6222.
- (71) Andreoni, W.; Ballone, P. *Phys. Scr.* **1987**, *T19*, 289.
- (72) Raghavachari, K.; Rohlfing, C. M. *Chem. Phys. Lett.* **1988**, *143*, 428.
- (73) Raghavachari, K.; Rohlfing, C. M. *J. Chem. Phys.* **1988**, *89*, 2219.
- (74) Chelikowsky, J. R.; Phillips, J. C.; Kamal, M.; Strauss, M. *Phys. Rev. Lett.* **1989**, *62*, 292.
- (75) Tomanek, D.; Sun, C.; Sharma, N.; Wang, L. *Phys. Rev. B*, **1989**, *39*, 5361.
- (76) Chelikowsky, J. R.; Phillips, J. C. *Phys. Rev. B*, **1990**, *41*, 5735.
- (77) Wang, H. X.; Messmer, R. P. *Phys. Rev. B*, **1990**, *41*, 5306.
- (78) Rohlfing, C. M.; Raghavachari, K. *Chem. Phys. Lett.* **1990**, *167*, 559.
- (79) Andreoni, W.; Pastore, G. *Phys. Rev. B*, **1990**, *41*, 10243.

- (80) Sankey, O. F.; Niklewski, D. J.; Drabold, D. A.; Dow, J. D. *Phys. Rev. B*, **1990**, *41*, 12750.
- (81) Patterson, C. H.; Messmer, R. P. *Phys. Rev. B*, **1990**, *42*, 7530.
- (82) Chelikowsky, J. R.; Glassford, K. M.; Phillips, J. C. *Phys. Rev. B*, **1991**, *44*, 1538.
- (83) Salk, S. H. S.; Lutrus, C. K.; Hagen, D. E.; Oshiro, T.; Beck, S.; Loper, G. L. *Phys. Rev. B*, **1992**, *45*, 1458.
- (84) Fournier, R.; Sinnott, S. B.; DePristo, A. E. *J. Chem. Phys.* **1992**, *97*, 4149.
- (85) Niessen, W. v.; Zakrzewski, V. G. *J. Chem. Phys.* **1993**, *98*, 1271.
- (86) Lee, I. H.; Chang, K. J.; Lee, Y. H. *J. Phys.: Condens. Matter* **1994**, *6*, 741.
- (87) Mittelbach, v. T.; Fritsche, H. G.; Muller, H. *Zeit. fur Physik. Chem.* **1994**, *187*, 45.
- (88) Zhao, J.; Chen, X.; Sun, Q.; Liu, F.; Wang, G. *Phys. Lett. A*, **1995**, *198*, 243.
- (89) Govind, N.; Mozos, J. L.; Guo, H. *Phys. Rev. B* **1995**, *51*, 7101.
- (90) Ramakrishna, M. V.; Bahel, A. *J. Chem. Phys.* **1996**, *104*, 9833.
- (91) Jackson, K.; Pederson, M. R.; Porezag, D.; Hajnal, Z.; Frauenheim, T. *Phys. Rev. B* **1997**, *55*, 2549.
- (92) Ho, K. M.; Shvartsburg, A. A.; Pan, B.; Lu, Z. Y.; Wang, C. Z.; Wacker, J. G.; Fye, J. L.; Jarrold, M. F. *Nature* **1998**, *392*, 582.

- (93) Shvartsburg, A. A.; Jarrold, M. F.; Liu, B.; Lu, Z. Y.; Wang, C. Z.; Ho, K. M. *Phys. Rev. Lett.* **1998**, *81*, 4616.
- (94) Liu, B.; Lu, Z. Y.; Pan, B.; Wang, C. Z.; Ho, K. M. *J. Chem. Phys.* **1998**, *109*, 9401.
- (95) Qiu, M.; Jiang, M.; Zhao, Y. J.; Cao, P. L. *J. Chem. Phys.* **1999**, *110*, 10738.
- (96) Lu, Z. Y.; Wang, C. Z.; Ho, K. M. *Phys. Rev. B*, **2000**, *61*, 2329.
- (97) Iwamatsu, M. *J. Chem. Phys.* **2000**, *112*, 10976.
- (98) Li, B. X.; Cao, P. L. *J. Phys.: Condens. Matter*, **2000**, *12*, 8357.
- (99) Li, B. X.; Cao, P. L. *Phys. Rev. B* **2000**, *62*, 15788.
- (100) Panda, B. K.; Mukherjee, S.; Behera, S. N. *Phys. Rev. B*, **2001**, *63*, 045404.
- (101) Li, B. X.; Cao, P. L.; Ye, Z.; Zhang, R. Q.; Lee, S. T. *J. Phys.: Condens. Matter* **2002**, *14*, 1723.
- (102) Zhu, X.; Zeng, X. C. *J. Chem. Phys.* **2003**, *118*, 3558.
- (103) Maroulis, G.; Begue, D.; Pouchan, C. *J. Chem. Phys.* **2003**, *119*, 794.
- (104) Yoo, S.; Zeng, X. C. *J. Chem. Phys.* **2003**, *119*, 1442.
- (105) Tekin, A.; Hartke, B. *Phys. Chem. Chem. Phys.* **2004**, *6*, 503.
- (106) Pouchan, C.; Begue, D.; Zhang, D. Y. *J. Chem. Phys.* **2004**, *121*, 4628.
- (107) Nigam, S.; Majumder, C.; Kulshreshtha, S. K. *J. Chem. Phys.* **2004**, *121*, 7756.
- (108) Majumder, C.; Kulshreshtha, S. K. *Phys. Rev. B* **2004**, *69*, 115432.
- (109) Nair, N. N.; Bredow, T.; Jug, K. *J. Comput. Chem.* **2004**, *25*, 1255.

- (110) Wang, L. S. & Wu, H. Probing the electronic structure of transition metal clusters from molecular to bulk- like using photoelectron spectroscopy in *Advances in Metal and Semiconductor Clusters. IV. Cluster Materials*, M.A. Duncan, Ed. (JAI Press, Greenwich, CT, 1998), pp.299-343.
- (111) L. S. Wang, H. S. Cheng, J. Fan, *J. Chem. Phys.* **1995**, *102*, 9480.
- (112) Alexandrova, A. N.; Boldyrev, A. I.; Fu, Y.-J.; Wang, X.-B.; Wang, L.-S. *J. Chem. Phys.* **2004**, *121*, 5709.
- (113) Parr R. G.; Yang W. Density-functional Theory of Atoms and Molecules (Oxford Univ. Press, Oxford, 1989).
- (114) Becke A. D. *J. Chem. Phys.* **1993**, *98*, 5648.
- (115) Perdew J. P.; Chevary J. A.; Vosko S. H.; Jackson K. A.; Pederson M. R.; Singh D. J.; Fiolhais C. *Phys. Rev. B* **1992**, *46*, 6671.
- (116) McLean A. D.; Chandler G. S. *J. Chem. Phys.* **1980**, *72*, 5639.
- (117) Clark T.; Chandrasekhar J.; Spitznagel G. W.; Schleyer P. v. R. *J. Comput. Chem.* **1983**, *4*, 294.
- (118) Frisch M. J.; Pople J. A.; Binkley J. S. *J. Chem. Phys.* **1984**, *80*, 3265.
- (119) Cizek, J. *Adv. Chem. Phys.* **1969**, *14*, 35.
- (120) Knowles, P. J.; Hampel, C.; Werner, H.-J. *J. Chem. Phys.* **1993**, *99*, 5219.
- (121) Raghavachari, K.; Trucks, G. W.; Pople, J. A.; Head-Gordon, M. *Chem. Phys. Lett.* **1989**, *157*, 479.
- (122) Head-Gordon, M.; Pople, J. A.; Frisch, M. J. *Chem. Phys. Lett.* **1988**, *153*, 503.

- (123) Bernardi, F.; Bottini, A.; McDougall, J. J. W.; Robb, M. A.; Schlegel, H. B. *Faraday Symp. Chem. Soc.* **1979**, *19*, 137.
- (124) Frisch, M. J.; Ragazos, I. N.; Robb, M. A.; Schlegel, H. B. *Chem. Phys. Lett.* **1992**, *189*, 524.
- (125) Cederbaum L. S. *J. Phys. B* **1975**, *8*, 290.
- (126) von Niessen W.; Shirmer J.; Cederbaum L. S. *Comput. Phys. Rep.* **1984**, *1*, 57.
- (127) Zakrzewski V. G.; von Niessen W. *J. Comput. Chem.* **1993**, *14*, 13.
- (128) (a) Ortiz, J.V.; *Int. J. Quant. Chem., Quant. Chem. Symp.* **1989**, *23*, 321;  
(b) Lin, J.S., Ortiz, J.V., *Chem. Phys. Lett.* **1990**, *171*, 197.
- (129) Zakrzewski, V.G., Ortiz, J.V., Nichols, J.A., Heryadi, D., Yeager, D.L., Golab, J.T., *Int. J. Quant. Chem., Quant.* **1996**, *60*, 29.
- (130) Bauernshmitt, R.; Alrichs, R. *Chem. Phys. Lett.* **1996**, *256*, 454.
- (131) Casida, M.E.; Jamorski, C.; Casida, K.C.; Salahub, D.R. *J. Chem. Phys.* **1998**, *108*, 4439.
- (132) Becke, A. D.; Edgecombe, K. E. *J. Chem. Phys.* **1990**, *92*, 5397.
- (133) Savin, A.; Silvi, B.; Colonna, F. *Can. J. Chem.* **1996**, *74*, 1088.
- (134) Savin, A.; Nesper, R.; Wengert, S.; Fassler, T. F. *Angew. Chem. Int. Ed. Engl.* **1997**, *36*, 1808.
- (135) Frisch, M. J.; et. al. *Gaussian 98*, revision A.7; Gaussian, Inc., Pittsburgh PA, 1998.
- (136) Frish, M.J.; et. al. *Gaussian 03*, version B. 02; Gaussian, Inc., Pittsburgh PA, 2003.

- (137) Noury, S.; Krokidis, X.; Fuster, F.; Silvi, B. TopMod Package, Universite Pierre et Marie Curie, **1997**; *Comp. Chem.* **1999**, *23*, 597.
- (138) MOLEKEL, Version 4.3. Stefan Portmann, CSCS/ETHZ (2002).
- (139) MOLDEN3.4. Schaftenaar, G. MOLDEN3.4, CAOS/CAMM Center, The Netherlands (1998).
- (140) Boldyrev, A. I.; Wang, L.-S. *J. Phys. Chem. A* **2001**, *105*, 10759.
- (141) King, B. R.; Heine, T.; Corminboeuf, C.; Schleyer, P. v. R. *J. Am. Chem. Soc.* **2004**, *126*, 430.
- (142) Wade, K. *Chem. Commun.* **1971**, 792.
- (143) Wade, K. *Adv. Inorg. Chem. Radiochem.* **1976**, *18*, 1.
- (144) Hirsch, A.; Chen, Z.; Jiao, H. *Angew. Chem. Int. Ed.* **2001**, *40*, 2834.
- (145) King, R. B.; Rouvray, D. H. *J. Am. Chem. Soc.* **1977**, *99*, 7834.
- (146) Aihara, J. J. *J. Am. Chem. Soc.* **1978**, *100*, 3339.



## CHAPTER 13

ON THE STRUCTURE AND CHEMICAL BONDING OF  $\text{Si}_6^{2-}$   
AND  $\text{Si}_6^{2-}$  IN  $\text{NaSi}_6^-$  UPON  $\text{Na}^+$  COORDINATION<sup>1</sup>**Abstract**

Photoelectron spectroscopy was combined with ab initio calculations to elucidate the structure and bonding in  $\text{Si}_6^{2-}$  and  $\text{NaSi}_6^-$ . Well-resolved electronic transitions were observed in the photoelectron spectra of  $\text{Si}_6^-$  and  $\text{NaSi}_6^-$  at three photon energies (355, 266, and 193 nm). The spectra of  $\text{NaSi}_6^-$  were observed to be similar to those of  $\text{Si}_6^-$  except that the electron binding energies of the former are lower, suggesting that the  $\text{Si}_6$  motif in  $\text{NaSi}_6^-$  is structurally and electronically similar to that of  $\text{Si}_6^-$ . The electron affinity of  $\text{Si}_6$  and  $\text{NaSi}_6$  were measured fairly accurately to be  $2.23 \pm 0.03$  eV and  $1.80 \pm 0.05$  eV, respectively. Global minimum structure searches for  $\text{Si}_6^{2-}$  and  $\text{NaSi}_6^-$  were performed using Gradient Embedded Genetic Algorithm followed by B3LYP, MP2 and CCSD(T) calculations. Vertical electron detachment energies (VDEs) were calculated for the lowest  $\text{Si}_6^-$  and  $\text{NaSi}_6^-$  structures at the CCSD(T)/6-311+G(2df), ROVGF/6-311+G(2df), UOVGF/6-311+G(2d), TD B3LYP/6-311+G(2df) levels of theory. Experimental VDEs were used to verify the global minimum structure for  $\text{NaSi}_6^-$ . Though the octahedral  $\text{Si}_6^{2-}$ , analogous to the closo-form of borane  $\text{B}_6\text{H}_6^{2-}$ , is the most stable form for the bare hexa-silicon dianion, it is not the kernel for the  $\text{NaSi}_6^-$  global minimum. The most stable isomer of  $\text{NaSi}_6^-$  is based on a  $\text{Si}_6^{2-}$  motif, which is distorted

---

<sup>1</sup> Coauthored by Dmitry Yu. Zubarev, Anastassia N. Alexandrova, Alexander I. Boldyrev, Li-Feng Cui, Xi Li and Lai-Sheng Wang. Reproduced with permission from *J. Chem. Phys.* **2006**, 124, 124305. Copyright 2006, American Institute of Physics.

into  $C_{2v}$  symmetry similar to the ground state structure of  $Si_6^-$ . The octahedral  $Si_6^{2-}$  coordinated by a  $Na^+$  is a low-lying isomer and was also observed experimentally. The chemical bonding in  $Si_6^{2-}$  and  $NaSi_6^-$  was understood using NBO, molecular orbital, and ELF analysis.

### 13-1. Introduction

Despite significant research efforts of many research groups, there is still not a consistent theory of chemical bonding to describe silicon clusters, which are important both in chemistry as potential material building blocks and in nanoscience relevant to device design in the future. Doubly charged  $Si_x^{2-}$  clusters offer a unique opportunity to use the isolobal analogy between an HB unit and a Si atom to allow the application of the chemical bonding models developed for deltahedral boranes  $(BH)_x^{2-}$ .<sup>1-3</sup> The isolobal analogy between HB and Si would suggest a series of stable deltahedral  $Si_x^{2-}$  clusters analogous to the deltahedral  $B_xH_x^{2-}$ . However, this straightforward approach does not appear to work, because even though  $Si_5^{2-}$  is stable enough to be obtained and characterized in the solid state,<sup>4</sup>  $B_5H_5^{2-}$  has not been synthesized.<sup>1-3</sup> On the other hand,  $Si_6^{2-}$  has not been synthesized yet, but  $B_6H_6^{2-}$  is well known for its stability.<sup>1-3</sup>  $B_{12}H_{12}^{2-}$ , the most famous borane, is icosahedral in its most stable form, but the corresponding  $Si_{12}^{2-}$  cage is not the global minimum, albeit it is a higher-lying isomer. According to our preliminary results, the global minimum of  $Si_{12}^{2-}$  has a lower symmetry structure. Thus we need to develop a chemical bonding model capable of explaining why valence isoelectronic systems have different structures. Such chemical models will be the first

step towards a comprehensive chemical bonding model for understanding the structure of silicon clusters.

The  $\text{Si}_6^{2-}$  cluster is the first system, which can be expected to have a highly symmetric octahedral structure, similar to the closo-borane  $\text{B}_6\text{H}_6^{2-}$ . However, a previous attempt to characterize the aromaticity of the octahedral  $\text{Si}_6^{2-}$  led to the conclusion that it is antiaromatic<sup>5</sup> and thus totally different from the corresponding aromatic  $\text{B}_6\text{H}_6^{2-}$  closo-borane. The difference was explained to be due to the mixing of the terminal hydrogen orbitals with the symmetry adapted skeletal MOs of  $\text{B}_6\text{H}_6^{2-}$ , which lowers their energies relative to the corresponding lone pair-dominated  $\text{Si}_6^{2-}$  MOs, where such mixing is not possible.<sup>5</sup>

The hexa-silicon cluster (neutral or with a negative charge) has been studied in numerous works with different theoretical methods.<sup>6-16</sup> It has also been extensively studied experimentally by mass-spectrometry,<sup>17-19</sup> IR and Raman spectroscopy,<sup>20-21</sup> and photoelectron spectroscopy.<sup>22-26</sup> The vertical detachment energies of  $\text{Si}_6^-$  have also been computed.<sup>27,28</sup> Of particular interest to the present work was the report by Kishi et al.<sup>23</sup> about the photoelectron spectrum of  $\text{NaSi}_6^-$  at 355 nm, which contained two broad spectral bands approximately at 2.1 and 3.0 eV. Theoretical analysis of the relative stability of several  $\text{Si}_6^{2-}$  and  $\text{NaSi}_6^-$  isomers at MP2/6-31G\* and MP4(SDTQ)/6-31G\* levels of theory was also carried out by the same authors, who concluded that the most stable structure of  $\text{NaSi}_6^-$  is based on a  $\text{C}_{2v}$   $\text{Si}_6^{2-}$  fragment, rather than the  $\text{O}_h$  motif. However, the experimentally determined VDE ( $2.10 \pm 0.04$  eV) and ADE ( $1.90 \pm 0.06$  eV) for  $\text{NaSi}_6^-$  differ significantly from the calculated VDE (1.518 eV) and ADE (1.446 eV) at MP4/6-31G\*. Li and co-workers<sup>29</sup> reported that according to their calculations at

the B3PW91/6-311G\* and MP2(full)/6-311+G\* levels of theory,  $\text{LiSi}_6^-$ ,  $\text{NaSi}_6^-$  and  $\text{KSi}_6^-$  clusters have a  $C_{3v}$  ( $^1A_1$ ) structure for all three species with a cation coordinated to one face of an octahedral  $\text{Si}_6^{2-}$ . Thus, the global minimum structure of the  $\text{NaSi}_6^-$  cluster is still not known.

In the current paper, we present a systematic study of  $\text{Si}_6^{2-}$  and  $\text{NaSi}_6^-$  both experimentally and theoretically focusing on elucidating their structures and chemical bonding. Well-resolved photoelectron spectra were obtained for  $\text{NaSi}_6^-$  at three photon energies (355, 266, 193 nm), which allow quantitative comparison with the accompanying ab initio calculations. The ground state structure of  $\text{NaSi}_6^-$  was established on the basis of good agreement between the photoelectron spectra and theoretical VDEs, calculated at several levels of theory: CCSD(T)/6-311+G(2df), ROVGF/6-311+G(2df), TD-B3LYP/6-311+G(2df), all at the B3LYP/6-311+G\* geometry. We further investigated the chemical bonding in the most stable isomer of  $\text{NaSi}_6^-$  and its silicon kernel  $\text{Si}_6^{2-}$ . Results of MO, NBO, and ELF analyses were compared with those for the octahedral  $\text{Si}_6^{2-}$  and  $\text{B}_6\text{H}_6^{2-}$  species. We also included photoelectron spectroscopic results on  $\text{Si}_6^-$  primarily to test theoretical methods used for  $\text{NaSi}_6^-$ .

### 13-2. Experimental Methods

Details of the photoelectron spectroscopy (PES) apparatus have been described elsewhere.<sup>30,31</sup> The silicon cluster anions and Na-Si mixed cluster anions were produced by laser vaporization of a pure Si and a Na/Si mixed target, respectively, in the presence of a helium carrier gas and analyzed by time-of-flight mass spectrometry. The  $\text{Si}_6^-$  and

NaSi<sub>6</sub><sup>-</sup> clusters of interests were mass-selected and decelerated before being photodetached by a pulsed laser beam, 355 nm (3.496 eV) and 266 nm (4.661 eV) from a Nd:YAG laser or 193 nm (6.424 eV) from an ArF excimer laser. Photoelectrons were collected at nearly 100% efficiency by a magnetic bottle and analyzed in a 3.5 m long electron flight tube. The PES spectra were calibrated using the known spectra of Au<sup>-</sup>, Pt<sup>-</sup>, or Cu<sup>-</sup>, and the electron energy resolution was  $\Delta E_k/E_k \approx 2.5\%$ , that is, approximately 25 meV for 1 eV electrons.

### 13-3. Theoretical Methods

The search for the global minimum on the potential energy surface of Si<sub>6</sub><sup>2-</sup> was started with the gradient embedded genetic algorithm (GEGA) program, developed by Alexandrova.<sup>32,33</sup> Semiempirical method PM3 (Refs. 34 and 35) was used for energy, gradient, and force computations, since it provides reasonable quality at low computational costs, which will be important for future studies of large silicon clusters. Our GEGA search produced several low-lying isomers, which were reoptimized at the hybrid B3LYP method<sup>36-38</sup> using the 6-311+G\* polarized split-valence basis set,<sup>39-41</sup> at the second order Moller-Plessett (MP2) method,<sup>42-46</sup> and at the coupled-cluster with single, double, and noniterative triple excitations [CCSD(T)] method<sup>47-51</sup> using the 6-311+G\* basis set. The total energies of the lowest structures were also estimated at the CCSD(T) level of theory using the extended 6-311+G(2df) basis set. Several levels of theory were used to obtain theoretical VDEs: R(U)CCSD(T)/6-311+G(2df), the equation of motion (EOM)-CCSD(T)/6-311+G(2df),<sup>52</sup> the restricted and unrestricted outer valence Green function [ROVGF/6-311+G(2df) and UOVGF/6-311+G(2d)] methods<sup>53-57</sup> (all at the

B3LYP/6-311+G\* or CCSD(T)/6-311+G\* geometries, where available), and the time-dependent (TD) density functional theory<sup>58,59</sup> B3LYP/6-311+G(2df) (at the B3LYP/6-311+G\* geometries). In the last approach the VDEs were calculated as a sum of the lowest transitions from the ground electronic state of the anion to the lowest electronic state of the neutral species (at the B3LYP level of theory) and the vertical excitation energies in the neutral species (at the TDB3LYP level of theory) at the anion geometry. At the CCSD(T) and ROVGF levels of theory the electron correlation was treated with frozen core electrons. Chemical bonding was investigated by means of NBO,<sup>60</sup> ELF,<sup>61-63</sup> and MO analyses. GAUSSIAN 98,<sup>64</sup> GAUSSIAN 03,<sup>65</sup> and MOLPRO 2000.1<sup>66</sup> *ab initio* software packages were used throughout this project. ELF analysis was carried out using the TOPMOD package.<sup>67</sup> MOLEKEL<sup>68</sup> and MOLDEN 3.4<sup>69</sup> programs were chosen for the visualization of the ELFs and molecular orbitals, respectively.

## 13-4. Experimental Results

### 13-4.1. Photoelectron Spectroscopy of $\text{Si}_6^-$

Figure 13-1 displays the photoelectron spectra of  $\text{Si}_6^-$  at three photon energies (355, 266, and 193 nm). Five distinct and intense spectral bands (X, A, B, C, D) were observed at 193 nm (Fig. 13-1c) and their VDEs measured from the peak maxima are given in Table 13-1. At 355 nm, the X band was better resolved with a well-defined onset, which yielded an ADE of  $2.23 \pm 0.03$  eV and VDE of  $2.35 \pm 0.05$  eV. Since no vibrational structures were resolved, the ADE which also represents the electron affinity (EA) of neutral  $\text{Si}_6$ , was measured by drawing a straight line at the leading edge of the X band and then adding the spectral resolution to the intersection with the binding energy

axis. The X band was quite broad, suggesting significant geometry changes between the ground state of  $\text{Si}_6^-$  and the corresponding neutral state. Weak and broad signals were observed in between bands X and A, in particular, the feature labeled “IS” was shown as a shoulder on the A band. These weak features could be either due to isomers or impurities. Since our mass resolution was high enough to resolve the isotopic pattern of  $\text{Si}_6^-$ , we could rule out the possibility of impurity contamination. Thus, these features were most likely due to another structural isomer, consistent with previous theoretical calculations.<sup>26,27</sup> The X-A band separation defines a HOMO-LUMO gap for the neutral  $\text{Si}_6$  as 1.05 eV. All the higher energy bands were all rather broad, due to either large geometry changes upon photodetachment or overlapping electronic transitions.

The photoelectron spectra of  $\text{Si}_6^-$  have been reported in a number of previous studies.<sup>22-26</sup> The current study presents a more systematic data set at different photon energies which is in general slightly better than or consistent with the previous measurements. The best resolved spectrum for  $\text{Si}_6^-$  was by Xu *et al.* at 355 nm.<sup>24</sup> Our obtained ADE (2.23 eV) and VDE (2.35 eV) are in good agreement with their corresponding values at 2.22 and 2.36 eV, respectively. However, the shoulder labeled as “IS” in Figure 13-1 was resolved as a vibrational progression by Xu *et al.*, who assigned it as the transition to the first excited state of  $\text{Si}_6$ . As discussed below, this weak feature is most likely due to the  $\text{D}_{4h}$  isomer of  $\text{Si}_6^-$  as shown via the molecular dynamics simulation by Binggeli and Chelikowsky.<sup>27</sup>

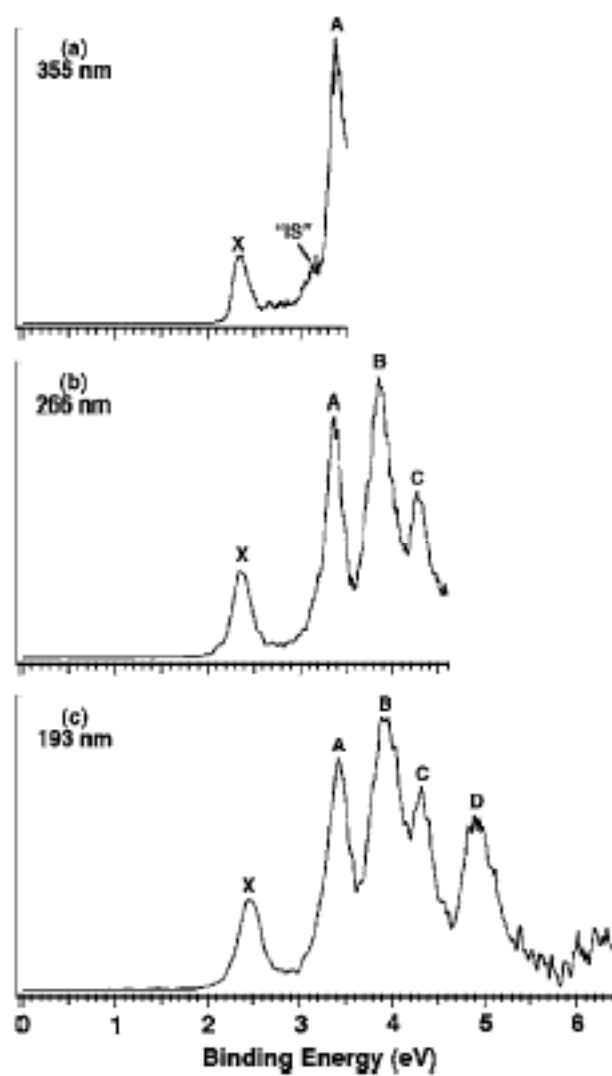


Figure 13-1. Photoelectron spectra of  $\text{Si}_6^-$  at (a) 355nm (3.496 eV), (b) 266 nm (4.661 eV), and (c) 193 nm (6.424 eV).



Table 13-1. Experimental and theoretical Vertical Detachment Energies for Si<sub>6</sub><sup>-</sup>. All energies are in eV.

Final Configuration		Exp. VDE <sup>a</sup>	TD B3LYP/6-311+G (2df)	UOVGF/6-311+G(2d)	EOM/ 6-311+G (2df)	CCSD(T)/ 6-311+G (2df)
Si <sub>6</sub> <sup>-</sup> C <sub>2v</sub> ( <sup>2</sup> B <sub>2</sub> )						
<sup>1</sup> A <sub>1</sub> (4a <sub>1</sub> <sup>2</sup> 1a <sub>2</sub> <sup>2</sup> 5a <sub>1</sub> <sup>2</sup> 3b <sub>2</sub> <sup>2</sup> 2b <sub>1</sub> <sup>2</sup> 6a <sub>1</sub> <sup>2</sup> 4b <sub>2</sub> <sup>0</sup> )	X	2.35±0.03	2.38	2.17 (0.84) <sup>b</sup>	2.31	2.29
<sup>3</sup> B <sub>2</sub> (4a <sub>1</sub> <sup>2</sup> 1a <sub>2</sub> <sup>2</sup> 5a <sub>1</sub> <sup>2</sup> 3b <sub>2</sub> <sup>2</sup> 2b <sub>1</sub> <sup>2</sup> 6a <sub>1</sub> <sup>1</sup> 4b <sub>2</sub> <sup>1</sup> )	A	3.38±0.03	3.23	3.15 (0.84) <sup>b</sup>	<sup>d</sup>	3.30
<sup>1</sup> B <sub>2</sub> (4a <sub>1</sub> <sup>2</sup> 1a <sub>2</sub> <sup>2</sup> 5a <sub>1</sub> <sup>2</sup> 3b <sub>2</sub> <sup>2</sup> 2b <sub>1</sub> <sup>2</sup> 6a <sub>1</sub> <sup>1</sup> 4b <sub>2</sub> <sup>1</sup> )	B	3.85±0.03	3.65	<sup>c</sup>	3.78	<sup>e</sup>
<sup>3</sup> A <sub>1</sub> (4a <sub>1</sub> <sup>2</sup> 1a <sub>2</sub> <sup>2</sup> 5a <sub>1</sub> <sup>2</sup> 3b <sub>2</sub> <sup>2</sup> 12b <sub>1</sub> <sup>2</sup> 6a <sub>1</sub> <sup>2</sup> 4b <sub>2</sub> <sup>1</sup> )			3.75	3.61 (0.84) <sup>b</sup>	<sup>d</sup>	3.78
<sup>3</sup> A <sub>2</sub> (4a <sub>1</sub> <sup>2</sup> 1a <sub>2</sub> <sup>2</sup> 5a <sub>1</sub> <sup>2</sup> 3b <sub>2</sub> <sup>2</sup> 2b <sub>1</sub> <sup>1</sup> 6a <sub>1</sub> <sup>2</sup> 4b <sub>2</sub> <sup>1</sup> )			3.80	3.67 (0.83) <sup>b</sup>	<sup>d</sup>	3.94
<sup>1</sup> A <sub>2</sub> (4a <sub>1</sub> <sup>2</sup> 1a <sub>2</sub> <sup>2</sup> 5a <sub>1</sub> <sup>2</sup> 3b <sub>2</sub> <sup>2</sup> 2b <sub>1</sub> <sup>1</sup> 6a <sub>1</sub> <sup>2</sup> 4b <sub>2</sub> <sup>1</sup> )			3.96	<sup>c</sup>	4.14	<sup>e</sup>
<sup>3</sup> B <sub>2</sub> (4a <sub>1</sub> <sup>2</sup> 1a <sub>2</sub> <sup>2</sup> 5a <sub>1</sub> <sup>1</sup> 3b <sub>2</sub> <sup>2</sup> 2b <sub>1</sub> <sup>2</sup> 6a <sub>1</sub> <sup>2</sup> 4b <sub>2</sub> <sup>1</sup> )			4.05	3.93 (0.83) <sup>b</sup>	<sup>d</sup>	<sup>e</sup>
<sup>1</sup> B <sub>2</sub> (4a <sub>1</sub> <sup>2</sup> 1a <sub>2</sub> <sup>2</sup> 5a <sub>1</sub> <sup>1</sup> 3b <sub>2</sub> <sup>2</sup> 2b <sub>1</sub> <sup>2</sup> 6a <sub>1</sub> <sup>2</sup> 4b <sub>2</sub> <sup>1</sup> )			C	4.26±0.03	4.21	<sup>c</sup>
<sup>1</sup> A <sub>1</sub> (4a <sub>1</sub> <sup>2</sup> 1a <sub>2</sub> <sup>2</sup> 5a <sub>1</sub> <sup>2</sup> 3b <sub>2</sub> <sup>1</sup> 2b <sub>1</sub> <sup>2</sup> 6a <sub>1</sub> <sup>2</sup> 4b <sub>2</sub> <sup>1</sup> )	4.23	<sup>c</sup>			4.42	<sup>e</sup>
<sup>3</sup> B <sub>1</sub> (4a <sub>1</sub> <sup>2</sup> 1a <sub>2</sub> <sup>1</sup> 5a <sub>1</sub> <sup>2</sup> 3b <sub>2</sub> <sup>2</sup> 2b <sub>1</sub> <sup>2</sup> 6a <sub>1</sub> <sup>2</sup> 4b <sub>2</sub> <sup>1</sup> )	D	4.89±0.03	4.69	4.61 (0.83) <sup>b</sup>	<sup>d</sup>	4.86
<sup>3</sup> B <sub>2</sub> (4a <sub>1</sub> <sup>1</sup> 1a <sub>2</sub> <sup>2</sup> 5a <sub>1</sub> <sup>2</sup> 3b <sub>2</sub> <sup>2</sup> 2b <sub>1</sub> <sup>2</sup> 6a <sub>1</sub> <sup>2</sup> 4b <sub>2</sub> <sup>1</sup> )			4.69	4.59 (0.83) <sup>b</sup>	<sup>d</sup>	<sup>e</sup>
<sup>1</sup> B <sub>1</sub> (4a <sub>1</sub> <sup>2</sup> 1a <sub>2</sub> <sup>1</sup> 5a <sub>1</sub> <sup>2</sup> 3b <sub>2</sub> <sup>2</sup> 2b <sub>1</sub> <sup>2</sup> 6a <sub>1</sub> <sup>2</sup> 4b <sub>2</sub> <sup>1</sup> )			4.92	<sup>c</sup>	5.11	<sup>e</sup>
<sup>1</sup> B <sub>2</sub> (4a <sub>1</sub> <sup>1</sup> 1a <sub>2</sub> <sup>2</sup> 5a <sub>1</sub> <sup>2</sup> 3b <sub>2</sub> <sup>2</sup> 2b <sub>1</sub> <sup>2</sup> 6a <sub>1</sub> <sup>2</sup> 4b <sub>2</sub> <sup>1</sup> )			5.32	<sup>c</sup>	5.49	<sup>e</sup>
Si <sub>6</sub> <sup>-</sup> D <sub>4h</sub> ( <sup>2</sup> A <sub>2u</sub> )						
<sup>1</sup> A <sub>1g</sub> (3a <sub>1g</sub> <sup>2</sup> 1e <sub>g</sub> <sup>4</sup> 1b <sub>2g</sub> <sup>2</sup> 2e <sub>u</sub> <sup>4</sup> 2a <sub>2u</sub> <sup>0</sup> )		~2.7 <sup>g</sup>	2.74	2.61 (0.92) <sup>b</sup>	<sup>f</sup>	2.63
<sup>3</sup> E <sub>g</sub> (3a <sub>1g</sub> <sup>2</sup> 1e <sub>g</sub> <sup>4</sup> 1b <sub>2g</sub> <sup>2</sup> 2e <sub>u</sub> <sup>3</sup> 2a <sub>2u</sub> <sup>1</sup> )		~3.1 <sup>g</sup>	3.04	3.05 (0.91) <sup>b</sup>	<sup>f</sup>	3.17
<sup>1</sup> E <sub>g</sub> (3a <sub>1g</sub> <sup>2</sup> 1e <sub>g</sub> <sup>4</sup> 1b <sub>2g</sub> <sup>2</sup> 2e <sub>u</sub> <sup>3</sup> 2a <sub>2u</sub> <sup>1</sup> )			3.08	<sup>c</sup>	<sup>f</sup>	<sup>e</sup>
<sup>3</sup> B <sub>1u</sub> (3a <sub>1g</sub> <sup>2</sup> 1e <sub>g</sub> <sup>4</sup> 1b <sub>2g</sub> <sup>1</sup> 2e <sub>u</sub> <sup>4</sup> 2a <sub>2u</sub> <sup>1</sup> )			4.49	4.53 (0.91) <sup>b</sup>	<sup>f</sup>	4.77
<sup>3</sup> A <sub>2u</sub> (3a <sub>1g</sub> <sup>1</sup> 1e <sub>g</sub> <sup>4</sup> 1b <sub>2g</sub> <sup>2</sup> 2e <sub>u</sub> <sup>4</sup> 2a <sub>2u</sub> <sup>1</sup> )			4.60	4.63 (0.90) <sup>b</sup>	<sup>f</sup>	4.91
<sup>1</sup> B <sub>1u</sub> (3a <sub>1g</sub> <sup>2</sup> 1e <sub>g</sub> <sup>4</sup> 1b <sub>2g</sub> <sup>1</sup> 2e <sub>u</sub> <sup>4</sup> 2a <sub>2u</sub> <sup>1</sup> )			4.61	<sup>c</sup>	<sup>f</sup>	<sup>e</sup>
<sup>3</sup> E <sub>u</sub> (3a <sub>1g</sub> <sup>2</sup> 1e <sub>g</sub> <sup>3</sup> 1b <sub>2g</sub> <sup>2</sup> 2e <sub>u</sub> <sup>4</sup> 2a <sub>2u</sub> <sup>1</sup> )			4.68	4.71 (0.91) <sup>b</sup>	<sup>f</sup>	4.92
<sup>1</sup> E <sub>u</sub> (3a <sub>1g</sub> <sup>2</sup> 1e <sub>g</sub> <sup>3</sup> 1b <sub>2g</sub> <sup>2</sup> 2e <sub>u</sub> <sup>4</sup> 2a <sub>2u</sub> <sup>1</sup> )			5.09	<sup>c</sup>	<sup>f</sup>	<sup>e</sup>
<sup>1</sup> A <sub>2u</sub> (3a <sub>1g</sub> <sup>1</sup> 1e <sub>g</sub> <sup>4</sup> 1b <sub>2g</sub> <sup>2</sup> 2e <sub>u</sub> <sup>4</sup> 2a <sub>2u</sub> <sup>1</sup> )			5.58	<sup>c</sup>	<sup>f</sup>	<sup>e</sup>

<sup>a</sup> The adiabatic detachment energy or the electron affinity of Si<sub>6</sub> is measured to be 2.23 ± 0.03 eV.

<sup>b</sup> The numbers in the parentheses indicate the pole strength, which characterizes the validity of the one-electron detachment picture.

<sup>c</sup> Singlet excited states have two-configurational character and therefore are not reported.

<sup>d</sup> EOM-CCSD(T) calculations for triplet excited states cannot be performed within our version of Molpro program.

<sup>e</sup> These states cannot be calculated using CCSD(T) method implemented in Gaussian.

<sup>f</sup> These computations were not performed.

<sup>g</sup> Broad features in Fig. 1a between bands X and A.

### 13-4.2. Photoelectron Spectroscopy of $\text{NaSi}_6^-$

The photoelectron spectra of  $\text{NaSi}_6^-$  are shown in Figure 13-2 at three photon energies (355, 266, and 193 nm). The electron binding energies of  $\text{NaSi}_6^-$  are lower than those of  $\text{Si}_6^-$ , but the overall spectral patterns for the two species are quite similar. Again five distinct and intense spectral bands (X, A, B, C, D) were observed for  $\text{NaSi}_6^-$ , which were slightly better spaced than those of  $\text{Si}_6^-$ . The VDEs of these bands are given in Table 13-2. There appeared two weak features, labeled as x and a, between bands X and A in the spectra of  $\text{NaSi}_6^-$ , similar to the weak features observed between the X and A bands in the spectra of  $\text{Si}_6^-$ . These two weak features are assigned to be due to a low-lying isomer (Table 13-2), analogous to  $\text{Si}_6^-$  (*vide infra*). The EA of  $\text{NaSi}_6^-$  was measured from the onset of the X band of the 355 nm spectrum to be  $1.80 \pm 0.05$  eV, which is 0.43 eV smaller than that of  $\text{Si}_6^-$ . The X-A band separation of 1.04 eV for  $\text{NaSi}_6^-$  is identical to that for  $\text{Si}_6^-$ . In fact, all the five main spectral features of  $\text{NaSi}_6^-$  line up well with those of  $\text{Si}_6^-$  with a shift of about 0.4 eV, suggesting that the geometrical and electronic structure of the  $\text{Si}_6$  motif in  $\text{NaSi}_6^-$  is similar to that in  $\text{Si}_6^-$ .

A very broad and diffuse photoelectron spectrum of  $\text{NaSi}_6^-$  at 355 nm was reported previously by Kishi *et al.*<sup>23</sup> The current spectra were considerably better resolved, making it possible to quantitatively compare with theoretical calculations (*vide infra*). As shown previously, the combination of PES with *ab initio* calculations is a powerful tool for elucidating the electronic structure and chemical bonding of novel clusters.<sup>70,71</sup> In the following, different levels of theories are employed to assist the interpretation of the observed photoelectron spectra and to elucidate the detailed structures and the underlying chemical bonding of  $\text{Si}_6^-$  and  $\text{NaSi}_6^-$  ( $\text{Si}_6^{2-}$ ).

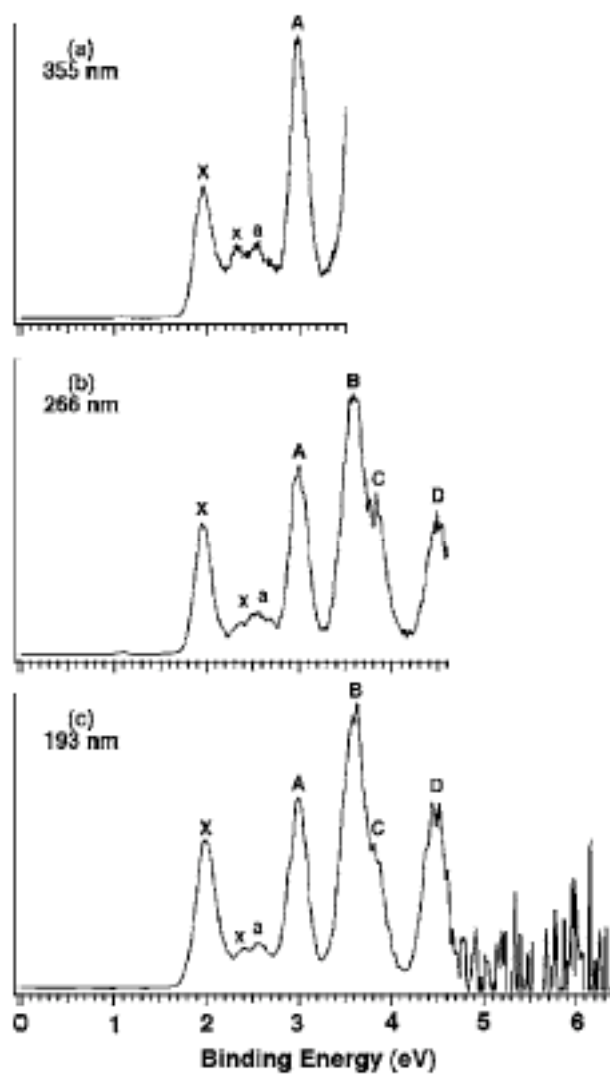


Figure 13-2. Photoelectron spectra of  $\text{NaSi}_6^-$  at (a) 355nm (3.496 eV), (b) 266 nm (4.661 eV), and (c) 193 nm (6.424 eV).

## 13-5. Theoretical Results

### 13-5.1. $\text{Si}_6^-$

The two lowest energy  $\text{C}_{2v}$  ( $^2\text{B}_2$ ) I and  $\text{D}_{4h}$  ( $^2\text{A}_{2u}$ ) II structures of  $\text{Si}_6^-$  (Figure 13-3 and Table 13-3) have been identified in the literature.<sup>6-16</sup> According to our calculations the  $\text{C}_{2v}$  ( $^2\text{B}_2$ ) I and the  $\text{D}_{4h}$  ( $^2\text{A}_{2u}$ ) II structures are almost degenerate. At our highest level of theory (CCSD(T)/6-311+G(2df)//CCSD(T)/6-311+G\*) the  $\text{D}_{4h}$  ( $^2\text{A}_{2u}$ ) II structure is slightly more stable (by 0.9 kcal/mol) than the  $\text{C}_{2v}$  ( $^2\text{B}_2$ ) I structure. Thus, we used both of these structures for our theoretical calculations of VDEs to help interpret the main PES spectral features of  $\text{Si}_6^-$  (Table 13-1).

### 13-5.2. $\text{Si}_6^{2-}$

For  $\text{Si}_6^{2-}$  we performed the GEGA search at the semiempirical PM3 level of theory, followed by geometry reoptimization and frequency calculations at higher levels of theory. Two isomers with close energies were obtained:  $\text{O}_h$  ( $^1\text{A}_{1g}$ ) III and  $\text{C}_{2v}$  ( $^1\text{A}_1$ ) IV (Table 13-4) as shown in Figure 13-3. The octahedral structure consistently remains the global minimum at B3LYP, MP2, and CCSD(T) levels of the theory (all at 6-311+G\* basis set). At our highest level of theory (CCSD(T)/6-311+G(2df)//CCSD(T)/6-311+G\*) the  $\text{O}_h$  ( $^1\text{A}_{1g}$ ) isomer is 12.2 kcal/mol more stable than the  $\text{C}_{2v}$  ( $^1\text{A}_1$ ) isomer. The  $\text{C}_{2v}$  ( $^1\text{A}_1$ ) isomer IV can be considered as a result of a distortion of the  $\text{O}_h$  ( $^1\text{A}_{1g}$ ) isomer III, leading to the cleavage of an “equatorial” Si-Si bond and the formation of a Si-Si bond between the two axial atoms. Alternation of other bond lengths occurs as well, the most noticeable is the increase of the distance between the axial ( $\text{Si}_{1,2}$ ) and bridging-equatorial

Table 13-2. Experimental and theoretical Vertical Detachment Energies for  $\text{NaSi}_6^-$ . All energies are in eV.

Feature	VDE (Exp.)	$\text{NaSi}_6^-$ ( $C_{2v}, {}^1A_1$ ) MO	ROVGF/6-311+G (2df) <sup>b</sup>	TD-B3LYP/6- 311+G (2df) <sup>b</sup>	CCSD(T)/6- 311+G(2df) <sup>b</sup>
X <sup>a</sup>	1.96 ±0.05	4b <sub>2</sub>	1.96 (0.88) <sup>c</sup>	1.88	1.92
A	3.00 ±0.05	6a <sub>1</sub>	2.78 (0.89) <sup>c</sup>	2.90	2.94
B	3.60 ±0.05	2b <sub>1</sub>	3.46 (0.88) <sup>c</sup>	3.32	3.45 <sup>d</sup>
		3b <sub>2</sub>	3.45 (0.88) <sup>c</sup>	3.46	
C	3.83 ±0.05	5a <sub>1</sub>	3.64 (0.88) <sup>c</sup>	3.65	<sup>d</sup>
D	4.50 ±0.05	1a <sub>2</sub>	4.42 (0.87) <sup>c</sup>	4.26	4.39 <sup>d</sup>
		4a <sub>1</sub>	4.48 (0.88) <sup>c</sup>	4.32	
Feature	VDE (Exp.)	$\text{NaSi}_6^-$ ( $C_{3v}, {}^1A_1$ ) MO	ROVGF/6-311+G (2df) <sup>b</sup>	TD-B3LYP/6- 311+G (2df) <sup>b</sup>	
x	2.32 ±0.03	5a <sub>1</sub>	2.29 (0.88) <sup>c</sup>	2.26	
a	2.55±0.03	4e	2.45 (0.88) <sup>c</sup>	2.48	
		3e	4.30 (0.88) <sup>c</sup>	4.32	
		4a <sub>1</sub>	4.35 (0.88) <sup>c</sup>	4.32	

<sup>a</sup> The adiabatic detachment energy or the electron affinity of  $\text{NaSi}_6$  is measured to be  $1.80 \pm 0.05$  eV.

<sup>b</sup> At B3LYP//6-311+G\* geometry.

<sup>c</sup> The numbers in the parentheses indicate the pole strength, which characterizes the validity of the one-electron detachment picture.

<sup>d</sup> These states cannot be calculated using CCSD(T) method implemented in Gaussian.

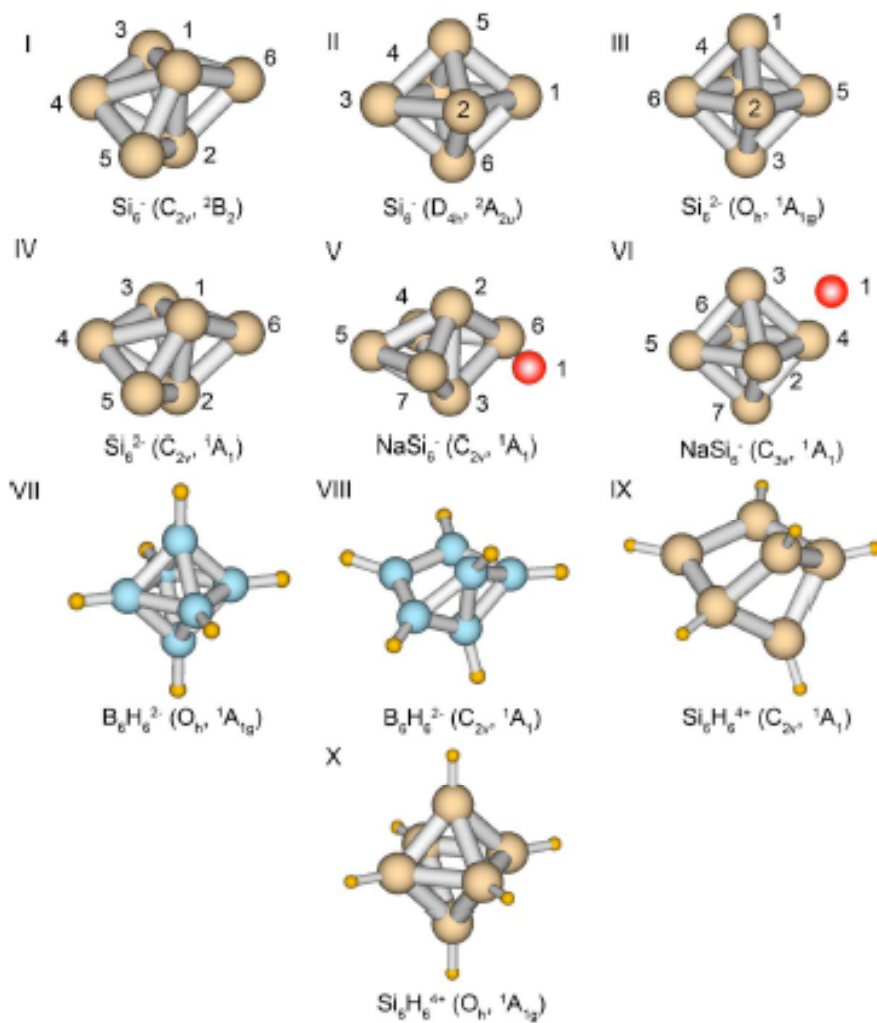


Figure 13-3. Structures of isomers for  $\text{Si}_6^-$  (I, II),  $\text{Si}_6^{2-}$  (III, IV),  $\text{NaSi}_6^-$  (V, VI),  $\text{B}_6\text{H}_6^{2-}$  (VII, VIII), and  $\text{Si}_6\text{H}_6^{4+}$  (IX, X).

Table 13-3. Calculated molecular properties of  $C_{2v}$  ( ${}^2B_2$ ) and  $D_{4h}$  ( ${}^2A_{2u}$ ) isomers of  $Si_6^-$ .

$C_{2v}$ ( ${}^2B_2$ ) Method	B3LYP/6- 311+G*	MP2/6- 311+G*	CCSD(T)/6- 311+G* <sup>c,d</sup>	$D_{4h}$ ( ${}^2A_{2u}$ ) Method	B3LYP/6- 311+G*	CCSD(T)/6- 311+G* <sup>e,f</sup>
-E, au	1737.107496	1734.128300	1734.184982	-E, au	1737.103268	1734.179554
$\Delta E$ , kcal/mol	0	0	0	$\Delta E$ , kcal/mol	2.7	3.4
$R(Si_1-Si_2)$ , Å	2.547	2.525	2.536	$R(Si_1-Si_5)$ , Å	2.433	2.414
$R(Si_1-Si_3)$ , Å	2.541	2.492	2.527	$R(Si_1-Si_2)$ , Å	2.607	2.594
$R(Si_1-Si_6)$ , Å	2.402	2.381	2.394	$\omega_1(a_{1g})$ , $cm^{-1}$	313 (0.0) <sup>a</sup>	
$R(Si_3-Si_6)$ , Å	2.497	2.471	2.484	$\omega_2(a_{1g})$ , $cm^{-1}$	424 (0.0) <sup>a</sup>	
$R(Si_3-Si_4)$ , Å	2.329	2.359	2.328	$\omega_3(a_{2u})$ , $cm^{-1}$	342 (0.2) <sup>a</sup>	
$\omega_1(a_1)$ , $cm^{-1}$	148 (0.1) <sup>a</sup>	163 (0.2) <sup>a</sup>		$\omega_4(b_{1g})$ , $cm^{-1}$	367 (0.0) <sup>a</sup>	
$\omega_2(a_1)$ , $cm^{-1}$	304 (0.2) <sup>a</sup>	332 (0.2) <sup>a</sup>		$\omega_5(b_{2g})$ , $cm^{-1}$	287 (0.0) <sup>a</sup>	
$\omega_3(a_1)$ , $cm^{-1}$	340 (0.0) <sup>a</sup>	355 (0.1) <sup>a</sup>		$\omega_6(b_{2u})$ , $cm^{-1}$	139 (0.0) <sup>a</sup>	
$\omega_4(a_1)$ , $cm^{-1}$	418 (0.5) <sup>a</sup>	427 (0.3) <sup>a</sup>		$\omega_7(e_u)$ , $cm^{-1}$	95 (0.1) <sup>a</sup>	
$\omega_5(a_1)$ , $cm^{-1}$	433 (0.0) <sup>a</sup>	458 (0.7) <sup>a</sup>		$\omega_8(e_u)$ , $cm^{-1}$	391 (10.3) <sup>a</sup>	
$\omega_6(a_2)$ , $cm^{-1}$	110 (0.0) <sup>a</sup>	111 (0.0) <sup>a</sup>		$\omega_9(e_g)$ , $cm^{-1}$	359 (0.0) <sup>a</sup>	
$\omega_7(a_2)$ , $cm^{-1}$	340 (0.0) <sup>a</sup>	406 (0.0) <sup>a</sup>				
$\omega_8(b_1)$ , $cm^{-1}$	207 (3.4) <sup>a</sup>	320 (2.7) <sup>a</sup>				
$\omega_9(b_1)$ , $cm^{-1}$	287 (0.1) <sup>a</sup>	6915 <sup>b</sup>				
$\omega_{10}(b_2)$ , $cm^{-1}$	235 (4.0) <sup>a</sup>	255 (1.2) <sup>a</sup>				
$\omega_{11}(b_2)$ , $cm^{-1}$	273 (1.5) <sup>a</sup>	306 (1.7) <sup>a</sup>				
$\omega_{12}(b_2)$ , $cm^{-1}$	436 (4.1) <sup>a</sup>	465 (0.6) <sup>a</sup>				

<sup>a</sup> Infrared intensities (km/mol) are given in parenthesis.

<sup>b</sup> Symmetry broken problem.

<sup>c</sup>  $E_{tot} = -1734.367370$  a. u. at CCSD(T)/6-311+G(2df)// CCSD(T)/6-311+G\*,  $\langle S^2 \rangle = 0.85$ .

<sup>d</sup>  $\langle S^2 \rangle = 0.83$

<sup>e</sup>  $E_{tot} = -1734.368752$  a. u. at CCSD(T)/6-311+G(2df)// CCSD(T)/6-311+G\*,  $\langle S^2 \rangle = 0.80$ .

<sup>f</sup>  $\langle S^2 \rangle = 0.78$

(Si<sub>3,4</sub>) atoms, and the decrease of the distance between the axial (Si<sub>1,2</sub>) and the non-bridging-equatorial (Si<sub>5,6</sub>) atoms.

### 13-5.3. *LiSi<sub>6</sub><sup>-</sup> and NaSi<sub>6</sub><sup>-</sup>*

Due to technical reasons semiempirical GEGA computations could be performed only for the LiSi<sub>6</sub><sup>-</sup> system, whose isomers were then taken as starting geometries for higher-level calculations for NaSi<sub>6</sub><sup>-</sup>. The low-lying LiSi<sub>6</sub><sup>-</sup> isomers from the GEGA search contained Si<sub>6</sub><sup>2-</sup> kernels with both the O<sub>h</sub> and C<sub>2v</sub> structures. Substitution of Li by Na and reoptimization of the obtained structures at B3LYP/6-311+G\* level of theory gave again two low-lying NaSi<sub>6</sub><sup>-</sup> isomers (Figure 13-3). Geometric parameters as well as harmonic frequencies for structures V and VI are summarized in Table 13-5, where total energies obtained in single-point calculations at CCSD(T)/6-311+G(2df) are also given. We found that while for bare Si<sub>6</sub><sup>2-</sup> the O<sub>h</sub> (<sup>1</sup>A<sub>1g</sub>) structure III is more stable than the C<sub>2v</sub> (<sup>1</sup>A<sub>1</sub>) isomer IV, for NaSi<sub>6</sub><sup>-</sup> the C<sub>3v</sub> (<sup>1</sup>A<sub>1</sub>) isomer VI with the O<sub>h</sub> motif is energetically less favorable than structure V with the C<sub>2v</sub> motif. At our highest level of theory (CCSD(T)/6-311+G(2df)//B3LYP/6-311+G\*) the C<sub>2v</sub> (<sup>1</sup>A<sub>1</sub>) isomer V of NaSi<sub>6</sub><sup>-</sup> is only 1.2 kcal/mol more stable than the C<sub>3v</sub> (<sup>1</sup>A<sub>1</sub>) isomer VI. We note that Kishi *et al.* obtained a similar ground state isomer for NaSi<sub>6</sub><sup>-</sup>.<sup>23</sup> But they did not obtain the C<sub>3v</sub> isomer; they considered two much higher energy isomers instead, in which the Na<sup>+</sup> is coordinated to either an axial Si atom or to two equatorial Si atoms of the O<sub>h</sub> Si<sub>6</sub><sup>2-</sup>. Comparison of the C<sub>2v</sub> and O<sub>h</sub> structures for the bare Si<sub>6</sub><sup>2-</sup> with the corresponding fragments in the two NaSi<sub>6</sub><sup>-</sup> isomers reveals relatively minor structural changes due to the Na<sup>+</sup> coordination, suggesting the robustness of the silicon kernel as a solid building block. In the global minimum C<sub>2v</sub>



Table 13-4. Calculated molecular properties of  $O_h$  ( $^1A_{1g}$ ) and  $C_{2v}$  ( $^1A_1$ ) isomers of  $Si_6^{2-}$ .

Method	B3LYP/6-311+G*	MP2/6-311+G*	CCSD(T)/6-311+G*
$Si_6^{2-} O_h (^1A_{1g})$			
-E, au	1737.044100	1734.054245	1734.112726 <sup>b</sup>
$\Delta E$ , kcal/mol	0	0	0
R(Si-Si), Å	2.498	2.464	2.475
$\omega_1(a_{1g})$ , $cm^{-1}$	405 (0.0) <sup>a</sup>	438 (0.0) <sup>a</sup>	431
$\omega_2(e_g)$ , $cm^{-1}$	334 (0.0) <sup>a</sup>	322 (0.0) <sup>a</sup>	332
$\omega_3(t_{1u})$ , $cm^{-1}$	364 (7.4) <sup>a</sup>	379 (9.7) <sup>a</sup>	378
$\omega_4(t_{2g})$ , $cm^{-1}$	333 (0.0) <sup>a</sup>	330 (0.0) <sup>a</sup>	328
$\omega_5(t_{2u})$ , $cm^{-1}$	137 (0.0) <sup>a</sup>	168 (0.0) <sup>a</sup>	146
$Si_6^{2-} C_{2v} (^1A_1)$			
-E, au	1737.031182	1734.045549	1734.099297 <sup>c</sup>
$\Delta E$ , kcal/mol	8.1	5.5	8.4
R(Si <sub>1</sub> -Si <sub>2</sub> ), Å	2.496	2.461	2.484
R(Si <sub>1</sub> -Si <sub>6</sub> ), Å	2.400	2.384	2.392
R(Si <sub>1</sub> -Si <sub>3</sub> ), Å	2.662	2.595	2.637
R(Si <sub>3</sub> -Si <sub>6</sub> ), Å	2.456	2.453	2.447
R(Si <sub>3</sub> -Si <sub>4</sub> ), Å	2.420	2.407	2.412
$\omega_1(a_1)$ , $cm^{-1}$	158 (4.5) <sup>a</sup>	177 (2.9) <sup>a</sup>	168
$\omega_2(a_1)$ , $cm^{-1}$	287 (4.7) <sup>a</sup>	312 (2.9) <sup>a</sup>	297
$\omega_3(a_1)$ , $cm^{-1}$	343 (2.1) <sup>a</sup>	346 (5.9) <sup>a</sup>	347
$\omega_4(a_1)$ , $cm^{-1}$	355 (0.1) <sup>a</sup>	375 (2.2) <sup>a</sup>	367
$\omega_5(a_1)$ , $cm^{-1}$	419 (2.4) <sup>a</sup>	449 (2.5) <sup>a</sup>	437
$\omega_6(a_2)$ , $cm^{-1}$	129 (0.0) <sup>a</sup>	132 (0.0) <sup>a</sup>	122
$\omega_7(a_2)$ , $cm^{-1}$	332 (0.0) <sup>a</sup>	375 (0.0) <sup>a</sup>	344
$\omega_8(b_1)$ , $cm^{-1}$	151 (6.7) <sup>a</sup>	182 (3.0) <sup>a</sup>	158
$\omega_9(b_1)$ , $cm^{-1}$	236 (0.0) <sup>a</sup>	260 (0.3) <sup>a</sup>	247
$\omega_{10}(b_2)$ , $cm^{-1}$	217 (0.2) <sup>a</sup>	227 (0.1) <sup>a</sup>	221
$\omega_{11}(b_2)$ , $cm^{-1}$	348 (0.2) <sup>a</sup>	345 (0.2) <sup>a</sup>	350
$\omega_{12}(b_2)$ , $cm^{-1}$	436 (3.7) <sup>a</sup>	461 (10.7) <sup>a</sup>	450

<sup>a</sup> Infrared intensities (km/mol) are given in parenthesis.

<sup>b</sup>  $E_{tot}=-1734.309096$  a.u. at CCSD(T)/6-311+G(2df)//CCSD(T)/6-311+G\*.

<sup>c</sup>  $E_{tot}=-1734.289598$  a.u. at CCSD(T)/6-311+G(2df)//CCSD(T)/6-311+G\*.

( $^1A_1$ )  $\text{NaSi}_6^-$ , the effect of the  $\text{Na}^+$  coordination appears to slightly increase the Si-Si bond length between the two axial atoms (Table 13-5). In the  $C_{3v}$  ( $^1A_1$ )  $\text{NaSi}_6^-$  isomer, the  $\text{Na}^+$  coordination has little effect on the three proximate Si atoms, but seems to increase the Si-Si bond distances for the three distal Si atoms (Table 13-5).

## 13-6. Interpretation of the Photoelectron Spectra

### 13-6.1. $\text{Si}_6^-$

Binggeli and Chelikowsky<sup>27</sup> first computed the PES spectra of  $\text{Si}_6^-$  using molecular dynamics simulation and compared with the slightly lower resolution PES spectra reported by Cheshnovsky *et al.*<sup>22</sup> They found that the simulated spectrum of the  $C_{2v}$   $\text{Si}_6^-$  structure was in excellent agreement with the experimental data, whereas a low-lying isomer with a distorted octahedral structure might also make minor contributions to the experimental data. Their study firmly established the  $C_{2v}$  ground state structure for  $\text{Si}_6^-$ . However, a quantitative interpretation of the PES spectra requires detailed calculations for each photodetachment transition from the  $C_{2v}$  and  $D_{4h}$  ground state structures to the neutral final states. In particular, since the ground state of  $\text{Si}_6^-$  is a doublet with an unpaired electron, both singlet and triplet final states are possible and they need to be computed in order to make quantitative comparison with the experimental PES spectra. In the current study, we calculated the VDEs for  $\text{Si}_6^-$  ( $C_{2v}$ ,  $^2B_2$ ) at the following levels of theory: CCSD(T)/6-311+G(2df)//CCSD(T)/6-311+G\*, EOM/6-311+G(2df)//CCSD(T)/6-311+G\*, TD B3LYP/6-311+G(2df)//B3LYP/6-311+G\*, and UOVGF/6-311+G(2d)//CCSD(T)/6-311+G\*. The final electron configurations and the

Table 13-5. Calculated molecular properties of the  $C_{2v}$  ( $^1A_1$ ) and  $C_{3v}$  ( $^1A_1$ ) isomers of  $NaSi_6^-$ .

$C_{2v}$ ( $^1A_1$ ) Method	B3LYP/ 6-311+G*	MP2/ 6-311+G*	$C_{3v}$ ( $^1A_1$ ) Method	B3LYP/ 6-311+G*	MP2/ 6-311+G*
-E, a. u.	1899.429907 <sup>b</sup>	1896.020071	-E, au	1899.424291 <sup>c</sup>	1896.009937
$\Delta E$ , kcal/mol	0.0	0.0	$\Delta E$ , kcal/mol	3.5	6.4
R(Na <sub>1</sub> -Si <sub>2</sub> ), Å	2.875	2.887	R (Na <sub>1</sub> -Si <sub>2</sub> )	2.861	2.864
R(Na <sub>1</sub> -Si <sub>6</sub> ), Å	2.915	2.913	R (Na <sub>1</sub> -Si <sub>5</sub> )	4.705	4.693
R(Na <sub>1</sub> -Si <sub>4</sub> ), Å	4.578	4.582	R (Si <sub>2</sub> -Si <sub>3</sub> ), Å	2.495	2.471
R(Si <sub>2</sub> -Si <sub>3</sub> ), Å	2.544	2.505	R (Si <sub>5</sub> -Si <sub>6</sub> ), Å	2.548	2.512
R(Si <sub>2</sub> -Si <sub>6</sub> ), Å	2.447	2.428	R (Si <sub>2</sub> -Si <sub>5</sub> ), Å	2.472	2.447
R(Si <sub>2</sub> -Si <sub>4</sub> ), Å	2.553	2.524	$\omega_1(a_1)$ , cm <sup>-1</sup>	213 (7.4) <sup>a</sup>	224 (19.0) <sup>a</sup>
R(Si <sub>4</sub> -Si <sub>6</sub> ), Å	2.443	2.444	$\omega_2(a_1)$ , cm <sup>-1</sup>	328 (5.7) <sup>a</sup>	342 (6.4) <sup>a</sup>
R(Si <sub>4</sub> -Si <sub>5</sub> ), Å	2.504	2.463	$\omega_3(a_1)$ , cm <sup>-1</sup>	359 (31.6) <sup>a</sup>	377 (28.1) <sup>a</sup>
$\omega_1(a_1)$ , cm <sup>-1</sup>	188 (6.9) <sup>a</sup>	203 (5.0) <sup>a</sup>	$\omega_4(a_1)$ , cm <sup>-1</sup>	410 (0.0) <sup>a</sup>	435 (1.7) <sup>a</sup>
$\omega_2(a_1)$ , cm <sup>-1</sup>	230 (19.1) <sup>a</sup>	235 (23.2) <sup>a</sup>	$\omega_5(a_2)$ , cm <sup>-1</sup>	140 (0.0) <sup>a</sup>	186 (0.0) <sup>a</sup>
$\omega_3(a_1)$ , cm <sup>-1</sup>	292 (4.0) <sup>a</sup>	314 (4.2) <sup>a</sup>	$\omega_6(e)$ , cm <sup>-1</sup>	74 (4.2) <sup>a</sup>	92 (4.9) <sup>a</sup>
$\omega_4(a_1)$ , cm <sup>-1</sup>	339 (0.4) <sup>a</sup>	346 (8.1) <sup>a</sup>	$\omega_7(e)$ , cm <sup>-1</sup>	162 (0.0) <sup>a</sup>	197 (0.0) <sup>a</sup>
$\omega_5(a_1)$ , cm <sup>-1</sup>	350 (3.0) <sup>a</sup>	368 (0.2) <sup>a</sup>	$\omega_8(e)$ , cm <sup>-1</sup>	321 (0.3) <sup>a</sup>	316 (0.4) <sup>a</sup>
$\omega_6(a_1)$ , cm <sup>-1</sup>	414 (4.5) <sup>a</sup>	441 (3.2) <sup>a</sup>	$\omega_9(e)$ , cm <sup>-1</sup>	342 (0.0) <sup>a</sup>	360 (0.0) <sup>a</sup>
$\omega_7(a_2)$ , cm <sup>-1</sup>	139 (0.0) <sup>a</sup>	142 (0.0) <sup>a</sup>	$\omega_{10}(e)$ , cm <sup>-1</sup>	375 (9.9) <sup>a</sup>	384 (11.4) <sup>a</sup>
$\omega_8(a_2)$ , cm <sup>-1</sup>	325 (0.0) <sup>a</sup>	360 (0.0) <sup>a</sup>			
$\omega_9(b_1)$ , cm <sup>-1</sup>	90 (2.1) <sup>a</sup>	94 (3.4) <sup>a</sup>			
$\omega_{10}(b_1)$ , cm <sup>-1</sup>	180 (6.2) <sup>a</sup>	204 (2.5) <sup>a</sup>			
$\omega_{11}(b_1)$ , cm <sup>-1</sup>	280 (0.0) <sup>a</sup>	290 (0.5) <sup>a</sup>			
$\omega_{12}(b_2)$ , cm <sup>-1</sup>	143 (3.4) <sup>a</sup>	154 (3.9) <sup>a</sup>			
$\omega_{13}(b_2)$ , cm <sup>-1</sup>	235 (11.6) <sup>a</sup>	247 (8.8) <sup>a</sup>			
$\omega_{14}(b_2)$ , cm <sup>-1</sup>	338 (0.1) <sup>a</sup>	339 (0.1) <sup>a</sup>			
$\omega_{15}(b_2)$ , cm <sup>-1</sup>	414 (1.8) <sup>a</sup>	435 (5.9) <sup>a</sup>			

<sup>a</sup> Infrared intensities (km/mol) are given in parenthesis.

<sup>b</sup>  $E_{tot} = -1896.261806$  a. u. at CCSD(T)/6-311+G(2df)//B3LYP/6-311+G\*

<sup>c</sup>  $E_{tot} = -1896.259976$  a. u. at CCSD(T)/6-311+G(2df)//B3LYP/6-311+G\*

corresponding detachment energies are given in Table 13-1, compared with the experimental VDEs. Results at different levels of theory generally agree well with each other and with the experiment.

As shown in Table 13-1, the LUMO of neutral  $\text{Si}_6$  is  $4b_2$ , which is singly occupied in  $\text{Si}_6^-$ . Detachment of the  $4b_2$  electron produces a singlet state ( $^1A_1$ ) for the neutral  $\text{Si}_6$ . There is a very good agreement between the calculated VDE values among the different theoretical methods (Table 13-1). The next detachment channel involves the  $6a_1$  orbital, which is the HOMO of the neutral  $\text{Si}_6$ . Detachment from this fully occupied MO produces both a triplet and singlet final state. The calculated VDEs for the triplet final state ( $^3B_2$ ) are in good agreement with the VDE of the A band observed experimentally. The A-X separation, which represents the excitation energy from the ground state of  $\text{Si}_6$  ( $^1A_1$ ) to the first excited triplet state ( $^3B_2$ ), is an experimental measure of the HOMO-LUMO gap of neutral  $\text{Si}_6$ . We note that the TD-B3LYP method underestimates the HOMO-LUMO gap, whereas the CCSD(T) method yields a HOMO-LUMO gap, which is in excellent agreement with the experimental measurement.

The next five detachment channels, including the singlet final state ( $^1B_2$ ) obtained by removing the  $6a_1$  electron, are congested within a narrow energy range from 3.65 to 4.05 eV from the TD-B3LYP calculations. All these detachment channels contributed to the B band, giving rise to the broad PES band. The next two detachment channels ( $^1B_2$  and  $^1A_1$ ) are nearly degenerate and their calculated VDEs are in good agreement with that of the C band. The next three detachment channels involve removal of an electron from the  $1a_2$  orbital and  $4a_1 \beta$  orbital. The calculated VDEs to the triplet and singlet states are in the range of the D band. The last detachment channel calculated was from the  $4a_1 \alpha$

orbital with a VDE of 5.32 eV, which could correspond to the tail part of the D band, although the signal-to-noise ratio was poor at the high binding energy part.

Overall, the computed VDEs from the  $C_{2v}$   $Si_6^-$  are in excellent agreement with the experimental PES spectral pattern, consistent with the previous molecular dynamics simulations by Binggeli and Chelikowsky. These authors were able to obtain simulated spectral patterns very similar to the experimental PES spectra, even though they did not do state-to-state calculations. This was because of the congested nature of the PES spectra and the limited spectral resolution. The current study represents the most quantitative interpretation of the PES spectra of  $Si_6^-$ . The spectrum for the low-lying isomer which is a distorted octahedral structure ( $D_{4h}$ ) was simulated by Binggeli and Chelikowsky. We also obtained theoretical spectra for  $D_{4h}$  ( ${}^2A_{2u}$ ) at CCSD(T)/6-311+G(2df)//CCSD(T)/6-311+G\*, TD-B3LYP/6-311+G(2df)//B3LYP-6-311+G\* and UOVGF/6-311+G(2d)//CCSD(T)/6-311+G\* levels of theory (Table 1). The theoretical VDE for the ground state transition was  $\sim 2.61$ - $2.74$  eV, consistent with weak signals in same energy range in Fig. 1. One main feature from this isomer (triplet final state  ${}^3E_g$ ) is in good agreement with the weak feature labeled as “IS” in Figure 13-1 with most of the simulated features that are buried in the features from the  $C_{2v}$  ground state of  $Si_6^-$ . Our calculations show effective degeneracy of the  $D_{4h}$  ( ${}^2A_{2u}$ ) and  $C_{2v}$  ( ${}^2B_2$ ) isomers; presence of the  $D_{4h}$  ( ${}^2A_{2u}$ ) structure is revealed in all the PES spectra of  $Si_6^-$  reported so far, including the current data. The feature labeled “IS” in Figure 13-1 was vibrationally resolved by Xu *et al.*, who did not recognize it as a contribution from an low-lying isomer and attributed it incorrectly to the first excited state transition from the main  $Si_6^-$  isomer. Our analysis showed that the theoretical spectrum of  $Si_6^-$   $C_{2v}$  ( ${}^2B_2$ ) was more consistent

with the experimental data, demonstrating that under the experimental conditions the  $C_{2v}$  structure was more abundant in the molecular beam than the  $D_{4h}$  one.

### 13-6.2. $NaSi_6^-$

The ground state of  $NaSi_6^-$  can be viewed as adding a Na atom to the  $C_{2v}$  ground state of  $Si_6^-$ , with an electron transfer from Na to the  $Si_6$  motif to produce the  $C_{2v}$   $Si_6^{2-}$  coordinated by a  $Na^+$ . The extra electron enters the  $4b_2$  SOMO of  $Si_6^-$ , producing a closed shell ground state of  $NaSi_6^-$  with a nearly identical MO ordering. The closed shell nature of  $NaSi_6^-$  means that the PES spectrum would be simpler because only doublet final states are produced and each occupied MO only yields one detachment channel, in contrast to  $Si_6^-$ , where both singlet and triplet final states can be produced after detachment from a fully occupied MO. Table 13-2 summarizes the calculated VDEs at several levels of theory for the  $C_{2v}$  ground state of  $NaSi_6^-$ , as well as those for the  $C_{3v}$  isomer, compared with the experimental values.

#### 13-6.2.1. $NaSi_6^- (C_{2v}, ^1A_1)$

The ground state transition corresponds to an electron detachment from the  $4b_2$  HOMO. The ROVGF and CCSD(T) methods yielded VDEs for the ground state transition in exact agreement with the experimental values within the experimental uncertainty (Table 13-2). The second detachment channel is from the  $6a_1$  HOMO-1. We note again the CCSD(T) method yielded a VDE in quantitative agreement with the experimental value of the A band. The X-A separation measured to be 1.04 eV is also well reproduced by both the TD-B3LYP and the CCSD(T) methods. It should be pointed out that the X-A separation measured in the spectra of  $NaSi_6^-$  is identical to that for  $Si_6^-$

(Figure 13-1 and Table 13-1), suggesting that the  $\text{Na}^+$  coordination has little electronic effect on these MOs. As can be clearly seen from Table 13-2, the next five detachment channels are in excellent agreement with the experimental pattern for the B, C, and D bands, with the B and D bands each containing two detachment channels. Comparison between the spectra of  $\text{Si}_6^-$  and  $\text{NaSi}_6^-$  suggests that the detachment channels of both species are similar. If all the excited singlet states were removed from  $\text{Si}_6^-$ , one would obtain almost identical spectra for these two species, which is why the spectra of  $\text{NaSi}_6^-$  were simpler and less congested. The excellent agreement between the calculated VDEs and the experimental PES data confirms unequivocally that the ground state of  $\text{NaSi}_6^-$  is the  $\text{C}_{2v}$  ( $^1A_1$ ) structure V.

#### 13-6.2.2. $\text{NaSi}_6^-$ ( $\text{C}_{3v}$ , $^1A_1$ )

The weak features in between the X and A bands clearly do not belong to the  $\text{C}_{2v}$  ground state isomer of  $\text{NaSi}_6^-$ . The low-lying  $\text{C}_{3v}$  ( $^1A_1$ ) isomer VI of  $\text{NaSi}_6^-$  (Figure 13-3) is only 1.2 kcal/mol higher in energy (at CCSD(T)/6-311+G(2df)//B3LYP/6-311+G\*) than the global minimum  $\text{C}_{2v}$  structure and thus could be populated experimentally. As shown in Table 13-2, our calculated VDEs for the first two detachment channels for the  $\text{C}_{3v}$  isomer are in excellent agreement with the observed weak features (x and a). The ground state transition from the  $\text{C}_{3v}$  isomer corresponds to electron detachment from the  $5a_1$  HOMO. The computed VDEs from both ROVGF and TD-B3LYP are in very good agreement with the experimental VDE from the x feature. The calculated VDE from the  $4e$  HOMO-1 gives rise to the feature a. The two higher binding energy transitions from

the  $C_{3v}$  isomer have similar binding energies with the D band of the main isomer and might be obscured.

Comparisons of the experimental PES data of  $\text{NaSi}_6^-$  with the theoretical calculations lead to several conclusions. First, two isomers were indeed observed experimentally for  $\text{NaSi}_6^-$ , similar to  $\text{Si}_6^-$ . Second, good agreement between the experimental and theoretical VDEs confirms the global minimum ( $C_{2v}$ ,  $^1A_1$ ) structure V for  $\text{NaSi}_6^-$  and the low-lying ( $C_{3v}$ ,  $^1A_1$ ) isomer VI. Third, the  $\text{Si}_6$  moiety in  $\text{NaSi}_6^-$  is very similar electronically and structurally to  $\text{Si}_6^-$ . Fourth, ROVGF/6-311+G(2df), TD B3LYP/6-311+G(2df), and CCSD(T)/6-311+G(2df) levels of theory, used to calculate VDEs, show good agreement with each other and with experiment. Thus, the first two methods, which do not require as much computer resources as CCSD(T) can be reliably implemented in the future in analyzing PES of larger Na-Si clusters. We note that the poor agreement ( $>0.5$  eV) between the calculated and experimental first VDE and ADE of  $\text{NaSi}_6^-$  reported by Kishi et al.<sup>23</sup> was most probably caused by the small basis sets used in their calculations.

### 13-7. Chemical Bonding in $\text{Si}_6^{2-}$ and $\text{NaSi}_6^-$

#### 13-7.1. NBO Analysis

We performed NBO analysis for the  $\text{Si}_6^{2-}$   $O_h$  ( $^1A_{1g}$ ),  $\text{Si}_6^{2-}$   $C_{2v}$  ( $^1A_1$ ),  $\text{NaSi}_6^-$   $C_{3v}$  ( $^1A_1$ ), and  $\text{NaSi}_6^-$   $C_{2v}$  ( $^1A_1$ ) species. Tables with NBO data are available from the authors upon request. The Si atoms in  $\text{Si}_6^{2-}$   $O_h$  ( $^1A_{1g}$ ) each carry an effective charge  $Q(\text{Si}) = -0.333 |e|$  and their hybridization is  $3s^{1.65}3p^{2.62}$ . Thus, the  $3s^2$  lone pairs on Si show some hybridization with the 3p-AOs in spite of the excessive  $-2$  charge on the cluster. From



$\text{Si}_6^{2-}$   $\text{O}_h$  ( $^1\text{A}_{1g}$ ) to  $\text{Si}_6^{2-}$   $\text{C}_{2v}$  ( $^1\text{A}_1$ ) some charge redistribution occurs. The two axial atoms with  $Q(\text{Si}_{1,2}) = -0.305 |e|$  (hybridization  $3s^{1.55}3p^{2.70}$ ) lose some electron density and some s-p promotion also occurs. The two bridging equatorial atoms with  $Q(\text{Si}_{3,4}) = -0.324 |e|$  (hybridization  $3s^{1.66}3p^{2.60}$ ) are almost the same as in the octahedral structure. The other two non-bridging equatorial atoms gain some extra negative charge with  $Q(\text{Si}_{5,6}) = -0.371 |e|$  and hybridization  $3s^{1.67}3p^{2.67}$ .

The major difference between the  $\text{O}_h$  ( $^1\text{A}_{1g}$ ) and  $\text{C}_{2v}$  ( $^1\text{A}_1$ ) structure is the transfer of electron density from lone pairs to Si-Si bonds. Occupation numbers in the six lone pairs in the  $\text{O}_h$  ( $^1\text{A}_{1g}$ ) isomer are 1.965  $|e|$  and 1.964  $|e|$ , compared to two lone pairs ( $\text{Si}_1$  and  $\text{Si}_2$ ) with occupation numbers 1.703  $|e|$ , two lone pairs ( $\text{Si}_3$  and  $\text{Si}_4$ ) with occupation numbers 1.914  $|e|$ , and two lone pairs ( $\text{Si}_5$  and  $\text{Si}_6$ ) with occupation numbers 1.931  $|e|$  in the  $\text{C}_{2v}$  ( $^1\text{A}_1$ ) isomer. Thus, about 0.5  $|e|$  were transferred from lone pairs in the  $\text{O}_h$  structure to Si-Si bonds (primarily to  $\text{Si}_3$ - $\text{Si}_6$  and  $\text{Si}_4$ - $\text{Si}_5$ ) in the  $\text{C}_{2v}$  structure.

NBO analysis of  $\text{NaSi}_6^-$   $\text{C}_{3v}$  ( $^1\text{A}_1$ ) and  $\text{C}_{2v}$  ( $^1\text{A}_1$ ) revealed that chemical bonding between  $\text{Na}^+$  and  $\text{Si}_6^{2-}$  is highly ionic. The NBO charge for Na is +0.823  $|e|$  in  $\text{NaSi}_6^-$   $\text{C}_{2v}$  ( $^1\text{A}_1$ ) and +0.709  $|e|$  in  $\text{NaSi}_6^-$   $\text{C}_{3v}$  ( $^1\text{A}_1$ ). In both isomers there is some charge redistribution in the corresponding  $\text{Si}_6^{2-}$  kernels due to the coordination of  $\text{Na}^+$ . In the  $\text{C}_{2v}$  structure the axial atoms become more negatively charged [ $Q(\text{Si}_{2,3}) = -0.419 |e|$ ; hybridization  $3s^{1.55}3p^{2.82}$ ], the bridging equatorial atoms lose some negative charge [ $Q(\text{Si}_{4,5}) = -0.103 |e|$ ; hybridization  $3s^{1.69}3p^{2.37}$ ], and there is almost no change of the charge on the two non-bridging equatorial atoms [ $Q(\text{Si}_{6,7}) = -0.391 |e|$ ; hybridization  $3s^{1.68}3p^{2.68}$ ]. In the  $\text{C}_{3v}$  structure, the Si atoms located on the face closest to  $\text{Na}^+$  gained some negative charge [ $Q(\text{Si}_{2,3,4}) = -0.402 |e|$ ; hybridization  $3s^{1.61}3p^{2.74}$ ], the other three

atoms become less negatively charged [ $Q(\text{Si}_{5,6,7}) = -0.168 |e|$ ; hybridization  $3s^{1.68}3p^{2.44}$ ].

### 13-7.2. MO Analysis

Figure 13-4 displays the MOs of  $\text{Si}_6^{2-} \text{C}_{2v} (^1\text{A}_1)$  IV and  $\text{NaSi}_6^- \text{C}_{2v} (^1\text{A}_1)$  V. Comparison of these two systems shows that the identical sets of orbitals are occupied. From this point of view the chemical bonding in  $\text{Si}_6^{2-} \text{C}_{2v} (^1\text{A}_1)$  and  $\text{NaSi}_6^- \text{C}_{2v} (^1\text{A}_1)$  can be assumed to be similar. The same is true for  $\text{Si}_6^{2-} (\text{O}_h, ^1\text{A}_{1g})$  III and  $\text{NaSi}_6^- (\text{C}_{3v}, ^1\text{A}_1)$  VI.

Upon transition from the  $\text{O}_h (^1\text{A}_{1g})$  isomer of  $\text{Si}_6^{2-}$  to the  $\text{C}_{2v} (^1\text{A}_1)$  isomer a HOMO-LUMO switch occurs, namely, one of the  $2t_{1u}$  triply degenerate HOMO ( $3b_1$  in the  $\text{C}_{2v}$  notation) switches with one of the  $1t_{2u}$  triply degenerate LUMO ( $4b_2$  in the  $\text{C}_{2v}$  notations). One can see from Figure 13-5 that the  $2t_{1u}$ -MO has a significant contribution from the 3s-AOs of the Si atoms, while the  $1t_{2u}$ -MO is primarily composed of 3p-AOs of Si. Thus, the  $2t_{1u}$ -MO ( $3b_1$ ) to  $1t_{2u}$ -MO ( $4b_2$ ) switch in the  $\text{C}_{2v}$  structure should result in decreasing 3s-AOs and increasing 3p-AOs occupations. That is consistent with our observation from the NBO analysis.

One can see from Figure 13-4 that the sodium cation can interact more favorably with the  $4b_2$ -MO rather than with the  $3b_1$ -MO and that makes the  $\text{NaSi}_6^- (\text{C}_{2v}, ^1\text{A}_1)$  V structure more stable than the  $\text{NaSi}_6^- (\text{C}_{3v}, ^1\text{A}_1)$  VI structure. Molecular orbitals of  $\text{B}_6\text{H}_6^{2-} \text{O}_h (^1\text{A}_{1g})$  VII and  $\text{Si}_6^{2-} \text{O}_h (^1\text{A}_{1g})$  III are shown at Figure 13-5. The sets of the occupied MOs are identical for both systems, but the ordering is slightly different: the HOMO of  $\text{B}_6\text{H}_6^{2-} \text{O}_h$  is a triply degenerate  $1t_{2g}$  orbital while in  $\text{Si}_6^{2-}$  it is  $2t_{1u}$ . Also,  $1e_g$  and  $2a_{1g}$  orbitals switch their positions.

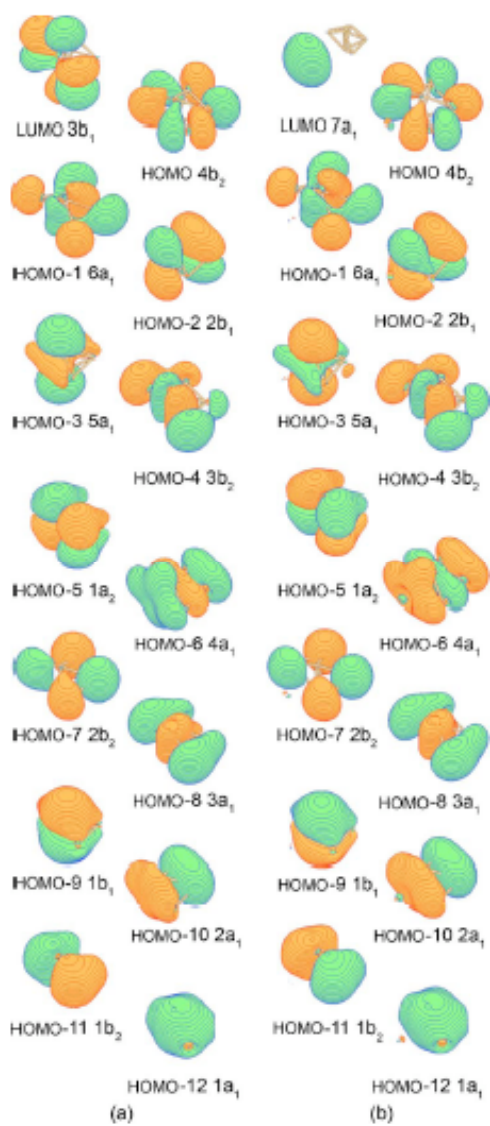


Figure 13-4. Molecular orbitals of  $\text{Si}_6^{2-}$   $C_{2v}$  ( $^1A_1$ ) and  $\text{NaSi}_6^-$   $C_{2v}$  ( $^1A_1$ ).

### 3-7.3. ELF Analysis

ELF analysis is a popular modern technique, which reveals the regions within a chemical system, where pairs of electrons with antiparallel spin can be localized. The local maxima of the ELFs define “localization attractors,” of which there are only three basic types: bonding, non-bonding, and core. Bonding attractors lie between the core attractors (which themselves surround the atomic nuclei) and characterize the shared-electron interactions. The spatial organization of localization attractors provides a basis for a well-defined classification of bonds. From any point in space the ELF gradient is followed to an attractor in that region, and this point is then attributed to this attractor. The collection of all the points in space which are assigned to a given attractor is called its basin. The synaptic order of a basin is determined as the number of atomic cores it is connected with. The criterion of discrimination between basins is provided by the reduction of reducible (containing more than one attractor) domains. The reduction of a reducible localization domain occurs at critical values (saddle points) of the bonding isosurface, over which the domain is split into domains containing fewer attractors. The localization domains are then ordered with respect to the ELF critical values, yielding bifurcations.

We studied the ELF of  $B_6H_6^{2-} O_h (^1A_{1g})$ ,  $Si_6^{2-} O_h (^1A_{1g})$ ,  $Si_6^{2-} C_{2v} (^1A_1)$ , and  $NaSi_6^- C_{2v} (^1A_1)$ . The ELF bifurcations, leading to the separation of regions with chemical significance, are shown in Figure 13-6. Let us start with the comparison of the two octahedral isoelectronic species,  $B_6H_6^{2-} O_h (^1A_{1g})$  and  $Si_6^{2-} O_h (^1A_{1g})$ , which are expected to have similar chemical bonding. The first bifurcation in  $B_6H_6^{2-}$  occurs at 0.49 and leads to the separation of 6 protonated basins (sphere-like regions), which correspond to 2e-2c

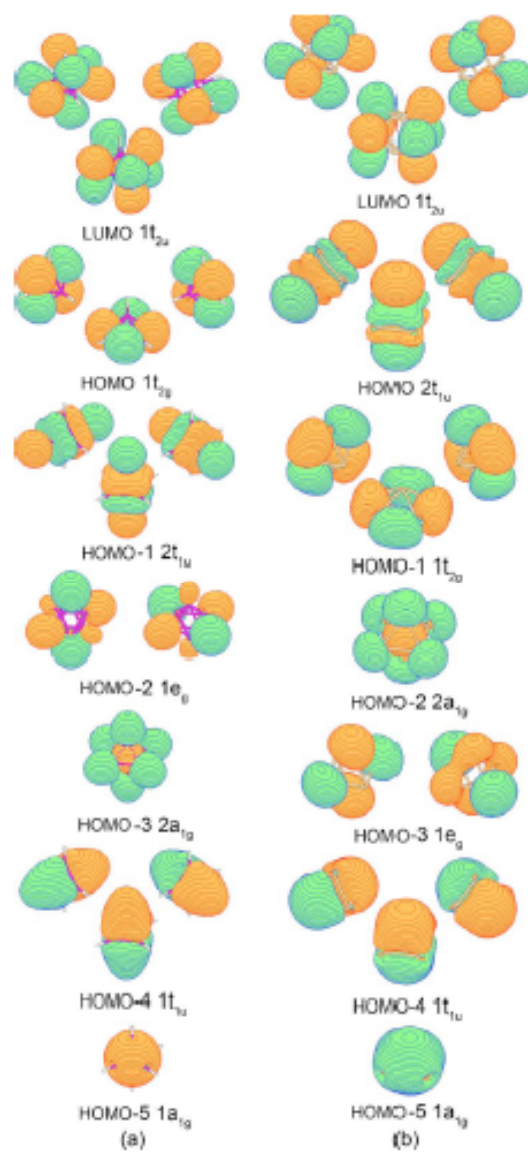


Figure 13-5. Molecular orbitals of  $B_6H_6^{2-} O_h (^1A_{1g})$  and  $Si_6^{2-} O_h (^1A_{1g})$ .

B-H bonds. There is a similar bifurcation in  $\text{Si}_6^{2-}$ , but it occurs at a higher ELF value (0.65), and the separated sphere-like domains correspond to 6 lone pairs of the silicon atoms. This means, that the interaction of the lone pairs and the skeletal bonds in  $\text{O}_h \text{Si}_6^{2-}$  is stronger than the interaction of the B-H bonds and the skeletal bonds in  $\text{O}_h \text{B}_6\text{H}_6^{2-}$ . The regions of skeletal bonds are different as well. Bifurcation, separating localization domains in the regions of B-B bonds occurs at 0.84, revealing 8 domains over the center of each of octahedron faces and 12 domains, connecting these central domains with each other. The bifurcational value is very close to the maximum value of ELF for these domains (0.85). Thus, there is very strong interaction between basins of the corresponding attractors, and effectively one 6-synaptic basin exists around single grid-like attractor, covering the entire boron cage. In  $\text{Si}_6^{2-}$  similar bifurcation occurs at 0.71 and gives rise to 12 separated localization domains. There are no domains over centers of triangular faces of the cluster, the maximum ELF value at the attractors within 12 disynaptic basins, corresponding to the skeletal Si-Si bonds, is 0.78. Thus, the skeletal bonding in  $\text{O}_h \text{Si}_6^{2-}$  is more “localizable” than in  $\text{O}_h \text{B}_6\text{H}_6^{2-}$ .

In the  $\text{C}_{2v} \text{Si}_6^{2-}$  the first bifurcation occurs at 0.64 and reveals a small bonding domain between the two axial atoms (scheme 0.64(a)), which can be tracked down to the ELF features of  $\sigma$ -antiaromatic  $\text{Si}_4^0 \text{C}_{2v} (^1\text{A}_1)$  cluster.<sup>72</sup> At 0.71 bonding domain between bridge-like Si atoms is separated. Bifurcation at 0.73 produces irreducible localization domains, corresponding to the lone pairs of the axial atoms, and the one at 0.76 finally separates lone pairs of the bridge equatorial atoms. There are two bonding domains in the regions of Si-Si bonding between equatorial atoms, and two more lone pairs, which can be seen after domain reduction at 0.85. So, the interaction between the lone pair domains

and the bonding domains is stronger in  $C_{2v}$ , than in the  $O_h$  isomer, which is consistent with our conclusions from the NBO and MO analysis. The last scheme demonstrates that maximal ELF values within the basins corresponding to the axial lone pairs are lower (0.93) than those of equatorial lone pairs (0.98). In other words, the axial lone pairs are less “localizable”, than the equatorial ones. Scheme 0.64(b) shows ELF saddle points, characterizing interaction of the axial lone pairs with the bond between bridge equatorial atoms. In the  $O_h$   $Si_6^{2-}$  isomer ELF maxima (attractors) can be found in the same regions, since irreducible domains exist there. These domains could have disappeared due to the strong interaction with the lone-pair domains as the  $O_h$  structure transforms into  $C_{2v}$ . The same can be true for bonding domains between the axial and non-bridge equatorial atoms, since they merge with axial lone pairs at 0.83, but the maximum ELF value for them is between 0.83 and 0.84.

The pattern of chemical bonding in  $Si_6^{2-}$   $C_{2v}$  somewhat changes after introduction of  $Na^+$  into the system according to the ELF bifurcational sequence for  $NaSi_6^-$   $C_{2v}$  isomer. The bonding domain between the axial atoms separates at 0.58 (vs. 0.64), the bonding domain between bridge equatorial atoms – at 0.70 (vs. 0.71). Separation of the axial and two equatorial lone pairs occurs at 0.72 (vs. 0.72) and 0.76 (vs. 0.76) correspondingly. But there are no bonding domains between bridge and non-bridge equatorial atoms any more (which appeared at 0.85 in  $Si_6^{2-}$   $C_{2v}$ ), they merge with lone pair domains of the non-bridge equatorial atoms. Finally, axial lone pairs have lower maximal ELF values (0.91) than the equatorial ones (0.98).

Chemical bonding analysis of the  $O_h$  ( $^1A_{1g}$ ) isomer of  $Si_6^{2-}$  and  $O_h$  ( $^1A_{1g}$ ) isomer of  $B_6H_6^{2-}$  revealed that like in our previous study of  $Si_5^{2-}$  and  $B_5H_5^{2-}$  species,<sup>73</sup>  $Si_6^{2-}$

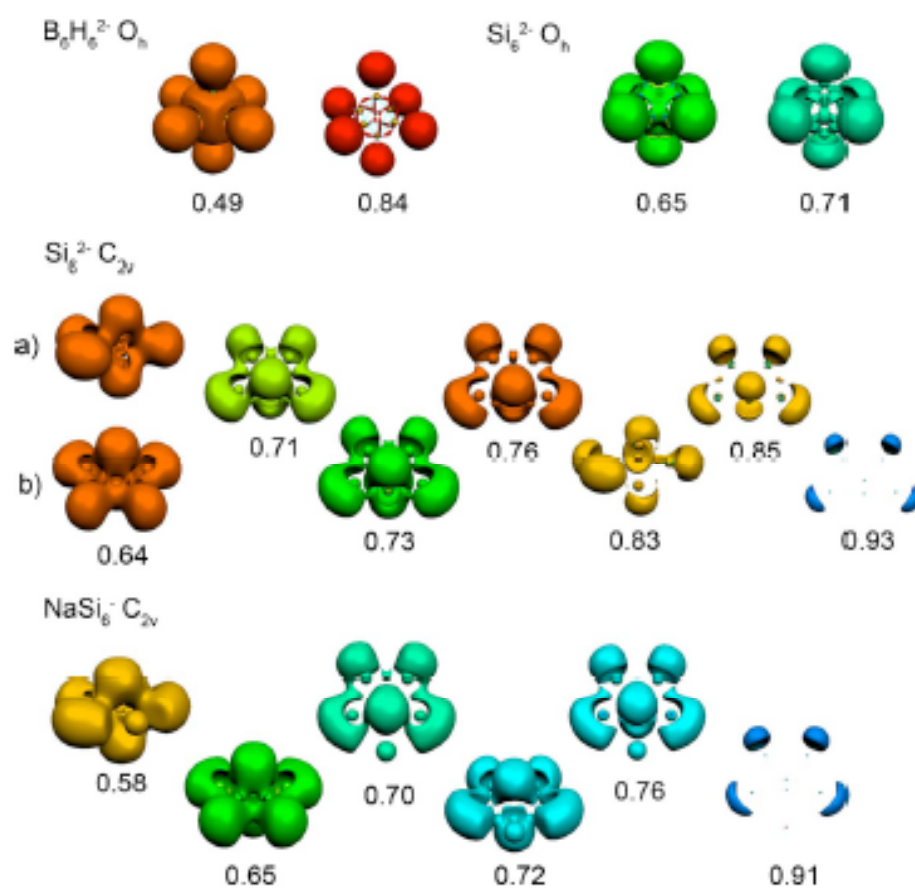


Figure 13-6. Bifurcations of ELF for  $B_6H_6^{2-}$  ( $O_h$ ,  $^1A_{1g}$ ),  $Si_6^{2-}$  ( $O_h$ ,  $^1A_{1g}$ ),  $Si_6^{2-}$  ( $C_{2v}$ ,  $^1A_1$ ), and  $NaSi_6^-$  ( $C_{2v}$ ,  $^1A_1$ ).



differs from  $B_6H_6^{2-}$  by involvement of the electron density, which is supposed to be “lone pairs” of the six silicon atoms in the skeletal bonding in  $Si_6^{2-}$ . This tendency of Si atoms in silicon clusters to favor s-p hybridization rather than  $3s^2$  lone pairs is also responsible for  $Si_6^{2-}$  having two low-lying  $O_h$  ( $^1A_{1g}$ ) and  $C_{2v}$  ( $^1A_1$ ) isomers. When sodium atom is attached to  $Si_6^{2-}$  the alteration in stability occurs. The most stable isomer of  $NaSi_6^-$  is based on the  $Si_6^{2-}$  kernel with the  $C_{2v}$  symmetry. The second most stable isomers  $NaSi_6^-$  is based on the  $Si_6^{2-}$  kernel with  $O_h$  symmetry.

The two low-lying  $O_h$  ( $^1A_{1g}$ ) and  $C_{2v}$  ( $^1A_1$ ) isomers of  $Si_6^{2-}$  inspired us to test the  $C_{2v}$  ( $^1A_1$ ) isomer of  $B_6H_6^{2-}$ . We found the  $C_{2v}$  ( $^1A_1$ ) isomer VIII of  $B_6H_6^{2-}$  (Figure 13-3) with the same electronic configuration is not a minimum, but a first order saddle point with the relative energy (compared to the  $O_h$  ( $^1A_{1g}$ ) isomer VII) of 65 kcal/mol (at B3LYP/6-311++G\*\*). Thus, even  $Si_6^{2-}$  and  $B_6H_6^{2-}$  are valence isoelectronic, they have somewhat different chemical bonding.

#### *13-7.4. Protonation as a Way to Increase the Relative Stability of the Octahedral $Si_6^{2-}$ ?*

From the above discussion we inferred that in order to stabilize the high symmetry  $O_h$  ( $^1A_{1g}$ ) structure of  $Si_6^{2-}$  over the  $C_{2v}$  ( $^1A_1$ ) structure one has to enforce  $sp^3$  hybridization on Si. In the isoelectronic  $B_6H_6^{2-}$  dianion, the external hydrogen atoms enforce almost  $sp^3$  hybridization on boron atoms. We tested if similar approach will work for silicon by calculating  $C_{2v}$  ( $^1A_1$ ) IX and  $O_h$  ( $^1A_{1g}$ ) X structures of  $Si_6H_6^{4+}$  at the B3LYP/6-311++G\*\* level of theory (Figure 13-3). We checked that both structures have the same electronic configurations as  $O_h$  ( $^1A_{1g}$ ) and  $C_{2v}$  ( $^1A_1$ ) structures of  $Si_6^{2-}$ . We found that both the  $C_{2v}$  ( $^1A_1$ ) IX and  $O_h$  ( $^1A_{1g}$ ) X structures of  $Si_6H_6^{4+}$  are true local

minima at our level of theory, but the  $C_{2v}$  ( $^1A_1$ ) IX structure of  $Si_6H_6^{4+}$  was found to be significantly more stable (by 19 kcal/mol at B3LYP/6-311+G\*) than the  $O_h$  ( $^1A_{1g}$ ) X of  $Si_6H_6^{4+}$  and that is different from  $Si_6^{2-}$  where the  $O_h$  ( $^1A_{1g}$ ) III structure is more stable than the  $C_{2v}$  ( $^1A_1$ ) IV structure. Thus, protonation is not a solution for stabilization of high symmetric  $Si_x^{2-}$  clusters.

### 13-8. Conclusions

Well-resolved photoelectron spectra were obtained for  $Si_6^-$  and  $NaSi_6^-$  at three photon energies (355, 266, and 193 nm) and compared with theoretical calculations to elucidate the structure and bonding in  $Si_6^-$  and  $Si_6^{2-}$  in  $NaSi_6^-$ . Global minimum structures of  $Si_6^{2-}$  and  $NaSi_6^-$  were identified first by using Gradient Embedded Genetic Algorithm followed by B3LYP/6-311+G\*, MP2/6-311+G\* and CCSD(T)/6-311+G\* (except  $NaSi_6^-$ ) geometry and frequency calculations. By comparing the theoretical VDEs with the experimental data we established the ground state structure for  $NaSi_6^-$  to be  $C_{2v}$  ( $^1A_1$ ), in which the  $Na^+$  is coordinated to a  $C_{2v}$   $Si_6^{2-}$ . Though the octahedral  $Si_6^{2-}$ , analogous to the closo-form of borane  $B_6H_6^{2-}$ , is the most stable form for the bare dianion, it is not the kernel of the  $NaSi_6^-$  global minimum geometry. However, the octahedral  $Si_6^{2-}$  coordinated by a  $Na^+$  with  $C_{3v}$  ( $^1A_1$ ) symmetry is a low-lying isomer only 1.2 kcal/mol higher in energy and it was observed experimentally.

Chemical bonding analysis of the two low-lying  $O_h$  ( $^1A_{1g}$ ) and  $C_{2v}$  ( $^1A_1$ ) isomers of  $Si_6^{2-}$  revealed that they differ by switching one of the  $2t_{1u}$  triply degenerate HOMO ( $3b_1$  in the  $C_{2v}$  notation) with one of the  $1t_{2u}$  triply degenerate LUMO ( $4b_2$  in the  $C_{2v}$  notations). Because the  $2t_{1u}$  triply degenerate HOMO in the  $O_h$  ( $^1A_{1g}$ ) isomer contains

significant contribution from 3s-AOs of Si and the  $1t_{2u}$  triply degenerate LUMO composed of primarily 3p-AOs of Si, such MO exchange resulted in s-p promotion with increasing sp-hybridization and increase in Si-Si chemical bonding in the  $C_{2v}$  ( $^1A_1$ ) isomer. When the  $Na^+$  is attached to the  $Si_6^{2-}$  cluster in  $NaSi_6^-$  it more strongly stabilizes the  $4b_2$ -MO than the  $3b_1$ -MO, making the  $C_{2v}$  ( $^1A_1$ ) isomer of  $NaSi_6^-$  with the  $C_{2v}$  ( $^1A_1$ )  $Si_6^{2-}$  kernel somewhat more stable than the  $C_{3v}$  ( $^1A_1$ ) isomer of  $NaSi_6^-$  with the  $O_h$  ( $^1A_{1g}$ )  $Si_6^{2-}$  kernel.

## References

- <sup>1</sup> W. N. Lipscomb, *Boron Hydrides* (Benjamin, New York, 1963).
- <sup>2</sup> E. L. Muetterties, *Boron Hydride Chemistry* (Academic Press, New York, 1975).
- <sup>3</sup> F. A. Cotton, G. Wilkinson, C. A. Murillo, M. Bochman, *Advance Inorganic Chemistry*, 6<sup>th</sup> ed. (Wiley-Interscience, New York, 1999).
- <sup>4</sup> J. M. Goicoechea, S. C. Sevov, J. Am. Chem. Soc. **126**, 6860 (2004).
- <sup>5</sup> R. B. King, T. Heine, C. Cornminboeuf, P. v. R. Schleyer, J. Am. Chem. Soc. **126**, 430 (2004).
- <sup>6</sup> K. Raghavachari, V. Logovinsky, Phys. Rev. Lett. **55**, 2853 (1985).
- <sup>7</sup> G. Pacchioni, J. Koutecky, J. Chem. Phys. **84**, 3301 (1986).
- <sup>8</sup> B. P. Feuston, R. K. Kalia, P. Vashishta, Phys. Rev. B, **35**, 6222 (1987).
- <sup>9</sup> O. F. Sankey, D. J. Niklewski,, D. A. Drabold, J. D. Dow, **41**, 12750 (1990).
- <sup>10</sup> K. Raghavachari, C. M. Rohlfing, J. Chem. Phys. **94**, 3670 (1991).
- <sup>11</sup> N. Binggeli, J. L. Martins, J. R. Chelikowsky, Phys. Rev. Lett. **68**, 2956 (1992).
- <sup>12</sup> M. V. Ramakrishna, A. Bahel, J. Chem. Phys. **104**, 9833 (1996).

- <sup>13</sup> S. Wei, R. N. Barnett, U. Landman, *Phys. Rev. B* **55**, 7935 (1997).
- <sup>14</sup> B. X. Li, P. L. Cao, *Phys. Rev. B* **62**, 15788 (2000).
- <sup>15</sup> B. X. Li, P. L. Cao, B. Song, Z. Z. Ye, *Phys. Lett. A* **307**, 318 (2003).
- <sup>16</sup> C. Majumder, S. K. Kulshreshtha, *Phys. Rev. B* **69**, 115432 (2004).
- <sup>17</sup> L. A. Bloomfield, M. E. Geusic, R.R. Freeman, W. L. Brown, *Chem. Phys. Lett.* **121**, 33 (1985).
- <sup>18</sup> W. D. Reents, V. E. Bondybey, *Chem. Phys. Lett.* **125**, 324 (1986).
- <sup>19</sup> D. E. Bergeron, A. W. Castleman, Jr. *J. Chem. Phys.* **117**, 3219 (2002).
- <sup>20</sup> S. Li, R. J. V. Zee, W. Weltner, Jr., K. Raghavachari, *Chem. Phys. Lett.* **243**, 275 (1995).
- <sup>21</sup> E. C. Honea, A. Ogura, D. R. Peale, C. Felix, C. A. Murray, K. Raghavachari, W. O. Sprenger, M. F. Jarrold, W. L. Brown, *J. Chem. Phys.* **110**, 12161 (1999).
- <sup>22</sup> O. Chesnovsky, S. H. Yang, C. L. Pettiette, M. J. Craycraft, Y. Liu, R. E. Smalley, *Chem. Phys. Lett.* **138**, 119 (1987).
- <sup>23</sup> R. Kishi, H. Kawamata, Y. Negishi, S. Iwata, A. Nakajima, K. Kaya, *J. Chem. Phys.* **107**, 10029 (1997).
- <sup>24</sup> C. Xu, T. R. Taylor, G. R. Burton, D. M. Neumark, *J. Chem. Phys.* **108**, 1395 (1998).
- <sup>25</sup> M. A. Hoffmann, G. Wrigge, B. V. Issendorff, J. Muller, G. Gantefor, H. Haberland, *Eur. Phys. J. D* **16**, 9 (2001).
- <sup>26</sup> L. Kronik, R. Fromherz, E. Ko, G. Gantefor, J. R. Chelikowsky, *Eur. Phys. J. D* **24**, 33 (2003).
- <sup>27</sup> N. Binggeli, J. R. Chelikowsky, *Phys. Rev. Lett.* **75**, 493 (1995).
- <sup>28</sup> C. Zhao, K. Balasubramanian, *J. Chem. Phys.* **116**, 3690 (2002).

- <sup>29</sup> S.-D. Li, G.-M. Ren, Z.-H. Jin, *J. Chem. Phys.* **119**, 10063 (2003).
- <sup>30</sup> L. S. Wang, H. S. Cheng, J. Fan, *J. J. Chem. Phys.* **102**, 9480 (1995).
- <sup>31</sup> L. S. Wang, H. Wu, in *Advances in Metal and Semiconductor Clusters. IV. Cluster Materials*, Ed. by M. A. Duncan (JAI Press, Greenwich, 1998), p. 299.
- <sup>32</sup> A. N. Alexandrova, A. I. Boldyrev, Y.-J. Fu, X.-B. Wang, L.-S. Wang, *J. Chem. Phys.*, **121**, 5709 (2004).
- <sup>33</sup> A. N. Alexandrova, A. I. Boldyrev, *J. Chem. Theory Comput.* **1**, 566 (2005).
- <sup>34</sup> J. J. P. Stewart, *J. Comput. Chem.* **10**, 209 (1989).
- <sup>35</sup> J. J. P. Stewart, *J. Comput. Chem.* **10**, 221 (1989).
- <sup>36</sup> R. G. Parr, W. Yang, *Density-Functional Theory of Atoms and Molecules* (Oxford Univ. Press, Oxford, 1989).
- <sup>37</sup> A. D. Becke, *J. Chem. Phys.* **98**, 5648 (1993).
- <sup>38</sup> J. P. Perdew, J. A. Chevary, S. H. Vosko, K. A. Jackson, M. R. Pederson, D. J. Singh, C. Fiolhais, *Phys. Rev. B* **46**, 6671 (1992).
- <sup>39</sup> R. Krishnan, J. S. Binkley, R. Seeger, and J. A. Pople, *J. Chem. Phys.*, **72**, 650 (1980).
- <sup>40</sup> A. D. McLean and G. S. Chandler, *J. Chem. Phys.* **72**, 5639 (1980).
- <sup>41</sup> T. Clark, J. Chandrasekhar, G. W. Spitznagel, P. v. R. Schleyer, *J. Comput. Chem.* **4**, 294 (1983).
- <sup>42</sup> M. Head-Gordon, J. A. Pople, and M. J. Frisch, *Chem. Phys. Lett.* **153**, 503 (1988).
- <sup>43</sup> M. J. Frisch, M. Head-Gordon, and J. A. Pople, *Chem. Phys. Lett.* **166**, 275 (1990).
- <sup>44</sup> M. J. Frisch, M. Head-Gordon, and J. A. Pople, *Chem. Phys. Lett.* **166**, 281 (1990).
- <sup>45</sup> M. Head-Gordon and T. Head-Gordon, *Chem. Phys. Lett.* **220**, 122 (1994).

- <sup>46</sup> S Saebo and J. Almlöf, *Chem. Phys. Lett.* **154**, 83 (1989).
- <sup>47</sup> J. Cizek, *Adv. Chem. Phys.*, **14**, 35 (1969).
- <sup>48</sup> G. D. Purvis and R. J. Bartlett, *J. Chem. Phys.* **76**, 1910 (1982).
- <sup>49</sup> G. E Scuseria, C. L. Janssen, and H. F. Schaefer, III, *J. Chem. Phys.* **89**, 7382 (1988).
- <sup>50</sup> G. E Scuseria and H. F. Schaefer, III, *J. Chem. Phys.* **90**, 3700 (1989).
- <sup>51</sup> J. A. Pople, M. Head-Gordon, and K. Raghavachari, *J. Chem. Phys.* **87**, 5968 (1987).
- <sup>52</sup> C. Hampel, K. Peterson, H.-J. Werner, *Chem. Phys. Lett.* **190**, 1 (1992).
- <sup>53</sup> L. S. Cederbaum, *J. Phys B* **8**, 290 (1975).
- <sup>54</sup> V. G. Zakrzewski, J. V. Ortiz, *Int. J. Quant. Chem.* **53**, 583 (1995).
- <sup>55</sup> J. V. Ortiz, *Int. J. Quant. Chem.*, *Quant. Chem. Symp.* **23**, 321 (1989).
- <sup>56</sup> For a review see: J. V. Ortiz, V. G. Zakrzewski, O. Dolgunitcheva, *Conceptual Trends in Quantum Chemistry* **3**, 463 (1997).
- <sup>57</sup> Yu. Dahnovsky, V. G. Zakrzewski, A. Klesov, J. V. Ortiz, *J. Chem. Phys.* **123**, 184711 (2005).
- <sup>58</sup> R. Bauernshmitt, R. Alrichs, *Chem. Phys. Lett.* **256**, 454 (1996).
- <sup>59</sup> M. E. Casida, C. Jamorski, K. C. Casida, D. R. Salahub, *J. Chem. Phys.* **108**, 4439 (1998).
- <sup>60</sup> F. Weinhold, C. Landis, *Valency and Bonding. A Natural Bond Orbital Donor-Acceptor Perspective* (Cambridge University Press, Cambridge, UK, 2005).
- <sup>61</sup> A. D. Becke, K. E. Edgecombe, *J. Chem. Phys.* **92**, 5397 (1990).
- <sup>62</sup> A. Savin, B. Silvi, F. Colonna, *Can. J. Chem.* **74**, 1088 (1996).

- <sup>63</sup> A. Savin, R. Nesper, S. Wengert, T. F. Fassler, *Angew. Chem. Int. Ed. Engl.* **36**, 1808 (1997).
- <sup>64</sup> Gaussian 98 (revision A.7). M. J. Frisch, G. M. Trucks, H. B. Schlegel, G. E. Scuseria, M. A. Robb, J. R. Cheeseman, V. G. Zakrzewski, J. A. Montgomery, Jr., R. E. Stratmann, J. C. Burant, S. Dapprich, J. M. Millam, A. D. Daniels, K. N. Kudin, M. C. Strain, O. Farkas, J. Tomasi, V. Barone, M. Cossi, R. Cammi, B. Mennucci, C. Pomelli, C. Adamo, S. Clifford, J. Ochterski, G. A. Petersson, P. Y. Ayala, Q. Cui, K. Morokuma, D. K. Malick, A. D. Rabuck, K. Raghavachari, J. B. Foresman, J. Cioslowski, J. V. Ortiz, A. G. Baboul, B. B. Stefanov, G. Liu, A. Liashenko, P. Piskorz, I. Komaromi, R. Gomperts, R. L. Martin, D. J. Fox, T. Keith, M. A. Al-Laham, C. Y. Peng, A. Nanayakkara, C. Gonzales, M. Challacombe, P. M. W. Gill, B. G. Johnson, W. Chen, M. W. Wong, J. L. Andres, M. Head-Gordon, E. S. Replogle and J. A. Pople (Gaussian, Inc., Pittsburgh PA, 1998).
- <sup>65</sup> Gaussian 03 (revision A.1). M. J. Frisch, G. M. Trucks, H. B. Schlegel, G. E. Scuseria, M. A. Robb, J. R. Cheeseman, J. A. Montgomery, T. Vreven, K. N. Kudin, J. C. Burant, J. M. Millam, S. S. Iyengar, J. Tomasi, V. Barone, B. Mennucci, M. Cossi, G. Scalmani, N. Rega, G. A. Petersson, H. Nakatsuji, O. Kitao, H. Nakai, M. Klene, X. Li, J. E. Knox, H. P. Hratchian, J. B. Cross, C. Adamo, J. Jaramillo, R. Gomperts, R. E. Stratmann, O. Yazyev, A. J. Austin, R. Cammi, C. Pomelli, J. W. Ochterski, P. Y. Ayala, K. Morokuma, G. A. Voth, P. Salvador, J. J. Dannenberg, V. G. Zakrzewski, S. Dapprich, A. D. Daniels, M. C. Strain, O. Farkas, D. K. Malick, A. D. Rabuck, K. Raghavachari, J. B. Foresman, J. V. Ortiz, Q. Cui, A. G. Baboul, S. Clifford, J. Cioslowski, B. B. Stefanov, A. Liu, A. Liashenko, P. Piskorz, I. Komaromi, R. L.

- Martin, D. J. Fox, T. Keith, M. A. Al-Laham, C. Y. Peng, A. Nanayakkara, M. Challacombe, P. M. W. Gill, B. G. Johnson, W. Chen, M. W. Wang, C. Gonzales, and J. A. Pople (Gaussian, Inc., Pittsburgh, PA, 2003).
- <sup>66</sup> H.-J. Werner, P. J. Knowles, with contributions from R. D. Amos, A. Bernhardsson, A. Berning, P. Celani, D. L. Cooper, M. J. O. Deegan, A. J. Dobbyn, F. Eckert, C. Hampel, G. Hetzer, T. Korona, R. Lindh, A. W. Lloyd, S. J. McNicholas, F. R. Manby, W. Meyer, M. E. Mura, A. Nicklass, P. Palmieri, R. Pitzer, G. Rauhut, M. Schutz, H. Stoll, A. J. Stone, R. Tarroni, T. Thorsteinsson, *MOLPRO-2000.1*.
- <sup>67</sup> S. Noury, X. Krokidis, F. Fuster, B. Silvi, TopMod Package, Universite Pierre et Marie Curie, **1997**; *Comp. Chem.* **1999**, *23*, 597.
- <sup>68</sup> MOLEKEL, Version 4.3. Stefan Portmann, CSCS/ETHZ (2002).
- <sup>69</sup> MOLDEN3.4. Schaftenaar, G. MOLDEN3.4, CAOS/CAMM Center, The Netherlands (1998).
- <sup>70</sup> A. I. Boldyrev, L. S. Wang, *J. Phys. Chem. A*, **105**, 10759 (2001).
- <sup>71</sup> A. I. Boldyrev, L. S. Wang, *Chem. Rev.*, **105**, 3716 (2005).
- <sup>72</sup> H.-J. Zhai, A. E. Kuznetsov, A. I. Boldyrev, L. S. Wang, *ChemPhysChem*, **5**, 1885 (2004).
- <sup>73</sup> D. Yu. Zubarev, A. I. Boldyrev, X. Li, L.-F. Cui, L. S. Wang, *J. Phys. Chem. A* **109**, 11385 (2005)



CHAPTER 14  
APPRAISAL OF THE PERFORMANCE OF NONHYBRID DENSITY  
FUNCTIONAL METHODS IN CHARACTERIZATION  
OF THE  $\text{Al}_4\text{C}$  MOLECULE<sup>1</sup>

**Abstract**

In three recent publications it was predicted that an  $\text{Al}_4\text{C}$  molecule is planar on the basis of nonhybrid density functional calculations. These conclusions contradict our earlier predictions that  $\text{Al}_4\text{C}$  is tetrahedral. In order to resolve the controversy we probed in this paper a potential energy surface of  $\text{Al}_4\text{C}$  using a large variety of theoretical methods including multiconfigurational methods and a variety of one-electron basis sets. We confirmed that the nonhybrid Becke's exchange with Perdew–Wang 1991 correlation functional density functional method predicts that  $\text{Al}_4\text{C}$  has a planar structure in agreement with the reports of the other three groups. However, in this paper we have shown that high level *ab initio* calculations at the coupled cluster with singles, doubles, and noniterative triples and at the complete active space self-consistent field followed by multireference configurational interaction levels of theory confirm our earlier prediction that  $\text{Al}_4\text{C}$  is indeed tetrahedral. The failure of nonhybrid density functional methods to correctly characterize the global minimum structure of  $\text{Al}_4\text{C}$  demonstrates that it is dangerous to rely solely on these density functional methods in characterization of new molecules and clusters, where experimental structure is not known.

---

<sup>1</sup> Coauthored by Dmitry Yu. Zubarev and Alexander I. Boldyrev. Reproduced with permission from *J. Chem. Phys.* **2005**, 122, 144322. Copyright 2005, American Institute of Physics.

### 14-1. Introduction

In quantum chemical characterization of new molecules and clusters density functional theory (DFT) is frequently a convenient choice. In this paper we present evidence that some nonhybrid DFT methods predict an incorrect global minimum structure of  $\text{Al}_4\text{C}$ . In 1999 we published a combined theoretical and experimental work,<sup>1</sup> where we characterized a  $\text{Al}_4\text{C}^-$  anion. On the basis of the extensive search, we concluded that the  $\text{Al}_4\text{C}^-$  anion has an almost planar structure ( $D_{2d}$ ,  $^2B_1$ ) with the inversion barrier through the planar structure ( $D_{4h}$ ,  $^2B_{2g}$ ) being 0.14 kcal/mol. Thus, when zero-point vibration motion is included, the vibrationally averaged structure is actually planar. In that paper we also concluded that a neutral  $\text{Al}_4\text{C}$  molecule is tetrahedral on the basis of Becke's three parameter hybrid functional using the Lee–Yang–Parr correlation functional (B3LYP), secondorder Moller–Plesset perturbation theory (MP2), and coupled cluster with singles, doubles, and noniterative triples [CCSD(T)] calculations, all with the 6-311+G\* basis sets. Our theoretical prediction was supported by a long tail in the experimental lowest electron detachment feature  $X$  in the photoelectron spectrum of  $\text{Al}_4\text{C}^-$ , which confirms a large geometry change from the quasiplanar structure of  $\text{Al}_4\text{C}^-$  to the tetrahedral structure of  $\text{Al}_4\text{C}$ . However, our conclusions on the tetrahedral structure of  $\text{Al}_4\text{C}$  molecule and the perfect square ( $D_{4h}$ ) or quasiplanar almost square structure of  $\text{Al}_4\text{C}^-$  were questioned by four different groups.<sup>2–5</sup>

Ashman, Khanna, and Pederson predicted<sup>2</sup> that  $\text{Al}_4\text{C}$  has a planar singlet  $C_{2v}$  structure [we call it  $C_{2v}$ , I in Fig. 14-1(c)]. Their calculations have been carried out using a nonhybrid density functional formalism. The molecular orbitals were formed from a linear combination of atomic orbitals, which were expanded as a sum of partially

contracted Gaussian functions located at the atomic sites. A gradient-corrected density functional proposed by Perdew, Burke, and Ernzerhof has been used to incorporate the exchange correlation effects. The calculations were carried out at the all-electron level and the multicenter integrals required to solve the Kohn–Sham equation were calculated by integrating numerically over a mesh of points. All the basis sets used in their paper have been previously optimized for density functional calculations. The basis sets consisted of  $6s$ ,  $5p$ , and  $3d$  Gaussians for Al and  $5s$ ,  $4p$ , and  $3d$  Gaussians for C. They started the search for the global minimum structure using several geometries, which were minimized by a conjugate gradient approach without any symmetry restrictions. They also probed several spin multiplicities. From these calculations they concluded that the global minimum structure is the singlet planar  $C_{2v}$ , I structure. They also reported that the tetrahedral structure was found to be 0.09 eV (2.1 kcal/mol) above the planar structure.

Rao and Jena predicted<sup>3</sup> two nearly degenerate isomers for  $Al_4C$ . A planar singlet  $C_{2v}$  structure [we call it  $C_{2v}$ , II in Fig. 14-1(e)] and a tetrahedral isomer [ $T_d$  in Fig. 14-1(a)]. We would like to stress that the planar structure  $C_{2v}$ , II reported by Rao and Jena<sup>3</sup> is different from the planar structure  $C_{2v}$ , I reported by Ashman, Khanna, and Pederson.<sup>2</sup> Rao and Jena also used the DFT method and the generalized gradient approximations (GGA) for the exchange correlation functional due to Becke, Perdew, and Wang (commonly referred to as BPW91) and they used a few basis sets: frozen core orbitals (LanL2DZ basis), all-electron basis (6-311G\*\*), and 6-311G\*\* basis with added diffuse functions. Rao and Jena also used geometry optimization without any symmetry restrictions for various multiplicities and for different random starting configurations.

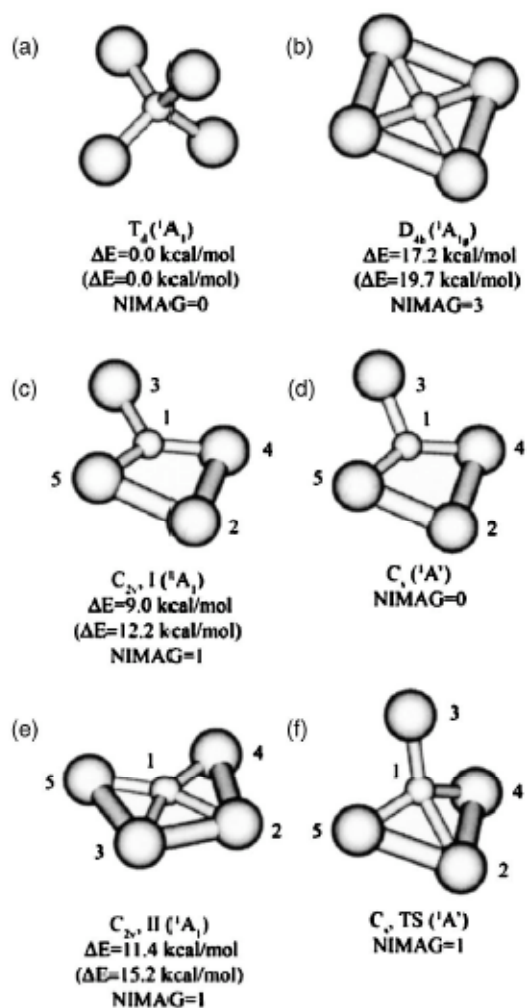


Figure 14-1. Optimized alternative structure of an  $Al_4C$  molecule. Relative energies are given at the CCSD(T)/6-311+G(2df)//CCSD(T)/6-311+G\* and at the CASSCF(8,10)-MRCISD(Q)/6-311+G\* levels of theory (in parentheses). NIMAG is the number of imaginary frequencies.

They found that the tetrahedral structure is more stable by 7.0 kcal/mol at BPW91/Lan12DZ basis set and by 0.2 kcal/mol at BPW91/6-311+ +G\*\* than the planar structure. However, the planar structure was found to be 0.15 kcal/mol more stable than the tetrahedral structure at BPW91/6-311G\*\*. Rao and Jena concluded that these energy differences are too small to be meaningful at this level of theory and it is, therefore, safe to conclude that the ground state of neutral  $\text{Al}_4\text{C}$  has two nearly degenerate structures, distorted tetrahedral and the planar.

Li and Gong also predicted<sup>5</sup> that  $\text{Al}_4\text{C}$  has a planar structure [ $\text{C}_{2v}$ , II in Fig. 14-1(e)] similar to what was previously reported by Rao and Jena. They used a DFT method with the spin-polarized GGA implemented in the Vienna *ab initio* simulation package. The wave functions were expanded in a plane wave basis with an energy cutoff of 286 eV. The atomic positions were optimized by conjugated gradient method with the energy convergence up to 0.005 eV. They used a large supercell with a lattice constant 14 Å in order to make interaction between the cluster and its periodic images negligible. The Vanderbilt ultrasoft pseudopotential was used to describe the interaction between the core and valence electrons. Only the G point was used in the summation of the Brillouin zone of the simulation cell. They mentioned in their search procedure that they used many initial structures with high and low symmetry. Additional structures with the atom positions randomly displaced also have been added. The conjugated gradient and simulated annealing methods have been used in search for the global minimum. Li and Gong<sup>5</sup> reported only one structure for  $\text{Al}_4\text{C}^-$  the singlet planar  $\text{C}_{2v}$ , II structure. Thus, four different groups reported that the  $\text{Al}_4\text{C}$  molecule has either the planar structure [ $\text{C}_{2v}$ , I (Ref. 2) or  $\text{C}_{2v}$ , II (Ref. 5)] or planar ( $\text{C}_{2v}$ , II) and tetrahedral structure with almost

degenerate energies<sup>3</sup> and that the  $\text{Al}_4\text{C}^-$  anion has a carbon-centered planar trapeziform structure of  $\text{Al}_4\text{C}^-$ .<sup>2-5</sup> These results contradict our conclusion<sup>1</sup> that the tetrahedral structure of  $\text{Al}_4\text{C}$  is in fact the global minimum structure and that the  $\text{Al}_4\text{C}^-$  anion has a vibrationally averaged  $D_{4h}$  planar structure. We noticed that in the four published papers, the authors used nonhybrid DFT methods and we decided to check if their disagreement with our results could be due to failure of these DFT methods to correctly describe an  $\text{Al}_4\text{C}$  potential energy surface. In this paper we present our extensive study of  $\text{Al}_4\text{C}$  using a variety of theoretical methods and our conclusion is that our previous statement, the  $\text{Al}_4\text{C}$  has a tetrahedral structure, is correct. Also, the reason why three other groups predicted a planar structure for this molecule is indeed due to inherent problems in the nonhybrid DFT methods that were used.

## 14-2. Theoretical Methods

In order to avoid human bias, we initially performed the search for the global minimum of the  $\text{Al}_4\text{C}$  molecule using an *ab initio* gradient embedded genetic algorithm (GEGA) program recently written in our group by Alexandrova.<sup>6</sup> The hybrid method, known as B3LYP,<sup>7-9</sup> with relatively small basis set 3-21G was employed throughout the execution of the GEGA. Briefly, within the GEGA procedure, the initial geometries of individuals in the population are randomly generated and further optimized to the nearest local minima on the potential energy surface, using the GAUSSIAN03 package.<sup>10</sup> If a saddle point is encountered the normal mode of the first imaginary frequency is followed until a local minimum is found. Further, the population, composed of the thus selected good individuals, undergoes breeding and mutations. The mating, implemented in

GEGA, is performed based on the robust technique originally proposed in 1995 by Deaven and Ho.<sup>11</sup> Probabilities to be bred are assigned according to the best-fit lowest-energy criterion. Based on the probabilities, couples of parents are randomly selected. The geometries of parents are cut by a random cutting plane, and the thus obtained halves are then recombined either in a simple or in a head-to-tail manner to form a new cluster (child). The number of atoms in the newly generated geometry is checked, and the new cluster is optimized to the nearest local minimum. After the number of individuals in the population is doubled within the breeding process, the best-fit group is selected and convergence of the algorithm is checked. The GEGA is considered converged if the current lowest-energy species is global minimum or at least very stable local minimum remains for 20 iterations. If the convergence is not yet met, the highest-energy species in the population undergo mutations with a mutation rate set to 33.33%. Mutations involve displacements of random atoms of a cluster in arbitrary directions, with the purpose of changing the initial geometry so as to push the structure out of the current local minimum to another well on the potential energy surface. Mutants are optimized to the nearest local minima. After that the algorithm proceeds with the new cycle of breeding. All low-lying isomers are detected and stored throughout the execution and they are reported to the user at the end of the run. A few runs of GEGA are done on the system in order to confirm the found global minimum structure.

The geometry and vibrational frequencies of the thus identified global minimum, as well as low-lying isomers, were further recalculated at higher levels of theory. The following set of theoretical methods have been employed: B3LYP/6-311+G\*, B3LYP/aug-cc-pvDZ, B3LYP/aug-cc-pvTZ, B3LYP/aug-cc-pvQZ, BPW91/6-311+G\*,

BPW91/aug-cc-pvDZ, BPW91/aug-cc-pvTZ, BPW91/aug-cc-pvQZ, MP2/6-311+G\*, CCSD(T)/6-311+G\*, and CCSD(T)/aug-cc-pvDZ. Single point energy calculations have been performed at CCSD(T)/aug-cc-pvTZ using the CCSD(T)/aug-cc-pv-DZ geometry [CCSD(T)/aug-cc-pvTZ//CCSD(T)/aug-cc-pv-DZ] and at the complete active space self-consistent field followed by multireference configurational interaction [CASSCF(8,10)-MRCISD(Q)/6-311+G\*] using the CCSD(T)/6-311+G\* geometry. The 6-311+G\* and 6-311+G(2*df*) basis sets were described in Refs. 12–15 and aug-cc-pvDZ, aug-cc-pvTZ, and aug-cc-pvQZ basis sets were described in Refs. 16–20. For a description of the nonhybrid density functional method BPW91 see Refs. 21 and 22. The description of the MP2 method can be found in Refs. 23–27. The coupled cluster CCSD(T) method was described in Refs. 28–32. The description of the CASSCF method can be found in Refs. 33–38. The number of electrons  $N$  and the number of orbitals  $M$  in the active space for CASSCF is specified following the keyword: CASSCF( $N,M$ ). Finally, the CASSCF( $N,M$ )-MRCISD(Q) method was described in Refs. 39 and 40.

Molecular orbitals were calculated at the RHF/6-311+G\* level of theory. RHF, B3LYP, BPW91, CCSD(T), and CASSCF( $N,M$ ) calculations were performed using GAUSSIAN03. The CASSCF( $N,M$ )-MRCISD(Q) calculations were done using the MOLPRO 2000.1 program.<sup>41</sup>

### 14-3. Results of Calculations and Discussion

Our GEGA search using the B3LYP/3-21G level of theory revealed only two singlet low-lying local minima: the tetrahedral structure ( $T_d$ , Fig. 14-1(a)] and the planar [ $C_{2v}$ , I, Fig. 14-1(c)]. The  $T_d$  structure was found to be the global minimum structure



with the  $C_{2v}$ , I structure being 15.1 kcal/mol higher in energy. That is because on the top of the gradient optimization procedure without any symmetry restrictions, GEGA runs frequency calculations for every optimized structure and it continues the optimization procedure further following imaginary frequency modes until it finds a true local minimum.

We then continued our study of  $Al_4C$  using the two local minima we found from the GEGA calculations:  $T_d$  ( ${}^1A_1, 1a_1^2 1t_2^6 2a_1^2 2t_2^6 1e^0$ );  $C_{2v}$ , I ( ${}^1A_1, 1a_1^2 2a_1^2 1b_2^2 3a_1^2 1b_1^2 2b_2^2 4a_1^2 5a_1^2 3b_2^0$ ); and two additional,  $D_{4h}$  ( ${}^1A_{1g}, 1a_{1g}^2 1e_u^4 2a_{1g}^2 1a_{2u}^2 1b_{1g}^2 2e_u^4 1b_{2g}^0$ ) and  $C_{2v}$ , II ( ${}^1A_1, 1a_1^2 1b_2^2 2a_1^2 3a_1^2 1b_1^2 2b_2^2 4a_1^2 3b_2^2 5a_1^0$ ), structures discussed in previous publications. For these four structures we used a variety of methods described in Sec. 14-2. Results of our calculations are summarized in Fig. 14-1 and Tables 14-1 – 14-5.

First, we performed calculations at the B3LYP level of theory using 6-311+G\*, aug-cc-pvDZ, aug-cc-pvTZ, and aug-cc-pvQZ basis sets. Our results at these four levels of theory were found to be in a good qualitative agreement with the B3LYP/3-21G results. At all four levels of theory we found only two local minima corresponding to the  $T_d$  ( ${}^1A_1$ ) and  $C_{2v}$ , I ( ${}^1A_1$ ) structures.  $T_d$  ( ${}^1A_1$ ) is the global minimum at these levels of theory with the planar  $C_{2v}$ , I ( ${}^1A_1$ ) structure being 7–9 kcal/mol higher in energy. The planar square  $D_{4h}$  ( ${}^1A_{1g}$ ) is a third-order saddle point at all four levels of theory as well as at the B3LYP/3-21G level of theory. The  $D_{4h}$  ( ${}^1A_{1g}$ ) structure was found to be 16–17 kcal/mol higher in energy than the  $T_d$  ( ${}^1A_1$ ) structure. The geometry optimization of the  $D_{4h}$  ( ${}^1A_{1g}$ ) structure following the doubly degenerate imaginary frequency [ $\omega_7(e_u)$ ] mode leads to the planar  $C_{2v}$ , II ( ${}^1A_1$ ) structure and following the nondegenerate imaginary frequency [ $\omega_5(b_{2u})$ ] mode leads to the tetrahedral structure  $T_d$  ( ${}^1A_1$ ). The planar  $C_{2v}$ , II

( $^1A_1$ ) structure reported as the global minimum structure by Rao and Jena and by Li and Gong was found to be a first-order saddle point 9–11 kcal/mol higher in energy than the  $T_d$  ( $^1A_1$ ) structure. The geometry optimization of the planar  $C_{2v}$ , II ( $^1A_1$ ) structure following the nondegenerate imaginary frequency [ $\omega_9(b_2)$ ] mode leads to the planar structure  $C_{2v}$ , I ( $^1A_1$ ).

Table 14-1. Calculated molecular properties of the  $T_d$  ( $^1A_1$ ) structure of  $Al_4C$ .

Method	B3LYP/ 6-311+G*	B3LYP/ aug-cc- pvqz	MP2/ 6-311+G*	CCSD(T)/ 6- 311+G** <sup>a,b</sup>	CCSD(T)/ aug-cc- pvdz <sup>c</sup>	BPW91/ 6-311+G*	BPW91/ aug-cc- pvqz
$-E_{tot}$ , a.u.	1007. 868295	1007. 904417	1005. 848076	1005. 914193	1005. 904173	1007. 793739	1007. 827974
$\Delta E$ , kcal/mol <sup>d</sup>	0.0	0.0	0.0	0.0	0.0	0.0	0.0
R(C-Al), Å	2.010	1.998	2.003	1.999	2.040	2.021	2.009
$\omega_1(a_1)$ , $cm^{-1}$	350 (0.0) <sup>e</sup>	350 (0.0) <sup>e</sup>	359 (0.0) <sup>e</sup>	363	342	340 (0.0) <sup>e</sup>	342 (0.0) <sup>e</sup>
$\omega_2(e)$ , $cm^{-1}$	97 (0.0) <sup>e</sup>	92 (0.0) <sup>e</sup>	96 (0.0) <sup>e</sup>	95	97	83 (0.0) <sup>e</sup>	76 (0.0) <sup>e</sup>
$\omega_3(t_2)$ , $cm^{-1}$	610 (246.2) <sup>e</sup>	608 (239.9) <sup>e</sup>	637 (268.8) <sup>e</sup>	640	590	590 (217.7) <sup>e</sup>	593 (212.7) <sup>e</sup>
$\omega_4(t_2)$ , $cm^{-1}$	170 (10.1) <sup>e</sup>	166 (10.0) <sup>e</sup>	175 (12.2) <sup>e</sup>	175	162	154 (9.2) <sup>e</sup>	148 (9.0) <sup>e</sup>

<sup>a</sup>  $E_{tot} = -1005.899090$  a.u. at the CASSCF(8,10)-MRCISD(Q)/6-311+G\*//CCSD(T)/6-311+G\* level of theory;  $E_{tot} = -1005.851570$  a.u. at the CASSCF(8,10)-MRCISD/6-311+G\*//CCSD(T)/6-311+G\* level of theory.

<sup>b</sup>  $E_{tot} = -1005.969079$  a.u. at the CCSD(T)/6-311+G(2df)//CCSD(T)/6-311+G\* level of theory.

<sup>c</sup>  $E_{tot} = -1005.994426$  a.u. at the CCSD(T)/aug-cc-pvtz//CCSD(T)/aug-cc-pvdz level of theory.

<sup>d</sup> Relative to the tetrahedral structure. Relative energies corrected for zero-point energy.

<sup>e</sup> Infrared intensities (km/mol) are given in parenthesis.

In order for the second local minimum, corresponding to the structure  $C_{2v}$ , I ( $^1A_1$ ), to be a viable isomer it should be separated by a high barrier from the global minimum  $T_d$  ( $^1A_1$ ) structure. We found a saddle point on the intramolecular rearrangement  $C_{2v}$ , I ( $^1A_1$ )  $\rightarrow$   $T_d$  ( $^1A_1$ ). The calculated barrier was found to be 3.7 and 3.2 kcal/mol when not including and including, respectively, the zero point energy (ZPE) correction (all at B3LYP/6-311+G\*). The transition state structure has a  $C_s$  ( $^1A'$ ) geometry [Fig. 14-1(f)],

Table 14-2. Calculated molecular properties of the  $D_{4h}$  ( $^1A_{1g}$ ) structure of  $Al_4C$ .

Method	B3LYP/ 6-311+G*	B3LYP/ aug-cc-pvqz	MP2/ 6-311+G*	CCSD(T)/ 6-311+G* <sup>a,b</sup>	CCSD(T)/ aug-cc-pvdz <sup>c</sup>
$-E_{tot}$ , a.u.	1007.838190	1007.876556	1005.816996	1005.882368	1005.873442
$\Delta E$ , kcal/mol <sup>d</sup>	17.1	15.7	17.7	18.2	17.6
R(C-Al), Å	2.034	2.024	2.033	2.029	2.078
$\omega_1(a_{1g})$ , $cm^{-1}$	345 (0.0) <sup>e</sup>	347 (0.0) <sup>e</sup>	354 (0.0) <sup>e</sup>	359	332
$\omega_2(a_{2u})$ , $cm^{-1}$	238 (0.4) <sup>e</sup>	232 (7.8) <sup>e</sup>	115 (5.1) <sup>e</sup>	118	208
$\omega_3(b_{1g})$ , $cm^{-1}$	232 (0.0) <sup>e</sup>	236 (0.0) <sup>e</sup>	252 (0.0) <sup>e</sup>	257	225
$\omega_4(b_{2g})$ , $cm^{-1}$	138 (0.0) <sup>e</sup>	140 (0.0) <sup>e</sup>	175 (0.0) <sup>e</sup>	186	174
$\omega_5(b_{2u})$ , $cm^{-1}$	65i	65i	92i	95i	71i
$\omega_6(e_u)$ , $cm^{-1}$	322 (17.0) <sup>e</sup>	326 (14.7) <sup>e</sup>	404 (34.2) <sup>e</sup>	408	351
$\omega_7(e_u)$ , $cm^{-1}$	479i	496i	223i	217i	250i

<sup>a</sup>  $E_{tot} = -1005.867751$  a.u. at the CASSCF(8,10)-MRCISD(Q)/6-311+G\*//CCSD(T)/6-311+G\* level of theory;  $E_{tot} = -1005.817351$  a.u. at the CASSCF(8,10)-MRCISD/6-311+G\*//CCSD(T)/6-311+G\* level of theory.

<sup>b</sup>  $E_{tot} = -1005.941679$  a.u. at the CCSD(T)/6-311+G(2df)//CCSD(T)/6-311+G\* level of theory.

<sup>c</sup>  $E_{tot} = -1005.966481$  a.u. at the CCSD(T)/aug-cc-pvtz//CCSD(T)/aug-cc-pvdz level of theory.

<sup>d</sup> Relative to the tetrahedral structure. Relative energies corrected for zero-point energy.

<sup>e</sup> Infrared intensities (km/mol) are given in parenthesis.

which is almost in between the two geometries of the  $C_{2v}$  I ( $^1A_1$ ) and the  $T_d$  ( $^1A_1$ ) structures. Thus, the second  $C_{2v}$  I ( $^1A_1$ ) isomer should have a rather short lifetime.

Then, we studied the same four structures using the nonhybrid BPW91 method with the same set of basis sets: using 6-311+G\*, aug-cc-pvDZ, aug-cc-pvTZ, and aug-cc-pvQZ basis sets (see Tables 14-I – 14-4). At this level of theory we have found three structures corresponding to three local minima:  $T_d$  ( $^1A_1$ ),  $C_{2v}$  I ( $^1A_1$ ),  $C_{2v}$  II ( $^1A_1$ ). We were not able to reach convergence at any of these levels of theory for the planar  $D_{4h}$  ( $^1A_{1g}$ ) structure. The planar  $C_{2v}$  I ( $^1A_1$ ) was found to be the global minimum at the BPW91/6-311+G\*, BPW91/augcc-pvDZ, BPW91/aug-cc-pvTZ, and BPW91/aug-cc-pvQZ levels of theory. The tetrahedral structure was found to be only slightly above the  $C_{2v}$  I ( $^1A_1$ ) structure: 0.3 kcal/mol (BPW91/6-311+G\*), 1.4 kcal/mol (BPW91/aug-cc-pvDZ), 1.5 kcal/mol (BPW91/aug-cc-pvTZ), and 1.5 kcal/mol (BPW91/aug-cc-pvQZ).

Table 14-3. Calculated molecular properties of the  $C_{2v,I}$ , ( $^1A_1$ ) structure of  $Al_4C$ .

Method	B3LYP/ 6-311+G*	B3LYP/ aug-cc- pvqz	MP2/ 6-311+G*	CCSD(T)/ 6-311+G* <sup>a,b</sup>	CCSD(T)/ aug-cc- pvdz <sup>c</sup>	BPW91/ 6-311+G*	BPW91/ aug-cc- pvqz
$-E_{tot}$ , a.u.	1007. 85497	1007. 89310	1005. 83295	1005. 89205	1005. 88642	1007. 79456	1007. 83071
$\Delta E$ , kcal/mol <sup>d</sup>	8.4	7.2	9.3	13.6	11.1	-0.3	-1.5
$R(C-Al_2)$ , Å	2.702	2.688	2.693	2.593	2.748	2.713	2.699
$R(C-Al_3)$ , Å	1.956	1.947	1.962	1.960	1.998	1.963	1.954
$R(C-Al_{4,5})$ , Å	1.914	1.906	1.930	1.928	1.956	1.927	1.918
$\angle Al_2CA_{4,5}$ , degrees	67.4	67.5	65.9	69.2	67.2	66.3	66.5
$\omega_1(a_1)$ , cm <sup>-1</sup>	731 (473.6) <sup>e</sup>	736 (473.7) <sup>e</sup>	761 (526.9) <sup>e</sup>	732	695	722 (351.6) <sup>e</sup>	726 (355.3) <sup>e</sup>
$\omega_2(a_1)$ , cm <sup>-1</sup>	392 (10.8) <sup>e</sup>	395 (10.2) <sup>e</sup>	394 (17.9) <sup>e</sup>	395	372	386 (8.5) <sup>e</sup>	389 (8.0) <sup>e</sup>
$\omega_3(a_1)$ , cm <sup>-1</sup>	255 (4.2) <sup>e</sup>	257 (4.1) <sup>e</sup>	266 (3.1) <sup>e</sup>	252	250	267 (3.2) <sup>e</sup>	268 (3.0) <sup>e</sup>
$\omega_4(a_1)$ , cm <sup>-1</sup>	112 (12.5) <sup>e</sup>	110 (13.1) <sup>e</sup>	144 (6.8) <sup>e</sup>	119	119	120 (5.9) <sup>e</sup>	117 (6.4) <sup>e</sup>
$\omega_5(b_1)$ , cm <sup>-1</sup>	218 (4.7) <sup>e</sup>	211 (1.9) <sup>e</sup>	130 (5.3) <sup>e</sup>	121	176	201 (4.4) <sup>e</sup>	195 (1.6) <sup>e</sup>
$\omega_6(b_1)$ , cm <sup>-1</sup>	51 (0.1) <sup>e</sup>	51 (0.2) <sup>e</sup>	100i	85i	47	52 (0.1) <sup>e</sup>	49 (0.3) <sup>e</sup>
$\omega_7(b_2)$ , cm <sup>-1</sup>	793 (23.1) <sup>e</sup>	801 (22.4) <sup>e</sup>	779 (22.6) <sup>e</sup>	787	742	766 (13.3) <sup>e</sup>	774 (13.2) <sup>e</sup>
$\omega_8(b_2)$ , cm <sup>-1</sup>	262 (20.6) <sup>e</sup>	266 (21.1) <sup>e</sup>	312 (8.6) <sup>e</sup>	279	263	282 (14.0) <sup>e</sup>	284 (14.2) <sup>e</sup>
$\omega_9(b_2)$ , cm <sup>-1</sup>	105 (2.0) <sup>e</sup>	102 (2.1) <sup>e</sup>	75 (1.6) <sup>e</sup>	88	99	81 (2.3) <sup>e</sup>	75 (2.4) <sup>e</sup>

<sup>a</sup>  $E_{tot}=-1005.879573$  a.u. at the CASSCF(8,10)-MRCISD(Q)/6-311+G\*//CCSD(T)/6-311+G\* level of theory;  $E_{tot}=-1005.828057$  a.u. at the CASSCF(8,10)-MRCISD/6-311+G\*//CCSD(T)/6-311+G\* level of theory.

<sup>b</sup>  $E_{tot}=-1005.954798$  a.u. at the CCSD(T)/6-311+G(2df)//CCSD(T)/6-311+G\* level of theory.

<sup>c</sup>  $E_{tot}=-1005.979732$  a.u. at the CCSD(T)/aug-cc-pvtz//CCSD(T)/aug-cc-pvdz level of theory.

<sup>d</sup> Relative to the tetrahedral structure. Relative energies corrected for zero-point energy.

<sup>e</sup> Infrared intensities (km/mol) are given in parenthesis.

Finally, the second planar structure  $C_{2v}$ , II ( ${}^1A_1$ ) was also found to be slightly higher in energy than the  $C_{2v}$ , I ( ${}^1A_1$ ) structure at these levels of theory: 0.7 kcal/mol (BPW91/6-311+G\*), 1.4 kcal/mol (BPW91/aug-cc-pvDZ), 0.5 kcal/mol (BPW91/aug-cc-pvTZ), 0.4 kcal/mol (BPW91/aug-cc-pvQZ). Thus, our findings using the nonhybrid DFT (BPW91) method generally agree with the previous DFT results reported by three other groups. However, they do not agree with our results with the hybrid DFT method (B3LYP).

As the next step we performed calculations using conventional *ab initio* methods such as MP2/6-311+G\*, CCSD(T)/6-311+G\*, and CCSD(T)/aug-cc-pvDZ. At these three levels of theory we found the  $T_d$  ( ${}^1A_1$ ) structure to be the global minimum structure. The planar  $C_{2v}$ , I ( ${}^1A_1$ ) structure was found to be a local minimum at the CCSD(T)/aug-cc-pvDZ level of theory being 11.1 kcal/mol higher in energy than the tetrahedral structure. It is, however, a first-order saddle point at the MP2/6-311+G\* and CCSD(T)/6-311+G\* levels of theory. Geometry optimization following the  $\omega_6(b_1)$  imaginary frequency mode ended up at the  $C_s$  ( ${}^1A'$ ) structure [Fig. 14-1(d) and Table 14-5], which is only slightly nonplanar. The barrier for planarity is 0.16 kcal/mol (MP2/6-311+G\*) and 0.14 kcal/mol [CCSD(T)/6-311+G\*] which is smaller than the difference in ZPE corrections between the planar  $C_{2v}$ , I ( ${}^1A_1$ ) and the quasiplanar  $C_s$  ( ${}^1A'$ ) structures: 0.22 kcal/mol (MP2/6-311+G\*) and 0.21 kcal/mol [CCSD(T)/6-311+G\*]. Therefore, when zero-point vibrational motion is considered, the vibrationally averaged structure is actually planar at these two levels of theory. The recalculated energy of the structure  $C_s$  ( ${}^1A'$ ) at the CCSD(T)/6-311+G(2df)//CCSD(T)/6-311+G\* level of theory was a little bit higher (0.2 kcal/mol) than the planar structure at the same level of theory. The deviation

Table 14-4. Calculated molecular properties of the  $C_{2v}, II, (^1A_1)$  structure of  $Al_4C$ .

Method	B3LYP/ 6-311+G*	B3LYP/ aug-cc- pvqz	MP2/ 6-311+G*	CCSD(T)/ 6- 311+G* <sup>a,b</sup>	CCSD(T)/ aug-cc- pvdz <sup>c</sup>	BPW91/ 6-311+G*	BPW91/ aug-cc- pvqz
$-E_{tot}$ , a.u.	1007. 851317	1007. 889884	1005. 827658	1005. 888292	1005. 880154	1007. 793453	1007. 830121
$\Delta E$ , kcal/mol <sup>d</sup>	10.5	9.0	12.6	15.7	14.7	0.4	-1.1
$R(C-Al_{2,3})$ , Å	2.135	2.123	2.167	2.129	2.188	2.147	2.137
$R(C-Al_{4,5})$ , Å	1.926	1.918	1.928	1.936	1.969	1.934	1.926
$\angle Al_2CA1_3$ , degrees	73.9	74.1	70.4	74.5	74.1	76.7	72.8
$\angle Al_4CA1_5$ , degrees	123.0	122.8	132.9	121.2	121.7	128.2	128.0
$\omega_1(a_1)$ , $cm^{-1}$	649 (351.7) <sup>e</sup>	654 (342.8) <sup>e</sup>	650 (495.4) <sup>e</sup>	658	611	639 (302.8) <sup>e</sup>	644 (296.3) <sup>e</sup>
$\omega_2(a_1)$ , $cm^{-1}$	370 (10.1) <sup>e</sup>	373 (10.2) <sup>e</sup>	380 (5.0) <sup>e</sup>	372	347	373 (7.0) <sup>e</sup>	376 (7.5) <sup>e</sup>
$\omega_3(a_1)$ , $cm^{-1}$	301 (11.4) <sup>e</sup>	306 (11.7) <sup>e</sup>	359 (17.0) <sup>e</sup>	296	281	328 (8.8) <sup>e</sup>	331 (8.9) <sup>e</sup>
$\omega_4(a_1)$ , $cm^{-1}$	174 (0.0) <sup>e</sup>	175 (0.1) <sup>e</sup>	169 (13.4) <sup>e</sup>	154	148	186 (1.5) <sup>e</sup>	188 (1.5) <sup>e</sup>
$\omega_5(a_2)$ , $cm^{-1}$	71 (0.0) <sup>e</sup>	71 (0.0) <sup>e</sup>	87 (0.0) <sup>e</sup>	42	58	85 (0.0) <sup>e</sup>	85 (0.0) <sup>e</sup>
$\omega_6(b_1)$ , $cm^{-1}$	213 (0.0) <sup>e</sup>	210 (0.3) <sup>e</sup>	122 (0.2) <sup>e</sup>	127	172	185 (0.0) <sup>e</sup>	183 (0.5) <sup>e</sup>
$\omega_7(b_2)$ , $cm^{-1}$	757 (81.7) <sup>e</sup>	762 (78.1) <sup>e</sup>	794 (44.2) <sup>e</sup>	755	701	759 (46.7) <sup>e</sup>	764 (45.5) <sup>e</sup>
$\omega_8(b_2)$ , $cm^{-1}$	238 (1.2) <sup>e</sup>	242 (1.5) <sup>e</sup>	266 (9.2) <sup>e</sup>	240	223	258 (2.4) <sup>e</sup>	262 (2.6) <sup>e</sup>
$\omega_9(b_2)$ , $cm^{-1}$	65i	53i	105i	111i	133i	69 (9.0) <sup>e</sup>	76 (8.8) <sup>e</sup>

<sup>a</sup>  $E_{tot}=-1005.874865$  a.u. at the CASSCF(8,10)-MRCISD(Q)/6-311+G\*//CCSD(T)/6-311+G\* level of theory;  $E_{tot}=-1005.823786$  a.u. at the CASSCF(8,10)-MRCISD/6-311+G\*//CCSD(T)/6-311+G\* level of theory.

<sup>b</sup>  $E_{tot}=-1005.950976$  a.u. at the CCSD(T)/6-311+G(2df)//CCSD(T)/6-311+G\* level of theory.

<sup>c</sup>  $E_{tot}=-1005.975784$  a.u. at the CCSD(T)/aug-cc-pvtz//CCSD(T)/aug-cc-pvdz level of theory.

<sup>d</sup> Relative to the tetrahedral structure. Relative energies corrected for zero-point energy.

<sup>e</sup> Infrared intensities (km/mol) are given in parenthesis.

from the planarity in the  $C_{2v}$ , I ( $^1A_1$ ) structure could be an artifact due to the 6-311+G\* basis sets. The planar structure  $C_{2v}$ , I ( $^1A_1$ ) is appreciably higher in energy than the  $T_d$  ( $^1A_1$ ) structure: 9.3 kcal/mol (MP2/6-311+G\*), 13.6 kcal/mol [CCSD(T)/6-311+G\*], 11.1 kcal/mol [CCSD(T)/aug-cc-pvDZ]. We also used more extended basis sets for evaluating the relative energy difference between the  $C_{2v}$ , I ( $^1A_1$ ) and the  $T_d$  ( $^1A_1$ ) structures. At our highest level of theory the  $C_{2v}$ , I ( $^1A_1$ ) is higher than the  $T_d$  ( $^1A_1$ ) structure by 9.0 kcal/mol [CCSD(T)/6-311+G(2df)//CCSD(T)/6-311+G\*] and by 9.2 kcal/mol [CCSD(T)/aug-cc-pvTZ//CCSD(T)/aug-cc-pvDZ]. The quasiplanar  $C_s$  ( $^1A'$ ) structure is higher than the  $T_d$  ( $^1A_1$ ) structure by 9.2 kcal/mol [CCSD(T)/6-311+G(2df)//CCSD(T)/6-311+G\*]. We also probed the multiconfigurational contribution to this difference. We used CASSCF(8,10)-MRCISD/6-311+G\* and CASSCF(8,10)-MRCISD(Q)/6-311+G\* methods. We found that  $C_{2v}$ , I ( $^1A_1$ ) is higher than  $T_d$  ( $^1A_1$ ) by 14.8 kcal/mol [CASSCF(8,10)-MRCISD/6-311+G\*//CCSD(T)/6-311+G\*] and by 12.2 kcal/mol [CASSCF(8,10)-MRCISD(Q)/6-311+G\*//CCSD(T)/6-311+G\*]. We used Davidson's corrections for accounting for higher order excitations. The Hartree-Fock functions were found to be dominant in the CASSCF expansions:  $C_{HF}=0.924$  for  $T_d$  ( $^1A_1$ ),  $C_{HF}=0.918$  for  $C_{2v}$ , I ( $^1A_1$ ). Thus, the use of the CCSD(T) method is justified. All our ab initio methods [MP2/6-311+G\*, CCSD(T)/6-311+G\*, and CCSD(T)/aug-cc-pvDZ] clearly demonstrated that the  $D_{4h}$  ( $^1A_{1g}$ ) structure is a third-order saddle point and the  $C_{2v}$ , II ( $^1A_1$ ) structure is a first-order saddle point.

At B3LYP, MP2, and CCSD(T) levels of theory the  $Al_4C$  potential energy surface is almost the same. There are two local minima  $T_d$  ( $^1A_1$ ) and  $C_{2v}$ , I ( $^1A_1$ ) [or  $C_s$  ( $^1A'$ )] with the tetrahedral structure being the global minimum and being appreciably more

Table 14-5. Calculated molecular properties of the  $C_s$ , ( $^1A'$ ) structure of  $Al_4C$ .

Method	MP2/6-311+G*	CCSD(T)/6-311+G** <sup>a</sup>
$-E_{tot}$ , a.u.	1005.833209	1005.892274
$\Delta E$ , kcal/mol <sup>b</sup>	9.4	13.6
R(C-Al <sub>2</sub> ), Å	2.693	2.596
R(C-Al <sub>3</sub> ), Å	1.962	1.959
R(C-Al <sub>4,5</sub> ), Å	1.931	1.928
$\angle Al_2CA_{4,5}$ , degrees	65.8	69.2
$\angle Al_4CA_5$ , degrees	131.7	138.3
$\angle Al_3CA_{4,5}$ , degrees	113.2	110.3
$\angle Al_2CA_3$ , degrees	165.7	165.5
$\omega_1(a')$ , $cm^{-1}$	757 (518.1) <sup>c</sup>	731
$\omega_2(a')$ , $cm^{-1}$	400 (16.1) <sup>c</sup>	399
$\omega_3(a')$ , $cm^{-1}$	269 (2.0) <sup>c</sup>	255
$\omega_4(a')$ , $cm^{-1}$	199 (8.7) <sup>c</sup>	196
$\omega_5(a')$ , $cm^{-1}$	147 (6.6) <sup>c</sup>	123
$\omega_6(a')$ , $cm^{-1}$	73 (0.2) <sup>c</sup>	61
$\omega_7(a'')$ , $cm^{-1}$	776 (22.2) <sup>c</sup>	786
$\omega_8(a'')$ , $cm^{-1}$	312 (8.7) <sup>c</sup>	278
$\omega_9(a'')$ , $cm^{-1}$	83 (1.7) <sup>c</sup>	95

<sup>a</sup>  $E_{tot} = -1005.954367$  a.u. at the CCSD(T)/6-311+G(2df)//CCSD(T)/6-311+G\* level of theory.

<sup>b</sup> Relative to the tetrahedral structure. Relative energies corrected for zero-point energy.

<sup>c</sup> Infrared intensities (km/mol) are given in parenthesis.



stable that the  $C_{2v}$ , I ( ${}^1A_1$ ) [or  $C_s$  ( ${}^1A'$ )] isomer. The barrier to the intramolecular rearrangement  $C_{2v}$ , I ( ${}^1A_1$ )  $\rightarrow$   $T_d$  ( ${}^1A_1$ ) was found to be rather small and the second,  $C_{2v}$  I ( ${}^1A_1$ ), isomer should have a rather short lifetime. The  $C_{2v}$  II ( ${}^1A_1$ ) structure, reported by Rao and Jena as a local minimum and by Li and Gong as the global minimum, is in fact a first-order saddle point. Finally, the perfect square  $D_{4h}$  ( ${}^1A_{1g}$ ) structure is a third-order saddle point. Calculated optimal geometric parameters, harmonic frequencies, and relative energies at the B3LYP, MP2, and CCSD(T) levels of theory agree reasonably well with each other (Tables 14-1 – 14-5).

On the basis of the confirmations of our previous results<sup>1</sup> for the neutral  $Al_4C$  molecule, we concluded that our prediction of the planar square ( $D_{4h}$   ${}^2B_{2g}$ ) structure for  $Al_4C^-$  at the B3LYP/6-311+G\* and MP2/6-311+G\* and quasiplanar almost square ( $D_{2d}$   ${}^2B_1$ ) structure [we would like to stress one more time that the energy difference between ( $D_{2d}$ ,  ${}^2B_1$ ) and ( $D_{4h}$ ,  ${}^2B_{2g}$ ) is very small and the vibrationally averaged structure is actually planar at this level of theory] at the CCSD(T)/6-311+G\* is also correct. Thus, we disagree with the conclusions about a carbon-centered planar trapeziform structure of  $Al_4C^-$  predicted by Ashman, Khanna, and Pederson,<sup>2</sup> Rao and Jena,<sup>3</sup> by Zhao and co-workers,<sup>4</sup> Li and Gong,<sup>5</sup> which were based on nonhybrid DFT methods.

#### 14-4. Conclusions

On the basis of all our calculations we conclude that a  $Al_4C$  molecule has the  $T_d$  ( ${}^1A_1$ ) global minimum structure, which is appreciably more stable than the planar or quasiplanar  $C_{2v}$  I ( ${}^1A_1$ ) [or  $C_s$  ( ${}^1A'$ )] isomer. The planar  $C_{2v}$  II ( ${}^1A_1$ ) structure, which was found to be a local or even a global minimum structure by Rao and Jena and Li and

Gong, is in fact a first-order saddle point. The reason why these groups failed to correctly identify the global minimum structure of  $\text{Al}_4\text{C}$  is a weakness in the nonhybrid DFT methods used in describing the  $\text{Al}_4\text{C}$  potential energy surface. Because nonhybrid DFT methods are frequently used for characterizing new molecules and clusters we believe it could be dangerous in such studies to solely rely on these methods.

## References

- <sup>1</sup>X. Li, L. S. Wang, A. I. Boldyrev, and J. Simons, *J. Am. Chem. Soc.* **121**, 6033 (1999).
- <sup>2</sup>C. Ashman, S. N. Khanna, and M. R. Pederson, *Chem. Phys. Lett.* **324**, 137 (2000).
- <sup>3</sup>B. K. Rao and P. Jena, *J. Chem. Phys.* **115**, 778 (2001).
- <sup>4</sup>J. Zhao, B. Liu, H. Zhai, R. Zhou, G. Ni, and Z. Xu, *Solid State Commun.* **122**, 543 (2002).
- <sup>5</sup>S. F. Li and X. G. Gong, *Phys. Rev. B* **70**, 075404 (2004).
- <sup>6</sup>A. N. Alexandrova, A. I. Boldyrev, Y.-J. Fu, X.-B. Wang, and L.-S. Wang, *J. Chem. Phys.* **121**, 5709 (2004).
- <sup>7</sup>R. G. Parr and W. Yang, *Density-Functional Theory of Atoms and Molecules* (Oxford University Press, Oxford, 1989).
- <sup>8</sup>A. D. Becke, *J. Chem. Phys.* **98**, 5648 (1993).
- <sup>9</sup>J. P. Perdew, J. A. Chevary, S. H. Vosko, K. A. Jackson, M. R. Pederson, D. J. Singh, and C. Fiolhais, *Phys. Rev. B* **46**, 6671 (1992).
- <sup>10</sup>M. J. Frisch, G. M. Trucks, H. B. Schlegel *et al.*, GAUSSIAN 03, Revision A.1, Gaussian, Inc., Pittsburgh, PA, 2003.
- <sup>11</sup>D. M. Deaven and K. M. Ho, *Phys. Rev. Lett.* **75**, 288 (1995).

- <sup>12</sup>R. Krishnan, J. S. Binkley, R. Seeger, and J. A. Pople, *J. Chem. Phys.* **72**, 650 (1980).
- <sup>13</sup>A. D. McLean and G. S. Chandler, *J. Chem. Phys.* **72**, 5639 (1980).
- <sup>14</sup>T. Clark, J. Chandrasekhar, G. W. Spitznagel, and P. v. R. Schleyer, *J. Comput. Chem.* **4**, 294 (1983).
- <sup>15</sup>M. J. Frish, J. A. Pople, and J. S. Binkley, *J. Chem. Phys.* **80**, 3265 (1984).
- <sup>16</sup>D. E. Woon and T. H. Dunning, Jr., *J. Chem. Phys.* **98**, 1358 (1993).
- <sup>17</sup>R. A. Kendall, T. H. Dunning, Jr., and R. J. Harrison, *J. Chem. Phys.* **96**, 6796 (1992).
- <sup>18</sup>T. H. Dunning, Jr., *J. Chem. Phys.* **90**, 1007 (1989).
- <sup>19</sup>K. A. Peterson, D. E. Woon, and T. H. Dunning, Jr., *J. Chem. Phys.* **100**, 7410 (1994).
- <sup>20</sup>A. Wilson, T. van Mourik, and T. H. Dunning, Jr., *J. Mol. Struct.: THEOCHEM* **388**, 339 (1997).
- <sup>21</sup>J. P. Perdew, J. A. Chevary, S. H. Vosko, K. A. Jackson, M. R. Pederson, D. J. Singh, and C. Fiolhais, *Phys. Rev. B* **46**, 6671 (1992).
- <sup>22</sup>J. P. Perdew, J. A. Chevary, S. H. Vosko, K. A. Jackson, M. R. Pederson, D. J. Singh, and C. Fiolhais, *Phys. Rev. B* **48**, 4978 (1993).
- <sup>23</sup>M. Head-Gordon, J. A. Pople, and M. J. Frisch, *Chem. Phys. Lett.* **153**, 503 (1988).
- <sup>24</sup>M. J. Frisch, M. Head-Gordon, and J. A. Pople, *Chem. Phys. Lett.* **166**, 275 (1990).
- <sup>25</sup>M. J. Frisch, M. Head-Gordon, and J. A. Pople, *Chem. Phys. Lett.* **166**, 281 (1990).
- <sup>26</sup>M. Head-Gordon and T. Head-Gordon, *Chem. Phys. Lett.* **220**, 122 (1994).
- <sup>27</sup>S. Saebo and J. Almlöf, *Chem. Phys. Lett.* **154**, 83 (1989).
- <sup>28</sup>J. Cizek, *Adv. Chem. Phys.* **14**, 35 (1969).
- <sup>29</sup>G. D. Purvis and R. J. Bartlett, *J. Chem. Phys.* **76**, 1910 (1982).
- <sup>30</sup>G. E. Scuseria, C. L. Janssen, and H. F. Schaefer III, *J. Chem. Phys.* **89**, 7382 (1988).

- <sup>31</sup>G. E. Scuseria and H. F. Schaefer III, *J. Chem. Phys.* **90**, 3700 (1989).
- <sup>32</sup>J. A. Pople, M. Head-Gordon, and K. Raghavachari, *J. Chem. Phys.* **87**, 5968 (1987).
- <sup>33</sup>D. Hegarty and M. A. Robb, *Chem. Phys. Lett.* **83**, 362 (1981).
- <sup>34</sup>E. M. Siegbahn, *Chem. Phys. Lett.* **109**, 417 (1984).
- <sup>35</sup>H. B. Schlegel and M. A. Robb, *Chem. Phys. Lett.* **93**, 42 (1982).
- <sup>36</sup>F. Bernardi, A. Bottoni, J. J. W. McDouall, M. A. Robb, and H. B. Schlegel, *Faraday Symp. Chem. Soc.* **19**, 137 (1984).
- <sup>37</sup>N. Yamamoto, T. Vreven, M. A. Robb, M. J. Frisch, and H. B. Schlegel, *Chem. Phys. Lett.* **250**, 373 (1996).
- <sup>38</sup>M. J. Frisch, I. N. Ragazos, M. A. Robb, and H. B. Schlegel, *Chem. Phys. Lett.* **189**, 524 (1992).
- <sup>39</sup>H.-J. Werner and P. J. Knowles, *J. Chem. Phys.* **89**, 5803 (1988).
- <sup>40</sup>P. J. Knowles and H.-J. Werner, *Chem. Phys. Lett.* **145**, 514 (1988).
- <sup>41</sup>H.-J. Werner and P. J. Knowles, with contributions from R. D. Amos, A. Bernhardsson, and A. Berning *et al.*, MOLPRO-2000.1.

CHAPTER 15  
GLOBAL MINIMUM STRUCTURE SEARCHES VIA  
PARTICLE SWARM OPTIMIZATION<sup>1</sup>

**Abstract**

Novel implementation of the evolutionary approach known as Particle Swarm Optimization (PSO) capable of finding the global minimum of the potential energy surface of atomic assemblies is reported. This is the first time the PSO technique has been used to perform global optimization of chemical systems. Significant improvements have been introduced to the original PSO algorithm to increase its efficiency and reliability and adapt it to chemical systems. The developed software has successfully found the lowest-energy structures of the LJ<sub>26</sub> Lennard-Jones cluster, anionic silicon hydride Si<sub>2</sub>H<sub>5</sub><sup>-</sup>, and triply hydrated hydroxide ion OH<sup>-</sup> (H<sub>2</sub>O)<sub>3</sub>. It requires relatively small population sizes and demonstrates fast convergence. Efficiency of PSO has been compared with Simulated Annealing, and the Gradient Embedded Genetic Algorithm (GEGA).

**15-1. Introduction**

Determination of the topography of potential energy surfaces of various atomic assemblies is a “hotspot” of modern computational chemistry. In certain cases it can be important to establish all the possible isomers of a given stoichiometry,<sup>1</sup> but generally only the lowest-lying isomers (the global minimum structures) and their closest competitors are of the practical interest. The number of stable atomic arrangements grows

---

<sup>1</sup> Coauthored Seth T. Call, Dmitry Yu. Zubarev and Alexander I. Boldyrev. Reproduced with permission from *J. Comput. Chem.* **2007**, 28, 1177-1186.

extremely fast as the size of the system increases, especially in the case of heteroatomic assemblies. As a result, manual search procedures become highly unreliable creating demand for automated procedures based on human-unbiased algorithms. For example, the search for isomers and conformers can be performed using fast and comprehensive “kick” method developed by Saunders,<sup>2</sup> or similar random search and minimization technique proposed by Lloyd and Johnston.<sup>3</sup> “Conformation flooding” by Grubmuller<sup>4</sup> may be used to study conformational transitions in macromolecular systems. The search for global minimum structures can utilize different implementations of several major algorithms, such as simulated annealing,<sup>5-14</sup> basin hopping,<sup>15,16,17</sup> multicanonical methods,<sup>18</sup> and genetic algorithms.<sup>18,19a,20-26</sup> Minima hopping algorithm has been proposed recently.<sup>27</sup>

This paper presents an original implementation of the Particle Swarm Optimization (PSO) strategy, which before now has not been used to solve the problem of finding the global minimum of the potential energy surface of chemical systems. PSO is a relatively new evolutionary approach, developed by Eberhart and Kennedy in 1995.<sup>28</sup> PSO has been the focus of much research including but not limited to References 29-36. In a survey paper,<sup>32</sup> the authors report that within only five years of its invention, the general-purpose algorithm was being actively researched and utilized in over twelve countries. PSO has been used with neural networks to diagnose patients with human tremor, including Parkinson’s disease. It has been used in a Japanese electric utility for optimizing discrete and continuous variables managing power control strategies. PSO has also been used to manage the mix of ingredients used for growing strains of microorganisms that secrete products of interest to manufacturing companies.

In adapting PSO to find global minimum structures, the work presented here has several notable benefits. These include

- flexible random initialization procedure controlling the quality of the initial population in terms of the fragmentation of the generated structures. Starting with non-fragmented structures helps to avoid exploring insignificant configurations.
- measurement of the similarity of structures using a distance metric. This metric ignores irrelevant translation and rotation information and solves the problem of revisiting configurations.
- enforcement of user-defined minimum distance constraints between atoms with different minimum distances between different types of atoms. This provides a flexible way to control the size of the search space.

This PSO application allows atoms to be grouped into sets that are moved and rotated as rigid units. This makes the application useful in analyzing chemical systems consisting of atomic groups preserving their structure, e.g. solvated molecules or ions. The Potential Energy Surface can be specified either explicitly by an analytical expression or via sampling performed by external quantum chemical software. The developed software runs in parallel and can be easily stopped and restarted. Previous research<sup>30</sup> indicates that PSO requires smaller population sizes to find global minimum structures than genetic algorithms. Population based methods are advantageous because they can be run in parallel.

Several chemical systems were chosen to test the ability of PSO to find lowest-energy structures, to estimate its performance, and to compare its efficiency with alternative algorithms. The first chemical system was the LJ<sub>26</sub> cluster. This is a

representative of a family of  $LJ_n$  clusters whose potential energy surface can be described by the Lennard-Jones potential and which serve as a model of, for example, noble gas clusters. The relative simplicity of Lennard-Jones clusters and significant number of studies on their possible low-energy structures up to  $n=1000$ <sup>15, 37-89</sup> make them an excellent test system for various global optimization techniques. Lennard-Jones clusters have been studied by means of genetic algorithms,<sup>51,62,64-67</sup> various hypersurface deformation methods,<sup>68-75</sup> annealing methods,<sup>15,76-84</sup> the “pivot method”,<sup>85-87</sup> the “taboo search”,<sup>88,89</sup> and other techniques.<sup>90</sup> The second studied system was  $Si_2H_5^-$  silicon hydride anion. Silicon hydrides  $SiH_x$  ( $x=1-3$ ) and  $Si_2H_x$  ( $x=1-6$ ) in both neutral and anionic forms are systems of high practical importance because they are used in semiconductor industry in silicon chemical vapor deposition processes.<sup>91</sup> They are believed to participate in the chemical reactions of circumstellar envelopes of dying carbon stars.<sup>92</sup> From the theoretical point of view, silicon hydrides are attractive due to their peculiar bonding characteristics in comparison with isovalent carbon congeners.<sup>93,94</sup> So, various silicon hydrides and corresponding anions have been actively studied experimentally<sup>95-109</sup> and theoretically.<sup>110-128</sup> Geometry of anionic  $Si_2H_5^-$  has been reported, for example, by Schaefer and co-workers.<sup>129</sup> The third test system was hydroxide ion coordinated with three water molecules  $OH^-(H_2O)_3$ . The  $OH^-$  anion and its solvation complexes play an essential role in aqueous chemistry.<sup>130</sup> Theoretical studies of the structure of the solvation complexes  $OH^-(H_2O)_n$  ( $n = 1 - 17$ ) have been performed by various groups. Parrinello and co-workers<sup>131, 132</sup> reported results of ab initio molecular dynamics investigations, while other authors<sup>133-135</sup> reported results of systematic manual searches for the lowest-energy isomers. In the combined experimental and theoretical work of Johnson and co-



workers<sup>136</sup> the composition and structure of complexes of OH<sup>-</sup> and water molecules were finally established.

All three test systems have been previously studied and their structures are known. Their size is big enough to make the search non-trivial but small enough to allow testing in a reasonable time. These systems represent different classes of atomic assemblies which can be successfully studied by the developed PSO software. LJ<sub>26</sub> is a cluster which is described by analytical Lennard-Jones potential and serves as a model of clusters of noble gases, Si<sub>2</sub>H<sub>5</sub><sup>-</sup> is a regular ion with covalent bonding, and OH<sup>-</sup>(H<sub>2</sub>O)<sub>3</sub> is a system consisting of three independent chemical subunits which preserve their chemical identity.

The structure of the present paper is as follows: Section 15-2 is an analysis of the size of the search space, Section 15-3 discusses current techniques for finding global minimum structures, Section 15-4 discusses the PSO algorithm, Section 15-5 discusses the details of the computational experiments on Si<sub>2</sub>H<sub>5</sub><sup>-</sup>, OH<sup>-</sup>(H<sub>2</sub>O)<sub>3</sub>, and LJ<sub>26</sub>, and Section 15-6 summarizes and concludes the work presented.

## **15-2. Size of the Search Space**

This section analyzes the size of the search space. This analysis supports previous results, which state that the problem is nondeterministic polynomial-time hard (NP-hard).<sup>19</sup> This means for every known algorithm, the function representing the time necessary to find the correct solution is non-polynomial (i.e. exponential) in terms of the number of atoms and the volume of space in which the atoms may roam. In this application, sets of one or more atoms are placed in groups that are moved and rotated

together as rigid units. Sometimes, these “units” are actually molecules, and in other situations, they are simply groups of one or more atoms. Most applications limit coordinates within a sphere or cube, and for simplicity, the newly developed application uses a cube. It is also helpful to measure the search space as discrete rather than continuous since continuous search spaces are infinite. Let the length, width, and height of the cube be  $w$ . Let the  $x$ ,  $y$ , and  $z$  coordinates of each unit’s center of mass be multiples of  $d$  lying in the range  $[0, Ld]$  where  $w = Ld$  and where  $L + 1$  is the number of possible values each coordinate can have. Note that in this analysis of the search space size, only the center of mass of each unit is confined within the cube, and some atoms may lie slightly outside the cube. Also note that the application itself requires that both atom coordinates and unit centers of mass are within the cube.

Three angles are used for representing the rotation of units. In aviation terms, these angles are roll, pitch, and yaw. Rotation around the vertical axis is called yaw. Rotation around the side-to-side axis is called pitch. Rotation around the front-to-back axis is called roll. Roll and yaw can have values in the range of  $[0, 2\pi)$ , while pitch can have values in the range of  $[0, \pi]$ . Letting angles be a multiple of some angle  $\theta$ , there are  $\left(\frac{2\pi}{\theta}\right)$  possible values for roll and yaw and  $\left(\frac{\pi}{\theta} + 1\right)$  possible values for pitch. The size of the search space  $S$  can be defined as follows:

$$S = (L + 1)^{3(n+m)} \left( \left( \frac{2\pi}{\theta} \right)^2 \left( \frac{\pi}{\theta} + 1 \right) \right)^m \quad (15-1)$$

where  $n$  is the number of units containing one atom and  $m$  is the number of units containing multiple atoms. It should be noted that this simple equation does not handle

duplicate solutions that arise due to translation and rotation, but it does provide a representative concept of how the search space grows.

In choosing  $\theta$  for the units with multiple atoms, it is desirable to have a choice not allowing changes in any atom's coordinates greater than  $d$ . Let  $U$  be the unit with atom  $F$  furthest from the unit's center of mass,  $f$  be the distance from  $F$  to  $U$ 's center of mass,  $C$  be a circle of radius  $f$ , and let  $R$  be an arc on  $C$  of length  $d$  and angle  $\theta$ . The angle  $\theta$  can be computed using the formula:

$$\theta = \frac{d}{f} \quad (15-2)$$

where  $\theta$  is measured in radians. Substituting Equation 15-2 into Equation 15-1 and simplifying yields:

$$S = (L + 1)^{3(n+m)} \left( \frac{4\pi^3 f^3}{d^3} + \frac{4\pi^2 f^2}{d^2} \right)^m \quad (15-3)$$

As indicated, the size of the search space grows exponentially as  $L$ ,  $m$ ,  $n$ , and  $f$  get larger and as  $d$  gets smaller. This means if an exhaustive search of every possible structure were to be tried, and if coordinates were a multiple of  $d$ , the number of times energies would have to be evaluated would increase exponentially with the number of units and the volume of the cube. Similarly, the time required for a successful PSO, genetic algorithm, basin hopping, or other run also grows exponentially with the number of units and with the volume of the search cube.

### 15-3. Current Techniques for Finding Global Minimum Structures

The most common methods for finding global minimum structures of chemical systems include simulated annealing, basin hopping, and genetic algorithms. Simulated annealing, basin hopping and multicanonical methods have a common foundation: a Markov process based on the Metropolis algorithm with a Boltzmann factor leads to a thermodynamic distribution. This means, that the ground state configuration will be dominant provided that the temperature is low enough. In principle, this guarantees success of the global minimum structure search. Simulated annealing<sup>5-14</sup> generally starts with a single random chemical structure. At each step a small perturbation is made to the structure, after which the energy value is recalculated. If the energy value is better, the perturbation is accepted. If it is worse, the perturbation is accepted with a certain probability, which is based on the temperature. At the start of a run, the temperature and the probability of accepting a bad perturbation are very high. The temperature decreases slowly over the course of the run. At the end, the temperature and the probability of accepting bad perturbations are very low. Essentially, the algorithm is a slow transition between a random search and a downhill search.

Another technique receiving recent attention is basin hopping.<sup>15,16,17</sup> Developed by Wales and Doye, this technique is like simulated annealing in that it starts with a single random structure, performs random perturbations, and accepts or rejects these probabilistically. It is different from simulated annealing, first of all, because it does not decrease the temperature, but fixes it at some value. Second, instead of using the energy values of the original and the perturbed structures, basin hopping uses the energy values

from copies of these structures that have been optimized to their nearest local minima using gradients. This helps ensure that the algorithm is not inhibited by high-energy barriers and that it always moves toward lower minima.

One problem with thermodynamic methods such as simulating annealing is that they are not guaranteed to achieve the equilibrium distribution within any given time. Moreover, it is more likely to obtain the thermodynamic equilibrium distribution if the process goes infinitely slow.

Genetic algorithms<sup>17,19a,20-26</sup> use a population of randomly generated candidate solutions, which evolve to form better solutions according to the Darwinian model of evolution. In this model, each candidate solution has a set of genes encoding the solution. Traditionally, the encoding is binary, though in many applications the solution is represented using a set of variables. Members of the population are mated producing children with characteristics of both parents. The best or fittest individuals are saved for the next generation. Genetic algorithms are implemented in a variety of ways, and the approach taken can have significant effects on how well the algorithm performs. The key ingredients of a genetic algorithm include the method for encoding the solution, the approach to performing mating, the algorithm that selects which candidate solutions to mate, and the technique for choosing which candidate solutions to keep and which to throw away. Genetic algorithms generally perform mutation of candidate solutions using a variety of approaches to help introduce diversity into the population. Also, many genetic algorithms such as the Gradient Embedded Genetic Algorithm (GEGA) by Alexandrova<sup>25,26</sup> optimize chemical structures to their nearest local minimum using gradients.

## 15-4. Particle Swarm Optimization

### 15-4.1. Generalized Particle Swarm Optimization

PSO<sup>28-36</sup> is based on observed behaviors of swarms of insects or flocks of birds, where each candidate solution or particle is guided by memory of the best solution it has seen and the best solution seen by the population. It is similar to a genetic algorithm in that it has a randomly initialized population, though it is different in that variables in candidate solutions have a velocity by which they are flown through the search space. Each variable's velocity is updated according to the formula:

$$x = x + v \quad (15-6)$$

where  $x$  is the given variable and  $v$  is its associated velocity. Each velocity  $v$  is influenced by the value of  $x$  in the best solution seen by the particle and in the best solution seen by the population of particles. More specifically, each velocity  $v$  is updated according to the formula:

$$v = wv + c_1r_1(b_p - x) + c_2r_2(b_i - x) \quad (15-7)$$

where the variables are defined below.

$w$  is the inertia value which is usually slightly less than 1.

$b_p$  is the value of the given variable from the best solution seen by the swarm.

$b_i$  is the value of the given variable from the best solution seen by the particle.

$c_1$  and  $c_2$  are constants indicating how much the particle is directed toward the best solution seen by the swarm and by the particle respectively.

$r_1$  and  $r_2$  are random numbers in the range  $[0, 1]$ .

PSO also has the benefit that all variables change at the same time, which means the search space is examined quickly. Velocities of solution variables are typically not allowed to exceed a predefined limit called  $V_{\max}$ . Having  $V_{\max}$  set high facilitates global rather than local exploration. Having  $V_{\max}$  set low restricts global exploration and encourages local exploration. The acceleration constants  $c_1$  and  $c_2$  determine the extent to which particles are directed toward the best solution seen by the swarm and by the particle respectively. Having a higher  $c_1$  value causes all particles to be most attracted toward the best solution seen by the swarm. Having a higher  $c_2$  value allows particles more time to roam away from the best solution seen by the swarm. The inertia weight  $w$  is designed to balance global and local exploration and, in some cases, eliminates the need for  $V_{\max}$ . The weight  $w$  is usually decreased linearly from 0.9 to 0.4 allowing a global search toward the beginning and a more local search toward the end.

#### *15-4.2. Particle Swarm Optimization for Finding Stable Chemical Structures*

The PSO algorithm as adapted for global optimization of chemical systems required some modifications. For example, the application uses two types of velocities, one for each unit's center of mass and the other for each unit's angles. Both of these have their own  $V_{\max}$ . In the case of a unit's center of mass, when the magnitude of the velocity vector exceeds the coordinate  $V_{\max}$ , the X, Y, and Z components of that vector are scaled to keep the magnitude within the coordinate  $V_{\max}$ . In the case of a unit's angles, each angle velocity is not allowed to exceed the angle  $V_{\max}$ , while the magnitude of the angle velocity vector may exceed the angle  $V_{\max}$ . In the case of the angles roll and yaw, these are attracted along the closest route to the destination angle. For example, if the current

roll angle is  $340^\circ$  and the target of attraction is  $20^\circ$ , the angle is attracted in the positive direction and takes the shorter route around the circle to the target angle.

Another novel feature that was added to this implementation of PSO is that the best solution seen by a particle is sometimes not updated with a newly discovered best solution seen in the current iteration. This update is not performed, if it places the particle's best solution within a user-defined distance of the best solution seen by particles in the population. Ensuring that the personal best and group best solutions seen by a particle are different helps prevent the particle from slowing down or stopping during the course of the algorithm. Other novel modifications of the general PSO algorithm and the incorporation of pre-existing advanced PSO techniques are described in subsequent sections.

#### *15-4.3. Random Initialization of Chemical Structures*

This PSO application has several methods for creating structures in the initial population. When creating the random initial population, the probability of generating linear or planar structures is very low. Linear and planar structures are chemically very important, however, so it is beneficial to create such structures in the initial population. Unit and atom coordinates in *linear structures* are initialized within a box having a length equal to the length of the search cube and a height and width equal to a small user-defined value. The centers of mass of *planar structures* are initialized in a box having a length and width equal to the length of the search cube and a height of zero.

It is also beneficial to eliminate species from the initial population that consist of several non-interacting fragments. For example, when the structure of an N-atomic



cluster is studied, there is no need to consider systems split into several smaller clusters with the same total number of atoms. This PSO software can also initialize random structures of these three types:

1. Fragmented structures
2. Partially non-fragmented structures
3. Completely non-fragmented structures

*Fragmented structures* contain units, groups of one or more atoms, in random locations within the search cube. *Partially non-fragmented structures* are created such that every atom is within the maximum distance of, at least, one other atom. In cases excluding noble gases, globally minimum structures rarely contain single atoms not close to, at least, one other atom. *Completely non-fragmented structures* can be best understood in terms of a graph wherein nodes are atoms and edges exist between each pair of atoms that are within the maximum distance of one another. A completely non-fragmented structure is one whose graph is connected or in which there is a path of consecutive edges between each pair of nodes. Figure 15-1 illustrates the differences between these three structure types. The methods initializing the two non-fragmented structure types are novel approaches.

Minimum distance constraints are always enforced between atoms. This allows escaping energy computations for chemically unrealistic systems, which are likely to have convergence problems. The user may specify different minimum distances between different types of atoms. The user also specifies the maximum distance constraint for partially and completely non-fragmented structures.

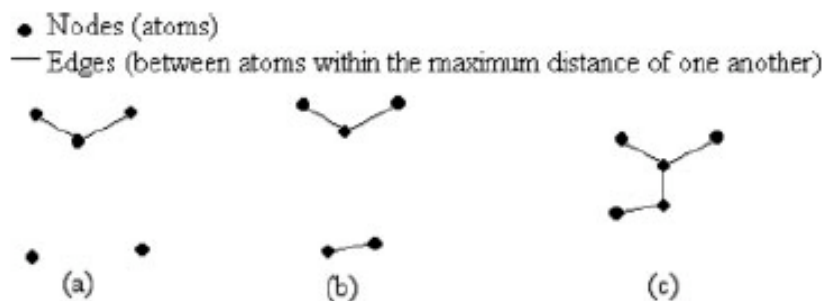


Figure 15-1. Example illustrations of (a) fragmented structures, (b) partially non-fragmented structures, and (c) completely non-fragmented (connected) structures.

A common function is used to initialize partially and completely non-fragmented structures and to enforce minimum distance constraints. This function positions one unit (unit 1) relative to another unit (unit 2) along a specified direction as seen in Figure 15-2. Let  $L$  be a line between the centers of mass of the two units, and let  $R$  be a line passing through atom 2 that is parallel to  $L$ . Let atoms 1 and 2 be the closest pair of atoms in the two units. These are found by moving unit 1 far away from unit 2 along  $L$ . All pairs of atoms, one from each unit, are examined to find the pair with the closest distance. Next, the value  $y$  is randomly assigned between the minimum and maximum limits, and the appropriate  $d$  value is calculated indicating the distance that should exist between the units' centers of mass which lie along  $L$ .

In some cases, the pair of atoms in the two units that are closest to one another differs when the units are far apart compared to when they are close together. In these cases, after  $d$  is calculated, the two units are moved apart a long  $L$  a little at a time, until the minimum distance constraints are satisfied.

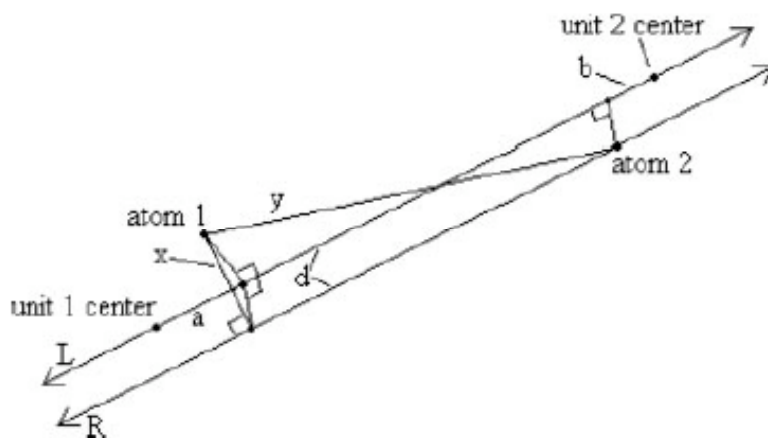


Figure 15-2. Diagram, illustrating how unit 1 is positioned relative to unit 2 along the line L. Atom 1 and atom 2 are the closest atoms in the two units.

#### 15-4.4. Enforcing Minimum Distance Constraints in PSO

PSO facilitates a faster exploration of the search space since all atoms in each structure are moving at the same time. One implementation challenge this poses is how to enforce the minimum distance constraints between atoms. This is necessary not only to reduce the size of the search space but also to help ensure that energy calculations converge as efficiently as possible. The following steps represent a simple method for solving this problem.

1. Detect pairs of units violating minimum atomic distance constraints
2. If no units violate the atomic distance constraints, quit
3. Randomly choose one pair of units violating the constraints
4. Move one randomly chosen unit in the pair away from the other unit in the pair
5. Go to Step 1

Step 4, which moves units apart, is performed using the technique described in the previous section. The above procedure represents a simple solution to the problem and is very fast with less than one hundred atoms. More complex and efficient approaches may be considered in cases with larger numbers of atoms.

Some might suggest that enforcing the minimum distance constraints modifies the progress of the algorithm. For example, two large units wanting to pass through one another could be prevented from doing so when minimum atom distances are enforced. To compensate for this, an option in the program will allow the minimum distance constraints to be enforced on a copy of each structure rather than on the original. This helps convergence of energy calculations without modifying the progress of the algorithm.

#### *15-4.5. Using a Local-Neighborhood with PSO*

In the original version of PSO, each particle is attracted toward the best solution it has seen to date, as well as to the best solution seen by the population. In a local-neighborhood version of PSO,<sup>31</sup> instead of being attracted toward the best solution seen by the population, each particle is attracted toward the best solution seen by particles within a given local neighborhood. Implementing this technique requires a distance metric to determine the degree of similarity of two chemical structures. This metric, described in the next section, ignores the translation, rotation, and mirror reflection of chemical structures when comparing them. Use of this metric reduces the size of the search space by placing truly similar chemical structures in the same local neighborhood.

A visibility distance determines the size of the local neighborhood within which each particle can see other particles. The user specifies a starting visibility distance and an amount by which the visibility distance will increase after each iteration. This allows the visibility to start low and grow during the course of the algorithm, thereby reducing the likelihood that PSO will become stuck in a local minimum.

#### *15-4.6. Distance Metric Comparing Pairs of Structures*

The distance metric in this application uses a matrix of interatomic distances. A distance matrix is advantageous because it is not dependent on position or rotation. The metric required ordering the atoms. This ordering is based first on the atomic number of each atom and second on the atom's distance from the center of mass. The metric calculates the root-mean-square (RMS) distance of the differences between pair wise atom distances according to Equation 15-8:

$$RMS(A,B) = \sqrt{\frac{1}{\left(\frac{n^2 - n}{2}\right)} \sum_{i=1}^{n-1} \sum_{j=i+1}^n (d(a_i, a_j) - d(b_i, b_j))^2} \quad (15-8)$$

where  $n$  is the number of atoms,  $d(a_i, a_j)$  is Euclidian distance,  $a_i$  and  $a_j$  are the the  $i$ 'th and  $j$ 'th atoms in structure A, respectively, and  $b_i$  and  $b_j$  are the the  $i$ 'th and  $j$ 'th atoms in structure B, respectively. The value  $\left(\frac{n^2 - n}{2}\right)$  is the number of unique pairs of atoms,

which is the same in both structures.

There is a similar method for comparing two proteins<sup>137</sup> that also uses a distance matrix wherein each element of the matrix is the distance between two amino acids, one

from each protein. This method performs translation and rotation of one protein to minimize the RMS distance to the other protein according to Equation 15-9:

$$RMS_{protein}(A,B) = \sqrt{\frac{1}{n} \sum_{i=1}^n d(a_i, b_i)^2} \quad (15-9)$$

where  $n$  is the number of amino acids,  $a_i$  is the primary carbon atom of the  $i$ 'th amino acid in protein A, and  $b_i$  is the primary carbon atom of the  $i$ 'th amino acid in protein B. The procedure performs translation and rotation of one protein to minimize explicitly the RMS distance between the two proteins. It then reports this minimum RMS distance as the measure of similarity between the proteins. The ability to do this relies on the fact that amino acids are ordered and that they are uniquely identified by number. In this application, however, atoms are not ordered and multiple atoms with the same atomic number are allowed. The distance metric presented here handles this.

#### *15-4.7. Attraction and Repulsion Phases to Preserve Diversity*

An additional enhancement to the traditional PSO algorithm is a method for managing diversity in the particle swarm population. Diversity management is important for population-based methods such as PSO. Low diversity is a two-edged sword that is beneficial in that it produces significant progress in a short time and hazardous because it may cause the algorithm to become stuck in a local minimum. To compensate for the adverse affects of low diversity, one suggestion<sup>33</sup> is to have attraction and repulsion phases. This is accomplished by adding a *dir* term to Equation 15-7 as follows:

$$v = w \cdot v + dir \cdot c_1 \cdot r_1(b_p - x) + dir \cdot c_2 \cdot r_2(b_i - x) \quad (15-10)$$

where *dir* can be either 1 or -1 for attraction or repulsion respectively.

Conditions for when to switch between attraction and repulsion phases depend on a metric measuring the diversity in the population. The method for measuring diversity suggested in the generic PSO algorithm<sup>33</sup> is as follows:

$$diversity(S) = \frac{\mathbf{1}}{|S| \cdot |L|} \sum_{i=1}^{|S|} \sqrt{\sum_{j=1}^N (p_{ij} - \bar{p}_j)^2} \quad (15-11)$$

where S is the swarm, |S| is the swarm size, |L| is the length of the longest diagonal in the search space, N is the dimensionality of the problem,  $p_{ij}$  is the j'th value of the i'th particle, and  $\bar{p}_j$  is the j'th value of the average point  $\bar{p}$ . This metric is independent of the swarm size and the dimensionality of the problem. The above diversity measure was adapted for chemical systems by using the distance metric in Equation 8 and taking the average distance between each pair of particles as follows:

$$diversity(S) = \frac{\mathbf{1}}{\left(\frac{|S|^2 - |S|}{2}\right) \cdot |C|} \sum_{i=1}^{|S|-1} \sum_{j=i+1}^{|S|} RMS(A_i, A_j) \quad (15-12)$$

where |C| is the length of the search cube diagonal, and  $\left(\frac{|S|^2 - |S|}{2}\right)$  is the number of pairs of particles. Equations 15-11 and 15-12 both measure population diversity in a way, that is independent of the swarm size and the dimensionality of the problem. Equation 15-12 is better adapted to chemical systems because it ignores the translation, rotation, and mirror reflection of two structures when comparing them. It also appropriately handles multiple atoms with the same atomic number by sorting them according to their distance to the center of mass. The transition from the attraction to the repulsion phase occurs when the diversity falls below some user-defined value and when no progress has been

made for a user-defined number of iterations. The transition from the repulsion to the attraction phase occurs when diversity has exceeded some user-defined limit.

When switching from repulsion to attraction, it is important to reset the best solution seen by each individual to ensure that the swarm doesn't simply move back to a previously visited local minimum. The need to do this is mentioned in Ref. 33, though no mention is made of how to accomplish this. This PSO application keeps a list of the  $n$  best solutions seen to date by the population, where  $n$  is user-defined, and each solution in the list is different from every other solution by some user-defined distance. This list is updated after each iteration. When switching from repulsion to attraction, this application resets the best individual solutions known to each particle with solutions from the list of best  $n$  solutions seen by the population during the entire run. Next, the visibility distance is reset to its initial low value and then increased at the same rate as before. Also, energy calculations are not performed during the repulsion phase to help speed the progress of the algorithm.

### 15-5. Computational Results

As mentioned, the  $\text{LJ}_{26}$ ,  $\text{Si}_2\text{H}_5^-$ , and  $\text{OH}^-(\text{H}_2\text{O})_3$  chemical systems were used to test PSO's performance. The performance of PSO was compared to un-enhanced PSO, simulated annealing, and the gradient embedded genetic algorithm (GEGA).<sup>25,26</sup> Un-enhanced PSO allowed an initial fragmented population, did not enforce minimum distance constraints between atoms, and did not have attraction and repulsion phases. PSO, un-enhanced PSO, and simulated annealing used in the current research were implemented within the same software package.



The comparison of performance was based on the number of iterations/energy calculations, necessary to achieve the final result rather than on the overall time of the search. This made it possible to compare population and non-population based searches and methods using gradient optimization with methods not using gradient optimization.

Parallel execution of code in the case of both versions of PSO and population-based simulated annealing did not involve parallelization of energy computations performed by external software.

With the exception of GEGA, the algorithms presented in this section did not use local optimization until the end of each run. PSO's performance could of course be improved upon using local optimization during the run, but this was not done in order to compare the efficiency of the algorithms themselves. GEGA for instance produced the global minimum structure for  $\text{Si}_2\text{H}_5^-$  after the first round of local optimization of the initial random population, but this provided no information concerning the efficiency of the genetic algorithm compared to other algorithms.

The calculations for Lennard-Jones clusters used the Lennard-Jones potential given by the formula:

$$E = 4\varepsilon \sum_{i < j} \left[ \left( \frac{\sigma}{r_{ij}} \right)^{12} - \left( \frac{\sigma}{r_{ij}} \right)^6 \right] \quad (15-13)$$

where  $\varepsilon$  and  $2^{1/6}\sigma$  are the pair equilibrium well depth and separation, respectively, and where  $r_{ij}$  is the Euclidean distance between atoms  $i$  and  $j$ . For simplicity,  $\varepsilon$  and  $\sigma$  are set to 1 as in Ref. 15. In case of  $\text{Si}_2\text{H}_5^-$  and  $\text{OH}^-(\text{H}_2\text{O})_3$  the sampling of the potential energy surfaces was performed utilizing Gaussian 03<sup>138</sup> single-point computations. Density functional theory (DFT) method known as B3LYP<sup>139</sup> with 3-21G ( $\text{Si}_2\text{H}_5^-$ ) and 6-

311++G\*\* (OH(H<sub>2</sub>O)<sub>3</sub>) basis sets was chosen as relatively inexpensive and providing reliable results. Visualization of the results was performed using Molden 3.4 software.<sup>140</sup>

As indicated in Table 15-1, simulated annealing and un-enhanced PSO failed to find the global minimum structure for LJ<sub>26</sub>, though simulated annealing came close. PSO found the T<sub>d</sub> global minimum structure for LJ<sub>26</sub> (Figure 15-3a) and did so with the fewest total number of energy calculations (Table 15-1). The energy of the T<sub>d</sub> LJ<sub>26</sub> is in excellent agreement with previously reported results.<sup>15</sup> It should be noted that LJ<sub>26</sub> is not the most challenging system among LJ<sub>n</sub> clusters due to peculiarities of the topology of PES of Lennard-Jones systems. For example, Wales and Doye<sup>15</sup> suggested that the efficiency of different methods should be estimated on their performance for LJ<sub>38</sub> and LJ<sub>75</sub> clusters, which have extremely complex PES. Definitely, these two computationally more demanding tasks are beyond the scope of the current article and can be addressed in future studies of the PSO technique.

PSO also found the C<sub>s</sub> <sup>1</sup>A' global minimum structure for Si<sub>2</sub>H<sub>5</sub><sup>-</sup> (Figure 15-3b), which is consistent with results reported by Schaefer and co-workers.<sup>129</sup> Gaussian 03 optimization of the structure reported by PSO lowered the energy only by 2.7 kcal/mol (Table 15-1). Simulated annealing failed to find the global minimum structure. Simulated annealing found it later when using a population of 40 where each individual in the population represented a simultaneous, independent run. This illustrates the complex nature of the Si<sub>2</sub>H<sub>5</sub><sup>-</sup> potential energy surface and the critical need for simulated annealing to have the right starting structure. As previously stated, GEGA also found the global minimum structure of this system.

Table 15-1. PSO Search Results for LJ<sub>26</sub>, Si<sub>2</sub>H<sub>5</sub><sup>-</sup>, OH<sup>-</sup>(H<sub>2</sub>O)<sub>3</sub>, and Si<sub>2</sub>H<sub>5</sub> OH<sup>-</sup>(H<sub>2</sub>O)<sub>3</sub>.

Algorithm	Population Size	Iterations	Number of Energy Calculations	Energy <sup>a</sup>	Found Global Min.
<b>LJ<sub>26</sub> Results</b>					
Simulated Annealing	1	1,000,000	1,000,000	-105.800559 (-106.794429) <sup>b</sup>	No
Un-enhanced PSO	1,000	10,000	10,000,000	-27.169052 (-39.531096) <sup>b</sup>	No
PSO	1,000	700	700,000	-108.315616 (-108.315616) <sup>b</sup>	Yes
<b>Si<sub>2</sub>H<sub>5</sub><sup>-</sup> Results</b>					
Simulated Annealing	1	13,000	13,000	-578.893002 (-578.89348) <sup>b</sup>	No
PSO	200	500	10,000	-578.932032 (-578.936337) <sup>b</sup>	Yes
<b>OH<sup>-</sup>(H<sub>2</sub>O)<sub>3</sub> Results</b>					
Simulated Annealing	1	11,000	11,000	-305.152599 (-305.222275) <sup>b</sup>	No
PSO	100	600	6,000	-305.152414 (-305.223383) <sup>b</sup>	Yes

<sup>a</sup> – energy units for LJ<sub>26</sub> are reduced units (r.u.); energy units for Si<sub>2</sub>H<sub>5</sub><sup>-</sup> and OH<sup>-</sup>(H<sub>2</sub>O)<sub>3</sub> are atomic units (a.u.).

<sup>b</sup> –values in parenthesis correspond to the local optimization results: LJ<sub>26</sub> used conjugant gradient local optimization; Si<sub>2</sub>H<sub>5</sub><sup>-</sup> and OH<sup>-</sup>(H<sub>2</sub>O)<sub>3</sub> used Gaussian 03 local optimization.

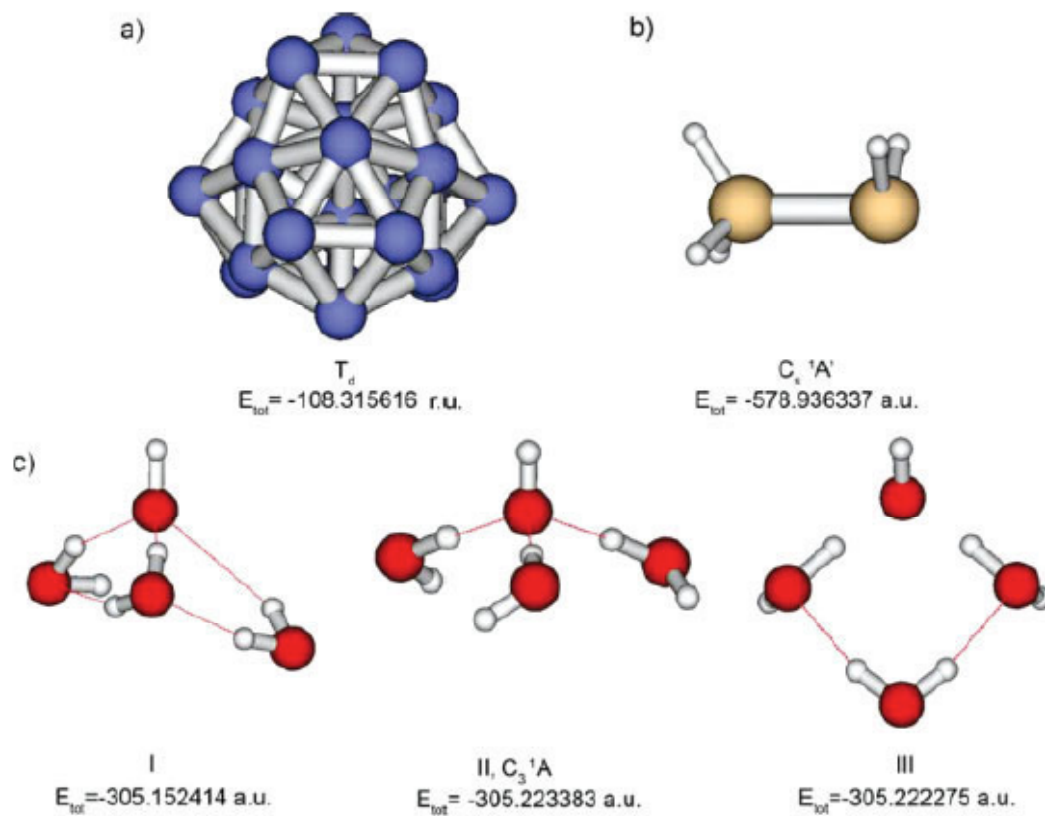


Figure 15-3. Global minimum structures of the test systems: (a)  $\text{LJ}_{26}$ , (b)  $\text{Si}_2\text{H}_5$ , and (c)  $\text{OH}(\text{H}_2\text{O})_3$ .

The  $\text{OH}^-(\text{H}_2\text{O})_3$  system contains four groups of atoms or units including three water molecules and one hydroxide ion. PSO found the structure I (Figure 15-3c), and local optimization transformed the structure to the  $C_3$   $^1A$  global minimum structure II (Figure 15-3c), which has a tetrahedral arrangement consistent with the results reported by Johnson and co-workers.<sup>136</sup> Though the structures are quite different geometrically, structure I is located in the basin of structure II, so the PSO search was considered to be successful. Simulated annealing did not find the global minimum structure I or a structure within its basin. After local optimization the structure found by simulated annealing converged to structure III (Figure 15-3c), which is 0.7 kcal/mol higher than the global minimum structure II. No run of the GEGA algorithm was attempted for this system because GEGA currently does not group atoms into sets or units.

The PSO algorithm found the global minimum structure for all three systems and did so with low numbers of energy calculations. These results are especially significant when considering that population-based methods such as PSO can run in parallel, while non-population-based methods such as simulated annealing must make one energy computation at a time. It is important to realize though, that no theoretical guarantee exists, that PSO search will be successful. So several runs of the PSO search are necessary to verify obtained result.

## 15-6. Conclusion

Particle Swarm Optimization (PSO) is a relatively new evolutionary algorithm, which until now has not been used to find global-minimum structures of chemical systems. Results from calculations on  $\text{LJ}_{26}$ ,  $\text{Si}_2\text{H}_5^-$ , and  $\text{OH}^-(\text{H}_2\text{O})_3$  demonstrate PSO's

ability to efficiently find global minimum structures for different types of chemical systems. PSO requires smaller population sizes than genetic algorithms. Also, PSO is advantageous because it is a population-based method, which can be run in parallel. This PSO application has several additional novel features including:

- flexible random initialization procedure controlling the quality of the initial population in terms of the fragmentation of the generated structures.
- enforcement of user-defined minimum/maximum distance constraints between atoms with different minimum/maximum distances between different types of atoms.
- measurement of the similarity of structures using a distance metric which ignores irrelevant translation, rotation, and reflection information.
- allowing groups of atoms that are moved and rotated as rigid units.
- capability of parallel execution.

This PSO application was written in C++ for the Linux platform and includes implementations of simulated annealing, basin hopping, and a basic genetic algorithm. It can perform multiple energy calculations at the same time and Gaussian 03 single point energy computations can be performed on multiple processors on a single workstation. The initial results presented here suggest that PSO has the potential to make valuable contributions in the search for global minimum and low energy structures.

## References

1. Bera, P. P.; Sattelmeyer, K. W.; Saunders, M.; Schaefer III, H. F.; Schleyer, P. v. R. *J Phys Chem A* 2006, 110, 4287.

2. Saunders, M. J *Comput Chem* 2004, 25, 621.
3. Lloyd, L. D.; Johnston, L. *Chem Phys* 1998, 236, 107.
4. Grubmuller, H. *Phys Rev E* 1995, 52, 1893.
5. Car, R.; Parrinello, M. *Phys Rev Lett* 1985, 55, 2471.
6. (a) Jones, R. O.; Gantefor, G.; Hunsicker, S.; Pieperhoff, P. *J Chem Phys* 1995, 103, 9549. (b) Jones, R. O.; Lichtenstein, A. I.; Hutler, J. *J Chem Phys* 1997, 106, 4556. (c) Jones, R. O. *J Chem Phys* 1999, 110, 5189.
7. Yourshaw, I.; Zhao, Y.; Neumark, D. M. *J Chem Phys* 1996, 105, 351.
8. Tomasulo, A.; Ramakrishna, M. V. *J Chem Phys* 1996, 105, 10449.
9. Lenzer, T.; Yourshaw, I.; Furlanetto, M. R.; Pivonka, N. L.; Neumark, D. M. *J Chem Phys* 2001, 115, 3578.
10. Corcelli, S. A.; Kelley, J. A.; Tully, J. C.; Johnson, M. A. *J Phys Chem A*, 2002, 106, 4872.
11. Haubein, N. C.; McMillan, S. A.; Broadbelt, L. J. *J Chem Inform and Comp Sci* 2003, 43, 68.
12. Haubein, N. C.; McMillan, S. A.; Broadbelt, L. J.; Snurr, R. Q. *J Chem Inform and Comp Sci* 2003, 43, 1820.
13. Bertolus, M.; Finocchi, F.; Millie, P. *J Chem Phys* 2004, 120, 4333.
14. Hamad, S.; Richard, C.; Catlow, A.; Spanó, E.; Matxain, J. M.; Ugalde, J. M. *J Phys Chem B* 2005, 109, 2703.
15. Wales, D. J.; Doye, J. P. K. *J Phys Chem A* 1997, 101, 5111.
16. Doye, J. P. K.; Wales, D. J.; Miller, M. *J Chem Phys* 1998, 109, 8143.

17. Back, T. *Evolutionary Algorithm in Theory and Practice: Evolutionary Programming, Genetic Algorithms*; Oxford University Press: Oxford, 1990.
18. Berg, B.; Neuhaus, T. *Phys Lett B* 1991, 267, 249.
19. (a) Deaven, D. M.; Ho, K. M. *Phys. Rev. Lett.* 1995, 75, 288. (b) Wille, L. T.; Vennik, J. *J Phys A: Math Gen* 1985, 18, L419.
20. White, R. P.; Niesse, J. A.; Mayne, H. R. *J Chem Phys* 1997, 108, 2208.
21. Kabrede, H.; Hentschke, R. *J Chem Phys B* 2002, 106, 10089.
22. Babadova-Parvanova, P.; Jackson, K. A.; Srinivas, S.; Horoi, M.; Kohler, C.; Seifert, G. *J Chem Phys* 2002, 116, 3576.
23. Lai, S. K.; Hsu, P. J.; Wu, K. L.; Liu, W. K.; Iwamatsu, M. *J Chem Phys* 2002, 117, 10715.
24. Zhao, J.; Xie, R. *Comput Theor Nanosci* 2004, 1, 117.
25. Alexandrova, A. N.; Boldyrev, A. I.; Fu, Y. J.; Yang, X.; Wang, X. B.; Wang L. S. *J Chem Phys* 2004, 121, 5709.
26. Alexandrova, A. N.; Boldyrev, A. I. *J Chem Theory Comput* 2005, 1, 566.
27. Goedecker, S. *J Chem Phys* 2004, 120, 9911.
28. Eberhart, R. C.; Kennedy, J. A. *Proceedings of the Sixth International Symposium on Micro Machine and Human Science*, 1995.
29. Kennedy, J.; Eberhart, R. C. *Proceedings IEEE International Conference on Neural Networks*, 1995, IV, 1942.
30. Shi, Y.; Eberhart, R. C. *Proceedings of the IEEE Congress on Evolutionary Computation*, 1999.



31. Suganthan, P. N. Proceedings of the IEEE Congress on Evolutionary Computation, 1999, 1958.
32. Eberhart, R. C.; Shi, Y. Proceedings of the IEEE Congress on Evolutionary Computation, 2001.
33. Riget, J.; Vesterstrom, J. S. EVALife Tech Report 2002-02.
34. Van der Bergh, F.; Engelbrecht, A. P. IEEE Trans on Evolut Comput 2004, 8, 225.
35. Eberhart, R. C.; Shi, Y. IEEE Trans on Evolut Comput 8, 2004, 201.
36. (a) Mohais, A. S.; Mendes, R.; Ward, C.; Posthoff, C. Lecture Notes in Artificial Intelligence 2005, 3809, 776. (b) Bergh, V. d. F.; Engelbrecht, A. P. Information Sciences 2006, 176, 937. (c) Chen, K.; Li, T. H.; Cao, T. C. Chemometrics and Intelligent Laboratory Systems 2006, 82, 248. (d) Ho, S.J.; Ku, W.Y.; Jou, J. W.; Hung M. H.; Ho, S.Y. Lecture Notes in Artificial Intelligence 2006, 3918, 790. (e) Kadirkamanathan, V.; Selvarajah, K.; Fleming, P. J. IEEE Trans. on Evolut. Comput 2006, 10, 245.
37. Hoare, M. R.; Pal, P. Adv Phys 1971, 20, 161.
38. Hoare, M. R.; Pal, P. Nature (Physical Science) 1971, 230, 645.
39. Hoare, M. R.; Pal, P. Nature (Physical Science) 1972, 236, 35.
40. Hoare, M. R.; Pal, P. Adv Phys 1975, 24, 645.
41. Hoare, M. R. Adv Chem Phys 1979, 40, 49.
42. Freeman, D. L.; Doll, D. J. J Chem Phys 1985, 82, 462.
43. Farges, J.; de Feraudy, M. F.; Raoult, B.; Torchet, G. Surf Sci 1985, 156, 370.
44. Wille, L. T.; Chem. Phys Lett 1987, 133, 405.

45. Northby, J. A. *J. Chem Phys* 1987, 87, 6166.
46. Coleman, T.; Shalloway, D. *J Global Optimization* 1994, 4, 171.
47. Xue, G. L. *J Global Optimization* 1994, 4, 425.
48. Pillardy, J.; Piela, L. *J Phys Chem* 1995, 99, 11805.
49. Doye, J. P. K.; Wales, D. J.; Berry, R. S. *J Chem Phys* 1995, 103, 4234.
50. Doye, J. P. K.; Wales, D. J. *Chem Phys Lett* 1995, 247, 339.
51. Deaven, D. M.; Tit, N.; Morris, J. R.; Ho, K. M. *Chem Phys Lett* 1996, 256, 195.
52. Tsai, C. J.; Jordan, K. D. *J Phys Chem* 1993, 97, 11227.
53. Mackay, A. L. *Acta Cryst* 1962, 15, 916.
54. Kunz, R. E.; Berry, R. S. *Phys Rev Lett* 1993, 71, 3987.
55. Kunz, R. E.; Berry, R. S. *Phys Rev E* 1994, 49, 1895.
56. Marks, L. D. *Phil Mag A* 1984, 49, 81.
57. Doye, J. P. K.; Wales, D. J. *J Chem Phys* 1996, 105, 8428.
58. Doye, J. P. K.; Wales, D. J. *Z Phys D* 1997, 40, 194.
59. Nelson, D. R.; Spaepen, F. *Solid State Phys* 1989, 42, 1.
60. Doye, J. P. K.; Wales, D. J. *Science* 1996, 271, 484.
61. Doye, J. P. K.; Wales, D. J. *J Phys B* 1996, 29, 4859.
62. Niesse, J. A.; Mayne, H. R. *J Chem Phys* 1996, 105, 4700.
63. Barron, C.; Gomez, S.; Romero, D. *Appl Math Lett* 1996, 9, 75.
64. Gregurick, S. K.; Alexander, M. H.; Hartke, B. *J Chem Phys* 1996, 104, 2684.
65. Hartke, B. *J Comput Chem* 1999, 20, 1752.
66. Mestres, J.; Scuseria, G. E. *J Comput Chem* 1995, 16, 729.
67. Xiang, Y.; Jiang, H.; Cai, W.; Shao, X. *J Phys Chem A* 2004, 108, 3586.

68. Stillinger, F. H.; Weber, T. A. *J Stat Phys* 1988, 52, 1429.
69. Piela, L.; Olszewski, K. A.; Pillardy, J. J. *Mol. Struct (Theochem)* 1994, 308, 229.
70. Kostrowicki, J.; Piela, L.; Cherayil, B. J.; Scheraga, H. A. *J Phys Chem* 1991, 95, 4113.
71. Scheraga, H. A. *Int. J Quant Chem* 1992, 42, 1529.
72. Stillinger, F. H.; Stillinger, D. K. *J Chem Phys* 1990, 93, 6106.
73. Head-Gordon, T.; Stillinger, F. H.; Stillinger, D. K. *Proc Natl Acad Sci USA* 1991, 88, 11076.
74. Pillardy, J.; Olszewski, K. A.; Piela, L. *J Phys Chem* 1992, 96, 4337.
75. Doye, J. P. K.; Wales, D. J. *J Chem Soc Faraday Trans* 1997, 93, 4233.
76. Kirkpatrick, S.; Gelatt, C. D.; Vecchi, M. P. *Science* 1983, 220, 671.
77. Wille, L. T. *Chem Phys Lett* 1987, 133, 405.
78. Ma, J.; Hsu, D.; Straub, J. E. *J Chem Phys* 1993, 99, 4024.
79. Ma, J.; Straub, J. E. *J Chem Phys* 1994, 101, 533.
80. Tsou, C.; Brooks, C. L. *J Chem Phys* 1994, 101, 6405.
81. Schelstrate, S.; Verschelde, H. *J Phys Chem A* 1992, 42, 1529.
82. Finnila, A. B.; Gomez, M. A.; Sebenik, C.; Stenson, C.; Doll, J. D. *Chem Phys Lett* 1996, 219, 343.
83. Maranas, C. D.; Floudas, C. A. *J Chem Phys* 1992, 97, 7667.
84. Maranas, C. D.; Floudas, C. A. *J Chem Phys* 1994, 100, 1247.
85. Stanton, A. F.; Bleil, R. E.; Kais, S. *J Comput Chem* 1997, 18, 594.
86. Serra, P.; Stanton, A. F.; Kais, S. *Phys Rev E* 1997, 55, 1162.
87. Serra, P.; Stanton, A. F.; Kais, S.; Bleil, R. E. *J Chem Phys* 1997, 106, 7170.

88. Cvijovic, D.; Klinowski, J. *Science* 1995, 267, 664.
89. Hong, S. D.; Jhon, M. S. *Chem Phys Lett* 1997, 267, 422.
90. (a) Xiang, Y.; Cheng, L.; Cai, W.; Shao, X. *J Phys Chem A* 2004, 108, 9516. (b) Shao, X. G.; Jiang, H. Y.; Cai, W. S. *J Chem Inf Comput Sci* 2004, 44, 193. (c) Lee, J.; Lee, I. H.; Lee, J. *Phys Rev Lett* 2003, 91, 080201.
91. Jasinski, J. M.; Meyerson, B. S.; Scott, B. A. *Annu Rev Phys Chem* 1987, 38, 109
92. (a) Sillars, D.; Bennett, C. J.; Osamura, Y.; Kaiser, R. I. *Chem Phys* 2004, 305, 141. (b) Kaiser, R. I.; Osamura, Y. *A&A* 2005, 432, 559.
93. Kutzelnigg, W. *Angew Chem Int Ed Engl* 1984, 23, 272.
94. Sannigrahi, A. B.; Nandi, P. K. *Chem Phys Lett* 1992, 188, 575.
95. Dubois, I. *Can J Phys* 1968, 46, 2485.
96. Kasdan, A.; Herbst, E.; Lineberger, W. C. *J Chem Phys* 1975, 62, 541.
97. Brown, J. M.; Robinson, D. *Mol Phys* 1984, 51, 883.
98. Ohno, K.; Matsuura, H.; Endo, Y.; Hirota, E. *J Mol Spectrosc* 1985, 111, 73.
99. Nimlos, M. R.; Ellison, G. B. *J Am Chem Soc* 1986, 108, 6522.
100. Boo, B. H.; Armentrout, P. B. *J Am Chem Soc* 1987, 109, 3549.
101. Berkowitz, J.; Greene, J. P.; Cho, H.; Ruscic, B. *J Chem Phys* 1987, 86, 1235.
102. Arnold, C. C.; Kitsopoulos, T. N.; Neumark, D. M. *J Chem Phys* 1993, 99, 766.
103. Liu, Z.; Davies, P. B. *Phys Rev Lett* 1996, 76, 596.
104. Liu, Z.; Davies, P. B. *J Chem Phys* 1996, 105, 3443.
105. Xu, C.; Taylor, T. R.; Burton, G. R.; Neumark, D. M. *J Chem Phys* 1998, 108, 7645.

106. Scheer, M.; Bilodeau, R. C.; Brodie, C. A.; Haugen, H. K. *Phys Rev A* 1998, 58, 2844.
107. Nimlos, M. R.; Harding, L. B.; Elison, G. B. *J Chem Phys* 1987, 87, 5116.
108. Kitsopoulos, T. N.; Chick, C. J.; Zhao, Y.; Neumark, D. M. *J Chem Phys* 1991, 95, 1441
109. Shotten. K. C.; Lee, A. G.; Jones, W. J. *J Raman Spectrosc* 1973, 1, 243.
110. Raghavachari, K.; Rohlfing, C. M. *J Chem Phys* 1991, 94, 3670.
111. Viswanathan, R.; Thompson, D. L.; Raff, L. M. *J Chem Phys* 1984, 80, 4230.
112. Allen, W. D.; Schaefer, H. F. *Chem Phys* 1986, 108, 243.
113. Colegrove, B. T.; Schaefer, H. F. *J Phys Chem* 1990, 94, 5593.
114. Shen, M.; Schaefer, H. F. *Mol Phys* 1992, 76, 467.
115. Curtiss, L. A.; Raghavachari, K.; Deutsch, P. W.; Pople, J. A. *J Chem Phys* 1991, 95, 2433.
116. Kalcher, J.; Sax, A. F. *Chem Phys Lett* 1992, 192, 451.
117. Becerra, R.; Walsh, R. *J Phys Chem* 1992, 96, 10856.
118. Hühn, M. M.; Amos, R. D.; Kobayashi, R.; Handy, N. C. *J Chem Phys* 1993, 98, 7107.
119. Kalcher, J.; Sax, A. F. *Chem Phys Lett* 1993, 215, 601.
120. Tada, T.; Yoshimura, R. *J Phys Chem* 1993, 97, 1019.
121. Taketsugu, T.; Gordon, M. S. *J Phys Chem* 1995, 99, 8462.
122. Ma, B.; Allinger, N. L.; Schaefer, H. F. *J Chem Phys* 1996, 105, 5731.
123. King, R. A.; Mastryukov, V. S.; Schaefer, H. F. *J Chem Phys* 1996, 105, 6880.

124. Yamaguchi, Y.; Van Huis, T. J.; Sherrill, C. D.; Schaefer, H. F. *Theor Chem Acc* 1997, 97, 341.
125. Gong, X. G.; Guenzburger, D.; Saitovitch, E. B. *Chem Phys Lett* 1997, 275, 392.
126. Feller, D.; Dixon, D. A. *J Phys Chem* 1999, 103, 6413.
127. Jursic, B. S. *J. Mol Struct (Theochem)* 2000, 497, 65.
128. Aarset, K.; Császár, A. G.; Sibert, E. L.; Allen, W. D.; Schaefer, H. F.; Klopper, W.; Noga, J. *J Chem Phys* 2000, 112, 4053
129. Pak, C.; Rienstra-Kiracofe, J. C.; Schaefer III, H. F. *J. Phys Chem A* 2000, 104, 11232.
130. Bernal, J. D.; Fowler, R. H. *J Chem Phys* 1933, 1, 515.
131. Tuckerman, M.; Laasonen, K.; Sprik, M.; Parrinello, M. *J Chem Phys* 1995, 103, 150.
132. Tuckerman, M. E.; Marx, D.; Parrinello, M. *Nature* 2002, 417, 925.
133. Xantheas, S. S. *J Am Chem Soc* 1995, 117, 10373.
134. Novoa, J. J.; Mota, F.; Perez del Valle, C.; Planas, M. *J Phys Chem* 1997, 101, 7842.
135. Chaudhuri, C.; Wang, Y.-S.; Jiang, J. C.; Lee, Y. T.; Chang, H.-C.; Niedner-Schatteburg, G. *Mol Phys* 2001, 99, 1161.
136. Robertson, W. H.; Diken, E. G.; Price, E. A.; Shin, J.-W.; Johnson, M. A. *Science* 2003, 299, 1367.
137. Carugo, O.; Pongor, S. *Protein Science* 2001, 10, 1470.
138. Gaussian 03 (revision A.1). Frisch, M. J.; Trucks, G. M.; Schlegel, H. B.; Scuseria, G. E.; Robb, M. A.; Cheeseman, J. R.; Montgomery, Jr., J. A.; Vreven,

- T.; Kudin, K. N.; Burant, J. C.; Millam, J. M.; Iyengar, S. S.; Tomasi, J.; Barone, V.; Mennucci, B.; Cossi, M.; Scalmani, G.; Rega, N.; Petersson, G. A.; Nakatsuji, H.; Hada, M.; Ehara, M.; Toyota, K.; Fukuda, R.; Hasegawa, J.; Ishida, M.; Nakajima, T.; Honda, Y.; Kitao, O.; Nakai, H.; Klene, M.; Li, X.; Knox, J. E.; Hratchian, H. P.; Cross, J. B.; Adamo, C.; Jaramillo, J.; Gomperts, R.; Stratmann, R. E.; Yazyev, O.; Austin, A. J.; Cammi, R.; Pomelli, C.; Ochterski, J. W.; Ayala, P. Y.; Morokuma, K.; Voth, G. A.; Salvador, P.; Dannenberg, J. J.; Zakrzewski, V. G.; Dapprich, S.; Daniels, A. D.; Strain, M. C.; Farkas, O.; Malick, D. K.; Rabuck, A. D.; Raghavachari, K.; Foresman, J. B.; Ortiz, J. V.; Cui, Q.; Baboul, A. G.; Clifford, S.; Cioslowski, J.; Stefanov, B. B.; Liu, G.; Liashenko, A.; Piskorz, P.; Komaromi, I.; Martin, R. L.; Fox, D. J.; Keith, T.; Al-Laham, M. A.; Peng, C. Y.; Nanayakkara, A.; Challacombe, M.; Gill, P. M. W.; Johnson, B. G.; Chen, W.; Wong, M. W.; Gonzales, C.; Pople, J. A., Gaussian, Inc., Pittsburgh PA, 2003.
139. (a) Parr, R. G.; Yang, W. *Density-functional theory of atoms and molecules*. 1989, Oxford Univ. Press, Oxford. (b) Becke, A. D. *J Chem Phys* 1993, 98, 5648. (c) Perdew, J. P.; Chevary, J. A.; Vosko, S. H.; Jackson, K. A.; Pederson, M. R.; Singh, D. J.; Fiolhais, C. *Phys Rev B* 1992, 46, 6671. (d) Clark, T.; Chandrasekhar, J.; Spitznagel, G.W.; Schleyer, P. v. R. *J Comput Chem* 1983, 4, 294. (e) Frisch, M. J.; Pople, J. A.; Binkley, J. S. *J Chem Phys* 1984, 80, 3265.
140. Schaftenaar, G. *MOLDEN3.4*, CAOS/CAMM Center, The Netherlands, 1998.

## CHAPTER 16

## SUMMARY

Fast development of the computational quantum chemical methods and user friendly scientific software in recent decades significantly changed the way theoretical chemistry works. It makes it relatively simple to determine structures of chemical objects and their energetic characteristics, e.g. ground-state or excitation energies, energetic profiles of the reactions, etc., thus obtaining pieces of data, which are not directly connected to each other. Rationalizing the obtained information, or building *chemical* theory of the experimentally observed facts and computationally obtained data is what makes chemistry a separate science distinct from physics.

The emphasis and the main result of this dissertation is development of a method of chemical bonding analysis applicable to main-group element and transition-metal clusters, that on one hand is closely related to the concept of a pair of electrons as the main object of chemical bonding<sup>1</sup> and on the other hand seamlessly incorporates the concept of the delocalized (aromatic/antiaromatic) bonding<sup>2</sup>. The new method is called Adaptive Natural Density Partitioning (AdNDP).<sup>3</sup> Within its framework chemical bonding is described in terms of n-center 2-electron (nc-2e) bonds where n ranges from one (core electrons, lone-pairs) to the total number of atoms in the system (completely delocalized bonding) through all the intermediate values (2c-2e Lewis bonds, 3c-2e, 4c-2e, and so on). The algorithm of the AdNDP, which is a generalization of the Natural Bonding Orbital (NBO) analysis,<sup>4</sup> is implemented in the software that is now the main



tool used in the group of Professor Alex Boldyrev (Department of Chemistry and Biochemistry, Utah State University) for deciphering chemical bonding in clusters.

The full-cycle studies of the main-group element and transition-metal clusters constitute the main body of the dissertation. These studies include photoelectron spectroscopy (PES) of anionic clusters in molecular beams performed by the group of Professor Lai-Sheng Wang (Pacific Northwest National Laboratory, Washington State University), establishing the global minimum structures and low-lying isomers of the corresponding anions using global optimization techniques (Gradient Embedded Genetic Algorithm (GEGA), Particle Swarm Optimization (PSO), Simulated Annealing), modeling PES of these structures by means of high-level ab-initio (Coupled-Cluster with Single, Double and non-iterative Triple excitations (CCSD(T)), Equation-of-Motion based on Coupled-Cluster (EOM-CCSD(T)), Outer Valence Green Function theory (OVGF)) and density functional theoretical (Time-Dependent Density Functional Theory (TD DFT)) methods, description of the chemical bonding in the species contributing to the experimentally observed spectra using Canonical Molecular Orbitals (CMO), Natural Bonding Orbital (NBO) analysis, and Electron Localization Function (ELF) analysis. The main results of this part of the dissertation can be summarized as follows.

A new mode of aromatic bonding never encountered previously - d-aromaticity, was identified in the experimentally observed  $\text{Ta}_3\text{O}_3^-$  cluster.<sup>5</sup> This type of bonding occurs only in multinuclear transition-metal systems.  $\text{Ta}_3\text{O}_3^-$  cluster was proved to have triangular Ta-atom core due to the simultaneous presence of p- and d- aromaticity originating from the d-atomic orbitals of Ta.

Heteroatomic main-group clusters  $\text{AlSi}_2^-$ ,  $\text{AlGe}_2^-$ , and  $\text{AlCGe}^-$  were found to have non-linear structures.<sup>6</sup> In case of  $\text{AlSi}_2^-$  and  $\text{AlGe}_2^-$  the non-linearity was attributed to the conflicting aromaticity (simultaneous presence of s-antiaromaticity and p-aromaticity) of the species.  $\text{AlCGe}^-$  cluster turned out to be a system with neither aromatic nor classical bonding.

A phenomenon of gold “aping” hydrogen in bonding with planar boron clusters was established in the study of  $\text{B}_7\text{Au}_2^-$ .<sup>7</sup> The bonding in this species and  $\text{B}_7\text{H}_2^-$  was explained on the basis of the strong covalent B-Au (H) bonding and the concepts of aromaticity/antiaromaticity. Together with Au/H analogy in bonding with silicon clusters this finding suggests that the analogy may actually be a general phenomenon typical for a wide range of chemical species. It was used to make a theoretical prediction of the viability of a new class of species, deltahedral closo-auroboranes  $\text{B}_x\text{Au}_x^{2-}$  ( $x=5-12$ ), analogous to the famous spherical closo-boranes  $\text{B}_x\text{H}_x^{2-}$  ( $x=5-12$ ).<sup>8</sup> The limit of Au/H analogy was tested in the joint experimental and theoretical study of  $\text{Au}_x\text{BO}^-$  ( $x=1-3$ ) species and their comparison with the borane oxides  $\text{H}_x\text{BO}^-$  ( $x=1-3$ ).<sup>9</sup> Interaction of a single Au atom with a bare BO unit was proved to mimic that of hydrogen. The neutral AuBO fragment remained unchanged in  $\text{Au}_2\text{BO}^-$  and  $\text{Au}_3\text{BO}^-$  upon addition of the second and third Au atoms, respectively. The studied  $\text{Au}_x\text{BO}^-$  ( $x=1-3$ ) species can also be viewed as  $\text{Au}_x^-[\text{BO}]$  complexes, with a significant charge transfer from  $\text{BO}^-$  to the  $\text{Au}_x$  fragment, analogous to the charge transfer in  $\text{Au}_x\text{CO}$  complexes.

The family of the known spherically symmetric clusters was expanded by the discovery that  $\text{Sn}_{12}^{2-}$  is an icosahedral cage that distorts just slightly upon addition of the  $\text{Na}^+$  cation within  $\text{NaSn}_{12}^-$  species.<sup>10</sup> The size of  $\text{Sn}_{12}^{2-}$  stannaspherene is comparable with

the size of  $C_{60}$  fullerene, so the stannaspherene potentially can host an atom inside its cage. The chemical bonding in the stannaspherene is closely related to that in the valence isoelectronic icosahedral closo-borane  $B_{12}H_{12}^{2-}$ .

Atoms of the fourth group in the periodic table (C, Si, Ge, Sn, Pb) and the BH structural unit of the deltahedral closo-boranes are valence isoelectronic. The studies of anionic silicon clusters were undertaken to explore if doubly charged silicon anions adopt high symmetric cage-like structures typical for the deltahedral closo-boranes. It was established,<sup>11</sup> that  $Si_5^-$  and  $Si_5^{2-}$  (within  $NaSi_5^-$  cluster) adopt trigonal bipyramidal structures. Though  $Si_5^{2-}$  and isoelectronic  $B_5H_5^{2-}$  clusters turned out to be isostructural, the analysis of chemical bonding in  $Si_5^{2-}$  showed significant involvement of lone-pairs into the skeletal bonding, not encountered in  $B_5H_5^{2-}$ . This apparent difference in the bonding patterns of boranes and silicon dianionic clusters manifested itself in structural peculiarities of the  $Si_6^{2-}$  cluster.<sup>12</sup> While the global minimum structure of the bare dianion  $Si_6^{2-}$  is octahedral just like  $B_6H_6^{2-}$ , the HOMO-LUMO switch and dramatic structural rearrangement occurs in the presence of  $Na^+$  in  $NaSi_6^-$  anion observed in molecular beams. Thus, the distorted  $Si_6^{2-}$  unit within the  $NaSi_6^-$  global minimum structure was shown to be spherically antiaromatic, despite the isolobal analogy with spherically aromatic  $B_6H_6^{2-}$ .

Comprehensive analysis of the chemical bonding in a family of planar boron clusters was performed to generalize the existing knowledge and formulate a chemical bonding model for these species.<sup>13</sup> It was shown that structure and properties of the planar or quasi-planar boron clusters are shaped by not only p-aromatic/antiaromatic (delocalized) bonding, but also by s-aromatic/antiaromatic (delocalized) bonding and

presence of the localized 2c-2e peripheral B-B bonds. Appropriate geometric fit was demonstrated to be important for choosing between empty cyclic structures or cycles with filled central cavity. Also, the possible types of the aromaticity, multifold nature of aromaticity, antiaromaticity, and conflicting aromaticity, as well as counting rules for  $\sigma$ -,  $\pi$ -, and  $\delta$ -aromaticity/antiaromaticity in transition metal clusters were analyzed and systematically reviewed.<sup>14</sup>

The last but not least aspect of the dissertation is methodological. Diversity of theoretical techniques for quantum chemical calculations sometimes leads to qualitative diversity of the obtained results. Availability of computationally inexpensive and fast density functional codes results in a huge number of theoretical predictions, contradicting each other or high level ab initio results. It was crucial for the present dissertation to single out the reliable DFT methods.<sup>15</sup> The hybrid DFT methods such as B3LYP were shown to provide reliable results in good agreement with high level CCSD(T) and CASSCF-MRCI computations unlike non-hybrid DFT methods, so B3LYP calculations were actively used throughout the projects that constitute the dissertation. Another methodological result of the dissertation is development of the software for the global optimization based on the Particle Swarm Optimization algorithm.<sup>16</sup> The author of the particular flavor of the algorithm that can be used for the global optimizations of chemical structures and the code is Seth T. Call (Computer Science major, Utah State University). The author of the present dissertation contributed to the project by refining the concept of the software, assisting in the development of the structure of the algorithm, picking up chemical systems for testing purposes, and testing the software. Application of the global optimization techniques for the search of the global minimum structures is de-

facto standard of the modern computational chemistry. As all the existing techniques are highly stochastic in nature and none can guarantee successful determination of the global minimum structure, it is very important to have access to a variety of tools, so that their results can be crosschecked and verified and erroneous conclusions avoided.

The results of the Dissertation have broader impact. The Dissertation significantly contributed to building up empirical knowledge of chemistry and material science by establishing structures of the main-group element and transition metal clusters observed in molecular beams. This task is very complicated and knowing structures of the clusters under specific experimental conditions is highly relevant to other spheres of the scientific activities, both fundamental and applied, and to engineering applications. The obtained empirical knowledge was used to formulate certain unified descriptive approach that can be utilized to rationalize the gathered data. This novel method called Adaptive Natural Density Partitioning has been successfully applied to a variety of chemical systems. Now the road is open to establish connections between the obtained descriptions and structural, physical, and chemical properties of clusters, molecules, polymers, bulk phases etc. Ultimately, it will lead to the predictions of the properties of the yet unknown chemical objects and rational design of materials and processes with preset properties. AdNDP will stimulate and increase the efficiency of the theoretical and experimental chemical research aimed at understanding the properties of the widest range of existing chemical systems, designing novel ones, and revealing mechanisms of complex processes. Some of the results of the Dissertation, such as predicted family of deltahedral closo-auroboranes, experimentally observed deltahedral stannaspherene, and  $\delta$ -aromatic  $\text{Ta}_3\text{O}_3^-$  might have immediate impact on the design of novel nano-catalysts, nano-machines, and

semiconducting nano-materials. Developed Particle Swarm Optimization software for the global optimization has a great potential to be used in molecular modeling for the bio-molecular and pharmaceutical research.

## References

1. (a) Lewis, G. N. *J. Am. Chem. Soc.* **1931**, *53*, 1367; (b) Weinhold, F.; Landis, C. R. Valency and Bonding: A Natural Bond Orbital Donor-Acceptor Perspective; Cambridge University Press: Cambridge, UK, **2005**.
2. Kekule, A. *Bull. Soc. Chim. Fr. (Paris)*, **1865**, *3*, 98; (b) Boldyrev, A. I.; Wang, L. S. *Chem. Rev.* **2005**, *106*, 3716
3. Zubarev, D. Yu.; Boldyrev, A. I. (in press)
4. Foster, J. P.; Weinhold, F. *J. Am. Chem. Soc.* **1980**, *102*, 7211.
5. Zhai, H.-J.; Averkiev, B. B.; Zubarev, D. Yu.; Wang, L. S.; Boldyrev, A. I. *Angew. Chem. Int. Ed.* **2007**, *46*, 4277.
6. Zubarev, D. Yu.; Boldyrev, A. I.; Li, X.; Wang, L. S. *J. Phys. Chem. B*, **2006**, *110*, 9743.
7. Zhai, H.-J.; Wang, L. S.; Zubarev, D. Y.; Boldyrev A. I. *J. Phys. Chem. A*, **2006**, *110*, 1689.
8. Zubarev, D. Yu.; Li, J.; Wang, L. S.; Boldyrev, A. I. *Inorg. Chem.* **2006**, *45*, 5269.
9. Zubarev, D. Yu.; Boldyrev, A. I.; Li, J.; Zhai, H.-J.; Wang, L. S. *J. Phys. Chem. A*, **2007**, *111*, 1648.

10. Cui, L. F.; Huang, X.; Wang, L. M.; Zubarev, D. Yu.; Boldyrev, A. I.; Li, J.; Wang L. S. *J. Am. Chem. Soc.* **2006**, *128*, 8390.
11. Zubarev, D. Yu.; Boldyrev, A. I.; Li, X.; Cui, L. F.; Wang, L. S. *J. Phys. Chem. A* **2005**, *109*, 11385.
12. Zubarev, D. Yu.; Alexandrova, A.; Boldyrev, A. I.; Cui, L. F.; Li, X.; Wang, L. S. *J. Chem. Phys.* **2006**, *124*, 124305.
13. Zubarev, D. Yu.; Boldyrev, A. I. *J. Comput. Chem.* **2006**, *28*, 251.
14. Zubarev, D. Yu.; Averkiev, B. B.; Zhai, H. -J.; Lai-Sheng Wang; Boldyrev, A. I. *Phys. Chem. Chem. Phys.* **2008**, *10*, 257
15. Zubarev, D. Yu.; Boldyrev, A. I. *J. Chem. Phys.* **2005**, *122*, 144322.
16. Call, S. T.; Zubarev, D. Yu.; Boldyrev, A. I. *J. Comput. Chem.* **2007**, *28*, 1177.

APPENDIX



PERMISSIONS

## American Chemical Society's Policy on Theses and Dissertations

If your university requires a signed copy of this letter see contact information below.

Thank you for your request for permission to include **your** paper(s) or portions of text from **your** paper(s) in your thesis. Permission is now automatically granted; please pay special attention to the implications paragraph below. The Copyright Subcommittee of the Joint Board/Council Committees on Publications approved the following:

### Copyright permission for published and submitted material from theses and dissertations

ACS extends blanket permission to students to include in their theses and dissertations their own articles, or portions thereof, that have been published in ACS journals or submitted to ACS journals for publication, provided that the ACS copyright credit line is noted on the appropriate page(s).

### Publishing implications of electronic publication of theses and dissertation material

Students and their mentors should be aware that posting of theses and dissertation material on the Web prior to submission of material from that thesis or dissertation to an ACS journal may affect publication in that journal. Whether Web posting is considered prior publication may be evaluated on a case-by-case basis by the journal's editor. If an ACS journal editor considers Web posting to be "prior publication", the paper will not be accepted for publication in that journal. If you intend to submit your unpublished paper to ACS for publication, check with the appropriate editor prior to posting your manuscript electronically.

If your paper has not yet been published by ACS, we have no objection to your including the text or portions of the text in your thesis/dissertation in **print and microfilm formats**; please note, however, that electronic distribution or Web posting of the unpublished paper as part of your thesis in electronic formats might jeopardize publication of your paper by ACS. Please print the following credit line on the first page of your article: "Reproduced (or 'Reproduced in part') with permission from [JOURNAL NAME], in press (or 'submitted for publication'). Unpublished work copyright [CURRENT YEAR] American Chemical Society." Include appropriate information.

If your paper has already been published by ACS and you want to include the text or portions of the text in your thesis/dissertation in **print or microfilm formats**, please print the ACS copyright credit line on the first page of your article: "Reproduced (or 'Reproduced in part') with permission from [FULL REFERENCE CITATION.] Copyright [YEAR] American Chemical Society." Include appropriate information.

**Submission to a Dissertation Distributor:** If you plan to submit your thesis to UMI or to another dissertation distributor, you should not include the unpublished ACS paper in your thesis if the thesis will be disseminated electronically, until ACS has published your paper. After publication of the paper by ACS, you may release the entire thesis (**not the individual ACS article by itself**) for electronic dissemination through the distributor; ACS's copyright credit line should be printed on the first page of the ACS paper.

**Use on an Intranet:** The inclusion of your ACS unpublished or published manuscript is permitted in your thesis in print and microfilm formats. If ACS has published your paper you may include the manuscript in your thesis on an intranet that is not publicly available. Your ACS article cannot be posted electronically on a publicly available medium (i.e. one that is not password protected), such as but not limited to, electronic archives, Internet, library server, etc. The only material from your paper that can be posted on a public electronic medium is the article abstract, figures, and tables, and you may link to the article's DOI or post the article's author-directed URL link provided by ACS. This paragraph does not pertain to the dissertation distributor paragraph above.

Questions? Call +1 202/872-4368/4367. Send e-mail to [copyright@acs.org](mailto:copyright@acs.org) or fax to +1 202-776-8112. 10/10/03, 01/15/04, 06/07/06

03/03/2008 11:17 FAX

JOHN WILEY &amp; SONS INC

001



Gale  
Krouser/Corp/Hoboken/Wile  
y  
02/20/2008 02:16 PM

To "Dmitry Yu. Zubarev" <dzoubarev@cc.usu.edu>  
cc bjohns@wiley.com  
bcc  
Subject Re: permission to reprint papers as a part of PhD dissertation

Hello,

"Dmitry Yu. Zubarev" <dzoubarev@cc.usu.edu>

02/20/2008 01:58 AM

To gkrouser@wiley.com  
cc

Subject permission to reprint papers as a part of PhD dissertation

Dear Mr. Gale Krouser,

my name is Dmitry Yu. Zubarev. I'm a senior graduate student in Utah State University currently finalizing my PhD dissertation. I'm hereby asking for the permission to reprint two articles co-authored by me and published in Journal of Computational Chemistry, as a part of this Dissertation. It would be more convenient for me to receive the permission by fax.

My mailing address:  
Department of Chemistry and Biochemistry,  
Utah State University,  
0300 Old Main Hill,  
Logan, UT 84322-0300

Phone number: (435) 797-7507  
Fax number: (435) 797-3390

The articles to be reprinted:

- 1) "Global Minimum Structure Searches via Particle Swarm Optimization", Call, S. T.; Zubarev, D. Yu.; Boldyrev, A. I. J. Comput. Chem. 2007, 28, 1177.
- 2) "Comprehensive Analysis of Chemical Bonding in Boron Clusters", Zubarev, D. Yu.; Boldyrev, A. I. J. Comput. Chem. 2006, 28, 251.

I'm not a correspondence author.

**PERMISSION GRANTED**  
BY: *[Signature]* 2/28/08  
Global Rights Dept., John Wiley & Sons, Inc.

**NOTE: No rights are granted to use content that appears in the work with credit to another source**

Brad Johnson, Permissions Assistant  
John Wiley & Sons Inc.  
111 River St  
Hoboken, NJ 07030  
[bjohns@wiley.com](mailto:bjohns@wiley.com)  
201-748-6786  
201-748-6008 [fax]

**AMERICAN INSTITUTE OF PHYSICS LICENSE  
TERMS AND CONDITIONS**

Jul 10, 2008

This is a License Agreement between Dmitry Yu Zubarev ("You") and American Institute of Physics ("American Institute of Physics"). The license consists of your order details, the terms and conditions provided by American Institute of Physics, and the payment terms and conditions.

License Number	1898211110419
License date	Feb 29, 2008
Licensed content publisher	American Institute of Physics
Licensed content title	Appraisal of the performance of nonhybrid density functional methods in characterization of the Al4C molecule
Licensed content author	Dmitry Yu. Zubarev and Alexander I. Boldyrev
Type of Use	Republish Entire Article
Requestor Type	Author
Title of your work	PhD dissertation
Publisher of your work	Utah State University
Publication date of your work	04/01/2008
PO Number	pending
Promotion code	
Total	\$0.00

**Terms and Conditions**

American Institute of Physics -- Terms and Conditions: Permissions Uses

American Institute of Physics ("AIP") hereby grants to you the non-exclusive right and license to use and/or distribute the Material according to the use specified in your order, on a one-time basis, for the specified term, with a maximum distribution equal to the number that you have ordered. Any links or other content accompanying the Material are not the subject of this license.

1. You agree to include the following copyright and permission notice with the reproduction of the Material: "Reprinted with permission from [FULL CITATION]. Copyright [PUBLICATION YEAR], American Institute of Physics." For an article, the copyright and permission notice must be printed on the first page of the article or book chapter. For photographs, covers, or tables, the copyright and permission notice may appear with the Material, in a footnote, or in the reference list.
2. If you have licensed reuse of a figure, photograph, cover, or table, it is your responsibility to ensure that the material is original to AIP and does not contain the copyright of another entity, and that the copyright notice of the figure, photograph, cover, or table does not indicate that it was reprinted by AIP, with permission, from another source. Under no circumstances does AIP, purport or intend to grant permission to reuse material to which it does not hold copyright.

3. You may not alter or modify the Material in any manner. You may translate the Material into another language only if you have licensed translation rights. You may not use the Material for promotional purposes. AIP reserves all rights not specifically granted herein.
4. The foregoing license shall not take effect unless and until AIP or its agent, Copyright Clearance Center, receives the Payment in accordance with Copyright Clearance Center Billing and Payment Terms and Conditions, which are incorporated herein by reference.
5. AIP or the Copyright Clearance Center may, within two business days of granting this license, revoke the license for any reason whatsoever, with a full refund payable to you. Should you violate the terms of this license at any time, AIP, American Institute of Physics, or Copyright Clearance Center may revoke the license with no refund to you. Notice of such revocation will be made using the contact information provided by you. Failure to receive such notice will not nullify the revocation.
6. AIP makes no representations or warranties with respect to the Material. You agree to indemnify and hold harmless AIP, American Institute of Physics, and their officers, directors, employees or agents from and against any and all claims arising out of your use of the Material other than as specifically authorized herein.
7. The permission granted herein is personal to you and is not transferable or assignable without the prior written permission of AIP. This license may not be amended except in a writing signed by the party to be charged.
8. If purchase orders, acknowledgments or check endorsements are issued on any forms containing terms and conditions which are inconsistent with these provisions, such inconsistent terms and conditions shall be of no force and effect. This document, including the CCC Billing and Payment Terms and Conditions, shall be the entire agreement between the parties relating to the subject matter hereof.

This Agreement shall be governed by and construed in accordance with the laws of the State of New York. Both parties hereby submit to the jurisdiction of the courts of New York County for purposes of resolving any disputes that may arise hereunder.

---

---

**AMERICAN INSTITUTE OF PHYSICS LICENSE  
TERMS AND CONDITIONS**

Jul 10, 2008

This is a License Agreement between Dmitry Yu Zubarev ("You") and American Institute of Physics ("American Institute of Physics"). The license consists of your order details, the terms and conditions provided by American Institute of Physics, and the payment terms and conditions.

License Number	1898210814565
License date	Feb 29, 2008
Licensed content publisher	American Institute of Physics
Licensed content title	On the structure and chemical bonding of Si and Si in NaSi upon Na coordination
Licensed content author	Dmitry Yu. Zubarev, Anastassia N. Alexandrova, Alexander I. Boldyrev, Li-Feng Cui, Xi Li, and Lai-Sheng Wang
Type of Use	Republish Entire Article
Requestor Type	Author
Title of your work	PhD dissertation
Publisher of your work	Utah State University
Publication date of your work	08/01/2008
PO Number	pending
Promotion code	
Total	\$0.00

**Terms and Conditions**

American Institute of Physics -- Terms and Conditions: Permissions Uses

American Institute of Physics ("AIP") hereby grants to you the non-exclusive right and license to use and/or distribute the Material according to the use specified in your order, on a one-time basis, for the specified term, with a maximum distribution equal to the number that you have ordered. Any links or other content accompanying the Material are not the subject of this license.

1. You agree to include the following copyright and permission notice with the reproduction of the Material: "Reprinted with permission from [FULL CITATION]. Copyright [PUBLICATION YEAR], American Institute of Physics." For an article, the copyright and permission notice must be printed on the first page of the article or book chapter. For photographs, covers, or tables, the copyright and permission notice may appear with the Material, in a footnote, or in the reference list.
2. If you have licensed reuse of a figure, photograph, cover, or table, it is your responsibility to ensure that the material is original to AIP and does not contain the copyright of another entity, and that the copyright notice of the figure, photograph, cover, or table does not indicate that it was reprinted by AIP, with permission, from another source. Under no circumstances does AIP, purport or intend to grant

permission to reuse material to which it does not hold copyright.

3. You may not alter or modify the Material in any manner. You may translate the Material into another language only if you have licensed translation rights. You may not use the Material for promotional purposes. AIP reserves all rights not specifically granted herein.
4. The foregoing license shall not take effect unless and until AIP or its agent, Copyright Clearance Center, receives the Payment in accordance with Copyright Clearance Center Billing and Payment Terms and Conditions, which are incorporated herein by reference.
5. AIP or the Copyright Clearance Center may, within two business days of granting this license, revoke the license for any reason whatsoever, with a full refund payable to you. Should you violate the terms of this license at any time, AIP, American Institute of Physics, or Copyright Clearance Center may revoke the license with no refund to you. Notice of such revocation will be made using the contact information provided by you. Failure to receive such notice will not nullify the revocation.
6. AIP makes no representations or warranties with respect to the Material. You agree to indemnify and hold harmless AIP, American Institute of Physics, and their officers, directors, employees or agents from and against any and all claims arising out of your use of the Material other than as specifically authorized herein.
7. The permission granted herein is personal to you and is not transferable or assignable without the prior written permission of AIP. This license may not be amended except in a writing signed by the party to be charged.
8. If purchase orders, acknowledgments or check endorsements are issued on any forms containing terms and conditions which are inconsistent with these provisions, such inconsistent terms and conditions shall be of no force and effect. This document, including the CCC Billing and Payment Terms and Conditions, shall be the entire agreement between the parties relating to the subject matter hereof.

This Agreement shall be governed by and construed in accordance with the laws of the State of New York. Both parties hereby submit to the jurisdiction of the courts of New York County for purposes of resolving any disputes that may arise hereunder.

---

---

**From:** VCH-RIGHTS-and-LICENCES <[RIGHTS-and-LICENCES@wiley-vch.de](mailto:RIGHTS-and-LICENCES@wiley-vch.de)>  
**To:** Dmitry Yu. Zubarev <[dzoubarev@cc.usu.edu](mailto:dzoubarev@cc.usu.edu)>  
**Subject:** Antwort: WG: permission to reprint a paper as a part of PhD dissertation  
**Date:** Wed, 20 Feb 2008 09:09:49 +0100 (01:09 MST)

Dear Customer,

Thank you for your email.

We hereby grant permission for the requested use expected that due credit is given to the original source.

Please note that we only grant rights for a printed version, but not the rights for an electronic/ online/ web/ microfiche publication.

If material appears within our work with credit to another source, authorisation from that source must be obtained.

Credit must include the following components:

- Books: Author(s)/ Editor(s) Name(s): Title of the Book. Page(s). Publication year. Copyright Wiley-VCH Verlag GmbH & Co. KGaA. Reproduced with permission.

- Journals: Author(s) Name(s): Title of the Article. Name of the Journal. Publication year. Volume. Page(s). Copyright Wiley-VCH Verlag GmbH & Co. KGaA. Reproduced with permission.

With kind regards

Bettina Loycke

\*\*\*\*\*

Bettina Loycke  
 Copyright & Licensing Manager  
 Wiley-VCH Verlag GmbH & Co. KGaA  
 Boschstr. 12  
 69469 Weinheim  
 Germany

Phone: +49 (0) 62 01- 606 - 280  
 Fax: +49 (0) 62 01 - 606 - 332  
 Email: [rights@wiley-vch.de](mailto:rights@wiley-vch.de)

-----  
 Wiley-VCH Verlag GmbH & Co. KGaA  
 Location of the Company: Weinheim  
 Chairman of the Supervisory Board: John Herbert Jarvis  
 Trade Register: Mannheim, HRB 432833  
 General Partner: John Wiley & Sons GmbH, Location: Weinheim  
 Trade Register Mannheim, HRB 432296  
 Managing Directors : Christopher J. Dicks, Bijan Ghawami, William



Pesce

----- Weitergeleitet von VCH-ANGEWANDTE/VCH/Wiley am 20.02.2008 08:08  
-----

Yu. "Dmitry

Zubarev"

<dzoubarev@cc.usu

.edu>

angewandte@wiley-vch.de

An

Kopie

20.02.2008

07:50

Thema

as a

dissertation

permission to reprint a paper  
part of PhD

Dear Madam/Sir,

my name is Dmitry Yu. Zubarev. I'm a senior graduate student in Utah State University currently finalizing my PhD dissertation. I'm hereby asking for the permission to reprint an article co-authored by me and published in Angewandte Chemie International Edition, as a part of this

Dissertation. It would be more convenient for me to receive the permission by fax.

My mailing address:

Department of Chemistry and Biochemistry,  
Utah State University,  
0300 Old Main Hill,  
Logan, UT, USA 84322-0300

Phone number: +1 (435) 797-7507

Fax number: +1 (435) 797-3390

The article to be reprinted:

1) "d-Aromaticity in Ta3O3-: A New Mode of Chemical Bonding", Zhai,

H.-J.; Averkiev, B.  
B.; Zubarev, D. Yu.; Wang, L. S.; Boldyrev, A. I. Angew. Chem. Int.  
Ed.  
2007, 46, 4277.

I'm not a correspondence author.

Thank you in advance.

Sincerely,

Dmitry Yu. Zubarev

---



Dmitry Zubarev &lt;dmitry.zubarev@aggiemail.usu.edu&gt;

---

**RE: Permission Request Form: Dmitry Yu. Zubarev**

---

**CONTRACTS-COPYRIGHT (shared)** <Contracts-Copyright@rsc.org>  
To: dmitry.zubarev@aggiemail.usu.edu

Fri, Jul 11, 2008 at 1:17 AM

Dear Mr Zubarev

I sent a fax to the number given below on 20 February 2008.

The Royal Society of Chemistry (RSC) hereby grants permission for the use of your paper(s) specified below in the printed and microfilm version of your thesis. You may also make available the PDF version of your paper(s) that the RSC sent to the corresponding author(s) of your paper(s) upon publication of the paper(s) in the following ways: in your thesis via any website that your university may have for the deposition of theses, via your university's Intranet or via your own personal website. We are however unable to grant you permission to include the PDF version of the paper(s) on its own in your institutional repository. The Royal Society of Chemistry is a signatory to the STM Guidelines on Permissions (available on request).

Please note that if the material specified below or any part of it appears with credit or acknowledgement to a third party then you must also secure permission from that third party before reproducing that material.

Please ensure that the published article states the following:

*Reproduced by permission of the PCCP Owner Societies*

Regards

Gill Cockhead

Contracts & Copyright Executive

Gill Cockhead (Mrs), Contracts & Copyright Executive

Royal Society of Chemistry, Thomas Graham House

Science Park, Milton Road, Cambridge CB4 0WF, UK

Tel +44 (0) 1223 432134, Fax +44 (0) 1223 423623

<http://www.rsc.org>

-----Original Message-----

From: [dmitry.zubarev@aggiemail.usu.edu](mailto:dmitry.zubarev@aggiemail.usu.edu) [mailto:[dmitry.zubarev@aggiemail.usu.edu](mailto:dmitry.zubarev@aggiemail.usu.edu)]

Sent: 10 July 2008 23:23

To: CONTRACTS-COPYRIGHT (shared)

Subject: Permission Request Form: Dmitry Yu. Zubarev

Name : Dmitry Yu. Zubarev

Address :

Department of Chemistry and Biochemistry,

Utah State University,

0300 Old Main Hill,

Logan, UT, USA 84322-0300

Tel : +1 (435) 7977507

Fax : +1 (435) 7973390

Email : [dmitry.zubarev@aggiemail.usu.edu](mailto:dmitry.zubarev@aggiemail.usu.edu)

I am preparing the following work for publication:

Article/Chapter Title : PhD Dissertation

Journal/Book Title :

Editor/Author(s) :

Publisher :

I would very much appreciate your permission to use the following material:

Journal/Book Title : PCCP

Editor/Author(s) : Zubarev, D. Yu.; Averkiev, B. B.; Zhai, H. -J.; Wang, L. S.; Boldyrev, A. I.

Volume Number : 10  
Year of Publication : 2008  
Description of Material : Aromaticity and antiaromaticity in transition-metal systems  
Page(s) : 257  
Journal/Book Title : PCCP (on-line)  
Editor/Author(s) : Zubarev, D. Yu.; Boldyrev, A. I.  
Volume Number : 10  
Year of Publication : 2008  
Description of Material : Developing paradigms of chemical bonding: adaptive natural density partitioning  
Page(s) : DOI: 10.1039/b804083d

Any Additional Comments :

Dear Madam/Sir,

I've recently defended PhD degree in Utah State University and now I'm finalizing the text of my PhD dissertation. I'm hereby asking for the permission to reprint two articles co-authored by me and published in Physical Chemistry Chemical Physics, as a part of this Dissertation. It would be more convenient for me to receive the permission by fax or e-mail. It should also be mentioned, that my first request for the permission was sent on February 20, 2008 and I still have not received any reply.

**DISCLAIMER:**

This communication (including any attachments) is intended for the use of the addressee only and may contain confidential, privileged or copyright material. It may not be relied upon or disclosed to any other person without the consent of the RSC. If you have received it in error, please contact us immediately. Any advice given by the RSC has been carefully formulated but is necessarily based on the information available, and the RSC cannot be held responsible for accuracy or completeness. In this respect, the RSC owes no duty of care and shall not be liable for any resulting damage or loss. The RSC acknowledges that a disclaimer cannot restrict liability at law for personal injury or death arising through a finding of negligence. The RSC does not warrant that its emails or attachments are Virus-free: Please rely on your own screening.

---

**Washington State University**

Department of Physics  
2710 University Drive  
Richland, WA 99354-1671

**Pacific Northwest National Laboratory**

Chemical & Materials Science Division  
MS K8-88, P.O. Box 999  
3020 Q Street  
Richland, WA 99352

**Lai-Sheng Wang**

Professor & Affiliate Senior Chief Scientist

Tel: 509-371-6138  
Fax: 509-371-6139  
E-mail: ls.wang@pnl.gov  
<http://www.tricity.wsu.edu/~physics>

31 January, 2008

Dear Mr. Dmitry Yu. Zubarev,

This letter is to confirm that you have my permission to use our nine common papers:

1. "Aromaticity and antiaromaticity in transition-metal systems" (Phys. Chem. Chem. Phys. 2008, 10, 257-267)
2. "δ-Aromaticity in  $Ta_3O_3^-$ : A New Mode of Chemical Bonding" (Angew. Chem. Int. Ed. 2007, 46, 4277-4280)
3. "On the Chemical Bonding of Gold in Auro-Boron Oxide Clusters  $Au_nBO^-$  ( $n=1-3$ )" (Phys. Chem. A, 2007, 111, 1648-1658)
4. " $Sn_{12}^{2-}$ : Stannaspherene" (J. Am. Chem. Soc. 2006, 128, 8390-8391)
5. "Theoretical Probing of Deltahedral Closo-Auro-Boranes  $B_xAu_x^{2-}$  ( $x = 5-12$ )" (Inorg. Chem. 2006, 45, 5269-5271)
6. "Observation of Triatomic Species ( $AlSi_2^-$  and  $AlGe_2^-$ ) With Conflicting Aromaticity" (J. Phys. Chem. B, 2006, 110, 9743-9746)
7. "On the Structure and Chemical Bonding of  $Si_6^{2-}$  and  $Si_6^{2-}$  in  $NaSi_6^-$  upon  $Na^+$  Coordination" (J. Chem. Phys. 2006, 124, 124305-1 – 124305-13)
8. "Gold apes hydrogen. The structure and bonding in the planar  $B_7Au_2^-$  and  $B_7Au_2$  clusters" (J. Phys. Chem. A, 2006, 110, 1689-1693)
9. "Chemical bonding in  $Si_5^{2-}$  and  $NaSi_5^-$  via Photoelectron Spectroscopy and Ab Initio Calculations" (J. Phys. Chem. A 2005, 109, 11385-11394)

in part or in full for preparation or presentation of your dissertation.

Sincerely,



Lai-Sheng Wang

**Washington State University****Pacific Northwest National Laboratory***Department of Physics*

2710 University Drive, Richland, WA 99354

*Chemical & Materials Sciences Division*

MS K8-88, P.O. Box 999, Richland, WA 99352

**Dr. Hua-Jin Zhai**  
Phone: 509-371-6148  
Fax: 509-371-6139  
E-mail: Hua-Jin.Zhai@pnl.gov

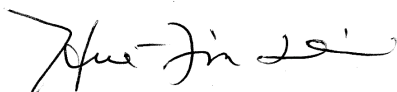
January 25th, 2008, Richland

Dear Dmitry Zubarev,

This letter is to confirm that you have my permission to use our common papers in part or in full for preparation or presentation of your PhD dissertation.

1. "Aromaticity and antiaromaticity in transition-metal systems" (*Phys. Chem. Chem. Phys.* 2008, 10, 257-267);
2. "delta-Aromaticity in Ta<sub>3</sub>O<sub>3</sub>:- A New Mode of Chemical Bonding" (*Angew. Chem. Int. Ed.* 2007, 46, 4277-4280);
3. "On the Chemical Bonding of Gold in Auro-Boron Oxide Clusters AunBO- (n=1-3)" (*J. Phys. Chem. A* 2007, 111, 1648-1658);
4. "Gold apes hydrogen. The structure and bonding in the planar B<sub>7</sub>Au<sub>2</sub>- and B<sub>7</sub>Au<sub>2</sub> clusters" (*J. Phys. Chem. A* 2006, 110, 1689-1693).

Sincerely,



Hua-Jin Zhai

01/23/08 15:49 FAX

001



To:

**Dmitry Zubarev**  
0300 Old Main Hill  
Department of Chemistry and Biochemistry, Utah State University  
Logan, Utah 84322-0300  
Phone number: (435) 797-7507  
Fax number: (435) 797-3390

I, Lei-Ming Wang, the 3rd author on the paper "Sn12 2-: Stannaspherene" (J. Am. Chem. Soc. 2006, 128, 8390-8391), hereby approve on my own behavior that my co-author, Dmitry Yu. Zubarev, can use this paper in part or in full for his PhD dissertation.

Lei-Ming Wang

01/23/08

Department of Physics, Washington State University  
2710 University Drive, Richland, WA 99354  
and Chemical & Materials Sciences Division, Pacific Northwest National Laboratory,  
MS K8-88, P. O. Box 999, Richland, WA 99352



5 February, 2008

Dear Mr. Dmitry Yu. Zubarev,

This letter is to confirm that you have my permission to use our three common papers:

1. "On the Chemical Bonding of Gold in Auro-Boron Oxide Clusters  $Au_nBO$  ( $n=1-3$ )" (J. Phys. Chem. A, 2007, 111, 1648-1658),
2. " $Sn_{12}^{2-}$ : Stannaspherene" J. Am. Chem. Soc. 2006, 128, (8390-8391)
3. "Theoretical Probing of Deltahedral Closo-Auro-Boranes  $B_xAu_x^{2-}$  ( $x=5-12$ )" (I. Inorg. Chem. 2006, 45, 5269-5271)

in part or in full for preparation or presentation of your dissertation.

Sincerely,



Dr. Jun Li

## THE ROWLAND INSTITUTE AT HARVARD

100 EDWIN H. LAND BOULEVARD  
CAMBRIDGE, MASSACHUSETTS 02142TEL: (617) 497-4600  
FAX: (617) 497-4627  
www.rowland.harvard.edu**Xi Li**Rowland Institute at Harvard  
Harvard University  
100 Edwin H. Land Blvd.  
Cambridge, MA 02142  
Tel: 617-497-4726  
Fax: 617-497-4627  
Email: [li@rowland.harvard.edu](mailto:li@rowland.harvard.edu)

January 26, 2008

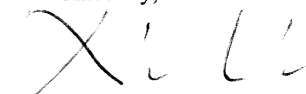
**Dmitry Yu. Zubarev**0300 Old Main Hill  
Department of Chemistry and Biochemistry  
Utah State University  
Logan, Utah 84322-0300  
Phone number: (435) 797-7507  
Fax number: (435) 797-3390

Dear Dmitry Yu. Zubarev:

You have my permission to use our three common articles (papers) "Observation of Triatomic Species (AlSi<sub>2</sub>- and AlGe<sub>2</sub>-) With Conflicting Aromaticity" (J. Phys. Chem. B, 2006, 110, 9743-9746), "On the Structure and Chemical Bonding of Si<sub>6</sub><sup>2-</sup> and Si<sub>6</sub><sup>2-</sup> in NaSi<sub>6</sub>- upon Na<sup>+</sup> Coordination" (J. Chem. Phys. 2006, 124, 124305-1 - 124305-13), and "Chemical bonding in Si<sub>5</sub><sup>2-</sup> and NaSi<sub>5</sub>- via Photoelectron Spectroscopy and Ab Initio Calculations" (J. Phys. Chem. A 2005, 109, 11385-1394) in part or in full in preparation or presentation of your PhD dissertation.

Please let me know if any questions arise.

Sincerely,

  
Xi Li, PhD

20 February, 2008

Dear Mr. Dmitry Yu. Zubarev,

This letter is to confirm that you have my permission to use our three common papers:

1. "Sn<sub>12</sub><sup>2-</sup>: Stannaspherene" (J. Am. Chem. Soc. 2006, 128, 8390-8391)
2. "On the Structure and Chemical Bonding of Si<sub>6</sub><sup>2-</sup> and Si<sub>6</sub><sup>2-</sup> in NaSi<sub>6</sub><sup>-</sup> upon Na<sup>+</sup> Coordination" (J. Chem. Phys. 2006, 124, 124305-1 – 124305-13)
3. "Chemical bonding in Si<sub>5</sub><sup>2-</sup> and NaSi<sub>5</sub><sup>-</sup> via Photoelectron Spectroscopy and Ab Initio Calculations" (J. Phys. Chem. A 2005, 109, 11385-11394)

in part or in full for preparation or presentation of your dissertation.

Sincerely,



3/3-2008

Dr. Li-Feng Cui

Yale University  
Department of Chemistry  
225 Prospect Street  
New Haven, CT 06520-8107  
Phone: 203-432-6288  
Fax: 203-432-6144



Anastassia Alexandrova, Ph.D.

23 January, 2008

Dear Mr. Dmitry Yu. Zubarev,

This letter is to confirm that you have my permission to use our common paper "On the Structure and Chemical Bonding of  $\text{Si}_6^{2-}$  and  $\text{Si}_6^{2-}$  in  $\text{NaSi}_6^-$  upon  $\text{Na}^+$  Coordination" (*J. Chem. Phys.* 2006, 124, 124305-1 - 124305-13) in part or in full for preparation or presentation of your dissertation.

Sincerely,

A handwritten signature in black ink, appearing to be 'A. Alexandrova', written in a cursive style.

Anastassia N. Alexandrova



January 30, 2008

Dear Mr. Zubarev

I am writing this letter in confirmation of my permission for you to use in your Dissertation any data and materials you wish from our common papers "Aromaticity and antiaromaticity in transition-metal systems" (*Phys. Chem. Chem. Phys.* 2008, 10, 257-267) and "δ-Aromaticity in Ta<sub>3</sub>O<sub>3</sub><sup>-</sup>: A New Mode of Chemical Bonding" (*Angew. Chem. Int. Ed.* 2007, 46, 4277-4280).

Yours sincerely,

Boris Averkiev

A handwritten signature in black ink, appearing to be "BA", written over a light blue horizontal line.



Dmitry Zubarev,

As a co-author of the article, "Global Minimum Structure Searches via Particle Swarm Optimization" (J. Comput. Chem. 2007, 28, 1177-1186), I hereby give you my permission to use material from the article in your PhD dissertation.

Seth Call



**Subject:** e-mails of co-authors  
**From:** "Dmitry Yu. Zubarev"  
**Date:** Wed, 23 Jan 2008 16:04:46 -0700  
**To:** [L.S.WANG@PNL.GOV](mailto:L.S.WANG@PNL.GOV)

Dear Lai-Sheng,

do you happen to have current emails of Li-Feng Cui, Xin Huang, Xi Li, and Jun Li? I need to get permissions from them as well. Thank you in advance.

With respect,

Dmitry Zubarev

**Subject:** recommendation letter  
**From:** "Dmitry Yu. Zubarev"  
**Date:** Tue, 19 Feb 2008 11:47:36 -0700  
**To:** wang

Dear Prof. Wang,

it looks like Prof. Bartlett is interested in my joining his group. Could you please send a recommendation letter to him? His email is [bartlett@qtp.ufl.edu](mailto:bartlett@qtp.ufl.edu). Also, do you keep in touch with Huang Xin? I need to contact him to get permission to use a common publication in my dissertation, but can't find his email. Thank you in advance.

With respect,

Dmitry Zubarev

## CURRICULUM VITAE

Dmitry Yu. Zubarev  
(February, 2008)

Department of Chemistry and Biochemistry, Utah State  
University, 0300 Old Main Hill, Logan, Utah, 84322-  
0300 Phone: (435) 764-1903  
E-mail: [dzoubarev@cc.usu.edu](mailto:dzoubarev@cc.usu.edu)  
Web: <http://www.chem.usu.edu/~boldyrev/dmitry.php>

## EDUCATION

PhD program, Utah State University, Department of Chemistry and Biochemistry,  
Logan, UT, USA, 2004-present (approximate time of graduation – March 2008),  
GPA=4.0

School of Graduate Studies, Department of Chemistry, Peoples' Friendship  
University of Russia, Moscow, Russia, 2000 - 2003, GPA=4.0

M.Sc in Chemistry Diploma with Excellency, Department of Chemistry, Peoples'  
Friendship University of Russia, Moscow, Russia, 1998-2000, GPA=4.0

B.Sc. in Chemistry Diploma with Excellency, Department of Physical-  
Mathematical and Natural Sciences, Peoples' Friendship University of Russia,  
Moscow, Russia, 1993-1998, GPA=4.0

Misc:

Graduate level “Quantum Mechanics” course, Utah State University, Spring 2006.



Summer School on Photoelectron Spectroscopy, University of Arizona, June 2005.

Workshop on parallel computations with Beowulf Clusters, Utah State University, Summer Semester, 2005.

## PROFESSIONAL EXPERIENCE

Research assistant, Department of Chemistry and Biochemistry, Utah State University, group of Prof. Boldyrev, Fall 2004-present.

- establishing ground state geometries of subnanoclusters in molecular beams, interpretation of the results of single-molecule photoelectron spectroscopy of subnanoclusters in molecular beams (in collaboration with the group of Prof. Lai-Sheng Wang, PNNL, WSU)
- development of the general theory of chemical bonding in the clusters of the main group and transitional elements and further extension of such a theory to the description of solid state.
- development of software capable of describing and analyzing the chemical bonding in chemical systems of general type, including electron-deficient systems (Adaptive Natural Density Partitioning (AdNDP)).

Graduate research assistant, Kurnakov's Institute of General and Inorganic Chemistry, group of academician Moiseev, 2003-2004.

- Computational studies of prototropic tautomerism for model systems relevant to the chemistry of the singlet dioxygen.

## TEACHING EXPERIENCE

Teaching assistant, General Chemistry, Department of Chemistry and Biochemistry, Utah State University, Fall 2007.

Full-time lecturer, Non-equilibrium thermodynamics, Division of Physical Chemistry, Department of Physical-Mathematical and Natural Sciences, People's Friendship University of Russia, Fall 2003-Spring 2004.

Teaching assistant, Programming in Chemistry (Laboratory), Division of Physical Chemistry, Department of Physical-Mathematical and Natural Sciences, People's Friendship University of Russia, Fall 2000-Spring 2003.

Teaching assistant, Physical Chemistry (Laboratory), Division of Physical Chemistry, Department of Physical-Mathematical and Natural Sciences, People's Friendship University of Russia, Fall 2000-Spring 2003.

Mentoring of undergraduate and graduate students, Department of Chemistry and Biochemistry, Utah State University, group of Prof. Boldyrev:

- Seth T. Call (M.Sc., computer science major, currently on PhD program in BYU), development of Particle Swarm Optimization software for the chemistry, publication #7.
- Deric Holden (B.Sc., chemistry major), ab-initio study of structure and photoelectron spectra of  $\text{Ge}_{12}^-$  system.

## PROJECTS AND SPECIAL ACTIVITIES

“Evolution of chemical bonding upon fusion of planar aromatic clusters into 2-D and 3-D clusters and into 3-D networks”: Prof. Boldyrev (Utah State University),

Prof. Wang (Washington State University, Pacific Northwest National Laboratory), funded by National Science Foundation.

“Probing aromaticity in transition metal clusters”: Prof. Boldyrev (Utah State University), Prof. Wang (Washington State University, Pacific Northwest National Laboratory), funded by Petroleum Research Foundation.

“Development of a new Natural Cluster Units (NCU) analysis for deciphering chemical bonding in clusters”: Prof. Boldyrev (Utah State University), Prof. Weinhold (University of Wisconsin - Madison), (submitted to National Science Foundation)

“Dioxygen reactivity of acireductons”: Prof. Boldyrev (Utah State University), Prof. Berreau (Utah State University)

## EXPERTISE AND SKILLS

### Computational Methods

1. general: *ab-initio*, DFT, semi-empirical;
2. global optimization: Genetic Algorithms, Monte-Carlo Simulated Annealing, Particle Swarm Optimization;
3. analysis of electronic structure: Canonical Molecular Orbitals, Natural Bonding Orbitals, Electron Localization Function;

### Software

- quantum chemical: Gaussian, MOLPRO, NWChem, ADF;
- global optimization: GEGA, PSO;
- analysis of electronic structure: NBO, TopMod, AdNDP;

- visualization: Molden, GaussView, VMD, Molekel;

#### Development

- programming languages: Fortran, C++, HTML, PERL;
- developed software: Adaptive Natural Density Partitioning (AdNDP)

#### Capabilities

- electronic structure calculations (single- and multi-configurational)
- global optimization
- simulation of the spectroscopic properties (IR, photoelectron)
- analysis of chemical bonding
- studies of the reaction pathways
- method development

### RESEARCH INTERESTS

Development of general theory of chemical bonding

Cluster growth and isomerization in condensed phases

Self-assembly of nanostructures

Structural and temporal ordering in the systems far from thermodynamic equilibrium

Abiogenesis

### AWARDS AND HONORS

Chemistry and Biochemistry Alumni Award, Department of Chemistry and Biochemistry, Utah State University, 2007.

One-year sponsored membership in AAAS/Science, the AAAS/Science Program for Excellency in Science, 2005-2006.

M.Sc. Diploma with Excellency, 2000.

B.Sc. Diploma with Excellency, 1998.

#### FELLOWSHIPS AND SCHOLARSHIPS

USU School of Graduate Studies Dissertation Fellowship, 2007 – 2008

Presidential Fellowship, Utah State University, 2004.

#### PROFESSIONAL AFFILIATIONS AND STUDENT ORGANIZATIONS

Graduate Student Senate representative for the Department of Chemistry and Biochemistry since November 2006.

Student Member of the American Chemical Society since May 2005.

Member of the USU Men's Volleyball Club team in 2004-2007.

#### LIST OF PUBLICATIONS AND PRESENTATIONS (January 24, 2008)

1. "Why Carbon Avoids High Coordination in Carbon-Boron Clusters", Averkiev, B. B.; Zubarev, D. Yu.; Wang, L. M.; Huang, W.; Wang, L. S.; Boldyrev, A. I. (submitted for the publication in *J. Am. Chem. Soc.*)
2. "Developing Paradigms of Chemical Bonding: Adaptive Natural Density Partitioning", Zubarev, D. Yu.; Boldyrev, A. I. (submitted for the publication in *J. Am. Chem. Soc.*)
3. "Aromaticity and antiaromaticity in transition-metal systems", Zubarev, D. Yu.;

- Averkiev, B. B.; Zhai, H. -J.; Lai-Sheng Wang; Boldyrev, A. I. *Phys. Chem. Chem. Phys.* 2008, *10*, 257 (cover page)
4. “Multiple Aromaticity, Multiple Antiaromaticity, and Conflicting Aromaticity in Planar Clusters”, Zubarev, D. Yu.; Boldyrev, A. I. (chapter in the book “Clusters - a Bridge Across Disciplines”, in press)
  5. “ $\delta$ -Aromaticity in  $Ta_3O_3^-$ : A New Mode of Chemical Bonding”, Zhai, H.-J.; Averkiev, B. B.; Zubarev, D. Yu.; Wang, L. S.; Boldyrev, A. I. *Angew. Chem. Int. Ed.* 2007, *46*, 4277 (highlighted in Chemical and Engineering News, May 7, 2007, 54).
  6. “On the Chemical Bonding of Gold in Auro-Boron Oxide Clusters  $Au_nBO^-$  ( $n=1-3$ )”, Zubarev, D. Yu.; Boldyrev, A. I.; Li, J.; Zhai, H.-J.; Wang, L. S. *J. Phys. Chem. A*, 2007, *111*, 1648.
  7. “Global Minimum Structure Searches via Particle Swarm Optimization”, Call, S. T.; Zubarev, D. Yu.; Boldyrev, A. I. *J. Comput. Chem.* 2007, *28*, 1177.
  8. “Comprehensive Analysis of Chemical Bonding in Boron Clusters”, Zubarev, D. Yu.; Boldyrev, A. I. *J. Comput. Chem.* 2006, *28*, 251 (Special Issue: 90 Years of Chemical Bonding; cover page of vol. 28, iss. 2-5).
  9. “ $Sn_{12}^{2-}$ : Stannaspherene”, Cui, L. F.; Huang, X.; Wang, L. M.; Zubarev, D. Yu.; Boldyrev, A. I.; Li, J.; Wang L. S. *J. Am. Chem. Soc.* 2006, *128*, 8390 (communication).
  10. “Theoretical Probing of Deltahedral Closo-Auro-Boranes  $B_xAu_x^{2-}$  ( $x = 5-12$ )”, Zubarev, D. Yu.; Li, J.; Wang, L. S.; Boldyrev, A. I. *Inorg. Chem.* 2006, *45*, 5269 (communication).

11. "Observation of Triatomic Species ( $\text{AlSi}_2^-$  and  $\text{AlGe}_2^-$ ) With Conflicting Aromaticity", Zubarev, D. Yu.; Boldyrev, A. I.; Li, X.; Wang, L. S. *J. Phys. Chem. B*, 2006, *110*, 9743 (communication).
12. "On the Structure and Chemical Bonding of  $\text{Si}_6^{2-}$  and  $\text{Si}_6^{2-}$  in  $\text{NaSi}_6^-$  upon  $\text{Na}^+$  Coordination." Zubarev, D. Yu.; Alexandrova, A.; Boldyrev, A. I.; Cui, L. F.; Li, X.; Wang, L. S. *J. Chem. Phys.* 2006, *124*, 124305.
13. "Gold apes hydrogen. The structure and bonding in the planar  $\text{B}_7\text{Au}^{2-}$  and  $\text{B}_7\text{Au}_2$  clusters." Zhai, H.-J.; Wang, L. S.; Zubarev, D. Y.; Boldyrev A. I. *J. Phys. Chem. A*, 2006, *110*, 1689 (communication, cover page).
14. "Chemical bonding in  $\text{Si}_5^{2-}$  and  $\text{NaSi}_5^-$  via Photoelectron Spectroscopy and Ab Initio Calculations." Zubarev, D. Yu.; Boldyrev, A. I.; Li, X.; Cui, L. F.; Wang, L. S. *J. Phys. Chem. A* 2005, *109*, 11385.
15. "Appraisal of the performance of nonhybrid density functional methods in characterization of the  $\text{Al}_4\text{C}$  molecule." Zubarev, D. Yu.; Boldyrev, A. I. *J. Chem. Phys.* 2005, *122*, 144322.

## PRESENTATIONS

1. "Evolution of the paradigms of chemical bonding", oral presentation, 22nd Austin Symposium on Molecular Structure, Austin, TX, March 1-4, 2008.
2. "Breakdown of the spherical symmetry in semiconducting sub-nanoclusters", talk at the Club Med seminar, Department of Chemistry, Yale University, November 16, 2006.
3. "Possibility of novel gold-boron compounds", poster session, 232nd ACS

National Meeting, San Francisco, CA, September 10-14, 2006.

4. "Peculiarities of chemical bonding in multiply charged silicon clusters: Joint ab-initio and photoelectron spectroscopy study", poster session, 231st ACS National Meeting, Atlanta, GA, March 26-30, 2006.